Quantitative mass spectrometry-based approaches for characterizing the immunopeptidome and tyrosine phosphoproteome in cancer

by

Lauren Elizabeth Stopfer

B.S. Biomedical Engineering
University of Wisconsin-Madison, 2015

Submitted to the Department of Biological Engineering in partial fulfillment of the requirements for the degree of

Doctor of Philosophy

at the

Massachusetts Institute of Technology

June, 2021

Author:

Lauren Elizabeth Stopfer
Department of Biological Engineering
January 26, 2021

Certified by:

Forest M. White
Ned C. and Janet Bemis Rice Professor of Biological Engineering
Thesis Supervisor

Certified by:

Douglas A. Lauffenburger
Ford Professor of Biological Engineering, Chemical Engineering, and Biology
Thesis Supervisor

Accepted by:

Katharina Ribbeck
Associate Professor of Biological Engineering
Chairman, Graduate Program Committee of Biological Engineering

This doctoral thesis dissertation has been examined by following thesis advisory committee members

Forest M. White, PhD
Ned C. and Janet Bemis Rice Professor of Biological Engineering
Thesis Supervisor

Douglas A. Lauffenburger, PhD
Ford Professor of Biological Engineering, Chemical Engineering, and Biology
Thesis Supervisor

K. Dane Wittrup, PhD
C.P. Dubbs Professor of Chemical Engineering and Biological Engineering
Committee Chairperson

Ryan Sullivan, MD
Massachusetts General Hospital Cancer Center and Harvard Medical School
Committee Member

Quantitative mass spectrometry-based approaches for characterizing the immunopeptidome and tyrosine phosphoproteome in cancer

by

Lauren Elizabeth Stopfer

Submitted to the Department of Biological Engineering June, 2021 in partial fulfillment of the requirements for the degree of Doctor of Philosophy in Biological Engineering

Abstract

Significant advancements in proteome-based analyses stem from innovations in the field of mass spectrometry (MS), an analytical method which allows for the sequencing, identification, and quantification of peptides and proteins in complex biological mixtures. MS enables a molecular and systems-wide understanding of the cell state, capturing post-translational modifications, protein turnover rates, protein-protein interactions, and other measurements that genetics cannot assess. Still, MS-based methods often require a compromise between reproducibility, quantitative accuracy, sensitivity, and depth of coverage, limiting their utility in research and translational settings alike. Here, I present a collection of MS-based platforms for targeted tyrosine phosphorylation signaling measurements and quantitative immunopeptidomics profiling, enabling novel biological findings in the field of cancer research. I describe how targeted tyrosine signaling assays can be leveraged to identify activated signaling pathways and assess immune infiltration in colorectal cancer. I also demonstrate how small molecules alter the peptide major histocompatibility complex repertoire in melanoma, and report copies-per-cell estimates of select treatment-modulated antigens using targeted MS, informing the development of targeted immunotherapies. Together, these findings highlight how innovations in MS-based methods can be used to advance a basic biology understanding of cancer and serve to demonstrate the clinical utility of using such assays to inform cancer therapy.

Thesis Supervisor: Forest M. White
Ned C. and Janet Bemis Rice Professor of Biological Engineering

Thesis Supervisor: Douglas M. Lauffenburger
Ford Professor of Biological Engineering, Chemical Engineering, and Biology

“Innovation, automation, and miniaturization.
Most advances in biology can usually be traced back to the development of a new technique.”

Peter James
Protein identification in the post-genome era: the rapid rise of proteomics, 1997

Acknowledgements

"I stand on the sacrifices of a million women before me
thinking what can I do to make this mountain taller
so the women after me can see farther?"

Legacy- Rupi Kaur

Where to begin. There are many (many) people who helped me navigate my way to this point.

I'd first like to thank my advisors, Forest and Doug, who have both served as mentors in and outside of the lab. I prioritized selecting research advisors that I felt were good people, and it's a decision I've never regretted. Your trust, understanding, encouragement, and pushing when necessary, has shaped me in more ways than you know. You made me feel important, even when I did not believe it myself. I'd also like to thank my committee chair, Dane, and committee member, Ryan, for your enthusiasm and support regarding science and life. The four of you have always made it clear that you care about my wellbeing and prioritize conversations about it before we talk about science. This has and continues to mean a great deal to me.

To the former research mentors, Pam and Dan, thank you for believing in me and giving me the push to get my PhD, and for writing recommendation letters (and Susan) that somehow got me into MIT. It's an honor to have been trained and mentored by you. To Molly, thank you for your training, mentorship, and friendship at Wisconsin and beyond.

To Linda, Diana, Jaime, Shelby, Catherine, Shalmalee, Jacqueline, and others who noticed when I wasn't okay, no thank you here will ever be enough.

A huge thank you to my lab mates from the White and Lauffenburger labs, especially Antje, Kristina, Daniel, Vibhuti, Nader, Jacqueline, Ishwar, JJ, Sean, Cam, and Elizabeth. You all have taught me so much, and I can honestly say working alongside you throughout the years has been great fun. In particular, I'd like to thank Antje and Kristina for helping me find my way as both a scientist and as a young adult. I adore you both. To my former UROP Josh, I think you probably taught me more than I taught you. I feel fortunate to have mentored you and can't wait to see where you take your career. I'd also like to thank Brian for your honest criticism and valuable suggestions, which has always propelled my work to a higher level, and to Toni, for always being willing to serve as a sounding board (mass spec related, or otherwise).

I'd be remiss not to thank all the fantastic collaborators I've had the pleasure of working with throughout the years, including Alex, Tim, Nick, Shelby, Catherine, Louis, Jen, and the team at Array biopharma. To the team at Thermo Fisher, especially Aaron, Sebastien, and Bhavin, what started as a week in San Jose has blossomed into more opportunities (presentations, conferences, webinars, articles) than I could have ever imagined. The SureQuant project fundamentally changed the way I think about mass spectrometry. Your

enthusiasm regarding my follow up MHC idea has allowed for the creation of a method I think is really special, and I so appreciate your help in turning the idea into a reality.

During my time at MIT, I had the privilege to be involved with the MIT Communication lab, to serve on the MIT grad blog's editorial board, and to begin the BEAAP program. These programs gave me purpose in a time when I greatly needed it, and I am glad to have met and worked alongside the members of these groups. I also served as an East Campus GRT for two years, which provided me with the most interesting stories and most wonderful friends—to my residents, who trusted me to have hard and thought-provoking conversations with, thank you. I learned a multitude of new things from you all, which continue to inform how I navigate life. To Mary, Rich, Lisa, Davi, Alexandria, and the rest of the EC team, it was an honor to have worked with and learned from you all. I'll miss being just steps away from an impromptu drink at the Muddy.

To my lab neighbors and classmates who have become close friends, thank you for sharing coffees and glasses of wine with me. A special thank you to Jared, my haiku co-author and someone whom I can always count on to be wearing a matching outfit to my own. You sparkle, and I adore being your friend.

To my dear college friends and KKG "sisters," especially Dana, Brooks, Weisberg, Davidson, Shelly, Chez, Annie, Taylor, Ficho, Sheenae, Hannan, Bailey, Ashley, Karol, Rocky, and Pena, having trips to visit you all in Chicago, California, Wisconsin, DC, Australia, etc. sprinkled through each semester helped make these 5.5 years fly by. I never laugh harder than when we're together, and I value your friendships immensely. Adolphe!

To my partner, Jon, thank you for being my rock. Thank you for your patience, your willingness to celebrate the smallest of victories, and your faithful support in my endeavors, past, present, and future. I look forward to seeing where our careers and lives take us, and I feel so lucky to have by my side.

Finally, I have to thank my family. To my parents, Lisa and Pete, thank you for your unconditional support. Whether you were helping me create the prettiest tri-fold board for a school project or building a car as close to the weight limit as possible for the pinewood derby, I always knew you cared, and you made sure I was equipped with the tools and the "chauffeuring" to give each and every opportunity my all. To my sister, Natalie, you have always provided me the most thoughtful and mature advice, all while managing to keep me a little hip. Your confidence is contagious, and I love being your sister. To my grandparents Jim, Dee, and Marilyn, to Brian and Lily, to Barb, you've all shaped me into who I am today, and I am so lucky to have so many family members that love and support me. To my late grandfather, "Papa," and my great-uncle Brian, I wish you were here. I dedicate this work in your memory.

Table of Contents

List of Figures

List of Tables

CHAPTER 1: Introduction

1-1 Therapeutic landscape for cancer patients

Cancer is driven by mutations, deletions, and amplifications in oncogenes or tumor suppressor genes, which can lead to uncontrolled cellular replication, migration, invasion, angiogenesis, and immune evasion, among others.[1,2] Despite advances in diagnostics and therapies, cancer remains the second leading cause of death in the united states, with over 600,000 deaths reported in 2019.[3] Beyond surgical resection, cancer therapies historically have been aimed at exploiting these cancer "hallmarks," such as radiation therapy, which cases DNA damage and limits tumor cell replication, or cytostatic chemotherapies which aim to disrupt the cell cycle by targeting the cytoskeleton (alkylating agents) and essential metabolic enzymes (antimetabolites).[4–6] Chemotherapy has demonstrated success in many types of cancer and remains the frontline therapeutic option for cancers including ovarian & cervical cancer, however chemotherapies have a documented low tumor specificity profile and often result in toxicity with serious side effects.[7,8] Furthermore, patients can develop resistant to chemotherapy through innate/adaptive mechanisms such as cells undergoing epithelial to mesenchymal transition, enrichment of cancer stem cells in the tumor, and tumor hypoxia.[9–11] A study from 2004 surveying published literature estimated chemotherapy's contribution to clinical trials with an observed 5-year survival benefit across 22 malignancies at just 2%, highlighting the relatively minor contribution of chemotherapy to patient survival.[12]

1-1-1 Targeted Therapy

Over the past two decades, a shift in the cancer treatment paradigm occurred with the emergence of targeted therapies. Targeted therapies come in two flavors: small molecule inhibitors (SMI) and monoclonal antibodies (mAbs), aimed at interfering with oncogenic signal transduction in tumor cells specifically, mitigating toxicity. SMI often bind to the ATP binding site on tyrosine kinases, which inactivates the kinase domain and halts aberrant downstream signal transduction.[13] There are a variety of SMIs approved for use across a range of cancer types, including gefitinib, a receptor tyrosine kinase inhibitor against the epidermal growth factor receptor (EGFR) for use in non-small cell lung carcinoma that demonstrated ~11 month PFS, and vemurafenib, a BRAF inhibitor approved in BRAF-mutant melanomas that extended PFS to ~7 months.[14–16]

Targeted mAb therapies have similar efficacies—the anti-EGFR mAb cetuximab extended overall survival in colorectal cancer patients by several months, and the anti-epidermal growth factor receptor 2 (ErbB2) mAb trastuzumab in combination with chemotherapy extended PFS to 7.4 months.[17,18] While multiple targeted therapies can be combined to further improve patient response, as is the case with BRAF/MEK combination therapy in BRAF-mutant melanomas, targeted therapies are generally non curative.[19] While targeted therapies have led to a significant extension of progression-free survival, responses are often transient. Most patients progress within a year of therapy due to innate or acquired resistance mechanisms. ,

At the center of therapeutic success is identifying the right drug & dose for each patient, i.e., “precision medicine,” which has been greatly aided by advances in genetics which allow for genetic sequencing of large target panels with ease. These data can detect mutations such as the BRAF or EGFR mutations previously described, which identify potential therapeutic targets. Still, the limited success of targeted therapies highlights a more complicated, less linear

relationship between identifying an oncogenic driver mutation and treated with an inhibitor of that that particular protein.[20] Dysfunctional signaling in cancer can arise not only from mutations, but also altered epigenetics and rewired signaling networks. Resistance to targeted therapies can similarly stem from the activation of alternate or parallel signaling pathways (by-pass signaling) or alterations/mutations of the therapeutic target or driver mutation.[21]

Utilizing signaling-level information such as the modification state of proteins (ex. phosphorylation), can identify activated signaling networks driving growth or resistance, which may be useful in both experimental and clinical applications to characterize/identify disease subtypes and biomarkers. Unfortunately, methods to make signaling-level measurements lag behind the ease and scale of genetics-based measurements. To improve the ease and reproducibility of making phosphorylation-based measurements, this work describes the development of SureQuant pTyr, a targeted mass spectrometry-based method for high density, quantitative phosphoproteomic measurements. This approach identifies activated signaling networks in human tumors, highlighting potential therapeutic targets.

1-1-2 Checkpoint blockade inhibitors

In recent years, the emergence of immunotherapy has revolutionized the standard of care for cancer patients, specifically though identifying cancer “checkpoints,” cell surface receptors that control the activation or inhibition of immune response.[22] The discovery and generation of monoclonal antibody inhibitors against the checkpoints cytotoxic T lymphocyte antigen 4 (CTLA-4) and programmed cell death protein 1 (PD-1) have been so pivotal in the field of immuno-oncology that immunologists James Allison and Tasuku Honjo received the novel prize in Psychology or Medicine in 2018. Antibodies that block these immune checkpoints “release the brakes” on the immune system, initiating anti-tumor immune response.

To date, checkpoint blockade immunotherapy (CBI) has had the greatest success in melanoma. Unfortunately, immunotherapies are often limited by immune-related adverse events (IRAEs), which are common as CBIs are general immune activators (i.e. *not* tumor-specific). While the combination CBI therapy showed increased efficacy in melanoma, the number of immune-related adverse events among patients nearly doubled. Furthermore, despite the success observed in metastatic melanoma, many cancer types have low objective response rates (~15-30%), and some have nearly nonexistent response rates.[23] Broadly, tumors that response well to immunotherapy have a high mutational burden. Colorectal tumors classified as DNA mismatch repair-deficient (dMMR) or microsatellite instable-high (MSI-high) have higher objective response rates to PD-1 therapy (34%), whereas microsatellite-stable tumors (MSI-low)/mismatch repair proficient (pMMR) are unresponsive.[24,25]

1-1-3 Therapeutic modalities alter tumor immunogenicity

Loss or downregulation of antigen presentation is a common mechanism used by cancer cells to escape immune recognition. This can have two consequences: first, it limits the direct priming of T cells by tumor antigen presenting cells, and second, it prevents recognition of tumor cells by antigen-specific immune cells.[26] As a result, there is a growing interest in identifying ways to increase the immunogenicity of “immunologically cold” tumors, or those with low antigen presentation and few infiltrating immune cells. One promising avenue is to combine CBI with other approved therapeutic modalities such as chemotherapy, radiotherapy, and targeted therapies to increase antigen expression and enhance tumor immunogenicity. This may sensitize patients to checkpoint inhibitors or other T-cell based immunotherapy by restoring or even “forcing” tumor cells to upregulate antigen signals.

Chemotherapy has several immuno-modulating effects, including inducing pro-inflammatory cytokine secretion in macrophages, which recruits and activates effector cells such as dendritic, natural killer and T cells, and decreasing the presence of suppressor cells such as T-regs.[27] Chemotherapy also increases major histocompatibility complex (MHC) class I presentation and tumor antigen presentation, increasing the antigenicity of the tumor.[28] Similarly, radiotherapy induces DNA damage, which increases immunostimulatory cytokine release, promotes antigen presentation by MHCs, and recruits antigen-presenting and effector immune cells.[29] Radiotherapy has also been shown to drive neoantigen generation, which may further improve CBI efficacy.[30]

Cells treated with various small molecule inhibitors have also displayed increased immunogenicity. MEK inhibitiors have been shown to increase surface levels of HLA, increase PD-L1 expression, reduce immunosuppressive cytokine secretion, an improve T cell killing by antibody dependent cellular cytotoxicity.[31–33] Other kinase inhibitors, such as EGFR, ErbB2, and PI3K inhibitors have also been shown to have similar immunomodulating effects.[34–36] In general, kinase inhibition has been shown to increase mRNA expression of HLA and other components in the antigen presentation pathway, and a knockdown experiment of STAT1 decreased surface HLA upregulation following MEKi, suggesting a role for STAT1 in regulating MHC upregulation.[31,37] Further studies have identified that type II interferons (IFN-g) bind to JAK1, which phosphorylates STAT1 and increases transcription of interferon regulated genes, including those involved in antigen presentation.[38,39]

Cyclin-dependent kinases 4 and 6 (CDK4/6) control cell cycle progression and is often dysregulated and overactive, therefore CDK4/6 inhibitors have emerged as promising therapeutic candidates across multiple cancer types[40,41]. In breast cancer, CDK4/6 inhibition has been shown to increase antigen presentation and suppress T reg proliferation, enhancing tumor immunogenicity.[42] CDK4/6 inhibition increased type III interferons instead of type II interferons,

but STAT1 signaling was also implicated in driving MHC upregulation. Beyond the examples detailed here, HDAC inhibitors, demethylating agents, cytokines, and other agonist therapies (toll-like receptors, CD40) have demonstrated enhanced MHC class I expression and other immunostimulatory effects upon treatment.[26]

These studies establish the therapeutic potential of utilizing traditional anti-cancer agents to enhance immunogenicity, and as a result an array of clinical trials evaluating therapies in combination with CBI are ongoing, some of which have shown promise.[43–45] Still, the combination of agents as well as the order and timing of treatment administration remain poorly understood, but is likely to be a critical element in clinical trial success. Therefore, to better understand how to optimally design synergistic combination regimes that enhance the efficacy of ICB, a deeper understanding of how different perturbations alter the cell signaling and immune landscape is required. Central to this is measuring how the antigen repertoire presented by class I MHCs shifts in response to therapy. Current efforts focus primarily on global changes in expression levels, but a precise, molecular understanding of relative and absolute quantitative changes in pMHC expression, on a per-antigen basis, is required to best understand how to rationally design combination treatments and identify new antigens as therapeutic targets. For improved quantitative accuracy over existing pMHC mass-spectrometry based methods, this thesis describes a novel platform for quantitative pMHC profiling using heavy isotope labeled MHCs (hipMHCs), which is applied to profile repertoire changes to CDK4/6 inhibitors and MEK inhibitors in melanoma. Furthermore, hipMHCs are utilized for absolute quantification of antigens of interest, which highlight treatment-modulated antigens that can be leveraged for targeted immunotherapy.

1-2 Antigen Presentation

1-2-1 MHC Class I Peptides

Major histocompatibility complex (MHC) class I molecules are expressed by all nucleated cells types, whose role is to present degraded protein fragments (i.e. peptides) on the cell surface for recognition by the immune system (**Figure 1-1**).[46] While the biology behind antigen processing is complex and remains an active area of study, most pMHCs are thought to be derived from proteins that are degraded by cytosolic and nuclear proteasomes. The degraded peptides are next translocated from the cytoplasm into the endoplasmic reticulum aided by the protein TAP (transporter associated with antigen presentation). TAP also assists in folding MHC I molecules, which are assembled from two subunits, the heavy alpha subunit and light B2-microglobulin (B2M).[47] MHC and TAP, together with additional chaperone proteins & cofactors, encompass the peptide loading complex (PLC), which facilitates peptide loading onto the MHC I molecules. The peptide-MHC (pMHC) class I complex is released from the PLC and is transported through the ER and golgi apparatus to reach the plasma membrane for surface expression. Cell surface complexes are relatively stable and are eventually ubiquinated by MARCH family proteins for internalization and degradation. Some fraction of MHC I molecules endocytosed are thought to be recycled and loaded with a new peptide for cell surface presentation, though the relative contribution of recycled molecules to the immunopeptidome is unknown.[48] Peptides that bind to class I MHC molecules are typically 9 amino acids in length, but can range from 8-15-mers while retaining high binding affinity and immunogenicity properties.[49]

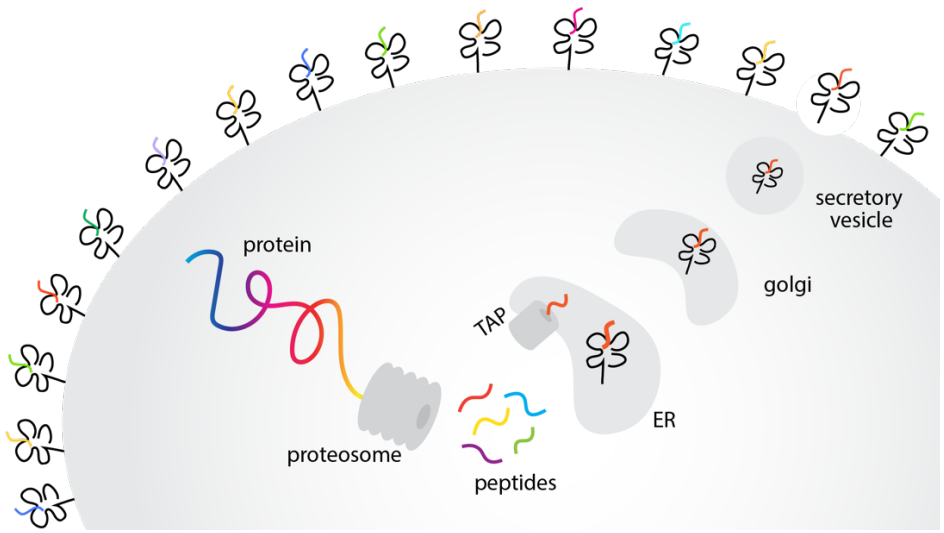

Figure 1-1*.Schematic of antigen processing and presentation for MHC-I.*

The three genes encoding class I MHCs are highly polymorphic, (*HLA-A*, *HLA-B*, and *HLA-C* in humans) with over 15,000 unique alleles identified in the world population.[50,51] Different alleles have different restricted binding epitopes, allowing for binding of peptides with different anchor residues or "binding motifs," though it should be noted that some alleles share overlapping peptide specificities.[52] This allelic diversity is important because it diversifies the repertoire of peptides presented for recognition by CD8+ T-cells, and consequently HLA allele homozygotes may be at an immunological disadvantage over HLA allele heterozygoes.[53,54]

1-2-2 MHC Class II Peptides

Class II MHC molecules are integral to the adaptive immune system maintaining immune tolerance. Unlike class I molecules which are ubiquitously expressed on nearly all nucleated cells, MHC class II molecules are predominantly presented by professional antigen presenting cells (APCs), including dendritic cells, B cells, and macrophages. Class II expression in non-

professional APCs can be induced by co-stimulatory molecules such as interferon-gamma, and class II molecules have been found on a variety of tumor types.[55]

Class II molecules also are composed of an alpha and beta chain, and genes encoding class II alleles are also highly polymorphic (*HLA-DR, HLA-DP, HLA-DQ* in human).[56] Class II molecules are similarly assembled in the endoplasmic reticulum, but unlike class I molecules which require a loaded peptide to exit the ER, class II molecules contain a class II associated Li peptide (CLIP) to stabilize the complex while exiting the ER.[57] In the golgi, the CLIP peptide is exchanged with an antigenic peptide aided by chaperone proteins. Molecules are then transported to the plasma membrane for recognition by CD4+ T cells. Like class I molecules, complexes are stable (with cell-type specific half-lives, and similarly degraded by ubiquitin tagging.[58]

Unique to class II molecules is the source of peptide antigens, which are of exogenous origin, and originate from proteins degraded in the endocytic pathway. They can also present tumor-specific antigens, including differentiation antigens, viral antigens, and neoantigens, similar to class I.[59] Class II molecules have an open-ended binding grove, which allows for the binding of peptides with greater length flexibility versus class I, though typically between 8-25 amino acids in length, with a majority being 15-mers.[60]

While the bulk of this work focuses on class I peptides, class II peptides are increasingly recognized as playing a critical role in the ant-tumor immune response, and related research areas such as class II binding prediction, the antigen processing pathway, and cross presentation remain active areas of interest in the field.

1-3 Mounting a response with immunotherapy

Immunotherapies against cancer can be defined by three categories: active, passive, and immunomodulating treatment modalities.[61] Active therapies augment a patient's immune system to initiate an immune response by recognizing tumor antigens. This is generally accomplished by targeting specific antigens or "epitopes," and can include polyvalent vaccines derived from dendritic cells pulsed with tumor peptides, or DNA/RNA/short peptide vaccines that deliver antigenic peptides which are secreted, processed by dendritic cells, and cross presented CD8+ T cells, both with the goal of activating an anti-tumor immune response against the specific antigen(s).[62]

Passive immunotherapies utilize exogenous components such as antibody-based therapies which can initiate cell killing through antibody-dependent cell-mediated cytotoxicity (ADCC), antibody-drug conjugates, or other antibody-mediated mechanisms.[63] Immunomodulated treatment modalities include checkpoint blockade therapy and other general immune activators (adjuvants). Another passive strategy the transfer of activated immune cells, such as adoptive T cell transfer, chimeric antigen receptor (CAR) T cell therapy, or activated lymphoblasts.

There are three categories of tumor antigens that have the potential to initiate an anti-tumor immune response: shared tumor antigens, viral antigens, and neoantigens. Each class contains several subtypes, which differ in their tumor specificity, abundance, tumor-type expression levels, and uniqueness across individuals. In general, a strong tissue antigen target has high tumor specificity, immunogenicity, and detectable expression levels optimal for the selected immunotherapy. Both active and passive immunotherapies leverage tumor antigens to initiate an anti-tumor immune response.

1-3-1 Shared tumor antigens

Cancer germline genes

*T*he first tumor-specific antigen recognized by T cells was idented in 1991, melanoma antigen family A,1 (MAGEA1), was found to expressed in many different tumor types, with no expression found in normal tissue.[64,65] The exception is in trophoblastic male germline cells (thus alternatively referred to as cancer-testis antigens), however these cells do not express class I HLA molecules and can therefore not present antigens to the immune system.[66] MAGEA1 belongs to a larger gene family of MAGE proteins, representing 25 different germline genes following an analogous pattern of tumor-specific expression. Other common germline genes include NY-ESO-1, and BAGE/GAGE gene families.[67] Expression of germline genes in tumors is thought to be the result of epigenetic mechanisms, specifically DNA demethylation of the promoter.[68]

Differentiation antigens

Differentiation antigens are derived from proteins overexpressed in tumors, are expressed in tumor cells and in the normal tissue of origin. Common in melanoma are differentiation antigens related to melanin synthesis, including gp100 (*PMEL*), MART-1 (*MLANA*), and tyrosinase (*TYR*).[69,70] Outside of melanoma, prostate specific antigen (PSA), mammoglobin-A, and carcinoembryonic antigen (CEA) are overexpressed in prostate, breast, and colon cancers, respectively.[62] T cell recognition and melanoma differentiation antigens are well documented, however it is thought that many T and B cells are removed due to central tolerance, limiting the immune system's response to this class of antigens.[71]

Overexpressed antigens

Proteins that are overexpressed in tumors, relative to healthy tissues including oncogenic drives, represent another source of tumor antigens.[72] These include growth factor

receptors like EGFR and ERBB2 (HER2), overexpressed in epithelial tumors including ovarian and breast carcinomas, p53, WT1, MUC1[73–75]. While a myriad of cancer vaccine trials has been deployed over previous years, aimed at activating the immune system against shared cancer antigens, they have shown little clinical benefit despite promising animal studies. For example, a gp100 targeted vaccine was tested in clinical trial with IL-2, an adjuvant, and found only modest improvement over IL-2 treatment alone (2.2 months versus 1.6) with low response rates of just 16%.[76] A peptide vaccine against MAGE-A3 failed to demonstrate efficacy over placebo.[77]

It is thought that the poor success of tumor antigen vaccines is due to low inherent immunogenicity, as these antigens are "self," increasing the likelihood that high-avidity T cell receptors against the tumor antigen targets were deleted from the immune repertoire during development to prevent autoimmunity.[61,62] Furthermore, cytotoxic T lymphocytes can also become anergic when the T cell receptors engage pMHCs on antigen presenting cells when costimulatory molecules are absent. These mechanisms of immune tolerance limit the efficacy of cancer vaccine efficacy.

In general, active immunotherapies target shared antigens can result in off-tumor, on-target toxicities, as many antigen targets are expressed to some degree on normal tissues, and T cells are remarkably sensitive, capable of recognizing a cell with a single copy of a peptide antigen.[78] For example, an adoptive T cell therapy trial using engineered T cells with an anti-MAGE-A3 TCR, where three of eleven patients experienced neurotoxicity resulting in death in 2 patients, due to expression of other MAGE family members in the brain, which had overlapping epitopes.[79]

There is also controversy over whether a single antigen is sufficient. Epitope spreading, referring to the development of an immune response against other distinct epitopes, is a phenomenon which may overcome limitations in single epitope therapies.[80] To circumvent the single antigen strategies previously deployed, researches from BioNTech developed FixVac, an

RNA vaccine targeting 4 tumor associated antigens (NY-ESO-1, MAGE-A3, TYR, and TMTE). Interim reported results from the Phase I clinical trial described a patient cohort of unresectable melanomas, almost all of which were previously treated with ICB. One arm of the study evaluated FixVac alone, while the other treated patients with FixVac and anti-PD1 therapy. Results showed expansion of antigen-specific T cells, with over 75% of patients demonstrating an immune response via ELIspot assay against one of the four tumor antigens. While the initial results are encouraging, either as a single agent therapy or in combination with immunotherapy, the final results have yet to be reported. Nevertheless, this study demonstrated usefulness of shared tumor antigens as vaccine targets, which remain attractive targets due to their abundant expression across many patients in contrast to patient specific neoantigens, representing an "off the shelf" strategy for targeted immunotherapy.

1-3-2 Viral antigens

It is estimated ~10% of cancers are the result of viral infection, including Hepatitis B and C, Epstein-Barr virus, human papilloma virus (HPV), among others.[81] Viral antigens integrate into the host's genome, and are subsequently processed and presented as surface antigens. Targeting viral cancer antigens has been successful, likely due to the foreign nature of oncolytic viruses.[82,83] For example, phase III trials of HPV vaccines designed to prevent cervical cancer demonstrated excellent safety profiles along with strong immunogenic response to the target antigens, leading to FDA approval in 2006.[84] Today, a variety of oncolytic viruses are under development for cancer therapy across many cancer types, attempting to specifically target and replicate in tumor cells (tumor "tropism") by targeting highly expressed cell surface receptors to guide viral antigens presentation on target cells.[85,86]

One of the first oncolytic virus vaccine approved, T-VEC (Imlygic) is used for unresectable melanomas. T-VEC is a genetically modified herpes simplex virus, and Phase III trials results (OPTiM) showed encouraging results, with 16% of patients demonstrating durable response (>6 months) vs. 2% for the GM-CSF control arm.A[87] While 16% is relatively low, a majority of patients had previously failed other systemic therapies. Currently, clinical trials are in progress evaluating T-VEC's efficacy in combination with CBI, with Dabrafenib/Trametinib for BRAF mutant patients, and in other cancer types.[88]

1-3-3 Neoantigens

Mutation containing neoantigens

Neoantigens arise from non-synonymous mutations occurring in tumor cells, giving rise to novel, tumor-specific antigen sequences that can be highly immunogenic, as tolerance mechanisms have not eliminated antigen-specific immune cells. Consequently, neoantigen-based therapies often result in lower toxicity than therapies directed at tumor associated "self" antigens and have stronger immunogenicity, as they are not affected by central tolerance.[89,90] In melanoma, the vast majority (~95%) of mutations in tumors are point mutations, however insert-deletions and frame-shift mutations have also been identified and can give rise to neoantigen peptide sequences.[91] One notable exception are oncogenic driver mutations which result in shared neoantigens among patients.[92,93]

Neoantigens are highly patient-specific and require a personalized therapeutic approach. One notable exception are oncogenic driver mutations which result in shared neoantigens among patients. Examples include neoantigens identified in TP53 and KRAS, however these neoantigens are still specific to a given allele and are therefore still not broadly generalizable across patient populations.

Neoantigens are commonly identified by performing whole exome sequencing on patient samples to identify mutations relative to normal tissue, followed by utilizing prediction algorithms to identify potential mutation-containing antigens that are likely to bind to a patient's allelic profile. This is accomplished using a variety of prediction algorithms developed for both HLA class I and II, which commonly use machine learning or artificial neural network algorithms trained on large experimental mass spectrometry datasets of HLA peptides.[94–99]

Beyond predictions, whether mutants materialize into tumor neoantigens depends on several criteria, including whether a mutated sequences is actually translated into protein, whether that protein is processed and presented as a peptide antigen on the MHC molecules (requires binding affinity to a patient's allelic profile), and whether the pMHC complex can initiate an antitumor immune response upon recognition by a T cell receptor.[100] Various prediction algorithms are capable of identifying thousands of mutations, predicting hundreds of potential MHC binders, however a majority of predictions are never validated by mass spectrometry and even fewer neoantigens are recognized in T-cell immunogenicity assays.[101] It remains challenging to validate which epitopes are immunogenic and should be selected for vaccine generation.

Still, immunotherapy vaccine strategies using neoantigens initially demonstrated efficacy in two small melanoma clinical trials, both published in 2017.[102,103] In a study by Ott et al., six patients received a custom neoantigen vaccine of twenty personalized tumor neoantigens, and four patients had no disease recurrence after 25 months, while two patients developed recurrent disease and were treated with PD-1 therapy, and subsequently regressed. Authors hypothesized that this was due to the expansion of neoantigen-specific T-cells generated through the neoantigen vaccination, though this cannot be explicitly confirmed. Sahin et al. dosed 13 patients with a custom neoantigen RNA vaccine, each containing 10 selected mutations. Of note, patients with NY-ESO-1 and/or TYR expression also received a vaccine with

the shared antigen. Two of five patients with metastatic disease had objective responses, while a third developed a complete response in combination with anti-PD-1 therapy.

One of the concerns with both neoantigen and shared antigen targeted immunotherapy strategies is the possibility of immune editing wherein cancer cells develop mechanisms of immune escape by eliminated antigens or downregulating antigen expression entirely.[104,105] Importantly, tumors with higher mutational burdens are correlated with better response to immune checkpoint blockade, as it is thought they process either a higher density or higher diversity of neoantigens which is particularly important given most neoantigens are unable to spontaneously elicit an immune response.[106–108] It has also been shown that neoantigen vaccines have higher response rates in high mutational burden tumors, such as melanoma, whereas tumors with low mutational burdens are not suitable for neoantigen or ICB therapies.[89] This underscores a critical question in immuno-oncology, which is how to modulate antigenicity in tumors to increase the number of patients who may benefit from immunotherapy, whether it be CBI or targeted methods.

Spliced neoantigen peptides

Another proposed source of neoantigens contributing to the non-natural, polymorphic immunopeptidome are spliced peptides.[109] These proteome-catalyzed spliced peptides, wherein peptide sequences are “cut and pasted” to generate novel sequences that could not be identified by mutation-based search spaces, was first described in 2004. In a study by Vigneron et al., researchers identified a T-cell clone which recognized a 9-mer peptide sequence from gp100 (RTKQLYPEW) that was a spliced sequence containing gp100 residues 40-42 and 46-52, excluding residues in the middle region of linear sequence.[110] Additional studies identified other immunogenic spliced peptides[111], however high throughput computational methods to probe the immunopeptidome for these sequences were not yet available.

In 2016, Liepe et al. reported a strategy to identify proteome-catalyzed peptide splicing, wherein peptide sequences are “cut and pasted” to generate novel sequences that could not be identified by mutation-based search spaces. Two flavors of spliced peptides are described: “cis-spliced” occur when peptides from the same protein are spliced, and “trans-spliced,” where proteins from two different molecules are combined.[112] Liepe et al. utilized a lymphoblastoid cell line (GR-LCL) and performed pMHC isolation and peptide fractionation using nearly $1e^{10}$ cells followed by LC-MS/MS analysis. Next, the mass specta were searched against the human proteome, along with all possible cis-spliced peptides between 9-12 amino acids, greatly expanding the experimental search space. Over 3000 unique spliced peptides were reported in this analysis, which represented 34% of HLA-ligands identified. In 2018, Faridi et al. claimed to have identified trans-spliced peptides using de-novo sequencing and reported over 15,000 spliced peptides contributing to ~29% of the immunopeptidome.[113]

These findings were controversial, and an additional investigation into the original dataset published by Liepe et al. alternatively reported that spliced peptides contributed to a much smaller fraction of the immunopeptidome than the initial report, ~3%, after imposing stricter quality control filters and de novo searching techniques.[114] The expanded search space created by considering all three or six frame translations increases false discovery rates, and FDR corrections have not always been rigorously and consistently applied.[115] Ultimately, large scale experimental confirmations, such as an analysis of isotopically labeled peptide standards to validate the “identified” spliced peptides, has not yet been performed beyond a handful of examples.[116] Still, the identification of spliced epitopes, accompanying software tools, and whether they carry immunological relevance remains an active area of research.

1-4 Mass Spectrometry

1-4-1 Types of Mass Spectrometers

Mass spectrometry (MS) has become a central analytical tool in the life sciences, analyzing samples across a wide range of industries & applications including pharmaceutical drug development, food sciences, petroleum composition, carbon dating, soil composition, as well as biomedical applications such as proteomics & metabolomics. Regardless of application, a mass spectrometer performs the core function of measuring the mass-to-charge (m/z) ratio of analytes of interest. From this measurement, one can determine the exact molecular weight of the analyte within a small mass error window, as well the potential to identify the abundance, structure or chemical properties of the component. While there are a variety of instrumentation configurations that accomplish this basic principle, all mass spectrometers contain three common components: an ionization source, a mass analyzer, and a detector.[117]

The ionization source serves to convert molecules to gas phase ions so they can be propelled into the mass analyzer. There are two primary methods of ionization: electrospray ionization (ESI) and matrix-assisted laser desorption/ionization (MALDI). In MALDI analyses, the sample is co-crystallized within a matrix and ionized with a pulsed laser beam.[118] ESI is performed by applying a high voltage charge a solution containing analytes of interest to create charged aerosol droplets. These droplets contain the solvent and negatively or positively charged analytes (depending on source polarity), and as the ions travel towards the ion source, the solvent evaporates leaving naked charged analytes, which enter the mass spectrometer.[119]

This body of work relies on ESI, which has several key advantages. First, ESI allows non-covalent interactions to remain intact, permitting analyses of protein complexes, small molecule-protein complexes, DNA-drug complexes, and other multi-molecule complexes.[120] Another important feature is the ability to couple MS with liquid-separation techniques such as high-performance liquid chromatography (HPLC), which distributes analytes using a stationary

phase (packing material) and mobile phase (elutant) for temporal separation of molecules for deeper analyiss of complex mixtures.[121]

There are two broad categories of mass analyzers commonly used: beam analyzers, where ions move through the ion source in a beam and travel through the analyzing field to the detector, and trapping analyzers, where ions are trapped within the analyzing prior to detection.[117] Popular beam analyzers include time of flight (TOF) mass spectrometers, quadrupoles, and common trap analyzers include the quadrupole ion trap, Fourier-transform ion-cyclotron resonance (FT-ICR), and orbitrap mass spectrometers. Importantly, these mass analyzers can be used in combination to perform tandem mass spectrometry, or MS/MS, which has two MS phases.

In MS/MS, after first measuring the mass of all precursor ions within a mass range entering the instrument, ions of a specific m/z are isolated from the ion source, and the precursor ion is subsequently disassociated. The most common dissociation method is collision-induced disassociation (CID), where the parent ion collides with a neutral gas such as nitrogen.[122] Next, the resulting ions (also referred to as “product ions,” “fragment ions,” or “transitions”) are analyzed. Scans of ions that result from MS/MS are called MS^2 scans, and in some instruments, it is possible to perform additional phases of MS, referred to as multi-stage or “MS^n” experiments.[123]

Hybrid MS/MS instruments are generally configured as “tandem-in-space” or “tandem-in-time” instruments. Tandem-in-space instruments use a distinct analyzer for each MS phase, whereas tandem-in-time MS/MS performs MS events in the same mass analyzer but separated by time. Popular tandem-in-space instruments (usually beam analyzers) include triple quadrupoles (QQQ) or quadrupole/time-of-flight (Q/TOF) systems. Tandem-in-time systems are commonly quadruple-ion traps and are generally more efficient due to the ions remaining in a

single analyzer throughout the analysis. All experiments in this body of work were performed using hybrid quadrupole-orbitrap mass spectrometers.

In quadropole-orbitrapl systems, ions enter the source with ESI and pass through a transfer tube, ion funnel, and flatapole before reaching the quadrupole mass filter. Next, ions pass through a second isolating quadropole and are stored in the C-trap. Ions are then fragmented in a higher-energy collision disassociation (HCD) cell and subsequently analyzed by the orbitrap mass analyzer. In this configuration, the orbitrap functions as both analyzer and a detector.[124] Ions in the orbitrap, a cylindrical outer electrode with a spindle-shaped inner electrode, oscillate with frequencies dependent on their respective *m/z* ratio and produce an electric current. The time-varying signal, also called a "transient," can be analyzed by the Fourier transform, from which a mass spectrum is derived.

The transient length affects the mass resolving power—the longer the ions oscillate in the orbitrap, the higher the mass accuracy. A principal benefit of an orbitrap system is that longer transient lengths do not affect measurement sensitivity (in contrast to TOF systems), however longer transient lengths reduce the number of scans allowed within a given cycle time, limiting the number of ions that can be analyzed within an analysis. Consequently, optimizing data acquisition parameters to balance data collection with mass accuracy is a critical element of developing efficient mass spectrometry methods.

1-4-2 Data Acquisition Modes

For "bottom-up" proteomics experiments, where peptides are analyzed following proteolytic digestion or other peptide-based experiments (ex. peptide-MHC profiling), there are three common data acquisition schemes: data dependent acquisition (DDA), data independent acquisition (DIA), and selected reaction monitoring (SRM).

Data Dependent Acquisition

In data dependent acquisition analyses, the MS acquires a full-scan mass spectrum ("MS1") which contains the mass-to-charge ratios of all precursor ions collected within either a fixed time window or ion count, whichever is reached first. The instrument next performs MS^2 analyses on a list of precursor ions selected from the first full-scan spectra. The number of MS^2 spectra collected following an MS1 event is dependent on either the specified cycle-time (in a 3 second cycle-time, MS2 events will be collected until 3 seconds is reached) or until a specified number of scans is reached ("topN"), depending on the method structure.

Precursor ions are selected for fragmentation on the basis of abundance; therefore this acquisition scheme may be biased against low-abundance ions.[125] Consequently, data-dependent acquisition incompletely samples among the peptide ions present. Furthermore, this introduces a stochastic element into peptide sampling, driven by minor changes in chromatography or the order peptides are selected for fragmentation, ensuring variability in peptides identified across even analyses of the sample.[126] DDA experiments result in "missing values" across replicate experiments, which can greatly impact quantitative studies that aim to compare the results of multiple analyses.[127] In complex mixtures, co-elution of peptides is also prevalent, therefore the width of chromatographic peaks, chromatographic gradient, and mixture complexity can greatly influence the depth of sample coverage.[128] Still, despite these limitations DDA remains a routine acquisition strategy for broad coverage, unbiased, discovery analyses. MS^2 spectrum are simpler to sequence than DIA spectral (discussed next), resulting in high confidence peptide-spectrum matches across a wide range of applications.

Data Independent Acquisition

In data independent acquisition (DIA) analyses, all peptides within a *m/z* window are simultaneously fragmented, resulting in a highly complex mass spectrum. This process is repeated across additional m/z windows, attempting to fragment all precursor ions in contrast to DDA analyses. Common DIA methods include all-ion fragmentation (AIF) and sequential window acquisition of all theoretical fragment-ion spectra (SWATH). The primary challenges with DIA data is deconvoluting the MS^2 spectrum, determining integration boundaries, removing background interferences, and controlling for false discovery rates.

Historically, DIA analysis required collecting sample-specific spectrum DDA to generate spectral libraries, which is laborious and spectra do not accurately capture the complexity and interferences of the real sample data collected with DIA.[129] A variety of tools have been developed to search DIA data, the most recent even eliminating the requirement for spectra libraries by using pseudo-MS^2 spectra from DIA data, yet analysis of the same sample with different tools yields vastly different results—a grave concern for maintaining accurate biological interpretation.[130,131] Additionally, studies comparing DDA to DIA for quantitative analysis have demonstrated DDA's superiority in quantitative accuracy.[132] Nevertheless, new data processing tools are continually released[133,134], which aim to improve peptide identification and quantification accuracy to expand the use of DIA across a wide range of suitable applications.

Selected & Parallel Reaction Monitoring (SRM/PRM)

In contrast to discovery-based acquisition studies, targeted assays aim to reproducibly identify and, in some cases, quantify, a panel of *m/z* targets within an MS analysis. Targeted assays can be especially helpful when trying to identify low-abundance ions, which may be challenging to identify by shotgun proteomics methods.

In selected reaction monitoring (SRM) experiments, typically performed in QQQ instruments, a specified precursor ion is isolated in the first quadropole, fragmented in the

second, and a predefined set of fragment ions (ex. 3-5) are filtered into the third quadrupole and transmitted to the detector. The integrated peak areas of transitions are used for quantitation and compared relative to other samples or to an isotopically labeled internal standard. While SRM approaches are highly sensitive, they often suffer from interfering signal from near-isobaric ions that co-elute with the target peptide, interfering with quantitative accuracy which is a particular concern in low abundance and/or complex mixtures.[135] Furthermore, SRM experiments are laborious to generate and optimize, as target masses, charge states, transitions, and retention times need be selected prior to analysis which requires iterative survey analyses.[136]

Using hybrid quadropole-orbitrap instrumentation, an analogous technique called parallel reaction monitoring (PRM) was developed, which has demonstrated improved mass filtering for increased sensitivity and selectivity, and an improvement in dynamic range limitations.[137,138] A targeted precursor ion is isolated in the quadrupole, fragmented in the HCD cell, and product ions are detected in the orbitrap. In contrast to SRM, a full, high resolution MS/MS spectra is acquired for each target that contains all protentional product ions, eliminating the need to pre-select transitions for isolation. The peak areas of the most abundant transitions are commonly used for quantitation, which is supported by targeted MS software platforms like Skyline.[139]

Still, despite using tight time scheduling and on-the-fly retention time adjustments, initial implementations of PRM were limited to reproducibly targeting ~50 precursor ions within a single analysis.[140] In its original implementation, expanding the number of targets requires a compromise on instrument performance and consequently, accuracy.[140] To circumvent these limitations, a new technique called internal standard triggered-parallel reaction monitoring (IS-PRM) was developed, which utilizes stable isotope-labeled (SIL) peptide to guide PRM measurements in real time.[141] Briefly, the instrument alternates between two modes: a low resolution mode (“watch mode”) where SIL peptides are monitored within their 1-minute

dynamic monitoring window (guided by landmark peptides), and a high resolution mode ("quantification mode") where SIL and endogenous peptides are monitored with high resolution for enhanced data quality. When a SIL peptide is detected in watch mode, quantification mode scans are triggered for the SIL and endogenous peptide within the peptide chromatographic elutions.

IS-PRM is similarly laborious to implement, requiring use of an application programming interface, retention time scheduling, and identification of optimal charge states for all targets. Nevertheless, the first implementation of IS-PRM by Gallien et al. demonstrated an increase in sensitivity over PRM and SRM, as well as the reproductible targeting of several hundred SIL-endogenous peptide pairs. A modified implementation of IS-PRM was recently released by Thermo Fisher Scientific, termed SureQuant, which utilizes internal standards to guide the reproducible acquisition of hundreds to thousands of endogenous targets without the need for retention time scheduling. Custom implementations of SureQuant acquisition software were utilized within this body of work, explained in detail within Chapters 2 and 5.

1-4-3 Quantitative Mass Spectrometry

While cancer is a historically viewed as a genetic disease, most cancer therapeutics target proteins. As a consequence, studying cancer at a systems level to identify overexpressed proteins, post-translational modifications, and more requires quantitative data, comparing abundances between samples or patients, healthy or diseased states, treated or untreated conditions, etc. Quantitative mass spectrometry can enable these measurements with a variety of strategies, each of which have strengths and limitations. Determining which technique to use requires consideration of throughput (time), quantitative accuracy, sensitivity, reproducibility, and cost.

Label free quantification

The most straightforward quantitative method is label-free quantification (LFQ) in discovery analyses, which relies on integrating the precursor ion signal over the chromatographic elution to obtain an intensity value.[142,143] While the "area under the curve" is not a representative of the absolute abundance of a given peptide, due to large variance in sequence-dependent signal intensities, these data can be used to compare abundances across samples. MS^2 spectra are used for peptide sequencing and identification but are not required for quantitation. Unlike isobaric strategies, LFQ is inexpensive, avoids additional sample handling/ chemical modification steps, and allows for theoretically unrestricted number of comparisons across analyses (unlike multiplexed analyses, discussed below). Disadvantages to LFQ include the requirement to perform individual analyses for each sample in a study, limited throughput, missing values and poor quantitative reproducibility due to many factors that vary due to sample handling as well as from run-to-run, across instruments, and across laboratories. Furthermore, low abundance peptides may be contaminated by neighboring peptide signaling, skewing quantitation.[144]

Targeted label free quantification

An alternative implementation of LFQ is in targeted analyses (ex. SRM/PRM), where quantitation is performed by integrating the area of selected transitions for quantitation. In applications that use an isotopically labeled internal standard peptide for triggering via mass offset (IS-PRM, SureQuant), quantitation can be performed by determining the ratio of light ("L," endogenous) signal to heavy ("H" peptide signal (L/H ratio).[141] This may allow for normalization across analyses, depending on the experimental setup.

Stable isotope labeling of amino acids in cell culture (SILAC)

For improved relative quantitative accuracy between samples, the stable isotope labeling by amino acids in cell culture (SILAC) method can be used.[145] SILAC uses cell culture medium lacking 1 or more standard amino acids and supplemented with heavy-isotope labeled amino acids (usually lysine and arginine for tryptic proteomic analyses), which are fully incorporated into the cell's proteome after ~6 doublings. Heavy isotope-labeled peptides (with deuterium as a notable exception) have near identical chemistry and elution times as their light peptide equivalents but are easily distinguished by their separated *m/z* ratios. As a result, both the isotopically labeled and light peptides can be analyzed and quantitatively compared within a single analysis, eliminating an element of run-to-run variability that afflicts LFQ analyses.

Notable drawbacks to using SILAC for quantitation is the limited capacity for multiplexing—both because of limited combinations of isotopically labeled amino acids, and because increasing samples increases complexity and reduces the number of scans measured for an individual sample.[146] Practically, this limits single experiment comparisons to 2 or 3 samples. Furthermore, SILAC cannot be used for quantitative analyses of most *in vivo* derived samples, such as human tissue. Outside of traditional applications, SILAC labeling can be a useful tool for pulse-chase styled experiments, including identifying newly translated proteins or investing how different cell types interact, such as looking at cross presented peptides on dendritic cells derived from tumor cells.[60,147]

Isobaric tags

For increased multiplexing capacity and throughput, chemical labeling methods such as isobaric tags for relative and absolute quantification (iTRAQ) and tandem mass tags (TMT) have become a staple for quantitative proteomic experiments.[148,149] Amine-reactive tandem mass tags are the most widely used, and consist of three functional groups: the amino reactive group

which utilizes NHS chemistry to covalently bind to N-terminal amino acids and lysine residues, the isotopic reporter group, and a linker between the two which balances the two groups, ensuring each tag has an identical mass. Peptides can be labeled with individual tags and combined together prior to analysis. Due to the isobaric nature of the tags, precursor ions of multiplexed samples appear as a single peak, however subsequent fragmentation generates reporter ion peaks as well as product ion peaks of the peptide. Quantification is accomplished by comparing the relative abundance of reporter ions between samples. Despite the minimal mass difference between reporter ion isotopologues, high resolution mass spectrometers such as hybrid quadrupole orbitrap systems are able to resolve the mass difference

The key benefit of multiplexing with TMT is the ability to compare a greater number of samples simultaneously without requiring separate scans for each sample, as is required with SILAC labeling. However, multiplexing capability is limited to 16 reporter ions with TMT-pro, which while representing a dramatic improvement over SILAC or iTRAQ-4plex, is minimal compared to sequencing technologies. The number of missing values significantly inflates as more multiplexed analyses are combined, and batch effects reduce quantitative precision.[150] Use of a common or "bridge" sample included in all analyses can reduce batch effects by normalizing all reporter ions to the common bridge channel, however this utilizes a TMT channel and can be subject to error propagation. Other data-driven normalization methods such as CONSTANd allow for cross-analysis comparisons without a bridge channel[151], but this does not address the primary issue of missing values.

Other disadvantages of TMT-labeling include additional sample handling steps which may result in sample losses. Furthermore, a comparison of TMT and SILAC-based quantification strategies of a standard whole cell digest demonstrated MS^2-based analysis of TMT data was affected by co-isolation, leading to dynamic range suppression and compromised quantitative accuracy.[152] Using the TMT complementary fragment ions (TMTc), resulting from

intact peptide attached to the balancing group, can alternatively be used for quantitation.[153] It has been suggested TMTc ions, in contrast to low m/z reporter ions, are precursor specific, thus co-eluting ions are less likely to interfere with the TMTc reporter ion signal. Quantitation with TMTc has been demonstrated to out-perform standard reporter ion quantitation in MS^2, though with several limitations. These include the inability to distinguish more than 5 isobaric labels, lowering multiplexing capacity, and poor complement ion formation.[143] Furthermore, software to support TMT-c quantitation is not readily available, therefore this approach has not been widely adopted. Another alternative is using MS^3 for TMT analyses, which have been shown to mitigate or even eliminate ion suppression. Unfortunately MS^3 can also lead to lower precision & speed, along with decreased sensitivity, likely attributed to sample losses taken in the additional mass analyzer event.[132,154]

1-5 Immunopeptidomics

1-5-1 Mass spectrometry-based methods for peptide MHC identification

Recognition of antigens presented by MHC molecules by the immune systems represents a crucial component of anti-tumor immunity, therefore identifying the collection of pMHCs tumor cells present is a fundamental biological question. The most common way to sequence peptide MHC repertoires, also referred to as the “immunopeptidome,” relies on mass spectrometry. However, unlike standard proteomic workflows which rely on peptides generated from enzymatic digestions of proteins, immunopeptidomic workflows pose several unique challenges, including how to isolate the peptide antigens first from whole cell lysate, and subsequently from the HLA/B2M complex at a level that is detectable by the instrumentation.

The first documented protocol detailing LC-MS/MS-based identification human MHC peptides was published in 1992, and utilized an antibody specific for HLA-A*02:01 to isolate

pMHCs by immunoprecipitation, which were further isolated by acid elution to release the peptide from complex and molecular weight size-exclusion filtration to further separate the peptides from the MHC light/heavy chains.[155] This initial protocol utilized $2x10^9$ cells and identified 200 peptides. Following this landmark publication, many more analyses followed which commonly utilized a pan-specific antibody for MHC immunoprecipitation, allowing for pMHC profiling of any sample, regardless of allelic profile.[156–158] An alternative strategy for pMHC profiling is incubating cells with a mild acid solution, which strips molecules off the surfaces of cells.[159] Due to the lack of specificity this technique provides, the approach has generally fallen out of favor. Some researchers favor using solid phase extraction instead of molecular weight cut off filtration for separating peptides from the MHC molecules, however both techniques are effective.[160]

An alternative strategy to profiling endogenous pMHCs are engineered, mono-allelic cell lines which present a given allele with an affinity purification tag at high expression levels.[161] This technique impressively identified over 24,000 unique peptide sequences from 16 class I alleles, requiring $5x10^7$-$1x10^8$ cells as input. While this technique cannot be used to inform immunologically relevant epitopes in clinical samples, it has been useful in generating large datasets of naturally processed and presented ligands across a range of alleles, which is particularly useful in training binding affinity and peptide prediction algorithms for alleles that are less commonly expressed.

One of the major hurdles in pMHC profiling is the large amount of cellular input material required for these analyses, ($1x10^9$-$1x10^{10}$ cells) which far exceeds the cellular input required for traditional proteomic assays and is well beyond the scope of material obtained in a clinical biopsy sample. Over the past decade, advances in pMHC isolation & sample processing, search algorithms, and instrumentation speed and sensitivity have dramatically improved the field of immunopeptidomics. Aa researchers used to identify only several hundred peptides from an analysis, these advances have enabled deeper sequencing of the immunopeptidome in cell line

samples using similar amounts of cellular input. Purcell, Ramarathinam, and Ternette detail a protocol utilizing up to $1x10^9$ cells to generate 10 peptide fractions for deep LC-MS/MS analysis.[162] Over 10,000 peptides were identified across five melanoma cell lines using 10^8 cells in Gloger et al. and over 22,000 peptides across 5 different cell types in work by Bassani-Sternberg et al. using $5x10^8$ cells.[163] While there has been an effort to reduce sample input, input amounts remain in the range of $5x10^7$ to $5x10^8$ cells which is equivalent to ~50 mg of cell lysate for epithelial tumor cells.[164,165]

1-5-2 Clinical pMHC profiling

Of critical importance in immunopeptidomics is to expand analyses beyond immortal cancer cell lines and into patient tissue samples. Again, tissue quantity remains a barrier to widespread profiling. Nevertheless, several successful applications of immunopeptidomics have been applied in recent years. In melanoma, pMHC repertoires of 25 human melanoma punch tissue biopsies were analyzed by LC-MS/MS, resulting in nearly 100,000 identified peptides.[158] These data were collected using 0.1 g to 4 g of tissue, and consequently peptide numbers per patients varied accordingly. The analysis using 4 g of tissue identified nearly 25,000 unique peptides whereas other analyses using lesser input identified under 1000. While even this minimal amount of cellular input exceeds what can be collected using a needle biopsy, this study successfully demonstrates the feasibility of using patient biopsies for antigen identifications.

To circumvent limited in vivo sample availability (as well as to avoid large scale cell culture required for deep pMHC profiling), Heather et al. proposed using immunodeficient mice as in vivo “bioreactors” to efficiently expand and grow large quantities of a cell sample for analysis.[166] Researches hypothesized that gene and protein expression, including phosphorylation patterns, would be conserved. Using a lymphoblast cell line (JY), Heather et al.

showcase peptide length/binding motif similarities between traditional cell culture and in vivo derived samples, along with similarity in source proteins of identified peptides. Rijensky et al. expand this method to patient samples and demonstrate similarity in pMHCs identified between samples (some level of non-overlap is expected due to the stochastic nature of mass spectrometry-based discovery analyses).[167] Unfortunately, neither study quantitatively compared expression levels between samples which would inform which applications this system may be effectively leveraged. Still, generating PDX samples weeks of incubation time and sometimes multiple mice to generate sufficient material and may not be a feasible solution to translating immunopeptidomics into the clinic.

1-5-3 Relative quantification of pMHC repertoires

There are several ways to obtain relative quantification data, each with strengths and limitations. Because cancer cells undergo a variety of changes that result in the dysregulation and mutation of proteins, using relative quantification techniques in mass spectrometry to characterize the immunopeptidome's response to perturbation is of interest, and may provide a window into pMHC repertoire changes that can be leveraged for immunotherapy.

Label-free quantification

Label-free quantification (LFQ) is the most common pMHC quantitative method, requiring samples for comparison to be analyzed individually. Quantitation is frequently performed by integrating the area under the chromatographic elution of the precursor ion in discovery mode analyses, though product ions may be used in the case of targeted analyses (**Figure 1-2A**). While LFQ offers the opportunity to compare quantitation across a theoretically unlimited number of samples and is straightforward to implement, it has several notable

limitations. First, data dependent acquisition methods suffer from poor overlap in peptide identifications across analyses. While the overlap across analyses may be slightly improved by calculating abundance values for precursor ions in the absence of an associated MS^2 spectrum, this can result in false positive data points, particularly because MHC peptides all have similar mass to charge ratios and biological properties.[168–170] This can be remedied with targeted acquisition methods like SureQuant, but requires a-priori knowledge of which peptides to target. Relative quantitation among class II MHC peptides adds an additional layer of complexity, as class II peptides form typically form nested sets of varying lengths and require peptides to be grouped into consensus epitopes to compare quantitation.[171,172] As an additional consideration, failing to normalizing for variations in sample input and processing across samples can result in variable and inaccurate quantitation.

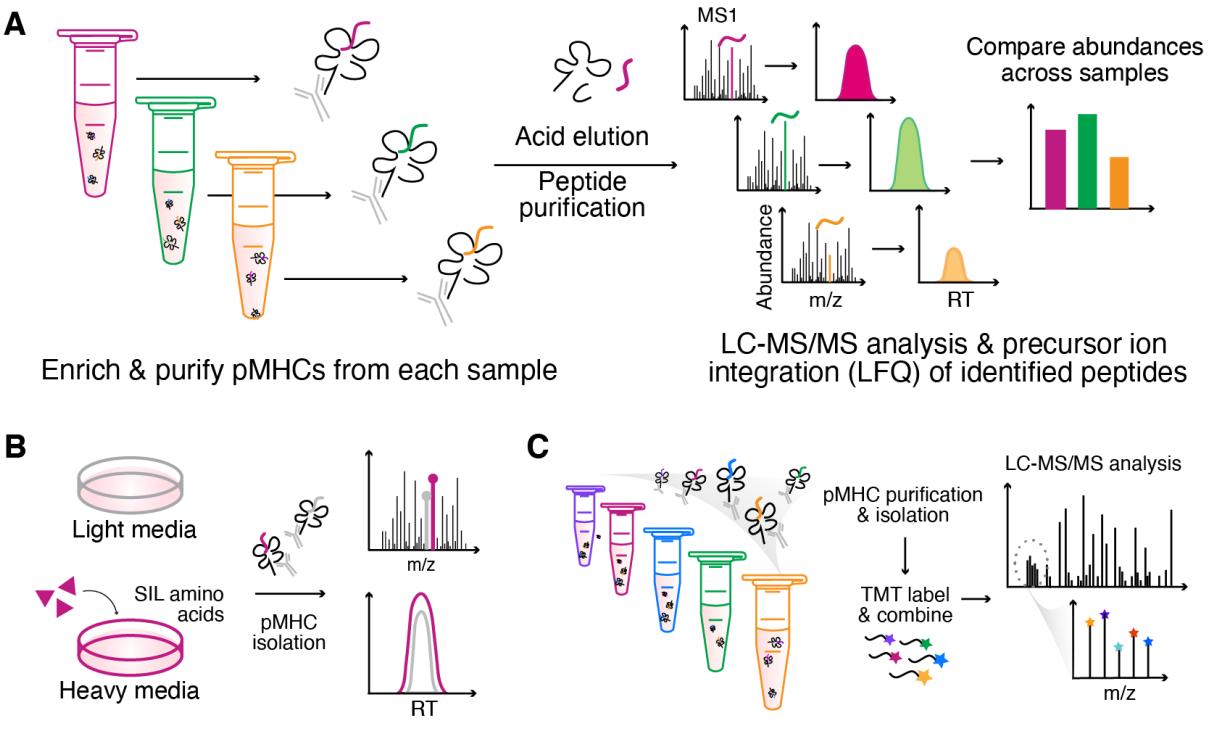

Figure 1-2. *Schematics of immunopeptidomics workflows.* ***A*** *label-free quantification,* ***B*** *SILAC,* ***C*** *multiplexed quantification with isobaric mass-tags.*

Nevertheless, LFQ data has provided novel insights. In 2011, Caron et al. published a quantitative dataset which displayed altered pMHC abundances in response to rapamycin therapy and described systems-level evidence for the immunopeptidome serving as an external representation of the cells state.[173] Several studies have probed how interferon gamma (IFN-γ) stimulation, alters the pMHC repertoire across human and mouse studies, and similarly found IFN-γ related pMHCs are upregulated in presentation following stimulation.[165,169,174,175] Other reports explore how perturbations like small molecule inhibitors[169] and oncolytic retroviruses[176] shape the immunopeptidome, and how different single-cell derived tumor organoids reveal inter-clonal variability[177]. Together, these data reveal therapeutically targetable pMHCs, and serve to better inform our understanding of the pMHC repertoire across different samples and conditions.

Multiplexed quantification

Utilizing isobaric labeling strategies can limit the number of "missing values" between analyses, as each peptide spectrum match contains quantitative information across all samples multiplexed. Traditional isobaric labeling strategies like SILAC (Stable isotope-labeling with amino acids of cells in culture)[145] may be used, which typically rely on labeling a cell population with heavy amino-acid medium and combining that sample with cells grown in light medium prior to analysis (**Figure 1-2Error! Reference source not found.-B**). While this allows for comparisons of precursor ion intensities between samples within a single analysis, multiplexing capacity is limited to just a few samples and SILAC cannot accommodate most in vivo samples. Furthermore, SILAC is not optimized for most immunopeptidomics experiments, as traditional heavy K/R medium is unable to fully label peptides across HLA alleles. Still, SILAC media has been used in pulse-chase experiments which profile the protein turnover kinetics of MHC

molecules and to study the cross presentation of tumor peptides on dendritic cells in vitro.[60,178,179] In these studies, Leucine is often heavy labeled, as it is an anchor residue in class I HLA-A*02:01 peptides. Custom SILAC media can be used to achieve higher labeling coverage of anchor residues, though it is challenging to reach complete labeling given the diversity of peptide sequences that bind to any given allele.[60,161]

Only a handful of studies have been published that utilize isobaric labeling such as iTRAQ and TMT in immunopeptidomics, likely because labeling MHC peptides has unique challenges not encountered in traditional proteomic workflows. Namely, the labeling must occur either before immunoprecipitation, which would require an exorbitant amount of isobaric reagent to label 10's to 100's of milligrams of cellular input, or alternatively, the peptides can be labeled after isolation. Labeling such small concentrations of peptide results in increased sample losses, likely attributed to the additional sample handling steps.[180]

The first study utilizing isobaric labeling in immunopeptidomics was published in 2010 by Bogunovic et al. and utilized iTRAQ isobaric labeling reagent to measure repertoire alterations in MHC class II peptides of mouse splenocytes with or without gamma interferon inducible lysosomal thiol (GILT).[181] In 2012, Shetty et al. utilized iTRAQ to profile the class I immunopeptidomes in sensitive and cisplatin-resistant ovarian cancer cells.[182] The authors identify pMHCs derived from proteins implicated in cancer pathways having increased presentation levels in cisplatin-resistant cells compared to the sensitive cells, presenting the first multiplexed quantitative pMHC analysis to identify pMHC repertoire alterations. Recently, a third study was reported where Murphy et al. utilized TMT-10plex for labeling pMHCs, expanding the multiplexing capacity from 4 samples with iTRAQ to 10 samples.[180]

There are several drawbacks to isobaric labeling strategies, including limited multiplexing capacity (11 with TMT, 16 with TMT-Pro), greater sample losses, as well as increased dynamic range suppression.[132] Additionally, quantitative pMHC methods lack a

normalization strategy to account for variations in sample input and processing. These losses are estimated to be as much as 99.5%, but vary across peptides and samples, further underscoring the need for normalization.[183]

An alternative approach is to utilize isobaric mass tags, allowing for the multiplexed quantitation of up to 18 samples[184] within a single analysis by labeling peptides after isolation and combining prior to analysis, minimizing missing values (**Figure 1-2-C**). Early studies by Bogunovic et al. and Shetty et al. utilized isobaric tags for relative and absolute quantification (iTRAQ) to multiplex up to four samples, demonstrating the utility of measuring repertoire alterations across different conditions.[181,182] Murphy et al. first extended this approach to tandem mass tags (TMT), multiplexing 10 samples to measure the immunopeptidome's response to doxorubicin treatment *in vitro* and *in vivo.* Other recent applications of this approach include using TMT to investigate the dynamics of HLA presentation following viral infection with SARS-CoV-2, and how perturbations in expression and degradation alter neoantigen expression.[185,186]

Multiplexed relative quantitation with isobaric mass tags like TMT has several unique advantages over LFQ, namely increased throughput and higher quantitative accuracy, even without hipMHC normalization. Multiplexing is also relatively inexpensive because of the small amount of labeling reagent required for immunopeptidomics samples, and may also yield better fragmentation due to the formation of multiply charge ions thereby enhancing peptide-spectrum matches for pMHC analyses.[187] Still, labeling has several drawbacks. First, additional sample handling steps to label peptides may result in additional samples losses and decrease data quantity. To circumvent this limitation, repeated sampling of a given multiplexed mixture (in contrast to running the entire sample in a "single shot" analysis) may increase the total number of quantifiable peptides[188], though this is likely dependent on the number of multiplexed samples and quantity of input material. Another consideration is that multiplexed analyses will always be

limited by multiplexing capacity of existing reagents, limiting the number of samples than can be easily compared without incorporating a bridge sample.

An additional concern with TMT multiplexing is that quantitation suffers from ratio compression to a greater extent than label-free, which may obscure subtler quantitative changes in the immunopeptidome.[188] Finally, existing multiplexed quantification strategies lack a normalization strategy to account for variations in sample input and processing therefore new strategies to mitigate sample losses and control for sample-to-sample variability are required to further advance quantitative immunopeptidomics.

1-6 Tyrosine phosphorylation

Post translational modifications (PTMs) provide an essential mechanism used by cells to diversity protein function by modulating protein-protein interactions. While over 200 types of PTMs have been identified that alter cell function, phosphorylation is the most common experimentally identified PTM.[189,190]

Phosphorylation is a reversible PTM, where protein kinases catalyze the transfer of a phosphate group to serine, threonine, or tyrosine residue side chains, and protein phosphatases hydrolyze the phosphate group to dephosphorylate amino acids (**Figure 1-3**). Approximately 90% of phosphorylation events occur on serine residues, 10% on threonine, and < 1% on tyrosine residues, as tyrosine phosphorylation (pTyr) is relatively rate and low level by comparison, however pTyr plays a critical role in regulating signaling networks that control metabolism, proliferation, apoptosis, migration, and more.[191–193] As a consequence, dysregulation of pTyr signaling though mutations or kinase hyperactivation can lead to and drive cancer, therefore a multitude of tyrosine kinase inhibitors have been developed for clinical use, as previously described.[194] Tyrosine phosphorylation measurements have proven valuable in

identifying targetable aberrantly activated signaling pathways and characterizing resistance mechanisms[195,196], however identifying and quantifying low abundance pTyr peptides remains challenging—particularly when sample input material is limited.

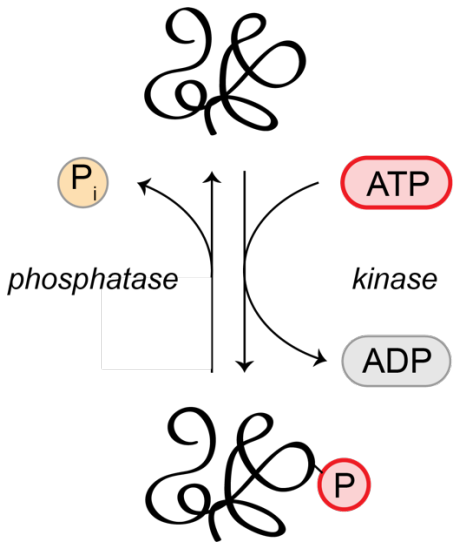

***Figure 1-3**. Schematic of protein phosphorylation and dephosphorylation.*

1-6-1 Quantification of pTyr signaling networks

Antibody-based assays (ex. immunoblots, reverse phase protein arrays) require both a pre-defined set of targets as well as high quality, modification-specific antibodies. While these assays are relatively straightforward, they suffer from limited sensitivity and quantitative accuracy, and it remains challenging to distinguish between similar phospho-epitopes on district proteins.[197,198]

Advances in high sensitivity, mass spectrometry (MS)-based pTyr methods provide an attractive alternative, allowing for hundreds to thousands of pTyr measurements within a single analysis without requiring phospho-specific antibodies. Generally, pTyr peptides are enriched from tryptic peptide digestions using anti-pTyr antibodies or motif-specific antibodies like the

SRC homology 2 (SH2) “superbinder” (immunoprecipitation), and this can be coupled with strong-cation exchange chromatography (SCX), immobilized metal affinity chromatography (Fe^{3+}-NTA), or Titanium dioxide (TiO_2) microspheres, for enhanced highest pTyr specificity.[199–203] While MS-based discovery analyses cataloging phosphorylation sites have been informative in identifying over 10,000 unique tyrosine phosphorylated peptides in discovery analyses utilizing grams of sample input or phosphatase inhibitor treated samples (pervanadate)[202,204], biological meaning is derived from making quantitative comparisons of pTyr levels: tumor versus non-tumor tissue, pre and post cytokine stimulation, drug sensitive versus drug resistant.

Label free quantitation allows for comparisons across replicates, but with poor run-to-run overlap and lower quantitative accuracy due to variable sample processing and chromatography across multiple analyses. Utilizing chemical labeling strategies, quantification can be performed by comparing abundance values between samples of iTRAQ or TMT, allowing for relative comparisons between samples within an analysis.[205,206] This enabled identification of activated signaling networks relative to a control condition or across a cohort of biological samples. For example, Randall et al. explored the pTyr response to erlotinib (EGFR inhibitor) treated GBM tumors in mice.[207] Hochgrafe et al. profiled a panel of basal and luminal breast cancer cell lines to identify biomarker signatures and potential therapeutic targets.[208] Each of these approaches rely on discovery-based MS and quantitative comparisons between 2 or fewer analyses. While this approach is informative for smaller scale studies, it is challenging to perform large studies that integrate many analyses together due to significant missing values and heterogeneity in sites identified within each analysis. Both systematic approaches as well as clinical applications rely on the ability to reproducibly measure the same phosphopeptide across replicate analyses, conditions, samples, timepoint, research centers, and more.

1-6-2 Targeted pTyr MS methods

Naturally, targeted methods such as PRM offer an attractive alternative to discovery MS, however the inherent challenges of phosphoproteomics (enrichment, low abundance) increases the difficulty of such approaches. For this reason, target phosphorylation methods have historically been limited to pSer/pThr sites and high abundance pTyr sites (ex. MAPK3/1).[193,209–211] Depth of coverage is also limited—Parker et al. targeted fifteen sites with isotopically labeled peptides and 98 with spectral libraries and DIA via LFQ; Lawrence et al. targeted 101 with PRM.

Studies from the White lab represent the only source of pTyr-specific targeted analyses. Wolf-Yadlin et al. quantified 222 pTyr sites across seven timepoints following EGF stimulation.[212] In this implementation, samples were multiplexed and labeled with iTRAQ, and targeted via MRM and retention time scheduling. Quantitation was determined from reporter ions intensities, allowing for targeted, relative quantitation. More recently, Curran et al. described Multiplex Absolute Regressed Quantification of Internal Standards (MARQUIS), a technique which allows for targeted absolute quantification of pTyr peptides via MRM and retention time scheduling.[213] Isotopically labeled pTyr peptides of targets are added to the tryptic peptide digest, labeled with iTRAQ, and endogenous/heavy labeled pTyr peptides were subsequently purified with two-step enrichment.

While both approaches described by Wolf-Yadlin and Curran offer significant advancements in targeted phosphoproteomics, these methods are difficult to implement and limited by the number of targets that can be reproducibly quantified.

1-7 Thesis overview

The body of this thesis aims to address existing limitations in MS-based methods by the development and/or modification of MS platforms, apply these methods to generate data

informing our understanding of cancer biology and highlight therapeutic targets, and demonstrate the potential utility of using these platforms clinically for personalized medicine.

Chapter 2 describes the development of SureQuant pTyr, a targeted tyrosine phosphorylation method which utilizes IS-PRM for rapid, reproducible quantitation of over 300 pTyr peptides in human tumors. I utilize the data to demonstrate the usefulness of pTyr data in identifying activated signaling pathways and potential therapeutic targets and use immune cell pTyr sites to estimate immune infiltration levels. Using other publicly available “omics” datatypes generated on the same tumors, I compare and contrast our findings to those made with sequencing and protein expression profiling datasets, identifying novel insights stemming from the inclusion of pTyr data.

Chapter 3 focuses on the development of a MS-based platform for multiplexed relative and absolute quantification of pMHC repertoires. I evaluate the method’s quantitative accuracy and benchmark it against other pMHC quantification strategies. I also apply the technique to study how pMHC repertoires are altered in response to CDK4/6 inhibitor treatment and find that treatment drives quantitative changes in pMHC expression of proteins mapping back to the known biological response to CDK4/6 inhibition, connecting intracellular changes to external immune presentation.

This work is expanded on in Chapter 4, where I measure changes in the pMHC repertoire in response to MEK inhibitor treatment in *NRAS* and *BRAF* mutant melanoma. These data demonstrate that melanoma differentiation antigens are selectively upregulated in expression following MEK inhibition, and an analysis of other omics datasets identifies E2F transcription factor switching and MITF expression as the mechanism responsible for this pMHC repertoire response. Tumor antigen upregulation is confirmed in cell line xenograft mouse models. Finally, an examination of published TCGA data on *BRAF* mutant melanoma patients identifies patients with lower MITF expression as having significantly lower HLA and tumor

antigen expression and experience worse clinical outcomes. Taken together, these data suggest that MEK inhibitor treatment may improve patient response by upregulating MHC and tumor antigen expression and combining MEK inhibitors with checkpoint blockade or targeted immunotherapy may improve therapeutic response.

Chapter 5 builds on the method developments of Chapter 2 (targeted quantification) and Chapter 3 (pMHC profiling), along with biological findings of Chapter 4, describing an improved method for absolute quantification of pMHCs. This approach, termed “SureQuant MHC,” uses IS-PRM and a series of isotopologues to generate an internal standard curve for targeted, label-free absolute quantification of eighteen MEK inhibitor modulated antigens of interest. Results determine copy-per-cell estimates of pMHC expression levels in cells treated with DMSO or MEK inhibitor, highlighting the wide range of endogenous expression in melanoma cell lines. Furthermore, we apply this method to estimate pMHC concentrations in human tumors, demonstrating the potential for targeted pMHC quantification in clinical settings.

In Chapter 6, MEK inhibitor-modulated antigen targets from chapter 4 and absolute quantification data form chapter 5 are combined for the development of pMHC-specific antibodies in collaborating with Nick Rettko and Jim Wells to target highly expressed pMHCs modulated by MEK inhibitor treatment. We leverage the antibodies as antibody-drug conjugates and highlight the potential of antigens highly expressed specifically on tumor cells as ADC drug targets, with the goal of limiting toxicity in non-tumor tissue.

Chapter 7 explores an emerging methodology in quantitative mass spectrometry, termed “boosting,” which aims to reduce sample input while increasing data quantity through the use of an isobaric protein carrier channel. This negative quantitative impact of utilizing a protein carrier in MS^2-based MHC and pTyr analyses is described, along with potential areas of exploration which may improve quantitation in these applications. Finally, Chapter 8 describes a collaboration with Stefani Spranger’s lab, utilizing a custom SILAC labeling scheme to study

cross presentation of peptide antigens between apoptotic tumor cells and dendritic cells. In conclusion, Chapter 9 details ongoing studies, and highlights areas for future exploration and methodological innovation in both tyrosine phosphorylation and immunopeptidomics workflows, along with insights on clinical uses of the described technologies.

“If signaling in tumors is so important and determines both the tumor cell state and the drugs to which the tumor would likely respond, why then is signaling information not being regularly used in clinical decision-making? The obvious reason is that these types of measurements are difficult, tedious, and nonstandardized and need to be fashioned individually for each pathway that is being queried—not exactly conducive to the design of personalized cancer treatments.”

Michael B. Yaffe
Why geneticists stole cancer research even though cancer is primarily a signaling disease, 2019

CHAPTER 2: High-density, targeted monitoring of tyrosine phosphorylation reveals activated signaling networks in human tumors.

2-1 Introduction

Protein posttranslational modifications (PTMs) provide a fundamental mechanism to regulate protein function. The most common PTM, phosphorylation, is reversibly mediated by a network of protein kinases and phosphatases. Phosphorylation can cause conformation changes that activate or inactivate proteins, while also recruiting adaptor proteins and substrates that initiate downstream signaling cascades, thus altering the cell state.[214–216] While over 250,000 unique phosphorylation sites have been reported, nearly all phosphorylation sites occur on serine and threonine residues, and less than ~1% occur on tyrosine residues.[193,217,218] Thus, deep profiling of tyrosine phosphorylation (pTyr)-mediated signaling requires pTyr enrichment and substantially higher sensitivity than standard phosphoproteomic or protein expression profiling approaches. Despite the rarity of pTyr, tyrosine kinases play a critical role in the signal transduction of pathways controlling proliferation, apoptosis, and survival, and their dysregulation through mutation, hyperactivation, or overexpression can lead to tumorigenesis.[191,219]

Many cancer therapeutics target oncogenic tyrosine kinases.[194] While kinase inhibitors have demonstrated clinical success, identifying patients that may benefit from specific therapies remains challenging, as a majority of clinical molecular characterization efforts rely on genomic-based methods, which do not necessarily reflect protein or pathway activation status and are unable to capture the complex dynamics of innate and acquired therapeutic resistance.[20,220] Tyrosine phosphoprotein measurements have proven valuable in identifying aberrantly activated

signaling pathways and characterizing therapeutic resistance mechanisms,[195,196,221,222] which should provide biomarkers to help inform personalized therapies. Unfortunately, measuring low abundance tyrosine phosphorylated peptides remains challenging, particularly from limited amounts of sample material.

Existing methods to profile pTyr levels are well documented, but each requires a compromise between sensitivity, reproducibility, broad coverage, and quantitative accuracy. Phosphorylation site-specific antibodies have been applied in a variety of formats, including multiplex immunoassays and reverse phase protein arrays, among others. While these assays are relatively straightforward and reproducible, it remains difficult to measure low abundance targets and distinguish between similar phospho-epitopes on distinct proteins due to poor antibody specificity.[198,223] High sensitivity, mass spectrometry (MS)-based pTyr methods provide an attractive alternative, although each of the three typical data acquisition strategies has limitations. Data-dependent acquisition (DDA) or “shotgun” MS-methods offer deep sequencing of the tyrosine phosphoproteome without requiring previous knowledge of peptide targets, enabling novel discovery.[195,200,224] However, DDA methods also result in inconsistent reproducibility of detected peptides, arising from stochastic sampling of precursor ions, and can be biased towards peptides of higher abundance.[212,225] Targeted methods like parallel or multiple-reaction monitoring (PRM/MRM) are well suited to quantify a known panel of peptides with high accuracy and reproducibility, but such traditional targeted acquisition schemes often require a tradeoff between the number of peptides that can be reliably measured and the sensitivity and selectivity of those measurements, restricting depth of coverage.[213] These methods also commonly require complex method acquisition structures and peptide retention-time scheduling, which limits ease of use.[212] Finally, pTyr data-independent acquisition (DIA) methods aim to improve run-to-run overlap while maintaining depth of coverage.[193,210] However the complexity of DIA spectra make quantitative accuracy challenging, and DIA methods have

demonstrated lower sensitivity than PRM approaches, a critical consideration with low abundance, tyrosine phosphorylated peptides.[226]

To address these limitations in existing pTyr profiling strategies, we describe a novel, high-density, targeted MS approach, termed “SureQuant pTyr,” that leverages isotopically labeled, tyrosine phosphorylated internal standard (IS) trigger peptides to efficiently guide MS acquisition in real-time. Adapted from traditional IS-PRM,[141] the use of trigger peptides eliminates the need for retention time scheduling to expand the capacity of targetable nodes, allowing for the reliable and accurate quantification of several hundred tyrosine phosphorylated peptide targets commonly dysregulated in cancer. This platform accommodates low sample input for pTyr enrichment and utilizes commercially available pTyr enrichment reagents, nano-HPLC columns, and data acquisition method templates for a streamlined, “plug and play” implementation.

We apply this approach to profile the pTyr signatures of human colorectal cancer (CRC) tumor specimens to identify dysregulated signaling pathways and reveal potential drug targets not identified with genomic or other proteomic measurements, such as tumors susceptible to anti-epidermal growth factor receptor (EGFR) therapy. Furthermore, we demonstrate the tumor-extrinsic nature of pTyr profiling on tumor specimens, quantifying T cell activation levels on low abundance immune cell-specific pTyr sites, which may be an effective indicator of immune cell infiltration and immunotherapy response. With the reproducibility and sensitivity of SureQuant pTyr, we highlight the potential of this approach to be used in clinical settings to rapidly profile pTyr signaling as a complementary strategy to enhance biomarker identification and tumor characterization for applications in precision medicine.

2-2 Results

2-2-1 Targeted pTyr proteomic workflow utilizing internal standard-driven data acquisition

In order to profile pTyr signaling events in cancer, we selected 340 tyrosine phosphorylated peptides to target and synthesized the corresponding synthetic isotope labeled (SIL) phosphopeptides to serve as ISs (**Figure 2-1**). Selected peptides were primarily chosen from discovery analyses performed on a cohort of CRC samples with matched adjacent normal tissue, with priority given to peptides identified across multiple analyses, sites with differential phosphorylation levels between tumor and non-tumor tissue, and sites known to be implicated in oncogenic signaling. Of note, the discovery analyses illustrate the central limitation of DDA: variation in the number and identify of peptides across multiple discovery analyses. Discovery analyses identified between 552 and 297 unique pTyr sites, yet only 127 sites mapping to 102 unique proteins were identified across all 4 analyses (**Supplementary Figure 2-1-A, B**). The poor reproducibility of this approach restricts depth of analysis across many samples, underscoring the need for a targeted approach. Selected pTyr sites from the discovery analyses primarily cover two branches of the kinome: tyrosine kinases and CMGC kinases (cyclin-dependent kinases (CDK), mitogen-activated protein (MAP) kinases, glycogen synthase kinases, and CDK-like kinases)[191]**.** This list was then supplemented with additional peptides from the literature mapping to EGFR and T cell signaling pathway, as EGFR inhibitors and immune checkpoint blockade (ICB) are two common therapies within CRC and other cancer types [206,227–229].

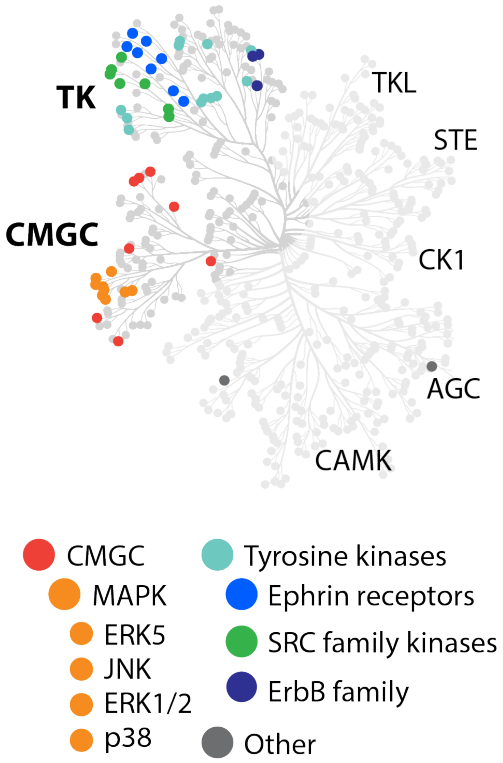

***Figure 2-1**. Kinome tree. Human kinome tree with peptides selected for SureQuant pTyr analysis colored according to kinase group.*

For SureQuant pTyr analysis, tumors or cell line samples were first digested into tryptic peptides, and stable isotope-labeled, tyrosine phosphorylated IS (*i.e.*, "heavy") peptides were added to the endogenous (*i.e.*, "light") peptide mixture. (**Figure 2-2-A**). Both light and heavy pTyr peptides were subsequently isolated using two-step enrichment, with an immunoprecipitation against pTyr residues, followed by immobilized metal affinity chromatography (IMAC). Enriched light and heavy pTyr peptides were next analyzed by LC-MS/MS using a custom IS-triggered targeted quantitation method, leveraging the "SureQuant" acquisition mode native to the Orbitrap Exploris 480 MS (Thermo Scientific).

During SureQuant acquisition, the MS alternates between a "watch" mode and a "quantitative" mode (**Figure 2-2-B**). In watch mode, the MS continuously monitors for the

presence of any heavy IS peptide. If an IS precursor ion is detected above a specified intensity threshold, a fast, low resolution MS^2 scan is performed and pseudo-spectral matching against six pre-selected product ions is applied to verify the presence of the IS for enhanced selectivity. If the MS^2 spectrum is a positive match, the MS initiates quantitative mode, triggering a high-quality MS^2 scan of the light, endogenous peptide. With this framework, IS-guided acquisition ensures high selectivity, high sensitivity measurements of the endogenous peptide for enhanced data quality and reproducibility.

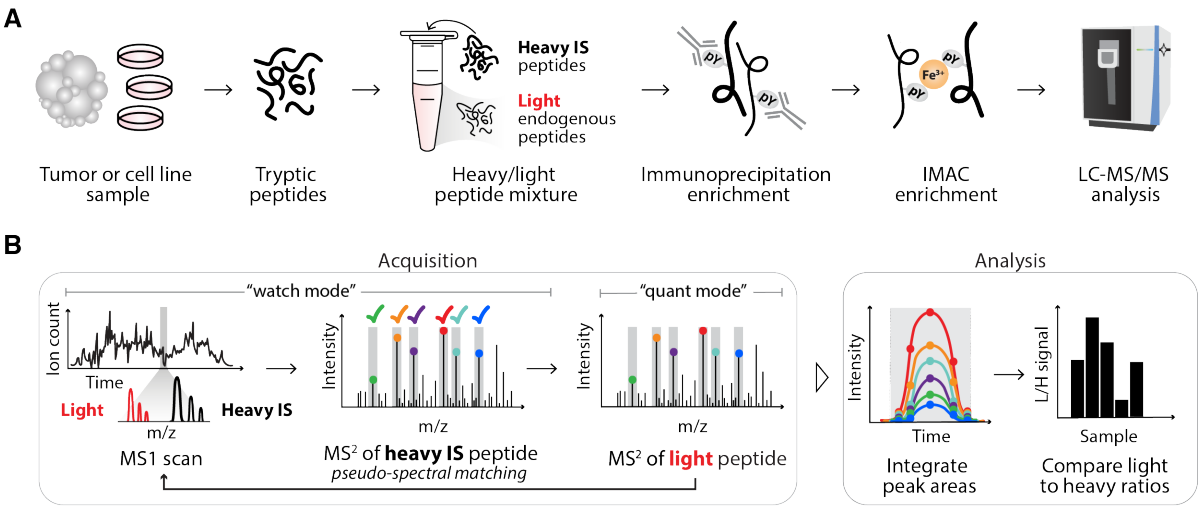

***Figure 2-2**. SureQuant pTyr workflow. **A** Sample processing workflow for pTyr enrichment and analysis. **B** Mass spectrometry acquisition method and analysis workflow for SureQuant pTyr IS-triggered quantitation.*

Product ions for both the heavy IS and light target peptides are monitored throughout the peptides' chromatographic elution, and signal intensity is quantified by integrating the area under the curve for both light and heavy peptide product ions. Next, the ratio of light signal to heavy signal (L:H) is calculated, and L:H ratios are used for quantitative comparisons across samples. Adding IS peptides at defined concentrations prior to pTyr enrichment provides a

number of additional benefits, serving as an embedded standard for concentration or copy number estimation using one-point calibration and enabling normalization across a theoretically unlimited number of samples and data-collection sites. IS peptides also double as a limit-of-detection control, as identification of the heavy IS but not the light peptide suggests the endogenous peptide was absent or below the limit-of-detection. Importantly, all parameters necessary to implement this workflow are readily determined in a single survey run analysis and can be used for all subsequent SureQuant analyses of the same peptide panel, streamlining assay implementation.

2-2-2 SureQuant pTyr provides reproducible quantitation across replicate analyses

We first applied this workflow to measure pTyr levels in A549 lung carcinoma cells stimulated with epidermal growth factor (EGF) as an *in vitro* control. We isolated light and heavy pTyr peptides from three technical replicate samples while varying the length of immunoprecipitation to assess the quantitative reproducibility of the SureQuant pTyr approach across replicate samples (**Figure 2-3-A**). Using a catenin delta-1 (CTTND1-pY904) peptide as an example, multiple MS^2 scans were captured across the chromatographic peptide elution profiles for both the light and heavy peptide (**Figure 2-3-B, C**). Between replicates, the product ion intensities varied, with replicate 3 having over 3-fold higher signal intensity than replicates 1 and 2, likely due to a longer incubation time during immunoprecipitation (**Figure 2-3-D**). Despite this dissimilarity in intensities, the L:H ratios across replicates remained consistent (**Figure 2-3-E**), demonstrating the ability of this workflow to account for variation in sample handling and absolute intensities. In fact, across all quantified peptides the correlation coefficient (r^2) between analyses was 0.96 or greater (**Figure 2-3-F**).

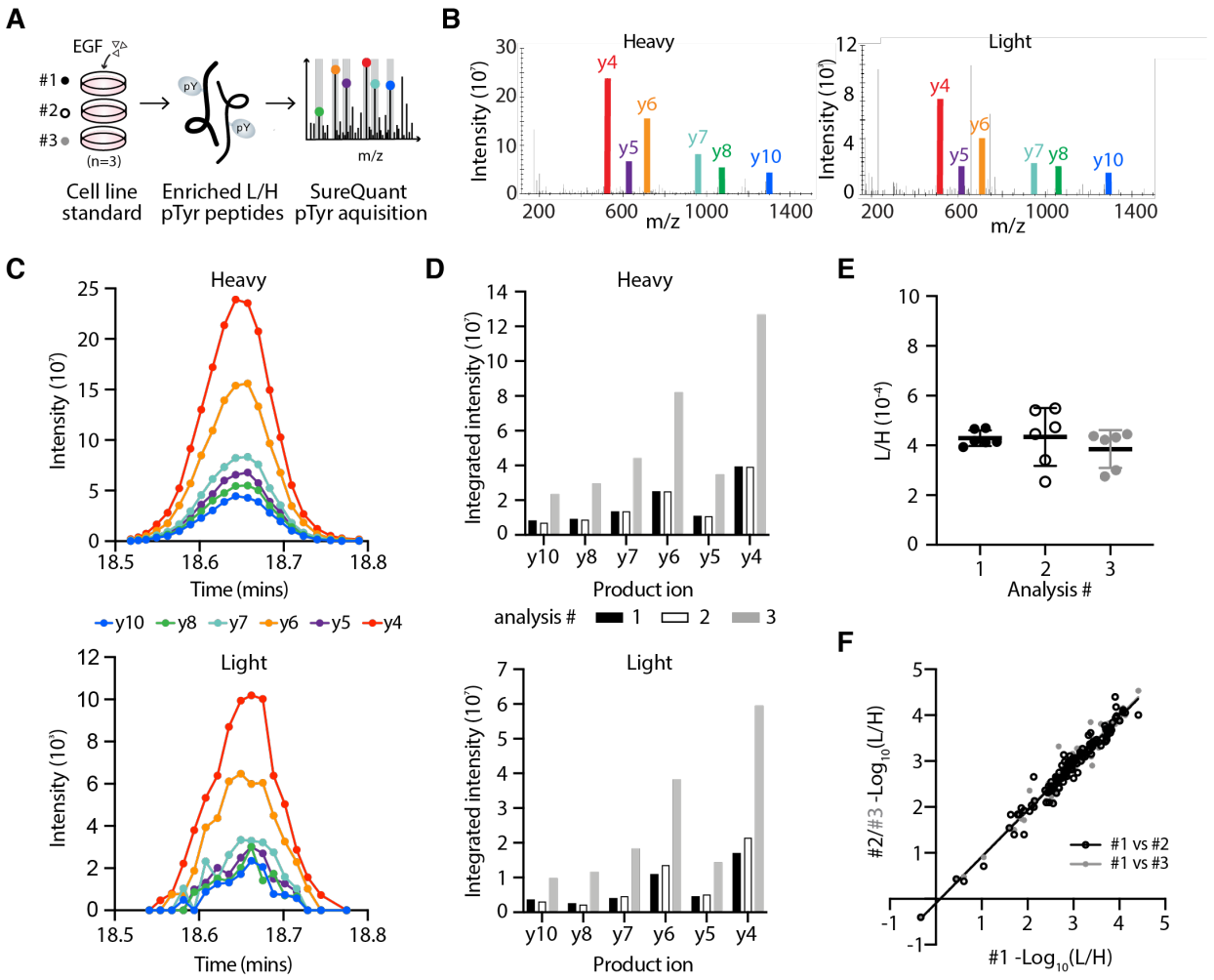

Figure 2-3. *Quantitative reproducibility with SureQuant pTyr.* ***A*** *Experimental setup. IS-trigger peptides were added to three biological replicates of A549 cell lysate stimulated with epidermal growth factor (EGF). Enriched light (L) and heavy (H) pTyr peptides were analyzing using SureQuant pTyr acquisition.* ***B*** *MS/MS spectra from analysis #3 of the heavy (left) and light (right) CTTND1 peptide, SLDNN[pY]STPNER-pY904, at peak intensity, where [pY] denotes the residue position with pTyr modification. Monitored product ions are uniquely colored and labeled with b/y ion.* ***C*** *Ion intensity over time for the 6 heavy (upper) and light (lower) product ions from CTTND1 pY904 in analysis #3. Each MS/MS event is represented by a point.* ***D*** *Integrated peak area intensities for each product ion in C. Bar color corresponds to analysis #.* ***E*** *Ratios of light to heavy signal intensity (L/H) of CTTND1 pY904 for each analysis, where each point represents the L/H value of a single product ion. Solid line and error bars represent the mean and standard deviation, respectively.* ***F*** *Correlation of (L/H) signals across 127 peptides between analysis #1 and #2 (r2=0.96, black) and analysis #1 and #3 (r2=0.97, grey).*

To benchmark SureQuant pTyr against existing acquisition methods, we analyzed three additional EGF stimulated A549 cell line replicates by label-free DDA and three labeled with TMT and found that SureQuant pTyr has comparable quantitative reproducibility to TMT-labeled DDA (r^2=0.97) and superior to label-free analysis (r^2=0.88 & 0.90) (**Figure 2-4-A**). We also analyzed three CRC tumor sample replicates with SureQuant pTyr, and found the method had equivalent quantitative accuracy in *in vivo* derived tissue (r^2=0.98) (**Figure 2-4-B**).

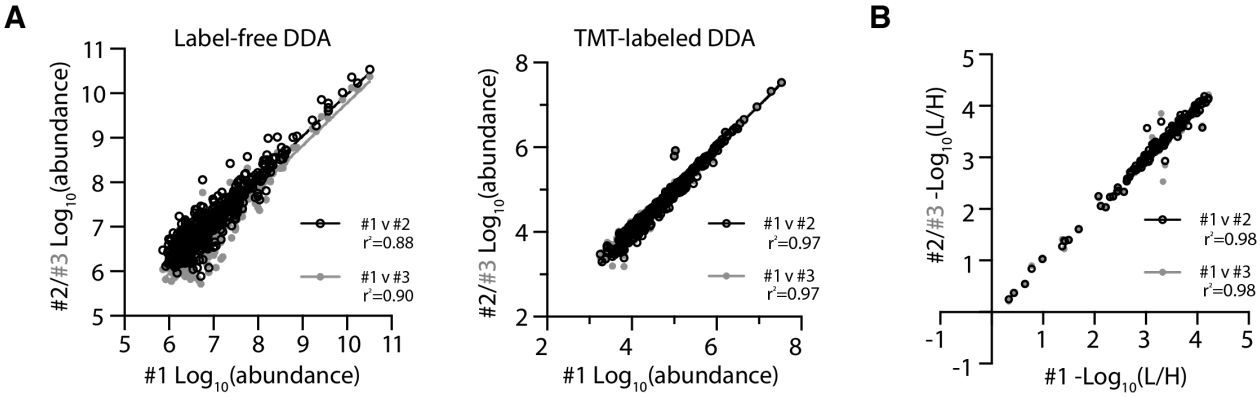

Figure 2-4*. Benchmarking SureQuant pTyr against other MS methods.* ***A*** *Correlation of peptide abundances for three label-free DDA analyses (left) and one multiplexed, TMT-labeled DDA (right) analysis. R-squared values were 0.88 and 0.90 for the label-free analysis, and* r^2*=0.97 for the TMT-labeled analysis.* ***B*** *Correlation of peptide L/H ratios between three technical replicate tumor samples,* r^2*=0.98.*

Finally, we assessed whether the L/H ratios, which can span several orders of magnitude, are able to accurately capture known quantitative dynamics, and whether the quantitation is comparable to traditional discovery and targeted MS acquisition methods. Three replicates of A549 cells were stimulated for 0, 0.5, or 2 minutes with EGF to create quantitative dynamics across the samples through activation of EGFR and downstream signaling nodes (**Figure 2-5-A**). These samples were then analyzed in one of three ways: labeled with TMT for multiplexed DDA, analyzed with SureQuant pTyr, and analyzed by PRM, where 20 pTyr targets

common to the SureQuant pTyr panel and the TMT-DDA analysis were selected for label-free, targeted analysis.

These data follow expected phosphorylation dynamics of EGFR receptor activation, as EGFR phosphorylation is greatly increased following EGF-stimulation, which recruits and phosphorylates the adapter protein GAB1, creating a docking site for SHP2 (PTPN11), which is required for ERK activation (MAPK3/1) (**Figure 2-5-B**)[230]. Importantly, the quantitation is highly similar between analysis techniques, with only the 0.5 min timepoint of EGFR-pY1197 being significant between SQ and TMT-DDA analyses, (21x vs. 24x average fold change, p=0.03), as replicates had low standard deviation. Noticeably, there is larger standard deviation between replicates in the label-free PRM data, as this acquisition method lacks an internal standard to account for variations in sample handling and analysis. Other peptides selected for PRM that exhibit dynamic changes in response to EGF stimulation likewise do not have statistically significant differences in quantitation across acquisition methods (**Figure 2-5-C**).

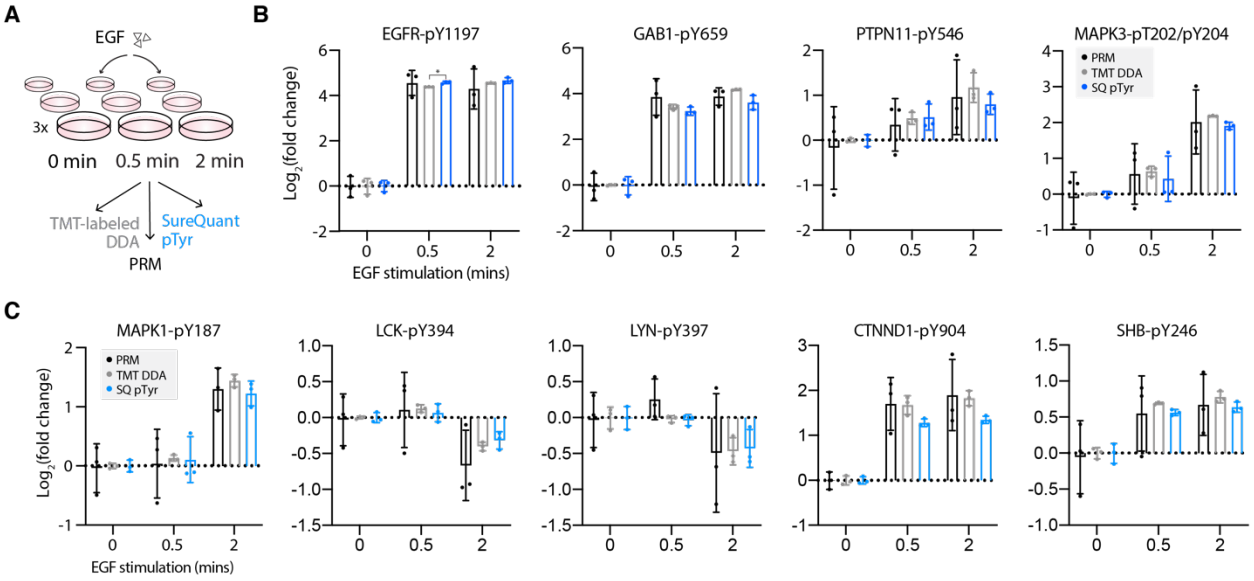

Figure 2-5*. Method comparison of quantitative dynamics.* ***A****, Experimental setup for quantitative comparison between TMT-labeled DDA, PRM, and SureQuant pTyr methods.* ***B,C*** *Log2 fold change values, relative to the mean peptide abundance at the 0-minute timepoint, of pTyr peptides for three data*

*acquisition methods: PRM (black), TMT-labeled DDA (grey) and SureQuant pTyr (blue). Significant differences in quantitation between PRM and TMT-DDA vs. SQ pTyr are represented as *p<0.05 (Dunnett's multiple comparisons test). Each sample includes n=3 biological replicates, error bars represent the standard deviation.*

2-2-3 Human colorectal tumors show distinct pTyr signatures

Thirty-one human CRC tumors that were previously characterized in a proteogenomic analysis by Vasaikar et al.[222] were selected for SureQuant pTyr profiling. The previous study did include a global phosphorylation analysis, but due to the lack of pTyr-specific enrichment, only 16/2183 sites (0.07%) measured across all 31 tumors were tyrosine phosphorylated, six of which were represented in the SureQuant pTyr panel. Consequently, we hypothesized a pTyr-targeted analysis could provide an additional dataset for further tumor characterization and may reveal novel insights.

Using our panel of 340 tyrosine phosphorylated ISs, we collectively detected & quantified 336 heavy peptides, representing 99% of the assay panel, and 325 light peptides, representing 96% of endogenous peptides from the assay panel across the tumor cohort (**Figure 2-6-A, B**). The four unmeasured heavy peptides exhibited fluctuating signal from run to run and did not systematically reach the signal intensity threshold defined in the initial survey analysis, while the eleven unquantifiable light peptides are assumed to be below the limit-of-detection, as the corresponding heavy peptide was detected. Across all tumors, an average of 91% of heavy peptides and 78% of light peptides were identified, highlighting the reproducibility of the method. While we did not see complete coverage of our panel in every tumor, this result was expected as pTyr peptides are often present at low levels, and some of the peptides included in the panel were hypothesis driven. For example, we included a T cell signaling peptide from ZAP70 (pY292) which was not identified in the discovery analyses but was

quantifiable in 16/31 tumors. Due to the tumor-specificity of some of the signaling nodes, we analyzed the pTyr signaling in two ways. First, L:H ratios of peptides identified across all 31 tumors were quantified and z-score normalized. Second, the L:H ratios for all sites identified in at least 50% of tumors were z-score normalized to expand the datasets for individual tumor signaling analyses.

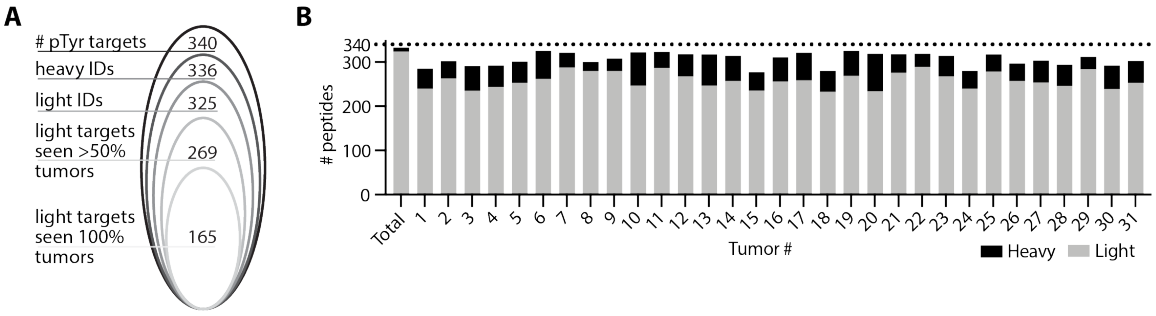

Figure 2-6*. pTyr sites quantified in human tumors.* ***A*** *Peptides identified and quantified across 31 tumors.* ***B*** *Number of unique heavy (black) and light (grey) peptides identified in each tumor.*

Approximately 97% of identified peptides had a L:H ratio between 1:1 and $1:10^4$, with just 0.7% of sites having a L:H ratio above 1 (**Figure 2-7**). These highly abundant sites (L:H > 1) include MAPK3/1 (ERK1/2), EGFR, and MAPK14 (p38α), each of which is implicated in oncogenesis [191,194]. Sites with the lowest L:H ratios include several T cell signaling associated peptides (CD3ζ, CD3δ, ZAP70), consistent with our hypothesis that a minority of cells in these tumors are infiltrating immune cells.

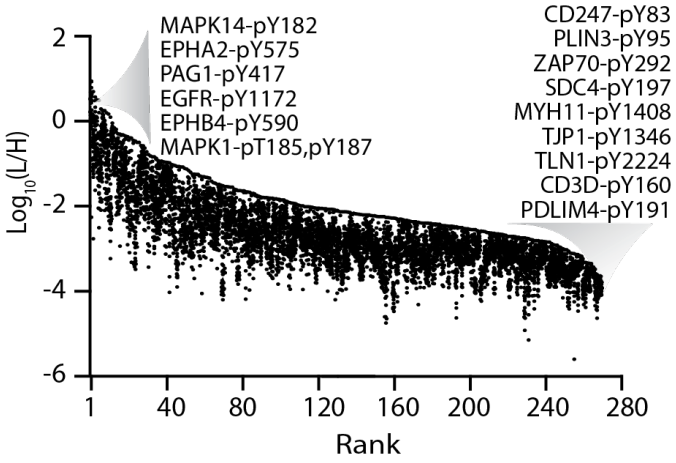

***Figure 2-7**. Range of L/H ratios across tumors. Distribution of tumor L/H ratios with peptides rank ordered from highest to lowest maximum abundance. Annotated peptides labeled by source protein and residue position with pTyr modification have the maximum and minimum abundances.*

The biological variation in peptide pTyr levels between tumors is evident upon comparing the L:H ratios measured by this platform. For example, EGFR and ErbB3, two receptor tyrosine kinases (RTKs) in the epidermal growth factor receptor family, appear to have coordinated levels of receptor phosphorylation in some tumors (Tumor 2 (T2), T7, T8, T21, T25), while others have differential levels (**Figure 2-8-A**). ErbB3 is a non-autonomous receptor, requiring dimerization with another ErbB family member or RTK for phosphorylation. Thus, the higher ErbB3 and lower EGFR phosphorylation levels of T5 and T6 suggest ErbB3 may be dimerizing with another ErbB family member or activated RTK. Alternatively, T1, T26, and T30 show the opposite trend, implying ErbB3 is playing a less dominant role in driving ErbB family signaling in these tumors. To assess whether observed pTyr abundance differences could be explained by variation in the overall amount of pTyr signal among tumors, potentially due to differences in protein loading or sample processing, we evaluated the distribution of L:H ratios across tumors (**Figure 2-8-B**). Only two tumors, T9 and T10 had a significantly higher and lower distribution, respectively, of L:H ratios from the mean signal across tumors, suggesting

differences in pTyr levels are indicative of biological variation as opposed to experimental variation.

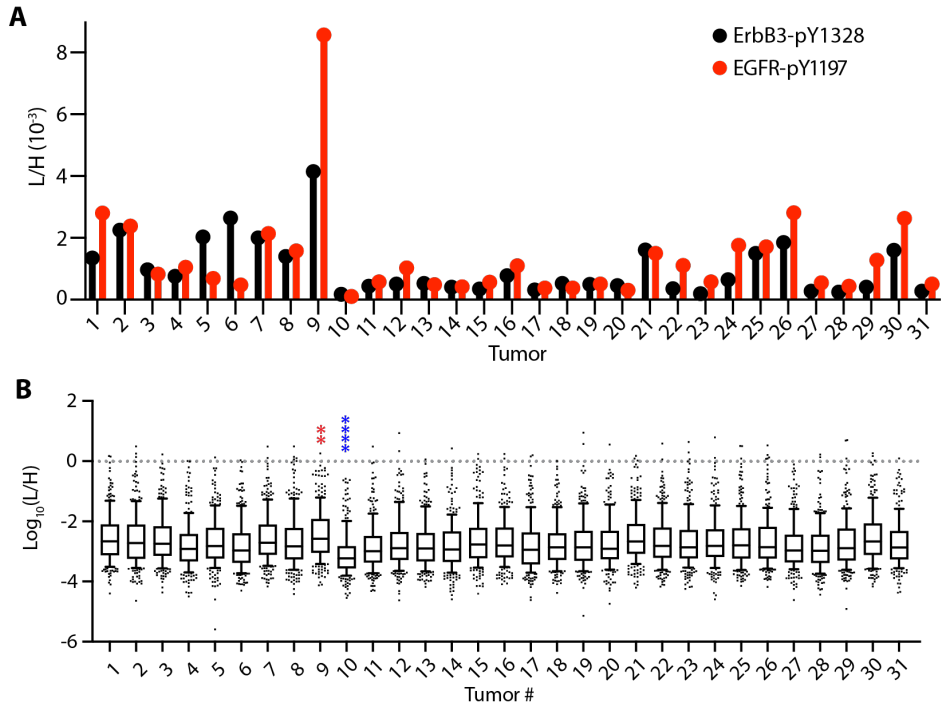

Figure 2-8*. L/H ratio distributions across tumors.* ***A*** *Light to heavy signal intensity ratios (L/H) for ErbB3 peptide (black), SLEATDSAFDNPD[pY]WHSR, and EGFR peptide (red), GSTAENAE[pY]LR, where [pY] denotes the residue position with pTyr modification.* ***B*** *Distributions of light to heavy signal ratios (L/H) for each tumor. Data is displayed as a box and whiskers plot, where the box describes the interquartile range and the whiskers define the 10-90 percentile of data. * Indicates significantly increased (red) or decrease (blue) from the mean distribution using Dunnett's multiple comparison test for significance. **p<0.01, ****=p<0.0001.*

To visualize the pTyr signaling profiles across tumors, phosphorylation sites quantified in all tumors were analyzed by hierarchical clustering (**Figure 2-9**). Two clear findings emerge from this analysis: each tumor possesses a unique pTyr signature, and tumor clustering is not readily explained by phenotypic information such as gender, histological subtype, or tumor stage (data file S5). Previous work by Vasaikar et al. assigned each tumor in our panel to one of

three unified multi-omics subtypes (UMS), characterizing tumors with microsatellite instability and hypermutation ("MSI"), chromosomal instability ("CIN"), and evidence of epithelial-to-mesenchymal transition ("mesenchymal"), based off of previous proteomic, genomic, and transcriptomic-based classifications developed for CRC tumors [222,231,232]. These classifications revealed some stratification with hierarchical clustering: CIN tumors are primarily located in clusters one and two, whereas a majority of mesenchymal and MSI tumors group together in clusters three and four, respectively. Still, hierarchical clustering of tumors with the same UMS illustrates the high degree of individuality in each tumor's pTyr signature, even within co-clustering subtypes (**Supplementary Figure 2-2**).

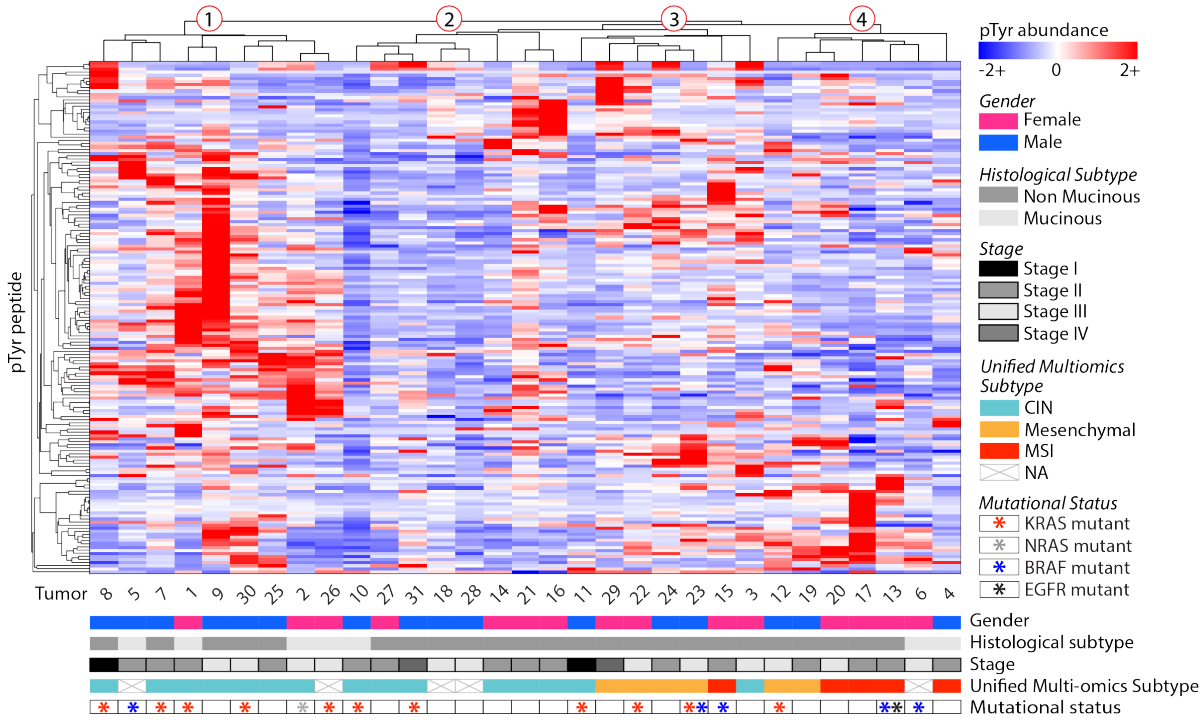

Figure 2-9*. Clustering of pTyr peptides in tumors. Peptide and tumor hierarchical clustering (distance metric = correlation), where pTyr abundance values are z-score normalized light to heavy signal ratios*

To understand which pTyr sites drive the UMS clustering of tumors, we utilized principal component analysis (PCA) (Fig. 3E). Principal component 1 (PC1), explaining 24% of the total variance, primarily separates T9 from the remaining tumors and is driven by T9's high pTyr levels of EGFR signaling peptides (Fig. 3F, fig. S1D). Interestingly, PC2, explaining 11% of the total variance, separates CIN tumors from the MSI and mesenchymal tumors. The 20 highest scoring pTyr peptides derived from unique proteins on PC2 show enrichment for pathways related to innate immunity (Fig. 3F, fig. S1E). Vasaikar et al. found that MSI and mesenchymal tumors had higher levels of immune cell infiltration, in agreement with our pTyr findings.

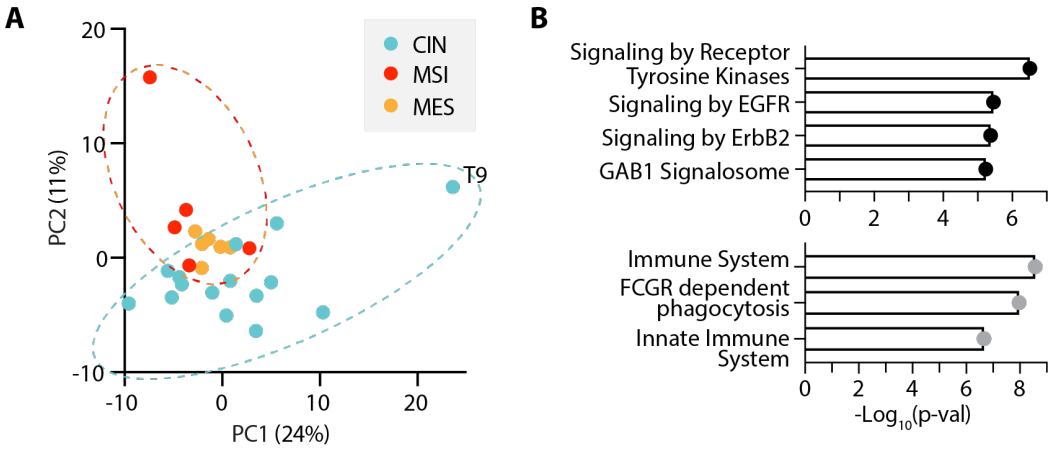

***Figure 2-10**. PCA analysis of pTyr peptides in tumors. **A** Tumors plotted by principal component 1 (PC1) and PC2 score, colored according to unified multi-omics subtype. **B** Significantly enriched reactome pathways from the top 20 peptides derived from unique proteins on PC1 (top, black) and PC2 (bottom, grey). Significance values are FDR adjusted.*

2-2-4 Tumor-specific pathway analysis reveals enriched signaling pathways

We next performed a correlation analysis on the full peptide matrix and clustered peptides on this basis to identify groups of co-regulated peptides across tumors (**Figure 2-11-A**). A protein-protein interaction network analysis on selected clusters revealed significantly enriched pathways and processes (**Supplementary Figure 2-4-A**). These included pathways

related to immunity in cluster 1 (**Figure 2-11-B)**, as well as cytoskeletal and actin binding proteins in cluster 2 (**Figure 2-11-C**). Cluster 3 maps to ErbB and Ras signaling pathways, (**Figure 2-11-D**), along with migration signaling pathways like adherins junctions, focal adhesions, and RAP1 signaling (**Figure 2-11-E**). Using these findings, we curated a custom library of twelve gene sets and performed a tumor-specific pathway enrichment analysis (TPEA).

Phosphorylation site source proteins from the expanded values matrix were rank ordered and used to identify tumors with positive or negative enrichment in the selected pathways and biological processes relative to the other tumors (**Figure 2-11-F**), showcasing the pathway level information obtained with SureQuant pTyr. For example, T16 and T10 have significant positive and negative enrichment in actin binding phosphopeptides, respectively, and correspondingly have the highest and lowest phosphorylation levels of peptides identified in cluster 2 (**Supplementary Figure 2-4-B)**. While some findings were redundant with insights obtained with hierarchical clustering, TPEA also identified signaling level similarities between tumors that were not obvious with clustering. For instance, T13 and T29 both have significant positive enrichment of RAP1 signaling but clustered separately in **Figure 2-9**.

Additionally, we applied kinase-substrate enrichment analysis (KSEA) to each tumor which, in contrast to TPEA, uses site-specific information to identify the enrichment of phosphorylated kinase substrates to infer kinase activity (**Figure 2-11-G**).[233] The results were complementary in some cases, with T9 showing an enrichment in ErbB signaling pathways with TPEA and ErbB substrates with KSEA, but KSEA also revealed novel findings. T1 did not contain any significantly enriched pathways, but showed significant enrichment in several kinase-substrate datasets, including SRC, LCK, and FYN, which have been explored as therapeutic targets in metastatic CRC.[234]

We subsequently combined the pTyr data with the global phosphorylation data generated by Vasaiker et al. and performed KSEA against a wider kinase-substrate library to evaluate whether this larger phospho-dataset might reveal additional kinase targets. Results identified CDK1/CDK1, previously reported by Vasaiker et al., along with ERK1/2, AKT1/MTOR, and PKCA, among others (**Supplementary Figure 2-4-C**). While some pathways contained a combination of pTyr/pSer/pThr sites (i.e., ERK1/2), SRC kinase enrichment was only identifiable using pTyr data (**Supplementary Figure 2-4-D**). SRC is a protein tyrosine kinase therefore all substrates have phosphorylated tyrosine residues, underscoring the importance of profiling the tyrosine phosphoproteome for deeper signaling network coverage. To better understand each tumor's unique pTyr signature and identify therapeutically targetable nodes, we next examined the sites driving pathway enrichment, focusing first on ErbB signaling and EGFR phosphorylation status.

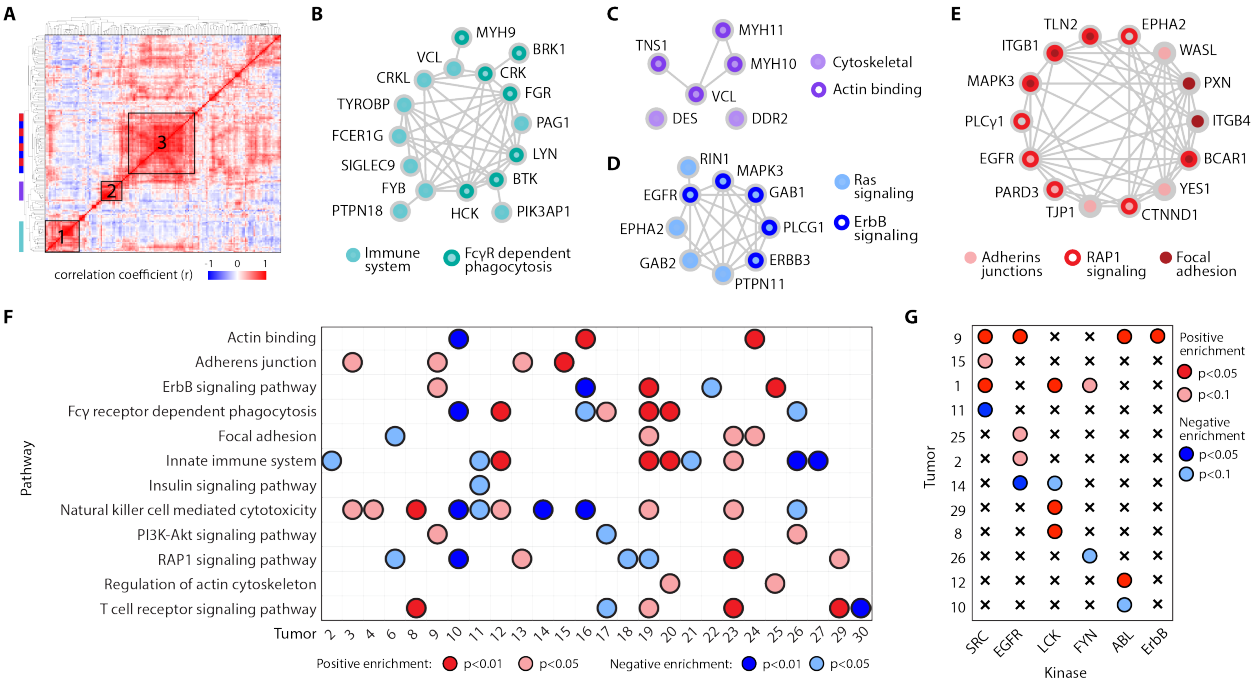

Figure 2-11*. Tumor-specific enrichment analysis.* ***A*** *Hierarchical clustering based on the correlation coefficients between phosphosites across all tumors (distance metric = correlation).* ***B-E*** *Protein-protein*

*interaction network of peptides within cluster 1 (**B**), cluster 2 (**C**) and cluster 3 (**D-E**). Node color(s) maps peptides to enriched pathway(s). **F** Significantly enriched pathways among tumors using tumor-specific pathway enrichment analysis. **G** Significantly enriched kinase-substrate interactions within tumors. Significance (p-value) and directionality indicated by color, q < 0.25 for all enrichment analyses. Tumors that did not have any significant enrichment are not shown.*

2-2-5 ErbB phosphorylation levels identify candidates for anti-EGFR therapy

EGFR is expressed in a majority of CRC, and its overexpression in many cancer types has been tied to more aggressive phenotypes and poor clinical prognosis, highlighting EGFR inhibitors as a promising therapeutic target.[235] Indeed, several anti-EGFR agents have been approved for CRC clinical use, though treatment is currently only recommended for patients with wild type KRAS/NRAS/BRAF, as mutations in these genes have been shown to confer EGFR inhibitor resistance.[236–238] Disappointingly, anti-EGFR agents are only effective in a fraction of qualifying patients, and those that do respond often still develop therapeutic resistance.[239] As EGFR expression levels have not been shown to correlate with clinical response to EGFR inhibitors[240] and RAS mutational status remains the principle biomarker for EGFR inhibitor efficacy, we hypothesized that measuring pTyr levels on EGFR and ErbB family signaling pathways could provide a more direct readout of EGFR activation status, thereby improving identification of those who may benefit from EGFR inhibition.

We identified three tumors with significant positive enrichment of the ErbB signaling pathway (T19, T25, and T9), and two with significant negative enrichment (T16 and T22). T19 had low pTyr levels of the ErbB family receptors, with pathway enrichment instead driven by common downstream signaling nodes including ERK1/2 phosphorylation (**Supplementary Figure 2-5-A**). As a result, T19 was excluded from subsequent analyses. Neither T25 nor T9 contained a RAS/RAF mutation, making both potentially eligible for anti-EGFR therapy under existing biomarker criteria. T25 displayed high levels of EGFR phosphorylation relative to the

other tumors, suggesting T25 may be a good candidate for an EGFR-inhibiting antibody like cetuximab (**Figure 2-12**). Alternatively, T9 had high levels of three ErbB RTKs: EGFR, ErbB2, and ErbB3, indicating EGFR inhibition alone may not be sufficient for T9, as ErbB2 amplification is predictive of anti-EGFR therapy resistance [229,240]. Instead, T9 may benefit from treatment with a pan-ErbB inhibitor like lapatinib, or combination therapy with cetuximab and the ErbB2 inhibitor, pertuzumab.

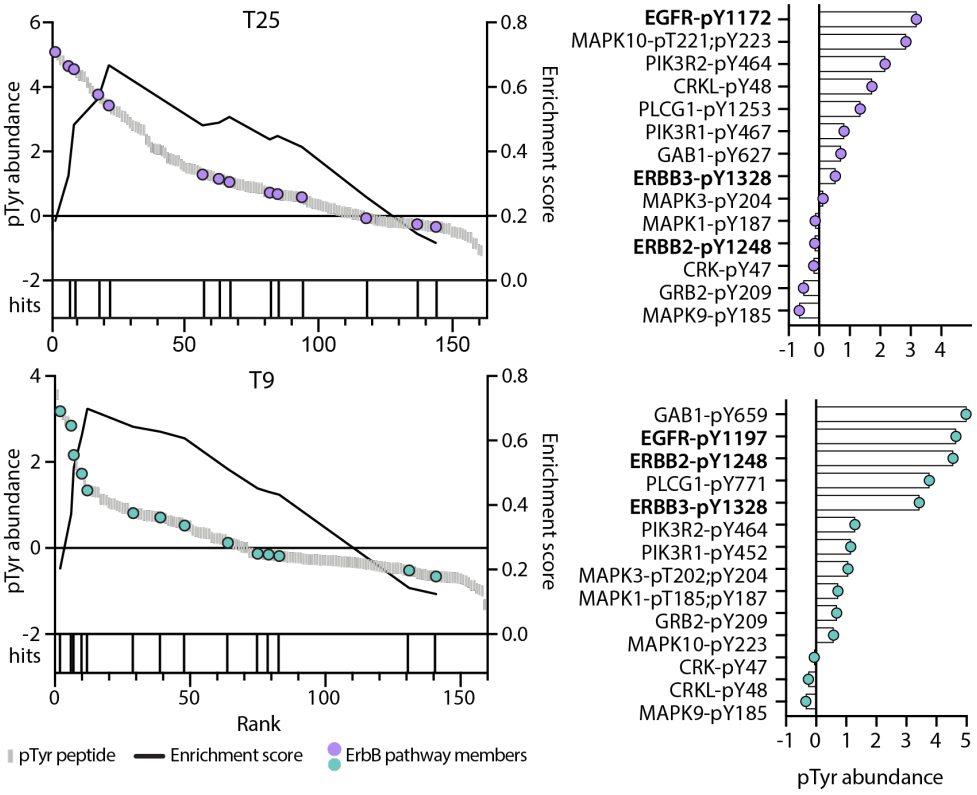

***Figure 2-12**. ErbB pathway enrichment. Enrichment plots (left) of ErbB signaling pathway in T25 (purple) and T9 (teal). Peptide rank (x-axis) versus pTyr abundance is plotted on the left y-axis, and the running enrichment score is plotted on the right y-axis. Each hit signifies a pTyr source protein present in the ErbB signaling pathway library. All pTyr peptides identified in the ErbB signaling pathway and their corresponding pTyr abundance (right), with ErbB family receptors annotated in bold. pTyr abundance values are z-score normalized light to heavy signal ratios.*

We next sought to determine whether these findings were predictable based on available transcriptomics and proteomics data for these same tumors [222]. Looking specifically at the sites driving ErbB enrichment, we observed a weak positive correlation between pTyr levels and corresponding gene expression levels in T9 but found no correlation with protein expression (**Figure 2-13-A, B**). T16 had no correlation between pTyr levels and gene/protein expression, whereas T25 and T22 surprisingly showed a weak negative correlation.

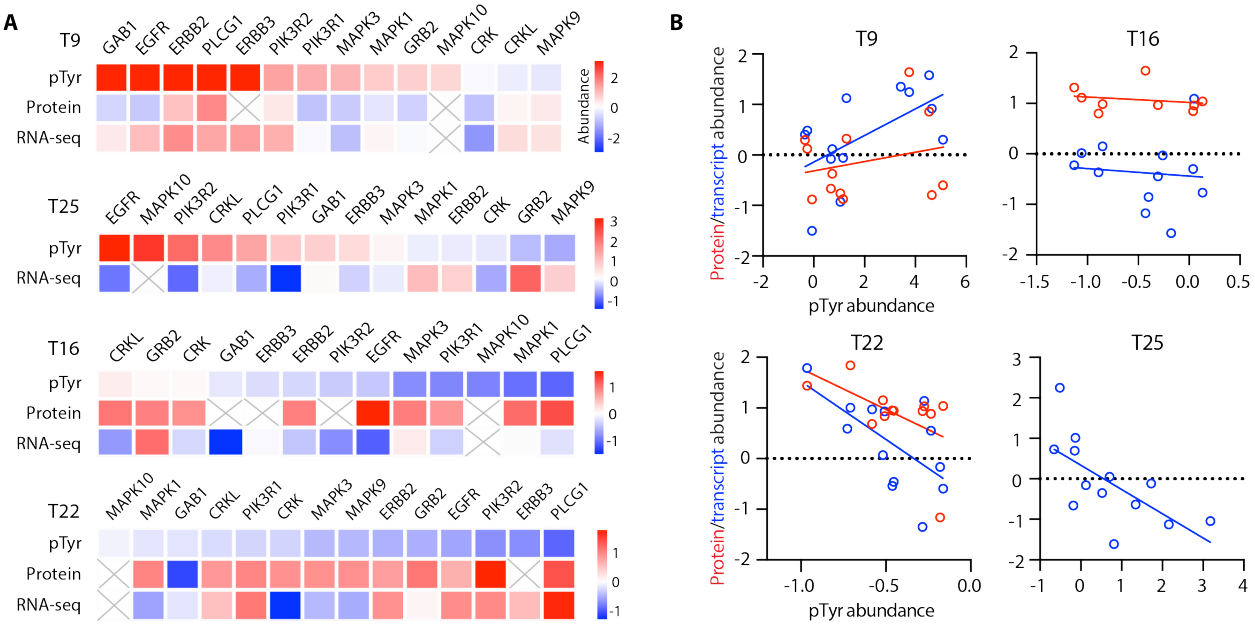

Figure 2-13*. Correlation between ErbB pathway pTyr and RNA/protein.* ***A*** *Z-score normalized pTyr abundance, protein expression and transcript expression levels of ErbB signaling pathway members.* ***B*** *Correlation between pTyr abundance and protein (red) or transcript (blue) expression of ErbB signaling pathway members. Protein and transcript abundance values are z-score normalized. Correlation coefficients for pTyr vs. protein for T9, T16, and T22 are r^2= 0.06, 0.05, 0.29, respectively. Correlation coefficients for pTyr vs. gene expression for T9, T16, T22, and T25 are r^2= 0.35, 0.01, 0.38, and 0.43, respectively. Protein expression data for T25 was unavailable.*

In line with these findings, gene set enrichment analysis (GSEA) of RNA-seq data from T9 identified significant enrichment in EGFR signaling genes, along with downstream pathways of EGFR activation including SHC1 and GAB1 signaling (**Figure 2-14-A, Supplementary Figure 2-5-B**). However, GSEA from T25, T16, and T22 showed no significant enrichment in EGFR/ErbB related signaling pathways using protein or gene expression data. In fact, an analysis of all pTyr sites and their corresponding protein and gene expression levels yielded no correlation (**Figure 2-14-B**), which taken together demonstrates the difficulty of using transcript expression or protein expression data to infer pTyr signaling dynamics and pathway activation.

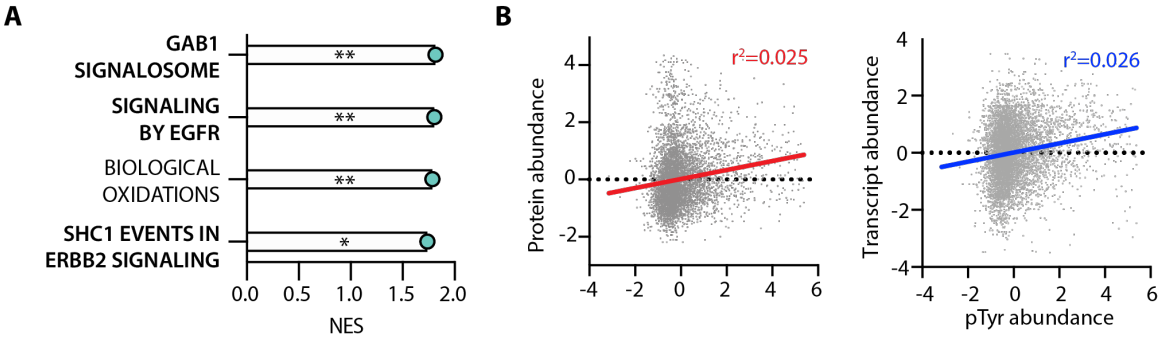

***Figure 2-14**. Global pTyr/RNA/protein correlation. **A** Normalized enrichment score (NES) for positively enriched reactome pathways in T9 using RNA-seq data. *= p<0.05, **= p<0.01, FDR q-value < 0.05 for all. **B** Correlation between all pTyr sites in the full matrix and corresponding protein expression (top) and gene expression (bottom) levels. All values are z-score normalized.*

Identifying anti-EGFR therapy candidates using TPEA requires enrichment among multiple nodes within the ErbB signaling pathway to achieve significance. To identify anti-EGFR therapy candidates that may have been missed using TPEA, we focused on two EGFR peptides containing autophosphorylation sites, pY1172 and pY1197 (pY1148 and pY1173, mature human isoform), which were most commonly quantified across tumors as an analogous approach. We identified twelve tumors with EGFR phosphorylation levels at least 1.5-fold higher

than the mean in either or both pTyr sites, termed “EGFR-high” (**Figure 2-15**). Half of EGFR-high tumors have a RAS mutation rendering them ineligible for anti-EGFR therapy, but the remaining six wild-type EGFR-high tumors (T3, T4, T21, T24, and previously identified T9 and T25) may be appropriate candidates. Similar to earlier findings, GSEA of transcriptomic and proteomic datasets for T3, T4, T21, and T24 did not identify enrichment in EGFR signaling pathways, highlighting the novel insight provided by pTyr profiling.

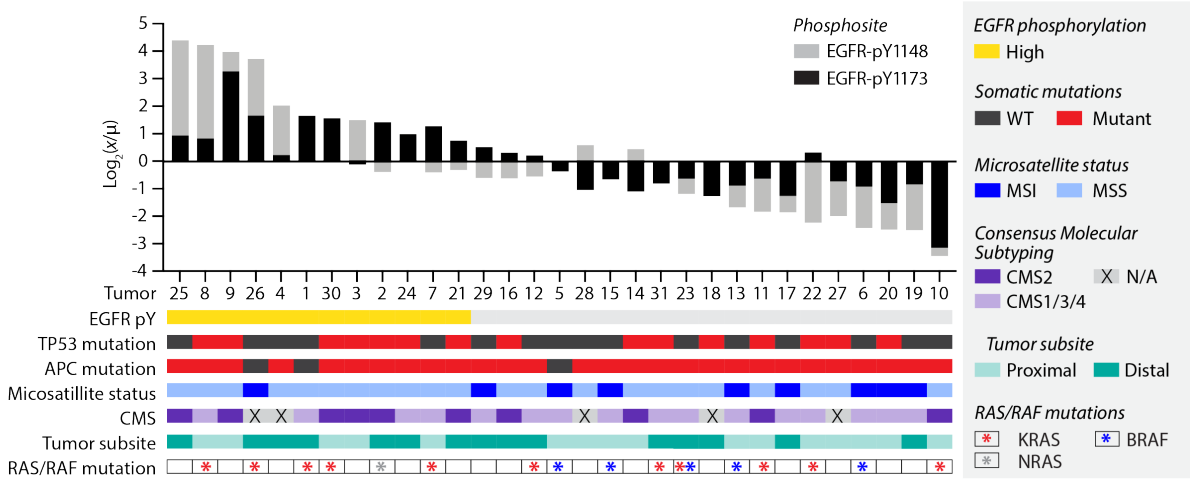

Figure 2-15*. EGFR pTyr signature across patients. Cumulative pTyr signal, calculated as the ratio of tumor light to heavy pTyr signal (x) to the mean light to heavy signal (μ) across tumors, log_2 transformed for two EGFR phosphopeptides rank ordered from highest to lowest signal. Tumor specific annotations are indicated by color, and pY1148 and pY1173 denote the EGFR residue position with pTyr modification.*

Beyond RAS mutational status, several other genomic and phenotypic classifications have been correlated with response to EGFR inhibitors, including tumors with a mutation in both *TP53* and *APC*, microsatellite stable (MSS) status, distally located CRC tumors, and those classified as consensus molecular subtype 2 (CMS2), an additional CRC molecular classification system [229,232,241]. Of the six wild-type EGFR-high tumors, only T21 matches these additional genomic criteria. In contrast, T18 and T16 possess all of the described biomarkers,

but also have lower levels of EGFR phosphorylation, indicating an alternative therapy has the potential to be more efficacious. These results suggest that pTyr analysis can provide critical information regarding target activation. When combined with genomic characterization, this information provides the potential to improve patient stratification for targeted therapeutics.

2-2-6 T cell phosphorylation suggests tumor immune cell activation & infiltration status

Following the demonstrated success of ICB in other solid tumors, immunotherapy has emerged as another therapeutic avenue in CRC with several ICB therapies approved for clinical use [24,25,242]. However, efficacy of ICB in CRC has been limited to mismatch-repair deficiency and microsatellite instability classified tumors (dMMR-MSI), which typically have higher immune cell infiltration and mutational burden than MMR proficient, microsatellite stable (pMMR-MSS) tumors, increasing their susceptibility to ICB therapy [243,244]. Nevertheless, dMMR-MSI tumors represent a minority (~15%) of CRCs [245] and overall response rates in recent clinical trials ranged from 30-55%, emphasizing the need for additional biomarkers of ICB efficacy [24,25,242]. Unlike other cancers, PD-L1 expression is not predictive of ICB response in CRC [25]. Still, better response rates have been observed in tumors with higher levels of CD8+ tumor-infiltrating lymphocytes, regardless of microsatellite status [246]. With this in mind, we investigated whether we could identify patients with high CD8+ T cell infiltration using the pTyr levels of immune cell-specific peptides to estimate ICB responsiveness.

The SureQuant pTyr IS panel contained T cell signaling-specific peptides derived from the T cell receptor CD3δ/γ, along with the T cell co-receptor CD3ζ (CD247) and zeta-chain associated protein kinase (ZAP70). These sites and other downstream signaling nodes comprised the T cell signaling pathway gene set used for TPEA; using this gene set we

identified six tumors with significant enrichment: four positive (T8, T19, T23, and T29) and two negative (T30 and T17) (**Figure 2-16**).

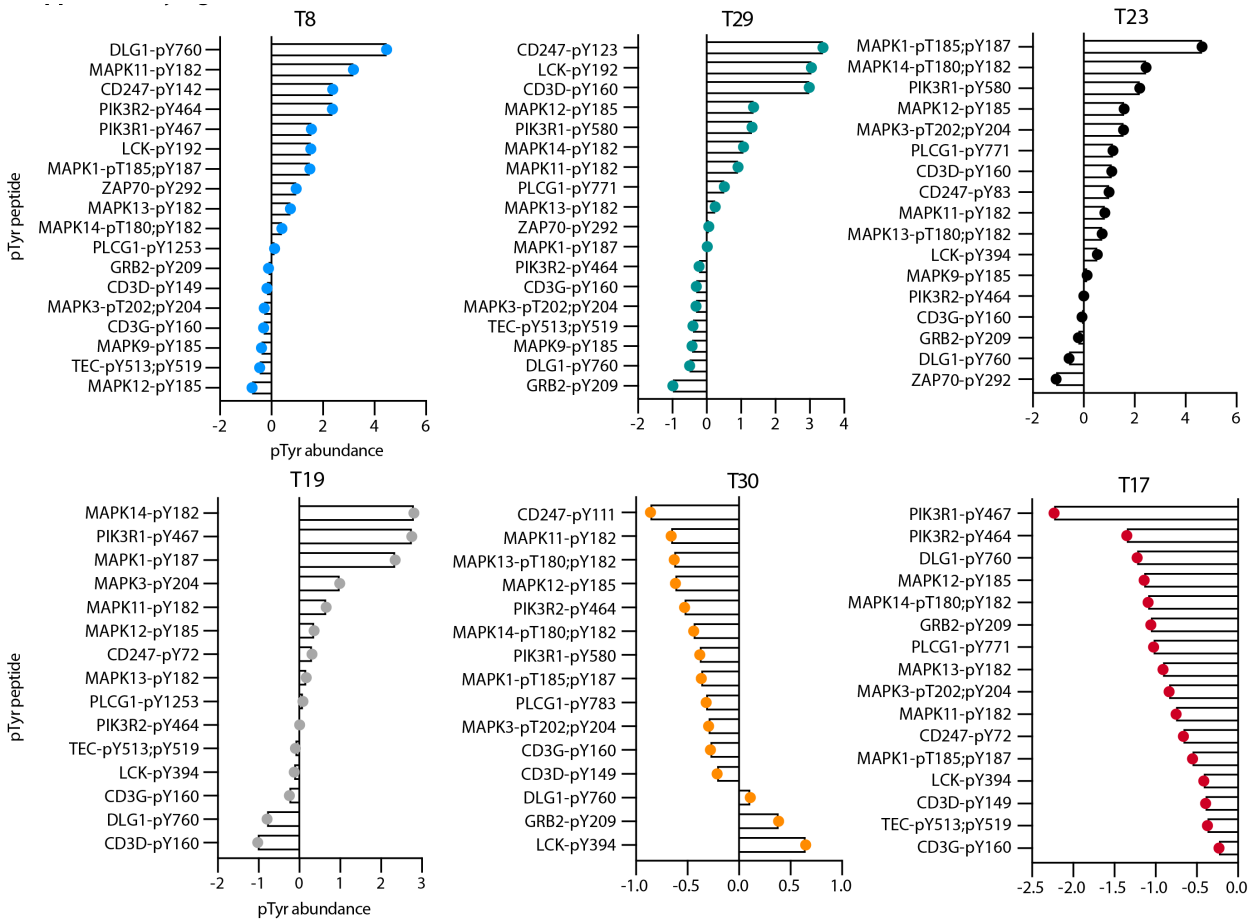

***Figure 2-16**. Tumor-specific pTyr signatures of T cell signaling peptides. pTyr abundance (z-score normalized light to heavy signal ratios) of T cell signaling peptides in tumors with significant pathway enrichment. Peptides are annotated by source protein.*

Examining the phosphosites driving enrichment, we observed high levels of CD3ζ phosphorylation across multiple pTyr sites and increased ZAP70 phosphorylation in T8 and T29, relative to the other tumors (**Figure 2-17**). Both tumors also show elevated LCK phosphorylation, a SRC kinase which phosphorylates immunoreceptor tyrosine-based activation motifs (ITAMS) on TCR/CD3 substrates including CD3ζ and ZAP70. Similarly, KSEA identified

significant positive enrichment of LCK substrate phosphorylation in T8 and T29 (**Figure 2-11-G**). In contrast, T cell signaling enrichment in T19 and T23 was primarily driven by downstream signaling nodes non-specific to T cells (p38 and ERK), which highlights the importance of evaluating pathway enrichment on a site-specific level.

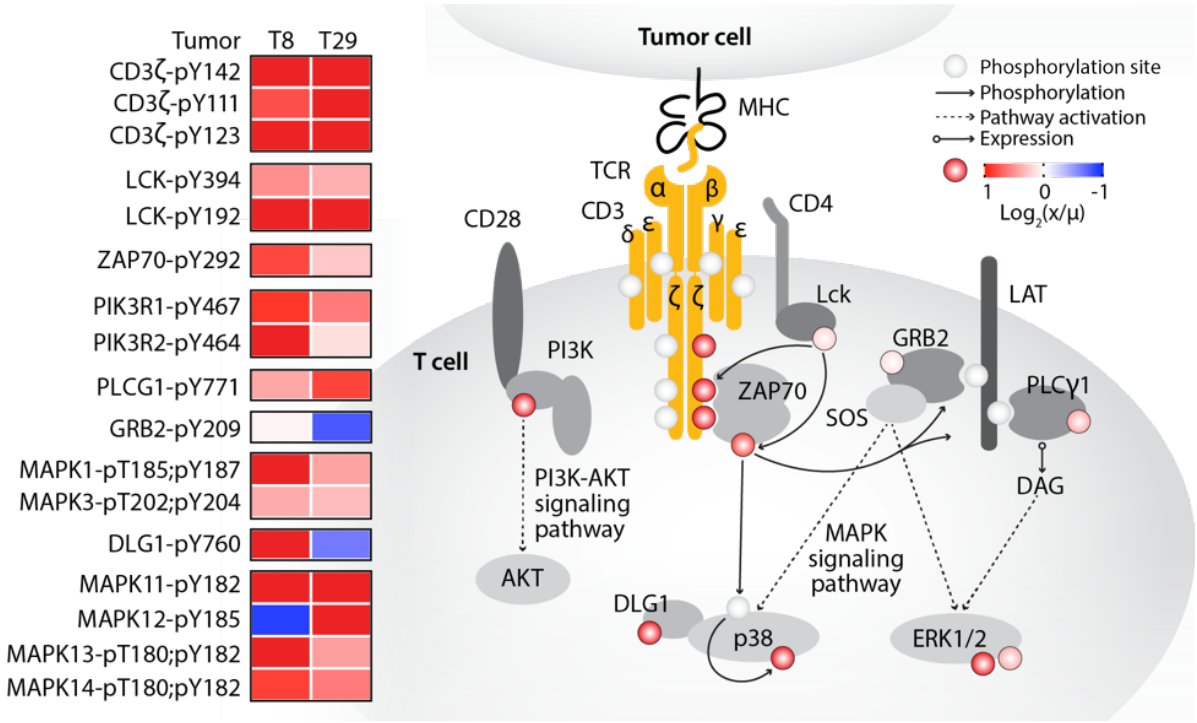

***Figure 2-17**. pTyr signal of T-cell signaling peptides, calculated as the ratio of tumor light to heavy pTyr signal (x) to the mean light to heavy signal (μ), for T8 and T9. Phosphorylation levels on the signaling diagram (colored circles) correspond to T8, and pY denotes the residue position with pTyr modification.*

Consequently, we applied a parallel, site-specific framework as used in the phospho-EGFR analysis to evaluate three CD3ζ phosphosites as a marker for T cell infiltration. We identified ten tumors with at least a 1.5-fold increase in CD3ζ phosphorylation relative to the mean, similarly termed “CD3ζ-high,” and twelve tumors with at least 1.5-fold lower phosphorylation, “CD3ζ-low” (**Figure 2-18**). Only two CD3ζ-high tumors (T29 and T5) were

classified as dMMR-MSI, while the others were pMMR-MSS. Mutations in DNA polymerase epsilon (POLE) have also been correlated with increase CD8+ T cell infiltration [247], but assessing POLE mutational status only identifies one additional tumor (T20) classified as CD3ζ-high. Other tumors including negatively enriched T cell signaling T17 and CD3ζ-low T4 may have been considered for ICB based on dMMR-MSI status, but low pTyr levels of CD3ζ suggest that they may not be strong candidates for ICB based on lack of activated T cell signaling within the tumor.

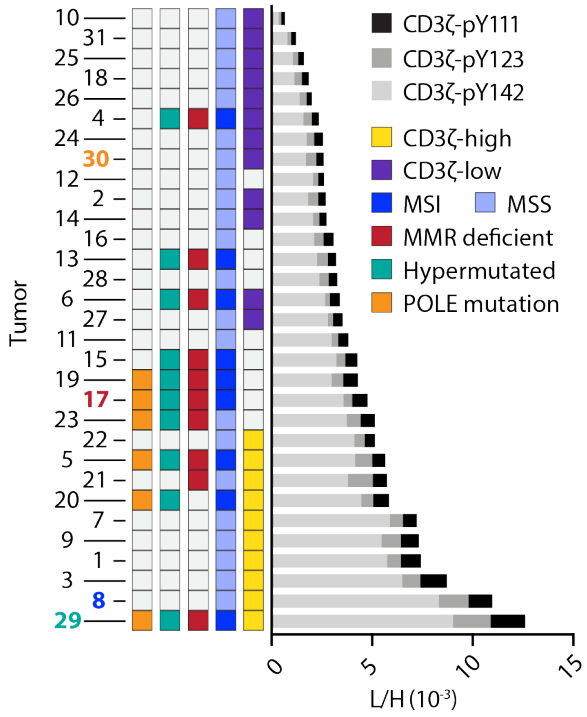

***Figure 2-18**. Cumulative CD3ζ pTyr levels (light to heavy signal) from three CD3ζ pTyr peptides. Tumor-specific biomarker statuses are indicated by color.*

We examined whether transcript expression or protein expression datasets would similarly identify T cell signaling pathway enrichment among positively enriched T8/T29 and negatively enriched T30/T17, but this analysis yielded no significant findings. However, GSEA

against the cancer hallmarks database using RNA-seq data identified interferon-γ (IFN-γ), IFN-α, and immune response pathways as significantly positively enriched in T8 and T29, and significantly negatively enriched in T30 (**Figure 2-19-A, B**). Tumor-infiltrating lymphocytes are the primary source of IFN-γ production in tumors and stimulates IFN response genes and immune activation, in agreement with our T cell signaling TPEA results [248]. We next looked at expression levels of antigen presentation machinery, hypothesizing that expression levels would mirror the directionality of T cell signaling and IFN-γ enrichment. Supporting this notion, we see corresponding increased (T8, T29) or decreased (T30) gene and protein expression levels of class I major histocompatibility complex (MHC-I) genes (HLA-A/B/C, β2M) and both transporters associated with antigen processing (TAP1/2) subunits (**Figure 2-19-C, D**).

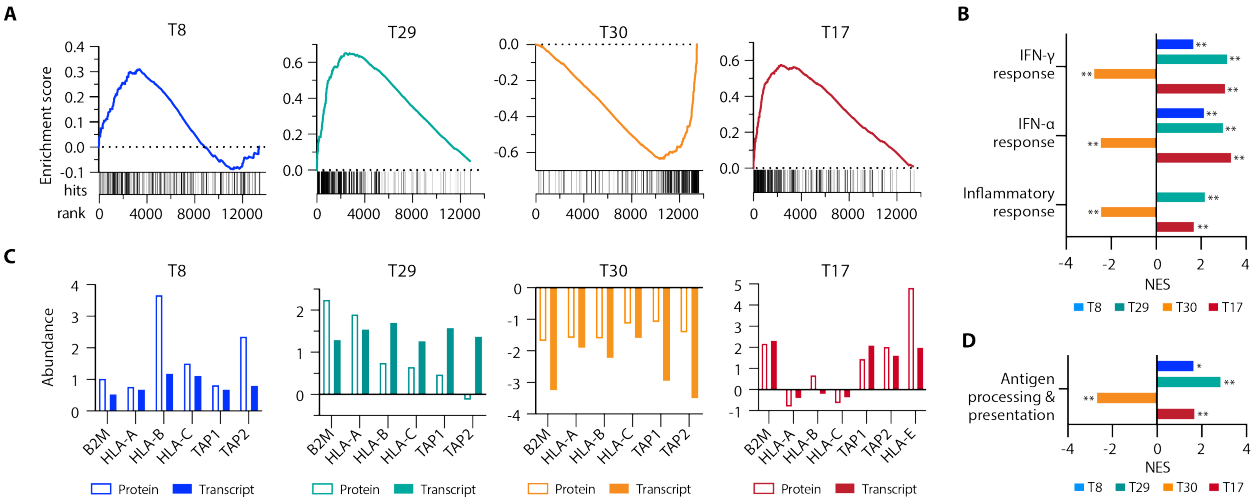

Figure 2-19*. Antigen presentation enrichment.* ***A*** *Gene set enrichment analysis (GSEA) plots for IFN-γ response, with gene rank (x-axis) versus running enrichment score (y-axis). Each hit signifies a gene present in the gene set.* ***B*** *Normalized enrichment scores (NES) from GSEA for selected significantly enriched pathways *p<0.05, **p<0.01, q<0.25 for all.* ***C*** *Z-scored normalized protein and transcript expression levels of antigen presentation genes.* ***D*** *GSEA NES for antigen processing and presentation gene ontology gene set (GO:0019882), *p<0.05, **p<0.01, q<0.25 for all.*

Intriguingly, negative T cell signaling enriched T17 has positive enrichment of IFN-γ/α, inflammatory response, and antigen processing and presentation genes, in contrast to the trend observed in the other tumors. Analysis of antigen presentation protein expression levels shows increased β2M and TAP1/2, but lower levels of classical HLA-A/B/C alleles with high expression of the non-classical allele, HLA-E. Similar to classical HLAs, HLA-E can be modulated by IFN-γ [249], but high expression of HLA-E can function as an inhibitory signal towards other immune cell types, attenuating tumor cell susceptibility to T cell mediated killing as a mechanism of immune escape [250,251]. Therefore, despite T17's enrichment for IFN-γ/antigen presentation and biomarker status, a deeper analysis of the genomic and proteomic data aligns with our pTyr-based assessment of T17 being a poor candidate for ICB therapy.

Previous analyses by Vasaikar et al. provided their own estimate of immune infiltration by using a gene expression signature to assign each tumor an "immune score," (**Figure 2-20-A**) representative of the fraction of immune cells within a tumor sample [222,252]. Tumors with the highest immune scores were largely dMMR-MSI and/or hypermutated, including negative T cell signaling enriched T17, while positively enriched T8 had an average score. Still, other tumors were similarly categorized. Both analyses predicted T29 to have the highest level of immune infiltration, whereas T2, T26, and T30 all have low predicted immune infiltration. To determine whether specific pTyr sites in our data were associated with tumor immune score, we assessed the correlation between these data. Although two CD3ζ pTyr sites were significantly correlated with the immune score, the correlations were weak, and other significantly correlated sites were not directly associated with T cell or immune function (**Figure 2-20-B, C)**. Collectively, these data further highlight the additional information provided by directly measuring activation status with SureQuant pTyr and suggest pTyr measurements applied in conjunction with genomic and/or proteomic data may improve identification of potential ICB or other immunotherapy responders, beyond classical MMR/MSI biomarkers.

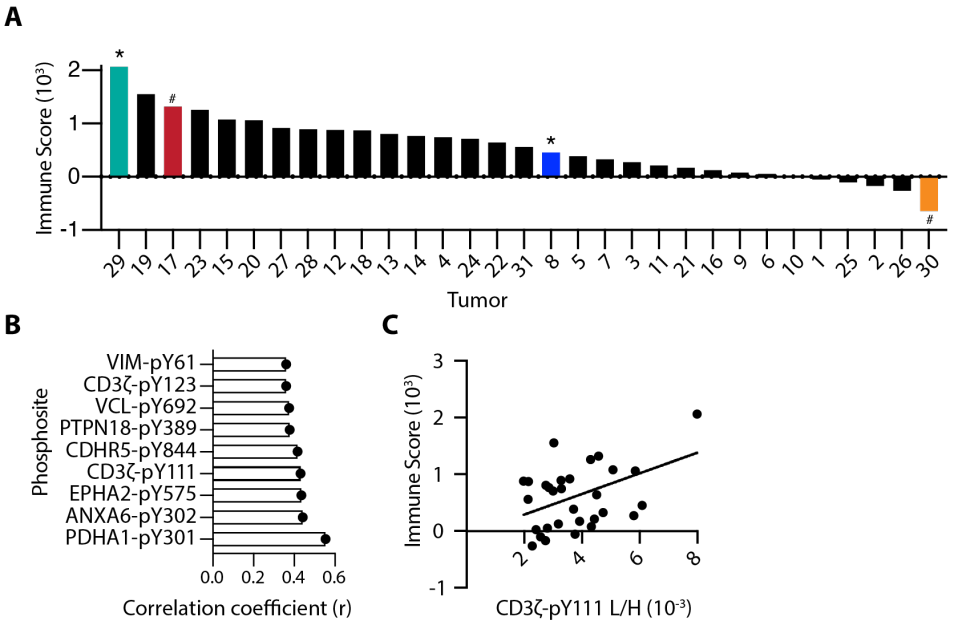

***Figure 2-20**. Immune score of tumors. **A** Immune score of tumors from Vasaikar et al., * = positively enriched # = negatively enriched in pTyr T cell signaling peptides. **B** Unique pTyr peptides with significant positive correlation to immune score ($p < 0.05$). **C** Correlation between immune score and the L/H signal of CD3ζ-pY111, $r^2 = 0.19$.*

2-3 Discussion

pTyr measurements are well suited to directly read out signaling network activation status and have the potential to identify therapeutically targetable protein kinases or signaling pathways in disease. To address the limitations of traditional shotgun and targeted MS-based pTyr approaches which require compromise between reproducibility, broad coverage, and quantitative accuracy, we developed SureQuant pTyr. This approach leverages isotopically labeled IS trigger peptides, similar to previously described methods, but here adapted to guide the acquisition of low abundance pTyr peptides in real-time for enhanced sensitivity and selectivity. In addition, SureQuant pTyr addresses significant analytical challenges compared to other MS-based approaches, as it does not rely on retention time scheduling, thus maximizing the number of targetable peptides and reducing the complexity of assay development. Here, we

utilized a panel of 340 tyrosine phosphorylated IS peptides to obtain highly reproducible, high-density coverage of pTyr signaling pathways implicated in cancer, while achieving accurate quantitation.

We established the quantitative reproducibility of SureQuant pTyr, by performing targeted pTyr profiling on three replicate in vitro samples. While peptide intensity responses varied across analyses and thus may have confounded label-free analysis, L:H ratios were consistent. The high quantitative reproducibility achieved with the SureQuant IS-triggered targeted workflow has many benefits, including the ability to readily analyze signaling network dynamics under various conditions [227], or to compare the signaling state of a patient derived tissue over time as therapeutic resistance or metastases develop [207]. Furthermore, using a set of reference standards for quantitation enables comparisons across research projects and data collection sites, paving the way for large scale, multi-site studies using pTyr levels for disease characterization.

To highlight the potential clinical utility of this platform, we applied SureQuant pTyr to measure pTyr signaling levels in CRC patient tumor tissues. Our analyses identified tumors with elevated ErbB signaling levels, as well as tumors with high levels of innate and adaptive immune cell infiltration. While some of our results reinforced complementary genomics-based classifiers used for treatment selection, in other cases our pTyr signaling data revealed therapeutic opportunities in tumors that would have been missed by traditional biomarkers. These results demonstrate the power of pTyr characterization as a complementary approach for selecting treatment strategies. Furthermore, this platform only requires 800 µg of total protein as sample input material, less than a standard 14G needle biopsy, making it highly amenable to clinical sample profiling [225].

While our initial study utilized just 340 pTyr targets selected with CRC application in mind, the current method framework could be applied to an alternate or expanded panel of

peptides for deeper profiling of the tyrosine phosphoproteome. This may include additional targets for applications in cancer research, such as broader coverage of receptor tyrosine kinases, or could incorporate other targets associated with non-oncological settings where dysregulated kinase signaling also plays a role. Implementing additions to the panel is easily accommodated by performing a new survey run analysis and importing the new acquisition parameters to the existing method structure. Furthermore, the same general framework could be applied to other non-tyrosine phosphosite panels to provide additional information regarding a sample's signaling status. Examples include peptides with pSQ/pTQ motifs for DNA damage response analysis, or other low-abundance PTMs such as lysine acetylation. Future studies may evaluate whether antibody enrichment is required for SureQuant-based analyses of these low abundance targets, or whether IMAC-only (in the case of pTyr) or possibly no enrichment is sufficient given the high specificity triggering of the SureQuant method. Finally, coupling SureQuant acquisition with isobaric labeling would greatly increase assay throughput, allowing for up to 16 samples analyzed simultaneously [253] while further decreasing sample input material required [207].

Though this assay is not approved by the Clinical Laboratory Improvement Amendments (CLIA) for clinical use at this time, implementation of targeted MS in clinical settings is beginning to emerge [254]. Importantly, while many targeted workflows require complex method structures and customized MS platforms, all aspects of pTyr SureQuant were performed with commercially available nano-HPLC columns, enrichment reagents, method templates, and instrumentation, thereby allowing for simplified implementation in other research or clinical settings. Executing this workflow simply requires the IS peptide mixture and a single survey analysis to determine intensity thresholds for IS peptide triggering, offering a turn-key solution for targeted pTyr profiling.

Improvements to assay accuracy, reproducibility, and ease of use may open new doors in the clinical setting to use utilize pTyr signatures in conjunction with existing technologies to obtain novel insights. Overall, we propose the broad application of targeted pTyr profiling with SureQuant pTyr in research and clinical settings, either as a standalone strategy or in combination with proteogenomic data, can aid in improving patient stratification and biomarker characterization, identification of drug targets, and designing personalized therapies in the context of oncology and beyond.

2-4 Materials and Methods

2-4-1 Cell lines

Lung cancer cell line A549 (CCL-185) was purchased from ATCC and routinely tested for mycoplasma contamination (Lonza). Cells were cultured in RPMI-1640 (Gibco) supplemented with 10% FBS (Gibco), 1% penicillin/streptomycin (Gibco) and maintained at 37°C, 5% CO_2. Prior to harvesting (passages 4-6), cells were stimulated with 5 nM EGF (PeproTech), and early time point samples (0, 0.5, and 2 minutes stimulation) were flash frozen in liquid nitrogen, as previously described.[227]

2-4-2 Tumor samples

Tumor samples were collected by several tissue source sites in strict accordance to the CPTAC-2 colon procurement protocol with an informed consent from the patients. The Washington University in St. Louis Institutional Review Board (IRB) reviewed the individual informed consent documents at each tissue source site and determined that the materials sent to the CPTAC biospecimen core resource met the requirements. All other information related to

procurement of these samples is detailed in Vasaikar et al. In this analysis, samples were obtained as tumor curls through the Clinical Proteomic Tumor Analysis Consortium (CPTAC) Biospecimen Core Resource and stored at -80°C prior to analysis.

2-4-3 Sample processing

Cell line samples/ frozen tissues samples were lysed/homogenized in lysis buffer [8 M urea, 1x HALT Protease/Phosphatase Inhibitor Cocktail (Thermo Scientific)]. Lysates were cleared by centrifugation at 5000 g for 5 min at 4°C and protein concentration was measured by bicinchoninic acid assay (BCA) (Pierce). In our hands, protein yield for frozen tumors is ~10% of the tumor wet weight. Proteins were reduced with 10 mM dithiothreitol for 30 min at 56°C, alkylated with 55 mM iodoacetamide for 45 min at room temperature (RT) protected from light, and diluted 4-fold with 100 mM ammonium acetate, pH 8.9. Proteins were digested with sequencing grade modified trypsin (Promega) at an enzyme to substrate ratio of 1:50 overnight at RT. Enzymatic activity was quenched by acidifying with glacial acetic acid to 10% of the final solution volume, and peptides were desalted using C18 solid phase extraction cartridges (Sep-Pak Plus Short, Waters). Peptides were eluted with aqueous 60% acetonitrile in 0.1% acetic acid and dried using vacuum centrifugation.

Protein concentration was again measured by BCA to account for variation in sample processing, and peptides were subsequently lyophilized in 800 µg aliquots for label-free DDA, PRM, & SureQuant analysis and stored at -80°C until analysis. Samples for TMT-labeled analyses were lyophilized in 150 ug aliquots and resuspended in 50 mM hepes (pH 8.5). TMT 10-plex (0,4 mg) (Thermo Scientific) was resuspended in 15uL of anhydrous acetonitrile and subsequently added to each sample, followed by a 1-hour incubation at RT. Reactions were

quenched with 0.3% hydroxylamine, pooled, dried by vacuum centrifugation, and stored at -80°C prior to analysis.

2-4-4 Peptide Synthesis

Peptides were purchased from Thermo Scientific Custom Peptide synthesis service. All synthetic peptides used in this study were produced as a PEPotec Custom Peptide Libraries using FMOC solid-phase technology. The peptides were synthesized with the following specifications: crude purity, synthetic isotope-labeled c-terminal lysine (K) or arginine (R) or proline (P) or alanine (A) or isoleucine (I) or valine (V). The crude peptides after synthesis were dissolved in 0.1% TFA in 50% (v/v) acetonitrile/water and stored at –20 °C. A pool of first heavy peptide mixture was prepared by mixing an equimolar amount of each peptide with the final concentration at 1pmol /μl in 0.1% TFA and 3% (v/v) acetonitrile and subjected to nanoLC-MS/MS analysis to determine the intensity response of 340 peptides. A final heavy peptide mixture was prepared by increasing the concentration of the 58 “low-intensity” heavy peptides with low intensity response values. The final concentration of 58 heavy peptides ranged from 1.8 to 5.5 pmol /μl. Exact concentrations are specified in **Table 2-1**. To avoid batch effects or repeated freeze/thaw cycles, upon receival the final heavy peptide mixture was divided into individual analyses aliquots and stored at -80 °C prior to use.

2-4-5 Tyrosine phosphorylated peptide enrichment

Lyophilized tryptic peptide aliquots were resuspended in 400 µL of immunoprecipitation (IP) buffer [100 mM Tris-HCl, 0.3% NP-40, pH 7.4] and supplemented with a mixture of ~1 pmol of each IS peptide standard. The light/heavy peptide mixture was incubated with 60 µL protein G agarose bead slurry (Calbiochem) conjugated to an antibody cocktail containing 12 µg 4G10

(Millipore), 12 µg PT66 (Sigma) and 6 µg of pY100 (Cell Signaling Technologies), rotating overnight at 4°C. Of note, samples 1 and 2 of the A549 enrichment analysis were only incubated for 6h at 4°C, whereas sample 3 followed the described protocol with overnight incubation. Beads were washed 1x with IP buffer, 3x with 100 mM Tri-HCl, pH 7.4, and eluted in 2 rounds of 25 µL 0.2% TFA. Phosphopeptides were further enriched using High-Select Fe-NTA Phosphopeptide Enrichment Kit (Thermo Scientific) following manufacturer's instructions with minor adjustments. Modifications include reducing the peptide volume initially added to the Fe-NTA column (50 µL) and reducing the elution volume to 2 rounds of 20 µL elutions. Peptide elutions were dried down using vacuum centrifugation to <2 µL total volume and resuspended in 5% acetonitrile in 0.1% formic acid for a total volume of 10 µL.

2-4-6 LC-MS/MS Analysis

Samples for SureQuant analyses were analyzed using an Orbitrap Exploris 480 mass spectrometer (Thermo Scientific) coupled with an Easy-nLC 1200 (Thermo Scientific) or UltiMate 3000 RSLC Nano LC system (Dionex), Nanospray Flex ion source (Thermo Scientific), and column oven heater (Sonation). A 10 µL injection volume of sample was directly loaded onto a 25 cm Aurora Series emitter column (IonOpticks) with a column oven temperature of 40°C. Peptides were eluted at a flow rate of 400 nL/min across a linear gradient consisting of 0.1% formic acid (buffer A) and 80% acetonitrile in 0.1% formic acid (buffer B). The gradient is as follows: 3-19% B from 1-37 mins, 19-29% B from 37-51 mins, 29-41% B from 51-60 mins, 41-95% B from 60-63 mins, and 95-3% B from 70-70:05 mins.

2-4-7 Survey MS analyses

A flowchart describing the pTyr SureQuant method build and analysis workflow can be found in **Supplementary Figure 2-6**. Prior to SureQuant acquisition, the IS peptides were first characterized by data dependent acquisition (DDA) with an inclusion list of the precursor ions under +2, +3, and +4 charge states for each IS trigger peptide to select optimal charge states and product ions for subsequent targeted experiments. For this analysis, a mixture containing approximately 700 fmol of each IS peptide was directly injected. Next, a "survey run" was performed, still based on directed DDA but with an inclusion list focused on the optimal charge state for each peptide, to capture the precursor ion intensity responses and derive the intensity thresholds for MS2 scan triggering in subsequent SureQuant analyses. To take sample losses from pTyr enrichment steps into account in determining triggering thresholds, a nominal amount (~1 pmol) of each IS peptide was added to 800 ug of the A549 processed cell line standard, followed by pTyr enrichment as a representative sample. Parameters obtained in these survey analyses were used in all subsequent pTyr SureQuant analyses. MS parameters can be found in the supplementary methods.

2-4-8 Targeted MS analyses for A549 and tumor samples

The SureQuant method combines various scan events and filters, depicted in **Supplementary Figure 2-7-A**. During SureQuant analyses, a high resolution MS1 scan is acquired to monitor the predefined optimal precursor ions of the IS heavy peptides, based on the list of associated m/z values and intensity thresholds. If any targeted m/z from the inclusion list is detected and meets the minimum intensity threshold specified, a short fill time, low resolution MS^2 scan of the IS peptide is performed in the subsequent MS cycle. If the scan contains at least 5 of 6 specified product ions, a high resolution MS^2 scan of the endogenous peptide at the defined mass offset is performed with longer fill times to improve measurement

sensitivity. In the current implementation of SureQuant acquisition on the Exploris 480 MS, all trigger peptides scans are performed first, followed by target peptide scans in any given MS cycle in order to optimize parallelization of trapping and Orbitrap-FT processing in sequential scans (**Supplementary Figure 2-7-B**).

To implement this method, the custom SureQuant acquisition template available in Thermo Orbitrap Exploris Series 1.0 was utilized. The template is structured such that the acquisition parameters for each unique isotopically labeled amino acid and charge state (defining the m/z offset) is contained within a distinct 4-node branch stemming from the full scan node (**Supplementary Figure 2-8**). We utilized the default template, which contains 6 branches for the +2, +3, and +4 charge states of SIL lysine and arginine residues and added four additional branches for the +2 charge states of SIL proline, valine, isoleucine, and alanine for a total of 10 branches. In each branch, the peptide m/z and intensity thresholds are defined in the "Targeted Mass" filter node. Next, parameters for the low resolution, IS peptide MS^2 scan are defined, followed by the "Targeted Mass Trigger" filter node, which defines the 6 product ions used for pseudo-spectral matching. To connect each set of product ions within the targeted mass trigger node to a given precursor mass, we utilize the group ID feature to define the precursor m/z associated with each group of product ions is related to. Finally, along with the scan parameters for the second MS^2 scan of the endogenous peptide, we define the isolation offset (m/z) within each node.

Standard mass spectrometry parameters for SureQuant acquisition are as follows: spray voltage: 1.5kV, no sheath or auxiliary gas flow, heated capillary temperature: 280°C. Full-scan mass spectra were collected with a scan range: 300-1500 m/z, AGC target value: 300% ($3e^6$), maximum IT: 50 ms, resolution: 120,000. Within a 5 second cycle time per MS1 scan, heavy peptides matching the m/z (within 10 ppm) and intensity threshold defined on the inclusion list were isolated [isolation width of 1.0 m/z] and fragmented [nCE: 28%] by HCD with a scan range:

100-1700 m/z, maximum IT: 10 ms, AGC target value: 1000% ($1e^6$), resolution: 7,500. A product ion trigger filter next performs pseudo-spectral matching, only triggering an MS^2 event of the endogenous, target peptide at the defined mass offset if $n \geq 5$ product ions are detected from the defined list. If triggered, the subsequent light peptide MS^2 scan has the same CE, scan range, and AGC target as the heavy trigger peptide, with a higher maximum injection time and resolution (for example, max IT: 180 ms, resolution, 60,000), however these parameters vary slightly across samples in order to optimize acquisition speed and sensitivity. Additional data acquisition parameters for the discovery colorectal tumor samples and DDA/PRM A549 analyses can be found in the Supplementary methods.

2-4-9 SureQuant data analysis

Peak area ratios of endogenous light peptides and corresponding heavy IS peptides for the 6 selected product ions were exported from Skyline, and peptides were filtered according to the following criteria: First, only IS peptides with an integrated peak area > 0 for $n \geq 5$ product ions were considered. Of these remaining targets, only endogenous targets with an integrated peak area > 0 for $n \geq 3$ product ions were considered. For quantification, the peak area values of the 3 highest intensity product ions present for both the light/heavy peptides were summed, and the ratio of light endogenous to heavy IS peptide signal was taken across samples. We selected 3 product ions for quantitation to balance specificity with the ability to retain lowly abundant targets. For tumor sample analysis, L:H ratios of peptides quantifiable in all tumors were included in the full matrix, and peptides quantifiable in ≥ 16/31 tumors were included in the expanded matrix. Both matrixes were z-score normalized for specified analyses. Analyses were performed using Python 3.6.0.

2-4-10 RNA-sequencing

RNA-sequencing data was analyzed by Vasaikar et al., as previous described [222]. RSEM upper-quartile normalized values for the tumor panel used in this study were extracted and z-score normalized for subsequent analyses.

2-4-11 Principal component analysis

PCA was performed in Matlab R2019b using z-score normalized L:H ratios of the 26 tumors with a defined unified molecular subtype. Only peptides identified across all tumors were used (165 unique sites).

2-4-12 Enrichment analysis

For tumor-specific pathway enrichment analyses (TPEA), Source proteins of phosphorylated peptides were rank ordered from highest to lowest z-score. In cases where more than one peptide mapped to the same source protein, the maximum/minimum was selected, depending on the directionality of the enrichment analysis. We utilized gene set enrichment analysis (GSEA) 4.0.3 [255] pre-ranked tool against a custom database of 12 pathways, obtained from gene ontology (GO) biological processes terms, Reactome pathways, and KEGG pathways with 1000 permutations, weighted enrichment statistic (p=1), and a minimum gene size of 12. Results were filtered according to $p < 0.05$, FDR q-value < 0.25.

Similarly, for pTyr-specific kinase-substrate enrichment analysis (KSEA) all peptides were ranked ordered by z-score and pre-ranked GSEA was performed using a custom library of 12 phosphosite specific kinase-substrate sets from the Substrate Kinase Activity Inference

(SKAI) library [233] using parameters listed above and a minimum gene set size of 10. Global phosphorylation/pTyr KSEA analysis used a minimum gene set size of 15, using the full kinase-substrate human library from Strasser et al. Results were filtered according to $p < 0.1$ and datasets with FDR q-value < 0.25.

GSEA using RNA-sequencing and protein-expression profiling data was similarly performed by rank-ordering genes by z-score and analyzed against the Molecular Signatures Database hallmarks gene sets with parameters listed for TPEA and a minimum gene size of 15. Results were filtered according to $p < 0.05$, FDR q-value < 0.25.

2-4-13 Protein-protein interaction network analysis

Significantly enriched pathways and biological processes (FDR q-value < 0.05) were identified within clusters of co-regulated phosphopeptides using STRING v11 and visualized using Cytoscape v3.7 [256,257]. Nodes are annotated by pTyr peptide gene name, and edges represent protein-protein associations experimentally determined.

2-5 Supplementary Information

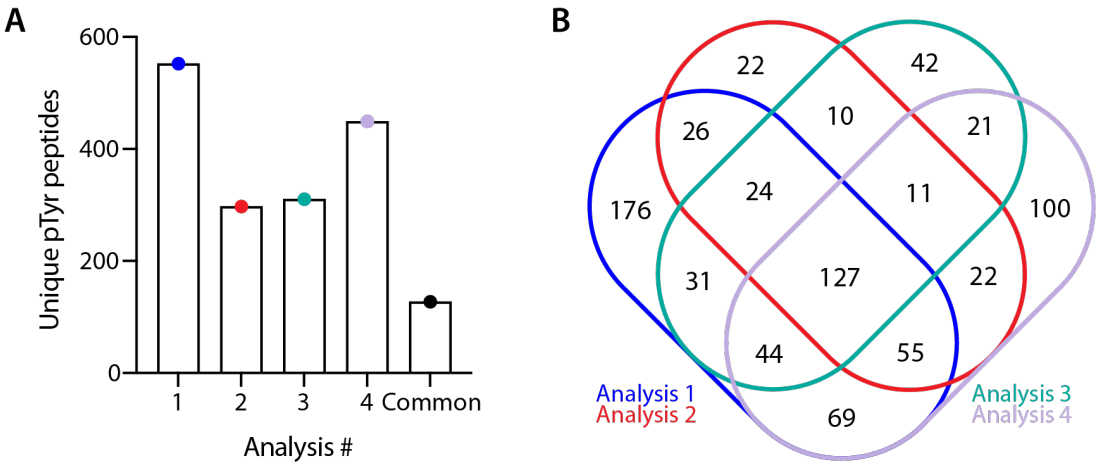

Supplementary Figure 2-1. A *Number of unique pTyr peptides in each discovery analysis.* ***B*** *Overlap in identified peptides between the four analyses.*

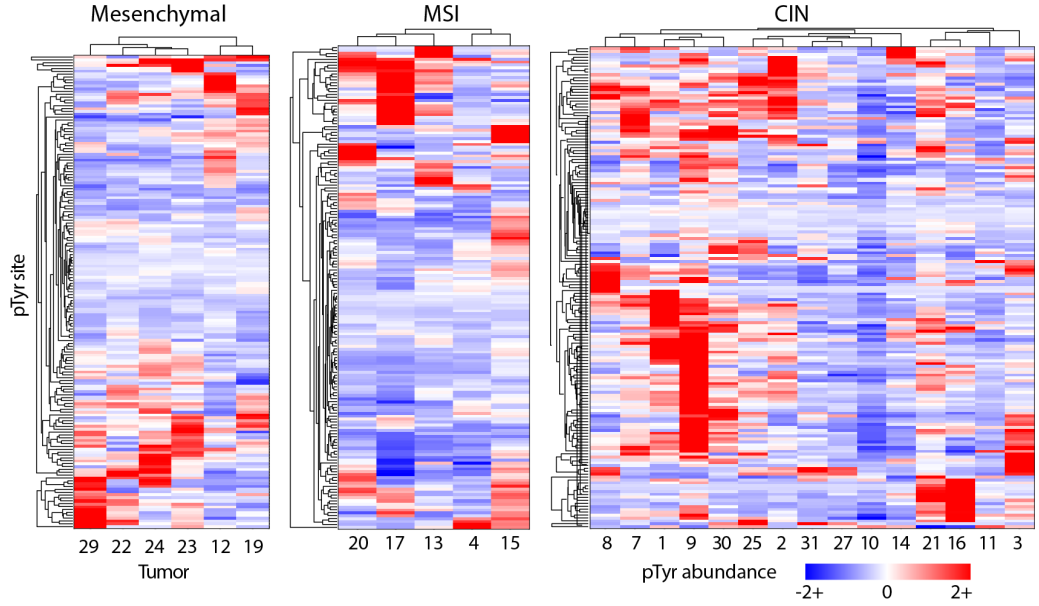

Supplementary Figure 2-2*. Hierarchical clustering of pTyr peptides within each unified multi-omics subtype defined by Vasaikar et al. Distance metrics for clustering of peptides and tumors, respectively, are Euclidean and correlation.*

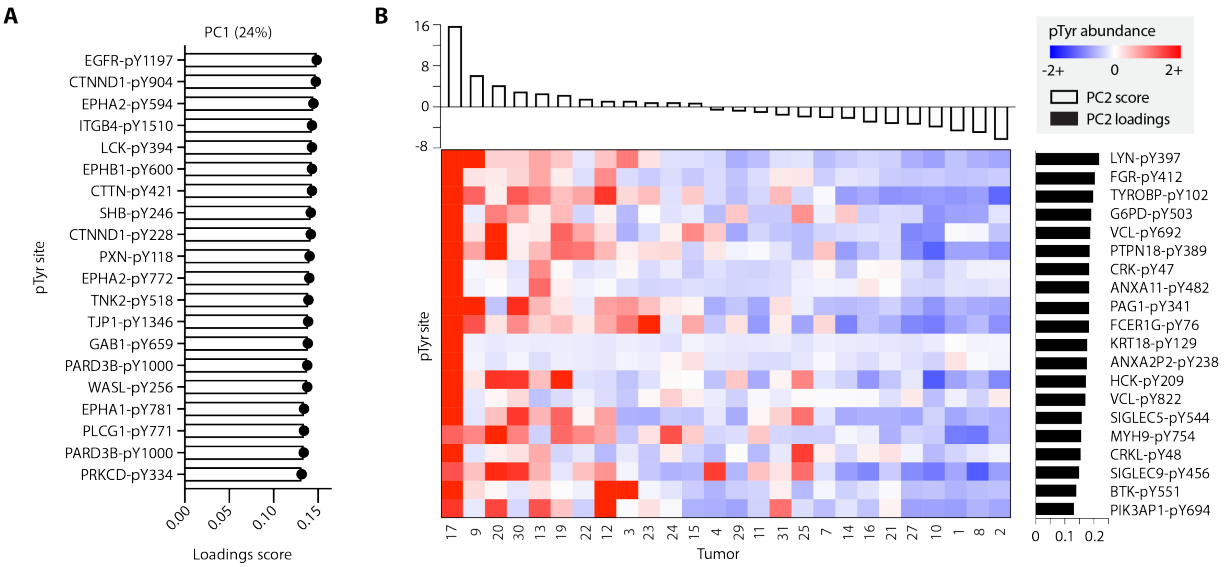

Supplementary Figure 2-3. ***A*** *Peptides with the top 20 loadings scores for PC1, pY denotes the residue position with pTyr modification.* ***B*** *Top 20 loadings scores of the peptides derived from unique proteins for PC2, ranked from highest to lowest PC2 score with corresponding pTyr abundance levels (z- score normalized L/H) across tumors.*

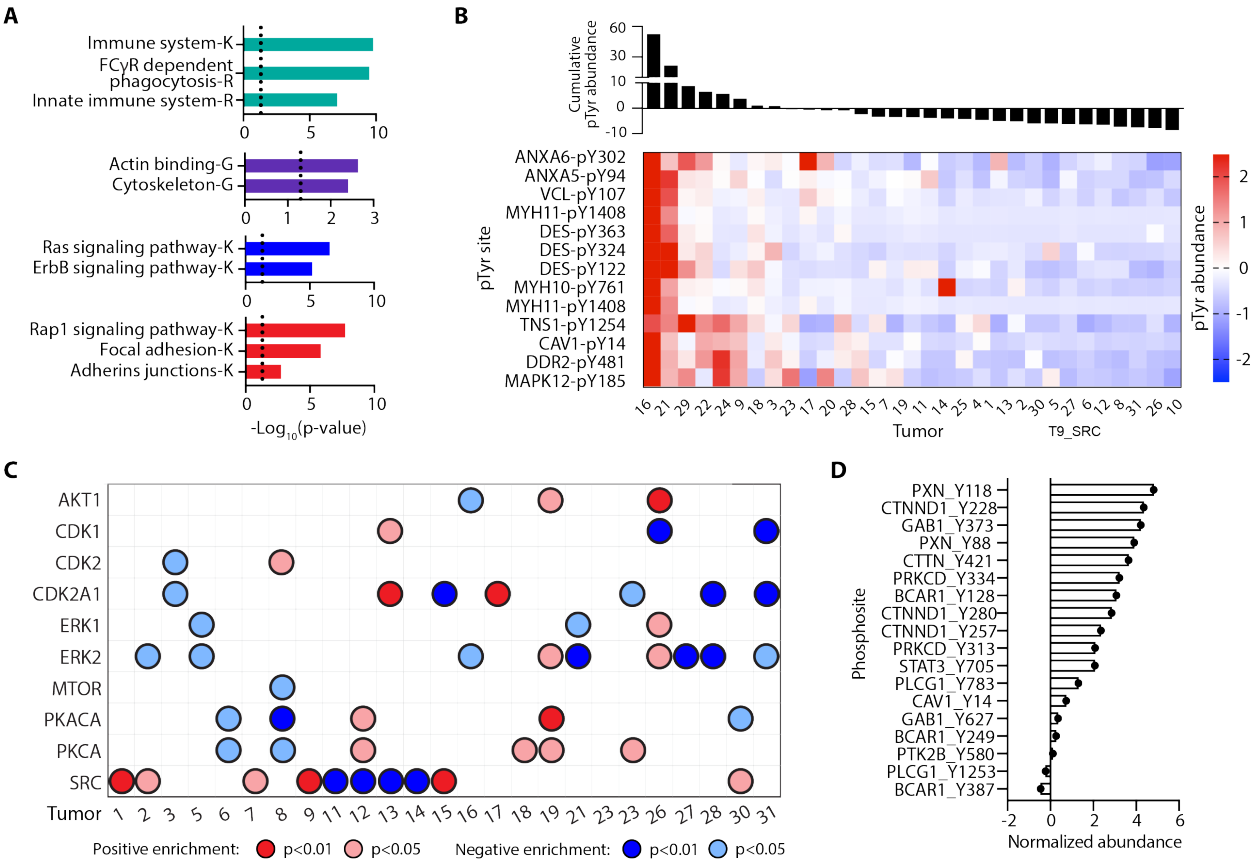

Supplementary Figure 2-4. ***A*** *Selected significantly enriched pathways identified in* ***Figure 2-11****. K=Kegg pathway, G=Gene Ontology term, R=reactome pathway. Significance values are FDR-adjusted, and a cutoff of p < 0.05 was used for filtering.* ***B*** *pTyr peptides from cluster 2, rank ordered from highest to lowest cumulative pTyr abundance, where abundance values are z-score normalized light to heavy signal ratios.* ***C*** *Significantly enriched kinase-substrate interactions within tumors using pTyr and pSer/pThr datasets. Significance (p-value) and directionality indicated by color, FDR q-value < 0.25 for all enrichment analyses. Tumors without any significant enrichment are not shown.* ***D*** *SRC kinase-substrate enrichment signature for T9. Normalized abundance corresponds to z-score normalized light to heavy signal ratios.*

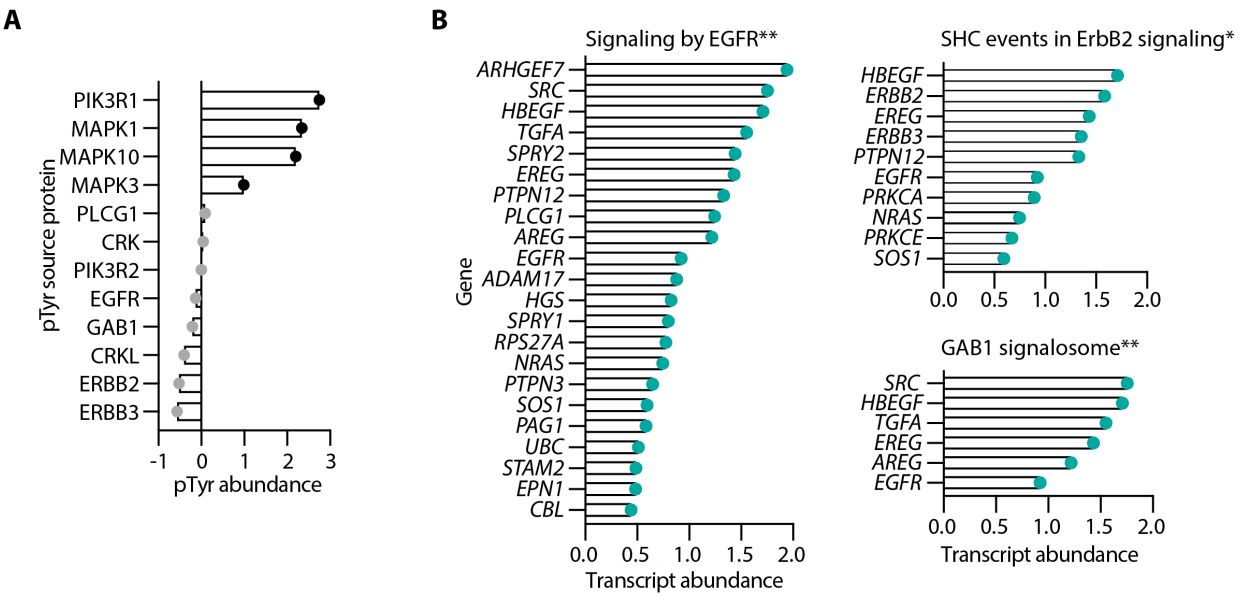

Supplementary Figure 2-5. ***A*** *Tumor 19 pTyr abundance of peptides in the ErbB signaling pathway. All peptides are annotated by source protein, with peptides in the enrichment core colored in black.* ***B*** *Tumor 9 positively enriched reactome pathways with corresponding transcript abundance levels (z-score normalized). *= p<0.05. **=p<0.01 FDR q-value < 0.05 for all.*

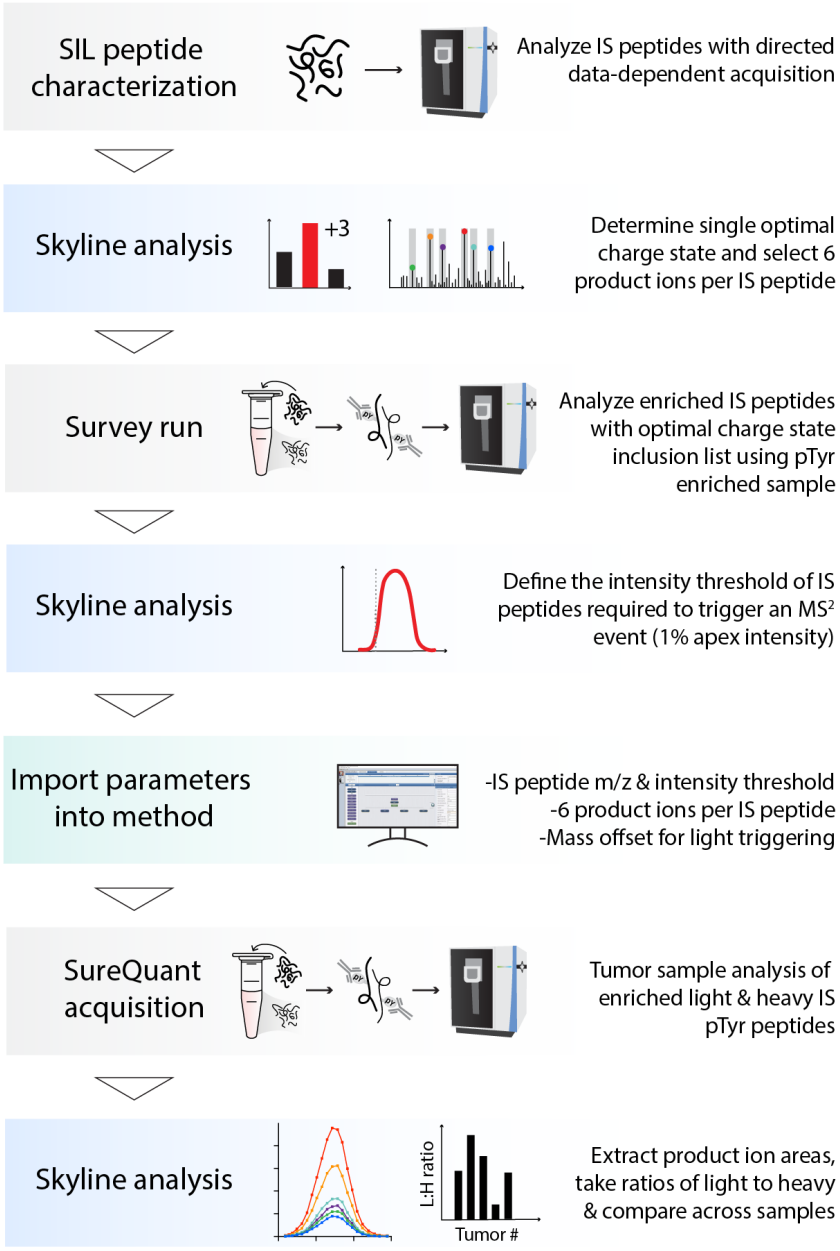

Supplementary Figure 2-6*. Flowchart of SureQuant pTyr workflow. SureQuant pTyr pipeline for method building, data acquisition, and data analysis.*

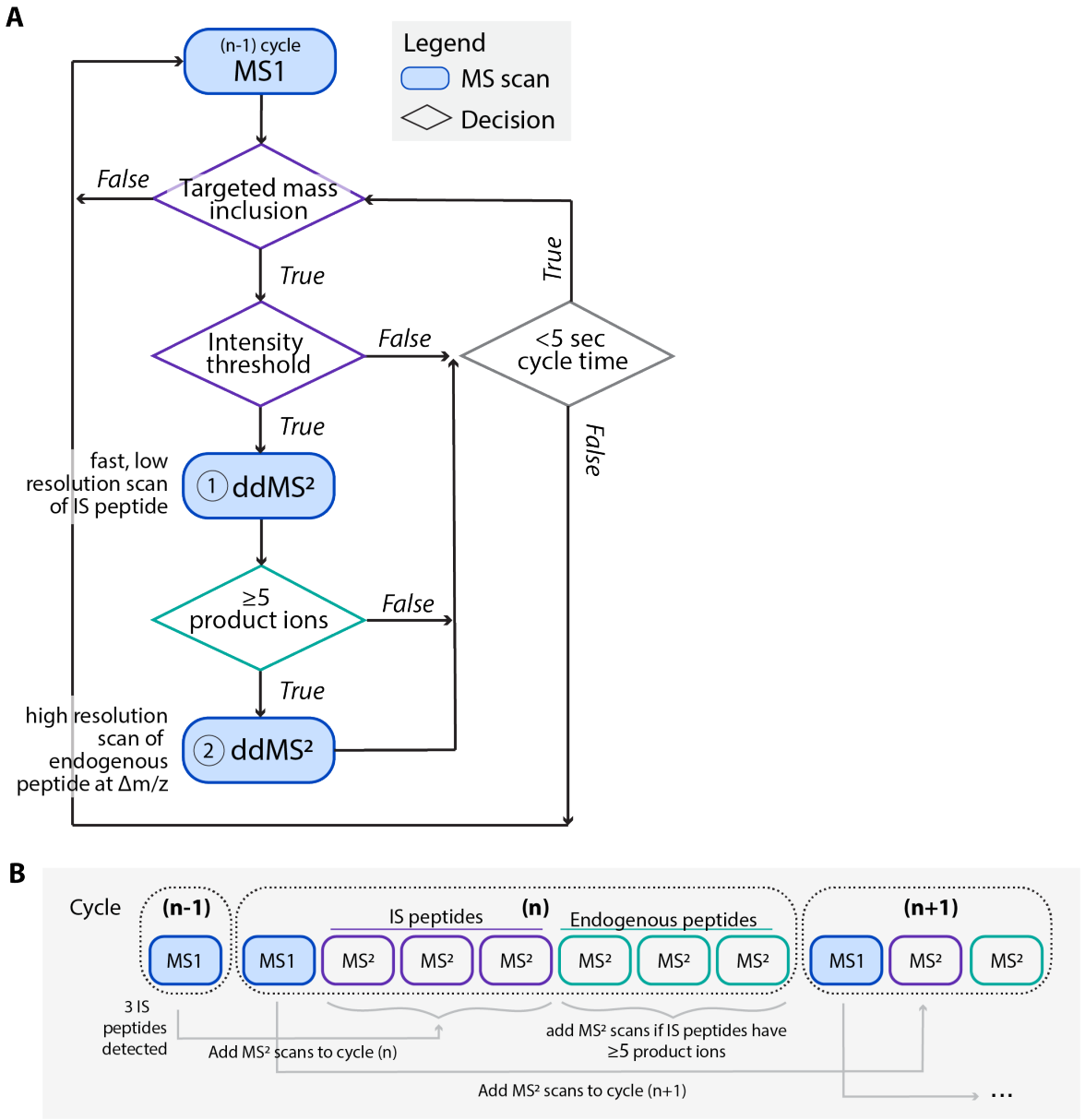

Supplementary Figure 2-7. ***A*** *Decision tree for SureQuant acquisition method framework.* ***B*** *Scan sequence for SureQuant analyses on the Exploris 480 MS. For example, if three internal standard (IS) peptides are detected in the MS1 scan of cycle (n-1), an MS² scan of each IS peptide is added to the scan sequence in cycle (n). If each IS MS2 scan contains ≥5 pre-defined product ions, MS² scans of each endogenous peptide at the defined m/z offset are added to the scan sequence in cycle (n). This scan structure repeats for each cycle.*

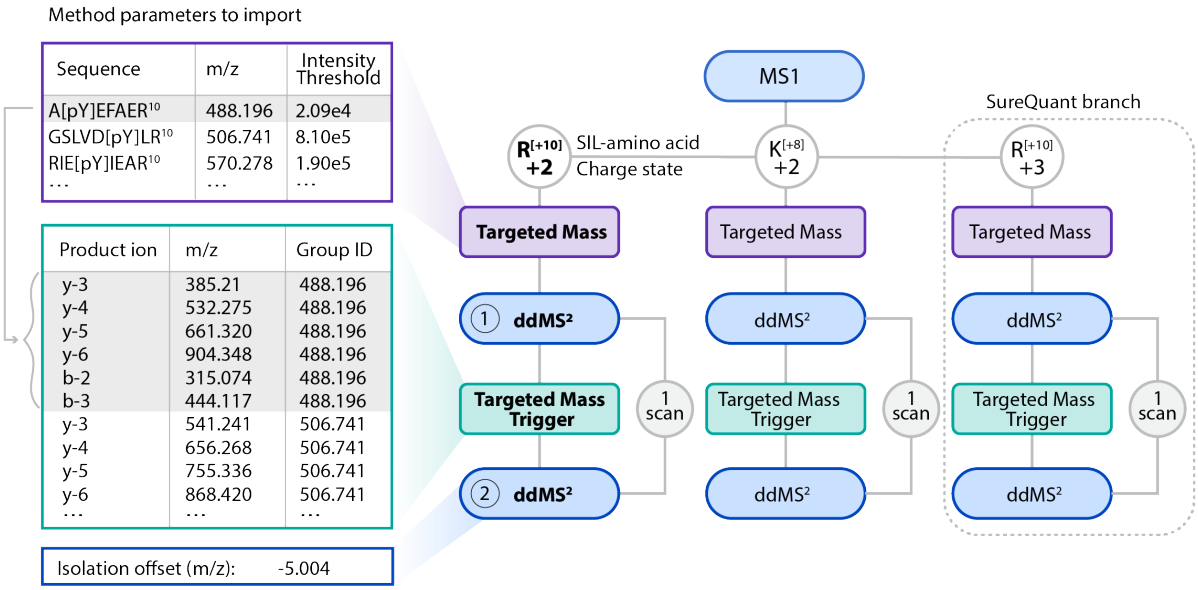

Supplementary Figure 2-8. *Method scan structure and parameters to import for SureQuant acquisition illustrated for three branches, however SureQuant pTyr uses ten branches. [pY] denotes the residue position with pTyr modification, and R^{10} and K^{8} denote stable isotope labeled (SIL) arginine (+10) and lysine (+8), respectively.*

2-6 Supplementary Methods

Internal standard peptide characterization and survey run analysis

All analyses were processed using Skyline software (version 20.1, daily build) [139]. The IS peptides properly detected in initial directed DDA analysis, *i.e.*, those for which at least one precursor ion yielded several MS^2 scans including at least 6 theoretical y- or b-type fragment ions, were retained for SureQuant method development. For peptides detected under multiple charge states, only the precursor ion yielding the highest signal response was retained. For each peptide, 6 associated optimal fragments ions were selected for psudo-spectral matching (typically the most intense ones showing sufficient specificity, *i.e.*, without neutral loss or low m/z value). Individual intensity thresholds for each IS peptide was set to 1% of the precursor MS1 intensity value at the apex of its chromatographic profile in the survey run analysis.

Mass spectrometry data acquisition parameters

Survey analysis

The mass spectrometry parameters used for these preliminary analyses were as follows: spray voltage: 1.9kV, no sheath or auxiliary gas flow, heated capillary temperature: 280°C. DDA analyzes collected full-scan mass spectra with m/z range 300-1200, AGC target value: 1000% (1e7), maximum injection time (IT): 50 ms, resolution: 120,000. For every scan, the top 40 most intense ions on the inclusion list (if above a 1e5 intensity threshold) were isolated [isolation width of 1.0 m/z] and fragmented [normalized collision energy (nCE): 28%] by higher energy collisional dissociation (HCD), scan range: 100-1700 m/z, maximum IT: 10 ms, AGC target value: 1000% (1e6), resolution: 7,500.

Multiplexed discovery analysis of colorectal tumors

Peptides were resuspended in 10 µL 0.1% acetic acid and onto an analytical capillary column with an integrated electrospray tip (~1 µm orifice) prepared in house ((50 µm ID × 12 cm with 5 µm C18 beads (YMC gel, ODS-AQ, 12 nm, S-5 µm, AQ12S05)). Peptides were eluted using a 140 minute gradient with 13-42% buffer B (70% Acetonitrile, 0.2M acetic acid) from 10-105 minutes and 42-60% buffer B from 105-115 minutes, 60-100% B from 115-122 minutes, and 100-0% B from 128-130 minutes at a flow rate of 0.2 mL/min for a flow split of approximately 10,000:1. Peptides were analyzed using a Thermo Fisher Q Exactive Plus Hybrid Quadrupole-Orbitrap mass spectrometer, and data was acquired using Thermo Fisher Scientific Xcalibur version 2.5.0.2042. Standard mass spectrometry parameters were as follows: spray voltage, 2 kV; no sheath or auxiliary gas flow; heated capillary temperature, 250 °C.

The Q Exactive Plus was operated in data-dependent acquisition (DDA) mode with the following scan settings: Full-scan mass spectrometry spectra (mass/charge ratio (m/z), 350 to 2,000; resolution, 70,000) were detected in the Orbitrap analyzer after accumulation of ions at $3e^6$ target value with a maximum injection time (IT) of 50 ms. For every full scan, the top 15 most intense ions were isolated (isolation width of 0.8 m/z) and fragmented (collision energy (nCE): 33%) by higher energy collisional dissociation (HCD) with a maximum IT 350 ms, AGC target $1e^5$, and 35,000 resolution. Unassigned and +1 charge states were excluded, and dynamic exclusion was set to 30 seconds.

Crude peptide analysis was performed on a Q Exactive Plus mass spectrometer to correct for variation in peptide loadings across TMT channels. Approximately 30 ng of the supernatant from pTyr IP was loaded onto an in-house packed precolumn (100 um ID x 10 cm) packed with 10 µm C18 beads (YMC gel, ODS-A, AA12S11) connected in series to an analytical column (as previously described) and analyzed with a 75 min LC gradient [0-30% B

from 0-40 minutes, 30-60% B from 40-50 minutes, 60-100% B from 50-55 minutes, and 100-0% B from 60-65 minutes]. MS1 scans were performed with m/z range: 350-2000; resolution: 70,000; AGC target: $3x10^6$; maximum IT: 50 ms. The top 10 abundant ions were isolated (isolation width 0.8 m/z) and fragmented (nCE = 33%) with 35,000 resolution, maximum IT 350 ms, AGC target $1e^5$. Unassigned and +1 charge states were excluded, and dynamic exclusion was set to 30 seconds.

Label-free DDA analysis of A549 cells

Three label-free replicate samples of A549 cells stimulated with 5 nM EGF were analyzed using an Orbitrap Exploris 480 mass spectrometer (Thermo Scientific) coupled with an UltiMate 3000 RSLC Nano LC system (Dionex), Nanospray Flex ion source (Thermo Scientific), and column oven heater (Sonation). A 10 µL injection volume of sample was directly loaded onto a 25 cm Aurora Series emitter column (IonOpticks) with a column oven temperature of 40°C. Peptides were eluted at a flow rate of 400 nL/min across a linear gradient consisting of 0.1% formic acid (buffer A) and 80% acetonitrile in 0.1% formic acid (buffer B). The gradient is as follows: 2-8% B from 2-15 mins, 8-35% B from 15-95 mins, 35-60% B from 95-105 mins, 60-100% B from 105-110 mins, and 100-2% B from 112-114 mins. Standard MS parameters were as follows: 1.5 kV; no sheath or auxiliary gas flow; heated capillary temperature, 275 °C.

The Exploris 480 was operated in DDA mode with the following scan settings: full-scan mass spectra were collected with m/z range 300-1600, AGC target value: 300% ($3e^6$), maximum IT: auto. For every MS1 scan, peptides were isolated during a 3 s cycle time [isolation width 0.4 m/z] and fragmented [nCE 30%] by HCD with 60,000 resolution, 150 ms maximum IT, AGC target 100% ($1e^5$). Charge states < 2 and > 6 were excluded., and peptides were excluded from MS^2 analysis for 30 s duration after fragmentation n=2 times within 20 s duration.

TMT-labeled DDA analysis of A549 cells stimulated with EGF

Multiplexed, A549 cells stimulated with 5 nM EGF for 0, 0.5, or 2 mins were analyzed using the Exploris 480 and UltiMate 3000 RSLC Nano LC system as previously described, using the SureQuant gradient.

Standard MS parameters were as follows: 2.5 kV; no sheath or auxiliary gas flow; heated capillary temperature, 275 °C.

The Exploris 480 was operated in DDA mode with the following scan settings: full-scan mass spectra were collected with m/z range 350-1600, AGC target value: 300% ($3e^6$), maximum IT: auto. For every MS1 scan, peptides were isolated during a 3 s cycle time [isolation width 0.4 m/z] and fragmented [nCE 33%] by HCD with 60,000 resolution, 150 ms maximum IT, AGC target 100% ($1e^5$). Exclusion parameters are as described with label-free DDA analysis of A549 cells.

Crude peptide analysis of the immunoprecipitation supernatant was performed on a Q Exactive Plus mass spectrometer to correct for variation in peptide loadings across TMT channels. Approximately 30 ng of the supernatant from pTyr IP was loaded onto an in-house packed precolumn (100 um ID x 10 cm) packed with 10 µm C18 beads (YMC gel, ODS-A, AA12S11) connected in series to an analytical column(as previously described) and analyzed with a 70 min LC gradient, as previously described. MS1 scans were performed with m/z range: 350-2000; resolution: 70,000; AGC target: $3x10^6$; maximum IT: 50 ms. The top 10 abundant ions were isolated (isolation width 0.4 m/z) and fragmented (nCE = 33%) with 70,000 resolution, maximum IT 150 ms, AGC target $1e^5$. Unassigned, >8, and +1 charge states were excluded, and dynamic exclusion was set to 30 seconds.

Label-free PRM analysis of A549 cells stimulated with EGF

A549 cells stimulated with 5 nM EGF for 0, 0.5, or 2 mins with analyzed by PRM using the Exploris 480 MS and UltiMate 3000 RSLC Nano LC system as previously described, using the SureQuant gradient. Standard MS parameters were as follows: 1.5 kV; no sheath or auxiliary gas flow; heated capillary temperature, 275 °C.

The Exploris 480 was operated using a targeted inclusion mass list, with an MS1 resolution of 60,000, scan range 3350-1600, AGC target value: 300% ($3e^6$). During a 3 s cycle time, targeted peptides were isolated [isolation width 0.4 m/z] and fragmented [nCE 30%] by HCD with 60,000 resolution, 150 ms maximum IT, AGC target 100% ($1e^5$).

Additional search space, filtering, and analysis details for MS analyses.

Multiplexed discovery analysis of colorectal tumors

Mass spectra were processed with Proteome Discoverer version 2.2 (PD 2.2) (Thermo Fisher) and searched against the human SwissProt database (2018_4) using Mascot version 2.4 (Matrix Science). Spectra were searched using the following parameters: enzyme: trypsin, maximum missed cleavages: 2, precursor mass tolerance: 10 ppm, fragment mass tolerance: 20 mmu. Static modifications included TMT-10-labeled lysine and N-terminal residues, as well as cysteine carbamidomethylation. Dynamic modifications included methionine oxidation, and tyrosine, serine, and threonine phosphorylation.

Peptide spectrum matches (PSMs) with phosphorylated tyrosine residues and no reporter ion missing values were filtered according to search engine rank = 1, ion score ≥ 20. Reporter ion intensities were summed across matching PSMs. Phosphotyrosine peptide reporter ion areas were corrected for variations in sample loading within each analysis using the median of peptide ratios in the crude peptide analysis for each channel relative to channel. Quantitation is represented as the fold change between the tumor and normal phosphorylation levels.

TMT-labeled DDA analysis of A549 cells stimulated with EGF

Mass spectra were processed with PD 2.5 and searched against the human SwissProt database (2020_4) using Mascot version 2.4. Spectra were searched and analyzed using the same parameters described in the multiplexed discovery analysis of colorectal tumors.
To evaluate the quantitative reproducibility of the SureQuant method, the three 2-minute EGF stimulated samples were used.

Label-free DDA analysis of A549 cells

Mass spectra were processed with PD 2.5 and searched against the human SwissProt database (2020_4) using Mascot version 2.4. Spectra were searched using the following parameters: enzyme: trypsin, maximum missed cleavages: 2, precursor mass tolerance: 10 ppm, fragment mass tolerance: 20 mmu. Cysteine carbamidomethylation was set as a static modification, and dynamic modifications included methionine oxidation, and tyrosine, serine, and threonine phosphorylation. MS1 integrated peak area quantitation was performed using the minora feature detector in PD 2.5 with match between runs enabled and filtered for ion score ≥ 20, search engine rank = 1. Only peptides containing phosphorylated tyrosine residue(s) were included in subsequently analyses.

Label-free PRM analysis of A549 cells stimulated with EGF

Mass spectra were processed with Proteome Discoverer version 2.5 (Thermo Fisher) and searched against a custom library containing the SureQuant pTyr panel, with precursor mass tolerance: 10, fragment mass tolerance: 20 mmu, along with the modifications as described in the label-free DDA analysis of A549 cells. MS1 integrated peak area quantitation was similarly performed using the minora feature detector. Spectra for targeted peptides were

verified by looking for the presence of the 6 preselection product ions using in the SureQuant pTyr analyses using Skyline software.

Protein expression profiling

LC-MS/MS raw files from the TMT-labeled global proteome analysis performed by Vasaikar et al. (15) were re-processed using Proteome Discoverer (version 2.2). All mass spectra were searched using Mascot (version 2.4) against the human SwissProt database (version 2019_6) with a tryptic enzymatic digestion, allowing for 2 missed cleavages, +/- 10 ppm parent ion tolerance. Static modifications of Cys carbamidomethylation and TMT on N-terminus and Lys residues were included, along with variable Met oxidation. Peptide spectrum matches (PSMs) were filtered according to the following criteria: Search engine rank = 1, isolation interference ≤ 30, ion score ≥ 20, peptide length ≥ 6. Relative protein abundance was calculated as the ratio of tumor abundance to reference channel abundance (TMT-131) using the summed TMT reporter ion intensities from all peptides uniquely mapped to a gene. Relative abundances were next divided by the median relative abundance ratio from each TMT channel to correct for sample loading variation within each analysis. Adjusted relative abundances for proteins quantified across all 31 tumors were z-score normalized for subsequent analyses.

SureQuant pTyr peptide panel selection

Discovery analysis data of colon cancer tumor samples and adjacent normal tissue identified nearly 800 unique pTyr peptides. This data was prioritized for panel selection by considering the following criteria: peptides identified across multiple analyses, sites with differential phosphorylation levels between tumor and non-tumor tissue, and sites known to be implicated in oncogenic signaling. Positional isomers were avoided, and sequences with a single pTyr phosphorylation event were prioritized over those with pTyr and a pSer/pThr

modification in most cases (MAPK3/1 peptides being a notable exception. We did not employ a set of strict criteria for panel selection, rather we considered the features described above and then manually curated the final list based on experience generating and analyzing tyrosine phosphorylation data. Additional peptides were then added to this list using EGFR and T cell signaling data previously generated by mass spectrometry in our group. For example, we did not identify ZAP70 in our discovery analyses, but we know from the literature ZAP70 is critical for T-cell signaling. Therefore, we selected a tyrosine phosphorylated tryptic sequence previously identified by mass spectrometry to add to our panel.

2-7 Acknowledgements

I would first like to thank Cameron Flower for agreeing to collaborate on this project with me, especially when it seemed initially like a far-fetched idea. Cam put in countless hours at the instrument, spearheaded the Skyline data wrangling, and was always willing to dive deep into the methods, the biology, the spectra, and more. A special thanks also goes out to the team at Thermo Scientific, Aaron Gajadhar, Bhavin Patel, and Sebastien Gallien, who were enthusiastic collaborators that opened my eyes to a whole new type of mass spectrometry and a method I was later able to leverage (again with their help) in my immunopeptidomics work. Your creativity, dedication, and positive attitudes made me so excited to be a proteomicist. I would also like to thank Andreas Huhmer at Thermo Scientific for funding the synthesis of the stable isotope labeled peptide standards, and for providing project guidance and manuscript feedback; The NCI Clinical Proteomic Tumor Analysis Consortium (CPTAC) for providing tumor samples and for data analysis guidance with RNA-sequencing and proteomics data (Bing Zang); Brian Joughin for data analysis recommendations; Jacqueline Gerritsen for assistance with EGFR peptide selection. Data used in this publication were generated by the Clinical Proteomic Tumor Analysis Consortium (NCI/NIH).

2-8 Tables

***Table 2-1**. Tyrosine phosphorylated peptides in SureQuant pTyr panel*

Peptide #	Heavy Peptide Sequence	pmol added	Gene	Rresidue number
Peptide1	ADY[+80]DTLSLR[+10]	1.00	PKP3	pY176
Peptide2	AEDGSVIDY[+80]ELIDQDAR[+10]	1.00	ANXA2	pY188
Peptide3	AEFAEY[+80]ASVDR[+10]	1.00	PAG1	pY227
Peptide4	AEGSDVANAVLDGADC[+57]IMLSGETAKGDY[+80]PLEAVR[+10]	1.00	PKM	pY370
Peptide5	AESGPDLRY[+80]EVTSGGGGTSR[+10]	1.00	DSP	pY28
Peptide6	AGSLPNY[+80]ATINGK[+8]	1.00	TNS1	pY1404
Peptide7	AHY[+80]THSDYQYSQR[+10]	1.00	PKP2	pY161
Peptide8	ALDY[+80]YMLR[+10]	1.00	TLN1	pY70
Peptide9	ALELDPNLY[+80]R[+10]	1.00	MYH10	pY761
Peptide10	ALELDSNLY[+80]R[+10]	1.00	MYH9	pY754
Peptide11	ALMDEEDMDDVVDADEY[+80]LIPQQGFFSSPSTSR[+10]	1.00	EGFR	pY1016
Peptide12	ALPQNDDHY[+80]VMQEHR[+10]	1.00	TNK2	pY284
Peptide13	ANDTQEFNLSAY[+80]FER[+10]	3.47	DUSP3	pY101
Peptide14	APTNEFY[+80](A)	1.00	SDC4	pY197
Peptide15	APYTC[+57]GGDSDQY[+80]VLMSSPVGR[+10]	1.00	IRS2	pY823
Peptide16	AQQGLY[+80]QVPGPSPQFQSPPAK[+8]	1.00	BCAR1	pY128
Peptide17	AQY[+80]EDIANR[+10]	1.00	KRT75	pY327
Peptide18	ARPSEY[+80]DLLWVPGR[+10]	1.00	PARD3B	pY1056
Peptide19	AY[+80]EFAER[+10]	1.00	CLTC	pY1096
Peptide20	AY[+80]TNFDAER[+10]	1.00	ANXA2P2	pY30
Peptide21	AY[+80]TNFDAERDALNIETAIK[+8]	1.00	ANXA2P2	pY30
Peptide22	DASSQDC[+57]Y[+80]DIPR[+10]	1.00	GAB1	pY406
Peptide23	DDAQY[+80]SHLGGNW(A)	1.00	CD3D	pY160
Peptide24	DDGMEEVVGHTQGPLDGSLY[+80]AK[+8]	1.00	TNS1	pY366
Peptide25	DGHPLSPERDHLEGLY[+80]AK[+8]	1.00	PARD3B	pY1000
Peptide26	DGNGY[+80]ISAAELR[+10]	1.00	CALM1	pY100
Peptide27	DGSSQQLQGY[+80]IPSNYVAEDR[+10]	1.00	FRK	pY99
Peptide28	DHLEGLY[+80]AK[+8]	1.00	PARD3B	pY1000
Peptide29	DIEQVPQQPTY[+80]VQALFDFDPQEDGELGFR[+10]	1.00	GRB2	pY160
Peptide30	DLEQPTY[+80]RYESSSYTDQFSR[+10]	1.00	TJP1	pY1059
Peptide31	DLEY[+80]LDLK[+8]	1.00	PLEKHA7	pY665
Peptide32	DNEVDGQDY[+80]HFVVSR[+10]	1.00	DLG3	pY673
Peptide33	DPHYQDPHSTAVGNPEY[+80]LNTVQPTC[+57]VNSTFDSPAHWAQK[+8]	1.00	EGFR	pY1138

Peptide34	DQEAPSTTEY[+80]SEIK[+8]	1.00	SIGLEC5	pY544
Peptide35	DQY[+80]LMWLTQK[+8]	1.00	PIK3R1	pY580
Peptide36	DSQMQNPY[+80]SR[+10]	1.00	MUC13	pY501
Peptide37	DSSTC[+57]PGDY[+80]VLSVSENSR[+10]	1.00	CRKL	pY48
Peptide38	DSSTSPGDY[+80]VLSVSENSR[+10]	1.00	CRK	pY47
Peptide39	DSTY[+80]DLPR[+10]	1.00	GAB2	pY266
Peptide40	DTY[+80]DALHMQALPPR[+10]	1.00	CD247	pY153
Peptide41	DVTIGGSAPIY[+80]VK[+8]	2.60	PARD3	pY489
Peptide42	DWSHY[+80]FK[+8]	2.91	KRT18	pY129
Peptide43	DY[+80]HFVTSR[+10]	1.00	DLG1	pY760
Peptide44	DY[+80]LIDGSR[+10]	3.46	VCL	pY107
Peptide45	DY[+80]SNFDQEFLNEK[+8]	1.00	PRKCD	pY630
Peptide46	DY[+80]STLTSVSSHDSR[+10]	1.00	ITGB4	pY1510
Peptide47	DYEVDGRDY[+80]HFVTSR[+10]	1.00	DLG1	pY760
Peptide48	DYSHY[+80]YTTIQDLR[+10]	1.00	KRT19	pY130
Peptide49	EAAY[+80]HPEVAPDVR[+10]	1.00	TLN1	pY2224
Peptide50	EATQPEPIY[+80]AESTK[+8]	2.25	PRAG1	pY413
Peptide51	EC[+57]DY[+80]SIDGINR[+10]	1.00	TLN2	pY1665
Peptide52	EDDQY[+80]SHLQGNQLR[+10]	1.00	CD3G	pY171
Peptide53	EEPEALY[+80]AAVNK[+8]	1.00	ITSN2	pY968
Peptide54	EEPIY[+80]IITEYMAK[+8]	1.00	LYN	pY316
Peptide55	EEY[+80]DVLDK[+8]	1.00	CD247	pY83
Peptide56	EGSDSY[+80]AITFR[+10]	1.00	PLCG2	pY680
Peptide57	EIDVSY[+80]VK[+8]	1.00	EPHB4	pY614
Peptide58	EIENLTQQY[+80]EEK[+8]	1.00	MYH11	pY1408
Peptide59	EILDEAY[+80]VMASVDNPHVC[+57]R[+10]	1.00	EGFR	pY764
Peptide60	EKPAQDPLY[+80]DVPNASGGQAGGPQRPGR[+10]	1.00	RIN1	pY36
Peptide61	ELGEY[+80]GFHEYTEVK[+8]	1.00	ALDH1A1	pY481
Peptide62	ELPPDQAEY[+80]C[+57]IAR[+10]	1.00	ACTN1	pY859
Peptide63	ELY[+80]GEVIR[+10]	1.00	INPP5D	pY221
Peptide64	ENDY[+80]ESISDLQQGR[+10]	1.00	PAG1	pY417
Peptide65	EQY[+80]DVPQEWR[+10]	1.00	MUC12	pY5413
Peptide66	ERDY[+80]AEIQDFHR[+10]	1.00	PARD3	pY1080
Peptide67	ERPPPVPNPDY[+80]EPIR[+10]	1.00	CD3E	pY188
Peptide68	ESMC[+57]STPAFPVSPETPY[+80]VK[+8]	2.89	TNS3	pY855
Peptide69	EVPIY[+80]ANR[+10]	2.82	ADAM9	pY769
Peptide70	EYDQLY[+80]EEYTR[+10]	1.00	PIK3R2	pY464
Peptide71	EYDRLY[+80]EEYTR[+10]	1.00	PIK3R1	pY467
Peptide72	FANY[+80]IDK[+8]	1.00	VIM	pY117

Peptide73	FANY[+80]IEK[+8]	2.61	DES	pY122
Peptide74	FASEASGY[+80]QDNIAR[+10]	1.00	DES	pY363
Peptide75	FASQQGMTAY[+80]GTR[+10]	2.56	CNN1	pY182
Peptide76	FAVPTY[+80]AAK[+8]	2.62	ADAM9	pY778
Peptide77	FEEPAPLSY[+80]DSRPR[+10]	1.00	TJP1	pY1140
Peptide78	FELSC[+57]Y[+80]SLAPQIK[+8]	1.00	ASS1	pY133
Peptide79	FHPEPY[+80]GLEDDQR[+10]	1.83	CTNND1	pY280
Peptide80	FIHQQPQSSSPVY[+80]GSSAK[+8]	2.08	PXN	pY88
Peptide81	FLEDDPSDPTY[+80]TSSLGGK[+8]	2.08	EPHB3	pY792
Peptide82	FQKEIENLTQQY[+80]EEK[+8]	1.00	MYH11	pY1408
Peptide83	GAY[+80]SLSIR[+10]	1.00	YES1	pY194
Peptide84	GDKQVEY[+80]LDLDLDSGK[+8]	1.00	GAB1	pY627
Peptide85	GDY[+80]PLEAVR[+10]	3.91	PKM	pY370
Peptide86	GEGLY[+80]ADPYGLLHEGR[+10]	2.74	SRCIN1	pY396
Peptide87	GEPNVSY[+80]IC[+57]SR[+10]	1.00	GSK3A	pY279
Peptide88	GGGPYDAPGGDDSY[+80](I)	1.00	CDHR5	pY844
Peptide89	GHDGLY[+80]QGLSTATK[+8]	1.00	CD247	pY142
Peptide90	GHEY[+80]TNIK[+8]	1.00	PTPN11	pY546
Peptide91	GIVVY[+80]TGDR[+10]	1.00	ATP1A1	pY260
Peptide92	GKVSYQDY[+80]EIEISDASEVEK[+8]	1.00	MX1	pY129
Peptide93	GLC[+57]TSPAEHQYFMT[+80]EY[+80]VATR[+10]	1.00	MAPK7	pT219; pY221
Peptide94	GLC[+57]TSPAEHQYFMTEY[+80]VATR[+10]	1.00	MAPK7	pY221
Peptide95	GLIDRDLY[+80]R[+10]	1.00	DSP	pY2159
Peptide96	GMSVY[+80]GLGR[+10]	1.00	CNN3	pY261
Peptide97	GMTVY[+80]GLPR[+10]	1.00	CNN1	pY261
Peptide98	GNFNY[+80]VEFTR[+10]	1.00	MYL9	pY156
Peptide99	GNPPHSAPC[+57]VPNGSALLLSNPAY[+80]R[+10]	1.00	DDR1	pY513
Peptide100	GPAVGIY[+80]NDNINTEMPR[+10]	1.00	CDCP1	pY707
Peptide101	GPAY[+80]GLSAEVK[+8]	1.00	CNN1	pY12
Peptide102	GQEATDTEY[+80]SEIK[+8]	1.00	SIGLEC9	pY456
Peptide103	GQESEY[+80]GNITYPPAMK[+8]	1.00	PTPN6	pY536
Peptide104	GQY[+80]HTLQAGFSSR[+10]	1.00	PKP3	pY84
Peptide105	GSHQIS[+80]LDNPDY[+80]QQDFFPK[+8]	1.00	EGFR	pY1172
Peptide106	GSLVDY[+80]LR[+10]	1.00	CSK	pY277
Peptide107	GSTAENAEY[+80]LR[+10]	1.00	EGFR	pY1197
Peptide108	GTGY[+80]IKTELISVSEVHPSR[+10]	1.00	STAT1	pY701
Peptide109	GTPTAENPEY[+80]LGLDVP(V)	1.00	ERBB2	pY1248
Peptide110	GVITDQNSDGY[+80]C[+57]QTGTMSR[+10]	1.00	DSP	pY56
Peptide111	GY[+80]AYVEFENPDEAEK[+8]	2.05	RNPS1	pY205

Peptide112	GY[+80]FFLDER[+10]	1.00	PDLIM4	pY293
Peptide113	GY[+80]VPATIK[+8]	4.83	STAT6	pY641
Peptide114	HADAEMT[+80]GY[+80]VVTR[+10]	1.00	MAPK13	pT180; pY182
Peptide115	HADAEMTGY[+80]VVTR[+10]	1.00	MAPK13	pY182
Peptide116	HAQDY[+80]VLTYNYEGR[+10]	1.00	DSC2	pY853
Peptide117	HELQANC[+57]Y[+80]EEVKDR[+10]	1.00	CFL1	pY140
Peptide118	HFDTY[+80]HR[+10]	1.00	PKP2	pY217
Peptide119	HLLAPGPQDIY[+80]DVPPVR[+10]	1.00	BCAR1	pY249
Peptide120	HPAGVY[+80]QVSGLHNK[+8]	1.00	TNS1	pY1254
Peptide121	HPDIY[+80]AVPIK[+8]	1.00	TJP2	pY1118
Peptide122	HTDDEMT[+80]GY[+80]VATR[+10]	1.00	MAPK14	pT180; pY182
Peptide123	HTDDEMTGY[+80]VATR[+10]	1.00	MAPK14	pY182
Peptide124	HYEDGYPGGSDNY[+80]GSLSR[+10]	1.00	CTNND1	pY228
Peptide125	IADPEHDHTGFLT[+80]EY[+80]VATR[+10]	1.00	MAPK3	pT202; pY204
Peptide126	IADPEHDHTGFLTEY[+80]VATR[+10]	1.00	MAPK3	pY204
Peptide127	IAIY[+80]ELLFK[+8]	1.00	RPS10	pY12
Peptide128	IDTLNSDGY[+80]TPEPAR[+10]	1.00	ZAP70	pY292
Peptide129	IEGVY[+80]AR[+10]	1.00	RPL35A	pY34
Peptide130	IEGY[+80]PDPEVVWFKDDQSIR[+10]	1.00	MYLK	pY1835
Peptide131	IFPLRPDY[+80]QEPSR[+10]	1.00	DDR2	pY481
Peptide132	IGEGT[+80]Y[+80]GVVYK[+8]	1.00	CDK2	pT14; pY15
Peptide133	IGEGTY[+80]GVVYK[+8]	1.00	CDK2	pY15
Peptide134	IGTAEPDY[+80]GALYEGR[+10]	1.00	PLCG1	pY771
Peptide135	IIQLLDDY[+80]PK[+8]	1.00	RPLP0	pY24
Peptide136	INLPIQTY[+80]SALNFR[+10]	1.00	DES	pY423
Peptide137	IQNTGDY[+80]YDLYGGEK[+8]	1.00	PTPN11	pY62
Peptide138	IY[+80]DEILQSK[+8]	1.00	CD84	pY296
Peptide139	IY[+80]EPLDVK[+8]	1.00	PLA2G4A	pY535
Peptide140	IY[+80]IDPFTYEDPNEAVR[+10]	1.00	EPHB1	pY594
Peptide141	IYIDPFTY[+80]EDPNEAVR[+10]	1.00	EPHB1	pY600
Peptide142	IYNGDY[+80]YR[+10]	1.00	AXL	pY702
Peptide143	IYQY[+80]IQSR[+10]	1.00	DYRK1B	pY273
Peptide144	KNPQEGLY[+80]NELQK[+8]	1.00	CD247	pY111
Peptide145	KPTY[+80]DPVSEDQDPLSSDFKR[+10]	1.00	TNK2	pY518
Peptide146	LC[+57]DFGSASHVADNDITPY[+80]LVSR[+10]	3.60	PRPF4B	pY849
Peptide147	LDNGGY[+80]YITTR[+10]	1.00	YES1	pY222
Peptide148	LEDYFETDSSY[+80]SDANNFIR[+10]	1.00	FRK	pY497
Peptide149	LEPQIASASEY[+80]AHR[+10]	1.00	PLIN3	pY95

Peptide150	LGEGTY[+80]ATVYK[+8]	2.06	CDK17	pY203
Peptide151	LGLDY[+80]EER[+10]	1.00	PHB2	pY128
Peptide152	LHEY[+80]NTQFQEK[+8]	1.00	PIK3R1	pY452
Peptide153	LIEDNEY[+80]TAR[+10]	1.00	LCK	pY394
Peptide154	LIKDDEY[+80]NPC[+57]QGSK[+8]	1.00	FGR	pY412
Peptide155	LIY[+80]LVPEK[+8]	2.62	ITSN2	pY553
Peptide156	LLDDFDGTY[+80]ETQGGK[+8]	3.05	EPHA1	pY781
Peptide157	LPQDDDRPADEY[+80]DQPWEWNR[+10]	1.00	SHB	pY336
Peptide158	LPSSPVY[+80]EDAASFK[+8]	1.00	CTTN	pY421
Peptide159	LQQY[+80]IAPGMK[+8]	3.32	EPHB3	pY600
Peptide160	LSLEGDHSTPPSAY[+80]GSVK[+8]	1.00	ANXA2P2	pY24
Peptide161	LVNEAPVYSVY[+80]SK[+8]	3.37	STAM2	pY374
Peptide162	LVQAAQMLQSDPYSVPARDY[+80]LIDGSR[+10]	2.60	VCL	pY107
Peptide163	LY[+80]AVVTR[+10]	1.00	LYN	pY306
Peptide164	LY[+80]DFVK[+8]	1.00	INPP5D	pY865
Peptide165	LY[+80]EEYTR[+10]	1.00	PIK3R1	pY467
Peptide166	LYDAY[+80]ELK[+8]	1.00	ANXA5	pY94
Peptide167	LYEEY[+80]TR[+10]	1.00	PIK3R1	pY470
Peptide168	LYGDADY[+80]LEER[+10]	2.48	CTPS1	pY473
Peptide169	LYPELSQY[+80]MGLSLNEEEIR[+10]	1.00	SDCBP	pY56
Peptide170	LYSNAY[+80]LNDLAGC[+57]IK[+8]	2.91	ALDH1A1	pY119
Peptide171	MAEAY[+80]SEIGMK[+8]	1.00	CD247	pY123
Peptide172	MDKNASTFEDVTQVSSAY[+80]QK[+8]	1.00	CTTN	pY334
Peptide173	MDY[+80]VEINIDHK[+8]	1.00	HDLBP	pY437
Peptide174	MHLPSPTDSNFY[+80]R[+10]	3.90	EGFR	pY998
Peptide175	NASTFEDVTQVSSAY[+80]QK[+8]	1.00	CTTN	pY334
Peptide176	NDQVY[+80]QPLR[+10]	1.00	CD3D	pY149
Peptide177	NHQLY[+80]C[+57]NDC[+57]YLR[+10]	1.00	LMO7	pY1667
Peptide178	NKDQGTYEDY[+80]VEGLR[+10]	1.00	MYL6	pY89
Peptide179	NLDNGGFY[+80]ISPR[+10]	1.00	LCK	pY192
Peptide180	NLIAFSEDGSDPY[+80]VR[+10]	1.00	ESYT2	pY824
Peptide181	NLIY[+80]DNADNK[+8]	1.00	PKP3	pY390
Peptide182	NPGFY[+80]VEANPMPTFK[+8]	1.00	PLCG1	pY783
Peptide183	NPGNQAAY[+80]EHFETMK[+8]	1.00	VCL	pY692
Peptide184	NPQEGLY[+80]NELQK[+8]	1.00	CD247	pY111
Peptide185	NQALNTDNY[+80]GHDLASVQALQR[+10]	1.00	SPTAN1	pY1261
Peptide186	NQETY[+80]ETLKHEK[+8]PPQ	3.28	FCER1G	pY76
Peptide187	NQGAHDPDY[+80]ENITLAFK[+8]	2.37	MCEMP1	pY38
Peptide188	NY[+80]VTPVNR[+10]	3.11	GRB2	pY209

Peptide189	NYQSSSPLPTVGSSYSSPDY[+80]SLQHFSSSPESQAR[+10]	1.00	TNS1	pY1149
Peptide190	QADEEMTGY[+80]VATR[+10]	1.00	MAPK11	pY182
Peptide191	QADSEMTGY[+80]VVTR[+10]	1.00	MAPK12	pY185
Peptide192	QAWFIENEEQEY[+80]VQTVK[+8]	5.49	ANXA1	pY21
Peptide193	QDVY[+80]GPQPQVR[+10]	1.00	CTNND1	pY257
Peptide194	QEEAEY[+80]VR[+10]	1.00	CRK	pY136
Peptide195	QEMMEY[+80]R[+10]	1.00	DES	pY324
Peptide196	QESTVSFNPY[+80]EPELAPWAADKGPQR[+10]	1.00	SYK	pY323
Peptide197	QISEGVEY[+80]IHK[+8]	1.00	MYLK	pY1575
Peptide198	QLHEY[+80]ETELEDER[+10]	1.00	MYH11	pY1601
Peptide199	QLLY[+80]SENK[+8]	1.00	FRK	pY132
Peptide200	QLVRGEPNVSY[+80]IC[+57]SR[+10]	1.00	GSK3A	pY279
Peptide201	QNLLSQSHAY[+80]QQFLR[+10]	1.00	SPTBN1	pY1171
Peptide202	QSPEDVY[+80]FSK[+8]	1.00	EPHA2	pY575
Peptide203	QTLLPNDQLY[+80]QPLK[+8]	3.35	CD3G	pY160
Peptide204	QVEELY[+80]HSLLELGEK[+8]	1.00	SPTAN1	pY1073
Peptide205	QVEY[+80]LDLDLDSGK[+8]	1.00	GAB1	pY627
Peptide206	QVY[+80]DAHTK[+8]	1.00	CAV1	pY42
Peptide207	QYFEQY[+80]SR[+10]	2.05	TJP1	pY1195
Peptide208	REEPEALY[+80]AAVNK[+8]	1.00	ITSN2	pY968
Peptide209	RGVITDQNSDGY[+80]C[+57]QTGTMSR[+10]	1.00	DSP	pY56
Peptide210	RIEY[+80]IEAR[+10]	1.00	BRK1	pY63
Peptide211	RPAGSVQNPVY[+80]HNQPLNPAPSR[+10]	1.00	EGFR	pY1110
Peptide212	RPGPGTLY[+80]DVPR[+10]	3.96	BCAR1	pY387
Peptide213	RSDSASSEPVGIY[+80]QGFEK[+8]	1.00	PRKCD	pY313
Peptide214	SADAPAYQQGQNQLY[+80]NELNLGR[+10]	1.00	CD247	pY72
Peptide215	SAEEAPLY[+80]SK[+8]	1.00	PTPN18	pY389
Peptide216	SAIY[+80]QLEEEYENLLK[+8]	1.00	DSP	pY249
Peptide217	SDSASSEPVGIY[+80]QGFEK[+8]	1.00	PRKCD	pY313
Peptide218	SDVY[+80]SDLNTQRPYYK[+8]	1.00	TYROBP	pY102
Peptide219	SEDIY[+80]ADPAAYVMR[+10]	1.00	PLEKHA6	pY492
Peptide220	SEQENPLFPIY[+80]ENVNPEYHR[+10]	1.00	PTPRB	pY1981
Peptide221	SFLDSGY[+80]R[+10]	1.00	VCL	pY822
Peptide222	SGDLPY[+80]DGR[+10]	1.00	LSR	pY586
Peptide223	SGQSLTVPESTY[+80]TSIQGDPQR[+10]	1.00	PAG1	pY341
Peptide224	SGY[+80]IPSGHSLGTPEPAPR[+10]	1.00	TNS1	pY766
Peptide225	SLDNGGYY[+80]ISPR[+10]	1.00	LYN	pY194
Peptide226	SLDNNY[+80]STPNER[+10]	2.83	CTNND1	pY904
Peptide227	SLEATDSAFDNPDY[+80]WHSR[+10]	3.16	ERBB3	pY1328

Peptide228	SLY[+80]HDISGDTSGDYR[+10]	1.00	ANXA11	pY482
Peptide229	SLY[+80]SMIK[+8]	3.02	ANXA6	pY302
Peptide230	SLYASSPGGVY[+80]ATR[+10]	1.00	VIM	pY61
Peptide231	SLYYY[+80]IQQDTKGDYQK[+8]	1.00	ANXA2P2	pY318
Peptide232	SNHY[+80]DPEEDEEYYR[+10]	1.00	TJP1	pY1346
Peptide233	SNHY[+80]DPEEDEEYYRK[+8]	1.00	TJP1	pY1346
Peptide234	SNTSPEELGPLANQLTSDY[+80]GR[+10]	3.91	TLN1	pY1893
Peptide235	SNY[+80]YDAYQAQPLATR[+10]	1.00	CLDN2	pY194
Peptide236	SQERPGNFY[+80]VSSESIR[+10]	1.00	PIK3AP1	pY570
Peptide237	SQSSHSY[+80]DDSTLPLIDR[+10]	1.00	CTNND1	pY865
Peptide238	SREYDQLY[+80]EEYTR[+10]	3.82	PIK3R2	pY464
Peptide239	SSGSGSSVADERVDY[+80]VVVDQQK[+8]	1.00	GAB1	pY659
Peptide240	SSPEQSYQGDMY[+80]PTR[+10]	1.00	GPRC5C	pY317
Peptide241	SSSAGGQGSY[+80]VPLLR[+10]	1.00	LSR	pY372
Peptide242	STGPGASLGTGY[+80]DR[+10]	1.00	CLDN3	pY214
Peptide243	STTNY[+80]VDFYSTK[+8]	3.00	PKP4	pY1168
Peptide244	SVLEDFFTATEGQY[+80]QPQ(P)	2.88	LCK	pY505
Peptide245	SVNESLNNLFITEEDY[+80]QALR[+10]	1.00	CLTC	pY1477
Peptide246	SYSPY[+80]DMLESIR[+10]	1.00	ANXA2P2	pY238
Peptide247	TAC[+57]TNFMMT[+80]PY[+80]VVTR[+10]	1.00	MAPK9	pT183;pY185
Peptide248	TAC[+57]TNFMMTPY[+80]VVTR[+10]	1.00	MAPK9	pY185
Peptide249	TAGTSFMMT[+80]PY[+80]VVTR[+10]	1.00	MAPK10	pT221;pY223
Peptide250	TAGTSFMMTPY[+80]VVTR[+10]	4.77	MAPK10	pY223
Peptide251	TASDTDSSY[+80]C[+57]IPTAGMSPSR[+10]	2.58	GAB1	pY373
Peptide252	TATESFASDPILY[+80]RPVAVALDTK[+8]	1.00	PKM	pY105
Peptide253	TEELIY[+80]LSQK[+8]	1.00	ARHGEF5	pY1370
Peptide254	TGVAGEDMQDNSGTY[+80]GK[+8]	2.99	PRKCD	pY334
Peptide255	THAVSVSETDDY[+80]AEIIDEEDTYTMPSTR[+10]	1.00	PTK2	pY397
Peptide256	TLDNGGFY[+80]ISPR[+10]	2.89	HCK	pY209
Peptide257	TMQFEPSTMVY[+80]DAC[+57]R[+10]	1.00	TLN1	pY26
Peptide258	TPLVLAAPPPDSPPAEDVY[+80]DVPPPAPDLY[+80]DVPPGLR[+10]	1.00	BCAR1	pY362;pY372
Peptide259	TPSSY[+80]GAGELLDFSLADAVNQEFLTTR[+10]	1.00	DES	pY83
Peptide260	TRDQY[+80]LMWLTQK[+8]	1.00	PIK3R1	pY580
Peptide261	TSIDAY[+80]DNFDNISLAQR[+10]	1.00	CLTC	pY1487
Peptide262	TTAVEIDY[+80]DSLK[+8]	1.00	FYB1	pY571
Peptide263	TTENNYC[+57]PHY[+80]EK[+8]	1.00	EFNB1	pY317
Peptide264	TVHDMEQFGQQQYDIY[+80]ER[+10]	2.12	PKP4	pY372
Peptide265	TY[+80]DMLK[+8]	1.00	PKP2	pY108

Peptide266	TY[+80]VDPHTY[+80]EDPNQAVLK[+8]	1.00	EPHA2	pY588; pY594
Peptide267	TY[+80]VDPHTYEDPNQAVLK[+8]	1.00	EPHA2	pY588
Peptide268	TYVDPHTY[+80]EDPNQAVLK[+8]	3.29	EPHA2	pY594
Peptide269	VADPDHDHTGFLT[+80]EY[+80]VATR[+10]	2.29	MAPK1	pT185; pY187
Peptide270	VADPDHDHTGFLTEY[+80]VATR[+10]	1.00	MAPK1	pY187
Peptide271	VAEDLESEGLMAEEVQAVQQQEVY[+80]GMMPR[+10]	1.00	SPTAN1	pY1176
Peptide272	VC[+57]AYGAQGEGPY[+80]SSLVSC[+57]R[+10]	1.00	ITGB4	pY1207
Peptide273	VDLGSEVY[+80]R[+10]	1.00	PDLIM4	pY191
Peptide274	VDNEDIY[+80]ESRHEIK[+8]	1.00	FRK	pY387
Peptide275	VDY[+80]VVVDQQK[+8]	1.00	GAB1	pY659
Peptide276	VEFGVY[+80]ESGPR[+10]	1.00	PIK3AP1	pY694
Peptide277	VENC[+57]PDELY[+80]DIMK[+8]	1.00	LYN	pY473
Peptide278	VGEEEHVY[+80]SFPNK[+8]	1.00	PXN	pY118
Peptide279	VGFQY[+80]EGTYK[+8]	1.00	G6PD	pY503
Peptide280	VGQGYVYEAAQPEQDEY[+80]DIPR[+10]	1.00	BCAR1	pY234
Peptide281	VGWFPANY(V)EEDYSEY[+80]C[+57]	1.00	VAV1	pY844
Peptide282	VIEDDPEAVY[+80]TTTGGK[+8]	3.13	EPHA7	pY791
Peptide283	VIEDNEY[+80]TAR[+10]	1.00	LYN	pY397
Peptide284	VIY[+80]DFIEK[+8]	1.00	WASL	pY256
Peptide285	VLEDDPEAAY[+80]TTR[+10]	1.00	EPHA4	pY779
Peptide286	VLEDDPEATY[+80]TTSGGK[+8]	1.00	EPHA2	pY772
Peptide287	VQIY[+80]HNPTANSFR[+10]	1.00	VASP	pY39
Peptide288	VSEKPSADY[+80]VLSVR[+10]	1.00	PTK6	pY114
Peptide289	VTIADDY[+80]SDPFDAK[+8]	1.00	SHB	pY246
Peptide290	VTPPEGY[+80]EVVTVFPK[+8]	1.00	PDLIM1	pY321
Peptide291	VVQEYIDAFSDY[+80]ANFK[+8]	3.05	PTPRA	pY798
Peptide292	VVY[+80]SAPR[+10]	1.00	CLDN3	pY198
Peptide293	VY[+80]AENAIR[+10]	1.92	CHMP1A	pY48
Peptide294	VY[+80]APASTLVDQPYANEGTVVVTER[+10]	3.04	DSG2	pY968
Peptide295	VY[+80]ENVGLMQQQK[+8]	1.00	PTPN11	pY584
Peptide296	VY[+80]IDPFTY[+80]EDPNEAVR[+10]	1.00	EPHB4	pY590; pY596
Peptide297	VY[+80]SEDGAC[+57]R[+10]	1.00	GRB7	pY107
Peptide298	VYNDGYDDDNY[+80]DYIVK[+8]	1.00	DYRK1A	pY145
Peptide299	VYTY[+80]IQSR[+10]	1.00	DYRK2	pY382
Peptide300	WDSYDNFSGHRDDGMEEVVGHTQGPLDGSLY[+80]AK[+8]	1.00	TNS1	pY366
Peptide301	WDSYENLSADGEVLHTQGPVDGSLY[+80]AK[+8]	1.00	TNS3	pY354
Peptide302	WDTGENPIY[+80]K[+8]	1.00	ITGB1	pY783
Peptide303	WTAPEAALY[+80]GR[+10]	1.00	YES1	pY446

Peptide304	WTAPEAIAY[+80]R[+10]	1.00	EPHA6	pY850
Peptide305	Y[+80]AALSDQGLDIK[+8]	1.00	PALLD	pY1348
Peptide306	Y[+80]AAPELEIAR[+10]	1.00	SERINC5	pY345
Peptide307	Y[+80]ANVIAYDHSR[+10]	1.00	PTPRF	pY1381
Peptide308	Y[+80]ATPQVIQAPGPR[+10]	1.00	TNK2	pY827
Peptide309	Y[+80]GDGIQLTR[+10]	3.24	DSP	pY95
Peptide310	Y[+80]IDLDK[+8]	2.68	MXRA8	pY429
Peptide311	Y[+80]LAEFATGNDR[+10]	1.00	YWHAE	pY131
Peptide312	Y[+80]LAEVAAGDDK[+8]	1.00	YWHAZ	pY128
Peptide313	Y[+80]LAEVAC[+57]GDDR[+10]	1.00	YWHAQ	pY128
Peptide314	Y[+80]LAEVATGEK[+8]	1.00	YWHAG	pY133
Peptide315	Y[+80]LPRPANPDEIGNFIDENLK[+8]	1.00	CDH1	pY797
Peptide316	Y[+80]LVIQGDER[+10]	1.00	EGFR	pY978
Peptide317	Y[+80]QQPFEDFR[+10]	1.00	PLCG1	pY1253
Peptide318	Y[+80]QTLPGR[+10]	1.00	PLEKHA7	pY1011
Peptide319	Y[+80]RPSMEGYR[+10]	1.00	CTNND1	pY241
Peptide320	Y[+80]SISDR[+10]	1.00	SOS1	pY1196
Peptide321	Y[+80]SSDPTGALTEDSIDDTFLPVPEY[+80]INQSVPK[+8]	1.00	EGFR	pY1069; pY1092
Peptide322	Y[+80]SSDPTGALTEDSIDDTFLPVPEYINQSVPK[+8]	1.00	EGFR	pY1069
Peptide323	Y[+80]SSMAASFR[+10]	1.00	PDZK1IP1	pY83
Peptide324	Y[+80]VDILPYDYNR[+10]	2.55	PTPRC	pY683
Peptide325	Y[+80]VLC[+57]PSTTPSPAQPADR[+10]	2.49	AXL	pY866
Peptide326	Y[+80]VLDDQY[+80]TSSSGAK[+8]	1.00	TEC	pY513; pY519
Peptide327	YADIESSNY[+80]MAPYDNYVPSAPER[+10]	1.00	PDGFRB	pY771
Peptide328	YAGEVY[+80]GMIR[+10]	1.00	PI4KA	pY1154
Peptide329	YC[+57]RPESQEHPEADPGSAAPY[+80]LK[+8]	1.00	STAT3	pY705
Peptide330	YGTC[+57]IY[+80]QGR[+10]	2.95	DEFA1	pY85
Peptide331	YHGHSMSDPGVSY[+80]R[+10]	1.00	PDHA1	pY301
Peptide332	YIEDEDYY[+80]KASVTR[+10]	1.00	PTK2B	pY580
Peptide333	YLSEMNY[+80]VHR[+10]	1.00	EPHB3	pY754
Peptide334	YSQNIY[+80]IQNR[+10]	1.00	PKP2	pY631
Peptide335	YSSDPTGALTEDSIDDTFLPVPEY[+80]INQSVPK[+8]	3.79	EGFR	pY1092
Peptide336	YTEFY[+80]HVPTHSDASK[+8]	1.00	PDLIM5	pY251
Peptide337	YTY[+80]SEWHSFTQPR[+10]	1.00	DSC3	pY818
Peptide338	YVDSEGHLY[+80]TVPIR[+10]	1.00	CAV1	pY14
Peptide339	YVLDDEY[+80]TSSVGSK[+8]	1.00	BTK	pY551

CHAPTER 3: Platform for multiplexed, quantitative pMHC profiling

3-1 Introduction

Cells present signals on the extracellular surface that serve as targets for immune cell recognition. These signals, peptides presented by class I MHCs, are typically derived from intracellular source proteins, and may therefore provide an external representation of the internal cell state.[258] As a reflection of this, the peptide MHC (pMHC) repertoire, or "immunopeptidome", of cancer cells may contain tumor-associated or mutation-containing antigens that serve as tumor-specific markers to activate T cells and initiate an anti-tumor immune response. This interaction can be strengthened with checkpoint blockade (CB) immunotherapies, however low response rates and toxicity remain barriers to their broad clinical success.[259,260] A growing body of evidence suggests that combining CB with other treatments such as small molecule inhibitors, cytotoxic agents, and radiotherapy could potentiate the response to CB, in part by augmenting tumor immunogenicity through increased surface pMHC expression.[31,261–263] While clinical trials in this space have shown promise[44,45], the optimal combination of agents, as well as the order and timing of administration, are only beginning to be understood. In order to improve combinatorial strategies, a quantitative, molecular understanding of how different perturbations shift the immunopeptidome is required. Furthermore, achieving absolute quantification of presented antigens is necessary to inform immunotherapy drug design, as targeted strategies have varying thresholds of antigen expression required for an optimal antitumor response.

Traditional data-dependent acquisition methods to profile pMHC repertoires using mass spectrometry (MS) are well-documented[155,157,264] but quantitative methods have critical

limitations. Specifically, most common relative quantification pMHC methods lack a normalization strategy to account for variations in sample input and processing.[168,170,180–182,265] Peptide losses during processing vary across peptide sequences, concentrations, and samples, underscoring the need for normalization.[164,183] Absolute quantification of pMHCs to date is most commonly performed by comparing endogenous levels of pMHCs to exogenous peptide standards, again failing to account for sample losses.[266–269] Losses can be accounted for with internal pMHC standards, but require laborious refolding of pMHCs for every target of interest.[183,270] Nevertheless this approach relies on single point calibration, ignoring the effects of ion suppression, thereby inaccurately estimating absolute pMHC levels in quantitative analyses.

To combat these challenges in quantitative immunopeptidomic profiling, we present a platform that utilizes ultraviolet (UV)-mediated peptide exchange of recombinant MHC monomers to generate on demand heavy isotope-labeled pMHCs for relative and absolute quantification of pMHC repertoires using low sample input. We demonstrate that the addition of heavy isotope pMHCs (hipMHCs) spiked into sample lysates for normalization improves quantitative accuracy between samples for both label-free and multiplexed (TMT-labeled) analyses and provides an estimate of ion suppression through regression against a titrated internal calibrant. Furthermore, we utilize hipMHC multipoint embedded standard curves coupled with isobaric mass tags to accurately quantify the absolute number of copies per cell of target antigens within a single analysis. We apply this platform to profile immunopeptidomic changes in melanoma cell lines, comparing treatment with palbociclib (a small molecule CDK4/6 inhibitor) and interferon-gamma (IFN-γ), both known modulators of antigen presentation.[263,271] Peptides derived from proteins implicated in the biological response to palbociclib and IFN-γ were selectively enriched in the pMHC repertoire following treatment, connecting the

intracellular response to extracellular immune presentation. Furthermore, peptides derived from the metabolic response to palbociclib, along with known tumor-associated antigens (TAAs), displayed significantly increased presentation with palbociclib treatment. We propose this platform can be broadly applied to profile immunopeptidomic changes in a high-throughput, low-input format across sample types and treatments to inform combination therapy strategies and can be used to identify and quantify treatment-modulated antigen targets for targeted immunotherapy.

3-2 Results

3-2-1 Platform for relative and absolute peptide MHC quantitation

We set out to develop a platform to provide accurate relative and absolute quantification of pMHCs across multiple samples while controlling for losses associated with sample processing and enrichment. Accurate quantitative analysis is best performed with internal standards and multi-point internal calibration curves. To generate internal standards, heavy isotope labeled MHC peptides of interest were synthesized and loaded onto biotinylated MHC monomers through UV-mediated peptide exchange (**Figure 3-1-A**).[272] To control for loading efficiency of synthetic peptides into recombinant MHC proteins, the concentration of stable hipMHC complexes was determined by an enzyme-linked immunosorbent assay (ELISA). Stable hipMHC complexes were then used in two ways: selected hipMHC complexes were spiked at the same concentration into whole cell lysate from each sample to provide a normalization correction for relative quantification across samples, while other hipMHC complexes were titrated at different concentrations into each sample to verify correction parameters, estimate dynamic range suppression for quantification, and/or create an internal standard curve for absolute quantification of a specific peptide. After adding hipMHCs,

endogenous and exogenous pMHCs were isolated by immunoprecipitation, acid elution, and molecular weight size exclusion filtration.

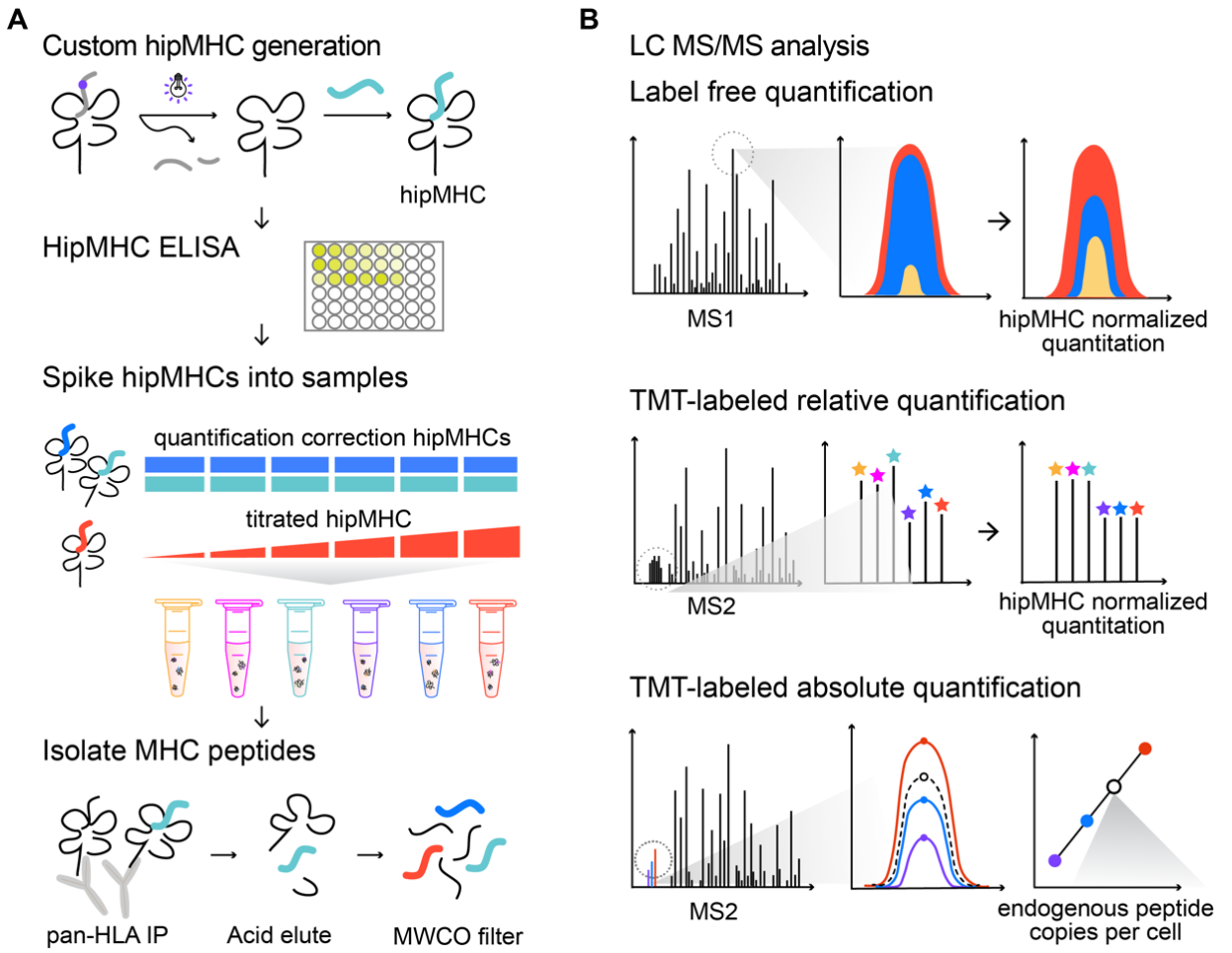

Figure 3-1. *Platform for quantitative immunopeptidomics using hipMHCs.* ***A*** *hipMHCs were generated through UV-mediated peptide exchange of HLA*A2:01 monomers with a heavy leucine HLA-A*02:01 binding peptide. Stable hipMHCs concentrations were measured with an ELISA, and hipMHC complexes were added to lysate samples prior to immunoprecipitation (IP), at the same concentration for quantification correction (blue/teal) or titrated in to create an internal standard curve (red). Heavy and light pMHCs were isolated with IP, acid elution, and molecular weight cut-off (MWCO) filters.* ***B*** *Peptides were analyzed by LC MS/MS three ways. Relative quantification label-free analyses were quantified by integrating the area under the curve (AUC) of the chromatographic elution across samples, and quantification was normalized by applying correction factors determined by hipMHC AUC intensity ratios between samples. Samples for multiplexed analysis were TMT-labeled and relative quantification was implemented using reporter ion intensities. Normalization was performed using hipMHC reporter ion*

intensity ratios across TMT channels. For absolute quantification, TMT-labeled samples containing a hipMHC internal standard curve were used to calculate the endogenous copies per cell of the pMHC of interest.

Peptide mixtures were next analyzed by liquid chromatography-tandem mass spectrometry (LC-MS/MS) in three different ways (**Figure 3-1-B**). For label-free (LF) analyses, samples were analyzed individually, and peptides were quantified by integrating the area under the curve (AUC) for the chromatographic elution of precursor masses for each peptide-spectrum match (PSM). Relative AUC intensities of quantification correction hipMHCs were used to normalize AUC intensities of endogenous peptides across analyses. To analyze multiple samples simultaneously, we labeled samples with tandem mass tags (TMT) and relative TMT ion intensity ratios of hipMHCs were used for normalization to correct the relative quantification in multiplexed samples. TMT-labeled titrated hipMHCs were also used for absolute quantification of endogenous peptides. Apex TMT intensities of hipMHCs generated a peptide specific multipoint calibration curve to calculate the average number of copies per cell. As a control, heavy isotope-coded synthetic peptides not complexed to MHC were spiked into whole cell lysate prior to immunoprecipitation. These peptides were not detected in the subsequent LC-MS/MS analysis, demonstrating that only peptides in stable complexes were isolated in our workflow and that excess free peptides did not displace endogenously presented peptides.

3-2-2 HipMHC standards improve quantitative accuracy

To demonstrate the improved quantitative accuracy obtained with hipMHCs, we used five LF and six TMT-labeled technical replicates of $1x10^7$ MDA-MB-231 breast cancer cells to measure variance between replicates before and after hipMHC correction (**Figure 3-2-A**). In both LF and TMT-labeled workflows, we spiked 30 fmol of two quantification correction

hipMHCs into each sample, as adding additional correction hipMHCs gave minimal improvement in quantitative accuracy. We also added 30-300 fmol of a titrated hipMHC across samples (**Figure 3-2-B**). A total of 2,369 unique pMHCs were identified in total across five LF analyses, 1,352 of which were quantifiable via AUC integration (**Figure 3-2-C**). Of these quantifiable peptides, only 589 were quantified in all five analyses, highlighting the poor run-to-run overlap of LF analyses, even with replicate samples (**Supplementary Figure 3-1-A**). By comparison, 1,754 unique peptides were quantifiable with TMT-labeled analyses.

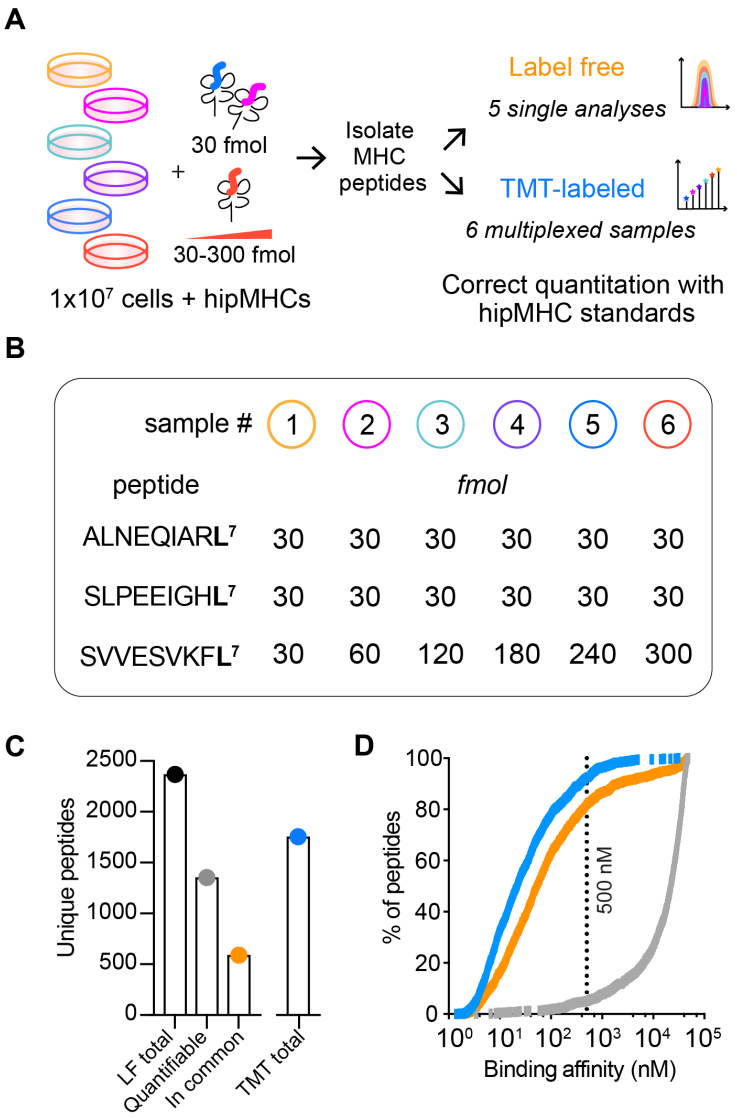

Figure 3-2. *hipMHCs improve quantitation in LF and TMT-labeled samples.* ***A*** *Experimental design. Five LF (orange) and six TMT (blue) technical replicates of 1x10⁷ cells + hipMHCs were used to compare LF & TMT quantification.* ***B*** *Peptide sequence and amount of hipMHC added into each sample. L7 denotes heavy isotope-labeled leucine (+7). ALNEQIARL and SLEEPIGHL were used as quantification correction hipMHCs, and SVVESVKFL was titrated in across samples. For LF analysis, sample #6 was omitted.* ***C*** *2,369 unique LF peptides identified across five analyses (black), 1,352 of which were quantifiable (grey) via AUC quantification, and 589 quantifiable peptides which were identified in all five analyses (orange). 1,754 unique peptides were quantified with TMT-labeled analyses combining six TMT fractions (blue).* ***D*** *92% of TMT, 82% of LF, and 5.6% of random peptide 9-mers derived from the proteome (grey) are predicted to bind to an HLA allele in MDA-MB-231 cells with an affinity < 500 nM*

The extra sample handling steps associated with TMT labeling can result in losses, so to achieve high coverage of the immunopeptidome, labeled samples were divided into six separate analyses, thereby increasing the number of unique identifications (**Figure 3-3-A**). In both LF and TMT analyses, peptides matched expected length distributions of 8 to 11 amino acids (**Figure 3-3-B**), and 82% of LF and 92% of TMT 9-mers were predicted to be binders with less than 500 nM predicted affinity (**Figure 3-2-D**).[99] The peptides were similarly apportioned across alleles between LF and TMT analyses, and the allele motifs aligned with those previously reported (**Figure 3-3-C,D**).[273] Further reducing the input material to $5x10^6$ cells still resulted in 86% of the number of unique peptides identified with $1x10^7$ cells in a single LF analysis, establishing the sensitivity of this method for low-input pMHC analyses (**Supplementary Figure 3-1-B**).

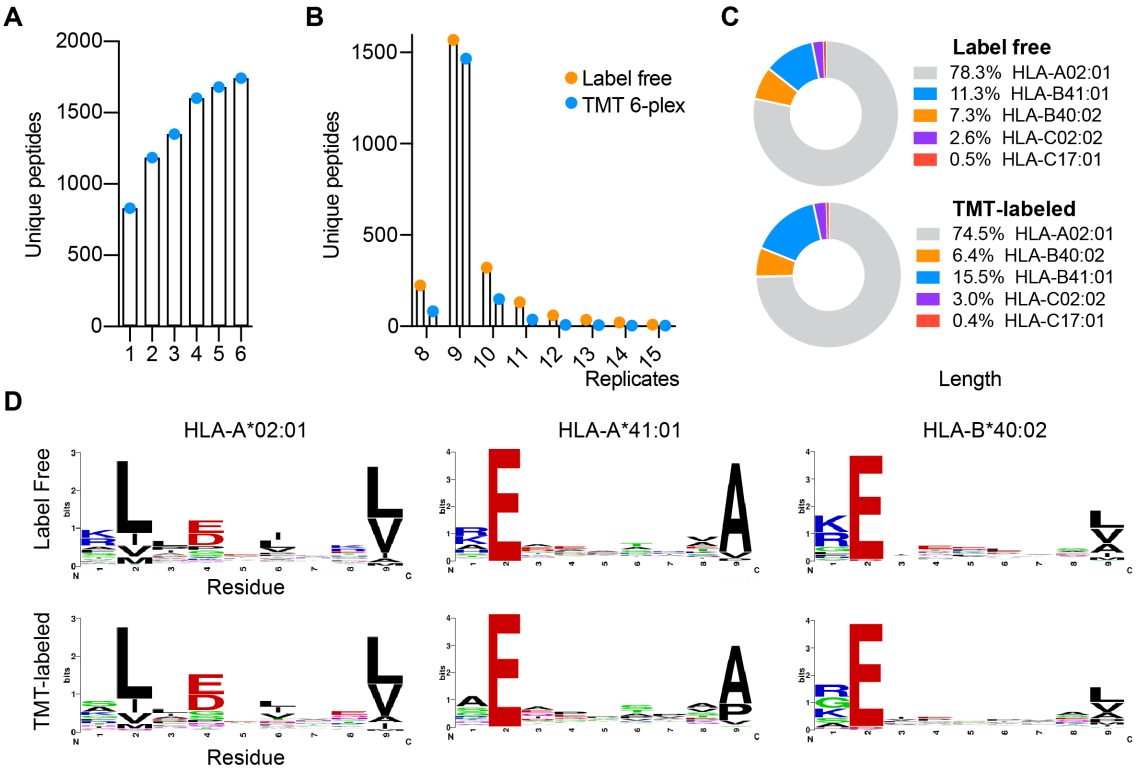

Figure 3-3. *MDA-MB-231 MHC peptide properties.* ***A*** *Total peptides identified combining the results from n=1 to n=6 independent analyses of TMT-labeled MDA-MB-231 cells, analyzing 15-20% of the peptide elution per analysis.* ***B*** *Length distribution of MDA-MB-231 peptides for LF and TMT-labeled samples.*

Unique peptides are identified from the union of n=5 LF technical replicates and n=6 TMT-labeled elution fractions. ***C*** *Distribution of 9-mer peptides across HLA alleles with a predicted affinity < 500 nM for LF (top) and TMT-labeled (bottom) analyses.* ***D*** *Binding motifs of alleles containing ≥ 5% of predicted binders for LF (top) and TMT-labeled (bottom) analyses*

To normalize LF and TMT-labeled datasets, we applied correction parameters calculated from the quantification correction hipMHCs. The titrated peptide, SVVESVKFL[7], displayed an improved linear fit after correction, with an even more pronounced effect in the LF samples (**Figure 3-4**). We observed dynamic range suppression for this peptide in TMT-labeled (4.7x) and LF (2.7x) datasets, demonstrating in both cases that quantitative differences are likely larger than what is measured.

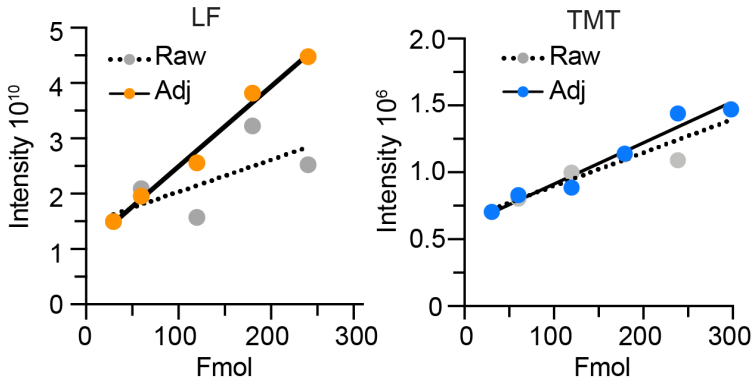

Figure 3-4. *Ion suppression in titrated hipMHC. Linear fit of titrated hipMHC peptide for LF (left) and TMT (right). Raw r^2 = 0.48 (LF) and r^2=0.91 (TMT), hipMHC adjusted (adj) r^2=0.99 (LF) and r^2=0.96 (TMT).*

In both analyses, hipMHC quantification correction reduced variation, for example, peptides from TMT-labeled sample 5 have lower intensities than the other samples, which was corrected by hipMHC normalization (**Figure 3-5-A**). The standard deviation from the mean for replicate samples decreased in LF and TMT-labeled samples (**Figure 3-5-B**), though TMT labeling showed lower variation between replicates (**Figure 3-5-C**), allowing for higher

confidence in small shifts within the immunopeptidome. We investigated whether peptides with lower abundance had higher quantitative variation across samples but found no correlation in LF or TMT-labeled analyses (Supplemental Fig. 1G).

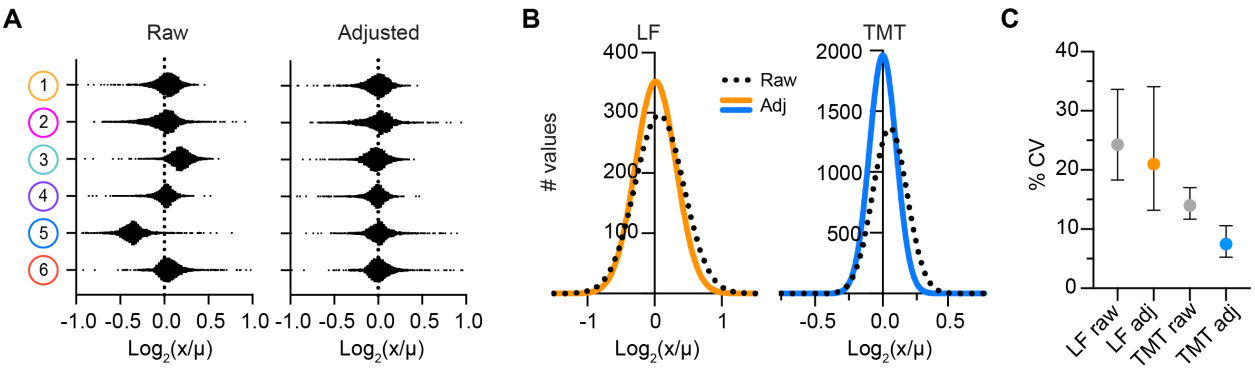

Figure 3-5. *hipMHC correction improves CV.* ***A*** *Distribution of the log_2 fold change (FC) of each peptide's quantification (x) over the mean (μ) peptide quantification across samples for raw (left) and hipMHC adjusted (right).* ***B*** *Gaussian fit of the frequency distribution of log_2(FC) of (x) over (μ) for raw and hipMHC adjusted LF and TMT samples. 99.7% of variance between peptide quantitation (3x SD) is captured within a 1.65 (raw) and 1.52 (adj) FC from the mean for LF samples, and 1.30 (raw) and 1.23 (adj.) for TMT samples.* ***C*** *Median coefficient of variation (CV) for LF (24.27% raw, 20.99% adj) & TMT (14.00% raw, 7.48% adj). Error bars represent the interquartile range.*

3-2-3 Absolute quantification of endogenous peptide MHCs

To demonstrate the ability of hipMHCs to quantify pMHC copies per cell, we selected two peptides identified in TMT-labeled MDA-MB-231 cells for absolute quantification: KLDVGNAEV derived from B cell receptor associated protein 31 (BCAP31) and KQVSDLISV from DEAD-box RNA helicase 5 (DDX5). BCAP31 regulates the transport of membrane proteins from the endoplasmic reticulum to the Golgi, a central component of antigen processing, and is a known TAA peptide.[163] DDX5 is important in gene expression regulation and has been implicated in proliferation, metastasis, and tumorigenesis in cancer.[274] These peptides were

detected at differing levels with the highly abundant BCAP31 peptide falling in the 98th percentile and DDX5 falling in the 33rd percentile of abundance (**Figure 3-6-A**). Both peptides were synthesized with heavy-isotope labeled leucine (+7), and hipMHC normalization standards were added to three replicates of 1x10^{7} MDA-MB-231 cells along with titrated amounts of BCAP31 and DDX5 hipMHC (**Figure 3-6-B**). We then labeled samples with TMT and performed LC-MS/MS analysis using an inclusion list, so only targeted peptides of interest were selected for fragmentation.

Chromatographic traces of the three TMT reporter ions for heavy BCAP31 and DDX5 peptides displayed increasing ion intensities with increasing amount of hipMHC added (**Figure 3-6-C**). In order to quantify peptide expression, the apex intensities of reporter ions were adjusted based on the normalization hipMHCs, and a linear fit was used to pMHC concentration present in the sample. Cells had an average of 1,740 copies per cell of the BCAP31 peptide, and 81 copies per cell of the DDX5 peptide (**Figure 3-6-D**). Concentrations of the DDX5 hipMHC as low as 100 attomole were detected (six copies per cell) showcasing the broad range of pMHC expression levels quantifiable by our method (**Supplementary Figure 3-3**). Furthermore, BCAP31 and DDX5 had a dynamic range suppression of 1.9x and 2.5x, respectively, illustrating that the ion suppression is not uniform across peptides and that peptide-specific internal standards may be required for absolute quantification of each pMHC of interest.

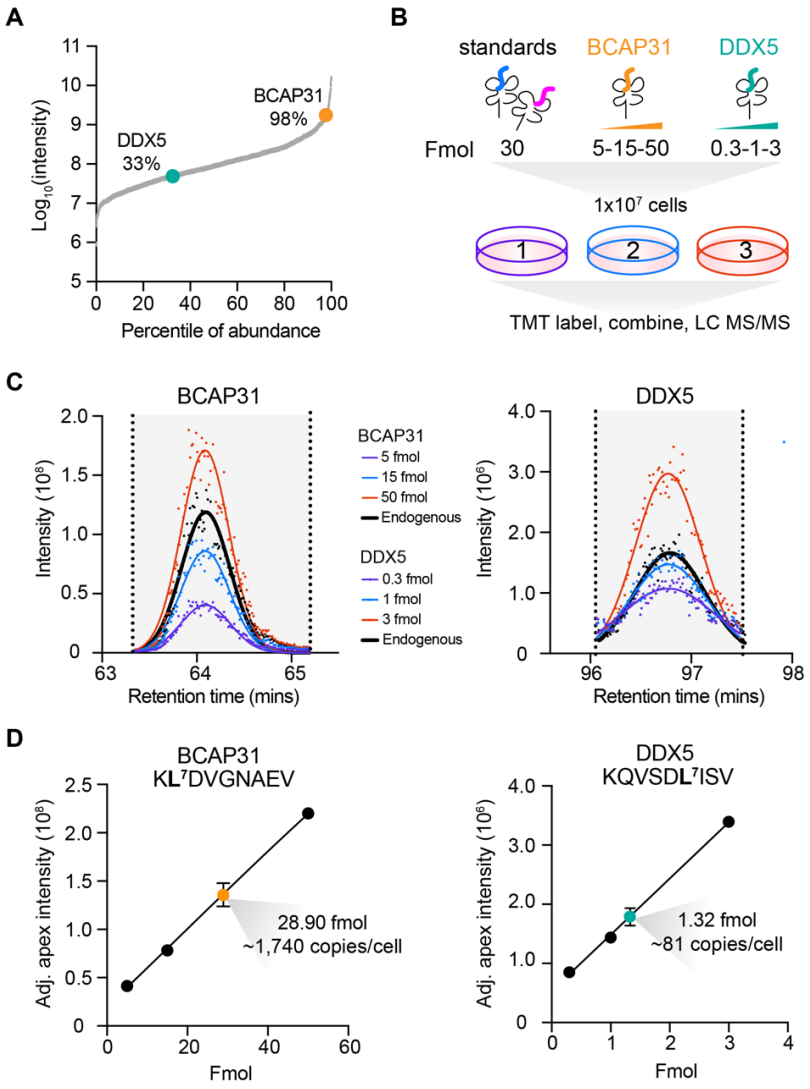

Figure 3-6. *Absolute quantification of pMHCs with hipMHC standards and isobaric labeling.* ***A*** *Peptide intensities for TMT-labeled MDA-MB-231 cells from Fig. 2 determined by AUC quantification. Percentile of abundance represents a peptide's rank relative to the most abundant peptide.* ***B*** *Experimental design. Normalization standards along with 5, 15, and 50 fmol of BCAP31 and 0.3, 1, and 3 fmol of DDX5 hipMHCs were added to three biological replicates of 1x107 MDA-MB-231 cells, and peptides from MHC complexes were isolated, labeled, and analyzed via LC-MS/MS.* ***C*** *Chromatographic elution profiles for the three TMT reporter ion intensities of the hipMHC standard curve (colored), along with the average (n=3) TMT reporter ion intensity trace of the endogenous peptide (black). Each MS2 scan is represented as a single point, and elution profiles are fitted with a gaussian distribution (line).* ***D*** *Adjusted (hipMHC normalized) apex intensity versus fmol of hipMHC added creates a standard curve from which the endogenous concentration of antigen is calculated. For both linear fits of BCAP31 and DDX5, r2 > 0.999. The endogenous peptide is presented as the mean value +/- SD for n=3 biological replicates.*

3-2-4 CDK4/6 inhibition alters the pMHC repertoire in melanoma

Cyclin-dependent kinases 4 and 6 (CDK4/6) control cell cycle progression by phosphorylating Rb1, thereby releasing the E2F family of transcription factors that drive progression through the G1 checkpoint.[275] CDK4/6 is often dysregulated and overactive in cancer, leading to uncontrolled proliferation (**Figure 3-7**).[40]

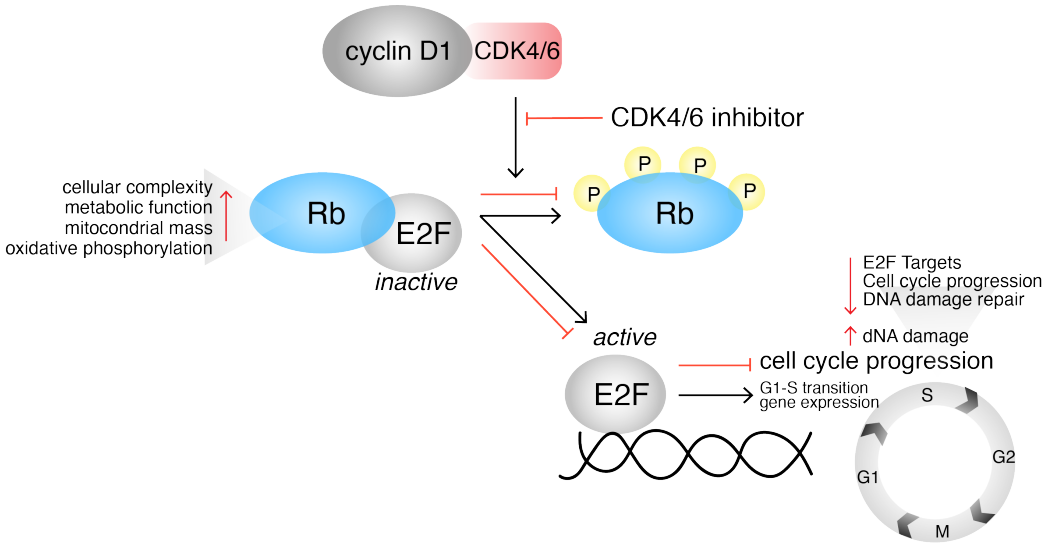

***Figure 3-7**. CDK4/6 mediated cell cycle control. Schematic of CDK4/6 mediated cell cycle control (black) and the effects of CDK4/6 inhibition (red).*

As such, CDK4/6 inhibitors have emerged as a potentially powerful class of anticancer agents, active against a spectrum of tumor types including melanoma.[41] In recent years, CDK4/6 inhibitors have also been shown to enhance tumor immunogenicity by increasing surface MHC class I expression and boosting T cell activation and infiltration.[42,263] These data highlight CDK4/6 inhibitors as an attractive candidate to combine with CB or other immunotherapies to augment immunotherapy response rates in melanoma. However, to date, the effect of CDK4/6 inhibition on the MHC class I peptide repertoire has not been

characterized. We therefore applied our platform to quantify how pMHC repertoires in melanoma change *in vitro* upon treatment with the CDK4/6 inhibitor, palbociclib, to better understand how CDK4/6 inhibitors could be leveraged in combination therapy regimes to improve patient outcomes.

We selected four melanoma cell lines for analysis: SKMEL5 and SKMEL28 (BRAF mutant), and SKMEL2 and IPC298 (NRAS mutant). Based on sensitivity analyses for each cell line (**Figure 3-8-A**), we selected two doses of palbociclib for further study: a low dose of 1 μM, below the IC_{50} of all four cell lines, and a high dose of 10 μM, near the IC_{50}. Three biological replicates of $1x10^7$ cells of each cell line were then treated with DMSO, low-dose, or high-dose palbociclib for 72h (**Figure 3-8-B**). Low-dose treatment increased surface class I MHC presentation, as measured by flow cytometry, by 1.5-2x across cell lines, whereas high-dose treatment had a milder effect (**Figure 3-8-C**).

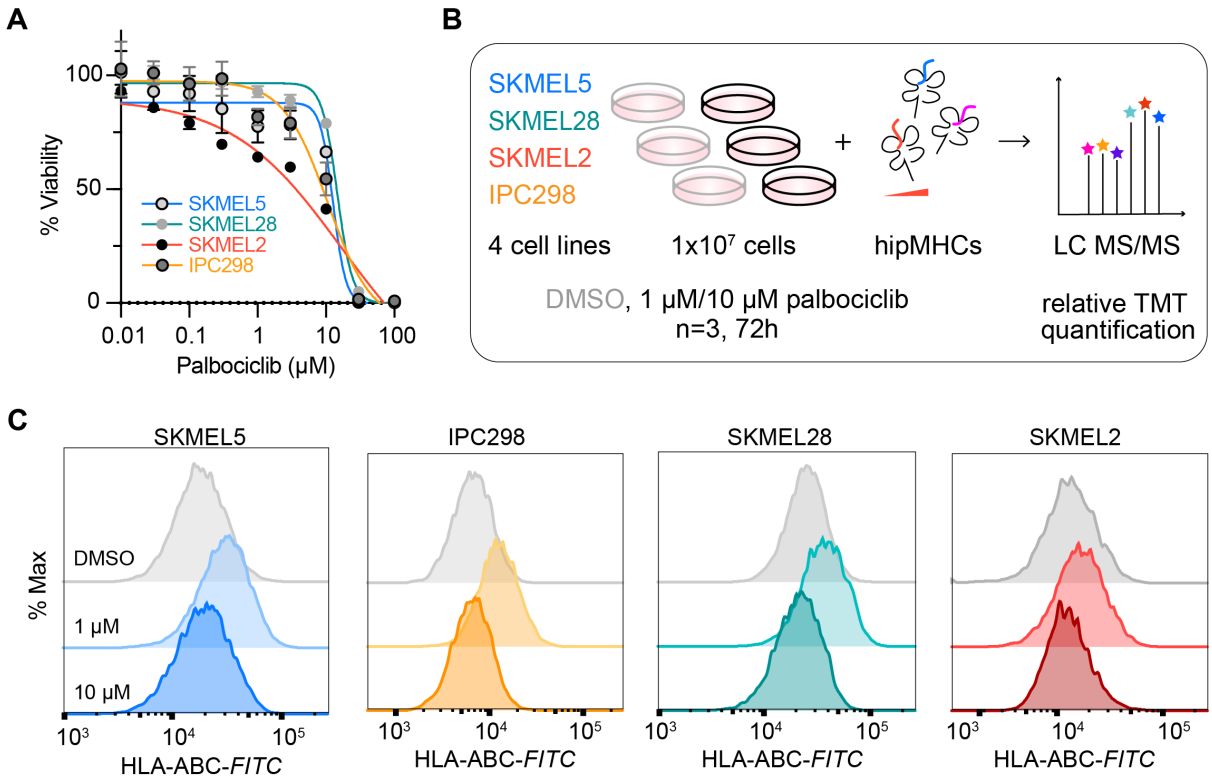

Figure 3-8. *Changes in HLA expression with CDK4/6i.* ***A*** *Viability at 72h after drug treatment, data is represented as a fraction (%) of the DMSO control. Calculated IC50s: for SKMEL5= 12.74 μM, SKMEL28=14.62 μM, SKMEL2=16.98 μM, IPC298=10.62 μM. Data is presented as mean values +/- SD for n=3 experimental replicates for all cell lines except SKMEL5 (n=4).* ***B*** *Experimental setup of TMT-labeled immunopeptidomics experiments in melanoma cell lines.* ***C*** *Flow cytometry measurements of surface HLA expression. Data is represented as % of maximum signal, and the distributions are representative of three independent experiments.*

To characterize the pMHC repertoire alterations induced by palbociclib, multiplexed relative quantitation was performed comparing low- and high-dose palbociclib to DMSO for each cell line, and data was normalized using hipMHC standards (**Supplementary Figure 3-4-A,B**). As with our previous analysis, identified peptides matched expected length distributions, and a majority were predicted to be MHC class I binders (**Supplementary Figure 3-4-C,D**). Immunopeptidomic analysis for each cell line and treatment showed a similar trend to the flow cytometry data: low-dose palbociclib shifted mean pMHC expression higher than DMSO

treatment in all cell lines, and a high dose showed a small increase in mean expression for SKMEL5 compared to DMSO and no significant change for the other cell lines (**Figure 3-9**). We measured a wider distribution of changes in peptide presentation following low dose treatment, with several peptides increasing eight to ten-fold, even before considering the effect of dynamic range suppression.

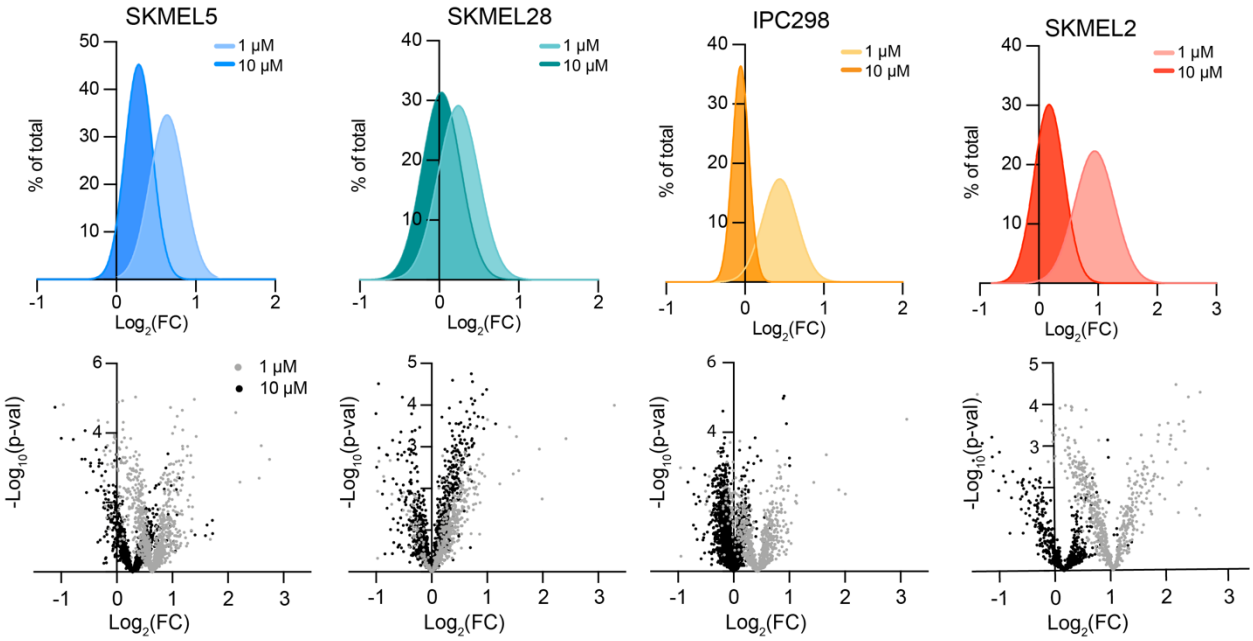

Figure 3-9. *pMHC response to CDK4/6i. Top: histogram distribution of log_2 fold change (FC) of (palbociclib/DMSO) for unique pMHCs, where FC is calculated from the mean intensity of n=3 biological replicates per condition. Data is represented as a % of total unique peptides identified. Bottom: volcano plots representing log2 fold change (FC) of pMHC presentation of (palbociclib/DMSO) versus significance (mean adjusted p-value, unpaired two-sided t test). Data points are colored by treatment, 1 μM (grey) and 10 μM (black).*

To gain insight into the biology underlying palbociclib modulated pMHC alterations, we analyzed our data in two ways. First, we determined which peptides and source proteins were significantly increased with palbociclib treatment over DMSO. Because many peptides were

significantly increased with low-dose treatment, we also identified the peptides and source proteins that were significantly enriched in presentation with treatment relative to the mean fold change of all peptides, highlighting peptides preferentially modulated by palbociclib.

Using these data, we performed GO term enrichment on the 127 peptides significantly enriched in low-dose treated SKMEL5 cells (**Figure 3-10-A**), and identified enriched biological processes of interest including ribosomal biogenesis, glucose metabolic process, and antigen processing, a reflection of the expected biological response to palbociclib (**Figure 3-10-B,C**).[263,276,277] We performed the same analysis with the raw, non-normalized values, and found only 66 of these peptides were significantly enriched without hipMHC quantification correction, altering the GO-term pathway analysis results (**Figure 3-10-D**). While peptides mapping to ribosomal biogenesis were still significantly enriched, the other two biological processes were not, underscoring the importance of using hipMHCs for quantification correction to accurately interpret alterations in pMHCs repertoires.

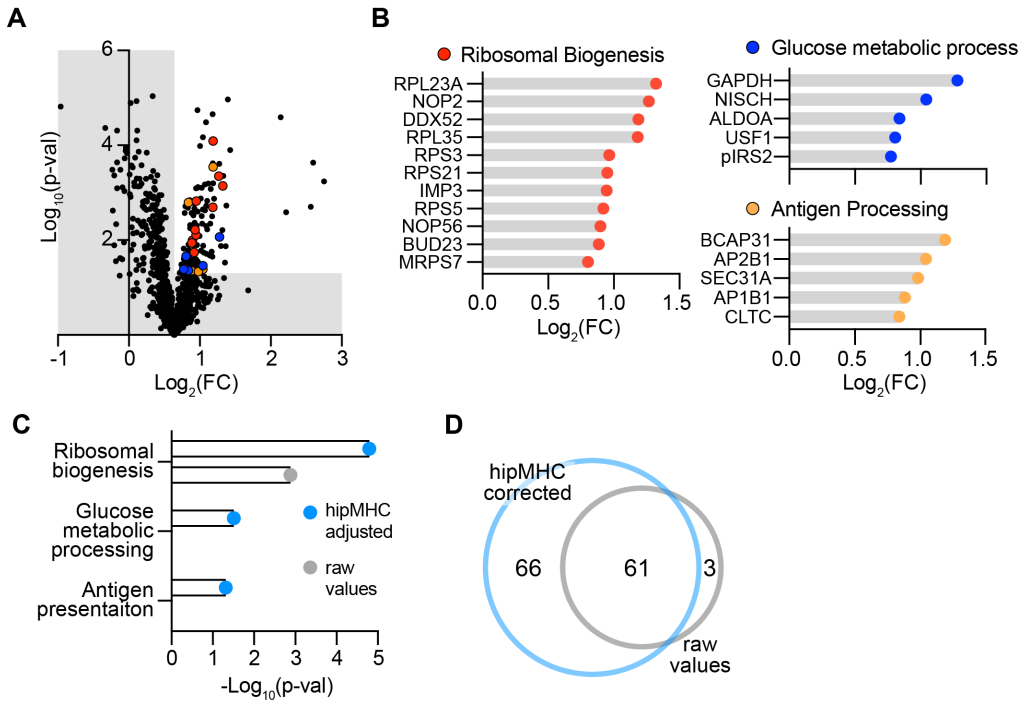

***Figure 3-10**. Enriched biological processes following CDK4/6i. **A** Volcano plot displaying log2(FC) of 1μM treated SKMEL5 cells versus significance (mean adjusted p-value, unpaired two-sided t-test). Colored points ($p < 0.05$, $Log2(FC) > 1.56$) correspond to processes in 4f. **B** Log2(FC) of significantly enriched peptides from GO term enrichment processes labeled with source protein name. FDR adj. p-value < 0.05. **C** Significantly enriched biological processes (GO term enrichment, FDR-adjusted $p < 0.05$) in SKMEL5 cells + 1 μM palbociclib using significantly enriched peptides from the raw data (grey) and hipMHC adjusted data (blue). **D** Number of significantly enriched peptides in raw data (grey) versus hipMHC adjusted data (blue) for SKMEL5 cells +/- 1 μM Palbociclib.*

To determine if the measured pMHC alterations to SKMEL5 cells were common across cell lines, we compared the source proteins of peptides that were significantly enriched with low-dose treatment compared to DMSO across all four cell lines. Surprisingly, a majority (72-88%) of enriched source proteins were unique to each cell line, and we discovered only three proteins in common: vimentin (VIM), putative beta-actin-like protein 3 (POTEKP), and SIL1 nucleotide exchange factor (SIL1) (**Figure 3-11-A, B**). Even when comparing source proteins of all peptides significantly increasing to any extent, just 17 proteins in common were identified,

further illustrating the uniqueness of the proteins altered by palbociclib in each immunopeptidomic landscape (**Figure 3-11-C**). We investigated whether the commonality of these 17 proteins could be explained by having high abundance in the peptide mixtures, but in SKMEL5 cells they were scattered throughout the distribution of AUC intensities (**Figure 3-11-D**).

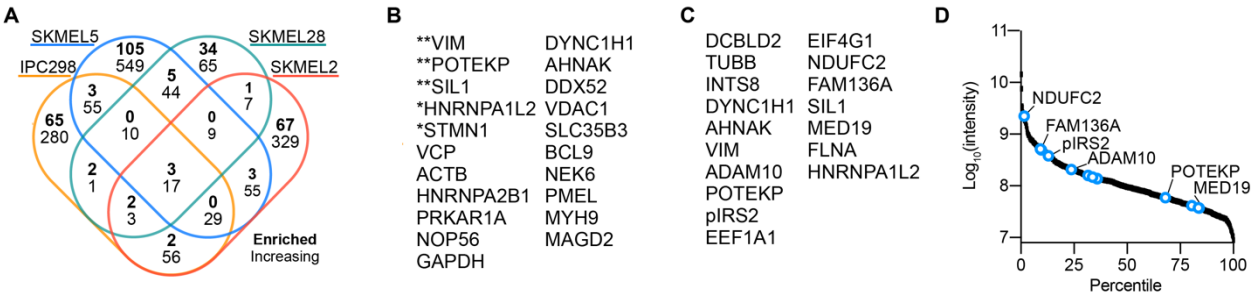

Figure 3-11*. Peptides identified across all 4 analyses.* ***A*** *4-way Venn-diagram of the number of source proteins of peptides significantly enriched or significantly increasing with 1 µM palbociclib.* ***B*** *Source proteins of peptides significantly enriched (mean adjusted p-value) following palbociclib treatment, **= significantly upregulated in four cell lines, *= three lines, all others were seen in at least two cell lines.* ***C*** *17 common source proteins significantly increasing in all four cell lines.* ***D*** *Average peptide AUC integrated abundance vs. percentile rank of abundance of all SKMEL5 +/- 1 µM palbociclib peptides. Blue points are peptides labeled by their source protein that are significantly increased in all four cell lines.*

While the list of shared pMHCs and source proteins in common is limited, of interest is the serine-phosphorylated IRS2 (pIRS2) peptide, RVA[pS]PTSGVK. This post-translationally modified sequence has previously been shown to be restricted to malignant cells, with only the phosphorylated form demonstrating immunogenic potential[278,279] Even though there are no alleles in common across the four cell lines (Supplementary Fig. 3k)[280], we observed the pIRS2 peptide increasing across all cell lines with low dose treatment (Fig. 4h). Furthermore, RVApSPTSGVK has high expression among pMHCs (**Figure 3-11-D**), and can be isolated without phospho-enrichment.[158] As a result, this peptide may be uniquely positioned as a

broadly targetable antigen whose expression can be modulated by CDK4/6 inhibition. As a general effect of palbociclib treatment, TAAs derived from proteins like MLANA (MART1), PMEL (gp100), and TYR, among others, also increased in presentation following treatment (Fig. 4i). While these antigens and their source proteins are not universally conserved across our cell lines, the effect of increased TAA presentation following 1 μM palbociclib treatment could be applied to increase antigen presentation prior to immunotherapies targeting these well-documented antigens.

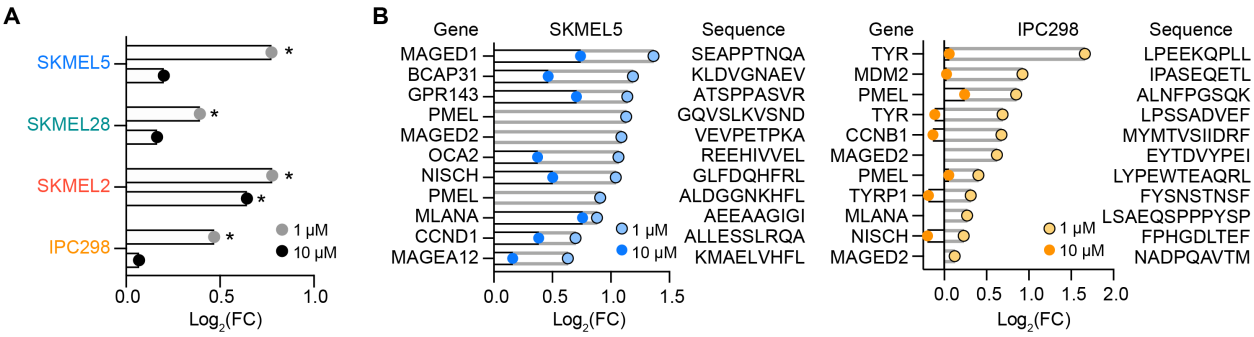

***Figure 3-12**. TAA expression changes with CDK4/6i. **A** Log$_2$(FC) of pIRS2 peptide following 1 μM (grey) or 10 μM (black) palbociclib, *p < 0.05, unpaired two-sided t-test. **B** Gene name, peptide sequence, and log$_2$(FC) of TAAs in SKMEL5 (left) and IPC298 (right) cells.*

3-2-5 Response to palbociclib is reflected in the immunopeptidome

To further assess whether quantitative differences in the immunopeptidome after palbociclib treatment are reflective of the cell signaling response to a perturbation, we performed a nonparametric test to identify positively- and negatively-enriched pathways. Gene names for source proteins were rank ordered according to fold change with treatment and searched against the MSigDB Hallmarks gene set database using Gene Set Enrichment Analysis (GSEA).[255,281,282] This analysis did not reveal any significantly enriched pathways for the low dose treatment, but high dose palbociclib showed significant enrichment among

downregulated pMHCs of E2F targets, G2M checkpoint, DNA repair, mitotic spindle, and MTORC1 signaling pathways in one or more cell lines (**Figure 3-13**).

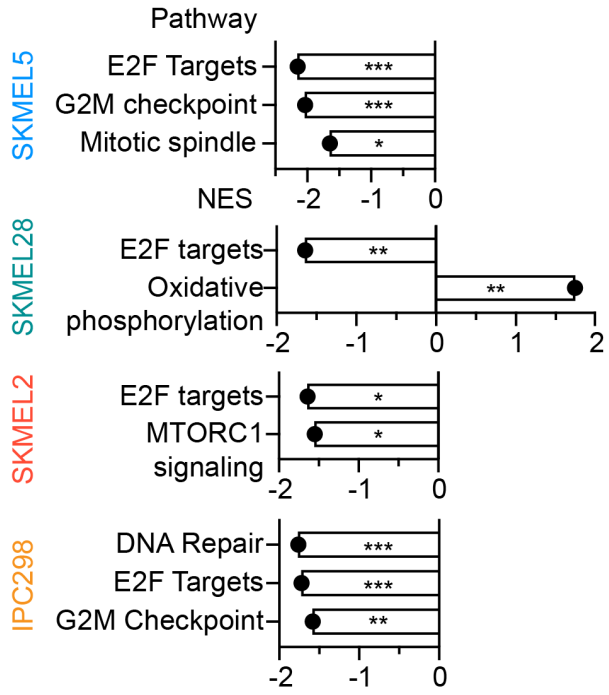

***Figure 3-13**. Enriched pathways using pMHC expression changes with CDK4/6i. Normalized enrichment score (NES) of significantly enriched pathways with 10 μM palbociclib, where +/- NES scores reflect enrichment directionality. For all, $q < 0.25$, and $^{*}p < 0.05$, $^{**}p < 0.01$, $^{***}p < 0.001$.*

These findings reflect the known biological effects of CDK4/6 inhibition. For instance, inhibiting CDK4/6 decreases expression of E2F targets, and peptides derived from E2F targets like Ki-67, a proliferation marker, were depleted in all four cell lines (**Figure 3-14-A**). E2F also controls genes involved in DNA damage repair, and consistently, γH2AX levels, a marker of DNA double-strand breaks, increased at 72h with palbociclib treatment in a dose dependent manner (**Supplementary Figure 3-6-A**).[283] Although similar biological processes are enriched across the four cell lines, source proteins for significantly depleted E2F peptides showed little

overlap between the cell lines (**Figure 3-14-A**), again emphasizing the individuality of the source proteins contributing to each cell line's detected pMHC repertoire.

Only one pathway, oxidative phosphorylation (OxPhos), was significantly upregulated in SKMEL28 cells. However, all cell lines presented peptides derived from the OxPhos pathway that increased significantly with palbociclib treatment, though this effect was more prominent with low-dose treatment in SKMEL5, IPC298, and SKMEL2 cells, in contrast to the results of SKMEL28 cells (**Figure 3-14-B**). OxPhos has been shown to increase with CDK4/6 inhibition due to increased ATP levels and mitochondrial mass, elevating metabolic activity. Comparably, all samples showed elevated mitochondrial levels following treatment, suggesting that enriched pMHC presentation of OxPhos derived peptides reflects a change in the metabolic cell state (**Figure 3-15-A**).

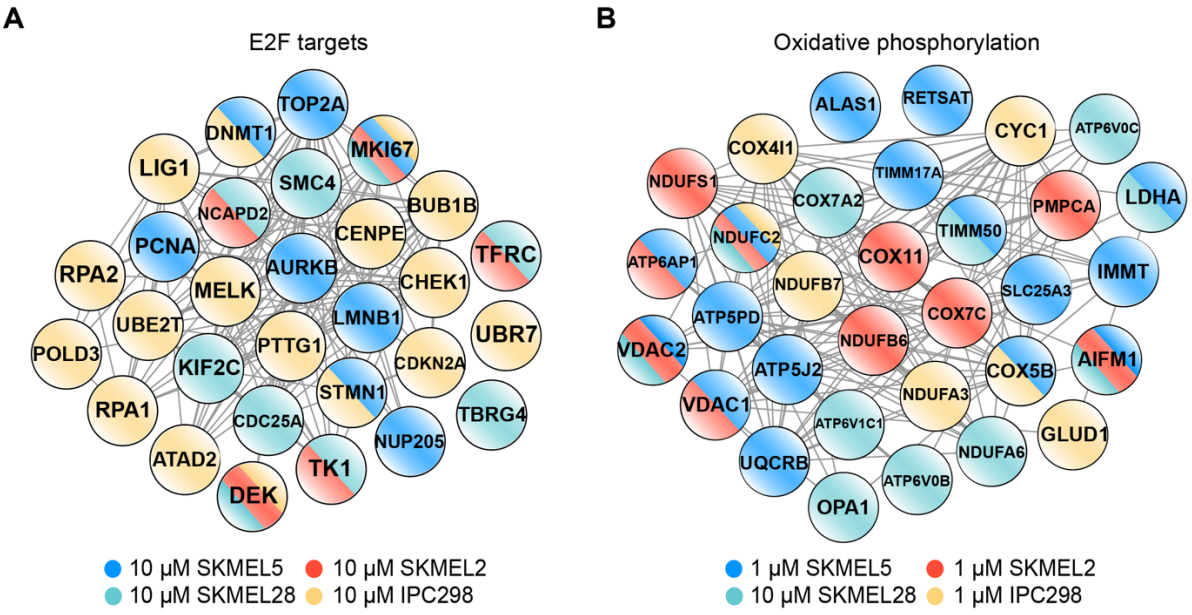

Figure 3-14*. Interaction networks of enriched E2F proteins. String network of protein-protein interactions of all source proteins from E2F peptides (**A**) significantly decreasing with 10 µM palbociclib, and OxPhos peptides (**B**) significantly increasing with 1 µM palbociclib for all cell lines except SKMEL28, where peptides from 10 µM are depicted. Node color corresponds to cell line.*

Because alterations to the pMHC repertoire align with previously characterized biological responses to CDK4/6 inhibition, we tested whether changes in RNA expression could predict the quantitative immunopeptidome changes. No bulk correlation (r^2=0.04) was observed between pMHC expression and RNA expression (**Figure 3-15-B**). This was unsurprising, as many mechanisms beyond gene expression regulate pMHC presentation, including protein synthesis, degradation, post-transitional modifications, processing, and more. Despite this poor correlation, significantly enriched gene sets in the immunopeptidome were also present in our RNA sequencing analysis (**Figure 3-15-C**). While E2F pMHCs significantly depleted in SKMEL5 cells correlated with significantly decreased gene expression of the same source proteins, (**Supplementary Figure 3-6-B**), only five of the 15 positively enriched OxPhos peptides displayed significantly higher gene expression with palbociclib treatment, with three decreasing in expression, and seven remaining unchanged (**Figure 3-15-D**). Collectively, these data suggest that while changes in gene expression and pMHC repertoires map to the same biological pathways, individual gene expression changes are not necessarily predictive of alterations in the immunopeptidome.

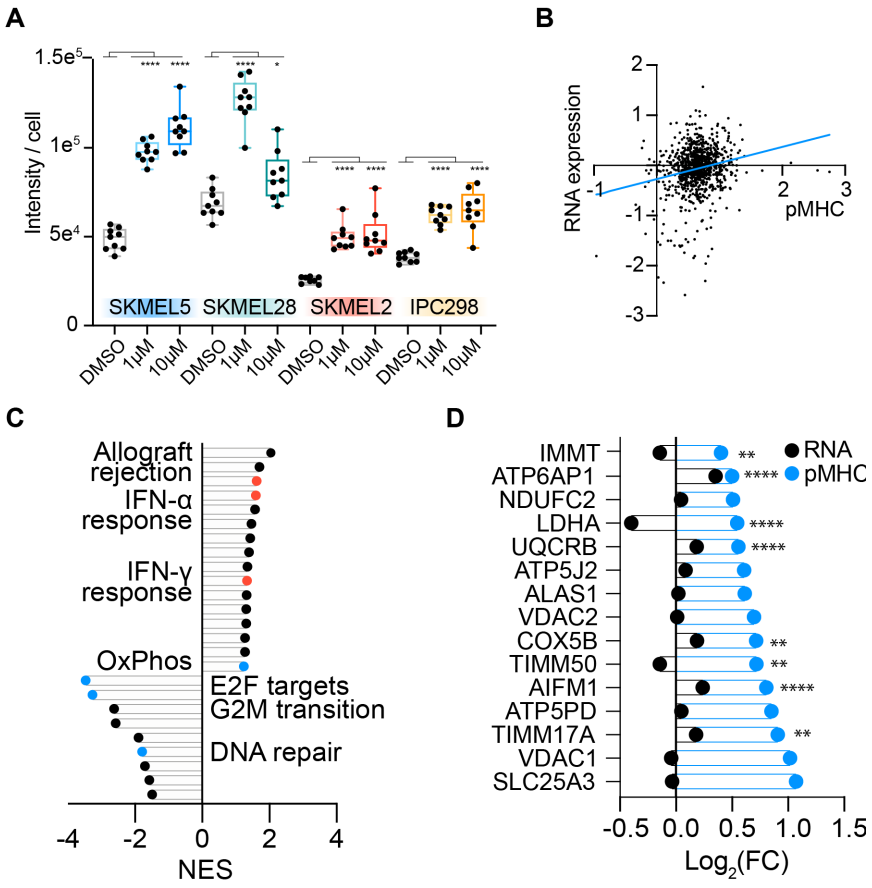

Figure 3-15. *pMHC changes reflect known response to CDK4/6i.* ***A*** *Quantification (n=9) of MitoTraker green intensity normalized to cell number following 72h palbociclib treatment. Data is represented as a box and whiskers plot with whiskers displaying minimum and maximum signal. Significance was determined using Dunnett's multiple comparisons test for each condition vs. DMSO. *p < 0.05, ****p < 0.0001.* ***B*** *Correlation between log_2 fold change (FC) of (palbociclib/DMSO) for RNA expression (y-axis) and pMHC presentation (x-axis) of SKMEL5 cells treated for 72h with 1 μM palbociclib, $r^2 = 0.04$. FC is calculated from the mean intensity of n=3 biological replicates per condition.* ***C*** *Significantly enriched pathways using RNA-seq data (p < 0.05, q < 0.25). Annotated pathways reflect pathways also identified in the immunopeptidome analysis (blue), and those that match with previous reported data (red).*[263] ***D*** *Log_2(FC) for SKMEL5 OxPhos peptides significantly increasing (p < 0.05, blue) with 1 μM palbociclib, and matched log_2(FC) of RNA expression (black). Significant differences in RNA-expression (palbociclib vs. DMSO) is indicated **p < 0.01, ****p < 0.0001 (Wald test, BH adjusted).*

3-2-6 IFN-γ induced pMHC alterations are distinct from palbociclib

Previous work has demonstrated that CDK4/6 inhibition stimulates interferon signaling, augmenting antigen presentation levels.[15] We also observed upregulation of IFN-γ response genes with low-dose palbociclib treatment, as well as increased expression of genes relating to antigen presentation (**Figure 3-16Error! Reference source not found.-A**). Consequently, we tested whether direct IFN-γ stimulation would shift the repertoire similarly to CDK4/6 inhibition. Cells were stimulated with DMSO or 10 ng mL^{-1} IFN-γ for 72h and the resulting pMHC repertoires were quantified using our multiplexed hipMHC platform. IFN-γ increased surface pMHC levels greater than 2x for each cell line (**Figure 3-16-B**), a trend that was reflected in the immunopeptidome, as nearly every identified pMHC increased in presentation with stimulation (**Figure 3-16-C-D**).

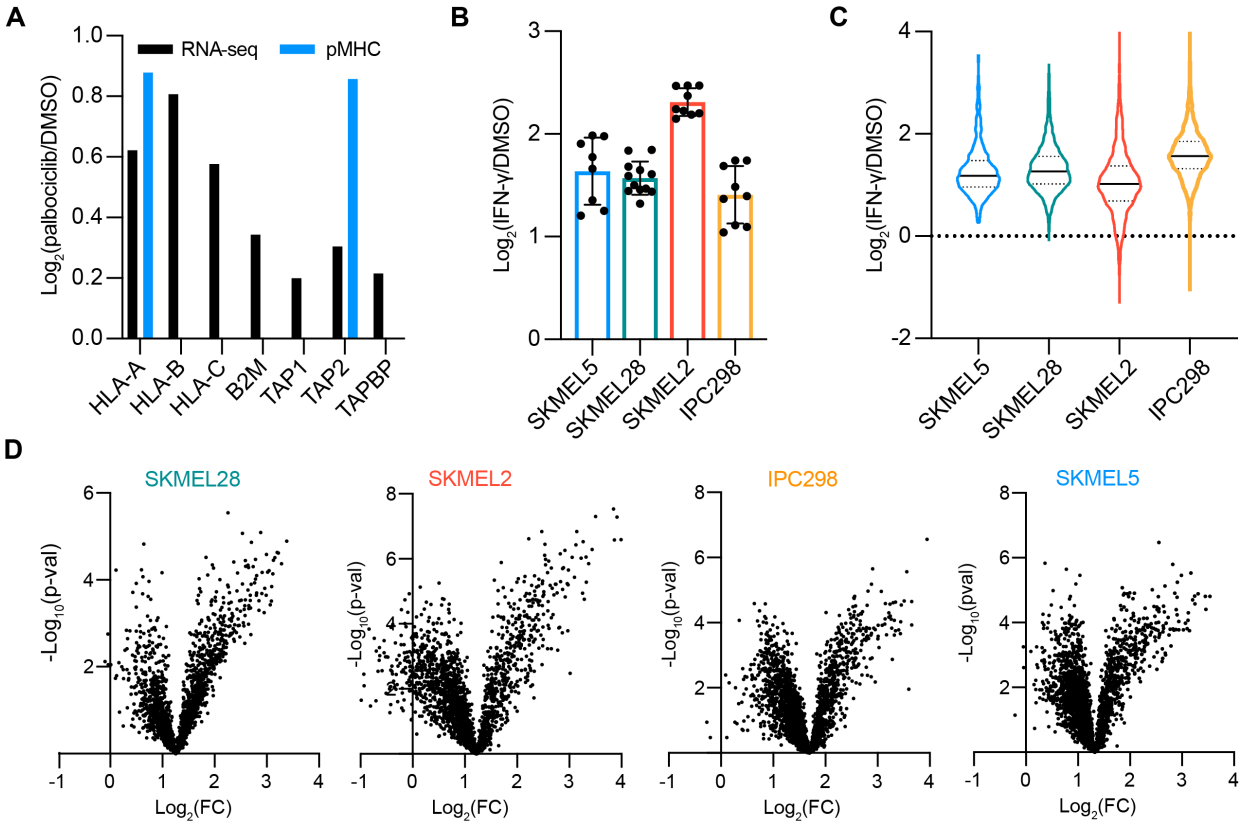

***Figure 3-16**. pMHC repertoire response to IFN-γ. **A** RNA-seq (black) and pMHC (blue) log₂ fold change (FC) of (1 μM Palbociclib/ DMSO), calculated from the mean intensity of n=3 biological replicates per condition, for antigen processing genes. **B** Surface HLA expression via flow cytometry (left) of cells treated with 72h IFN-γ shown as log2(FC) (IFN-γ/DMSO). Errors bars represent +/- SD, biological replicates are n=8, 11, 9, and 9 for SKMEL5, SKMEL28, SKMEL2, and IPC298, respectively. **C** Immunopeptidome log2(FC) (right), dotted lines display quartiles, and mean fold changes (solid line) are 2.42, 2.50, 2.08, and 3.04 for SKMEL5, SKMEL28, SKMEL2, and IPC298 cells, respectively. **D** Volcano plots of the IFN-γ regulated peptides. Data points display the log2 fold change (FC) of IFN-γ stimulated pMHC abundances over DMSO versus significance (mean adjusted p-value, unpaired two-sided t-test).*

To determine the similarity of response to palbociclib treatment, we again performed GSEA against the hallmark gene sets. The most significantly upregulated pathway in SKMEL5 cells with IFN-γ stimulation was the "IFN-γ response," including peptides derived from proteins involved in antigen processing like STAT1 and HLA-A, in line with previous findings (**Figure**

3-17-A,B).[165] In fact, IFN-γ response was the top enriched pathway in every cell line, reiterating that the cellular response to stimulus is reflected in quantitative differences in pMHC presentation, and that IFN-γ related peptides are preferentially upregulated by IFN-γ stimulation (**Figure 3-17-C**). Other pathways such as G2M checkpoint and mitotic spindle were positively enriched in IFN-γ stimulated cells, in contrast to the results of palbociclib treatment.

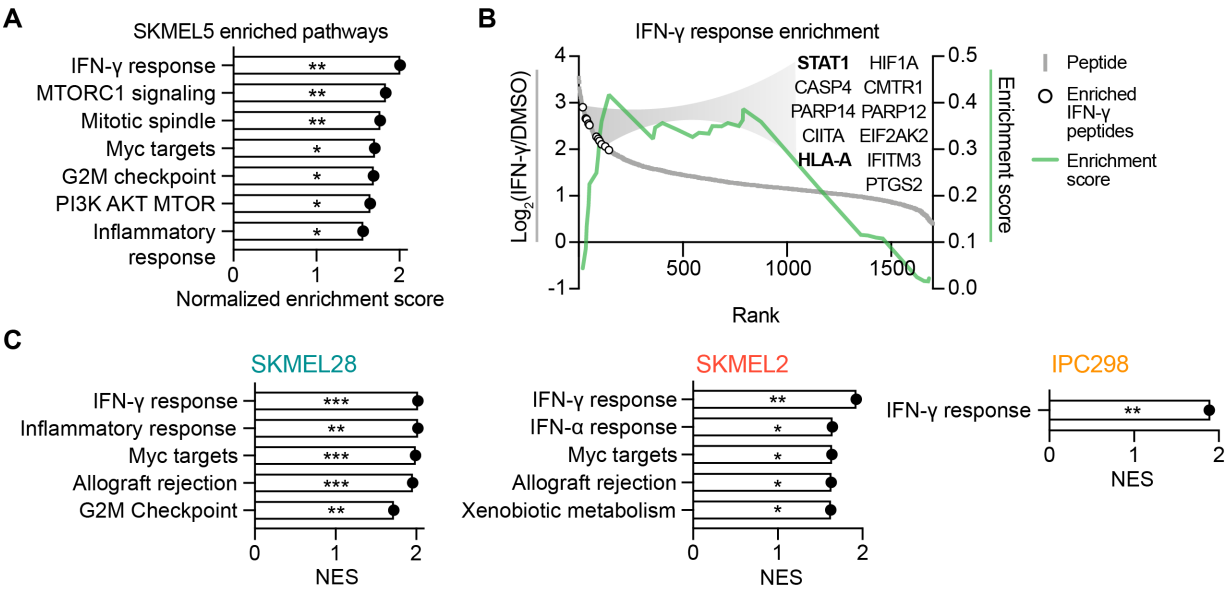

Figure 3-17*. IFN-γ-related pMHCs upregulated following IFN-γ stimulation.* ***A*** *Significantly enriched pathways in SKMEL5 cells with 72h IFN-γ, q < 0.25, *p < 0.05, **p < 0.01.* ***B*** *Enrichment plot of IFN-γ response enrichment in SKMEL5 cells displays running enrichment score (green, right y-axis), and the log₂(FC) (left y-axis) vs. rank (x-axis) for each peptide (grey). Open circles show significantly enriched IFN-γ peptides.* ***C*** *Significantly enriched pathways of IFN-γ stimulated cells. Plots represent normalized enrichment score (NES), q < 0.25, *p < 0.05, **p < 0.01, ***p < 0.001. No pathways were negatively enriched.*

Although the cell lines showed differential pMHC pathway enrichment upon CDK4/6 inhibition with palbociclib and IFN-γ stimulation, we tested whether any pMHCs or source proteins were commonly enriched in response to these perturbations. In SKMEL5 cells we

identified just 20 peptides and 31 source proteins significantly enriched in both conditions (Fig. 6f-g), which primarily map to the cytoplasm and contain multiple ribosomal and translation initiation proteins frequently overrepresented in immunopeptidomic datasets (i.e., DRiPs) (Fig. 6h).[178] These data demonstrate that while CDK4/6 inhibition may induce an IFN-γ response, stimulating cells with IFN-γ does not recapitulate the distinct peptide repertoire alterations observed with palbociclib treatment. Instead, IFN-γ stimulation alters the repertoire by augmenting the presentation of IFN-γ related peptides.

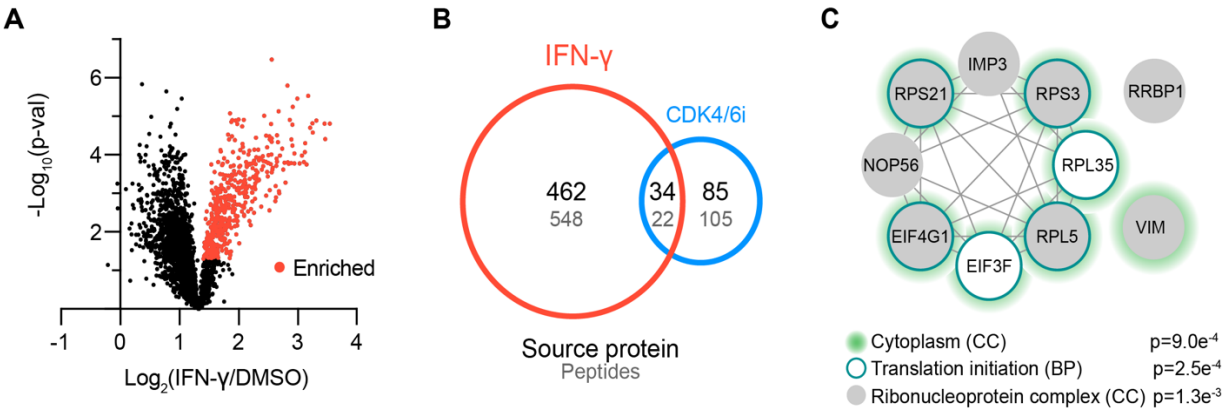

***Figure 3-18**. Minimal overlap in IFN-γ and CDK4/6i induced pMHC changes. **A** Volcano plot of IFN-γ induced changes in SKMEL5 cells. Peptides are presented as the log_2(FC) versus mean adjusted p-value (unpaired two-sided t-test). Red points represent peptides significantly enriched, ($p < 0.05$, fold change > 2.42). **B** Venn diagram of significantly enriched source proteins (black) or peptides (grey) between IFN-γ and 1 μM palbociclib treated SKMEL5 cells. **C** Protein-protein interaction network of significantly enriched source proteins in common, annotated by enriched gene ontology cellular components (CC) and/or biological professes (BP).*

3-3 Discussion

The addition of hipMHCs as internal standards improves relative quantitative accuracy for both LF and multiplexed labeled analyses, though multiplexed labeling with TMT showed superior accuracy and peptide binding specificity and yielded a higher number of quantifiable

unique peptides using equivalent sample input. These internal hipMHC standards, which travel through the entire pMHC workflow, also account for variation across samples and provide an estimate for dynamic range suppression, which varies across peptides. We demonstrate that hipMHC correction alters the biological interpretation of quantitative pMHC repertoire changes, even in a relatively simple, in vitro system. Utilizing hipMHCs will be increasingly beneficial in accounting for variation in sample losses across heterogenous in vivo samples, and in large studies to compare and correct quantitation across many multiplexed analyses or clinical sites. While we use TMT 6-plex in our analyses, this method is compatible with other isobaric labeling strategies, including iTRAQ, TMT 11-plex and TMTpro, to analyze up to 16 samples simultaneously.

For rapid profiling of immunopeptidome changes, we elected to use minimal sample input, making this protocol easily translatable for in vivo-derived tissue (*e.g.*, clinical and animal) samples. While further reductions in sample input mirroring the amount obtained with a 14-gauge needle biopsy[225] resulted in a notable decrease in the number of unique peptides identified (Supplementary Fig. 1F), we believe advancements in the speed and sensitivity of mass spectrometers, as well as in sample preparation techniques to reduce sample losses will enable pMHC profiling at even lower sample inputs in the future. Alternatively, using this same general platform of hipMHCs and isobaric multiplex labeling, the sample amount could be increased and coupled with fractionation for deeper sequencing of the pMHC repertoire, including neoantigen identification.[162]

In addition to improved relative quantification, we also demonstrated the utility of hipMHCs for pMHC absolute quantification by generating an embedded multipoint standard curve. Using targeted mass spectrometry to detect attomole levels of antigen from just $1x10^7$ cells and regressing this signal against the titrated hipMHC standard, we were able to extract accurate absolute quantification in terms of copies per cell for two pMHC's with ~20-fold

difference in abundance. While absolute quantification is limited to just two peptides in this study, applying advanced targeted MS methods could enable the quantitation of hundreds of peptides in a single analysis.[141] The ability to readily determine the absolute quantification of detectable antigens of interest without the need for a pMHC-specific antibody will aid in targeted immunotherapy design. For instance, peptides of lower abundances may be better suited for engineered TCR-based therapies, as TCRs have been shown to be incredibly sensitive with as few as one pMHC complex being capable of initiating detectable T cell activation.[284] Alternatively, antibody-based therapies targeting specific pMHCs, *e.g.*, bi-specific T cell engagers (BiTES) or antibody-drug conjugates (ADCs), may benefit from higher antigen expression levels, though results vary across antigen targets and antibody affinities.[285]

Moreover, absolute quantification of pMHC expression can help to untangle the biological relationships among antigen processing, epitope abundances, immunogenicity, and off-target toxicity (*e.g.*, tumor vs. non-tumor abundance).

It is worth noting that one existing restriction to using hipMHCs is the commercial availability of UV-mediated MHC monomers and ELISA control reagents, which are limited to a handful of common human class I alleles. While matched allele hipMHCs are not required for normalization correction if MHC molecules are isolated using a pan-specific antibody, they are necessary for accurate absolute quantification with embedded standard curves. An analogous technology, disulfide-stabilized HLA molecules, could be used in place of UV-mediated exchange.[286] These HLA-B2M complexes show increased stability and higher exchange efficiency of lower-affinity peptides, potentially eliminating the need for an ELISA to quantify exchange efficiency and simplifying MHC refolding to expand this protocol to other alleles and species.

We applied our quantitative multiplexed hipMHC normalization to determine the pMHC repertoire response to CDK4/6 inhibition with palbociclib treatment in melanoma. These results

indicate that extracellular changes in pMHC abundance are reflective of the intracellular response to CDK4/6 inhibition. Moreover, palbociclib treatment increased the presentation of TAAs and peptides derived from metabolic processes. Recently, high tumor antigen and metabolic protein expression levels have been shown to be predictive of checkpoint inhibitor response in melanoma, suggesting that palbociclib could be used in conjunction with checkpoint blockade or TIL-based therapies to increase tumor immunogenicity.[287] As an alternate therapeutic strategy, peptide antigens whose surface expression was selectively increased by palbociclib could be utilized for targeted immunotherapy, either alone or in combination.

Indeed, the landscape of clinical trials exploring combination treatment regimens coupling checkpoint blockade with other therapies is rapidly expanding.[43,288,289] Quantifying the molecular consequences of these combination regimes with our platform could provide insight into these trials and enable the informed design of new therapeutic combinations, potentially with targeted immunotherapies. Taken together, our relative and absolute quantitative immunopeptidomic data demonstrate the utility of quantitative immunopeptidomics in evaluating the pMHC repertoire response to therapy. The multiplexed nature of this platform allows for analyses of many samples in a short timescale, an important feature in the context of clinical trials. Further analyses of pMHC repertoire changes will be useful in understanding the order and timing of therapies to achieve optimal success and may enable predictions as to how to tune the immunopeptidome to be most applicable to immunotherapy targeting.

3-4 Materials and methods

3-4-1 Human cell lines

SKMEL5, SKMEL28, and MDA-MB-231 cell lines were obtained from ATCC [ATCC HTB-70, ATCC HTB-72, and HTB-26, respectively] and maintained in DMEM medium (Corning). IPC298 and SKMEL2 cells were provided by Array Biopharma and maintained in RPMI 1640 (Gibco) and MEM-α (Gibco) mediums, respectively. All medium was supplemented with 10% FBS (Gibco) and 1% penicillin/streptomycin (Gibco). Cells were routinely tested for mycoplasma contamination, and maintained in 37 °C, 5% CO_2.

3-4-2 Phenotypic assays

Half-maximal inhibitory concentrations (IC_{50}) of palbociclib (Selleckchem, PD-0332991) were determined for each cell line using CellTiter-Glo luminescent cell viability assay (Promega). Cells were seeded at density of 10,000 (SKMEL2, SKMEL28, IPC298) or 5,000 (SKMEL5) cells/well in a 96 well plate and allowed to adhere overnight. Cells were then treated with palbociclib or DMSO as a vehicle control in fresh medium for 72h and assayed. Data was acquired using a Tecan plate reader Infinite 200 with Tecan icontrol version 1.7.1.12. IC_{50} values were calculated using a 4-parameter logistic curve in Prism 8.4.1.

Mitochondrial content was measured using a fluorescent mitochondrial stain. Cells were seeded at a density of 20,000 cells per well in a 24 well plate and allowed to adhere overnight. Cells were then treated with 1 µM or 10 µM palbociclib or DMSO vehicle control in fresh medium for 72h. Cells were assayed by incubating 200 nM of MitoTracker Green FM (Thermo Scientific) and a 1:1000 dilution of NuclearID Red DNA stain (Enzo Life Biosciences) for 15 minutes in serum free medium at 37 °C. After staining medium exchange, cells were imaged and analyzed using the Incucyte live cell analysis system (IncuCyte Zoom version 6.2.9200.0,

Essen BioScience). The integrated intensity of MitoTracker dye was calculated for each image (n=3 experimental replicates, n=3 images per sample) and divided by the number of cells (counted using Nuclear counterstain) to determine the mitochondrial intensity per cell. A one-way ANOVA followed by Dunnett's multiple comparisons statistical test was performed in Prism to compare significance of treated cells versus vehicle DMSO control. Significance values represent multiplicity-adjusted p-values.

3-4-3 Flow cytometry

For analysis of cells by flow cytometry, cells were lifted with 0.05% Trypsin-EDTA and 10^6 cells/mL were spun at 300 g for 3 minutes, washed with ice cold PBS supplemented with 1% FBS and 0.1% sodium azide (flow buffer) and incubated with fluorophore-conjugated antibody at 0.5 µg mL^{-1} in flow buffer for 30 minutes on ice. After incubation, cells were washed again, and resuspended in flow buffer plus 5 µL of propidium iodide staining solution (10 µg mL^{-1}, Invitrogen) per sample. Analyses were performed on an LSRII (BD Biosciences) and data analyzed using FlowJo (version 10.6.2). All antibodies were purchased from Biolegend: Alexa Fluor 488 HLA-A, B, C, clone W6/32 [cat # 311413], Alexa Fluor 488 anti-H2A.X Phospho (Ser139), clone 2F3 [cat # 613406]. The gating strategy used for all experiments is provided in **Supplementary Figure 3-7**.

3-4-4 UV-mediated peptide exchange for hipMHCs

UV-mediated peptide exchange was performed using recombinant, biotinylated Flex-T HLA-A*02:01 monomers (BioLegend), using a modified version of the commercial protocol. Briefly, 4 µL of 500 µM peptide stock, 2 µL of Flex-T monomer, and 32 µL of 1X PBS were combined in a 96-well U bottom plate. On ice, plates were illuminated with ultraviolet light (365

nm) for 30 minutes, followed by a 30 minute incubation at 37 °C protected from light. Concentration of stable complexes following peptide exchange was quantified using the Flex-T HLA class I ELISA assay (Biolegend) per manufacturer's instructions for HLA-A*02:01. ELISA results were acquired using a Tecan plate reader Infinite 200 with Tecan icontrol version 1.7.1.12.

3-4-5 Peptide MHC isolation

Cultured cells were seeded in 10 cm plates, allowed to adhere overnight, and treated for 72h with palbociclib, 10 ng mL^{-1} human recombinant IFN-γ (ProSpec Bio), or DMSO vehicle control. At the time of harvest, cells were washed with 1x PBS, and lifted using 0.05% Trypsin-EDTA (Gibco). Cells were pelleted at 500 g for 5 minutes, washed twice more in 1x PBS, and pelleted again. Cells were resuspended in 1 mL lysis buffer [20 nM Tris-HCl pH 8.0, 150 mM NaCl, 0.2 mM PMSO, 1% CHAPS, and 1x HALT Protease/Phosphatase Inhibitor Cocktail (Thermo Scientific)], followed by brief sonication (3 x 10 second microtip sonicator pulses) to disrupt cell membranes. Lysate was cleared by centrifugation at 5000 g for 5 minutes and quantified using bicinchoninic acid protein assay kit (Pierce).

Peptide MHCs were isolated from $1x10^7$ cells per condition with immunoprecipitation (IP) and size exclusion filtration, as previously described.[169] Briefly, for each condition 0.5 mg of pan-specific anti-human MHC Class I (HLA-A, HLA-B, HLA-C) antibody (clone W6/32, Bio X Cell [cat # BE0079]) was bound to 20 µL FastFlow Protein A Sepharose bead slurry (GE Healthcare) for 3 hours rotating at 4 °C. Beads were washed 2x with IP buffer (20 nM Tris-HCl pH 8.0, 150 mM NaCl) prior to lysate and hipMHC addition, and incubated rotating overnight at 4 °C to isolate pMHCs. Beads were washed with 1x TBS and water, and pMHCs were eluted in 10% formic acid for 20 minutes at room temperature (RT). Peptides were isolated from antibody and MHC

molecules using a passivated 10K molecule weight cutoff filters (PALL Life Science), lyophilized, and stored at -80 °C prior to analysis.

3-4-6 pMHC labeling with Tandem Mass Tags and SP3 cleanup

For labeled analyses, 100 µg of pre-aliquoted Tandem Mass Tag 6-plex (TMT) was resuspended in 30 µL anhydrous acetonitrile, and lyophilized peptides were resuspended in 100 µL 150 mM triethylammonium bicarbonate, 50% ethanol. Both were gently vortexed, centrifuged at 13,400 g for 1 minute, and combined. TMT/peptide mixtures were incubated on a shaker for 1 hour at RT, followed by 15 minutes of vacuum centrifugation. After combining labeled samples, we washed tubes 2x with 25% acetonitrile (MeCN) in 0.1% acetic acid (AcOH) and added it to the labeled mixture, which was subsequently centrifuged to dryness.

Sample cleanup was performed using single-pot solid-phase-enhanced sample preparation (SP3) as previously described.[290] Briefly, a 1:1 mix of hydrophobic/hydrophilic Sera-mag carboxylate-modified speed beads (GE Healthcare) was prepared at a final bead concentration of 10 µg μL^{-1}. Labeled samples were resuspended in 30 µL of 100 mM ammonium bicarbonate (pH 7-8) and added to 500 µg of bead mix with 1 mL MeCN. Peptides were allowed to bind for 10 minutes at RT, washed 2x with MeCN, and eluted with 2% DMSO for 1 minute of sonication in a bath sonicator. TMT-labeled peptides were transferred to a fresh microcentrifuge tube and centrifuged to dryness.

3-4-7 Synthetic peptide standards

Heavy leucine-containing peptides were synthesized at the MIT Biopolymers and Proteomics Lab using standard Fmoc chemistry using an Intavis model MultiPep peptide synthesizer with HATU activation and 5 µmol chemistry cycles. Starting resin used was Fmoc-

Amide Resin (Applied Biosystems). Cleavage from resin and simultaneous amino acid side chain deprotection was accomplished using: trifluoroacetic acid (81.5% v/v); phenol (5% v/v); water (5% v/v); thioanisole (5% v/v); 1,2-ethanedithiol (2.5% v/v); 1% triisopropylsilane for 1.5 hr. Standard Fmoc amino acids were procured from NovaBiochem and Fmoc-Leu ($^{13}C_6$, ^{15}N) was obtained from Cambridge Isotope Laboratories.

Peptides were quality controlled by mass spectrometry and reverse phase chromatography using a Bruker MiroFlex MALDI-TOF and Agilent model 1100 HPLC system with a Vydac C18 column [300 angstrom, 5 micron, 2.1 x 150 mm] at 300 μL/min monitoring at 210 and 280 nm with a trifluoroacetic acid/ H_2O/MeCN mobile phase survey gradient. All peptides contain c-terminal amidation, with the exception of the BCAP31 and DDX5 peptides used for absolute quantification. For amidated peptides, we observe c-terminal amidation and c-terminal carboxyl groups on peptides synthesized with an amide group. Therefore, both are considered in downstream analyses.

3-4-8 RNA sequencing

RNA was isolated from 10 cm plates of SKMEL5 cells with 3 biological replicates per condition. Prior to harvest, cells were washed with ice-cold 1X PBS over ice and lysed in TRIzol reagent (Thermo Fisher Scientific). Total RNA was isolated from each sample using Direct-zol RNA miniprep kit (Zymo Research) according to manufacturer's instructions.

RNA were confirmed for quality using the Agilent Fragment Analyzer and 300 ng of material was polyA-selected using NEBNext Poly(A) mRNA Magnetic Isolation Module (E7490) modified to include two rounds of polyA binding and 10 minute incubations. cDNA was generated using the NEB Ultra II directional kit (E7760) following manufacturers protocol using 12 cycles of PCR and an 0.9X SPRI clean. The resulting libraries were quality assessed using

the Fragment Analyzer and quantified by qPCR prior to be sequenced on the Illumina HiSeq2000. The 40nt single-end reads with an average depth of 5 million reads per sample were sequenced for all conditions.

RNAseq reads were aligned to the human transcriptome prepared with the hg38 primary assembly and the Ensembl version 95 annotation using STAR version 2.5.3a.[291] Gene expression was summarized with RSEM version 1.3.0 and SAMtools version 1.3.[292,293] Differential expression analysis was performed with DESeq2 version 1.24.0 running under R version 3.6.0 with normal log fold change shrinkage.[294] Significance values (adjusted p value) are determined using the Wald test, and are multiple hypothesis corrected using Benjamini-Hochberg (BH) method. The resulting data were parsed and assembled using Tibco Spotfire Analyst version 7.11.1.

3-4-9 Mass spectrometry data acquisition

For MS analysis, peptides were resuspended in 0.1% acetic acid and loaded on a precolumn packed in-house (100 µm ID × 10 cm packed with 10 µm C18 beads (YMC gel, ODS-A, 12 nm, S-10 µm, AA12S11)). The precolumn was then washed with 0.1% acetic acid and connected in series to an analytical capillary column with an integrated electrospray tip (~1 µm orifice) with 5µM C18 beads, prepared in house ((50 µm ID × 12 cm with 5 µm C18 beads (YMC gel, ODS-AQ, 12 nm, S-5 µm, AQ12S05)).

Peptides were eluted using a 130 minute gradient with 10-45% buffer B (70% Acetonitrile, 0.2M acetic acid) from 5-100 minutes and 45-55% buffer B from 100-120 minutes at a flow rate of 0.2 mL/min for a flow split of approximately 10,000:1. Peptides were analyzed using a Thermo Q Exactive HF-X Hybrid Quadrupole-Orbitrap mass spectrometer, and data was acquired using Thermo Fisher Scientific Xcalibur version 2.9.0.2923. Standard mass

spectrometry parameters were as follows: spray voltage, 2.5 kV; no sheath or auxiliary gas flow; heated capillary temperature, 250 °C.

The HF-X was operated in data-dependent acquisition (DDA) mode for LF and TMT analyses. LF: Full-scan mass spectrometry spectra (mass/charge ratio (*m/z*), 350 to 2,000; resolution, 60,000) were detected in the Orbitrap analyzer after accumulation of ions at $3e^6$ target value with a maximum IT of 50 ms. For every full scan, the top 20 most intense ions were isolated (isolation width of 0.4 *m*/*z*) and fragmented (collision energy (CE): 28%) by higher energy collisional dissociation (HCD) with a maximum injection time of 300 ms, AGC target $1e^5$, and 60,000 resolution. Charge states < 2 and > 4 were excluded, and dynamic exclusion was set to 30 seconds. TMT: Full-scan mass spectrometry spectra (mass/charge ratio (*m/z*), 400 to 2,000; resolution, 120,000) were detected in the Orbitrap analyzer after accumulation of ions at $3e^6$ target value with a maximum IT of 50 ms. For every full scan, the 20 most intense ions were isolated (isolation width of 0.4 *m*/*z*) and fragmented (collision energy (CE): 29%) by higher energy collisional dissociation (HCD) with a maximum injection time of 350 ms, AGC target $1e^5$, and 30,000 resolution. Charge states < 2 and > 4 were excluded, and dynamic exclusion was set to 60 seconds. To ensure fragmentation of normalization standards, one fraction may be analyzed using targeted selected ion monitoring (t-SIM) used in tandem with DDA with an inclusion list of hipMHC standards. For absolute quantification, the HF-X was operated in DDA mode with inclusion list enabled. Parameters mirror those of the TMT DDA method, with several exceptions. Full scan mass spectra m/z range: 300-1200, maximum MS2 injection time 200 ms, only charge states of 2 and 3 were considered. Inclusion list masses and charge states are located in (**Table 3-1**).

3-4-10 Mass spectrometry search space and filtering

All mass spectra were analyzed with Proteome Discoverer (PD, version 2.2) and searched using Mascot (version 2.4) against the human SwissProt database. No enzyme was used, and variable modifications included oxidized methionine for all analyses and phosphorylated serine, threonine, and tyrosine for cell treatment analyses. Treatment analyses were also searched against a previously published catalog of over 40,000 predicted antigenic mutations in cancer cell lines.[295] Heavy leucine-containing peptides were searched for separately with heavy leucine (+7), c-terminal amidation, and methionine oxidation as dynamic modifications against a custom database of the synthetic peptide standards. All analyses were filtered with the following criteria: search engine rank =1, isolation interference ≤ 30%, and length between 8 and 15 amino acids. Label-free analyses were filtered with ion score ≥ 20, and labeled samples were filtered with ion score ≥ 15 and percolator q-value ≤ 0.05. Area under the curve (AUC) quantitation was performed using the minora feature detector in PD with match between runs enabled and filtered for ion score ≥ 20. For targeted, absolute quantification analyses, total ion count (TIC) values for each scan and peak intensities were extracted using Skyline (version 19.1.0.193).[139]

3-4-11 Mass spectrometry data analysis with hipMHC correction

For LF analyses, correction parameters were determined by calculating the ratio of AUC intensities in each sample against a reference sample and taking the mean across hipMHCs. For TMT-labeled samples, ratios against a reference channel (usually TMT126) were calculated and the median of all ratios for correction hipMHCs was used to determine the final correction parameters. Only PSMs of heavy leucine-coded peptides with an average reporter ion intensity within 10-fold of the interquartile range of endogenous PSM reporter ion intensities were used for correction, as we observed drift in the correction factors when PSM TMT intensities were

well beyond endogenous levels. For absolute quantification analyses, correction factors were generated as described for TMT analyses, and used to normalize maximum peak intensity values for DDX5 and BCAP31. Notably, with mean fold changes greater than 2x between samples (ex. IFN-γ stimulation), in our hands hipMHCs are no longer able to correct between conditions despite narrow isolation window (0.4 m/z). This inaccuracy may be due to co-isolation, as the calculated correction factors reflect median fold-changes of endogenous peptides. In this case, we generated correction factors for each treatment condition separately.

Correction factors were applied to AUC values in label-free analyses for all peptides that were quantifiable across samples. For labeled samples, ion intensities of PSMs for each unique peptide across analyses of the same sample were summed, after which normalization factors were applied. To evaluate differences between conditions, the $\log_2$ transformed ratio of arithmetic mean intensity for drug- and DMSO-treated samples (n=3) was calculated. To determine if peptides were significantly increasing, an unpaired, 2-sided t-test was performed, and peptides with $p \leq 0.05$ were considered significantly increasing. To evaluate which peptides were significantly enriched above the mean, treated samples were mean centered by dividing the ion intensity of each peptide by the mean fold-change across all peptides, after which a student's 2-tailed t-test was performed on adjusted values. Peptides with a mean-adjusted p-value ≤ 0.05 were considered significantly enriched. Mean centering was not performed on samples where the mean $\log_2$ fold change was between -0.07 and 0.07. Data analyses were performed using Matlab version R2019b, and Microsoft Excel version 16.34.

3-4-12 Peptide MHC binding affinity

Binding affinity of pMHCs was estimated using NetMHCpan-4.0 against each cell line's allelic profile (Supplementary Fig. 3k).[99,280] Only 9-mers were evaluated, and the minimum

predicted affinity (nM) of each peptide was used to assign peptides to their best predicted allele. The threshold for binding was set to 500 nM. Binding motifs for the alleles were generated using 9-mers with predicted affinity < 500nM, and visualized using WebLogo 2.8.2.[296] To estimate the proportion of peptides predicted to be binders by chance, 10 sets of 2,000 random 9-mers were created by selecting with equal probability any amino acid (aa) more than 8aa from a protein C-terminus as a start site from human proteins in SwissProt version 2019_2, and binding affinity prediction was performed against the alleles of MDA-MB-231 cells. Data presented in Fig. 2d is a representative example.

3-4-13 Enrichment analyses

For pMHC pathway enrichment analyses, gene names from peptide source proteins were extracted and rank ordered according to the average $\log_2$ fold change over DMSO treated cells. In cases where more than one peptide mapped to the same source protein, the maximum/minimum was chosen, depending on the directionality of enrichment analysis. For RNAseq data, gene sets were rank ordered according to the mean $\log_2$ fold change value with only protein encoding genes considered. We utilized gene set enrichment analysis (GSEA) 4.0.3 pre-ranked tool against the Molecular Signatures Database hallmarks gene sets with 1000 permutations, weighted enrichment statistic (p=1), and a minimum gene size of 8 for pMHC analyses and 15 for RNAseq.[255,281,282] Results were filtered for FDR q-value ≤ 0.25, and nominal p-value ≤ 0.05.

Significantly enriched peptides (mean-adjusted p-value ≤ 0.05) were analyzed using STRING v11 for Gene Oncology (GO) term enrichment against biological processes and cellular components datasets.[256,297] Enriched categories were filtered according to FDR-q value ≤ 0.05.

3-4-14 Data availability

RNA-sequencing data have been deposited into the NCBI Gene Expression Omnibus (GSE144373). The mass spectrometry proteomics data have been deposited to the ProteomeXchange Consortium via the PRIDE partner repository with the dataset identifier PXD017407.

3-5 Acknowledgements

We thank Array Biopharma for providing melanoma cell lines; Cristine Devlin and Michael Birnbaum for providing recombinant MHC monomers; Joe Card (Marto lab, Dana-Farber) for kindly providing guidance on the SP3 protocol; the MIT BioMicro Center (Stuart Levine) and the Swanson Biotechnology Center for technical support, specifically the Flow Cytometry (Glenn Paradis), Biopolymers & Proteomics (Richard Cook & Antonius Koller), and the Barbara K. Ostrom (1978) Bioinformatics (Charlie Whittaker) core facilities.

3-6 Supplementary Information

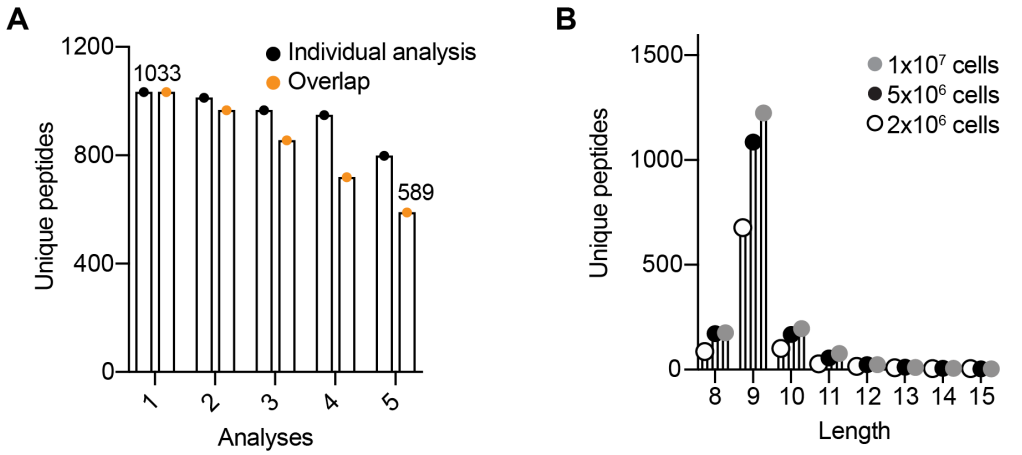

Supplementary Figure 3-1. A *LF analyses (n=5 technical replicates) of MDA-MB-231 cells show poor overlap of quantifiable peptides observed across multiple analyses (orange) compared to the number of peptides identified in any given single analysis (black).* ***B*** *Number of unique peptides identified using different amounts of MDA-MB-231 cells as sample input. Values represent a single analysis using 20% of the peptide elution.*

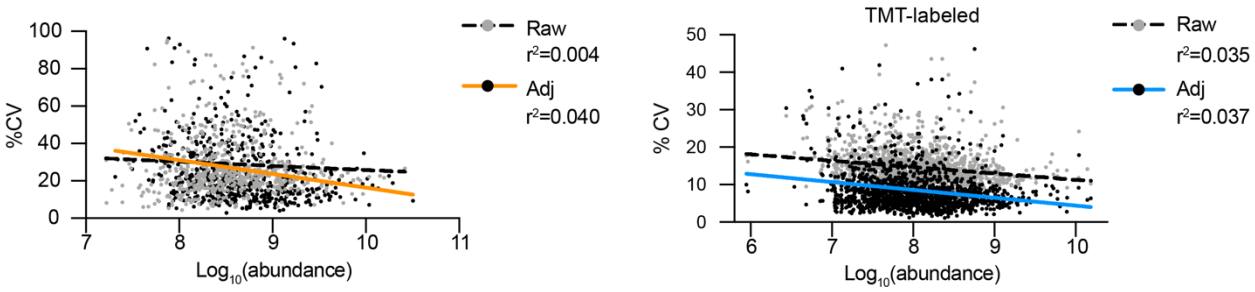

Supplementary Figure 3-2. *Correlation of each peptide's coefficient of variation (CV) versus abundance for LF (left) and TMT-labeled (right) analyses.*

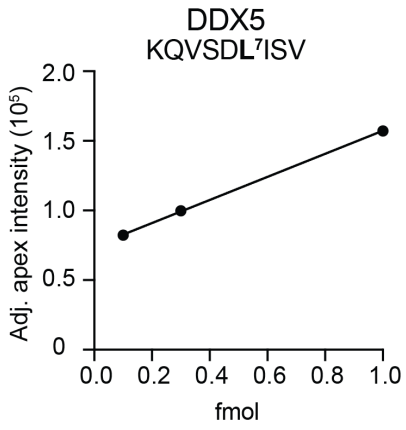

Supplementary Figure 3-3. *Calibration curve of the DDX5 peptide (KLDVGNAEV) added into 1x107 MDA-MB -231 cells from 0.1 fmol to 1 fmol. 0.1 fmol corresponds to ~6 copies per cell.*

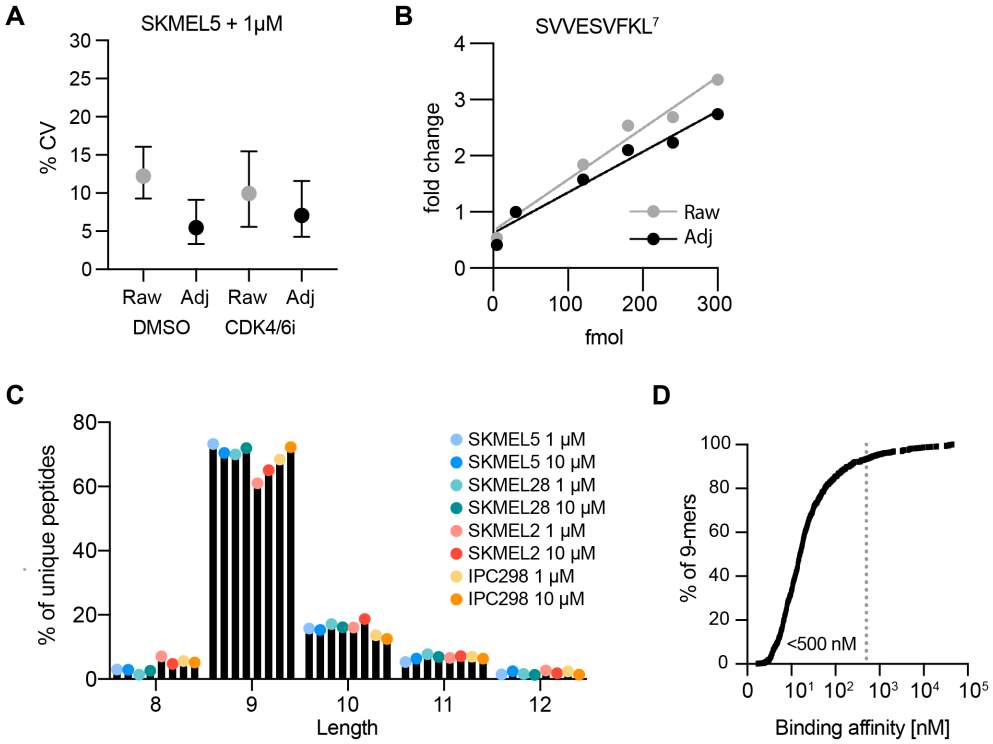

Supplementary Figure 3-4. A *Applying hipMHC correction factors decreases the coefficient of variation in both DMSO and 1 µM palbociclib SKMEL5 cells, where data are presented as mean values +/- SD for n=3 biological replicates.* ***B*** *The titrated peptide, SVVESVFKL, displays 3.6x dynamic range suppression.* ***C*** *Length distribution of peptides identified in each cell line and treatment. Data is represented as % of total peptides identified.* ***D*** *Predicted binding affinity of 9-mer peptides in SKMEL5 cells with DMSO or 1 µM palbociclib. 93.3% have a predicted affinity of <500 nM.*

	HLA-A	HLA-B	HLA-C
SKMEL5	02:01 11:01	40:01 07:02	03:04 07:02
SKMEL28	11:01	40:01	03:04
IPC298	24:02 03:01	07:02 35:02	04:01 07:02
SKMEL2	26:01 03:01	38:01 35:08	04:01 12:03

Supplementary Figure 3-5. *Class I allelic profiles of each cell line.*

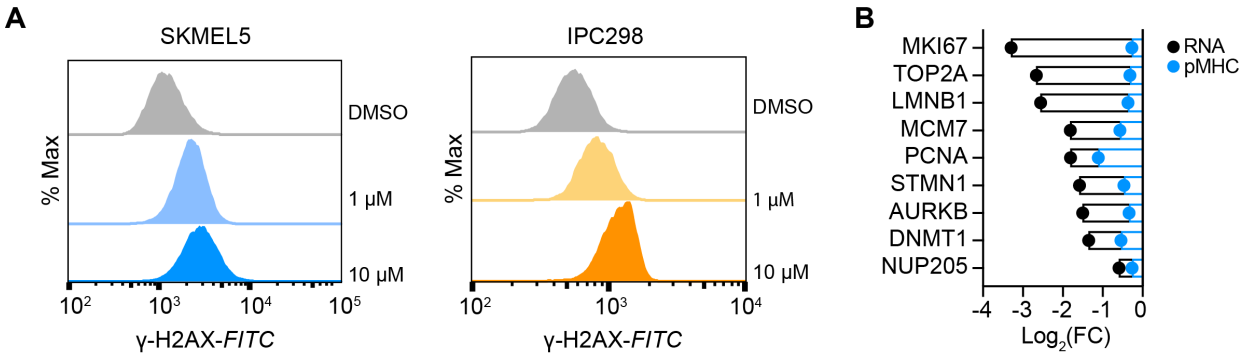

Supplementary Figure 3-6. A *Histogram of γ-H2AX levels determined by flow cytometry in cells treated with DMSO or 1 μM / 10 μM palbociclib for 72h. Data is represented as % of maximum signal, and results are representative of those obtained in a second independent experiment.* ***B*** *Log_2 fold change (FC) for SKMEL5 E2F peptides significantly decreasing in presentation (blue) with 10 μM palbociclib for 72h and matched RNA expression of SKMEL5 cells treated with 1 μM palbociclib for 72h (black). Immunopeptidomics and RNA-sequencing experiments each contained n=3 biological replicates for each condition. RNA sequencing was not performed on SKMEL5 cells treated with 10 μM palbociclib.*

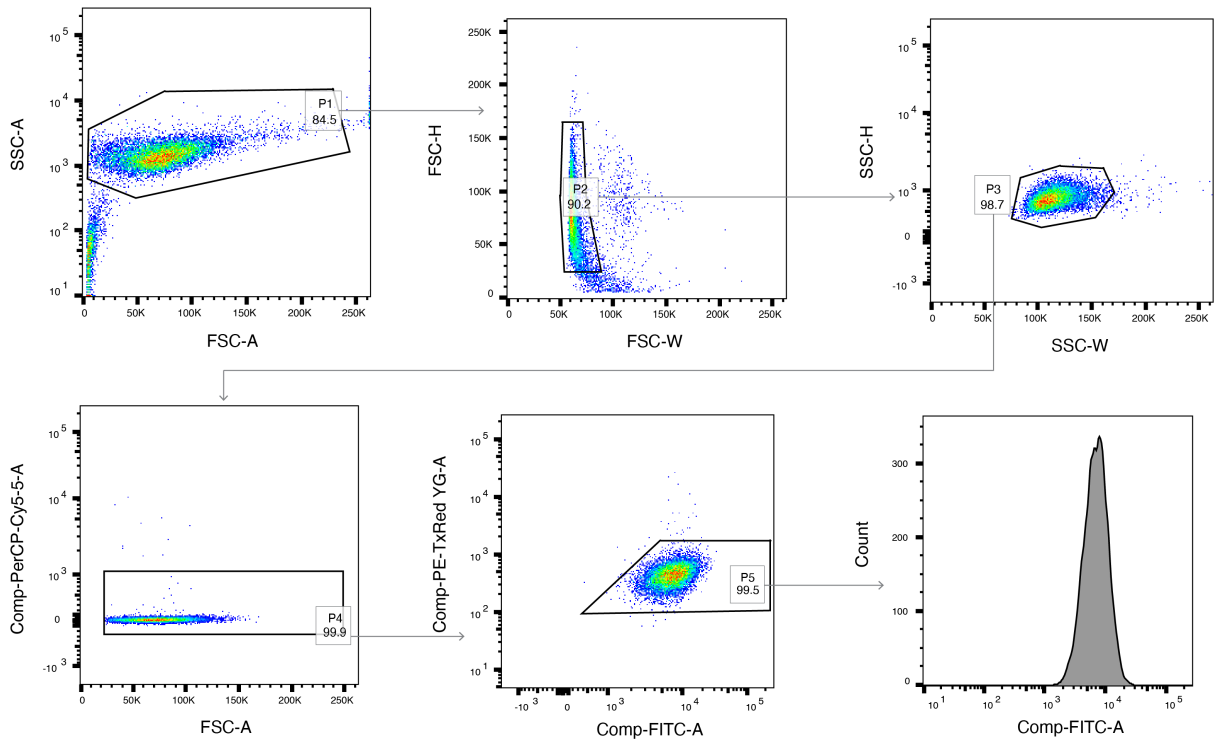

Supplementary Figure 3-7. *Gating strategy for all flow cytometry experiments. FSC-A/SSC-A gating was used to eliminate debris, and doubles were discarded with FSC-W/FSC-H gating followed by SSC-W and SSC-H gating. Living cells were gated by propidium iodide exclusion using FSC-A/PerCP-CY5-5A. FITC positive cells were gated against TX-red, using unstained cells to distinguish FITC positive vs. FITC negative cells.*

Tables

Table 3-1. *Peptides used for hipMHCs. L7 denotes heavy isotope labeled peptides with heavy leucine (+7), N denotes amidated peptides.*

m/z	charge	peptide
723.9510	2	DDX5
701.9200	2	BCAP31
727.4596	2	DDX5-L7
705.4276	2	BCAP31-L7
615.3600	2	SLPEE
615.8540	2	SLPEE-N
631.8960	2	ALNE-N
632.3890	2	ALNE

CHAPTER 4: MEK inhibition enriches TAA presentation in NRAS/BRAF mutant melanomas

4-1 Introduction

4-1-1 MAPK pathway mutation are key drivers in melanoma

Melanomas arise from melanocytes, neural crest-derived cells that produce pigment, and are found in the skin, eyes, and other tissues throughout the body.[298] Many different phenotypes of melanomas exist, but the most common cutaneous melanomas are categorized into two groups: chronically sun damaged (CSD) or non-CSD melanomas. UV rays are known to damage DNA in cells, resulting in gene mutations that are responsible for unchecked proliferation of melanocytes leading to cancer metastasis. Non-CSD melanomas may be due to a combination of factors including environmental and genetic influences. While melanomas account for less than one percent of skin cancer diagnoses, melanomas are responsible for the majority of skin cancer deaths.[299] In the past, melanomas were treated with traditional chemotherapeutics including Dacarbazine, but achieved limited success due to low object response rates of ~20% and minimal impact on progression free survival (PFS).[300]

In 2002, the Cancer Genome Project/Sanger Institute identified an activating mutation in the serine/threonine BRAF kinase in ~50% of melanoma patients, thereby revolutionizing the course of treatment strategies by enabling targeted therapeutic-based approaches. The identified mutation was a single amino acid substitution, switching a valine (V) to glutamic acid (E) at position 600 (e.g., V600E) in the BRAF kinase, a kinase present in the MAPK pathway.[301] Signaling through the MAPK pathway (i.e., Ras-Raf-MEK-ERK pathway) is critical for regulating the balance between melanocyte proliferation, differentiation, and survival, and dysregulation

occurring through mutations or other mechanisms can drive oncogenesis. While BRAF mutations at codon 600 are the most common, occurring in over 90% of reported instances, other RAF mutations have been implicated as oncogenic drivers, allowing for unchecked growth independent of upstream stimulation.[302] The V600E mutation occurs on the activation loop of the BRAF kinase domain, locking BRAF into a constitutively active position, leading to hyper-activation of the MAPK pathway as BRAF become insensitive to negative feedback and regulation.[303] Other reported mechanisms of BRAF mutations implicated in melanoma progression include evasion of apoptosis and sentences, unchecked proliferation & migration, metastasis, as well as angiogenic and invasive phenotypes.[304]

The second most common activating mutation occurs in NRAS, a small GTPase, which is mutated in ~20% of patients.[305] NRAS mutations typically increase the ratio of active GTP-bound RAS to the inactive GDP-bound RAS, leading to constitutive activation of downstream pathways that drive amplified proliferation and migration, and can give rise to therapeutic resistance. While a variety of mutations have been reported, over 80% frequently occur at codon 61 (Q61K).[306307] Active NRAS also stimulates the MAPK pathway, along with the phosphatidylinositol 3-inase (PI3K/ protein kinase B (AKT) signaling pathways. While melanoma patients are typically stratified into the BRAF mutant, NRAS mutant, and wild type populations, it should be noted that other subgroups exist, including ~10% with a loss of PTEN which activates PI3K/AKT and 12% with a NF1 mutation, a negative regulator of RAS[308–310]. With a vast majority of patients harboring MAPK pathway mutations, much attention has been put into developing kinase inhibitors of mutant BRAF and downstream nodes such as MEK and ERK.

4-1-2 Targeting MAPK driver mutations in BRAF mutant melanoma

FDA approved BRAF small molecule kinase inhibitor therapies such as vemurafenib and dabrafenib both target V600E BRAF mutations by binding to the ATP pocket, and obstructing

BRAF activation which causes decreased proliferation and increased apoptosis in cell lines, along with tumor growth delay in mouse studies.[311,312] Both of these compounds have shown impressive ~50% response rates in clinical trials for BRAF mutant patients with median PFS of 5.1 to 5.3 months, and a median overall survival of 13.6 months.[313] MEK inhibitor (MEKi) monotherapies such as trametinib had a lower response rate, though still an improvement over standard chemotherapy with PFS times of 4.8 months vs. 1.5 months.[314] In BRAF patients, intrinsic resistance is rare (~10% of patients), but acquired resistance is almost universal with the majority of patients developing resistance within ~6 months of BRAF inhibitor (BRAFi) treatment.[315] Similarly, 70% of MEKi monotherapy patients experienced disease progression within a year.[313]

Many studies have investigated the resistance mechanisms associated with BRAF mutant melanoma patients on BRAF or MEK inhibitors, reactivation of ERK through NRAS mutations, or loss of the RAS suppressor NF1. Additionally, overexpression or mutation of MEK activators such as CRAF and COT have been shown to bypass BRAF inhibition.[313,316] Reactivation of the MAPK pathway through other receptor tyrosine kinases (RTKs) like PDGFR, MET, IGF-1R, and EGFR is found in relapsed melanomas as well.

Activation of alternative signaling networks or reactivation of the MAPK pathway has prompted combination treatment with BRAF and MEK inhibitors in the hopes of delaying MAPK-driven acquired resistance and to extend response rates. Dabrafenib and trametinib was the first combination in clinical trials, and phase II data yielded a PFS of 9.4 months on BRAFi/MEKi vs. 5.8 months for patients on dabrafenib monotherapy.[19,314] Two subsequent phase III trials gave similarly encouraging results, with median PFS of ~11 months in both trials on the combination treatment, versus 7-8 months on dabrafenib monotherapy.[317,318] Overall response rates also improved with combination therapy versus monotherapy, at ~70% versus ~50%, respectively. Intriguingly, sequential dosing with MEKi following progression on a BRAFi was not

a beneficial strategy, yielding a PFS of only 1.8 months, suggesting the dosing sequences is a critical for therapeutic efficacy.[319]

While several other trials have been performed over the past decade with different MEK and BRAF inhibitors[320], the best results to date were reported from the Phase III COLUMBUS trial combining binimetinib (MEKi) & encorafenib (BRAFi), reporting a 14.9 month median PFS versus 7.3 months on vemurafenib monotherapy.[321] These combinations prolong responses, but unfortunately patients commonly develop resistance in 50% of patients within 9-10 months.[320,322] In fact, a 5-year follow up of the COMBI-d/v trials suggest that only one third of patients had durable responses to the MEKi/BRAFi combination.[323] Mechanisms of resistance mirror those observed in monotherapy studies, including BRAF amplifications, MEK1/2 mutations and oncogenic NRAS mutations.[324] Nevertheless, BRAF/MEK inhibitor combinations are now accepted as a standard of care treatment for BRAF-mutant advanced melanoma. Further investigation of biomarkers indicative of certain resistance mechanisms and exploring other combination therapy regimes may further enhance overall survival while decreasing or prolonging the emergence of resistance.

4-1-3 Targeting MEK in NRAS mutant melanoma

NRAS mutant melanoma patients have fewer options than BRAF mutant patients, as there are no approved targeted therapies presently available. NRAS mutant patients also appear to take on a more aggressive disease course than BRAF mutant patients, with thicker primary tumors, increased mitotic rate, and poorer overall survival.[313] Current approaches are focused on targeting downstream signaling nodes from RAS, as RAS initiates the MAPK cascade through RAF, activating MEK and ERK. Blocking RAF in wild type or NRAS mutant tumors is ineffective, as BRAF inhibitors initiate a paradoxical activation of ERK signaling

through transactivation of CRAF dimerization.[311,325] As a result, efforts to halt MAPK signaling have focused on MEK inhibition.

First generation MEK inhibitors were promising in preclinical models, but yielded high toxicity and low objective response rates (~10%), conferring minimal clinical benefit.[326] Newer MEKi show a more favorable safety profile, but clinical trials did not stratify by NRAS mutational status, instead only excluding BRAF mutant patients, and results showed no clinical benefit over standard chemotherapies.[327,328] Third generation MEK inhibitors, including trametinib and binimetinib, have favorable pharmacokinetic profiles, though still have yet to demonstrate strong efficacy. A Phase I trial of trametinib showed no clinical benefit in NRAS mutant patients.[329]

In 2016, Array BioPharma's phase III clinical trial NEMO of binimetinib demonstrated an improved mean PFS of 2.8 months over dacarbazine (1.5 months).[330] Still, only 41% of patients responded to the drug. Despite the statistically significant improvement of patients on binimetinib, overall survival (OS) did not improve and Array eventually withdrew its new drug application (NDA) due to a lack of observed clinical benefit.[331] These findings have led to interest in combination therapies, including with CDK4/6 and PI3K inhibitors.[305] In an ongoing clinical trial with ribociclib (CDK4/6i) plus binimetinib, 33% of patients demonstrating a partial response and 52% with no response. PI3K inhibitor combination results show minimal efficacy and high toxicity, despite promising pre-clinical studies.[332] Taken together, the lack of approved, targeted therapies for NRAS-mutant patients underscores the substantial unmet need for NRAS-mutant patients. Consequently, immunotherapy is the recommended first-line treatment for NRAS mutant melanoma and is often used as second line or even first line in BRAF mutant melanoma treatment strategies.

4-1-4 Checkpoint blockade immunotherapy in melanoma

The first attempt to use immunotherapy for advanced melanoma patients used high-dose interleukin-2 treatment (HD IL-2), a cytokine known to induce T-cell activation and proliferation. Promising success was seen in mouse models of HD IL-2 treatment, but phase III clinical trials showed low response rates of ~6% and high toxicity, therefore is rarely used today.[333–335] Identification of the immune checkpoints, cytotoxic T-lymphocyte antigen-4 (CTLA-4) and programmed death 1/ligand-1 (PD-1/PD-L1), are the targets of current checkpoint blockade immunotherapies (CBI) today and have revolutionized melanoma standard of care. In antitumor immunity, a T-cell is first activated by binding an antigen presented by MHCs. A second stimulating signal is needed to initiate T-cell proliferation. CTLA-4 inhibits activation by binding to stimulatory molecules on antigen presenting cells.[336] Similarly, PD-1 is an inhibitory receptor expressed on activated T-cells, and PD-L1 is its ligand expressed on epithelial, endothelial, and immune cells. These checkpoints serve to prevent the immune system from attacking healthy cells. Tumors are thought to exploit this regulatory function and express PD-L1 to evade a T-cell response. CTLA-4 signals are required early in the lymph node during the initiation of an immune response, and PD-1 acts later at the tissue site to decrease T-cell activity.[337]

The first therapeutic checkpoint inhibitors were monoclonal antibodies (mAbs) against CTLA-4, including ipilimumab which showed survival benefit in melanoma patients (57.5% PFS after 4 months of ipilimumab), leading to FDA approval in 2011.[338] Unfortunately, treatment also resulted in significant and sometimes lethal autoimmune toxicity, likely due to the general immune activating nature of CTLA-4 inhibition.[339]

Soon thereafter, a mAb against PD-1, nivolumab, was developed and tested across a range of malignancies including colon and non-smell lung cancer, melanoma, and renal cell carcinoma, and showed promising tumor regression.[340] Studies aimed at evaluating nivolumab in melanoma specifically demonstrated superiority over dacarbazine in BRAF wild-type patients (PFS 5.1 vs. 2.2 months).[341] Nivolumab, along with a second PD-1 mAb, pembrolizumab, both demonstrated an improvement in toxicity profiles over anti-CTLA-4 therapies, and both were FDA approved in 2014.

The differences in timing and location of CTLA-4 and PD-1 signals suggest co-targeting these checkpoints is non-redundant and potentially synergistic. In a 2015 Phase III clinical trial comparing combination nivolumab (PD-1 inhibitor) and ipilimumab (CTLA-4 inhibitor) versus monotherapy, results showed a median PFS of 11.5 with the combination, compared to 2.9 on ipilimumab and 6.9 months on nivolumab.[342] In a separate study evaluating the same compounds in combination or with ipilimumab-monotherapy, BRAF wild-type tumors had a median PFS of 5.7 months vs. 2.8 with monotherapy, and BRAF V600E mutant patients had a median PFS of 8.5 months versus 2.7 on monotherapy.[343] Despite conferring an additional clinical benefit, the combination was associated with high immune-related toxicity, drawing into question the feasibility of administer the combination therapy over either agent alone. Ultimately, a subset of melanoma patients have achieved remarkable and durable results on ICB therapy, not all patients respond (10-15% response rates with anti-CTLA-4 and 30-50% with anti-PD-1, 50-60% with combo), and those that do suffer from toxicity and side effects.[344] Furthermore, approximately half of patients treated with ICIs will develop resistance, either primary or acquired, and/or relapse within several years, with no accurate biomarkers to predict such a response.[345,346]

As a result, there is a growing interest in combining checkpoint immunotherapy in synergistic combinations to improve patient response and expand the population benefiting from

the immunotherapy. Two primary avenues are being explored: combining ICB with other targeted immunotherapies such as anti-cancer vaccines, and with small molecule inhibitors for optimal anti-tumor efficacy.

4-1-5 Immunotherapy + kinase inhibitors in melanoma

Due the inherent limitations of targeted therapy & immunotherapy namely that targeted tends to be associated with a high response rate but short term efficacy, and immunotherapies tend to have a low response rate with long term efficacy in patients who do respond, it has been proposed that the most effective strategy may be to combine the two.[347] This is especially true due to an increasing pool of evidence suggesting that oncogenes may affect the immune environment, and thus optimal combinations may prove synergistic.

For example, BRAF V600E cell lines secrete immunosuppressive factors like IL-10, IL-6, and VEGF and suppressed TNF-a production by dendritic cells. These effects were reversed with MEK inhibition in vitro.[32,348] Furthermore, BRAF inhibition on BRAF mutant cell lines and tumors have been found to upregulate antigen expression via major histocompatibility complex (MHC) expression, increase melanoma differentiation antigen expression, and elevated interferon gamma gene expression.[349–351] BRAF and MEK inhibitors were shown to increase recognition of these antigens by antigen specific T lymphocytes, though the literature has conflicting findings on how MEK alters MHC expression.[349,352] While an initial 2010 study found that MEK inhibition adversely impacts T-cell function, more recent studies have indicated that MEK inhibitors increase expression of MHCs, enhance antigen recognition by T-cells, and increase CD8+ T cell infiltration.[31,315,353] Importantly, MEK inhibition did not alter HLA expression on normal peripheral blood mononuclear cells which suggests MEKi modulation is limited to cells with activated MAPK signaling, though this remains to be exhaustively explored.[31]

Several preclinical models demonstrated that BRAF and MEK inhibitors could be effectively combined with CBI and highlighted the potential for a triple combination. A small clinical trial combining dabrafenib, trametinib, and pembrolizumab was undertaken to explore the triplet therapy efficacy, and initial results demonstrated high objective response rates (73%), however 73% of patients also experienced grade immune-related adverse events.[354] Still, median PFS was 15.4 months, substantially longer than MEKi/BRAFi or anti-PD-1 therapies alone. Analysis of patient biopsies demonstrated an increase in CD8+ T cells in tumors following therapy, as well as MHC expression. These data support the preclinical data and confirm MEK inhibition does not negatively impact intratumoral immune response. Still, the toxicity observed is of concern, thus several trials are in progress testing different dosing sequences of the same agents, in both wild type and BRAF mutant melanomas.

In NRAS mutant patients, a retrospective analysis found that NRAS mutant patients, despite having more aggressive disease course versus wild-type and BRAF mutant melanomas[355], had superior disease control rates of 50% vs. 31% in patients treated with either CTLA-4 or PD-1 inhibitors.[356] A separate retrospective analysis found the survival benefit in NRAS mutant and wild-type melanoma patients on ipilimumab to be more comparable, with equivalent response rates of ~40% in both treatment groups.[357] A striking finding was observed in the binimetinib NEMO study, which found that NRAS mutant patients that had received prior immunotherapy had a superior survival benefit over patients without prior immunotherapy (5.5 vs. 2.8 months).[330] A separate study had a similar finding, though not statistically significant.[357] Intriguingly, patients in this clinical trial failed immunotherapy, but it appeared to confer some benefit during the MEK inhibitor treatment, suggesting efficacy for an “immunotherapy then kinase inhibitor” treatment regimen. One possibility is that prior immunotherapy increased T-cell infiltration so that when kinase inhibitors were given the increase antigen expression, the

immune system was primed for attack. Another possibility is that the benefit seen was due to delayed onset of ICB.

In contrast, in a 2016 study, authors designed a supramolecular MEK inhibitor (SPI), increasing selumetinib's stability and treated mice with two schedules. In the "immediate" schedule, PD-1 inhibitors were administered on alternating days with the SPI.[35] In the "after" schedule, the PD-1 inhibitor was given after the 5-day SPI treatment cycle was complete. Interestingly, the after schedule was more efficacious, resulting in significantly lower tumor volume after treatment and a longer average survival time. [35] This result suggests that kinase inhibition increases antigen expression, so secondary immunotherapy is more effective. As is demonstrated by these two examples, optimal sequencing of these agents remains controversial and poorly understood. Consequently, a plethora of clinical trials are ongoing, looking at various permutations and combinations of available approved therapies.[358]

Ultimately, despite the promising initial results in both BRAF and NRAS mutant melanomas combining targeted therapies with ICB, there remains much to learn about how exposure of cells to kinase inhibitors alters the immune system, and how these alterations can be leveraged to confer the largest clinical benefit.[359]

4-2 Results

4-2-1 MEK inhibition increases MHC-I expression in melanoma cell lines

To evaluate how MEK inhibition alters pMHC expression in *NRAS* and *BRAF* mutant melanomas, we selected 2 *NRAS* and 4 *BRAF* mutant cell lines (V600E) are treated cells for 72 hours with the MEK inhibitor binimetinib, at two doses: 100 nM or 1 μM. Cell lines exhibited a range of sensitivities to binimetinib: NRAS mutant lines IPC298 and SKMEL2, along with BRAF

V600E SKMEL28 had half maximal inhibitor concentrations of approximately 120 nM, whereas other BRAF mutant lines had higher IC_{50} values, and RPMI-7951 was largely unresponsive at even 10 μM of binimetinib (**Supplementary Figure 4-1**).

We next measured class-I MHC surface expression by flow cytometry and found that 72 hours of treatment resulted in a maximal increase in expression over a DMSO treated control without requiring cell passaging (**Supplementary Figure 4-3**), therefore we selected 72 hours as the timepoint for all subsequent immunopeptidomics experiments. As measured by flow cytometry, all cell lines showed elevated surface MHC-I expression with binimetinib treatment at 72 hours, and increases were dose-dependent in most cases (**Figure 4-1**, **Supplementary Figure 4-3**). This stands in contrast to our previously reported results with palbociclib, a CDK4/6 inhibitor, where a lower, sub-cytotoxic dose increased expression to a greater extent than a higher concentration.[188] Of note, previously reported results demonstrated that treatment of normal PBMCs with trametinib did not affect surface HLA expression, demonstrating that this effect is specifically seen in cells with activated signaling[31]

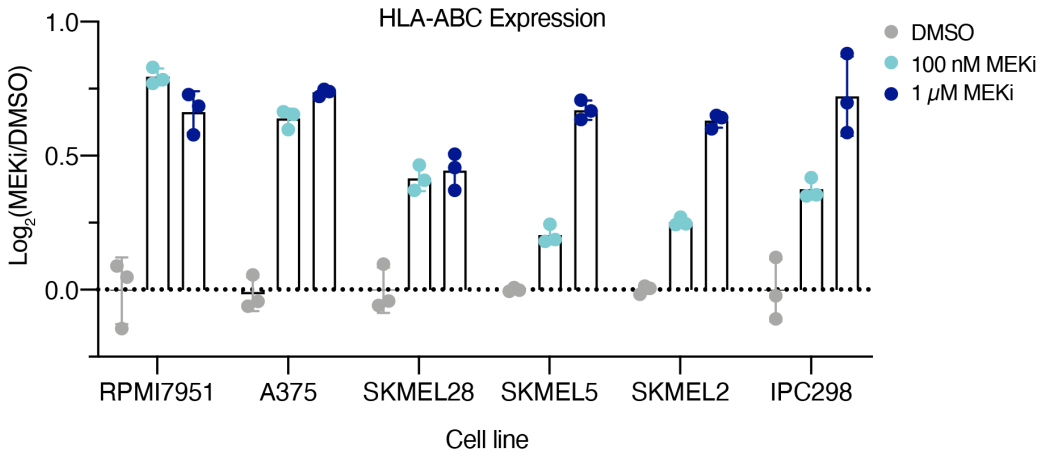

Figure 4-1. *Changes in surface HLA expression with MEKi. Fold change in median surface expression levels (over average DMSO control condition) of HLA-A/B/C in cell lines treated with vehicle control or binimetinib (MEKi) for 72hr. Error bars represent standard deviation of n=3 biological replicates.*

We next sought to investigate quantitatively how the pMHC repertoires presented on these six cell lines were altered in response to MEKi treatment. Do this end, we employed our previously described framework for multiplexed, quantitative profiling of pMHC repertoires utilizing isobaric labeling (TMT) and heavy isotope-labeled peptide MHCs (hipMHC) standards for accurate relative quantitation of endogenous pMHCs. In triplicate, $1x10^7$ cells were treated with DMSO, 100 nM, or 1 μM (BRAF mutant only) binimetinib for 72 hours (**Figure 4-2-A**). Cells were lysed, and three hipMHC standards were spiked into the lysate mixture prior to immunoprecipitation. Isolated endogenous and isotopically labeled normalization standards were subsequently labeled with TMT, combined together, and analyzed with LC-MS/MS for quantitative immunopeptidomic profiling.

We identified between 1470 and 4,982 unique peptides per analysis (**Figure 4-2-B**), totaling 15,450 unique peptides derived from 6,292 unique proteins. Peptides matched expected class I length distributions, and a majority of peptides were predicted to be binders of each cell

line's allelic profile (**Supplementary Figure 4-4**. Intriguingly, nearly 80% of peptides were identified in only a single analysis, despite several cell lines having some allelic overlap (**Figure 4-2-C, Supplementary Figure 4-5**). Unsurprisingly, highly abundant proteins like vimentin and beta-actin were the source of many unique pMHCs across analyses, however most unique source proteins (60%) produced just 1 or 2 MHC peptides (**Figure 4-2-D**). These data highlight the uniqueness of the immunopeptidome, as not only the peptides sequences but also the proteins they are derived from are highly variable, despite the cell type and disease phenotype similarities.

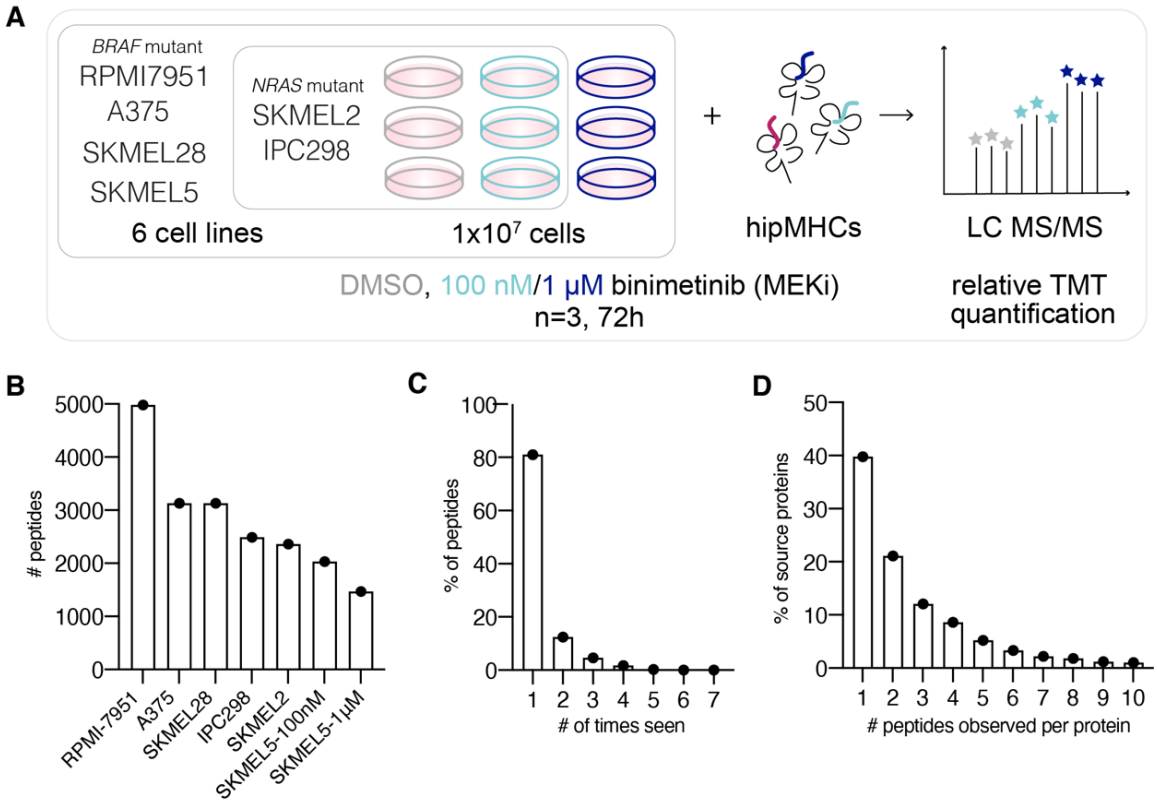

Figure 4-2. *Quantitative immunopeptidomics experiments in vitro.* ***A*** *Experimental setup for quantitative immunopeptidomics experiments.* ***B*** *Number of unique peptides identified in each sample.* ***C*** *Distribution*

of the number of times each peptide was observed across analyses. ***D*** *Distribution of the number of peptides derived from each gene across analyses.*

In most cases, there was a median increase in pMHC expression levels with binimetinib treatment (**Figure 4-3**). Some cell lines mirrored the flow cytometry data such as RPMI-7951s and SKMEL28s, with had similar expression level changes, ~2x and ~1.4x respectively with both 100 nM and 1 μM binimetinib treatment. Alternatively, A375 cells showed larger changes in expression with the immunopeptidomics analysis than by flow cytometry, however flow cytometry measurements represent an average change in signal, whereas MS data measures each peptide's altered expression. Notably, there was a wide distribution in expression level changes (**Supplementary Figure 4-6**). While the average fold change of A375 cells treated with 1 μM binimetinib was 2.45x, some peptides increased 16-fold or higher, while others decreased 4-fold. Even in SKMEL2 cells where there was no mean fold change in expression, some peptides increased and decreased 3-4x in expression. We examined whether increase pMHC presentation with binimetinib was also observed trametinib, a more potent MEK inhibitor than binimetinib. We find trametinib similarly increases presentation, though to a greater extent, in line with the dose-dependent response observed with binimetinib (**Supplementary Figure 4-7-A**). Furthermore, we treated SKMEL5 cells with 100 nM binimetinib for 10 days, and find that expression remains elevated, and to a further extent than treatment for 72 hours (μ=2x change), (**Supplementary Figure 4-7-B**).

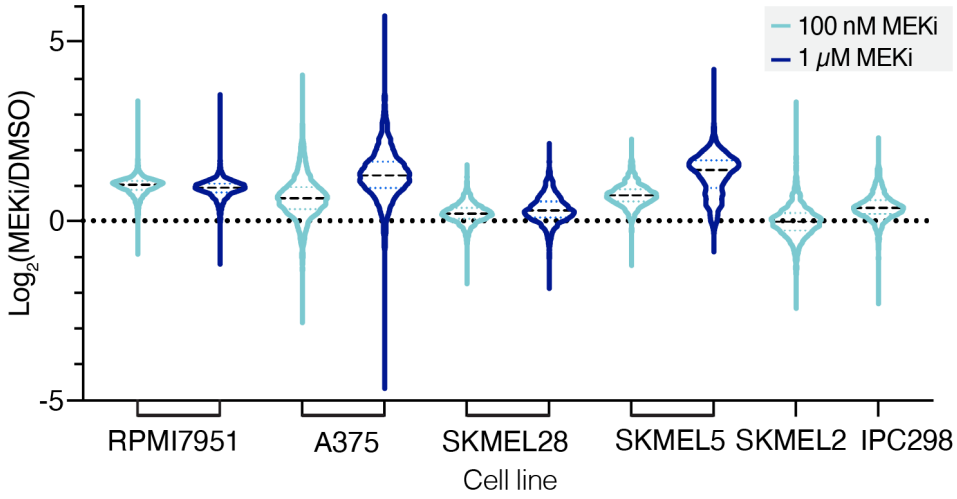

***Figure 4-3**. Changes in pMHC expression with MEKi. Violin plot of relative changes in pMHC expression for each cell line. Black dashed line = median, colored dotted lines = quartiles.*

As ratio compression is a known feature of multiplexed, MS^2-based analyses, we performed an additional analysis of SKMEL5 cells treated with DMSO or 100 nM MEKi (n=3) and performed six label-free LC-MS/MS analyses. We find that while the mean change in expression is similar between unlabeled and TMT-labeled analyses (1.88x vs. 1.65x), there was a much wider distribution in expression levels in the label-free analysis (**Figure 4-4-A**). There were also more quantifiable peptides identified in total, 3354, however only 1087 peptides were quantifiable across all six replicates (**Figure 4-4-B**). This represents nearly half the number of peptides quantified in the labeled analysis (2033), highlighting a significant benefit of multiplexing.

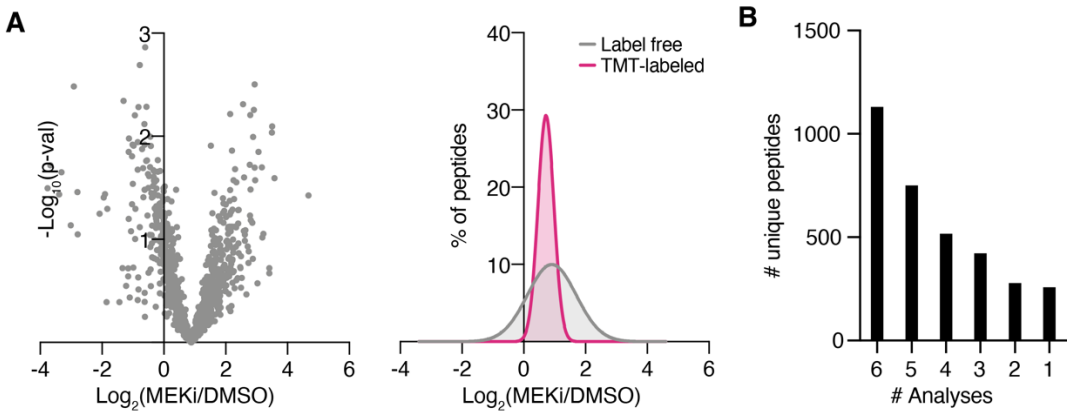

***Figure 4-4**. Comparison of LF and TMT-labeled pMHC analyses for SKMEL5 +/- MEKi. **A** (Left) Volcano plot of the average fold change in pMHC expression with 100 nM binimetinib treatment in SKMEL5 cells (n=3 biological replicates for DMSO and MEKi treated cells) versus significance (mean-adjusted p value, unpaired two-sided t test). (Right) Frequency distributions of changes in pMHC expression in TMT-labeled and unlabeled analyses of SKMEL5 +/- 100 nM binimetinib. **B** Distribution of the number of analyses each peptide was observed in for the six label-free analyses of SKMEL5 +/- 100 nM binimetinib.*

4-2-2 TAAs are selectively enriched in presentation with MEK inhibition

We next investigated which peptides were significantly increasing relative to the median change in expression, to determine if any pMHCs were selectively enriched following MEK inhibition. We noticed two peptides derived from known tumor antigens, DCT (TRYP2) and PMEL (gp100) were two pMHCs in the SKMEL5 + 100 nM MEKi analysis that had the largest increase in expression, increasing 2.8 and 5.3-fold, respectively (**Figure 4-5-A**). These peptides were also two of the most abundant pMHCs in the analysis, ranking in the 99th percentile of precursor ion abundance (**Figure 4-5-B**).

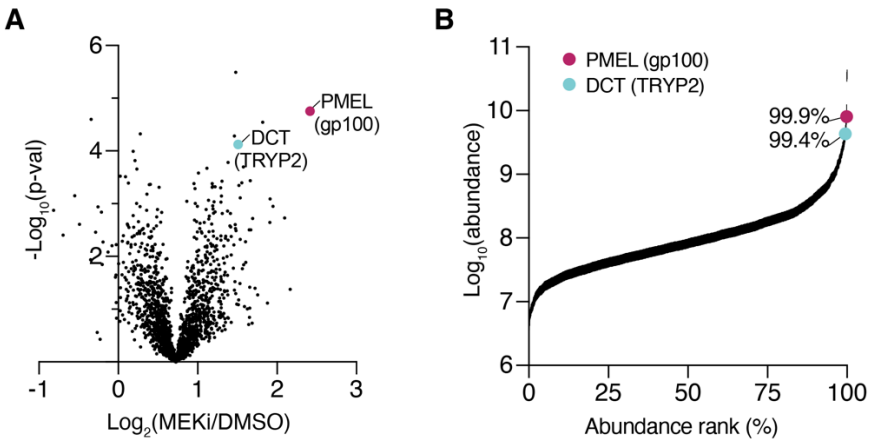

Figure 4-5*. TYRP2/gp100 pMHCs increase following MEKi.* ***A*** *Volcano plot of the average fold change in pMHC expression for SKMEL5 cells treated with 100 nM binimetinib for 72hr (n=3 biological replicates for DMSO and MEKi treated cells) versus significance (mean-adjusted p value, unpaired two-sided t test).* ***B*** *pMHCs ranked by precursor ion area abundance.*

To determine whether this observation of enriched presentation of DCT and PMEL peptides transcends to TAA-derived peptides broadly, we performed a non-parametric test to determine TAA enrichment significance in response to MEK inhibitor treatment. For this analysis, we complied a custom tumor associated antigen library derived from the literature in mass spectrometry analyses and immunogenicity assays as well as and online databases.[163,360–362] This list, featuring over 1000 unique pMHC sequences, was biased towards more well studied alleles (ex. HLA-A2*01), therefore we utilized the peptide's source proteins to generate a protein-based TAA library (**Table 4-1**, **Table 4-2**).

We next rank-ordered peptide source proteins by fold change in presentation with MEKi. In cases where multiple peptides were derived from the same source protein, the maximal fold change was selected. Enrichment was assessed using the Gene Set Enrichment Analysis (GSEA) algorithm against the custom TAA library. In both SKMEL5 and SKMEL28 cells with 100 nM MEKi, we see significant enrichment ($p = 0.003$ & $p<0.001$, respectively) of known tumor antigens (**Figure 4-6-A**). These TAAs include the previously noted examples (DCT and

PMEL) along with many others, including melanoma differentiations from the MAGE family, MLANA (MART-1), and TYR (**Supplementary Figure 4-8**). Of interest, these antigens showed increasing expression with increasing MEK inhibitor dosing, with peptides derived from TRYP1, DCT (TRYP2), and PMEL (gp100) increasing over 10-fold with 1 μM binimetinib treatment (**Figure 4-6-B**). This is particularly exciting, as these antigens are well studied, have known immunogenicity, and are existing targets for targeted immunotherapies which may benefit from increase expression.[363,364] Furthermore, this dose dependent response occurs regardless of whether bulk expression increases proportionally: SKMEL5 cells have increasing expression with increasing MEKi, whereas SKMEL28 cells have little variation in mean expression between the two MEKi doses (**Figure 4-6-C**). When we applied the enrichment analysis framework to all cell lines and binimetinib treatment doses, binimetinib significantly enriched ($p<0.05$) tumor associated antigen presentation in all cases (**Figure 4-7**), suggesting a mechanistic basis for this response.

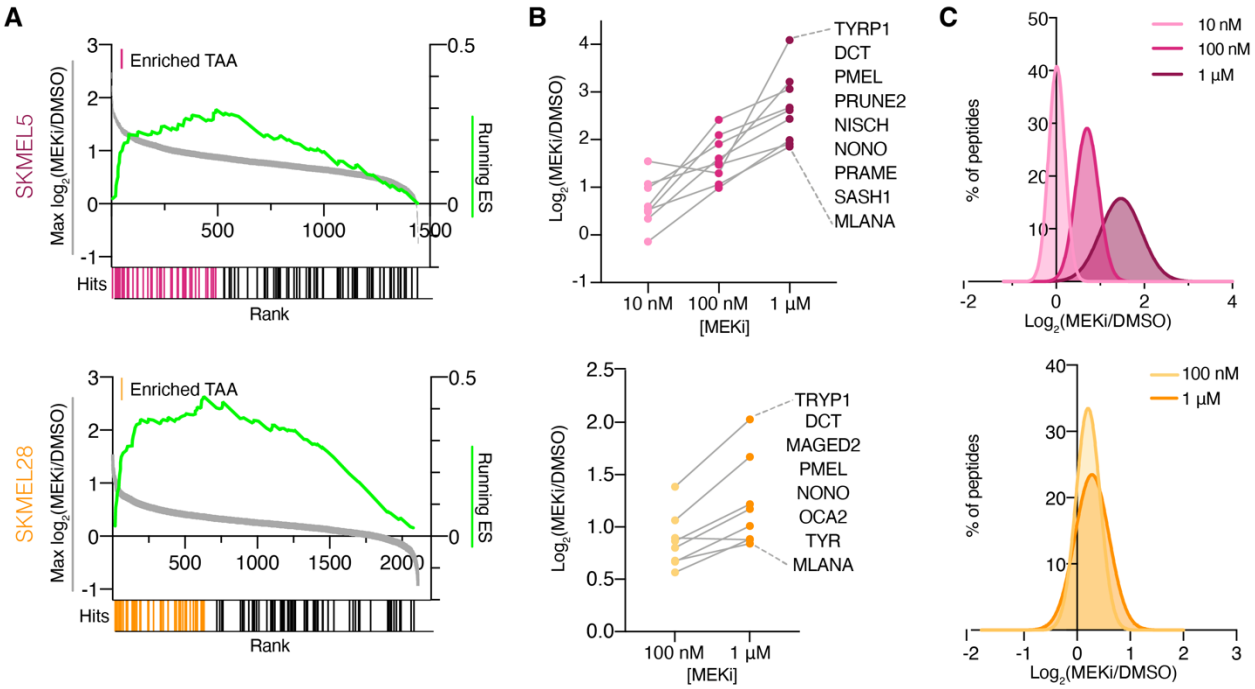

Figure 4-6*. TAAs are significantly enriched following MEKi.* ***A*** *Enrichment plots of TAA enrichment in SKMEL5 +/- 100 nM MEKi (top, pink) and SKMEL28 +/- 100 nM MEKi (bottom, orange), displaying running enrichment scores (green, right y-axis), and fold change in pMHC presentation (left y-axis) versus rank (x-axis) for each peptide (gray). Hits denote TAA peptides, and colored hits represent enriched TAAs.* ***B*** *Selected enriched TAA peptides in SKMEL5 (top) and SKMEL28 (bottom) analyses.* ***C*** *Frequency distribution of pMHC fold change with MEK inhibition. SKMEL5: 10 nM: μ=0.01, 100 nM: μ=0.70, 1μM: μ=1.47. SKMEL28: 100 nM: μ=0.21, 1μM = μ=0.28.*

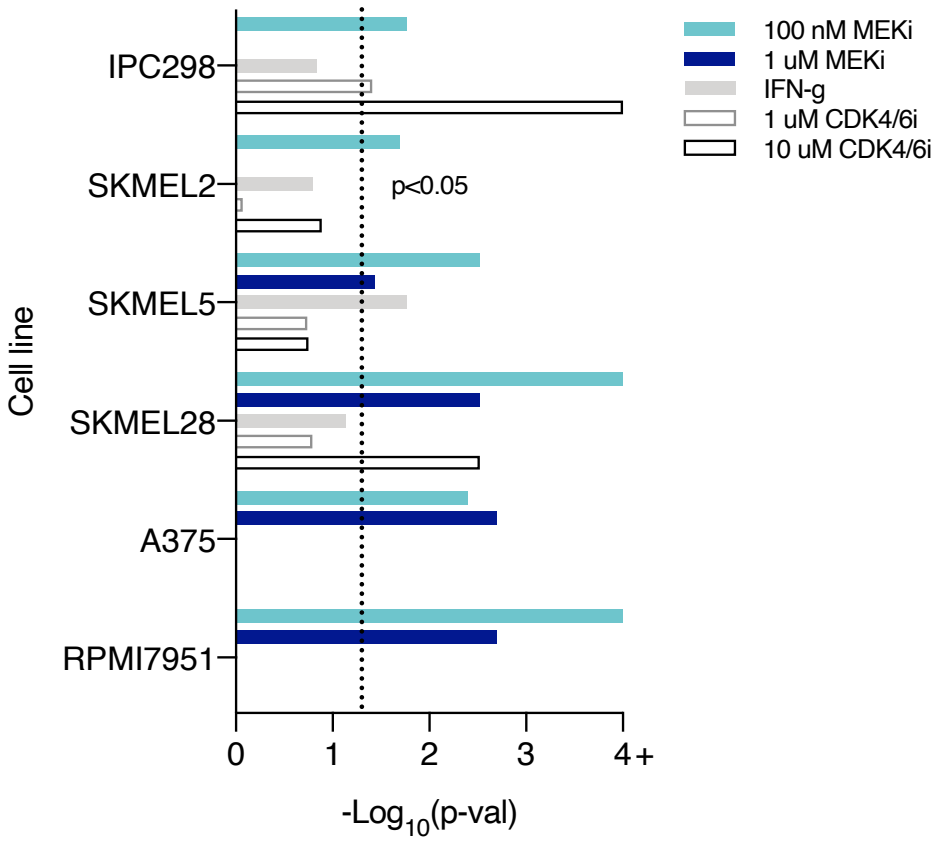

***Figure 4-7**. MEKi robustly enriches for TAA pMHC expression. Significance values for TAA pathway enrichment. Values greater 4 (Log_{10} adjusted) represent p<0.0001.*

We performed the same enrichment analysis on SKMEL5 +/- 100 nM MEKi peptides rank ordered by precursor abundance (**Supplementary Figure 4-9-A**), and again found that TAAs were enriched amongst the peptides of highest abundance. Interestingly, there was no correlation between pMHC fold change in expression and peptide abundance, suggesting that TAAs are both some of the most abundant peptide presented and change the most in presentation with MEK inhibition (**Supplementary Figure 4-9-B**). We also applied the same analysis to the label free data of 100 nM SKMEL5 cells and discover significant TAA enrichment (**Supplementary Figure 4-9-C**). Finally, we used the TAA peptide database (not source proteins) and curated a sub library of TAA peptides predicted to bind to SKMEL5's allelic profile

(<500 nM predicted affinity. Again, TAA peptides were significantly enriched in pMHCs ranked according to expression fold change and abundance, underscoring the robustness of this finding (**Supplementary Figure 4-9-C**).

We also compared the results of the multiplexed SKMEL5 +/- 100 nM MEKi analysis to the label free data, to assess whether the unlabeled analyses showed similar or greater changes in TAA presentation provided the known impact of ratio compression. The changes in expression levels of TAAs was correlated (r=0.63), however as previously described the TMT-labeled samples showed lower relative changes in pMHC expression (**Figure 4-8-A**). For example, a DCT-derived peptide had a 12-fold change in the unlabeled analysis compared to a 2.85-fold change in the TMT-labeled analysis (**Figure 4-8-B**), suggesting that TAA expression level changes may be much larger across cell lines than what is reported in the multiplexed analyses.

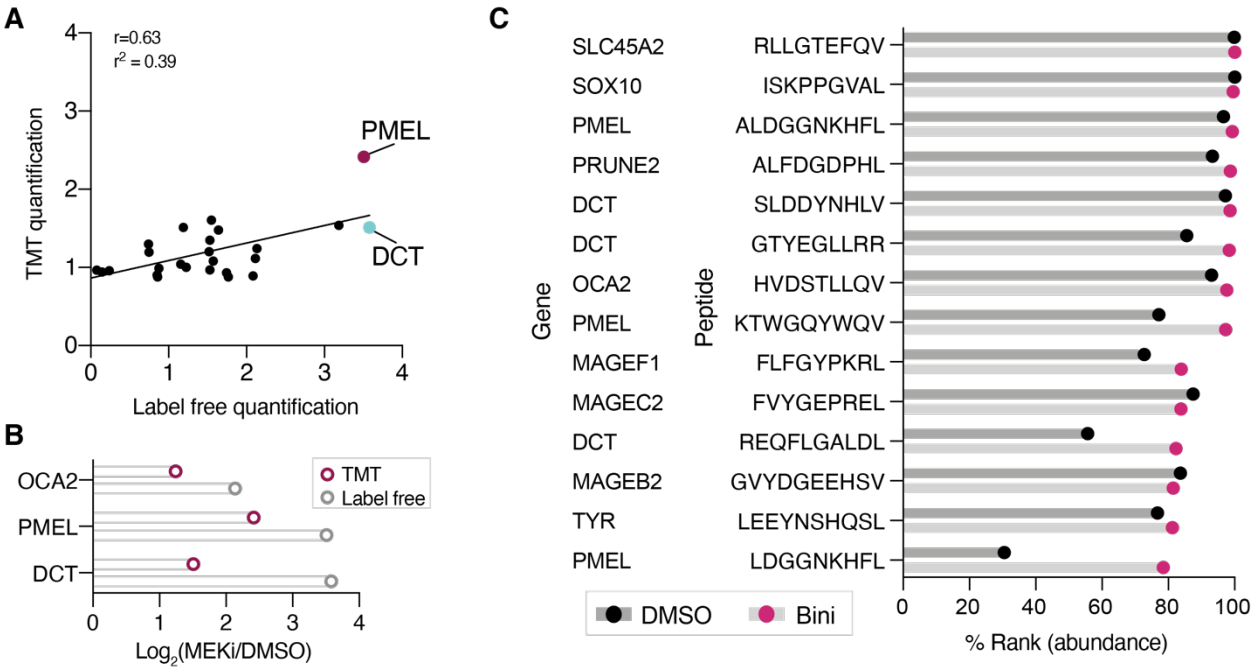

***Figure 4-8**. TMT-labeled analyses underestimate fold changes in expression. **A** Correlation between the fold change in pMHC expression (Log_2(MEKi/DMSO)) between unlabeled and TMT-labeled analysis of SKMEL5 cells +/- 100 nM binimetinib. **B** Selected pMHCs from **A**. **C** Ranked median abundance (integrated precursor area) of selected TAAs in DMSO and 100 nM binimetinib treated SKMEL5 cells from the label free analysis.*

Finally, the label-free data of SKMEL5 cells +/- 100 nM binimetinib provided a unique dataset to assess whether enrichment of TAAs amongst peptide abundances was a result of high endogenous expression, or whether MEK inhibition further drove increases in TAA abundance, above median changes. This cannot be assessed in the labeled data, as the precursor ion intensity is the summed intensity of the replicates. We determine that in both the DMSO and binimetinib treated cells, TAAs were of high abundance. However, most TAAs were of higher ranked abundance, relative to other peptides within the same treatment condition, in the binimetinib treated cells (**Figure 4-8-C**). For some pMHCs the difference was small—the SLC45A2 peptide RLLGTEFQV" is one of the top 5 most abundant peptides in untreated

SKMEL5 cells, and while binimetinib further increases expression, it does significant change its already high ranked order. Alternatively, the PMEL peptide “KTWGQYWQV” moves from the 77th percentile in DMSO treated cells to the 97th percentile with MEK inhibition, consistent with our finding that tumor antigens are selectively enriched.

4-2-3 IFN-γ and MEKi drive distinct pMHC repertoire alterations

It has been proposed that ERK is a negative regulator for IFN- γ/STAT1 signaling, and that inhibition of ERK via MEK inhibitors can drive an interferon regulatory factor resonse.[365,366] IFN-g binds to the Janus kinase 1 and 2 receptors, phosphorylating STAT1, which can then bind to IFN-g activated site (GAS) located at the promoter region of primary interferon response genes, increasing their transcription. Interferon-regulatory factor 1 (IRF1) can subsequently bind to the interferon-stimulated response element (IRSE), which increases transcription of response genes involved in immunomodulatory functions including HLA-A/B/C and B2M.[367,368] It has also been proposed that MEK inhibitors drive IRF1-mediated upregulation of pMHCs via STAT3 or NF-kB.[365,369] Interestingly, siRNA knockdowns of STAT1, STAT3, and RelA (NF-kB component), all of which show increase transcription following MEKi, all suppressed MEK inhibitor-induced upregulation of HLA expression, though to varying degrees.[31,37] In two separate studies, STAT1 knockdown had the largest effect, though MEKi was still able to upregulate expression to some degree. This suggests MEK inhibitors can upregulate pMHC expression through multiple or overlapping routes.

Previous work profiled the pMHC repertoire’s response to IFN-γ stimulation in SKMEL2, IPC298, SKMEL5, and SKMEL28 cells[188], therefore we investigated whether TAAs were also selectively enriched following IFN-γ treatment. In 3 cell lines TAA’s were not significantly enriched, with SKMEL5 cells being the only exception. Upon closer inspection, even when IFN-γ stimulation increases pMHC expression to a greater extend than MEK inhibition (**Figure 4-9-A**), melanoma differentiation tumor antigens like TRYP1, DCT, and PMEL all show a larger

change in expression with MEK inhibition (**Figure 4-9-B**). Interestingly, peptides derived from STAT1 and HLA show a large increase in presentation in IFN-g treated cells, but very little change in MEK inhibitor treated cells **Figure 4-9-C**). Our previously results demonstrate that quantitative alterations in the immunopeptidome are reflective of cells state changes, so the IFN-γ mediated response makes sense, and the lack of response with binimetinib treatment suggests MEK inhibition drives MHC upregulation through a mechanism district from IFN-γ /STAT1.

An enrichment analysis of the MSigDB cancer hallmarks pathways showed significant enrichment of IFN-g response in IFN-γ stimulated cells (described in Stopfer et al.), however cell lines treated with binimetinib did not show positive IFN-γ response pathway enrichment among upregulated pMHCs, further contrasting the biological response between the two drivers of MHC presentation. Furthermore, upregulated expression of the TAAs highlighted here were not significantly enriched above the mean increase in expression, highlighting a MEK inhibitor specific mechanism driving TAA presentation. CDK4/6 inhibitor treatment, such as palbociclib, has also been shown to increase antigen presentation, including TAAs (Stopfer et al.).[188,263] We again performed the TAA enrichment analysis, and found that in just a few cases (IPC298 cells, SKMEL28 + 10 uM palbociclib), there was significant enrichment. In most cases, including both SKMEL5 treatment conditions, TAAs were not significantly enriched in presentation. Taken together, we find MEK inhibitors uniquely drive upregulation of TAAs, district from other perturbations known to alter pMHC expression levels.

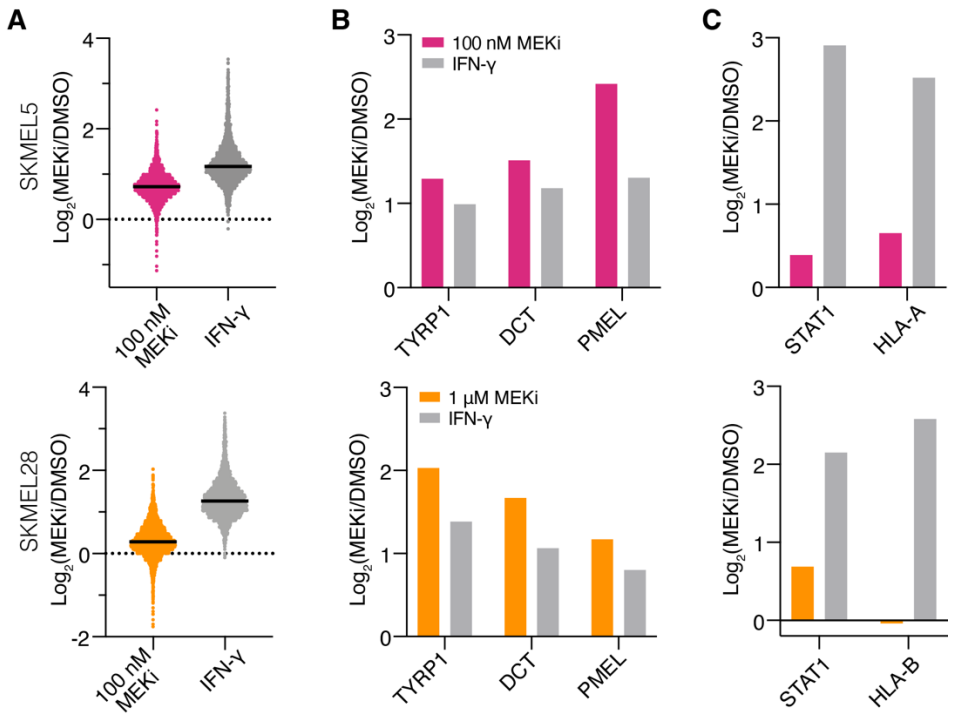

***Figure 4-9**. Comparison of MEKi/IFN-g induced pMHC changes. **A** Distribution of pMHC changes in expression with binimetinib (100 nM) or IFN-g (10 ng/mL) for 72hr. **B**. Changes in pMHC expression for selected TAA peptides. **C** Changes in pMHC expression for STAT1 and HLA-derived peptides.*

4-2-4 ZEB2/SNAIL2 expression drives melanoma differentiation antigen expression

In melanoma cell lines treated with the CDK4/6 inhibitor palbociclib, quantitative changes in pMHC peptides reflected the known biological response to CDK4/6 inhibition. For example, peptides derived from proteins involved in E2F transition and G2M checkpoints were decreased in presentation following treatment, whereas peptides derived from oxidative phosphorylation proteins showed increased presentation. To this end, we looked at the enrichment results against the MSigDB cancer hallmarks pathways to identify groups of peptides derived from signaling pathways that showed significant enrichment with binimetinib treatment (**Table 4-3**). In SKMEL5, A375, and RPMI-7951 cells, epithelial to mesenchymal transition (EMT)-derived peptides were positively enriched ($p<0.05$, $q<0.25$) in presentation (**Figure 4-10-A)**. IPC298,

SKMEL28, and SKMEL2 cells also showed positive enrichment at $p < 0.01$, with pMHCs derived from EMT peptides increasing in each condition regardless of significance value (**Supplementary Figure 4-10**).

Across all cell lines/conditions, enriched EMT pMHCs were derived from 51 unique source proteins, including pMHCs derived from SNAI2 (Slug), an EMT transcription factor (EMT-TF), as well as Integrin αv (ITGAV) and Vimentin (VIM), which showed enrichment across 7 and 8 multiplexed pMHC analyses, respectively (**Figure 4-10-B**). At first glance, increased pMHC expression of these sites appears to be consistent with an epithelial to mesenchymal transition. Slug is an EMT transcription factor (EMT-TF) that has been shown to regulate expression of genes responsible for EMT and serve as a transcriptional repressor of e-cadherin.[370,371] Integrins are cell surface receptors mediating cell attachment to the ECM. Previous work has shown that Integrin signaling potentiate TGF-B1 dependent down regulation of e-cadherin, a critical component of the epithelial to mesenchymal transition.[372] Increased vimentin expression is a mesenchymal marker, and correlates with loss of E-cadherin, more invasive phenotypes, and poor clinical outcomes.[373] EMT is a known adaptive response/resistance mechanism to MEK inhibition in KRAS mutant lung cancer, therefore we similarly hypothesized MEK inhibition of NRAS/BRAF mutant melanoma cell lines was inducing EMT.[374,375]

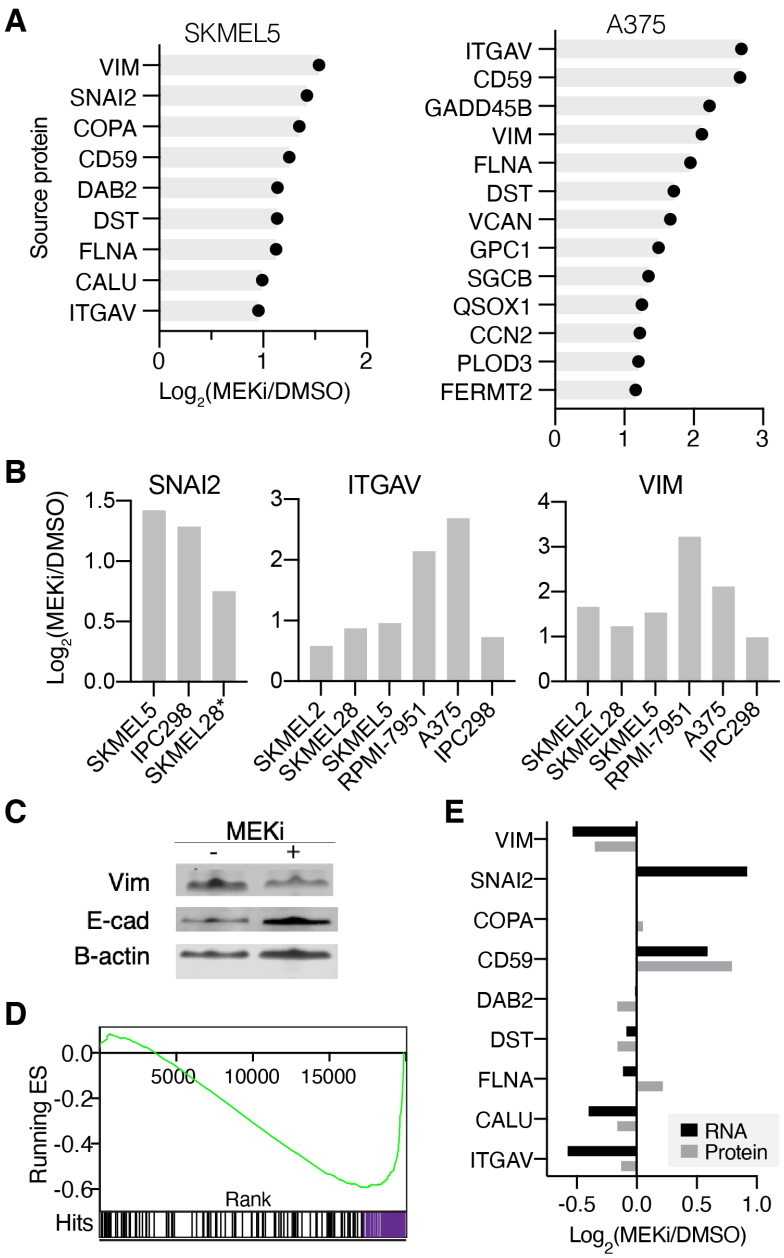

Figure 4-10. *EMT enrichment among pMHCs in MEKi treated cells.* ***A*** *Enriched pMHCs derived from EMT source proteins with their change in expression for SKMEL5 and A375 cells +/- 100 nM binimetinib.* ***B*** *Change in pMHC expression for peptides derived from SNAI2, ITGAV, and VIM in 100 nM treated cells. *denotes pMHC not significantly enriched 1 μM MEKi.* ***C*** *Protein expression of vimentin, e-cadherin expression in SKMEL5 cells +/- 100 nM binimetinib.* ***D*** *Enrichment plot of EMT genes using for RNA-seq data, SKMEL5 cells +/- 100 nM binimetinib. p & q-values < 0.0001.* ***E*** *RNA and protein expression of EMT genes/proteins enriched in pMHC presentation (**A**).*

To assess this hypothesis, we first measured E-cadherin and vimentin protein expression in SKMEL5 cells +/- 100 nM binimetinib. Intriguingly, Vimentin protein expression decreased, and e-cadherin expression increased with MEK inhibition, in contrast to our hypothesis (**Figure 4-10-C**). We next examined transcript expression data for SKMEL5 cells +/- 100 nM or 1 μM binimetinib and found the EMT cancer hallmarks pathway to be significantly negatively enriched in both treatment conditions (**Figure 4-10-D**). We next compared the source gene and protein expression levels of enriched EMT pMHCs and found that, in agreement with the western blot data, vimentin expression decreases with MEKi, along with ITGAV and others, in contrast to the pMHC data (**Figure 4-10-E**). Intriguingly, SNAI2 (slug) and CD59 expression are the only proteins/genes to increase in expression with MEKi, matching the pMHC data.

Of note, while traditionally classified as an EMT-TF responsible for loss of e-cadherin, Slug expression does not always correlate with complete EMT and regulation of EMT-TFs in malignant melanoma may be uniquely regulated compared to other epithelial tumors.[376,377] In 2013, Caramel et al. proposed a new EMT program in melanoma, where the expression of EMT-TFs are under the control of oncogenic signaling pathways.[378,379] During melanomagenesis, SNAI2 and ZEB2 act as oncosuppressive proteins during melanocyte differentiation under MITF control. In response to MAPK pathway activation, EMT-TFs undergo a reorganization and ZEB1 and TWIST are upregulated to promote dedifferentiation and tumorigenesis. This change in EMT-TF expression, termed “EMT-TF switching” correlates with pERK levels. Consequently, we next assessed changes in gene expression of these key EMT-TF switch markers, and found that in addition to SNAI2, ZEB2, E-cadherin, and MITF expression were all increased following MEKi and TWIST, ZEB1, N-cadherin, and vimentin were all decreased (**Figure 4-11-A**) Under this mechanism, treatment with binimetinib inhibited pERK which likely initiated the switch back to the “differentiation” phenotype.

MITF expression induces gene expression patterns of melanocyte differentiation and pigment production/melanin biosynthesis, therefore in this “differentiation” phenotype expression of differentiation antigens such as Tyrosinase (TYR) , Dopachrome tautomerase (DCT or TRYP2), Tyrosinase-related protein 1 (TYRP1), premelanosome protein (PMEL), and SLC45A2 have been shown to increase in expression.[378,380] As previously described, pMHCs derived from these proteins are also known tumor associated antigens. Using RNA-seq and protein expression profiling data, we found that MEK inhibitor treatment increased expression of these differentiation genes/proteins, which correlates with pMHC expression (**Figure 4-11-B**). As previously highlighted, vimentin pMHC expression increases with MEKi, whereas gene/protein expression decreases, suggesting that elevated pMHC expression is a likely due to other post-translational processing.

To assess this, we performed a quantitative analysis of the “ubiquitylome”, which measures peptides tagged for degradation with ubiquitination modifications by purifying peptides containing two remnant glycine residues (di-Gly) of ubiquitin on lysine residues peptides following tryptic digestion (**Supplementary Figure 4-11**).[381] We found that while the tumor antigens displayed increased degradation tagging following MEKi, so did vimentin, therefore increased vimentin pMHCs may be the result of higher degradation rates rather than protein/gene expression (**Figure 4-11-C**). Taken together, these data highlight a likely mechanism responsible for the select enrichment of TAAs following MEKi, driven by elevated ZEB2/SNAI2/MITF expression, which coordinates the upregulation of differentiation antigens expression and translates to elevated pMHC levels.

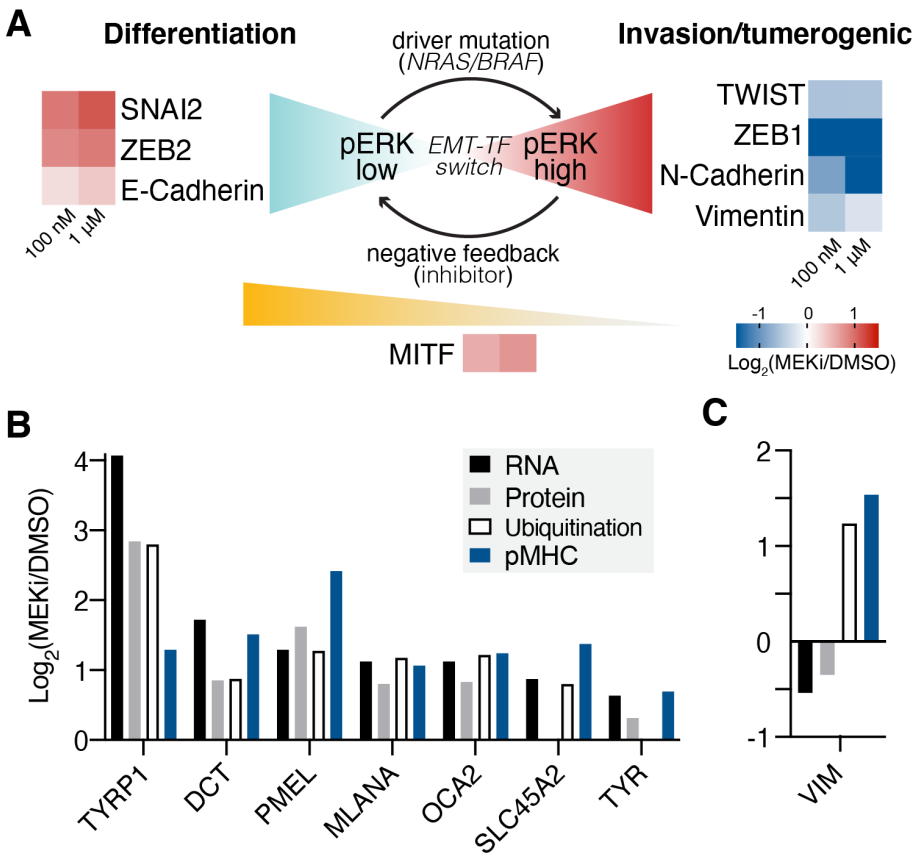

***Figure 4-11**. Proposed mechanism of EMT-TF switching. **A** Schematic of EMT-TF switching, with changes in transcription with MEK inhibitor treatment in SKMEL5 cells shown next to gene names. **B,C** Changes in RNA, protein, ubiquitination, and pMHC expression of selected targets.*

4-2-5 Predicting pMHC expression from central dogma

Previous work has demonstrated that HLA-I sampling for pMHC presentation correlates with source protein length (longer proteins result in more unique pMHCs presented, with protein abundance (more abundant proteins lead to more unique pMHCs), and protein half-life (faster turnover rates leader to a higher concentration of pMHCs).[157] However, whether changes in protein or transcript abundance in response to a perturbation such as MEKi can predict changes in pMHC expression remain poorly understood. Furthermore, the previous work focused on the number of peptides derived from a particular protein rather than focusing on protein and pMHC

abundances. Given the data presented in **Figure 4-11-B,** where melanoma differentiation antigen pMHC expression correlates with protein/transcript/ubiquitin abundances, we investigated whether there was a broader correlation across up and down-regulated pMHCs.

To this end, SKMEL5 cells treated with 100 nM binimetinib were processed four different ways, with three replicates for each condition (**Figure 4-12-A**). First, cells were lysed in Trizol, and RNA was isolated for RNA-sequencing. Next cells were treated for 1 hour with 100 nM Bortezomib, a protease inhibitor, lysed, and di-gly residues were immunoprecipitated using an anti-di-gly antibody (**Supplementary Figure 4-11**). Di-gly modified peptides were next TMT-labeled, combined, and analyzed by LC-MS/MS. Next, pMHCs were lysed in the MHC lysis buffer, and pMHCs were isolated and labeled as previously described. The unbound fraction (global protein expression) following anti-HLA-A/B/C IP was then digested into tryptic peptides, processed with C18 cleanup, labeled with TMT, distributed between twenty fractions, and analyzed by LC-MS/MS. Together, data is presented as the change in expression of the MEK inhibitor samples versus the DMSO treated samples (**Figure 4-12-B**). We quantified nearly 20,000 protein encoding genes, 5,183 proteins, and obtained ubiquitination data on 701 unique proteins. We used this data in combination with the pMHC data for SKMEL5 cells +/- 100 nM binimetinib for quantitative comparisons.

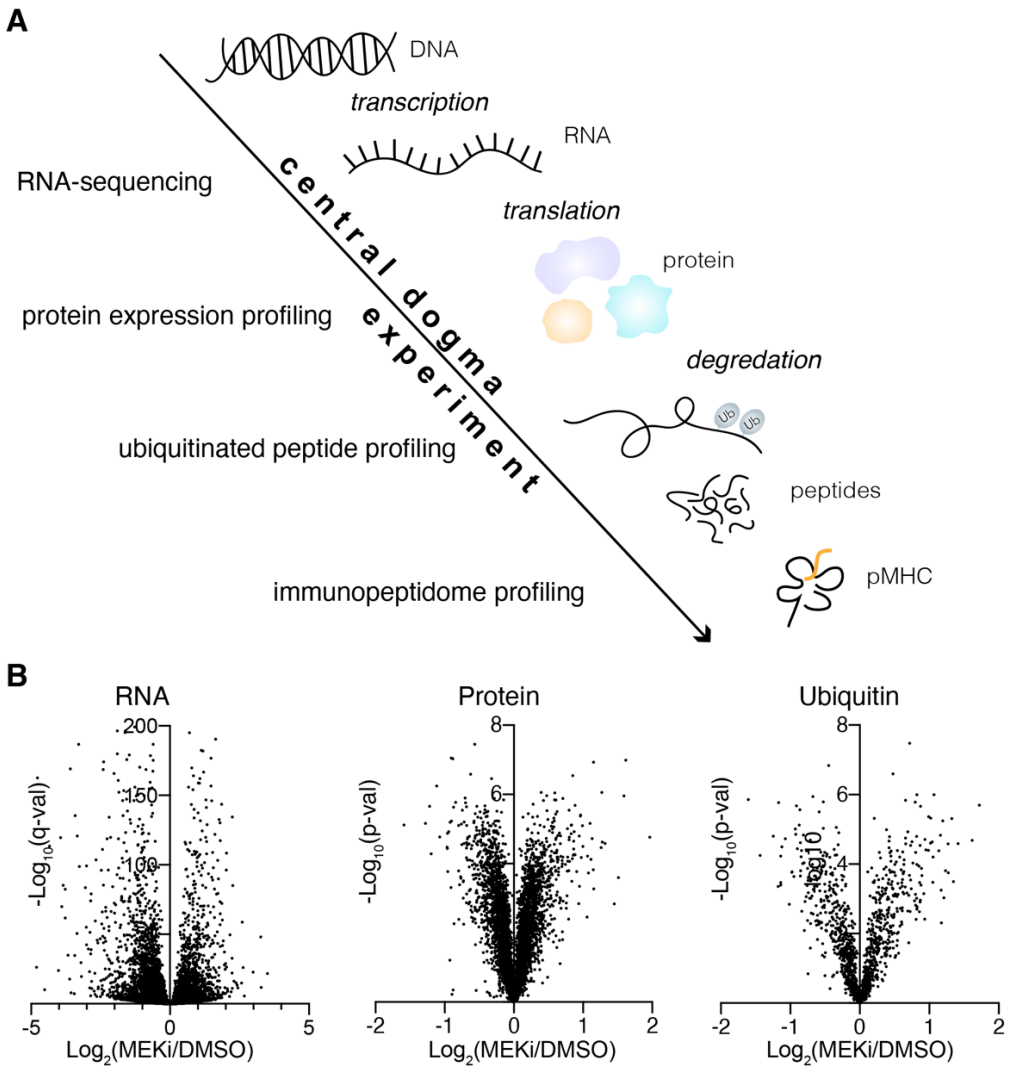

***Figure 4-12**. Probing central dogma for global understanding of MEKi induced pMHC changes. **A** Experimental setup for investigating relationship between pMHC expression and central dogma. **B** Volcano plots of changes in RNA and protein expression, and abundance of ubiquitin tagged peptides. The y-axis represents significance values. Significance: RNA: Wald test, Benjamini Hochberg adjusted. Protein and Ubiquitin: unpaired two-sided T-test.*

Generally, there was no bulk correlation between changes in gene/protein expression and changes in pMHC expression in response to MEK inhibitor treatment (**Figure 4-13-A**), whereas protein and transcript expression do have a weak positive correlation (**Figure 4-13-B**). To visualize whether there were groups of pMHCs with similar patterns of pMHC/RNA/protein

expression, we first performed hierarchical clustering of the combined dataset. In this analysis, RNA/protein abundances are matched to pMHCs based on their source protein/gene, therefore some RNA/protein values are duplicated if there are multiple pMHCs derived from the same protein. As not all pMHCs had protein expression values, the matrix contained values for 1,483 unique pMHCs.

At first glance, while most pMHC levels increase in presentation, many corresponding transcript and protein expression levels remain unchanged, or do not show coordinates expression level changes (**Figure 4-13-C**) . Several clusters emerge, including the orange cluster (**Supplementary Figure 4-12-A**), containing primarily TAA peptides, which have increased expression across pMHC/RNA/ and protein expression, consistent with the examples highlighted earlier (**Figure 4-11-B**). Alternatively, the blue cluster shows significant positive increases in pMHC expression, with small changes in RNA or protein expression, and contains tumor antigens NISCH, pIRS2, NONO, as well as vimentin (**Supplementary Figure 4-12-B**). The green cluster shows high pMHC expression, with lower RNA expression and unchanging protein expression. This cluster contains EMT-related ITGAV, as well as multiple PRKDC peptides (**Supplementary Figure 4-12-C**). It has previously been shown that MEK inhibition can lead to phosphorylation of the kinase PRKDC, involved in cell cycle regulation and DNA damage response, therefore PRKDC may be upregulated by pMHCs through alterations in protein phosphorylation or another processing mechanism not captured in these datasets.[382]

As TAAs were one of the most prominent clusters with coordinating changes in pMHC/RNA/protein expression, we next assessed whether all tumor associated antigens (including TAAs derived from overexpressed proteins, germline genes, etc.) all showed strong correlation. We found that broadly, most RNA and protein levels did not predict changes in pMHC expression beyond those derived melanocyte differentiation genes likely due to their upregulation via ZEB2/SNAIL2/MITF (**Figure 4-13-D**). This suggests that while transcript or

protein expression assays may be used to predict upregulated pMHC expression in MEKi treated cells, changes in abundance of other tumor antigen targets of interest cannot necessarily be predicted using protein/transcript abundance data alone.

We next compared the pMHC/RNA/protein expression data to the ubiquitination data, however only 192 source proteins of pMHCs had ubiquitination quantitation. Still, this comparison revealed similar findings to the analyses between RNA/protein expression data—a majority of quantitative pMHC changes cannot be explained by changes in ubiquitination (**Supplementary Figure 4-13-A, B**). The only notable exception are melanoma differentiation antigens, which showed increased degradation tagging in addition to increased RNA/protein (**Supplementary Figure 4-13-C)**. Other pMHCs increasing in presentation showed no change or decreased degradation (**Supplementary Figure 4-13-D, E**), with decreased RNA/protein expression well. Together, this suggests that other post translational modifications, turnover rates, peptide processing, or other mechanisms are likely responsible for the bulk of changes in pMHC, as these three datasets fail to comprehensively explain alterations beyond the melanoma differentiation antigens.

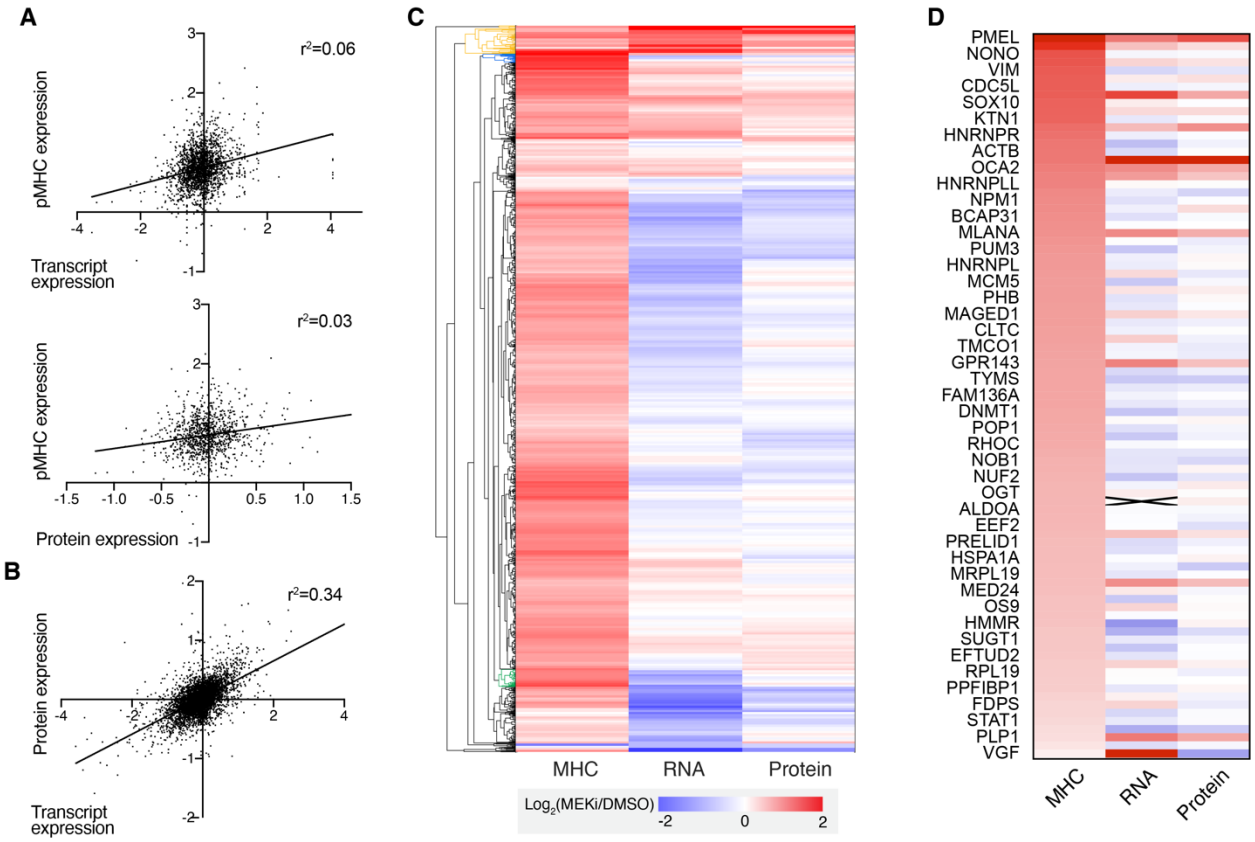

Figure 4-13*. Correlation between pMHC/RNA/protein expression changes with MEKi.* ***A*** *Correlation between pMHC expression and transcript (top) and protein (expression levels) for unique pMHCs in SKMEL5 cells +/- 100 nM MEKi.* ***B*** *Correlation between protein and transcript expression levels for SKMEL5 cells +/- 100 nM MEKi.* ***C*** *Hierarchical clustering of pMHC, RNA, and protein expression, represented as the change in expression following 100 nM MEKi.* ***D*** *Changes in expression (color bar from* ***C****) for TAAs, where every other pMHC is labeled by the corresponding source protein.*

4-2-6 In vivo analyses of MEKi induced pMHC alterations

While enrichment of TAAs, specifically melanoma differentiation antigens, was enriched upon MEK inhibition *in vitro*, we wanted to see if these findings translated *in vivo*. Four melanoma cell lines were inoculated in immunocompromised mice, IPC298/SKMEL2 (*NRAS* mutant) and SKMEL5/SKMEL28 *(BRAF* mutant), and mice were treated with vehicle control or binimetinib for 1, 2, 3, or 5 days in triplicate prior to tumor harvesting (**Figure 4-14-A**). For *BRAF* mutant lines, three additional mice were treated for 3 days with encorafinib (BRAF inhibitor) or

encorafinib and binimetinib as a combination therapy, as is common in the clinic for *BRAF* mutant melanomas. Harvested tumors were homogenized, and class-I MHCs were isolated by immunoprecipitation, purified by molecular weight size exclusion, labeled with TMT-Pro to accommodate labeling of 15 samples within a single analysis, and analyzed by LC-MS/MS. Encorafinib and combination treated tumors for SKMEL5/SKMEL28 were run in a separate analysis and utilized either replicate control samples or a bridge channel for comparison between the analyses (**Table 4-4**). A time course of early response to these two kinase inhibitors was selected to better understand when expression levels reach their peak, and how long the duration of that response lasts. While the time courses are not expansive, this information is useful in understanding how and when to combine targeted therapies like kinase inhibitors with other types of immunotherapies for optimal efficacy.

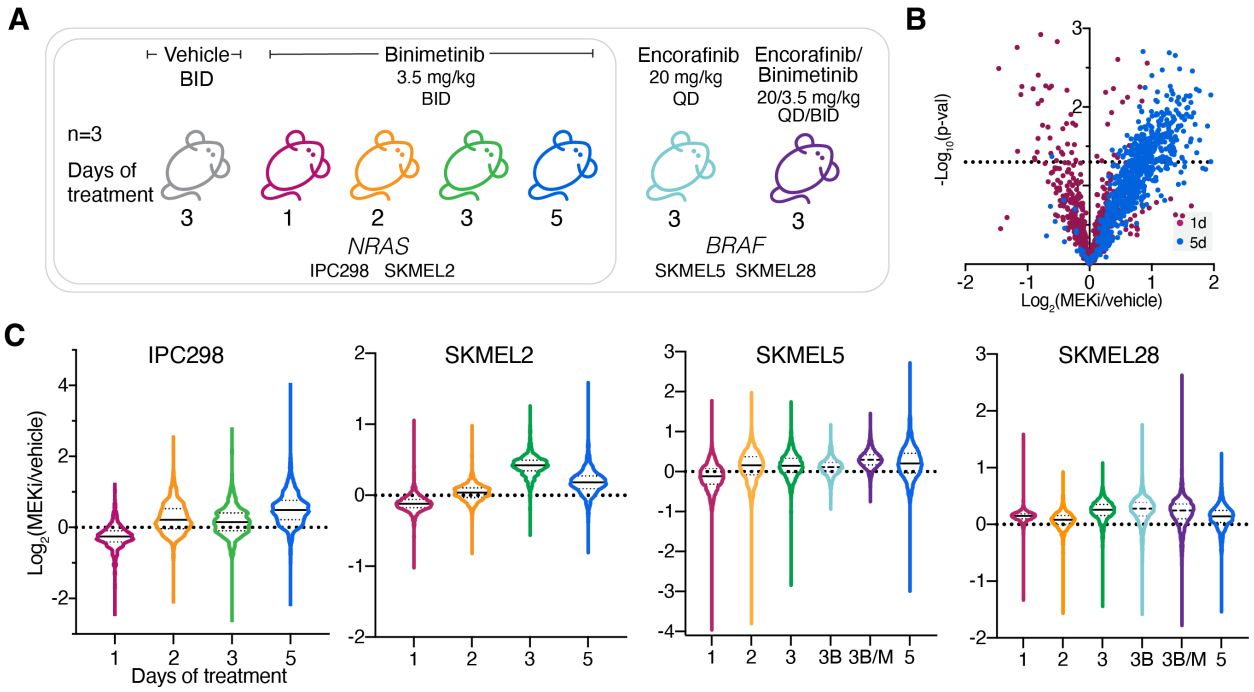

Figure 4-14*. In vivo CLX MEKi-induced pMHC expression changes.* ***A*** *Experimental setup for cell line xenograft studies of mice + binimetinib or encorafinib. BRAF inhibitor (BRAFi, encorafinib) treated mice*

treated mice are subsequently labeled "3B" for BRAFi and encorafinib/binimetinib combination mice are subsequently labeled "3B/M" (BRAFi/MEKi).

Combined, we identified a total of 6,767 unique pMHCs derived from 3,653 source proteins, which followed the expected class I length distribution (**Supplementary Figure 4-14**). Across cell lines, treatment with binimetinib for just 1 or 2 days showed a minimal effect on bulk increases to HLA presentation levels. In IPC298, SKMEL2, and SKMEL5 cells, on average pMHC levels actually slightly decreased. (**Figure 4-14-B,C**). For IPC298 and SKMEL5 cells, the peak change in expression with MEKi only was observed at 5 days of dosing, whereas the maximum increase was seen at 3 days for SKMEL2 and SKMEL28 cells. This suggests that longer treatment may continue to increase expression in some cases, but in others pMHC levels may actually start to decline. In BRAF mutant melanoma cell lines treated with a BRAF inhibitor or MEKi/BRAFi combo, the median fold change was highest with the combination therapy compared to any other treatments or time points in SKMEL5 cells, and about equivalent in SKMEL28 cells. These data suggest that the combination therapy may further improve antigenicity of tumors in some cases, or at the very least not hinder pMHC upregulation.

We next performed an enrichment analysis for TAAs but found that only SKMEL28 cells robustly demonstrated TAA enrichment at all timepoints except the 3d encorafinib condition ($p < 0.05$), while the other CLXs each had a single condition with significant enrichment (**Figure 4-15-A**). Nevertheless, melanoma differentiation antigens showed positive increases in presentation following MEK and BRAF inhibition, often above median fold-changes (**Figure 4-15-B,C**). For example, the PMEL peptide "ALDGGNKHFL" had a nearly four-fold increase in presentation after 5 days of MEKi treatment, far exceeding the median pMHC fold-change value of 1.15x. Still, changes in expression generally followed the trends of bulk expression—SKMEL2 CLXs showed the highest change in presentation levels at 3d of MEKi, and correspondingly

TAAs also show the largest change at 3d. SKMEL5 cells were a notable exception, as TAAs showed the highest expression at 5d despite the 3d MEKi/BRAFi combo giving the median change in expression, suggesting that continued MEKi treatment continues to increase differentiation tumor antigens, regardless of bulk expression. Furthermore, it's possible that the combination treatment at 5d may have a similar expression profile, and the duration of MAPK pathway inhibition rather than the drug itself may be primary driver or select upregulated TAAs.

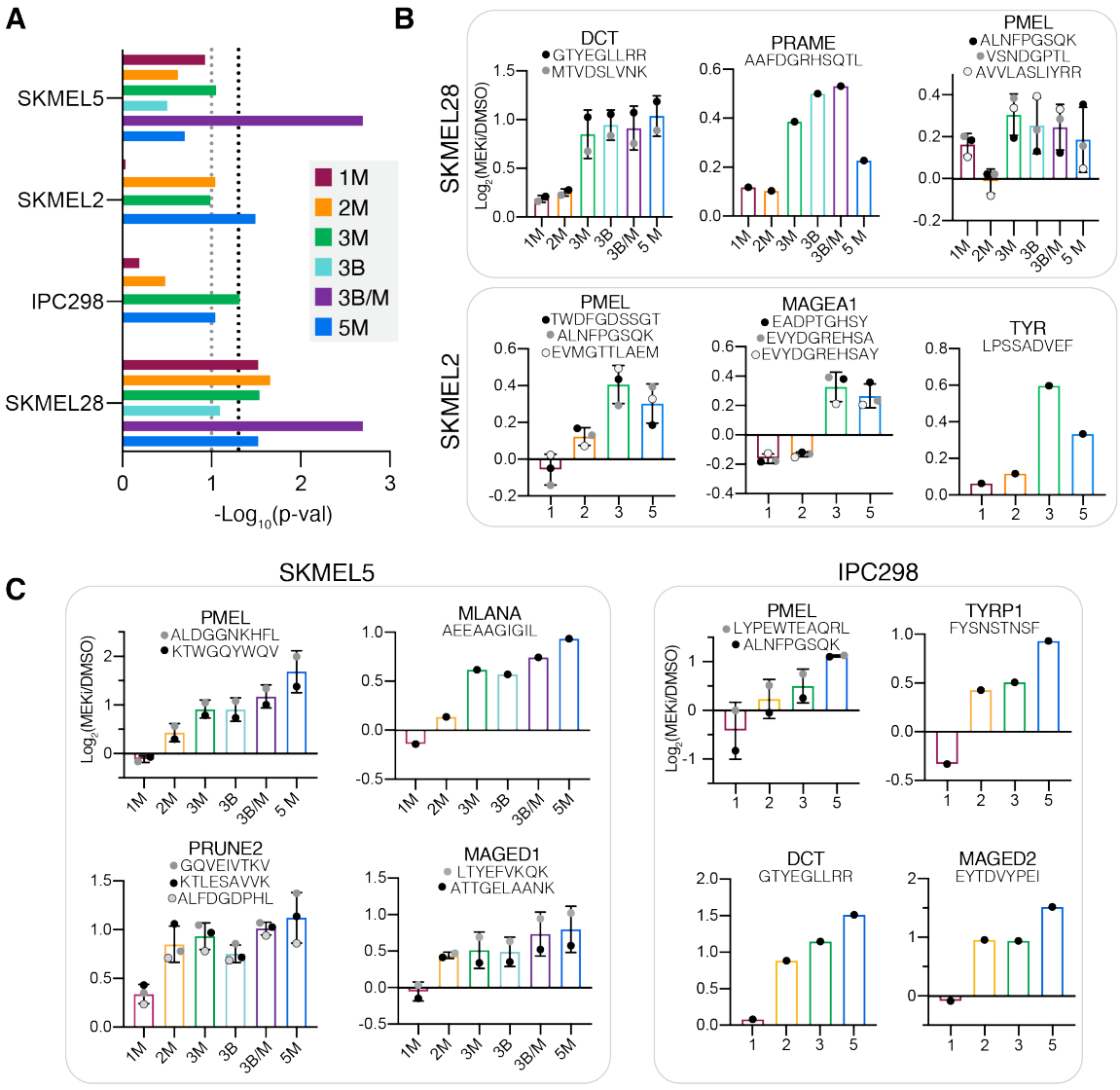

Figure 4-15*. CLX TAA enrichment.* ***A*** *TAA enrichment significance values for each analysis. Black dotted line represents p ≥ 0.05, grey = p ≥ 0.01. M = MEKi treated, B = BRAFi treated.* ***B,C*** *Changes in pMHC*

expression for select melanoma differentiation antigens. Errors bars represent standard deviation when >1 peptide from each source protein was identified.

We next rank ordered the pMHCs in SKMEL5 and SKMEL28 CLXs by integrated peak area abundance, and found that for both analyses, TAAs were significantly enriched in abundance ($p<0.0001$), comparable to the in vitro analyses of the same cell lines (**Figure 4-16-A**). Some of the most abundant enriched TAAs mapped to sequences and source proteins that also had the highest changes in expression, further confirming our initial observations of TAAs being the most abundant and differentially expression pMHCs in tumors following MEK inhibition **Figure 4-16-B**).

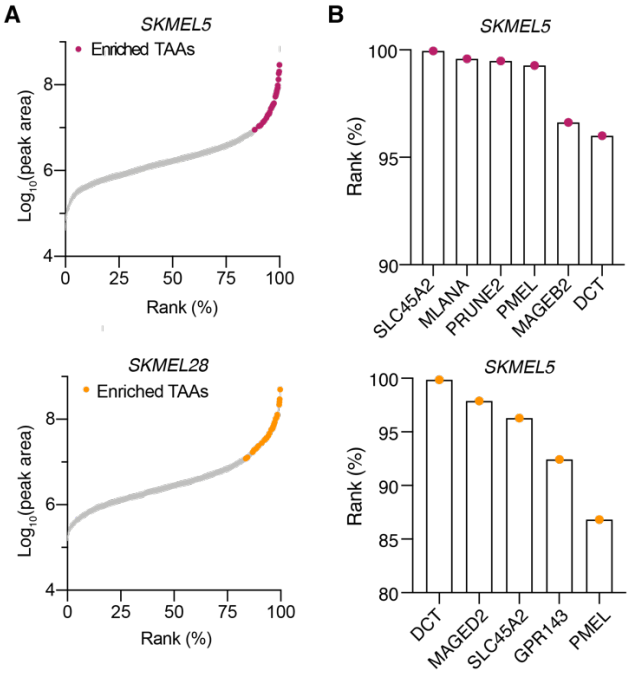

Figure 4-16*. TAAs are of high abundance in CLX models. Rank-ordered abundance of pMHCs in SKMEL5 + MEKi (top) and SKMEL28 + MEKi (bottom) analyses. Positively enriched TAAs are highlighted in color.* ***B*** *Select TAA peptide rank-ordered abundance.*

4-3 CLX models show evidence of EMT-TF switching

We next assessed whether upregulation of melanoma differentiation antigens was driven by ZEB2/SNAI2 EMT-TF switching and upregulated MIF, as was suggested by the *in vitro* SKMEL5 analyses. While enrichment analysis did not identify the EMT pathway as significantly enriched in any of the CLX analyses, EMT-related sites highlighted in the cell line analysis showed pMHC upregulation following MEKi. Increased pMHC expression of ZEB2-derived peptides was seen across all four CLXs, however this pMHC, "GSYSSHISSK," has sequence homology to ZEB1, therefore we are unable to verify it solely came from ZEB2 (**Figure 4-17-A**). SKMEL28 cells contained a second ZEB2-derived pMHC (no sequence homology with ZEB1) that had comparable quantitation. Similarly, SKMEL28 and IPC298 cell line samples contained additional specific ZEB2-derived pMHCs (3 and 2, respectively) that increased in presentation with MEKi with similar dynamics to the non-specific "GSY" peptide (**Figure 4-17-B**), however the "GSY" peptide had the highest quantitation of the ZEB2 pMHCs. As a result, it is likely that the increases in pMHC presentation of the "GSY" peptide in the CLXs is at least partially ZEB2-derived, as increases mirror those of the specific pMHCs. We also observed increases in vitro and in vivo of MITF-derived pMHCs (**Figure 4-17-C**, **Supplementary Figure 4-15-A**), as well as SNAI2 peptides (**Supplementary Figure 4-15-B**), further suggesting an EMT-TF switch that leads to select TAA upregulation following MAPK pathway inhibition with either MEKi or BRAFi. Other significantly enriched pathways include negatively enriched E2F targets and G2M checkpoints (**Table 4-5**), which have some overlap with the cell line negative enrichment results (**Supplementary Figure 4-16**).

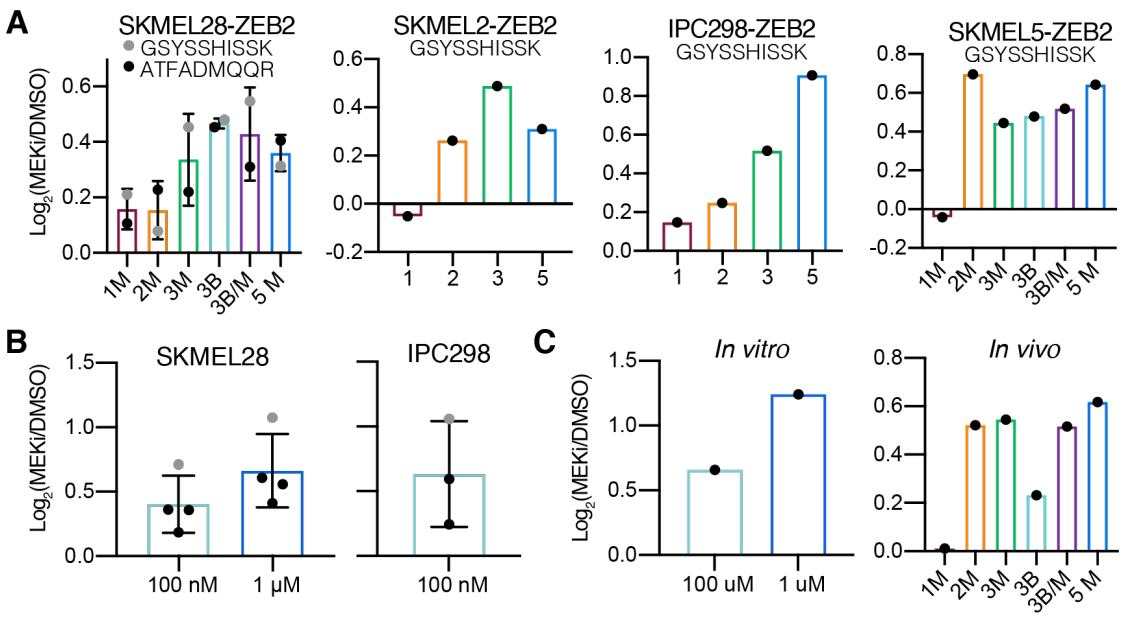

Figure 4-17. *EMT-TF switching in CLX models.* ***A*** *Changes in ZEB2-derived pMHC expression levels with treatment for 1-5 days in CLX models. M = MEK inhibitor treated, B = BRAF inhibitor treated, M/B = combination therapy.* ***B*** *Change in expression of ZEB2-derived pMHCs in SKMEL28 (left) and IPC298 (right) in vitro.* Grey data point represents the "GSYSSHISSK" peptide. **C** Changes in expression of MITF-derived peptide in SKMEL5 cell lines treated with MEKi (left) for 3 days or SKMEL5 CLX treated with MEKi, BRAFi, or combo for 1-5days.

4-4 Correlation of TAAs and MITF expression in human melanoma

In vitro and *in vivo* analyses have highlighted an increase in MHC expression and provided evidence of EMT-TF switching as a mechanism that selectively drives increased melanoma differentiation antigen expression. We next queried transcriptional data from a TCGA study of cutaneious melanoma to investigate whether there was a relationship between tumor antigen expression and EMT-TF phenotypes.[383] Previous work by Akbani et al. performed a hierarchical clustering analysis of differentially regulated gene and identified three subclasses termed "immune" for those with high immune infiltration, "MITF-low" for tumors with low MITF expression of MITF target genes including pigmentation and epithelial expression, and a "keratin" subtype. Interestingly, MITF-low tumors had a higher proportion of *BRAF* mutations,

which aligns with the predicted phenotype for MAPK mutant, high pERK tumors as described in the EMT-TF switching model.

We investigated the 150 *BRAF* mutant tumors and found that the MITF-low tumors had a lower probability (p=0.07) of survival compared to the “immune” tumors, though not as statistically significant as the analysis reported by Akbani et al. comparing all ~300 tumors in the study (

Figure 4-18-A). The MITF-low classified tumors had low expression of genes mapping to the “differentiation” phenotype (MITF, E-cadherin, ZEB2, and SNAI2), with higher expression of the “invasion/tumorigenesis” phenotype (N-cadherin, ZEB1, TWIST1) (

Figure 4-18-B). In line with this finding, “immune” classified tumors had significantly higher expression of SNAI2, E-cadherin, and MITF, and significantly lower expression of N-cadherin than MITF- tumors (

Figure 4-18-C). Tumors with higher immune infiltration scores also have significantly higher HLA expression, and HLA expression is significantly positively correlated with MITF expression & E-cadherin, and negatively correlated with N-cadherin (

Figure 4-18-D,E, Supplementary Figure 4-17), While the treatment courses for each patient aren’t available, it is possible that treatment with a MAPK pathway inhibitor (BRAFi or MEKi) in *BRAF* mutant patients with low MITF expression may drive an increase in HLA expression and tumor antigen presentation and increase tumor immunogenicity and susceptibility to cancer immunotherapy.

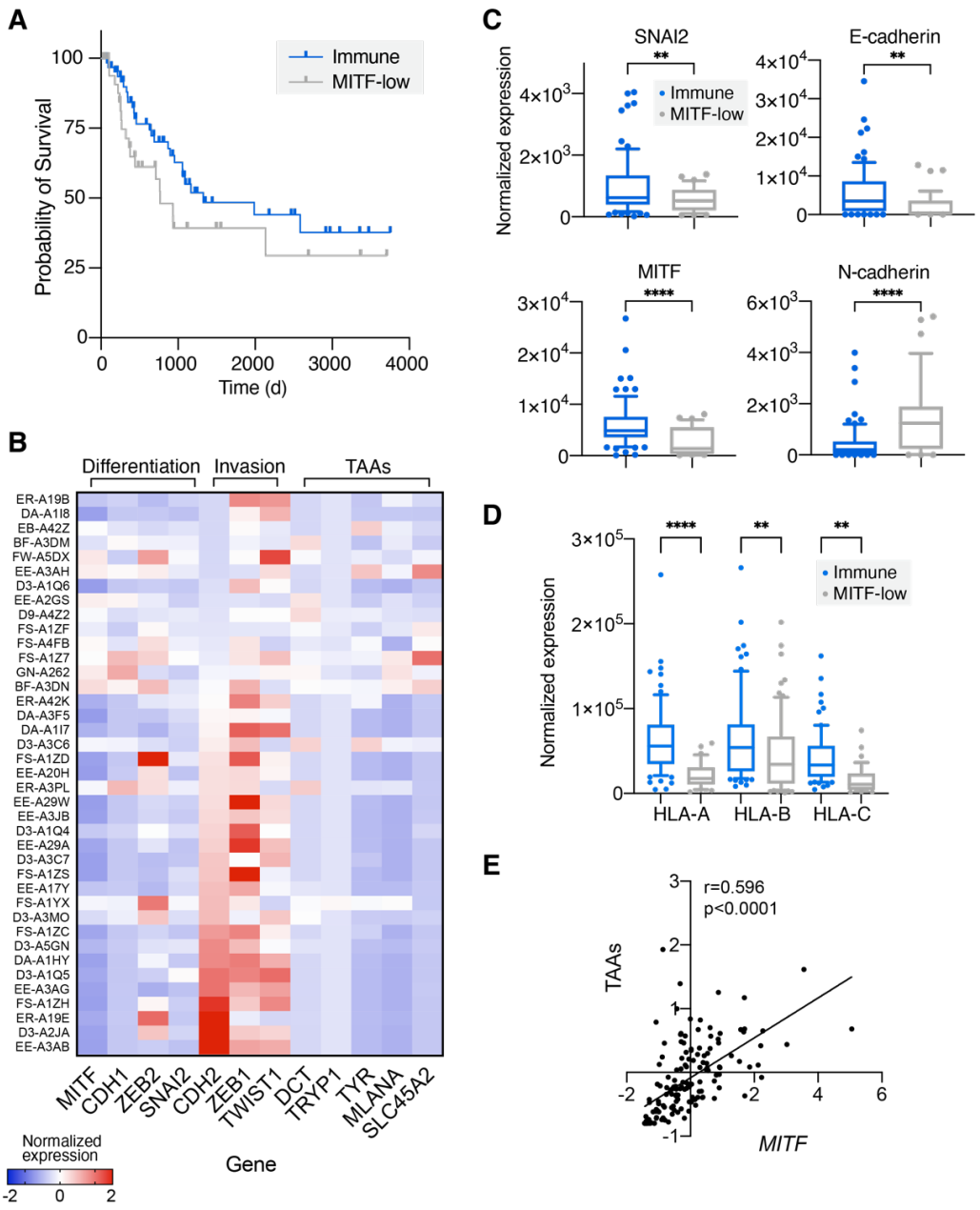

Figure 4-18. *EMT-TF switching evidence in TCGA melanoma tumors.* ***A*** *Kaplan Meier curve of BRAF mutant melanomas from TCGA subcutaneous melanoma study.* ***B*** *Heatmap of select genes from BRAF mutant melanoma TCGA patients. Normalized expression is z-scored against all tumors in the study.* ***C*** *Normalized expression of EMT genes and MITF.* ***D*** *Normalized expression of HLA-A/B/C in Immune and MITF-low tumors.* ***E*** *Correlation in expression of MITF and average TAA Z-scored expression. **p<0.01, ****p<0.0001.*

4-5 Discussion

Mitogen activated pathway kinase (MAPK) inhibitors such as MEK and BRAF inhibitors have demonstrated success at extending progression free survival in *BRAF* and *NRAS* mutant melanoma patients, however the therapeutic response is often short lived, and resistance quickly develops. Immunotherapies have longer lasting efficacy, but only a subset of patients respond. To expand therapeutic efficacy, combining targeted therapies like MEK and BRAF inhibitors with and immunotherapy, though the optimal dosing and timing remains an open area of research. Previous work has demonstrated that MEK and BRAF inhibitors can increase the gene and protein expression of some tumor antigens, and class-I MHC expression is upregulated. However, how the pMHC repertoire is altered in response to MEK inhibition has not been robustly explored.

Here, we apply multiplexed, quantitative pMHC profiling to determine the expression level changes of thousands of pMHCs within a single analysis. We confirm that MEK inhibition increases pMHC expression levels with mass spectrometry and flow cytometry across a panel of six cell lines, even if the dose is substantially below the half maximal inhibitory concentration (100 nM treatment in SKMEL5 cells increased pMHC expression 1.65x with a 12 μM IC_{50}.) We found that TAAs were significantly upregulated in expression compared to the median change following MEK inhibition, and that the TAAs represented some of the most abundant pMHCs presented. An in vivo analysis of CLXs found the same results.

We next explored potential mechanisms of selective TAA upregulation and found evidence of EMT-TF switching, with increased levels of epithelial markers and SNAI2/ZEB2 following MEKi. This is suspected to increase MITF expression, which drives expression of differentiation antigens like TYRP1, gp100, and TYR. Of interest, high ZEB2 expression is associated with better clinical outcomes in an analysis of 178 primary melanomas, and similarly

low MITF expression is associated with worse clinical outcomes and tumors have lower levels of immune infiltration in *BRAF* mutant tumors from the TCGA study.[380,383] Together, this suggests that MEK inhibitor treatment in MAPK-mutant melanomas may drive increases in pMHCs and TAA presentation, as well as increase immune cell infiltration. These changes may improve the efficacy of immunotherapy, however future studies, including the release of data from ongoing clinical trials exploring dosing schedules, will be important in evaluating how to combine these therapies together.

While pMHC changes in expression mirrors transcriptional and protein expression changes for melanoma differentiation antigens, most pMHC changes did not correlate with RNA/protein data, suggesting other mechanisms including post translational modifications, protein processing and turnover, protein cellular compartment, etc. that may dictate pMHC presentation differences. We explored degradation rates, using qualitative ubiquitination mass spectrometry to measure peptides tagged for degradation, and highlight Vimentin as a protein that's increase in pMHC expression levels may be explained by altered degradation rather than transcription/translation. Still, this remains an open area of research, and combining quantitative pMHC datasets with other quantitative data types may further elucidate how pMHC presentation is regulated, and whether other datatypes may predict pMHC changes. This could be useful clinically, as pMHC analyses require large sample input, so a targeted assay for transcript or protein expression to predict upregulated antigens would be advantageous.

Ultimately, MEK inhibitor-induced upregulation of known melanoma antigens provides compelling evidence to combine MEKi treatment with checkpoint blockage or other targeted immunotherapies which target these antigens. Relative and absolute quantitative pMHC analyses exploring different durations of treatment, dosing schedules, and how the repertoire is altered when therapeutic resistance emerges will enable a deeper understanding of repertoire alterations that can be leveraged.

4-6 Materials and Methods

4-6-1 Human cell lines

SKMEL5, SKMEL28, A375, and RPMI-7951 cell lines were obtained from ATCC [ATCC HTB-70, ATCC HTB-72, CRL1619, and HTB-66, respectively] and maintained in DMEM medium (Corning). IPC298 and SKMEL2 cells were provided by Array Biopharma and maintained in RPMI 1640 (Gibco) and MEM-α (Gibco) mediums, respectively. All medium was supplemented with 10% FBS (Gibco) and 1% penicillin/streptomycin (Gibco). Cells were routinely tested for mycoplasma contamination, and maintained in 37 °C, 5% CO_2. Experiments were performed on passages 4-8.

4-6-2 Cell line xenografts

SKMEL5, SKMEL28, SKMEL2, and IPC298 cell lines were used for cell line xenograft (CLX) analyses in collaboration with Array Biopharma. 100 μL containing $5x10^6$ cells in 50% Matrigel via subcutaneous injection was implanted into 30 NCr nu/nu mice on the right flank. Tumors were allowed to grow to a starting size of ~200-400mg, after which animals were measured/weighed and randomized into study groups based on tumor volume. BID and QD dosing orally was subsequently initiated: Binimetinib (MEK162): 3.5 mg/kg, Vehicle (1% CMC/0.5% Tween80), Encorafenib: 20 mg/kg. Compound doses were prepared (MEK162: 0.35 mg/mL, LGX818: 2.0mg/mL) and resuspended in 1% CMC/ 0.5% Tween80, vortexed, and sonicated for 10 minutes prior to dosing. Dosing continued for 5 days, and at the end of each time course tumors were harvested and flash frozen in liquid nitrogen. Animals were housed in groups of 3. Food, water, temperature and humidity are according to Pharmacology Testing Facility performance standards (SOP's) which are in accordance with the 1996 Guide for the Care and Use of Laboratory Animals (NRC) and AAALAC-International. Dosing schedules are listed in **Table 4-6**.

4-6-3 Dose response assays

Half-maximal inhibitory concentrations (IC_{50}) of binimetinib (Selleckchem, MEK162) were determined for each cell line using CellTiter-Glo luminescent cell viability assay (Promega). Cells were seeded at density of 10,000 (SKMEL2, SKMEL28, IPC298) or 5,000 (SKMEL5, A375, RPMI-7951) cells/well in a 96 well plate and allowed to adhere overnight. Cells were then treated with binimetinib or DMSO as a vehicle control in fresh medium for 72h and assayed. Data was acquired using a Tecan plate reader Infinite 200 with Tecan icontrol version 1.7.1.12. IC_{50} values were calculated using a 4-parameter logistic curve in Prism 9.0.0.

4-6-4 Flow cytometry

For analysis of cells by flow cytometry, cells were lifted with 0.05% Trypsin-EDTA and 10^6 cells/mL were spun at 300 g for 3 minutes, washed with ice cold PBS supplemented with 1% FBS and 0.1% sodium azide (flow buffer) and incubated with fluorophore-conjugated antibody at 0.5 µg mL^{-1} in flow buffer for 30 minutes on ice. After incubation, cells were washed again, and resuspended in flow buffer plus 5 µL of propidium iodide staining solution (10 µg mL^{-1}, Invitrogen) per sample. Analyses were performed on an LSRII (BD Biosciences) and data analyzed using FlowJo (version 10.6.2). Antibodies: Alexa Fluor 488 HLA-A, B, C, clone W6/32 [Biolegend, cat # 311413].The gating strategy used for all experiments is located in the supplemental information in Stopfer et al.[188]

4-6-5 UV-mediated peptide exchange for hipMHCs

UV-mediated peptide exchange was performed using recombinant, biotinylated Flex-T HLA-A*02:01 monomers (BioLegend), using a modified version of the commercial protocol. Briefly, 4 µL of 500 µM peptide stock, 2 µL of Flex-T monomer, and 32 µL of 1X PBS were combined in a 96-well U bottom plate. On ice, plates were illuminated with ultraviolet light (365

nm) for 30 minutes, followed by a 30 minute incubation at 37 °C protected from light. Concentration of stable complexes following peptide exchange was quantified using the Flex-T HLA class I ELISA assay (Biolegend) per manufacturer's instructions for HLA-A*02:01. ELISA results were acquired using a Tecan plate reader Infinite 200 with Tecan icontrol version 1.7.1.12.

4-6-6 Peptide MHC isolation

Cultured cells were seeded in 10 cm plates, allowed to adhere overnight, and treated for 72h with binimetinib or DMSO vehicle control. At the time of harvest, cells were washed with 1x PBS, and lifted using 0.05% Trypsin-EDTA (Gibco). Cells were pelleted at 500 g for 5 minutes, washed twice more in 1x PBS, and pelleted again. Cells were resuspended in 1 mL lysis buffer [20 nM Tris-HCl pH 8.0, 150 mM NaCl, 0.2 mM PMSO, 1% CHAPS, and 1x HALT Protease/Phosphatase Inhibitor Cocktail (Thermo Scientific)], followed by brief sonication (3 x 10 second microtip sonicator pulses) to disrupt cell membranes. Lysate was cleared by centrifugation at 5000 g for 5 minutes and quantified using bicinchoninic acid protein assay kit (Pierce). For in vitro analyses, $1x10^7$ cells were used for each condition. Frozen CLX tumor samples were homogenized in lysis buffer, cleared by centrifugation, and quantified using BCA as described in the in vitro analyses. For each sample, 7 mg of lysate was used.

Peptide MHCs were isolated by immunoprecipitation (IP) and size exclusion filtration, as previously described.[188] Briefly, for each condition 0.5 mg of pan-specific anti-human MHC Class I (HLA-A, HLA-B, HLA-C) antibody (clone W6/32, Bio X Cell [cat # BE0079]) was bound to 20 µL FastFlow Protein A Sepharose bead slurry (GE Healthcare) for 3 hours rotating at 4 °C. Beads were washed 2x with IP buffer (20 nM Tris-HCl pH 8.0, 150 mM NaCl) prior to lysate and hipMHC addition (*in vitro analyses)*, and incubated rotating overnight at 4 °C to isolate pMHCs.

For hipMHCs: 30 fmol of the following isotopically labeled pMHC standards were added prior to IP for quantification correction: ALNEQIARL[7], SLPEEIGHL[7], and SVVESVKFL[7]. Beads were washed with 1x TBS and water, and pMHCs were eluted in 10% formic acid for 20 minutes at room temperature (RT). Peptides were isolated from antibody and MHC molecules using a passivated 10K molecule weight cutoff filters (PALL Life Science), lyophilized, and stored at -80°C.

4-6-7 pMHC labeling with Tandem Mass Tags and SP3 cleanup

For labeled analyses, 100 µg of pre-aliquoted Tandem Mass Tag (TMT) 6-plex, 10-plex, or TMT-pro was resuspended in 30 µL anhydrous acetonitrile, and lyophilized peptides were resuspended in 100 µL 150 mM triethylammonium bicarbonate, 50% ethanol. Both were gently vortexed, centrifuged at 13,400 g for 1 minute, and combined. TMT/peptide mixtures were incubated on a shaker for 1 hour at RT, followed by 15 minutes of vacuum centrifugation. After combining labeled samples, we washed tubes 2x with 25% acetonitrile (MeCN) in 0.1% acetic acid (AcOH) and added it to the labeled mixture, which was subsequently centrifuged to dryness.

Sample cleanup was performed using single-pot solid-phase-enhanced sample preparation (SP3) as previously described.[290] Briefly, a 1:1 mix of hydrophobic/hydrophilic Sera-mag carboxylate-modified speed beads (GE Healthcare) was prepared at a final bead concentration of 10 µg μL^{-1}. Labeled samples were resuspended in 30 µL of 100 mM ammonium bicarbonate (pH 7-8) and added to 500 µg of bead mix with 1 mL MeCN. Peptides were allowed to bind for 10 minutes at RT, washed 2x with MeCN, and eluted with 2% DMSO for 1 minute of sonication in a bath sonicator. TMT-labeled peptides were transferred to a fresh microcentrifuge tube and centrifuged to dryness.

4-6-8 Global protein expression profiling sample preparation

For a quantitative global proteomics analysis, 300 ug of supernatant from DMSO and 100 nM MEKi sample for SKMEL5 cells was diluted 8-fold in 8M urea, reduced with 10 mM dithiothreitol in 100 mM ammonium acetate (pH 8.9) at 56°C for 45 minutes, and subsequently alkylated with 50 mM iodoacetamide for 45 minutes rotating at RT in the dark. Lysates were diluted 4-fold with 100 mM ammonium acetate and digested with sequence-grade trypsin (Promega) overnight at RT at an enzyme:substrate ratio of 50:1 (w/w). The reaction was quenched with formic acid (5% total volume) and desalted on C18-based STAGE tips. Solvents: 0.1% formic acid, 90% acetonitrile (MeCN) in 0.1% formic acid, and 60% acetic MeCN in 0.1% formic acid. Volumes were reduced with vacuum centrifugation and lyophilized in 150 ug aliquots. Peptide aliquots were labeled with TMT10-plex reagents in 70% ethanol/150 mM triethylammonium bicarbonate (TEAB) for 1 hour at room temperature, pooled, brought to dryness with vacuum centrifugation, and stored at -80°C.

The labeled mixture was resuspended in 0.1% formic acid, and 25% was loaded onto an Agilent Zorbax 300Extend-C18 5 µm 4.6 × 250 mm column on an Agilent 1200 operating at 1 ml/min for fractionation, as previously described.[384] Briefly, peptides were eluted with the following gradient: 1% B to 5% B for 10 mins, 5–35% B for 60 mins, 35-70% B for 15 min, held at 70% B for 5 mins, and was followed by equilibration back to 1% B. Fractions were collected with a Gilson FC203B fraction collector at 1 minute intervals and fractions 10-90 were concatenated to 20 fractions. The fraction volumes were next reduced by vacuum centrifugation, lyophilized, and stored at -80°C prior to analysis.

4-6-9 Ubiquitination sample preparation

SKMEL5 cells were seeded in 10 cm plates and allowed to adhere overnight. Cells were then treated with DMSO or 100 nM binimetinib for 72 hours. Prior to harvest, cells were treated with 100 nM bortezomib (PS-341, SelleckChem) to halt protease activity. Cells were next washed with ice cold 1X PBS and lysed in 8M Urea. Lysates were processed to tryptic peptides as described in the global protein expression methods and desalted using SepPak plus cartridges. Five mg aliquots per sample were lyophilized and stored at 80 °C prior to analysis.

PRMScan ubiquitin remnant motif (anti–K-ε-GG) antibody beads (Cell Signaling Technology, #5562) were crosslinked as previously described.[385] Briefly, beads were washed 3x with 100 mM sodium borate pH 9, incubated in cross linking buffer (20 mM DMP in 100 mM sodium borate pH9) for 30 mins (RT, rotation). Beads were next washed 3x with blocking buffer (200 mM ethanolamine, pH 8) and incubated for 2 hours at 4°C rotating. Crosslinked beads were washed 3x with immunoprecipitation buffer (100 mmol/l Tris–HCl, 1% Nonidet P-40 at pH 7.4) and stored in 1X PBS with 0.02% sodium azide at 4°C prior to use.

Each sample was resuspended in 1 mL IP buffer and added to 40 uL bead slurry of conjugated anti–K-ε-GG beads and incubated for 2 hours rotating at 4°C.[386] Peptides were washed 2x with IP buffer and 3x with 1X PBS, and diGly peptides were eluted 2x with 0.2% TFA for 5 minutes. To improve specificity, each lysate was IP'd twice, following the same IP protocol with the first elution. Finally, peptides were dried with vacuum centrifugation and lyophilized.

Lyophilized samples were next labeled with 100 ug of TMT-6plex, as described in the MHC labeling methods section. A high pH reverse-phase peptide fraction kid was used to separate labeled peptides into six fractions, according to manufacturer's instructions (17.5%, 20%, 22.5%, 25%, 30%, and 70% MeCN). Volumes of peptide fractions was reduced with vacuum centrifugation, lyophilized and stored at -80°C prior to analysis.

4-6-10

4-6-11 RNA-sequencing

RNA was isolated from 10 cm plates of SKMEL5 cells with 3 biological replicates per condition (DMSO, 100 nM binimetinib, 1 μM binimetinib). Prior to harvest, cells were washed with ice-cold 1X PBS over ice and lysed in TRIzol reagent (Thermo Fisher Scientific). Total RNA was isolated from each sample using Direct-zol RNA miniprep kit (Zymo Research) according to manufacturer's instructions.

RNA were confirmed for quality using the Agilent Fragment Analyzer and 300 ng of material was polyA-selected using NEBNext Poly(A) mRNA Magnetic Isolation Module (E7490) modified to include two rounds of polyA binding and 10 minute incubations. cDNA was generated using the NEB Ultra II directional kit (E7760) following manufacturers protocol using 12 cycles of PCR and an 0.9X SPRI clean. The resulting libraries were quality assessed using the Fragment Analyzer and quantified by qPCR prior to be sequenced on the Illumina HiSeq2000. The 40nt single-end reads with an average depth of 5 million reads per sample were sequenced for all conditions.

RNAseq reads were aligned to the human transcriptome prepared with the hg38 primary assembly and the Ensembl version 95 annotation using STAR version 2.5.3a.[291] Gene expression was summarized with RSEM version 1.3.0 and SAMtools version 1.3.[292,293] Differential expression analysis was performed with DESeq2 version 1.24.0 running under R version 3.6.0 with normal log fold change shrinkage.[294] Significance values (adjusted p value) are determined using the Wald test, and are multiple hypothesis corrected using Benjamini-Hochberg (BH) method. The resulting data were parsed and assembled using Tibco Spotfire Analyst version 7.11.1.

4-6-12 HF-X LC-MS/MS data acquisition

Chromatography:

Peptides were resuspended in 0.1% acetic acid and loaded on a precolumn packed in-house (100 µm ID × 10 cm packed with 10 µm C18 beads (YMC gel, ODS-A, 12 nm, S-10 µm, AA12S11)). The precolumn was then washed with 0.1% acetic acid and connected in series to an analytical capillary column with an integrated electrospray tip (~1 µm orifice) with 5µM C18 beads, prepared in house ((50 µm ID × 12 cm with 5 µm C18 beads (YMC gel, ODS-AQ, 12 nm, S-5 µm, AQ12S05)).

Labeled pMHC analyses:

Peptides were eluted using a 130 minute gradient with 10-45% buffer B (70% Acetonitrile, 0.2M acetic acid) from 5-100 minutes and 45-55% buffer B from 100-120 minutes at a flow rate of 0.2 mL/min for a flow split of approximately 10,000:1. Peptides were analyzed using a Thermo Q Exactive HF-X Hybrid Quadrupole-Orbitrap mass spectrometer, and data was acquired using Thermo Fisher Scientific Xcalibur version 2.9.0.2923. Standard mass spectrometry parameters were as follows: spray voltage, 2.5 kV; no sheath or auxiliary gas flow; heated capillary temperature, 250 °C.

The HF-X was operated in data-dependent acquisition (DDA) mode for LF and TMT analyses. LF: Full-scan mass spectrometry spectra (mass/charge ratio (*m/z*), 350 to 2,000; resolution, 60,000) were detected in the Orbitrap analyzer after accumulation of ions at $3e^6$ target value with a maximum IT of 50 ms. For every full scan, the top 20 most intense ions were isolated (isolation width of 0.4 *m*/*z*) and fragmented (collision energy (CE): 28%) by higher energy collisional dissociation (HCD) with a maximum injection time of 350 ms, AGC target $1e^5$,

and 30,000 resolution. Charge states < 2 and > 4 were excluded, and dynamic exclusion was set to 45 seconds. TMT: Full-scan mass spectrometry spectra (mass/charge ratio (*m/z*), 400 to 2,000; resolution, 60,000) were detected in the Orbitrap analyzer after accumulation of ions at $3e^6$ target value with a maximum IT of 50 ms. For every full scan, the 20 most intense ions were isolated (isolation width of 0.4 *m*/*z*) and fragmented (collision energy (CE): 31%) by higher energy collisional dissociation (HCD) with a maximum injection time of 350 ms, AGC target $1e^5$, and 30,000 resolution. Charge states < 2 and > 4 were excluded, and dynamic exclusion was set to 60 seconds.

Global protein expression profiling:

Peptides were analyzed using a Thermo Q Exactive HF-X Hybrid Quadrupole-Orbitrap mass spectrometer. Standard mass spectrometry parameters were as follows: spray voltage, 2.5 kV; no sheath or auxiliary gas flow; heated capillary temperature, 250°C. Peptides were eluted with 80% acetonitrile in 0.1% formic acid (solvent B) in following gradient: 0–10% buffer B for 5 min, 10–30% for 100 min, 30–40% for 14 min, 40–60% for 5 min, 60–100% for 2 min, held at 100% of 10 mins, and equilibrated back to 0.1% formic acid. All twenty fractions were analyzed back-to-back to minimize effects from instrument performance variation.

The HF-X was operated in data-dependent acquisition (DDA) mode. Full-scan mass spectrometry spectra (mass/charge ratio (*m/z*), 300 to 2,000; resolution, 60,000) were detected in the Orbitrap analyzer after accumulation of ions at $3e^6$ target value with a maximum IT of 50 ms. For every full scan, the 15 most intense ions were isolated (isolation width of 0.4 *m*/*z*) and fragmented (collision energy (CE): 31%) by HCD with a maximum injection time of 350 ms, AGC target $1e^5$, and 30,000 resolution. Charge states of 1 and >7 were excluded, and dynamic exclusion was set to 20 seconds.

Ubiquitination analyses:

The same gradient and standard instrument parameters from global protein expression profiling were used for ubiquitination analyses. The HF-X was operated in data-dependent acquisition (DDA) mode. Full-scan mass spectrometry spectra (mass/charge ratio (m/z), 400 to 1,250; resolution, 60,000) were detected in the Orbitrap analyzer after accumulation of ions at 5e5 target value with a maximum IT of 100 ms. For every full scan, the 20 most intense ions were isolated (isolation width of 0.4 m/z) and fragmented (collision energy (CE): 33%) by HCD with a maximum injection time of 300 ms, AGC target 1e5, and 60,000 resolution. Charge states of <3 and >7 were excluded, and dynamic exclusion was set to 30 seconds. The six fractions were analyzed back-to-back to minimize effects from instrument performance variation.

4-6-13 Exploris 480 LC-MS/MS data acquisition

pMHC samples were analyzed using an Orbitrap Exploris 480 mass spectrometer (Thermo Scientific) coupled with an UltiMate 3000 RSLC Nano LC system (Dionex), Nanospray Flex ion source (Thermo Scientific), and column oven heater (Sonation). Samples were resuspended in 0.1% formic acid and directly loaded onto a 10-15 cm analytical capillary chromatography column with an integrated electrospray tip (~1 µm orifice), prepared and packed in house (50 µm ID × 20 cm & 1.9 µM C18 beads, ReproSil-Pur). pMHC elutions were injected in 15-25% fractions for improved coverage of the immunopeptidome.

TMT-6/10: Peptides were eluted using a gradient with 8-25% buffer B (70% Acetonitrile, 0.1% formic acid) for 50 minutes, 25-35% for 25 minutes, 35-55% for 5 minutes, 55-100% for 2 minutes, hold for 1 minutes, and 100% to 3% for 2 minutes.

TMT-Pro: Peptides were eluted using a gradient with 8-25% buffer B (70% Acetonitrile, 0.1% formic acid) for 50 minutes, 25-45% for 30 minutes, 45-100% for 2 minutes, hold for 1 minutes, and 100% to 3% for 2 minutes.

Standard mass spectrometry parameters were as follows: spray voltage, 2.0 kV; no sheath or auxiliary gas flow; heated capillary temperature, 275 °C. The Exploris was operated in data dependent acquisition (DDA) mode. Full scan mass spectra (350-1200 m/z, 60,000 resolution) were detected in the orbitrap analyzer after accumulation of $3e^6$ ions (normalized AGC target of 300%) or 25 ms. For every full scan, MS^2 were collected during a 3 second cycle time. Ions were isolated (0.4 m/z isolation width) for a maximum of 150 ms or 75% AGC target and fragmented by HCD with 32% CE (TMT-6/10) or 30% (TMT-pro) at a resolution of 45,000. Charge states < 2 and > 4 were excluded, and precursors were excluded from selection for 30 seconds if fragmented n=2 times within 20 second window.

4-6-14 LC-MS/MS data analysis:

All mass spectra were analyzed with Proteome Discoverer (PD, version 2.5) and searched using Mascot (version 2.4) against the human SwissProt database. MS/MS spectra were matched with an initial mass tolerance of 10 ppm on precursor masses and 20 mmu for fragment ions. Data analyses were performed using Matlab version R2019b, and Microsoft Excel version 16.34

pMHC analyses: No enzyme was used, static modifications included N-terminal and lysine TMT, and variable modifications included oxidized methionine for all analyses and phosphorylated serine, threonine, and tyrosine for cell treatment analyses. Treatment analyses were also searched against a previously published catalog of over 40,000 predicted antigenic mutations in cancer cell lines.[295] Heavy leucine-containing peptides were searched for

separately with heavy leucine (+7), c-terminal amidation, and methionine oxidation as dynamic modifications against a custom database of the synthetic peptide standards. All analyses were filtered with the following criteria: search engine rank =1, isolation interference ≤ 30%, and length between 8 and 15 amino acids. Label-free analyses were filtered with ion score ≥ 20, and labeled samples were filtered with ion score ≥ 15 and percolator q-value ≤ 0.05. Area under the curve (AUC) quantitation was performed using the minora feature detector in PD with match between runs enabled and filtered for ion score ≥ 20.

For TMT-labeled *in vitro* samples, ratios against a reference channel (usually TMT126) were calculated and the median of all ratios for correction hipMHCs was used to determine the final correction parameters. Only PSMs of heavy leucine-coded peptides with an average reporter ion intensity within 10-fold of the interquartile range of endogenous PSM reporter ion intensities were used for correction. To evaluate differences between conditions, the $\log_2$ transformed ratio of arithmetic mean intensity for drug- and DMSO-treated samples (n=3) was calculated. To determine if peptides were significantly increasing, an unpaired, 2-sided t-test was performed, and peptides with $p \leq 0.05$ were considered significantly increasing/decreasing. To evaluate which peptides were significantly enriched above the mean, treated samples were mean centered by dividing the ion intensity of each peptide by the mean fold-change across all peptides, after which a student's 2-tailed t-test was performed on adjusted values. Peptides with a mean-adjusted p-value ≤ 0.05 were considered significantly enriched. Mean centering was not performed on samples where the mean $\log_2$ fold change was between -0.07 and 0.07.

Global protein expression profiling: Enzyme: trypsin, allowing for up to 2 missed cleavages. Cysteine carbamidomethylation, TMT-labeled lysine, and peptide N-termini were searched as fixed modifications, and oxidated methionine was set as a variable modification. PSMs from all fractions were filtered according to search engine rank = 1, ion score ≥ 20,

precursor isolation interference ≤30%. Reporter ion abundances for peptides mapping to the same protein were summed, and quantification was corrected by normalizing with the median fold change in TMT abundances over TMT-126 to account for variations in sample input. To determine differences in protein expression, an unpaired, 2-sided t-test was performed, and peptides with $p \leq 0.05$ were considered significantly changing.

Ubiquitination analysis: Enzyme: trypsin, allowing for up to 2 missed cleavages. Cysteine carbamidomethylation was set as a static modification, and dynamic modifications were set as diGly-TMT on lysine residues (monoisotopic: 343.20), and N-terminal TMT. PSMs from 6 fractions were filtered to the following criteria: di-Gly modification, search engine rank = 1, ion score ≥ 15, precursor isolation interference ≤ 30%. Reporter ion intensities were summed for PSMs mapping to the same peptide, and the fold change in abundance was calculated by taking the average reporter ion abundance for n=3 replicates per condition. Variation in sample input was account for by normalizing each reporter channel to the median fold change over TMT-126 across all peptides. When multiple peptides mapped to a source protein, the maximal fold change value was used for pMHC comparisons. Significance values were calculated using an unpaired, 2-sided t-test was performed, and peptides with $p \leq 0.05$ were considered significantly changing.

4-6-15 Peptide MHC binding affinity

Binding affinity of 9-mer pMHCs was estimated using NetMHCpan-4.0 against each cell line's allelic profile (**Supplementary Figure 4-5**).[99,280] The minimum predicted affinity (nM) of each peptide was used to assign peptides to their best predicted allele. The threshold for binding was set to 500 nM.

4-6-16 Enrichment analyses

For pMHC pathway and TAA enrichment analyses, gene names from peptide source proteins were extracted and rank ordered according to the average $\log_2$ fold change over DMSO treated cells. In cases where more than one peptide mapped to the same source protein, the maximum/minimum was chosen, depending on the directionality of enrichment analysis. For RNAseq & protein expression data, data sets were rank ordered according to the mean $\log_2$ fold change value with only protein encoding genes considered.

We utilized gene set enrichment analysis (GSEA) 4.0.3 pre-ranked tool against the Molecular Signatures Database hallmarks gene sets with 1000 permutations, weighted enrichment statistic (p=1), and a minimum gene size of 15.[255,281,282] Results were filtered for FDR q-value ≤ 0.25, and nominal p-value ≤ 0.05. P-values > 0.05 in reported analyses are noted. Significantly enriched peptides (mean-adjusted p-value ≤ 0.05) were analyzed using STRING v11 for Gene Oncology (GO) term enrichment against biological processes and cellular components datasets.[256,297] Enriched categories were filtered according to FDR-q value ≤ 0.05.

4-7 TCGA data analysis

mRNASeq normalized gene expression data (MD5) from the TCGA skin cutaneous melanoma study (SKCM) for was obtained from Firebrowse (Broad Institute).[383] Expression for all tumors was z-score normalized, and *BRAF* mutant tumor data was extracted for subsequent analyses. Pairwise gene expression significance comparisons were calculated using an un-paired, two-taled T test, and significance values for HLA expression between MITF-low and immune subtypes were calculated using Sidak's multiple comparisons test.

4-8 Acknowledgements

I'd like thank Eric Brown, Shannon Winski, and Lenka Sinik of Array Biopharma (currently Pfizer Boulder) for collaborating on this project and providing cell line xenograft tumors for analyses and engaging in discussions regarding MEK inhibitor-modulated immunopeptidomes. I'd also like to thank the MIT BioMicro Center (Stuart Levine) and the Swanson Biotechnology Center for technical support, specifically the Flow Cytometry (Glenn Paradis), Biopolymers & Proteomics (Richard Cook & Antonius Koller), and the Barbara K. Ostrom (1978) Bioinformatics core facilities (Charlie Whittaker).

4-9 Supplementary Information

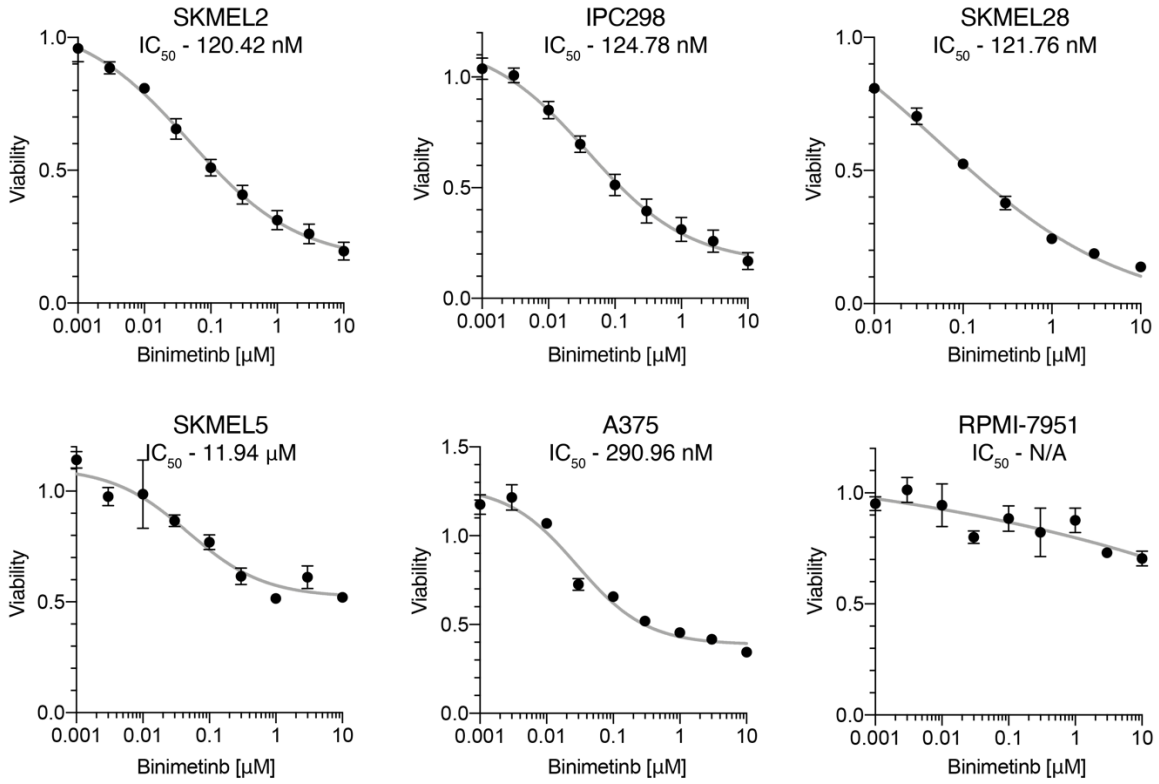

Supplementary Figure 4-1*. Viability assessment (fraction of DMSO control) for cell lines treated with binimetinib for 72hr.*

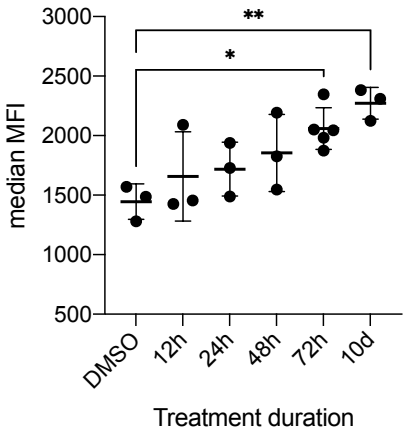

Supplementary Figure 4-2. *Surface MHC expression following 100 nM binimetinib treatment in SKMEL5 cells. Significance: *p<0.05, **p<0.01, Dunnett's multiple comparisons test against DMSO control.*

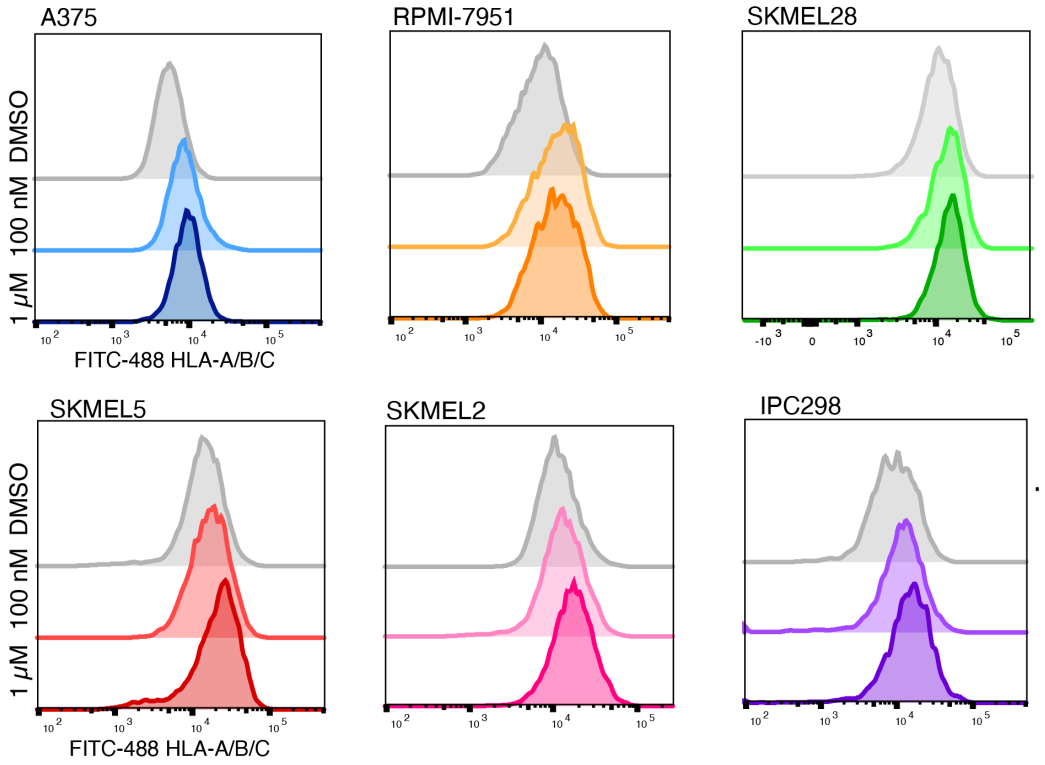

Supplementary Figure 4-3. *Flow cytometry analysis of HLA-ABC expression in melanoma cell lines treated with DMSO, 100 nM or 1 μM binimetinib for 72h.*

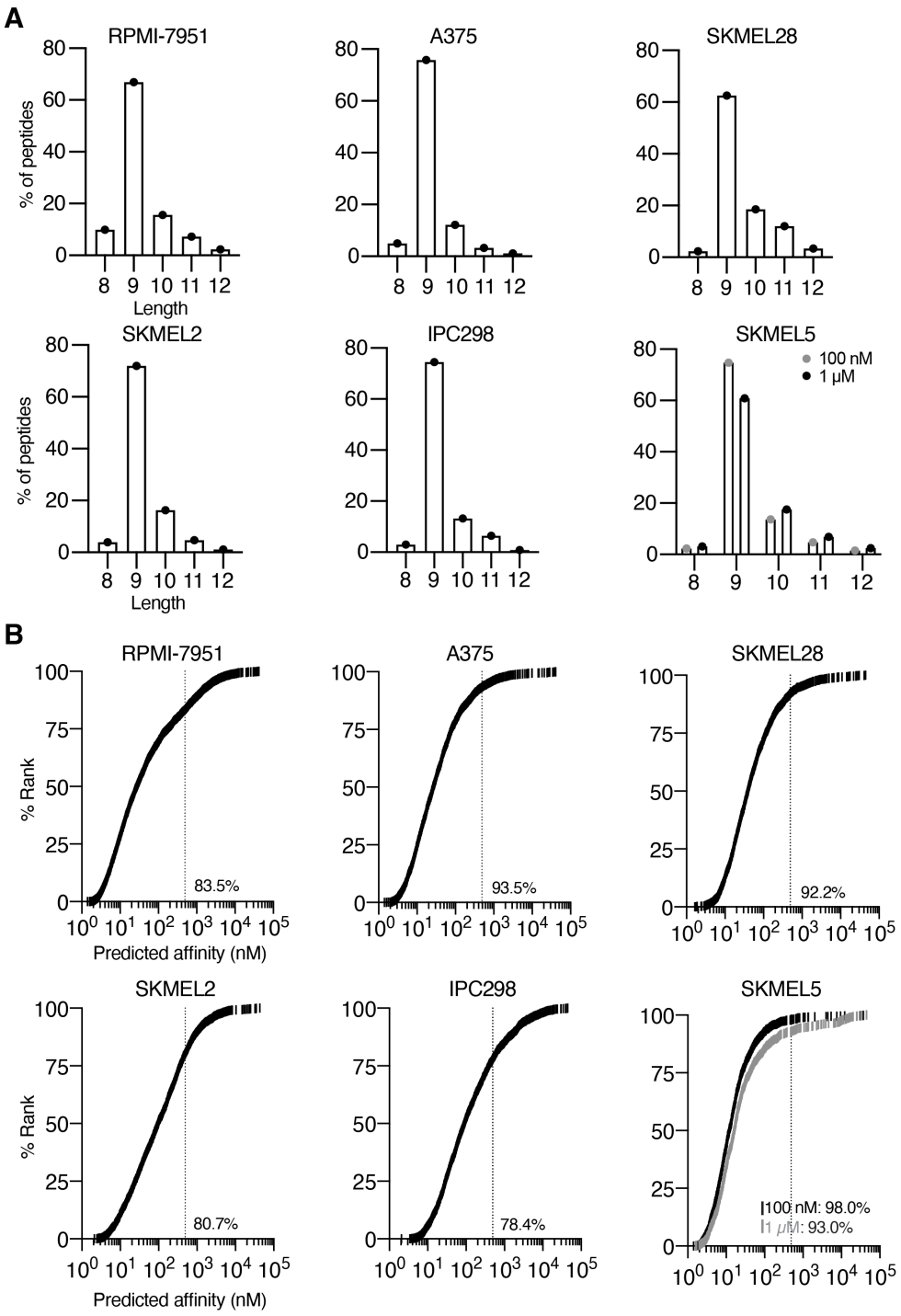

Supplementary Figure 4-4. ***A*** *Peptide length distribution for each cell line.* ***B*** *Predicted binding affinity of 9-mer peptides, rank ordered. Dotted line represents threshold for binding at ≤500 nM. Percentage of peptides ≤500 nM are listed on each plot.*

	HLA-A	HLA-B	HLA-C
SKMEL5	02:01 11:01	40:01 07:02	03:04 07:02
SKMEL28	11:01	40:01	03:04
IPC298	24:02 03:01	07:02 35:02	04:01 07:02
SKMEL2	26:01 03:01	38:01 35:08	04:01 12:03
A375	01:01 02:01	44:03 57:01	06:02 16:01
RPMI-7951	01:01 02:01	08:01 13:02	07:01 06:02

Supplementary Figure 4-5. *HLA alleles for each cell line.*

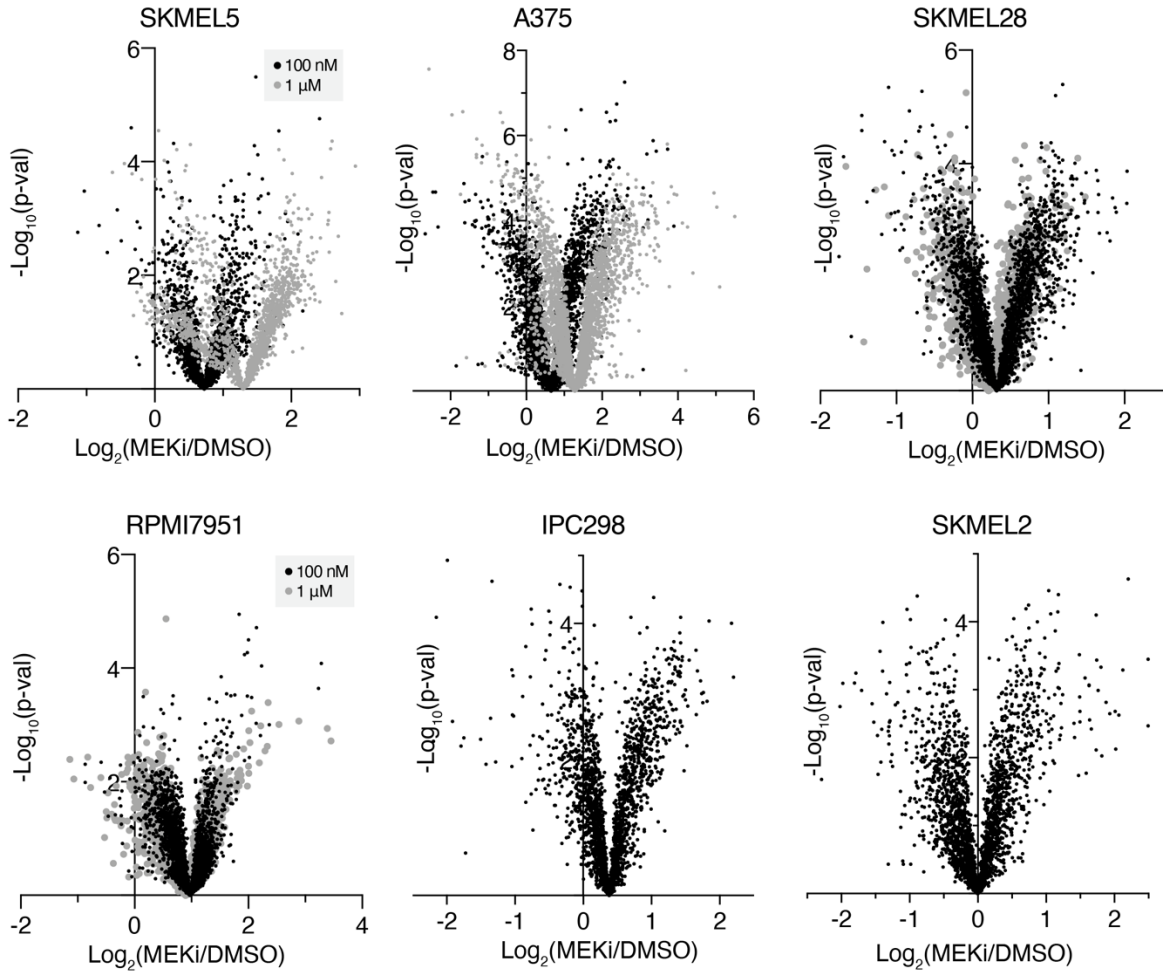

Supplementary Figure 4-6*. Volcano plots of the average fold change in pMHC expression with binimetinib treatment (n=3 biological replicates for DMSO and MEKi treated cells) versus significance (mean-adjusted p value, unpaired two-sided t test).*

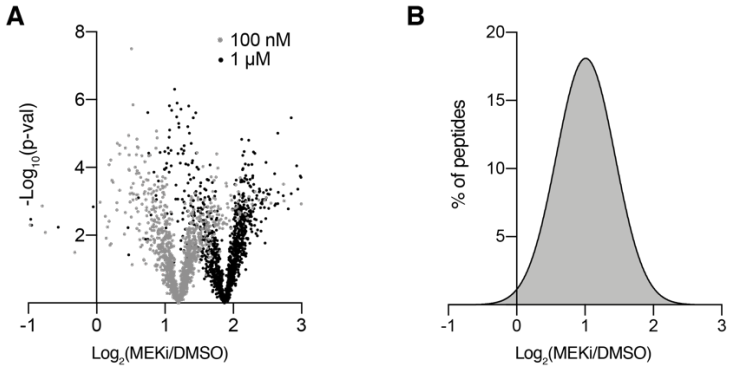

Supplementary Figure 4-7. A *Volcano Plot for SKMEL5 cells +/- Trametinib, plotted as described in* ***Supplementary Figure 4-6. B*** *Histogram of fold changes in pMHC expression for SKMEL5 cells +/- 100 nM MEKi for 10 days. μ=2.0 fold change.*

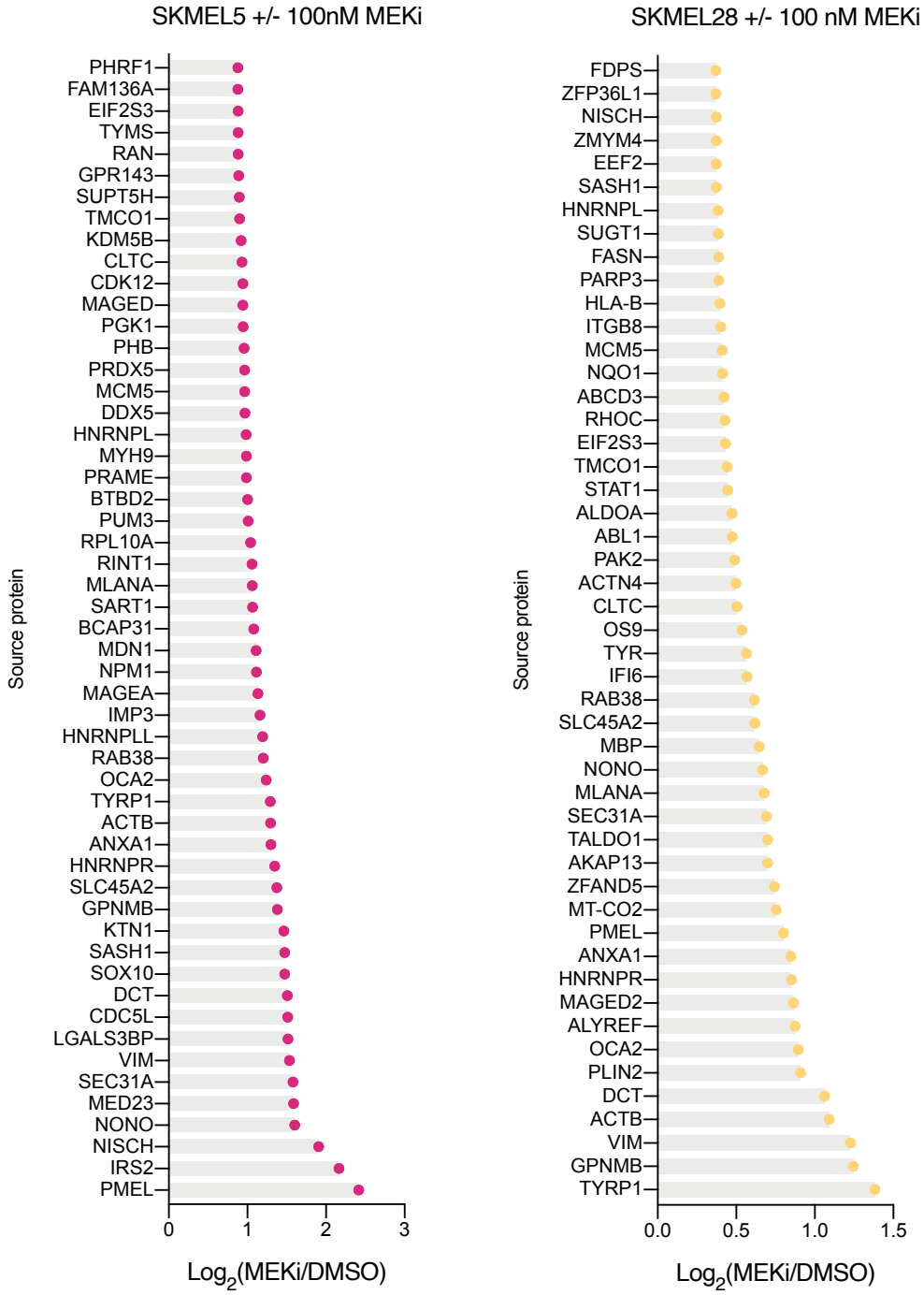

***Supplementary Figure 4-8**. Enriched tumor associated antigen pMHC expression changes with 100 nM MEKi.*

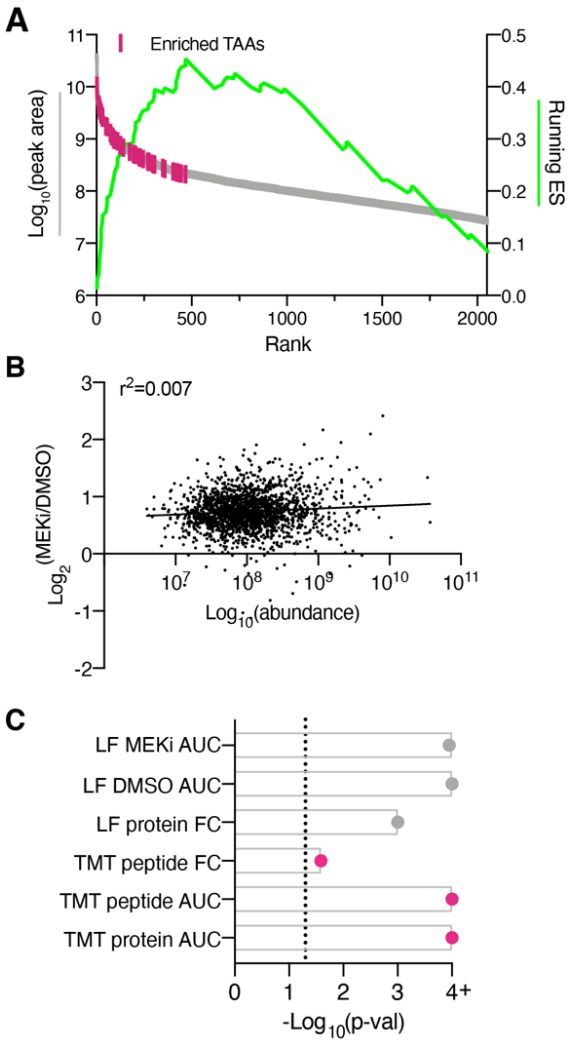

Supplementary Figure 4-9. ***A*** *Tumor associated antigen (TAA) enrichment plot of SKMEL5 cells +/- 100 nM MEKi, ranked by precursor ion abundance (peak area).* ***B*** *Correlation between fold change in pMHC expression and precursor ion abundance for SKMEL5 +/- 100 nM binimetinib.* ***C*** *Significance value of TAA enrichment analysis, where LF = label free analysis, TMT = multiplexed analysis, AUC = ranked according to precursor ion abundance (area under the curve, AUC), peptide = ranked by peptide fold change and searched against SKMEL5 peptide MHC database, gene = ranked by maximal fold change for each source protein. Significance values at 4 represent p<0.0001.*

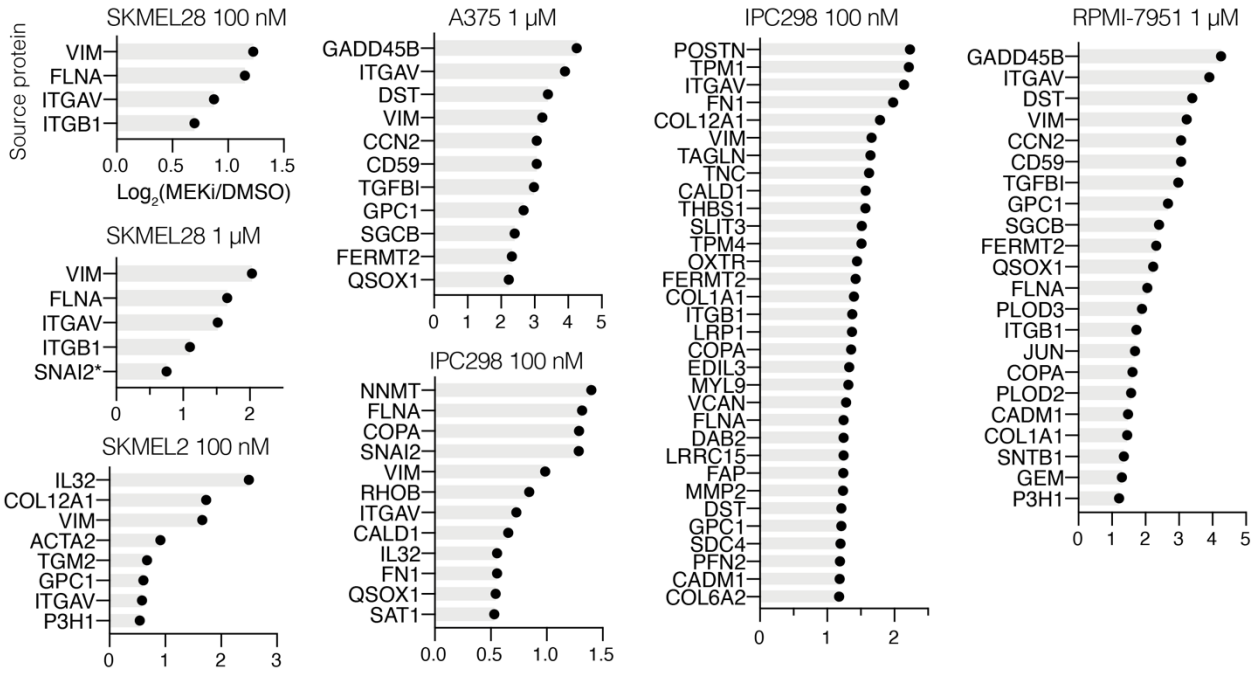

***Supplementary Figure 4-10**. Enriched pMHCs derived from EMT-related proteins.*

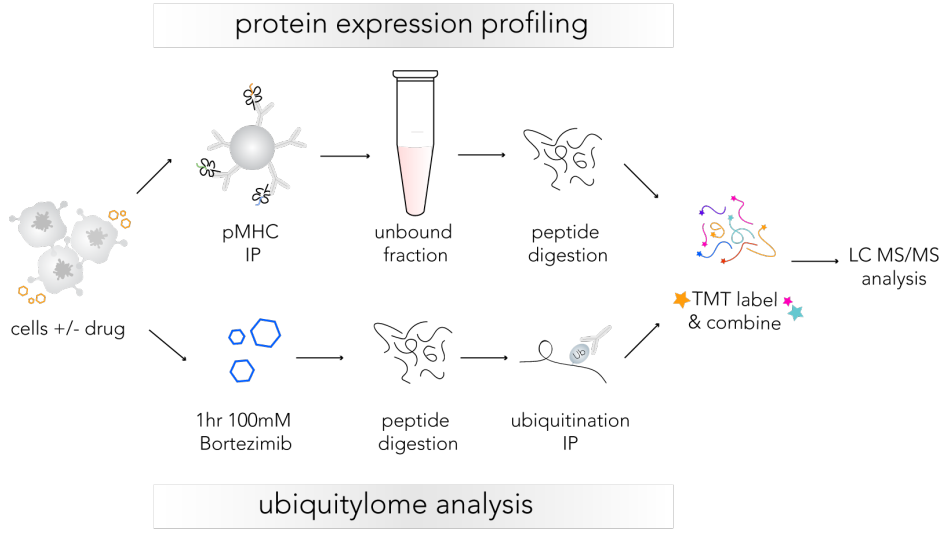

***Supplementary Figure 4-11**. Proteomics LC-MS/MS workflow for quantitative protein expression profiling (top) and ubiquitination analysis (bottom).*

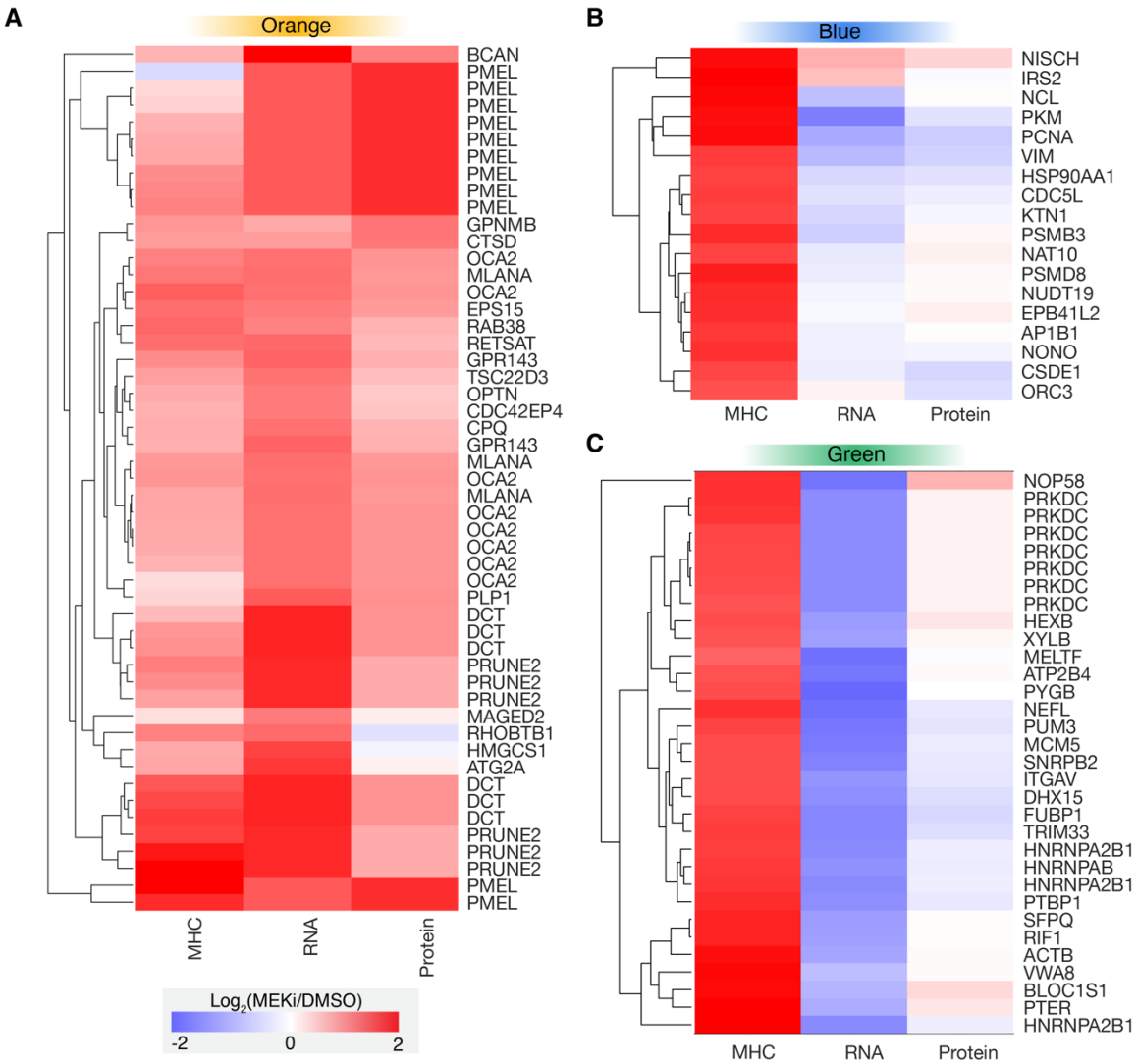

Supplementary Figure 4-12*. Changes in pMHC, RNA, and protein expression following 100 nM binimetinib treatment for 72 hours.*

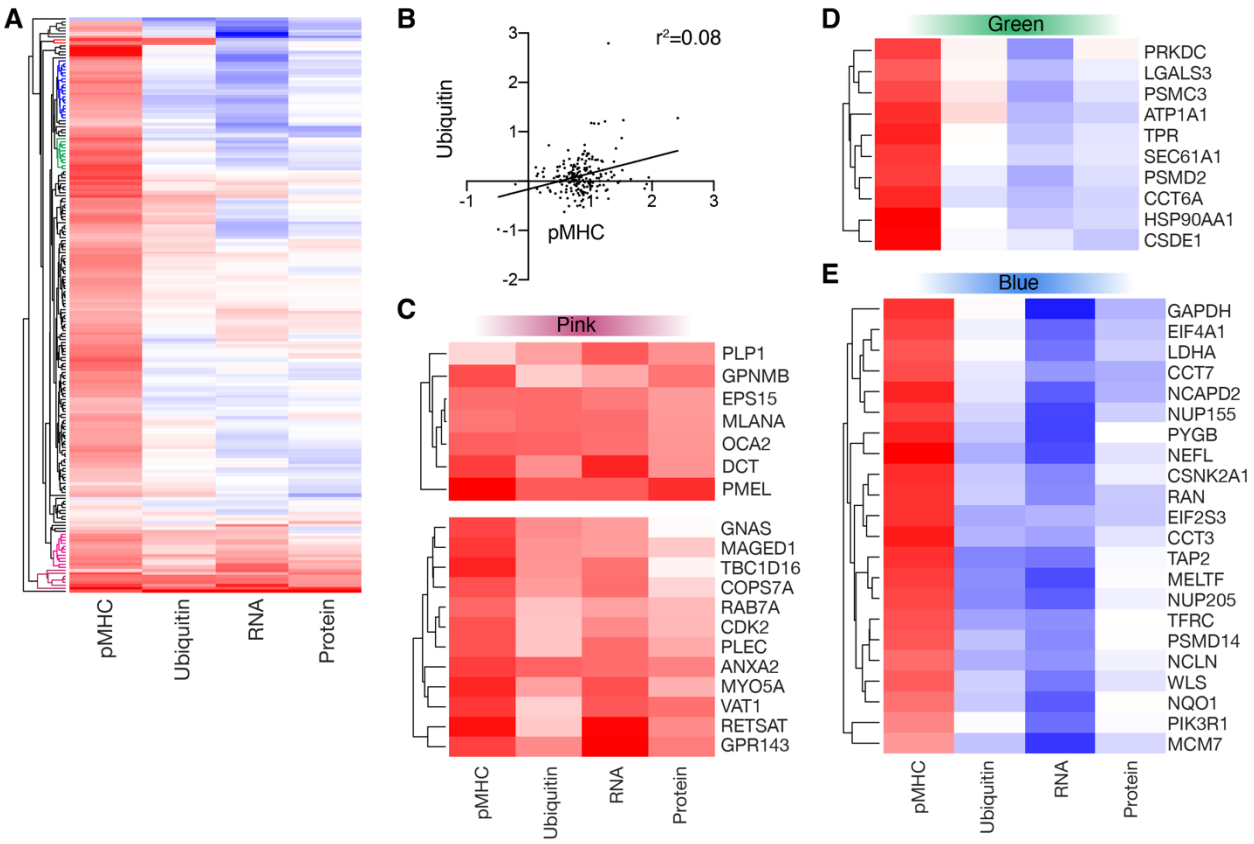

Supplementary Figure 4-13. ***A*** *Clustergram of maximum changes in pMHC expression and corresponding changes in ubiquitination (maximum if >1 peptide quantified), RNA, and protein expression.* ***B*** *Correlation of maximum change (Log_2(MEKi/DMSO)) in ubiquitination and pMHC for each source peptide.* ***C-E****, select clusters from* ***A****.*

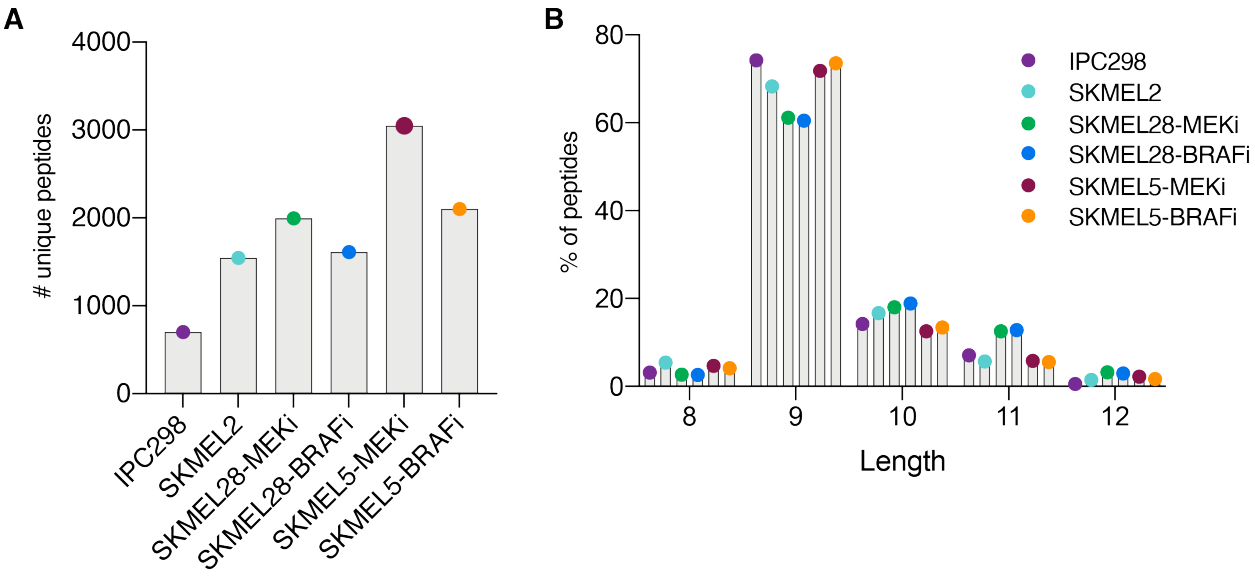

***Supplementary Figure 4-14**. **A** Number of unique pMHCs identified in each analysis. **B** Length distribution of pMHCs represented as a percentage of the total pMHCs identified.*

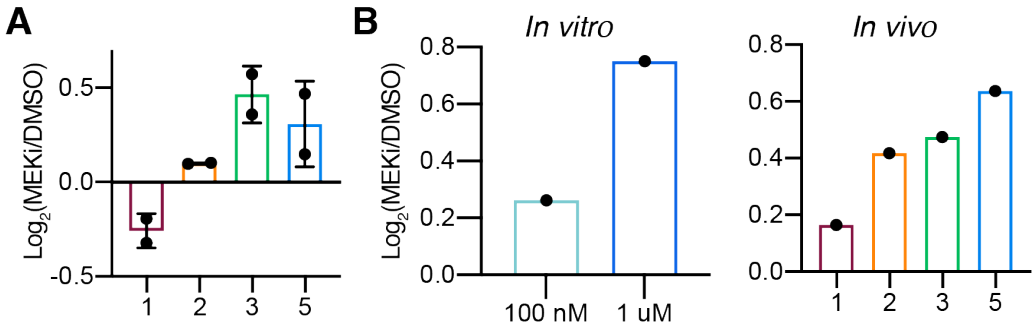

***Supplementary Figure 4-15**. **A** Change in pMHC expression with MEKi of MITF-derived peptides in SKMEL2 CLX model after 1-5d of treatment. **B** SKMEL28 cell line (left) and CLX (right) changes in pMHC expression of an SNAI2-derived pMHC.*

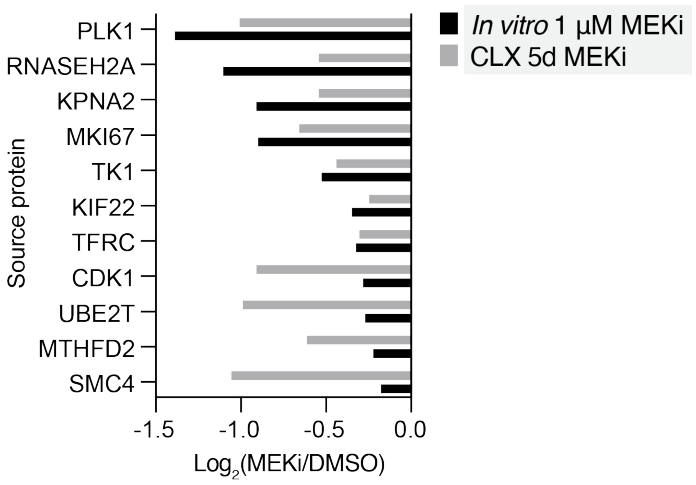

***Supplementary Figure 4-16**. Source proteins of negatively enriched E2F targets in the in vitro (black) and CLX (grey) analyses.*

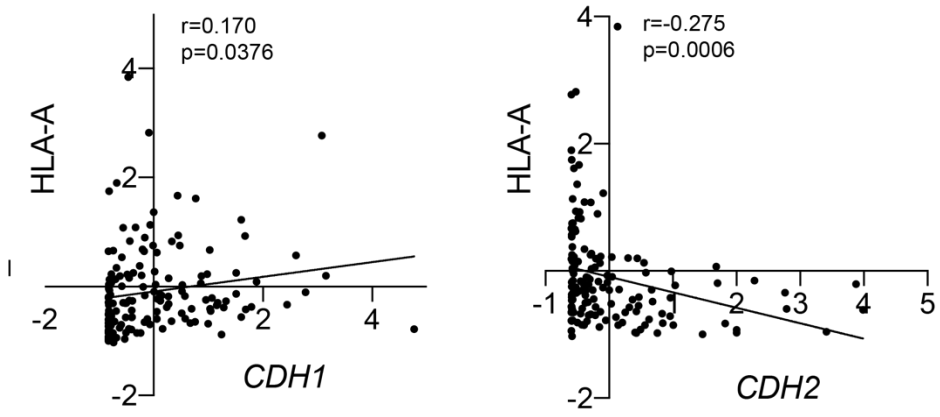

***Supplementary Figure 4-17**. Correlation between HLA-A expression and E-cadherin (CDH1) and N-cadherin (CDH2) expression.*

4-10 Tables

***Table 4-1**. Custom library of tumor associated antigen source proteins.*

ABCA1	BING4	CLTC	DUSP22	GNTK	IMP3
ABCA6	BIRC5	CLYBL	EEF2	GPC3	INPP5D
ABCC3	BIRC7	CML28	EFTUD2	GPCPD1	INS
ABCD3	BIRC8	CNMD	EGFR	GPNMB	INSM2
ABL1	BIRC9	COA1	EHD2	GPR143	INTS11
ACPP	BRAF	COL2A1	EIF2S3	HAO2	INTS13
ACRBP	BST2	COL4A3	EIF3D	HAUS3	IQGAP2
ACTB	BTBD2	COL6A2	ELAC2	HBD	IRS2
ACTN4	BTG1	CORO1A	ELAVL1	HCG	ITGAL
ADAM17	BTK	COX2	ELAVL4	HDAC1	ITGAM
ADAMTSL5	C18orf21	CPSF	EML6	HDGF	ITGB2
ADRP	C2CD4A	CPSF1	ENAH	HEPACAM	ITGB8
AFP	C5	CPVL	EPCAM	HHAT	KAAG1
AIM2	CA9	CR2	EPHA2	HIFPH3	KCNAB1
AIMP1	CACNG	CRABP1	ERAP1	HIST4H4	KDM2B
AKAP13	CADH3	CRNKL1	ERBB2	HIVEP1	KDM5B
ALDH1A1	CALCA	CSAG2	ERVK3-1	HLA-A	KDM5C
ALDOA	CALR	CSF1	ETV5	HLA-B	KDM5D
ALK	CAMP	CSF3R	EVI2B	HLA-DOB	KDR
ALYREF	CASP5	CSNK1A1	EZH2	HLA-DPA1	KIAA1551
AML1	CASP8	CSPG4	EZR	HMMR	KIF20A
AMZ2	CCDC110	CT83	FAM136A	HMOX1	KLK10
ANKRD30A	CCL3	CTAG1A	FASN	HMSD	KLK3
ANO7	CCL3L1	CTDP1	FBXW11	HNF4G	KLK4
ANXA1	CCLA2	CTNNB1	FCER1A	HNRNPL	KRAS
APOBEC3H	CCNA1	CTPS1	FDPS	HNRNPLL	KRI1
ARF1	CCNB1	CTSH	FGF5	HNRNPR	KRT16
ARHGAP15	CCND1	CYP1B1	FGF6	HOXD3	KRT18
ARHGAP25	CCNI	CYP21A2	FLT3	HPN	KRT6C
ARHGAP4	CD19	CYP2A6	FLT3LG	HPSE	KTN1
ARHGAP45	CD274	CYP2A7	FMOD	HSDL1	LAGE1
ARL4D	CD33	CYP2C8	FMR1NB	HSP90AB1	LAGE3
ART4	CD48	CYP2C9	FNDC3B	HSPA1A	LAS1L
ART5	CD69	CYP2D6	FOLH1	HSPA1B	LCK
ASH1L	CD79B	CYPB	FOXO1	HSPA1L	LCP2
ATIC	CDC5L	DAPK2	G3BP1	HSPA6	LGALS1
ATP2A3	CDCA7L	DCT	G6PC2	HSPB1	LGALS3BP
ATXN10	CDH13	DDX21	GAD2	HSPD1	LGSN
B2A2	CDK12	DDX3Y	GAGE1	ICAM3	LPGAT1
B3A2	CDK4	DDX5	GAS7	ICE	LRMP
BA46	CDKN1A	DKK1	GATA2	IDNK	LRRC8A
BAD	CDKN2A	DLAT	GC	IDO1	LTB
BAGE1	CDR2	DMD	GCGR	IER3	LY6K
BCAP31	CEACAM5	DMXL1	GEMIN4	IFG2BP3	LYN
BCHE	CELF6	DNAJC2	GFAP	IFI30	MAG
BCL2	CELSR1	DNMBP	GINS1	IFI6	MAGEA1
BCL2A1	CENPM	DNMT1	GLRX3	IGF2BP2	MAGEA12
BCL2L4	CEP55	DOCK2	GLS	IGF2BP3	MAGEB2
BFAR	CLCA2	DOK2	GNAO1	IL13RA2	MAGEC1
BID	CLP	DSE	GNL3L	IL2RG	MAGEC2

Table 4-1 continued

MAGEC2	NELFA	PSMB1	SIRT2	UBE2C
MAGED2	NFYC	PSMB10	SLC25A5	UBE2D2
MAGEE1	NISCH	PTHLH	SLC30A8	UGT2B17
MAGEF1	NLRP5	PTPN11	SLC41A3	UQCR10
MAGEF1	NOB1	PTPN21	SLC45A2	UQCRH
MALL	NONO	PTPRC	SLC45A3	USP11
MAP4K1	NPM1	PTPRN	SLCO2A1	USP9X
MARK3	NQO1	PTTG1IP	SNRNP70	USP9Y
MATN2	NRAS	PUM3	SNRPD1	UTY
MBP	NUDCD1	PWWP3A	SNX14	VEGFA
MC1R	NUF2	PXDN	SOX10	VENTXP1
MCF2	NUF3	RAB38	SP110	VGF
MCM5	NUP210	RAN	SPA17	VIM
MCMBP	NUP37	RASGRF1	SPARC	VIPR1
MDK	OCA2	RASGRP2	SPATA5L1	VPS13B
MDM2	OGT	RASSF10	SSX1	VSIG10L
MDN1	OS9	RBAF600	SSX2	WNK2
ME1	P2RX5	RBBP4	STAT1	WT1
MED23	PAK2	RBL2	STEAP1	XAGE1B
MED24	PARP10	RFA1	SUGT1	XBP1
MET	PARP3	RGS5	SUPT5H	ZFAND5
METTL21A	PASD1	RHOC	SYNGR1	ZFHX3
MFGE8	PAX3	RINT1	TAG1	ZFP36L1
MICA	PAX5	RNF19B	TALDO1	ZFY
MLANA	PCDH11Y	RNF43	TBC1D22A	ZMYM4
MMP2	PCDH20	RPA1	TCHH	ZNF395
MMP7	PDGFRA	RPL10A	TEK	
MOK	PFKM	RPL19	TEP1	
MPL	PGK1	RPS2	TERT	
MRPL19	PHB	RPS4Y1	TG	
MS4A1	PHRF1	RPSA	TGRBR2	
MSCP	PIM1	RUBCNL	THEM6	
MSLN	PLAC1	SAGE1	TMCO1	
MT-ATP6	PLIN2	SART1	TMED4	
MT-CO2	PLP1	SART3	TMSB10	
MTRR	PMEL	SASH1	TMSB4Y	
MUC1	POP1	SCGB2A2	TOP1	
MUC16	PP2A	SCGB2A7	TOP2A	
MUC5AC	PPFIBP1	SCRN1	TP53	
MUM2	PPIB	SEC31A	TP53I11	
MUM3	PPP1R3B	SELL	TPBG	
MYH1	PRAME	SELPLG	TPO	
MYH2	PRDM1	SEPT2	TRIM22	
MYH9	PRDX2	SEPT6	TRIM68	
MYO1G	PRDX5	SERPINB5	TTK	
N4BP2	PRELID1	SF1	TTN	
N4BP2L1	PRKCB	SFMBT1	TYMS	
NACA2	PRTN3	SGT1B	TYR	
NCF4	PSD4	SH3GLB2	TYRP1	
NECTIN4	PSMA3	SIRPD	UBD	

***Table 4-2**. Tumor associated antigen peptide library for enrichment analyses.*

AAAAAIFVI	ALIHHNTHL	AMLDLLKSV	AVFDGAQVTSK	DLTSFLLSL	ESDPIVAQY
AAANIIRTL	ALISKNPV	AMLERQFTV	AVLTKQLLH	DLWKETVFT	ESFSGSLGHL
AAFDGRHSQTL	ALKDSVQRA	AMLGTHTMEV	AVMALENNYEV	DNGAKSVVL	ESLFRAVITK
AAGIGILTV	ALKDVEERV	AMLGTHTMEVTV	AVQEFGLARFK	DPARYEFLW	ESVMINGKY
AARAVFLAL	ALLALTSAV	AMTKDNNLL	AVTNVRTSI	DPKDAEKAI	ETAGPQGPPHY
AAVEEGIVLGGG	ALLAVGATK	AMVGAVLTA	AVVDLQGGGHSY	DPSTDYYQEL	ETFTEGQKL
ACDGERPTL	ALLEIASCL	AMYDKGPFRSK	AVVGILLVV	DPYKATSAV	ETHLSSKRY
ACDPHSGHFV	ALLESSLRQA	ANADLEVKI	AVYGQKEIHRK	DQYPYLKSV	ETILTFHAF
AEEAAGIGIL	ALLKDTVYT	ANDPIFVVL	AWISKPPGV	DRASFIKNL	ETLGFLNHY
AEEAAGIGILT	ALLMPAGVPL	APAGRPSAS	AWLVAAAEI	DSDPDSFQDY	ETVELQISL
AEEHSIATL	ALLNIKVKL	APAGRPSASR	AYACNTSTL	DSFPMEIRQY	ETVSEQSNV
AEHIESRTL	ALLPSLSHC	APAGVREVM	AYDFLYNYL	DSFPMEIRQYL	EVAPDAKSF
AEINNIIKI	ALLPTALDAL	APDGAKVASL	AYGLDFYIL	DTEFPNFKY	EVAPPASGTR
AELESKTNTL	ALMDKSLHV	APLLRWVL	AYIDFEMKI	DVNGLRRVL	EVDPASNTY
AELLNIPFLY	ALMEQQHYV	APLQRSQSL	AYTKKAPQL	DVTSAPDNK	EVDPIGHLY
AELVHFLLL	ALMVRQARGL	APNTGRANQQM	AYVPQQAWI	DVWSFGILL	EVDPIGHLYIF
AEPINIQTW	ALNFPGSQK	APRGVRMAV	CHILLGNYC	DYIGPCKYI	EVDPIGHVY
AFLPWHRLF	ALPPPLMLL	APVIKARMM	CIAEQYHTV	DYKSAHKGF	EVFEGREDSVF
AFLRHAAL	ALPSFQIPV	AQAEHSITRV	CILGKLFTK	DYLQCVLQI	EVFPLAMNY
AGDGTTTATVLA	ALQDIGKNIYTI	AQCQETIRV	CITFQVWDV	DYLQYVLQI	EVFPLAMNYL
AGFKGEQGKGEP	ALQKAKQDL	AQDPHSLWV	CLAFPAPAKA	DYLRSVLEDF	EVFQNANFRSF
AGYLMELCC	ALRCASPWL	AQPDTAPLPV	CLGHNHKEV	DYPSLSATDI	EVHNLNQLLY
AHVDKCLEL	ALREEEEGV	AQYEHDLEVA	CLLSGTYIFA	DYSARWNEI	EVIGRGHFGCVY
AIDELKECF	ALSDHHIYL	ARGPESRLL	CLLWSFQTSA	EAAGIGILTV	EVIPYTPAM
AIIDPLIYA	ALSEDLLSI	ARGQPGVMG	CLVFLAPAKA	EADPTGHSY	EVIPYTPAMQR
AIISGDSPV	ALSVMGVYV	ARHRRSLRL	CLVFPAPAKA	EAFIQPITR	EVIPYTPAMQRY
AISANIADI	ALTAVAEEV	ARSVRTRRL	CLVFPAPAKAV	EEFGRAFSF	EVIQWLAKL
AIYDHINEGV	ALTDIDLQL	ARTDLEMQI	CMHLLLEAV	EEKLIVVLF	EVISCKLIKR
AIYDHVNEGV	ALTEHSLMGM	ASERGRLLY	CMLGDPVPT	EEYLQAFTY	EVISSRGTSM
AIYKQSQHM	ALTERSLMGM	ASFDKAKLK	CMTWNQMNL	EEYNSHQSL	EVITSSRTTI
AKYLMELTM	ALTPVVVTL	ASGPGGGAPR	CQWGRLWQL	EFKRIVQRI	EVKLSDYKGKYV
ALAGLSPV	ALVDAGVPM	ASLDSDPWV	CTACRWKKACQ	EFQKMRRDL	EVLDSLLVQY
ALAPAPAEV	ALVSIIKV	ASLIYRRRLMK	CTACRWKKACQR	EGDCAPEEK	EVLLRPGLHFR
ALARGAGTVPL	ALWGPDPAAA	ASSTLYLVF	CYMEAVAL	EILGALLSI	EVMSNMETF
ALASHLIEA	ALWGPDPAAAF	ASYLDKVRA	CYTWNQMNL	ELAEYLYNI	EVRGDVFPSY
ALAVLSVTL	ALWKEPGSNV	ATAGDGLIELRK	DAKNKLEGL	ELAGIGILTV	EVTFVPGLY
ALCQNGYHGT	ALWMRLLPL	ATAGIIGVNR	DALVLKTV	ELAPIGHNRMY	EVTSSGRTSI
ALCQNGYHGTI	ALWMRLLPLL	ATAQFKINK	DCLVFLAPA	ELFQDLSQL	EVVEKYEIY
ALCRWGLLL	ALWPWLLMA	ATATPCWTWLL	DEKQQHIVY	ELHLLQDEEV	EVVHKIIEL
ALDEKLLNI	ALWPWLLMA(T)	ATFSSSHRYHK	DELEIKAY	ELHLLQDKEV	EVVRIGHLY
ALDGGNKHFL	ALWPWLLMAT	ATGFKQSSK	DEVYQVTVY	ELSDSLGPV	EVYDGREHSA
ALDVYNGLL	ALYGDIDAV	ATIIDILTK	DFMIQGGDF	ELTLGEFLK	EYILSLEEL
ALEEANADL	ALYLVCGER	ATLPLLCAR	DIKAKMQAS	ELTLGEFLKL	EYLQLVFGI
ALENNYEVL	ALYSGVHKK	ATQIPSYKK	DLDVKKMPL	ELVRRILSR	EYLSLSDKI
ALFDIESKV	ALYVDSLFFL	ATSPPASVR	DLILELLDL	ELWKNPTAF	EYRGFTQDF
ALGDLFQSI	AMAPIKVRL	ATTNILEHY	DLKGFLSYL	EPLARLEL	EYSKECLKEF
ALGGHPLLGV	AMAQDPHSL	ATVGIMIGV	DLLSHAFFA	EQYEQILAF	EYSRRHPQL
ALIDCNPCTL	AMAQDPHSLWV	AVAANIVLTV	DLPAYVRNL	ERGFFYTPK	EYTAKIALL
ALIEVGPDHFC	AMARDPHSL	AVASLLKGR	DLPPPPPLL	ERLERQERL	EYYLQNAFL
ALIGGPPV	AMARDPHSLWV	AVCPWTWLR	DLSPGLPAA	ERSPVIQTL	FALQLHDPSGY

Table 4-2 continued

FATPMEAEL	FLPETEPPEM	FVGEFFTDV	GLWRHSPCA	HTMEVTVYHR	IMIHDLCLA
FATPMEAELAR	FLPETEPPEML	FVSGSGIAIA	GLYDGMEHL	HTRTPPIIHR	IMIHDLCLV
FAWERVRGL	FLPHFQALHV	FVSGSGIATA	GMVTTSTTL	HTYLEPGPVTAQ	IMIHDLCLVFL
FEITPPVVL	FLPRNIGNA	FVWLHYYSV	GMWESNANV	HVDSTLLQ	IMLCLIAAV
FGLATEKSR	FLQDVMNIL	FYTPKTRRE	GPFGAVNNV	HVDSTLLQV	IMNDMPIYM
FGLFPRLCPV	FLRAENETGNM	GADGVGKSA	GPFGPPMPLHV	HVYDGKFLAR	IMPGQEAGL
FIASNGVKLV	FLRNFSLML	GADGVGKSAL	GPRESRPPA	HYTNASDGL	IMPKAGLLI
FIDKFTPPV	FLRNFSLMV	GAFEHLPSL	GQHLHLETF	IALNFPGSQK	IPSDLERRIL
FIDNTDSVV	FLRNLVPRT	GAIAAIMQK	GRAPQVLVL	IARNLTQQL	IPSNPRYGM
FIDSYICQV	FLSSANEHL	GASGVGSGL	GSHLVEALY	ICLHHLPFWI	IQATVMIIV
FIFPASKVYL	FLSTLTIDGV	GCELKADKDY	GSPATWTTR	IESRTLAIA	IRRGVMLAV
FIFSILVLA	FLTGNQLAV	GDFGLATEK	GSSDVIIHR	IEVDGKQVEL	ISGGPRISY
FIIENLKAA	FLTKRGGQV	GEISEKAKL	GTAAIQAHY	IIGGGMAFT	ISKPPGVAL
FILPVLGAV	FLTKRGRQV	GERGFFYT	GTADVHFER	IIMFDVTSR	ISSVLAGASCPA
FINDEIFVEL	FLTKRSGQV	GEVDVEQHTL	GTATLRLVK	IISAVVGIL	ISTQQQATFLL
FIQVYEVERA	FLTKRSGQVCA	GFKQSSKAL	GTMDCTHPL	IITEVITRL	ITARPVLW
FKNIVTPRT	FLTKRSRQV	GIMAIELAEL	GTMDCTHSL	ILAKFLHWL	ITDFGLAKL
FLAELAYDL	FLTPKKLQCV	GIPPAPHGV	GTSSVIVSR	ILAKFLHWLE	ITDFGLARL
FLAKLNNTV	FLTPLRNFL	GIPPAPRGV	GTWESNANV	ILAVDGVLSV	ITDQVPFSV
FLALIICNA	FLTSGTQFSDA	GIVEQCCTSI	GTYEGLLRR	ILDEKPVII	ITKKVADLVGF
FLAPAKAVV	FLWGPRALA	GLAPPQHLIRV	GVALQTMKQ	ILDFGLAKL	ITQPGPLAPL
FLAPAKAVVYV	FLWGPRALV	GLASFKSFLK	GVFIQVYEV	ILDKKVEKV	ITQPGPLVPL
FLASESLIKQI	FLWGPRAYA	GLCEREDLL	GVLVGVALI	ILDKVLVHL	IVDCLTEMY
FLDEFMEGV	FLWSVFMLI	GLEALVPLAV	GVNPVVSYAV	ILDSSEEDK	IVDSLTEMY
FLDRFLSCM	FLWSVFWLI	GLEKIEKQL	GVRGRVEEI	ILDTAGREEY	IYMDGTADFSF
FLEGNEVGKTY	FLYDDNQRV	GLFDEYLEMV	GVYDGREHTV	ILFGISLREV	KAFLTQLDEL
FLFAVGFYL	FLYGALLLA	GLFGDIYLA	GYCASLFAIL	ILGALLSIL	KAFQDVLYV
FLFDGSPTY	FLYTLLREV	GLGLPKLYL	GYDQIMPKI	ILHNGAYSL	KAKQDLARL
FLFLLFFWL	FMHNRLQYSL	GLGNRWTSRT	GYDQIMPKK	ILIDWLVQV	KALRLSASALF
FLGMESCGI	FMNKFIYEI	GLGPVAAV	HAIPHYVTM	ILKDFSILL	KASEKIFYV
FLGYLILGV	FMTRKLWDL	GLIEKNIEL	HIAGSLAVV	ILLEAPTGLA	KAYGASKTFGK
FLHHLIAEIH	FMTSSWWGA	GLKAGVIAV	HLCGSHLVEA	ILLEAPTGLV	KCDICTDEY
FLIIWQNTM	FMTSSWWRA	GLLDKAVSNV	HLFGYSWYK	ILLRDAGLV	KCQEVLAWL
FLIVLSVAL	FMTSSWWRAPL	GLLDQVAAL	HLLTSPKPSL	ILLWAARYD	KEADPTGHSY
FLLDILGAT	FMVEDETVL	GLLETTVQKV	HLSTAFARV	ILMEHIHKL	KEAGNINTSL
FLLENAAYL	FMVELVEGA	GLLGQEGLVEI	HLSYHRLLPL	ILMEHIHKLK	KECVLHDDL
FLLENAAYLD	FPALRFVEV	GLLQVHHSCPL	HLSYHWLLPL	ILMEHIHKLKA	KECVLRDDL
FLLFIFKVA	FPSDSWCYF	GLMDVQIPT	HLVEALYLV	ILMHCQTTL	KEFEDDIINW
FLLGLIFLL	FPYGTTVTY	GLPAGAAAQA	HLWVKNMFL	ILNAMIAKI	KEFEDGIINW
FLLKAEVQKL	FQRQGQTAL	GLPGQEGLVEI	HLWVKNVFL	ILPLHGPEA	KEFKRIVQR
FLLKLTPLL	FRSGLDSYV	GLPPDVQRV	HLYQGCQVV	ILSAHVATA	KEFTVSGNILTI
FLLQMMQICL	FSIDSPDSL	GLPPDVQRVH	HMYHSLYLK	ILSLELMKL	KELEGILLL
FLLQMMQVCL	FSYMGPSQRPL	GLPPPPPLL	HPLVFHTNR	ILTVILGVL	KELPSLHVL
FLLSLFSLWL	FTHNEYKFYV	GLQHWVPEL	HPRQEQIAL	ILVLASTITI	KEPSEIVEL
FLMLVGGSTL	FTWAGKAVL	GLQLGVQAV	HPRYFNQLST	ILYENNVITV	KEWMPVTKL
FLMSSWWPNL	FTWAGQAVL	GLREDLLSL	HQILKGGSGTY	ILYENNVIV	KFHRVIKDF
FLNQTDETL	FTWEGLYNV	GLREREDLL	HRWCIPWQRL	IMAIELAEL	KFLDALISL
FLPATLTMV	FVEHDDESPGL	GLRRVLDEL	HSATGFKQSSK	IMDQVPFSV	KGSGKMKTE
FLPEFGISSA	FVEHDLYCTL	GLSPNLNRFL	HSSSHWLRLP	IMFDVTSRV	KIADPICTFI
FLPETEPPEI	FVFLRNFSL	GLSTILLYH	HSWITRSEA	IMIGVLVGV	KIDEKTAELK

Table 4-2 continued

KIFDEILVNA	KLQELNYNL	KTWDQVPFS	LLDGTATLRL	LLMPAGVPL	LMLGEFLKL
KIFGSLAFL	KLQQKEEQL	KTWDQVPFSV	LLDKAVSNVI	LLMPAGVPLT	LMLQNALTTM
KIFSEVTLK	KLQVFLIVL	KTWDQVPFSVSV	LLDRFLATV	LLMWITQCF	LMVLMLAAL
KILDAVVAQK	KLSEGDLLA	KTWGQYWQ	LLDTNYNLF	LLNAFTVTV	LMWAKIGPV
KINKNPKYK	KLSEQESLL	KTWGQYWQV	LLDTNYNLFY	LLNATIAEV	LNIDLLWSV
KIQEILTQV	KLTQINFNM	KVAELVHFL	LLDVAPLSL	LLNLPDKMFL	LNIYEKDDKL
KIQRNLRTL	KLVERLGAA	KVAELVRFL	LLDVPTAAV	LLNLPVWVL	LNLPDKMFL
KIWEELSVLE	KLVMSQANV	KVFGSLAFV	LLEAPTGLV	LLNQPDKMFL	LPAVVGLSPGEQ
KIWEELSVLEV	KLVVVGAVGV	KVHPVIWSL	LLEEMFLTV	LLPENNVLSPV	LPGEVFAI
KIYSENLKL	KLYSENLKL	KVIDQQNGL	LLESAFPGGL	LLPPLLEHL	LPHAPGVQM
KIYSENLKLA	KLYSENLKLA	KVLEFLAKL	LLFETVMCDT	LLQAEAPRL	LPHNHTDL
KIYSENLTL	KLYSENLTL	KVLEHVVRV	LLFGLALIEV	LLQDSVDFSL	LPHSEITTL
KIYSENLTLA	KLYSENLTLA	KVLEYVIKV	LLFLLQMMQI	LLQEEEEEL	LPHSSSHWL
KLADQYPHL	KMAAFPETL	KVLHELFGMDI	LLFLLQMMQV	LLQEYNWEL	LPLLALLAL
KLAEAERVGLHK	KMAELVHFL	KVNIVPVIAK	LLFPYILPPKA	LLQGWVMYV	LPMEVEKNSTL
KLAKPLSSL	KMDAEHPEL	KVSAVTLAY	LLFSFAQAV	LLQLGYSGRL	LPPPPPLLDL
KLATAQFKI	KMFVKGAPDSV	KVVEFLAML	LLGATCMFV	LLQLYSGRL	LPQKKSNAL
KLCKVRKITV	KMFVKGAPESV	KYDCFLHPF	LLGCPVPLGV	LLQMMQICL	LPRWPPPQL
KLCPVQLWV	KMISAIPTL	KYIQESQAL	LLGDLFGV	LLQMMQVCL	LPSSADVEF
KLDETGNSL	KMLDHEYTT	KYLATASTM	LLGNCLPTV	LLQVHHSCPL	LQSRGYSSL
KLDETGNSLK	KMLKSFLKA	KYLKLSSSEL	LLGPGRPYR	LLRGYHQDAY	LRAGRSRRL
KLDETGNSLKV	KMNVFDTNL	KYVGIEREM	LLGPTVML	LLSAEVQQHL	LRRYLENGK
KLDVGNAEV	KMQASIEKA	LAALPHSCL	LLGRFELIGI	LLSAVLPSV	LSIGTGRAM
KLEGLEDAL	KMRRDLEEA	LAAQERRVPR	LLGRNSFEV	LLSDDDVVV	LSRLSNRLL
KLFGSLAFV	KMVELVHFL	LALWGPDPAA	LLHVHHSCPL	LLSDEDVAL	LTLGEFLK
KLFGVLRLK	KMYAFTLES	LAMPFATPM	LLIADNPQL	LLSDEDVALM	LTLGEFLKL
KLGDCIWTYL	KMYAFTLESV	LAPAKAVVYV	LLIDLTSFL	LLSDEDVALMV	LTLTTGEWAV
KLGDCIWTYLS	KNKRILMEH	LASEKVYTI	LLIDLTSFLL	LLSDEDVEL	LTYNDFINK
KLGDCIWTYPS	KPIVVLHGY	LATEKSRWS	LLIGATIQV	LLSDEDVELM	LTYVSFRNL
KLIETYFSK	KPQQKGLRL	LATEKSRWSG	LLIGATIQVT	LLSDEDVELMV	LVALLACLTV
KLIGDPNLEFV	KPRQSSPQL	LAVDGVLSV	LLIGATMQV	LLSETVMCDT	LVALLVCLTV
KLIKDGLIIRK	KPSGATEPI	LCGSHLVEAL	LLIGATMQVT	LLSGQPASA	LVCGERGFFY
KLKHYGPGWV	KPSPPYFGL	LDKVRALEE	LLIGGFAGL	LLSHGAVIEV	LVFGIELMEV
KLLDISELDMV	KQDFSVPQL	LEEKKGNYV	LLIKKLPRV	LLSILCIWV	LVFLAPAKAVV
KLLEYIEEI	KQDNSTYIMRV	LEEYNSHQSL	LLLDDLLVSI	LLSLFSLWL	LVHFLLLKY
KLLGPHVEGL	KQLPEEKQPLL	LEKQLIEL	LLLEAVPAV	LLSPLHCWA	LVLKRCLLH
KLLGPHVLGV	KQPAIMPGQSY	LGYGFVNYI	LLLELAGVTHV	LLSPLHCWAV	LVMAPRTVL
KLLMVLMLA	KQSSKALQR	LGYGFVNYV	LLLGIGILV	LLSSGAFSA	LVQENYLEY
KLLQIQLCA	KRIQEIIEQ	LHHAFVDSIF	LLLGPLGPL	LLTSRLRFI	LVVVGAVGV
KLLQIQLCAKV	KRTLKIPAM	LIAHNQVRQV	LLLGTIHAL	LLTTLSNRV	LWMRLLPLL
KLLQIQLRA	KSEMNVNMKY	LIFDLGGGT	LLLHCPSKTV	LLVALAIGCV	LYATVIHDI
KLLQIQLRAKV	KSLNYSGVK	LIFDLGGGTFD	LLLLDVAPL	LLVSEIDWL	LYAWEPSFL
KLLSSGAFSA	KSMNANTITK	LIYDSSLCDL	LLLLTVLTV	LLWWIAVGPV	LYLVCGERGF
KLMPPDRTAV	KTCPVQLWV	LIYRRRLMK	LLLPAEVQQHL	LLYKLADLI	LYSACFWWL
KLMSPKLYVW	KTIHLTLKV	LKLSGVVRL	LLLPALAGA	LMAGCIQEA	LYSDPADYF
KLNVPATFML	KTLGKLWRL	LLAAVAALL	LLLPGPSAA	LMALPPCHAL	LYVDSLFFL
KLPNSVLGR	KTLTSVFQK	LLAGIGTVPI	LLLRSPAGV	LMASSPTSI	LYVDSLFFLC
KLQAPVQEL	KTPFVSPLL	LLAGPPGV	LLLSAEVQQHL	LMETHLSSK	MALENNYEV
KLQATVQEL	KTVDLILEL	LLASSMSSQL	LLMEGVPKSL	LMFWSPSHSCA	MAQKRIHAL

KLQEELNKV	KTVNELQNL	LLDDSLVSI	LLMEKEDYHSL	LMGDKSENV	MAVPPCCIGV

Table 4-2 continued

MEGEVWGL	NLFDTAEVYA	PLTSIISAV	RAPPTTPAL	RLLYPDYQI	RTFHHGVRV
MEIFIEVFSHF	NLFDTAEVYAA	PPSACSPRF	RASHPIVQK	RLMKQDFSV	RTGEVKWSV
MEKEDYHSL	NLFETPVEA	PTLDKVLEL	RAYQQALSR	RLNAALREK	RTIAPIIGR
MEVDPIGHLY	NLFLFLFAV	PTLDKVLEV	RCHELTVSL	RLPRIFCSC	RTIPTPLQPL
MFPEVKEKG	NLIKLAQKV	QCSGNFMGF	RELEETNQKL	RLQGISPKI	RTKQLYPEW
MGNIDSINCK	NLKLKLHSF	QFITSTNTF	REPVTKAEML	RLQREWHTL	RTLAEIAKV
MIAVFLPIV	NLLDSLEQYI	QGQHFLQKV	REQFLGALDL	RLQTPMQVGL	RTLDKVLEV
MIHDLCLAFPA	NLLEREFGA	QIAKGMSYL	RESEEESVSL	RLQVPVEAV	RTNWPNTGK
MIHDLCLVFL	NLLGRFELI	QIEGLKEEL	RFEEKHAYF	RLRAPEVFL	RTTEINFKV
MIMQGGFSV	NLLGRFELIGI	QILKGGSGT	RFKMFPEVK	RLRPLCCTA	RVFQGFFTGR
MLAVISCAV	NLPDKMFLPGA	QILPLHGPEA	RIAECILGM	RLSCPSPRA	RVHAYIISY
MLGDPVPTPT	NLQGSPVYV	QIRPIFSNR	RIDITLSSV	RLSCSSPRA	RVKAPNKSL
MLGTHTMEV	NLSALGIFST	QLARQQVHV	RIGQRQETV	RLSSCVPVA	RVLRQEVAAPL
MLLAVLYCL	NLSSAEVVV	QLCAKVPLL	RIKDFLRNL	RLTSTNPTM	RVLRQEVEAPL
MLLDKNIPI	NLVRDDGSAV	QLCPICRAPV	RILGPGLNK	RLTSTNPTT	RVPGVAPTL
MLLKTSEFL	NLWDLTDASVV	QLEERTWLL	RILMEHIHKLK	RLVDDFLLV	RVQEAVESMVK
MLLSVPLLLG	NLYPFVKTV	QLFEDNYAL	RINEFSISSF	RLVELAGQSLLK	RVRFFFPSL
MLMAQEALAFL	NMQDLVEDL	QLFNHTMFI	RIVQRIKDF	RLWQELSD	RVSLPTSPR
MLPSQPTLL	NMVAKVDEV	QLFNKHTMFI	RLAEYQAYI	RLWTTTRPRV	RVTSIRLFEV
MLTNSCVKL	NPATPASKL	QLGPTCLSSL	RLARLALVL	RLYDEKQQHI	RVWDLPGVLK
MLVGGSTLCV	NPIVVFHGY	QLGPVGGVF	RLASFYDWLP	RLYDEKQQHIVY	RWPSCQKKF
MLWSCTFCRI	NPKAFFSVL	QLGRISLLL	RLASSVLRCGK	RLYEMILKR	RYAMTVWYF
MLWSCTFCRM	NSELSCQLY	QLIMPGQEA	RLASYLDKV	RLYPWGVVEV	RYCNLEGPPI
MLYYPSVSR	NSQPVWLCL	QLLALLPSL	RLDFNLIRV	RMFPNAPYL	RYGSFSVTL
MMKMMCIKDL	NTDSPLRY	QLLDGFMITL	RLDQLLRHV	RMLPHAPGV	RYMPPAHRNF
MMLPSQPTL	NTYASPRFK	QLLDQVEQI	RLFAFVRFT	RMMEYGTTMV	RYQLDPKFI
MMLPSQPTLL	NTYASPRFKf	QLLIKAVNL	RLFFYRKSV	RMMLPSQPTL	RYQQWMERF
MMLPSQPTLLT	NVIRDAVTY	QLLKLNVPA	RLFVGSIPK	RMPEAAPPV	SACDVSVRV
MMLPSRPTL	NVLHFFNAPL	QLLNSVLTL	RLGGAALPRV	RMTDQEAIQ	SACDVSVRVV
MMLPSRPTLL	NVMPVLDQSV	QLMAFNHLV	RLGLQVRKNK	RMTDQEAIQDL	SAFPTTINF
MMLPSRPTLLT	NYARTEDFF	QLQGLQHNA	RLGNSLLLK	RNGYRALMDKS	SAGPPSLRK
MMQICLHHL	NYKHCFPEI	QLSLLMWIT	RLGPTLMCL	RPHVPESAF	SASVQRADTSL
MMQVCLHHL	NYKRCFPVI	QLSSGVSEIRH	RLGPVARTRV	RPKSNIVL	SAWISKPPGV
MMSEGGPPGA	NYNNFYRFL	QLVFGIEVV	RLIDLGVGL	RPKSNIVLL	SAYGEPRKL
MMYKDILLL	NYSVRYRPGL	QLVIQCEPL	RLIGDAAKNQV	RQAGDFHQV	SEHLDTQKELL
MPFATPMEA	PAFSYSFFV	QLYALPCVL	RLLASLQDL	RQFVTQLY	SEIWRDIDF
MPFATPMEAEL	PLADLSPFA	QMFFCFKEL	RLLCALTSL	RQKKIRIQL	SEIWRDIDFd
MPGEATETV	PLALEGSLQK	QMMQICLHHL	RLLDLAQEGL	RQKRILVNL	SELFRSGLDSY
MQLIYDSSL	PLDGGVAAA	QMMQVCLHHL	RLLIKKLPRV	RQLAQEQFFL	SESIKKKVL
MSLQRQFLR	PLFDFSWLSL	QQITKTEV	RLLKEYQEL	RQVGDFHQV	SESLKMIF
MTSALPIIQK	PLFQVPEPV	QQLDSKFLEQV	RLLPLLALL	RRFFPYYV	SFSYTLLSL
MTVDSLVNK	PLHCWAVLL	QRPYGYDQIM	RLLPLLALLAL	RRKWRRWHL	SGMGSTVSK
MVIGIPVYV	PLHCWVVLL	QVFPGLLERV	RLLPLWAAL	RRQRRSRRL	SHETVIIEL
MVKISGGPR	PLLALLALWG	QVLDLRLPSGV	RLLPLWAALPL	RRRWHRWRL	SHLVEALYLV
MVWESGCTV	PLLENVISK	QYSWFVNGTF	RLLQETELV	RSCGLFQKL	SIFDGRVVAK
MVYDLYKTL	PLPEAPLSL	RAGLQVRKNK	RLLSDEDVAL	RSDSGQQARY	SIFTWAGKAVL
MYIFPVHWQF	PLPPARNGGL	RALAETSYV	RLLSDEDVALM	RSKFRQIV	SIFTWAGQAVL
NCLKLLESL	PLPPARNGGLg	RALAKLLPL	RLLSDEDVEL	RSRRVLYPR	SILEDPPSI

NLAQDLATV	PLQPEQLQV	RALEEANADLEV	RLLSDEDVELM	RSYHLQIVTK	SIQNYHPFA
NLATYMNSI	PLTEYIQPV	RALRLTAFASL	RLLVPTQFV	RSYVPLAHR	SISVLISAL

Table 4-2 continued

SIVKIQSWFRM	SLMSWSAIL	SQGFSHSQM	THFPDETEI	TMTRVLQGV	VLHDDLLE
SLAAGVKLL	SLNYSGVKEL	SQKTYQGSY	TIADFWQMV	TPGNRAISL	VLHDDLLEA
SLAAYIPRL	SLPGGTAS	SQLTTLSFY	TIHDSIQYV	TPNQRQNVC	VLHELFGMDI
SLADEAEVYL	SLPKHSVTI	SQQAQLAAA	TILLGIFFL	TPRLPSSADVEF	VLHWDPETV
SLADTNSLAV	SLPPPGTRV	SRASRALRL	TIMIHDLCLA	TPRTPPPQ	VLLESAFPGGL
SLADTNSLAVV	SLPRGTSTPK	SRDSRGKPGY	TINPQVSKT	TQPGPLAPL	VLLESAFPGRL
SLAMLDLLHV	SLQALKVTV	SRFGGAVVR	TIPTPLQPL	TQPGPLVPL	VLLGMEGSV
SLASLLPHV	SLQDVPLAAL	SRFTYTALK	TIRYPDPVI	TRPWSGPYIL	VLLLVLAGV
SLAVVSTQL	SLQEEIAFL	SSADVEFCL	TLADFDPRV	TRVLAMAIY	VLLQAGSLHA
SLCPWSWRAA	SLQEKVAKA	SSDNYEHWLY	TLAKYLMEL	TSALPIIQK	VLLRHSKNV
SLDDYNHLV	SLQKRGIVEQ	SSDYVIPIGTY	TLDEKVAELV	TSDQLGYSY	VLMIKALEL
SLDDYNHLVTL	SLQPLALEG	SSFGRGFFK	TLDSQVMSL	TSEHSHFSL	VLNSLASLL
SLDKDIVAL	SLQRMVQEL	SSKALQRPV	TLDWLLQTPK	TSEKRPFMCAY	VLNSVASLL
SLEEEIRFL	SLQRTVQEL	SSLSLFFRK	TLEEITGYL	TSTTSLELD	VLPDVFIRC
SLEENIVIL	SLQSMVQEL	SSPGCQPPA	TLEGFASPL	TTINYTLWR	VLPDVFIRCV
SLFEGIDIYT	SLQSTVQEL	SSSGLHPPK	TLGEFLKL	TTLITNLSSV	VLPDVFIRCV
SLFEGVDFYT	SLRILYMTL	SSVPGVRLL	TLITDGMRSV	TTNAIDELK	VLQELNVTV
SLFGKLQLQL	SLSKILDTV	STALRLTAF	TLKCDCEIL	TVASRLGPV	VLQVGLPAL
SLFLGILSV	SLSPLQAEL	STAPPAHGV	TLKKYFIPV	TVFDAKRLIGR	VLQWLPDNRL
SLFPNSPKWTSK	SLSRFSWGA	STAPPVHNV	TLLASSMSSQL	TVSGNILTIR	VLQWLSDNRL
SLFRAVITK	SLVEELKKV	STDPQHHAY	TLLIGATIQV	TYACFVSNL	VLRDDLLEA
SLFVSNHAY	SLWGGDVVL	STIKFQMKK	TLLIGATIQVT	TYLPTNASL	VLRENTSPK
SLGEQQYSV	SLWSSSPMA	STLCQVEPV	TLLIGATMQV	TYSEKTTLF	VLRKEEEKL
SLGIMAIEL	SLWSSSPMAT	STLQGLTSV	TLLIGATMQVT	VAANIVLTV	VLRQEVAAPL
SLGSPVLGL	SLWSSSPMATT	STMPHTSGMNR	TLLLEGVMAA	VAELVHFLL	VLSVNVPDV
SLGWLFLLL	SLYHVYEVNL	STPPPGATRV	TLLNLPDKMFL	VAVKAPGFGD	VLTSESMHV
SLIAAAAFCLA	SLYKFSPFPL	STSQEIHSATK	TLLNQPDKMFL	VCGERGFFYT	VLVEGSTRI
SLIKQIPRI	SLYQLENYC	STVASRLGPV	TLLPATMNI	VCLHHLPFWI	VLVPPLPSL
SLKLLESLTPI	SLYSFPEPEA	STVASWLGPV	TLLSNIQGV	VEETPGWPTTL	VLWDRTFSL
SLLDRFLATV	SMCRFSPLTL	SVAQQLLNGK	TLMSAMTNL	VEGSGELFRW	VLYGPDAPTV
SLLGLALLAV	SMLIRNNFL	SVASLLPHV	TLPGYPPHV	VEIEERGVKL	VLYPRVVRR
SLLGQLSGQV	SMPPPGTRV	SVASTITGV	TLPPAWQPFL	VFLPCDSWNL	VLYRYGSFSV
SLLKFLAKV	SMPQGTFPV	SVGSVLLTV	TLPPRPDHI	VIMPCSWWV	VLYRYGSFSVTL
SLLLELEEV	SMSKEAVAI	SVHSLHIWSL	TLRTGEVKWSV	VISNDVCAQV	VMALENNYEV
SLLMWITQA	SMSSQLGRISL	SVKPASSSF	TLSSRVCCRT	VIVMLTPLV	VMIIVSSLAV
SLLMWITQC	SNDGPTLI	SVPQLPHSSSHW	TLTNIAMRPGL	VIWEVLNAV	VMLDKQKEL
SLLMWITQCFL	SPASSRTDL	SVQGIIIYR	TLTTGEWAV	VLAGGFFLL	VMNILLQYV
SLLNLPVWV	SPAVDKAQAEL	SVSPVVHVR	TLWVDPYEV	VLAGVGFFI	VMNILLQYVV
SLLNLPVWVLM	SPGSGFWSF	SVVKIQSWFRM	TLYEAVREV	VLASIEAEL	VPGWGIALL
SLLPAIVEL	SPHPVTALL	SVYDFFVWL	TLYNPERTITV	VLASIEAELPM	VPLDCVLYRY
SLLQHLIGL	SPLFQRSSL	SYLDKVRA	TMASTSVSRSA	VLASIEPEL	VPRSAATTL
SLLQSREYSSL	SPQNLRNTL	SYLDSGIHF	TMESMNGGKLY	VLASIEPELPM	VPYGSFKHV
SLLQSRGYSSL	SPRFSPITI	SYRNEIAYL	TMGGYCGYL	VLCSIDWFM	VRIGHLYIL
SLLSGDWVL	SPRPPLGSSL	SYTRLFLIL	TMHSLTIQM	VLDFRLPSGV	VRLGSLSTK
SLLSLPVWV	SPRWWPTCL	TALRLTAFASL	TMKIYSENLTL	VLDGLDVLL	VRSRRCLRL
SLLSLPVWVLM	SPSKAFASL	TCQPTCRSL	TMKLYSENLTL	VLEGMEVV	VSDFGGRSL
SLLSPLHCWA	SPSSNRIRNT	TEAASRYNL	TMLARLASA	VLFGLGFAI	VSLLSLPVWV

SLLSPLHCWAV	SPSVDKARAEL	TETEAIHVF	TMLGRRAPI	VLFSSDFRI	VTLLIGATIQV
SLLTSSKGQLQK	SPTSSRTSSL	TFDYLRSVL	TMLGRRPPI	VLFYLGQY	VTLLIGATMQV
SLMASSPTSI	SQFGGGSQY	TFPDLESEF	TMNGSKSPV	VLFYLGQYI	VTTDIQVKV

Table 4-2 continued

VVEGTAYGL	YLDPAQQNL	YVDPVITSI
VVHFFKNIV	YLEPGPVTA	YVFTLLVSL
VVLGVVFGI	YLEYRQVPV	YVIPIGTYGQM
VVMSWAPPV	YLFSEEITSG	YYNAFHWAI
VVMVNQGLTK	YLGSYGFRL	YYSVRDTLL
VVPCEPPEV	YLIELIDRV	YYWPRPRRY
VVPEDYWGV	YLLKPVQRI	RVASPTSGVK
VVQNFAKEFV	YLLLRVLNI	
VVTGVLVYL	YLLPAIVHI	
VVVGAVGVG	YLLPEAEEI	
VYDFFVWLHY	YLLQGMIAAV	
VYDYNCHVDL	YLMDTSGKV	
VYFFLPDHL	YLNDHLEPWI	
VYGIRLEHF	YLNKEIEEA	
VYLDKFIRL	YLQGMIAAV	
VYSDADIFL	YLQLVFGIEV	
VYVKGLLAKI	YLQQNTHTL	
WATLPLLCAR	YLSGANLNL	
WGPDPAAA	YLSGANLNLG	
WLDEVKQAL	YLSGANLNV	
WLDPNETNEI	YLVGNVCIL	
WLEYYNLER	YLVPQQGFFC	
WLLPLWAAL	YLYDRLLRI	
WLLPLWAALPL	YLYGQTTTY	
WLPFGFILI	YMDGTMSQV	
WLPKILGEV	YMFDVTSRV	
WLQYFPNPV	YMFPNAPYL	
WLSLKTLLSL	YMIAHITGL	
WLSLLFKKL	YMIDPSGVSY	
WMRLLPLLAL	YMIMVKCWMI	
WQYFFPVIF	YMIPSIRNSI	
WYEGLDHAL	YMMPVNSEV	
WYQTKYEEL	YMNGTMSQV	
YAVDRAITH	YMNSIRLYA	
YEDIHGTLHL	YPFKPPKV	
YEGSPIKVTL	YQGSYGFRL	
YGHSGQASGLY	YQLDPKFIV	
YGYDNVKEY	YRPRPRRY	
YIDEQFERY	YRYGSFSVTL	
YIFAVLLVCV	YSDHQPSGPYY	
YIGEVLVSV	YSLEYFQFV	
YLAMPFATPME	YSLKLIKRL	
YLAPENGYL	YSWMDISCWI	
YLCDKVIPG	YTCPLCRAPV	
YLCDKVVPG	YTDFHCQYV	
YLCSGSSYF	YTDFVGEGL	
YLCSGSSYFV	YTDQPSTSQIAY	
YLDLFGDPSV	YTLDRDSLYV	
YLDLLFQIL	YTMKEVLFY	

YLDLLFQILL YVDFREYEYY

***Table 4-3**. Enriched signaling pathways in melanoma cells +/- MEKi. Positively & negatively enriched cancer hallmarks signaling pathways in pMHC analyses of melanoma cell lines + binimetinib. + NES scores are positively enriched, - NES scores are negatively enriched.*

	NES	p-val	q-value < 0.25?
SKMEL5-100 nM			
EMT	1.77	0.011	y
A375-100 nM			
EMT	1.65	0.003	y
Glycolysis	1.58	0.001	y
A375-1 uM			
EMT	1.82	0.001	y
Hypoxia	1.63	0.009	y
RPMI-7951 100 nM			
EMT	3.15	<0.0001	y
MYC targets	2.08	<0.0001	y
Unfolded protein response	2	0.002	y
Protein Secretion	1.81	0.011	y
Androgen response	1.79	0.011	y
MTORC1 signaling	1.65	0.023	y
Myogenesis	1.62	0.037	y
Apical Junctioln	1.58	0.046	y
RPMI-7951 1uM			
EMT	3.12	<0.0001	y
MYC targets	2.08	<0.0001	y
Unfolded protein response	1.95	0.003	y
Androgen response	1.77	0.017	y
Protein Secretion	1.76	0.016	y
MTORC1 signaling	1.68	0.016	y
Myogenesis	1.63	0.029	y
Apical Junction	1.59	0.041	y

	NES	p-val	q-value < 0.25?
IPC298-100 nM			
EMT	1.39	0.069	n
SKMEL28-100 nM			
Apical junction	1.77	0.002	y
Androgen response	1.74	0.002	y
Cholesterol homeostasis	1.56	0.018	y
Myogenesis	1.45	0.032	y
EMT	1.29	0.117	n
SKMEL28-1 uM			
Apical junction	1.71	0.015	y
Androgen response	1.56	0.006	y
Myogenesis	1.46	0.02	y
Oxidative phosphorylation	1.45	0.009	y
Protein Secretion	1.42	0.039	y
Hypoxia	1.39	0.041	y
EMT	1.37	0.061	n
SKMEL2-100 nM			
Myogenesis	2.16	<0.0001	y
EMT	1.45	0.064	n

Table 4-3 continued.

SKMEL28- 1 uM	NES	p-val
E2F TARGETS	-1.63	<0.0001
TNFA SIGNALING VIA NFKB	-1.61	0.04
G2M CHECKPOINT	-1.52	<0.0001

A375- 100 nM	NES	p-val
E2F TARGETS	-2.06	<0.0001
G2M CHECKPOINT	-1.38	<0.0001

SKMEL2- 100 nM	NES	p-val
E2F TARGETS	-2.13	<0.0001
G2M CHECKPOINT	-1.96	<0.0001
MTORC1 SIGNALING	-1.68	0.002
INTERFERON GAMMA RESPONSE	-1.56	0.014

SKMEL5- 100 nM	NES	p-val
MTORC1 SIGNALING	-1.68	<0.0001
E2F TARGETS	-1.64	<0.0001

***Table 4-4**. Labeling scheme for CLX tumors.*

SKMEL2, IPC298

Treatment	Label
C1	126
C2	127N
C3	127C
1d1	128N
1d2	128C
1d3	129N
2d1	129C
2d2	130N
2d3	130C
3d1	131N
3d2	131C
3d3	132N
5d1	132C
5d2	133N
5d3	133C

SKMEL5

Treatment	Label
C1	126
1d1	128N
1d2	128C
1d3	129N
2d1	129C
2d2	130N
2d3	130C
3d1	131N
3d2	131C
3d3	132N
5d1	132C
5d2	133N
5d3	133C

SKMEL5

C3	126
C4	127N
C5	127C
3d1	128N
3dB1	128C
3dB2	129N
3dB3	129C
3dBM1	130N
3dBM2	130C
3dBM3	131N

Bridge channel

SKMEL28

Treatment	Label
C1	126
C2	127N
C3	127C
1d1	128N
1d2	128C
1d3	129N
2d1	129C
2d2	130N
2d3	130C
3d1	131N
3d2	131C
3d3	132N
5d1	132C
5d2	133N
5d3	133C

SKMEL28

C1	126
C2	127N
C3	127C
3d1	128N
3dB1	128C
3dB2	129N
3dB3	129C
3dBM1	130N
3dBM2	130C
3dBM3	131N

Bridge channel

Table 4-5. *Cancer hallmarks enrichment results for CLX analyses. All reported results are q < 0.25, conditions with no listed results did not have any significant findings.*

SKMEL28 - Positive enrichment	p-vals					
PATHWAY	1d	2d	3d	5d	3dB	3dB/M
HYPOXIA	0	0.001				
ESTROGEN RESPONSE LATE	0.029					
P53 PATHWAY	0.026					
GLYCOLYSIS	0.022					
MTORC1 SIGNALING	0.012					
DNA REPAIR	0.042					
PROTEIN SECRETION			0.001	0.002		
ALLOGRAFT REJECTION			0.029			
APICAL JUNCTION				0.024		

SKMEL28- Negative enrichment	p-vals					
PATHWAY	1d	2d	3d	5d	3db	3dbm
ESTROGEN RESPONSE LATE		0.012		0.044		
E2FTARGETS				<0.0001	<0.0001	<0.0001
G2MCHECKPOINT				<0.0001		0.009
MTORC1SIGNALING				<0.0001		0.012
ANDROGENRESPONSE				0.009		
MITOTICSPINDLE				0.009		
GLYCOLYSIS				0.015		
MYCTARGETSV1				0.006		
HYPOXIA				0.031		0.095
ESTROGENRESPONSEEARLY				0.043		
IL2 STAT5 SIGNALING						0.021

SKMEL5 - Positive enrichment	p-val
PATHWAY	3dB
UV-RESPONSE	0.016

SKMEL5 - Negative enrichment	p-val
PATHWAY	3dB
G2MCHECKPOINT	<0.0001
E2FTARGETS	<0.0001
APOPTOSIS	0.027

SKMEL2- Negative enrichment	p-vals			
PATHWAY	1d	2d	3d	5d
DNA REPAIR	0.002			
G2M CHECKPOINT		0.017		
HYPOXIA			0.047	
MITOTIC SPINDLE				<0.0001

***Table 4-6**. CLX treatment groups and dosing schedule. Groups 6 and 7 were not included in SKMEL2/IPC298 studies.*

Study groups:	Schedule	Route	Animal #
1. Vehicle (1%CMC/0.5%Tween80)	BID1-3, 2hr	PO	3
2. 3.5 mg/kg MEK162	QD, 2hr	PO	3
3. 3.5 mg/kg MEK162	BID1-2, 2hr	PO	3
4. 3.5mg/kg MEK162	BID1-3, 2hr	PO	3
5. 3.5mg/kg MEK162	BID1-7, 2hr	PO	3
6. 20mg/kg LGX818	QD1-3, 2hr	PO	3
7. 3.5 mg/kg MEK162/ 20 mg/kg LGX818	BID1-3, 2hr QD1-3	PO	3

CHAPTER 5: Absolute quantification of pMHCs with isotopologues

5-1 Introduction

Achieving absolute quantification of presented peptide antigens is necessary to inform immunotherapy drug design, as targeted strategies have varying thresholds of antigen expression required for an optimal antitumor response. For example, it has been reported that T cells can recognize and elicit an anti-tumor immune response against a single pMHC, and just ~100-200 pMHCs are required for cytokine secretion to activate/stimulate T cells.[78,387–389] Engineered pMHC-specific therapies like ImmTACs (immune-modulizing monoclonal TCRs against cancer) require 15-45 pMHCs for cytokine release and ~50% specific lysis, whereas TCR-like ADCs require tens of thousands of pMHCs for a similar level of cytotoxicity.[390–392] It is thought that neoantigens are lowly expressed, and many tumor antigens derived from germline or differentiation genes have much higher expression levels in tumor cells, though this has not been thoroughly characterized (**Figure 5-1**). Nevertheless, the expression level of an antigen may dictate which type of targeted immunotherapy may be most efficacious, however methodologies to accurately and robustly quantify pMHC expression levels have significant limitations.

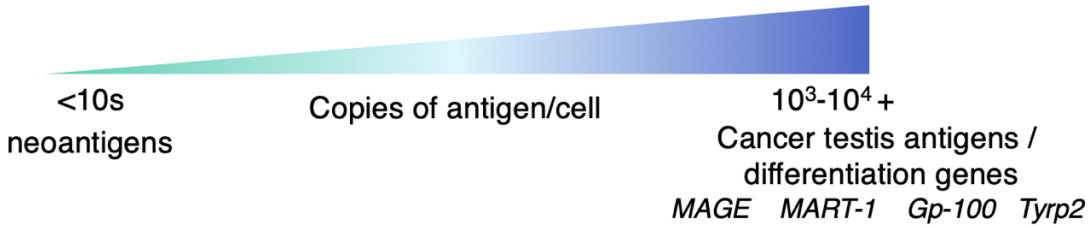

***Figure 5-1**. Schematic of proposed antigen presentation scale.*

To date, absolute quantification of pMHCs with mass spectrometry is most commonly performed by comparing endogenous levels of pMHCs to exogenous peptide standards, which fail to account for losses taken throughout the pMHC workflow. The initial 1992 publication by Hunt and colleagues attempts to quantify copies-per-cell of endogenous peptides using exogenous synthetic standards. They estimated the lower limit of detection on their instrument at 30 fmol, and estimated 10% of identified peptides were present at 150-600 fmol, whereas the rest were present at 30-150 fmol, representing a range of peptide presentation levels from ~100 to 3000 complexes/cell.[155]

Hogan et al. similarly performed copy number estimations of three HLA-A*02:01 peptides, but utilized exogenous deuterated peptide standards and SRM, which do not co-elute with endogenous peptides and therefore are not optimal for use as internal standards.[266] Bozzacco et al. used a similar strategy for absolute quantification of MHC II peptides presented on mouse dendritic cells by generating 7 synthetic, isotopically labeled peptides added exogenously prior to DDA LC-MS/MS analysis.[269] Similar to previous work, estimations were generated through single-point calibration, which rely on a linear intensity response across pMHC concentrations. Authors estimate concentrations ranging from to 13-20,000 copies per cell. Wu et al apply a similar technique, and like Hunt, Hogan, and Bozzacco, fail to consider losses incurred throughout sample processing. Consequently, reported values are inaccurate and likely underestimations of the true presentation levels.[268]

These suspected losses were first estimated by Hassan et al. using a set of two isotopologue peptides (termed heavy and medium-labeled) for two different peptides the authors identify as HLA-A*02:01 binders.[183] The authors folded recombinant HLA alpha chain and β2m with the isotopically labeled peptides to generate pMHC complexes with the heavy-labeled peptide. These complexes were added to cell lysates prior to immunoprecipitation, and

the medium labeled peptide was exogenously added prior to LC-MS/MS analysis. Using SRM acquisition, authors estimated pMHC losses by calculating the ratio of heavy to medium peptide signal across three replicates. While this study failed to capture measurements across a diversity of sequences or pMHC concentrations, these data highlight pMHC losses ranging from ~97.2-99.5%, underscoring the need for internal reference standards to make copy number estimations. An optimized experimental system for pMHC absolute quantification has not yet been developed and would ideally utilize internal standards and an embedded multipoint calibration curve for quantification.

It is worth noting that an alternate technique has been previously employed to estimate pMHC surface levels, utilizing pMHC-specific antibodies or TCR-mimic antibodies which specifically bind pMHC epitopes.[31,389,393,394] The antibodies, bound to pMHCs, are detected by microscopy or more commonly, flow cytometry, where a linear curve can be generated using QuantiBRITE calibration beads to estimate copies per cell. This technique relies on having a high-affinity pMHC-specific antibody for each target of interest and is limited to the dynamic range of QuantiBRITE beads (~1,700-133,000 molecules/cell) and the sensitivity of a flow cytometer for quantitative estimates. As a result, this technique is not scalable for high-throughput, high sensitivity quantification, and cannot capture low abundance pMHCs.

We previously reported a technique to perform absolute quantification with an embedded internal standard curve, combining heavy isotope-labeled MHCs (hipMHCs) with TMT.[188] While this method was successful in capturing endogenous expression levels of target pMHCs, it has several limitations. First, it requires running three replicate samples to generate three internal standard data points. This is not an obstacle for renewable samples like immortalized cell lines, however for *in vivo* animal or patient-derived samples there may not be enough material to perform three replicates. The method, which utilizes an inclusion list, is also less sensitive as many MHC peptides have similar amino acid compositions and molecular weights and there are

frequently false triggering events. Finally, due to significant ion suppression with TMT-MS^2 analyses of the immunopeptidome, standard curves can only span a 10-fold range therefore it is challenging to determine the range required to capture the endogenous peptide.

To circumvent these limitations, we have developed SureQuant MHC, a method that uses a series of isotopologues and SureQuant internal standard (IS)-triggered PRM to generate an embedded standard curve along with sensitive and selective measurements of the endogenous peptide for 18 peptide targets. This label-free analysis utilizes less than $1e^7$ cells for protein input and utilizes a 100-fold standard curve range, eliminating the requirement for tedious range-finding. We apply this method to profile changes in pMHC expression levels in melanoma cell lines treated with binimetinib, a MEK inhibitor, and translate the approach to profiling antigen levels in human tumors.

5-2 Results

5-2-1 Peptide panel selection

Peptides selected for absolute quantification with isotopologues were identified from discovery analyses of SKMEL5 cells treated with MEK inhibitors. Initially, SKMEL5 +/- 100 nM binimetinib that were predicted to be HLA-A2*01 binders (< 500 nM predicted affinity) were considered. Synthetic standards of 50 possible targets (**Table 5-1**). were synthesized and binding affinity was tested T2 cells, which are defective in presenting exogenous antigens due to a deletion in genes encoding transporters associated with antigen presentation (TAP1/TAP2). As a result, addition of exogenous peptide is taken up by cells and loaded onto newly synthetized MHC molecules. As control peptides, we synthesized a known high affinity flu peptide binder (GILFGVFTL) and a low affinity MART1-derived binder (AAGIGILTV). Most peptides demonstrated an increase in fluorescent intensity over DMSO treated T2 cells, with

expected MFI increases corresponding to an increase in peptide loading (**Figure 5-2**). Several peptides were initially selected that we saw large increases in pMHC expression with like the serine phosphorylated IRS2-derived peptide "RVASPTSGVK," which showed little change in MFI compared to the DMSO T2 vehicle control.

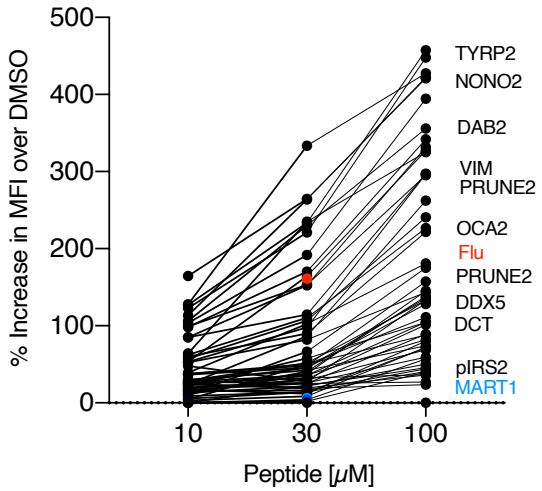

***Figure 5-2**. pMHC binding in T2 cells. Increase in median fluorescent intensity (MFI) of synthetic peptide stimulated T2 cells over DMSO treated T2 cells. Positive control Flu peptide is shown in red, negative control MART1 in blue.*

Using this data, eighteen peptides (termed "Iso18" panel) were selected, most of which are known tumor associated antigens and follow the previously defined criteria of being nine or ten amino acids in length, predicted high affinity HLA-A2*01 binders (**Table 5-2**), and had at least a 2-fold change in expression with MEK inhibition (**Figure 5-3-A**). Of note, several were selected that were no included in the T2 analysis. Priority was given to peptides that were of high abundance relative to the other peptides, including peptides derived from PMEL, DCT, PRUNE2, SLC45A2 and BCAP31, all of which were in the 99th percentile of abundance across multiple analyses (**Figure 5-3-B**). While many of the Iso18 peptides are well studied tumor antigens (ex. PMEL/gp100 and DCT/TRYP2), several were selected that are less well studied.

One set of targets of particular interest was derived from SLC45A2, a highly tissue-specific melanocyte membrane associated transporter protein. A previous study by Park et al. identified pMHCs derived from SLC45A2 in a 16/ 55 melanoma cell line lines screened for tumor antigens.[395] Two peptides, SLYSYFQKV and RLLGTEFQV, were predicted HLA-A2*01 binders and were identified in 6 and 8 cell lines, respectively, in the study. We similarly identified both epitopes and noted that RLLGTEFQV was one of the top 10 most abundant peptides in our analyses. Park et al. also detected CD8+ T cells specific to SLC45A2 peptides, and showed immunogenicity using a chromium 51 release assay. Of particular interest, authors showed that BRAF inhibitors in BRAF V600 E mutant melanomas increased SLC45A2 gene expression by q-PCR, and this led to enhanced tumor cell recognition and killing by SLC45A2-specific CD8+ T-cells. Together, this highlights peptide derived from SLC45A2 as promising candidates for targeted immunotherapy, particularly due to their high tissue specificity, high expression, and ability to be modulated by MEK inhibition.

PRUNE2-derived peptides were also of interest due to similar features, however PRUNE2 is poorly studied. PRUNE 2 is a tumor suppressor gene first identified in prostate cancer, wherein prostate cancer antigen 3 (PCA3) is thought to downregulate PRUNE2 expression, promoting malignant growth.[396] Another study reported expression in melanoma cell lines in association with the AP2 protein and describes an involvement for vesicle trafficking.[397,398] It is not been investigated a tumor-antigen target; however, these mass spectrometry analyses highlight it's potential due to high abundance (99%) and high changes in expression (4-fold or more) in cells treated with a MEK inhibitor. Achieving absolute quantitation estimates of copies-per-cell with and without MEK inhibition will provide better resolution as to which targeted immunotherapies may be best exploited to target antigens such as SLC45A2, PRUNE2, and other well described antigens.

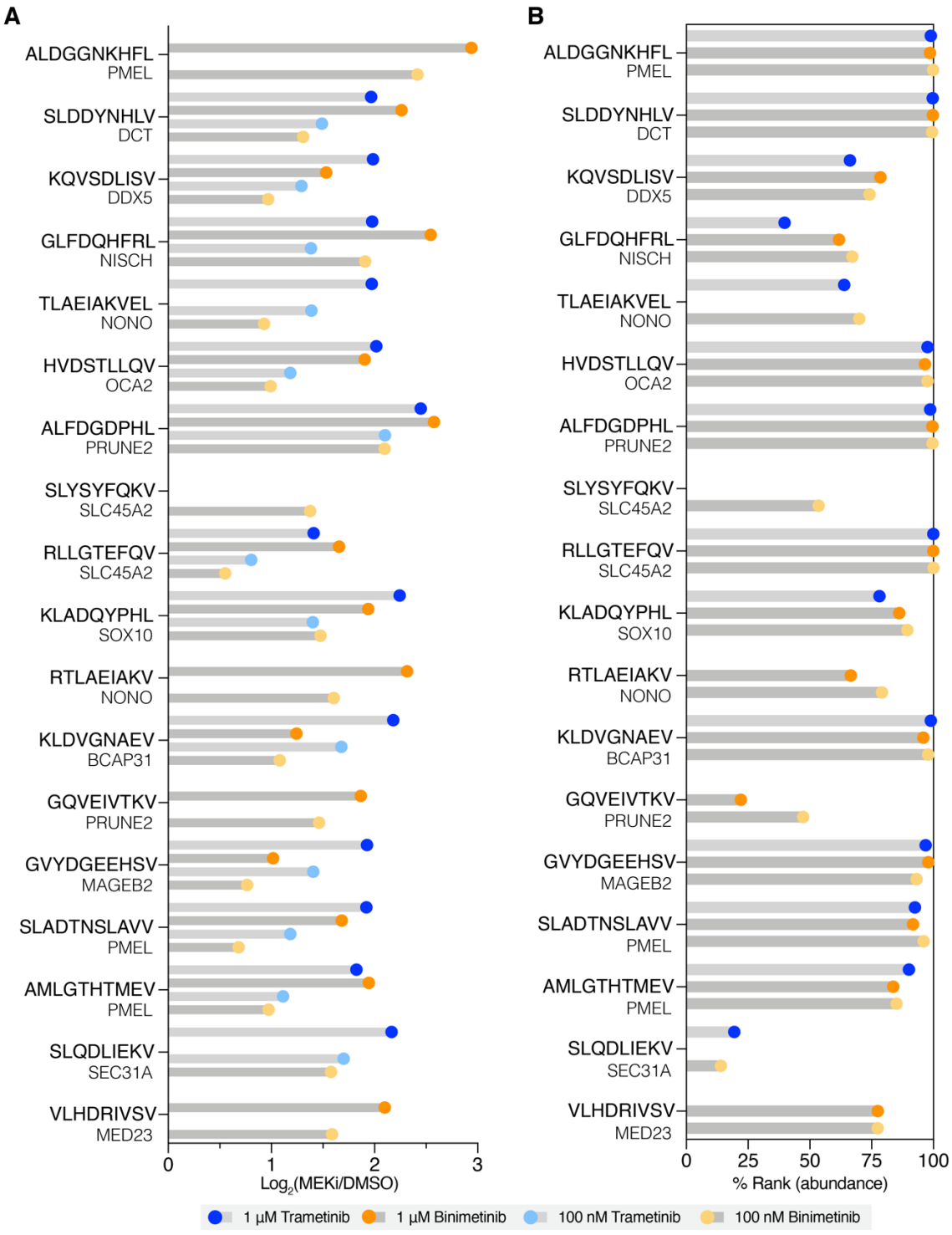

Figure 5-3. *Changes in pMHC expression of Iso18 peptides.* ***A*** *Fold change in pMHC expression measured with multiplexed LC-MS/MS with binimetinib or trametinib (MEK inhibitors) for peptides in the Iso18 panel.* ***B*** *Ranked abundance (integrated precursor area) values of peptides across three analyses, where 100% is the most abundant peptide.*

5-2-2 SureQuant MHC platform for absolute quantification of pMHCs

For absolute quantification of the Iso18 panel, we combined our previous framework of utilizing hipMHCs as internal standards with SureQuant internal standard (IS)-based triggering (SureQuant MHC). In contrast to SureQuant pTyr, a series of four isotopologue peptides is synthesized per target rather than one. Each set of isotopologues contained a differing number of heavy isotopically labeled amino acids (usually one to four), therefore all “heavy” peptides as well as the endogenous peptide co-elute but are still distinguishable by their unique mass-to-charge (m/z) ratio (**Figure 5-4**). Ten amino acids were used for heavy labeling: I, L, F, Y, K, V, A, G, R and P (

Table 5-3), where the isotopologue with a single heavy labeled amino acid is referred to as “1H,” two heavy amino acids, “2H,” etc. Three isotopologues create an internal standard curve for absolute quantification of endogenous targets, and the fourth is used as the IS trigger peptide for SureQuant triggered quantitation. Amino acid compositions for all Iso18 peptides can be found in **Table 5-4**.

	DCT (TYRP2)
	SLDDYNHLV
1H	S**L**[+7]DDYNHLV
2H	S**L**[+7]DDYNHL**V**[+6]
3H	S**L**[+7]DDYNH**L**[+7]**V**[+6]
4H	S**L**[+7]DDY**N**[+6]H**L**[+7]**V**[+6]

Figure 5-4. *Isotopologue series for DCT peptide "SLDDYNHLV"*

The workflow for SureQuant MHC is follows (**Figure 5-5**): three isotopologue peptides (1H, 2H and 3H) are loaded into HLA-A2*01 MHC complexes via UV-mediated peptide exchange (hipMHCs). Concentrations of stable hipMHCs are determined by ELISA for each peptide, and hipMHCs are subsequently titrated into whole cell lysate. As pMHCs have a broad range of expression, peptides were commonly titrated in at 1 (1H), 10 (2H), and 100 (3H) fmol for each peptide. For a cellular input of $7.5e^6$ cells, as was used with SKMEL5, this results in a range of ~80-8000 copies-per-cell for a given pMHC target. Several peptides of high expression in SKMEL5 cells (ex. SLC45A2) required a range of 10-1000 fmol or higher, though broadly 1-100 fmol captured most peptides in the pMHC target panel. For endogenous peptides with lower expression than 1 fmol, results were interpolated. Next, endogenous and hipMHCs were isolated by pan-HLA immunoprecipitation, acid elution, and molecular weight size exclusion filtration. Prior to SureQuant analysis, ~250 fmol of the trigger peptide (4H) is spiked into the

peptide elution. This allows for consistent intensity levels of the trigger peptide for reproducible triggering with the SureQuant method.

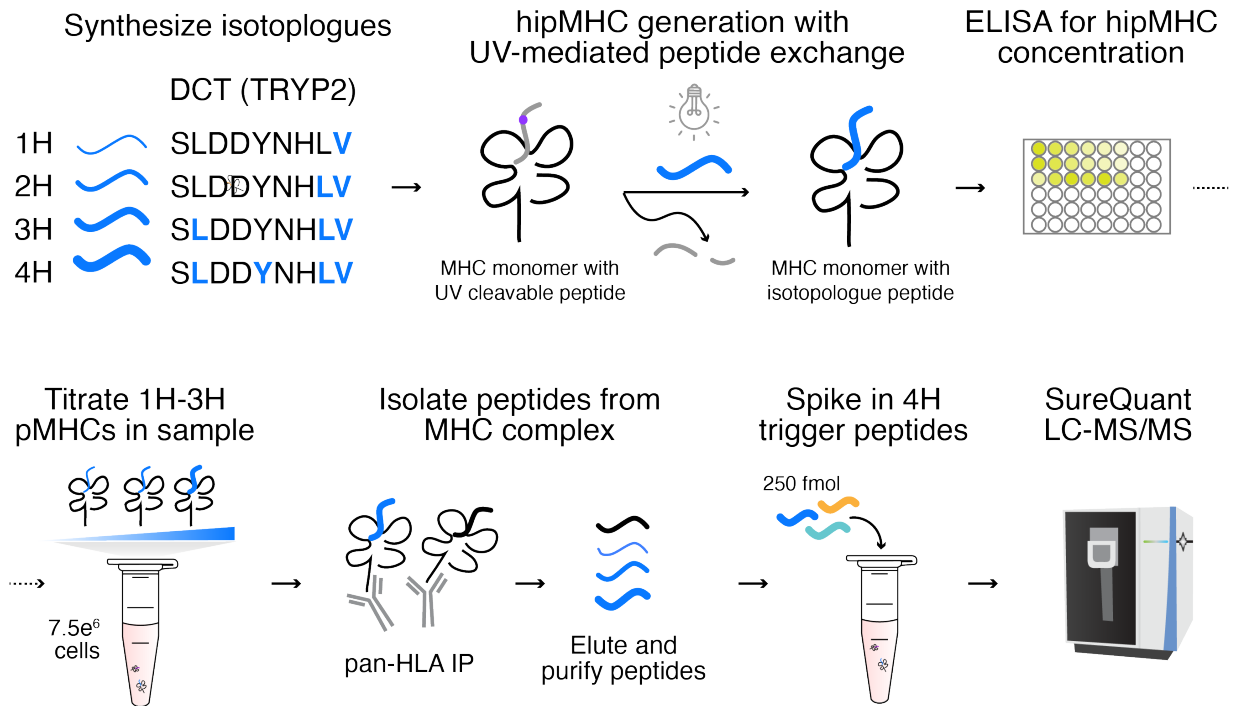

***Figure 5-5**. Sample preparation and experimental workflow for SureQuant MHC.*

SureQuant MHC acquisition follows a similar framework to SureQuant pTyr, where the target peptides are monitored with MS1 scans. When a target reaches a defined intensity threshold, a low-resolution MS^2 scan is performed. If six pre-defined product ions are present (pseudo-spectral matching), this triggers the acquisition of the endogenous target, as well as the 3H, 2H, and 1H peptides at defined m/z offsets (**Table 5-4**). To accomplish this, a custom acquisition method of SureQuant was implemented.

First, all 4H trigger peptides were analyzed with a targeted analysis containing the +2 and +3 charge states for each peptide to determine the most abundant charge state for targeting (**Figure 5-6**).

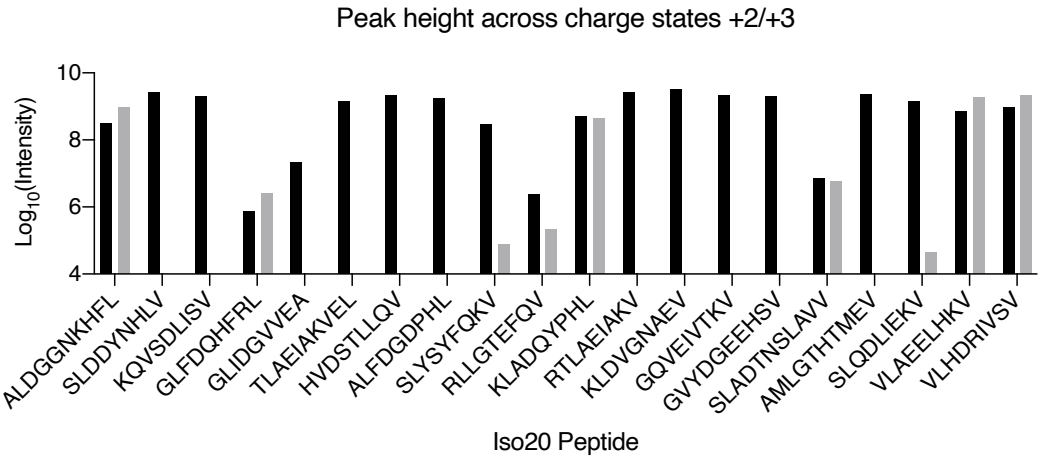

Figure 5-6. *Selecting optimal charge states. Peak heights for +2 (black) and +3 (grey) charge states for each peptide in the panel.*

Next, the six transitions were for each charge state were selected for pseudo-spectral matching in a survey analysis targeting each peptide's optimal charge state (**Table 5-5**). Here, 4H peptides were analyzed against a representative matrix of SKMEL5 pMHCs to mirror the background interference from other MHC peptides in SureQuant MHC analyses. The 6 most abundant product ions were selected using Skyline software and templates generously provided by Sebastien Gallien. Additionally, intensity thresholds were set at 1% of the precursor ion apex intensity.

These data were added to a custom SureQuant method build (**Figure 5-7**), where the "targeted mass" and "targeted mass trigger" nodes mirror those for SureQuant pTyr. In this implementation however, each branch contains the parameters for a unique peptide, as m/z triggering offsets are unique for each series of isotopologues. As a result, four MS^2 scans are triggered following identification of the trigger peptide at m/z offsets for the 1H, 2H, 3H, and endogenous peptides.

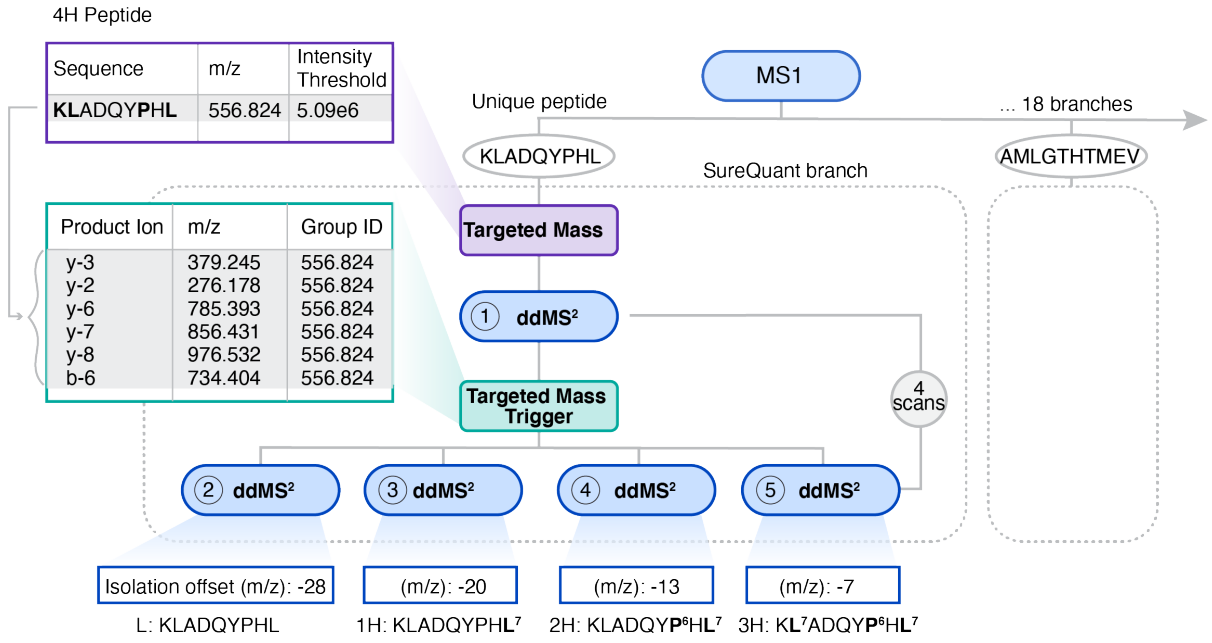

Figure 5-7. *SureQuant MHC acquisition schematic. Method built and import parameters for SureQuant MHC for implementation on the Exploris 480 mass spectrometer.*

Data is acquired using the standard SureQuant framework (**Figure 5-8**), alternating between “watch mode’ for the trigger peptide and “quantification mode” for high resolution scans of the target peptides (1-3H, endogenous). For quantification, the area of selected transitions is integrated and summed, and endogenous concentrations can be subsequently determined using a linear fit of the internal standard curve containing the 1-3H isotopologues.

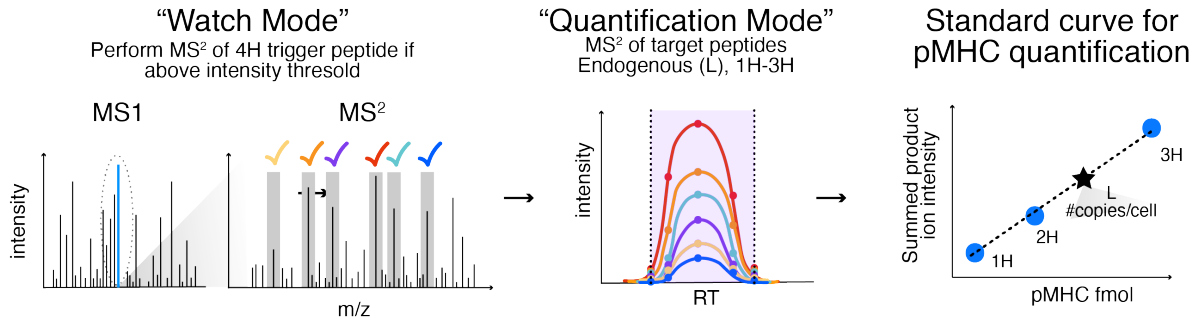

Figure 5-8. *SureQuant MHC LC-MS/MS acquisition and data analysis for pMHC absolute quantification.*

5-3 Method validation of SureQuant MHC

After the method was built, the method was first tested by exogenously adding 1-4H peptides at a 1:1:1:1 concentration (125 fmol) to a background matrix of SKMEL5 pMHCs (**Figure 5-9-A**). The 4H trigger peptide successfully initiated scans of the endogenous and 1H-3H peptides (**Figure 5-9-B**), with similar intensity values in both the precursor ions (CV = 9.0%), as well as the summed transitions (CV = 10.7%) (**Figure 5-9-C**). To determine whether peptides could similarly be detected when added to cell lysate as hipMHCs prior to the immunoprecipitation, 60 fmol of 1-3H hipMHCs of each target were added to SKMEL5 cell lysate, and the 4H peptide was spiked in as the trigger prior to analysis (**Figure 5-9-D**). Reassuringly, all endogenous and 1-3H peptides were successfully targeted and quantified, and intensities between the isotopologues were comparable (**Figure 5-9-E**).

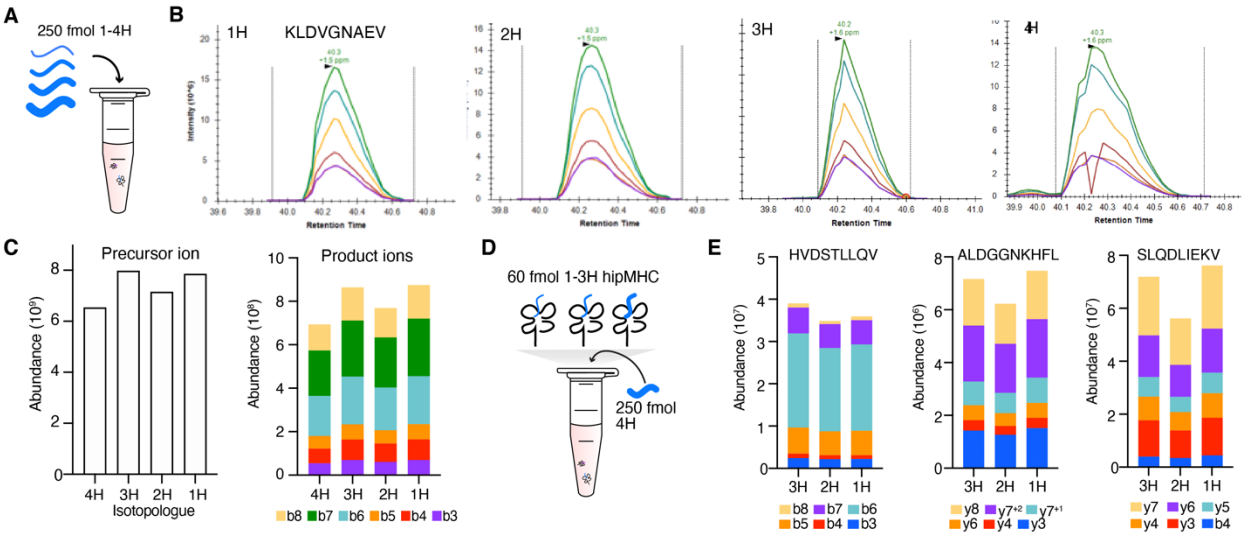

Figure 5-9*. SureQuant pMHC validation with exogenous peptides.* ***A*** *Exogenously added 1-4H peptides for method validation.* ***B*** *Product ion traces for 1-4H KLDVGNAEV peptides.* ***C*** *Integrated precursor ion intensities and product ions for KLDVGNAEV.* ***D*** *Experimental setup for hipMHC method validation.* ***E*** *Integrated product ions of 1-3H peptides added as hipMHCs.*

We next sought to characterize the linearity of peptide intensity response and limit of detection (LOD) for peptides in the target panel. To this end, we built another method where only the 1H peptide was targeted and analyzed all 1H peptides added exogenously to the SKMEL5 pMHC matrix at 0.1, 1, 10, and 100 fmol concentrations in triplicate. All peptides were quantifiable at 0.1 fmol with the exception of GLFDQHFRL We integrated and summed the transition areas for each peptide and assessed the intensity response linear fit for each peptide (**Figure 5-10**). All peptides had a coefficient of determination (r^2) 0.95 or higher with the exception of AMLGTHTMEV, which had an r^2 value 0.94. All peptides were quantifiable at 0.1 fmol, with GLFDQHFRL being the only exception.

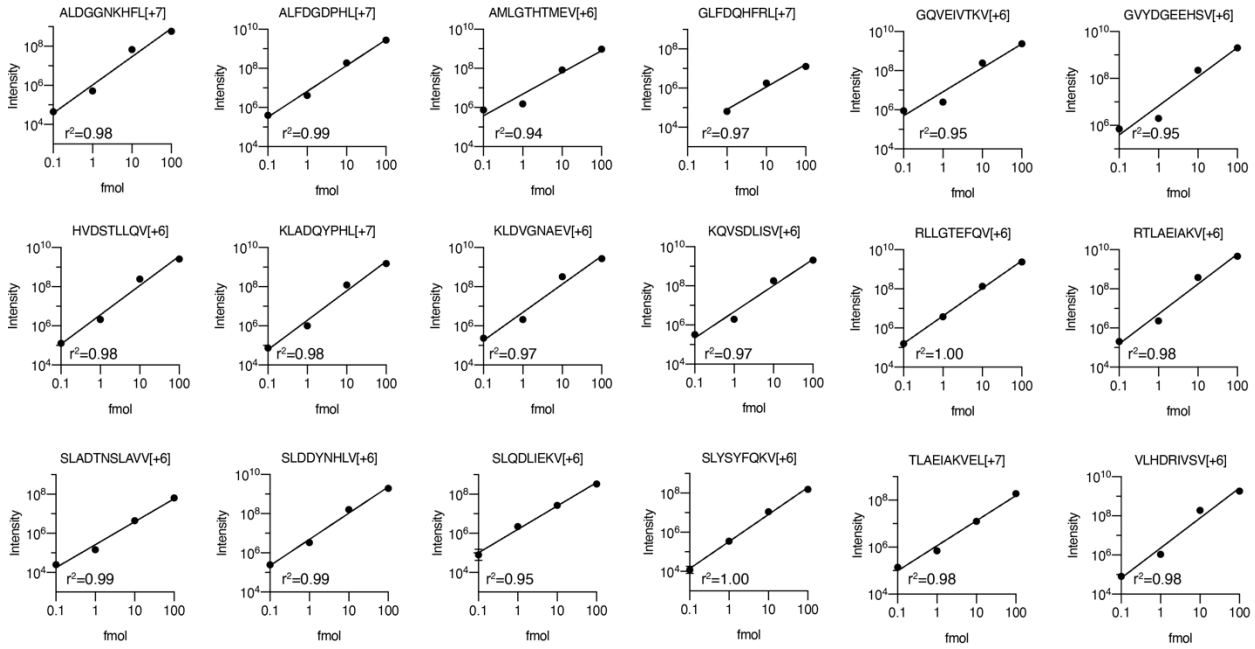

Figure 5-10*. Intensity response of 1H peptide added exogenously with 4H trigger peptide, n=3. Error bars (if visible) represent the standard deviation.*

As it's been previously established that immunoprecipitations and sample processing result in substantial sample losses (up to 99%), we sought to assess the limit of detection and linearity of response with hipMHCs.[399] We assessed the quantitation in half of the isotopologue panel (n=9), where 0.1 to 1000 fmol of the 2H hipMHC was added to an immunoprecipitation of $7.5e^6$ SKMEL5 cells (5mg) and analyzed by a modified SureQuant MHC method, where only the 2H peptide was targeted by the 4H trigger (**Figure 5-11-A**). All concentrations were performed in triplicate with the exception of the 100 fmol condition (n=2). The concentration range was selected as it spans 10-fold higher and lower than the range used in SureQuant MHC experiments, and spans ~8-80,000 pMHC copies/cell. In a case where the endogenous peptide falls outside the 1-100 fmol range, we sought to determine whether interpolation at higher or lower concentrations would be accurate.

We find that in each case, increased concentrations of hipMHC lead to a higher intensity response, and all coefficients of determination for the 1-100 fmol linear fit are r^2=0.92 or higher (**Figure 5-11-B)**. In most cases, the peptides exhibited a linear response at the higher (1000 fmol) and lower (0.1 fmol) concentration (ex. RLLGTEFQV), allowing for high confidence in estimating pMHC concentrations 10-fold outside the standard curve. Exceptions include SLADTNSLAVV and SLDDYNHLV, where these additional data points do not exhibit the same linear response. Consequently, interpolated values should be viewed cautiously, with a replicate experiment performed with an adjusted standard isotopologue standard curve if possible, for the most accurate quantitation. As all peptides in this panel were quantifiable at 0.1 fmol, we performed a separate analysis to determine whether we could quantify hipMHCs at 10 attomol concentration. In 15 peptides, all six transitions were quantifiable, 2 had five transitions, and 1 had four, suggesting that for a majority of peptides in this panel, attomole sensitivity can target peptides at ~1 copy/cell (**Table 5-6**).

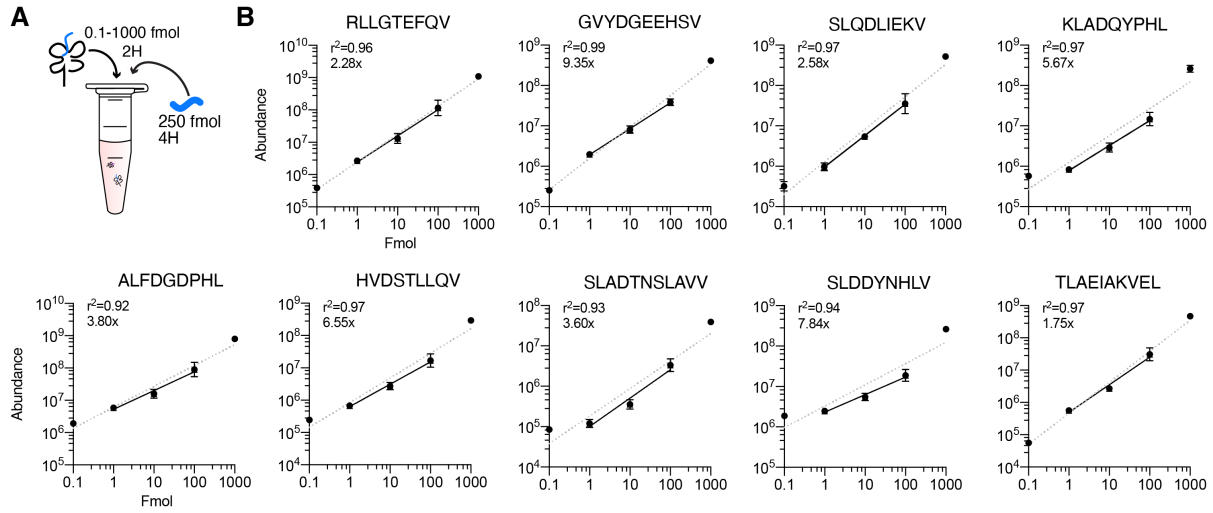

Figure 5-11*. SureQuant pMHC hipMHC intensity response of 2H.* ***A*** *Experimental setup for 2H hipMHC intensity response analyses.* ***B*** *Intensity responses for 2H hipMHCs. Solid line represents linear fit of 1-100 fmol peptides (r^2, upper left), and dotted line the liner fit of 0.1-1000 fmol peptides. Magnitude of ratio compression for the exprected 100-fold difference of the 1 and 100 fmol peptides is reported in the upper left corner. Error bars represent the standard deviation.*

We have also previously reported the varying effects of ion suppression, even in label free analyses, therefore we next assessed the magnitude of ratio suppression from the expected 100-fold intensity difference between the 1 and 100 fmol pMHCs.[188] Across the nine peptides, ratio compression varies greatly, from 1.75x in TLAEIAKVEL to 9.35x in GVYDGEEHSV, suggesting there are peptide-specific variations that cannot be estimated with a single value. Together, these data further underscore that need for pMHC-specific multipoint calibration curves for absolute quantification, as even one-point calibration estimates are likely to be inaccurate.

5-3-1 Absolute quantification of pMHCs in SKMEL5 cells

To assess copy number expression levels of peptides in the Iso18 panel, SKMEL5 cells were treated with DMSO, 100 nM binimetinib, or 1 μM binimetinib for 72h. Cells were subsequently lysed, and Iso18 hipMHCs were titrated into 5 mg of cell lysate ($7.5e^6$ SKMEL5 cells) at 1-100 fmol with the exception of HVDSTLLQV (10-1000 fmol) and RLLGTEFQV (20-2000 fmol) for the MEK inhibitor treated conditions. Endogenous and hipMHCs were purified by immunoprecipitation and size exclusion filtration, and the 4H trigger peptide was added exogenously to the peptide mixture prior to SureQuant MHC analysis.

Similar to method validation experiments, the 1-3H and endogenous (L, light) peptides were triggered by the 4H peptide (**Figure 5-12-A**). The area of each peptide's product ions was integrated and summed, and for SLDDYNHLV, isotopologue intensities roughly followed expected ratios (**Figure 5-12-B,** Supplementary Figure 5-1). A linear fit of these intensities was used to generate a standard curve from which the endogenous concentration was interpolated (**Figure 5-12-C**). For the first DMSO replicate, SLDDYNHLV was present at 15.5 fmol, or ~1200 molecules/cell (**Equation 5-1**).

When comparing the transition areas of endogenous peptides between treatment conditions, it is evident that pMHC expression of SLDDYNHLV increases with MEK inhibition, in line with our discovery pMHC analyses (**Figure 5-12-D**). Of note, replicate 1 of the 100 nM MEKi treated condition had about half the signal intensity as replicate 3. However, replicate 1 had lower signal across isotopologue standards as well, and because each L peptide's concentration is determined using the embedded standard curve from the same analysis, the peptides concentration estimates were comparable across the three replicates (**Figure 5-12-E**). This feature accounts for variation in signal intensity across analyses, which can result from variations in sample processing, immunoprecipitation efficiency, or chromatography. This is in stark contrast to analyses which utilize calibration curves generated through separate injections

of a single isotopically labeled peptide, which does not allow for such run-to-run variation to be accounted for.

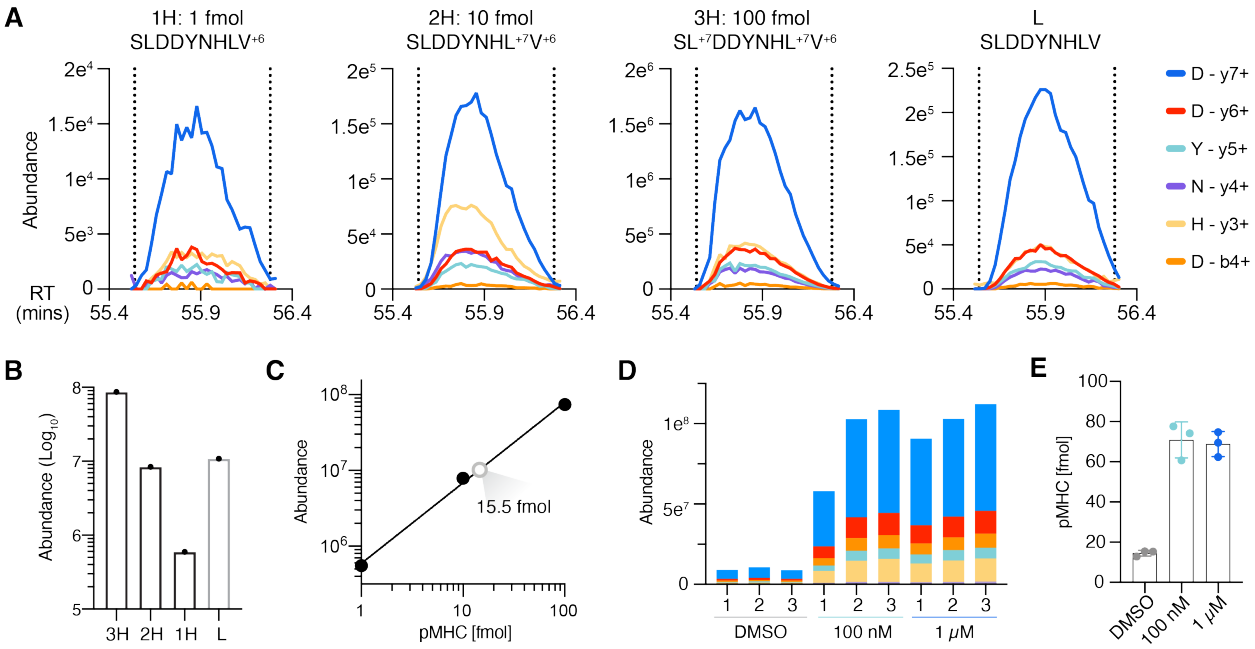

Figure 5-12**. Absolute quantitation of SLDDYNHLV.* ***A *Product ion traces for SLDDYNHLV 1-3H and endogenous (L) peptides for DMSO treated cells (replicate #1).* ***B*** *Summed intensities of 1-3H and L peptides (DMSO, replicate #1).* ***C*** *Linear fit of summed intensities (r^2=0.997) of the 1-3H standards, and quantification of endogenous level from standard curve.* ***D*** *Transition abundance for DMSO, 100 nM and 1 μM binimetinib treated cells, numbered by replicate.* ***E*** *Estimated abundance of endogenous peptides. Error bars represent standard deviation.*

***Equation 5-1**. Equation for determining molecules/cell.*

$$\left(\frac{\text{pMHC concentration } (15.5e^{-15}\text{ mol}) \times \text{Avagadro's number } (6.022*10^{23}\text{ molecules/mol})}{\underset{\text{\# of cells}}{7.5e6\text{ cells}}}\right) = \textbf{1244 molecules/cell}$$

Standard curves were similarly generated for all peptides in the Iso18 panel across treatment conditions in SKMEL5 cells (**Supplementary Figure 5-2**), and endogenous levels were calculated using a linear fit. Four DMSO treated peptides (SLQDLIEKV, TLAEIAKVEL,

GQVEIVTKV, and GLFDQHFRL) had endogenous peptide signals below the 1 fmol 1H peptide, therefore values were interpolated using the linear fit of the 1-3H standard curve. Importantly, while discovery analyses of 1 μM binimetinib-treated cells did not identify the two least abundant peptides (SLQDLIEKV and TLAEIAKVEL, **Figure 5-3-A**), every peptide was identified and quantified with SureQuant MHC, showcasing the sensitivity and reproducibility of utilizing targeted methodologies for monitoring targets of interest.

Endogenous pMHC levels spanned a wide range. PRUNE2 peptide, "GQVEIVTKV," had an estimated 20 molecules/cell in DMSO treated cells, whereas SLC45A2 peptide, "RLLGTEFQV," had approximately 150,000 molecules-per-cell in SKMEL5 cells treated with 1 μM binimetinib. This represents nearly 4 orders of magnitude, highlighting the wide diversity in expression levels of tumor antigens in the immunopeptidome.

As expected, MEK inhibition increased the expression of every peptide in the panel, though to carrying degrees (**Figure 5-14**). On the low end, 100 nM of binimetinib increased the BCAP31 peptide, "KLDVGNAEV" 1.7-fold, and 1 μM of binimetinib increased the PRUNE2 peptide, "GQVEIVTKV" 19-fold. The array of endogenous expression coupled with the perturbagen-induced expression changes showcase the wide range of expression levels and patterns the immunopeptidome can possess. Next, we were curious has to how calculated changes in quantification of the Iso18 peptides, performed label-free, compared to the multiplexed discovery datasets quantitation, as we've previously characterized the dynamic range suppression prevalent in TMT-MS^2 analyses of the immunopeptidome. We find that in cases where the SureQuant-based quantitation showed fold changes up to 4-fold, the quantitation between the two analyses was comparable. However, in peptides with SureQuant MHC-measured fold changes higher than 4x, ex. HVDSTLLQV and GQVEIVTKV, the multiplexed fold changes were much smaller than the SureQuant MHC measured, suggesting a limited dynamic range of the multiplexed assay. As ratio compression has been demonstrated in

label-free and multiplexed analyses, the only accurate way to measure changes in expression is through multipoint calibration curves described here. This allows for a wider dynamic range in measurements of absolute levels of expression and changes in expression.

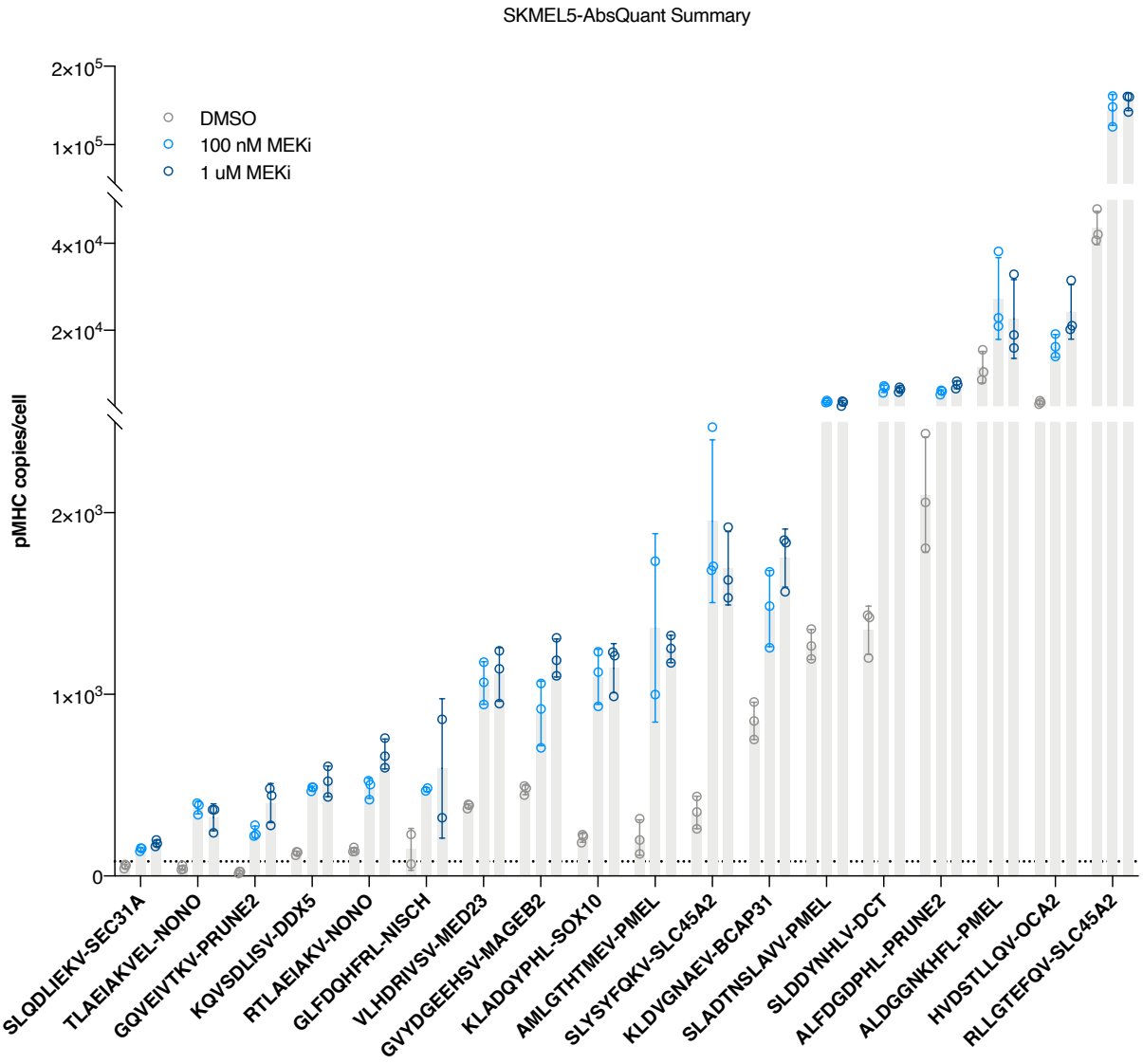

Figure 5-13. *SKMEL5 endogenous copies-per-cell estimates of peptides in the Iso18 panel for DMSO (grey), 100 nM (blue) and 1 μM binimetinib treated cells (n=3). Error bars represent standard deviation. Dotted line = 1 fmol, lower limit of quantitation of the standard curve.*

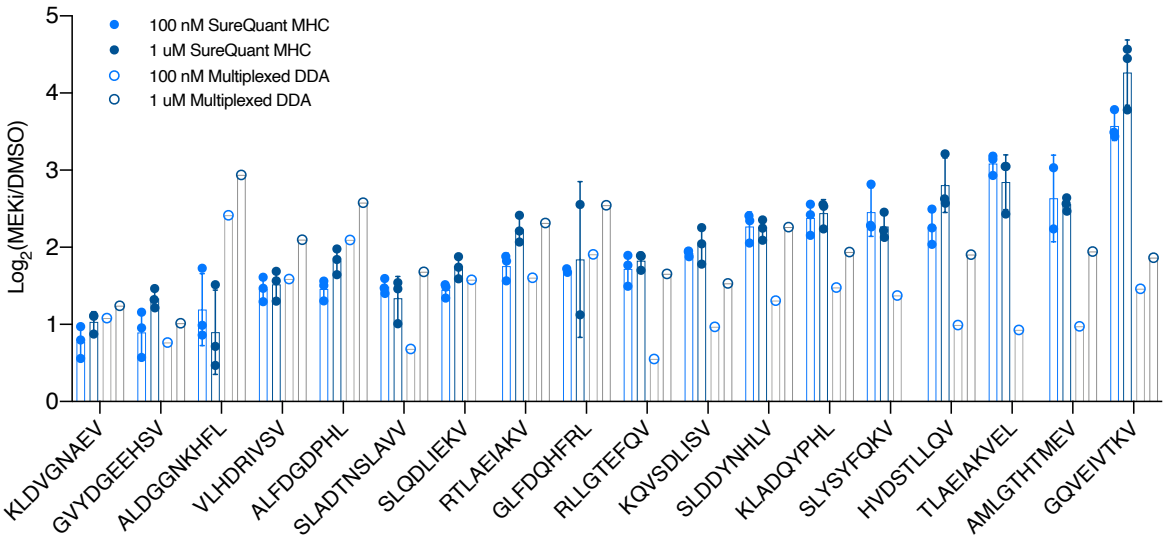

Figure 5-14*. DDA and SQ-MHC quantitative comparison of MEKi-induced expression changes. Fold change in expression of pMHCs in SureQuant MHC and multiplexed DDA-based quantitation strategies.*

5-3-2 Iso18 quantitation in other melanoma cell lines

We next wanted to utilize the Iso18 panel, generated from peptides identified in the SKMEL5 cell line, to determine if we could quantify endogenous levels of pMHCs with and without MEK inhibition in other melanoma cell lines. We selected A375 and RPMI-7951, both BRAF V600E mutant lines that are HLA-A2*01 positive. In discovery analyses, we identified 7 of the Iso18 peptides in A375 cells and 9 in RPMI-7951 cells (**Figure 5-15**). Though we would not expect all Iso18 peptides to be present in each cell line due to differences in their proteomes, we anticipated that due to the sensitivity of SureQuant MHC, if the peptide was present, we would be able to detect and quantify it. In a similar setup to SKMEL5 experiments, cell lines were treated with DMSO, 100 nM or 1μM binimetinib for 72h, and each condition was analyzed with SureQuant MHC in triplicate.

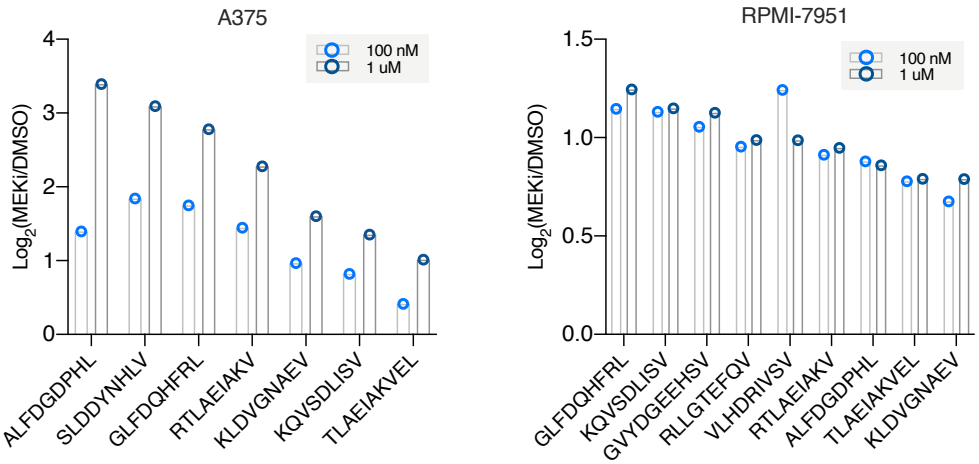

Figure 5-15*. A375/RPMI-7951 pMHC changes in Iso18 peptides. Mean fold change (n=3) in pMHC expression of Iso18 panel peptides in multiplexed, DDA analyses of cells treated with 100 nM or 1 μM binimetinib.*

We quantified 13 of the Iso18 peptides in A375 cells and 11 in RPMI cells (**Figure 5-16**, **Supplementary Figure 5-3,4**). The abundances again spanned a wide range: 6-1730 pMHCs-per-cell in RPMI-7951 cells and 5-8500 in A375 cells. Several of the least abundant endogenous peptides in A375 cells (derived from MAGEB2 and SLC45A2) were not detected in discovery analyses, again illustrating the sensitivity of SureQuant MHC in detecting low-abundance pMHCs with IS-PRM. The same trend was observed in RPMI-7951 cells: two of the three peptides present at levels below 1 fmol were not detected in discovery analyses. However, the remaining RPMI-7951 peptides were detected. Upon further investigation, RPMI-7951 cells had much lower absolute quantification values than A375 and SKMEL5 cells (maximum expression detected was ~1700 copies/cell in a MED23 peptide). Higher abundance peptides dominate discovery analyses, so in the case of RPMI-7951, where there were not really high abundant peptides present, discovery analyses were able to pick up more peptides of low abundance. Of note, neither cell line detected endogenous levels of any of the three

PMEL (gp100) peptides, suggesting the cells did not present pMHCs derived from PMEL at levels above ~1 copy-per-cell.

One peptide of particular interest was the PRUNE2 derived epitope, “ALFDGDPHL,” which showed the highest change in expression in A375 cells in discovery, TMT-labeled analyses (2.6x with 100 nM and 10.5x with 1 μM MEKi). In SureQuant MHC analysis, endogenous levels of this epitope were below the 1 fmol limit of detection (<80 copies/cell) and interpolated to be ~22 copies/cell. With 100 nM MEKi, endogenous levels were measured at ~1050 copies/cell, and ~8,500 copies/cell with 1μM MEKi, representing 46x and 377x increases in expression, respectively. If these data are accurate, it would suggest that the dynamic range limitations in multiplexed analyses of A375 cells is about 10-fold, therefore one would not be able to determine the true magnitude in expression change with discovery analyses.
This substantial change in expression is striking, and MEK inhibition of these cells could push this antigen into being able to be targeted by certain antibody-based therapies requiring higher expression. Utilizing SureQuant MHC can capture such dynamic changes, highlighting novel, therapy-induced targets for immunotherapy targeting.

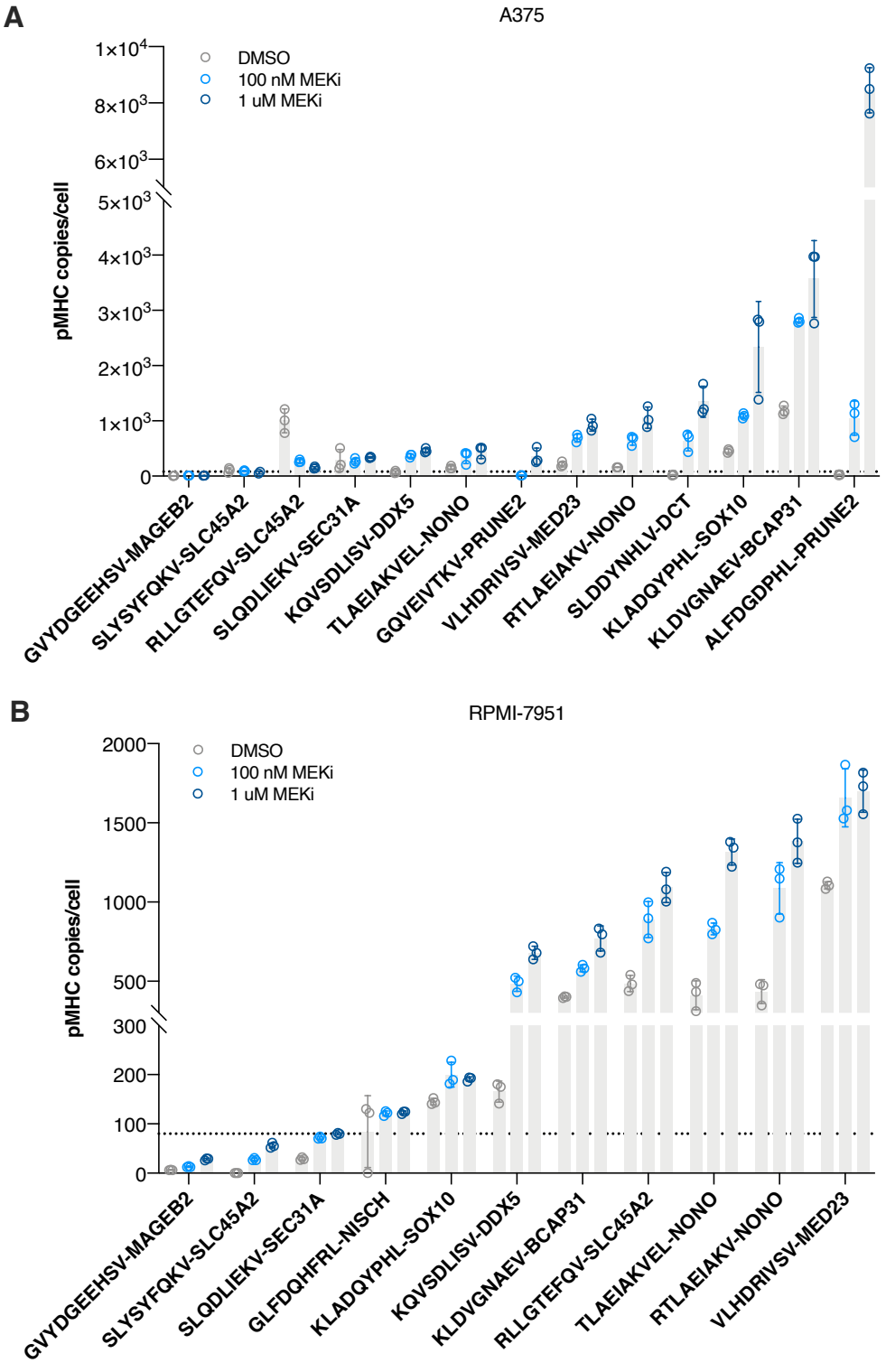

***Figure 5-16**. Absolute quantification in A375 and RPMI-791 cells. Copies-per-cell estimates of pMHCs in A375 (**A**) and RPMI-7951 (**B**) cells. Dotted line represents limit of quantitation (1 fmol).*

We quantified 13 of the Iso18 peptides in A375 cells and 11 in RPMI cells (**Figure 5-16**). The abundances again spanned a wide range: 6-1730 pMHCs-per-cell in RPMI-7951 cells and 5-8500 in A375 cells. Several of the least abundant endogenous peptides in A375 cells (derived from MAGEB2 and SLC45A2) were not detected in discovery analyses, again illustrating the sensitivity of SureQuant MHC in detecting low-abundance pMHCs with IS-PRM. The same trend was observed in RPMI-7951 cells: two of the three peptides present at levels below 1 fmol were not detected in discovery analyses. However, the remaining RPMI-7951 peptides were detected. Upon further investigation, RPMI-7951 cells had much lower absolute quantification values than A375 and SKMEL5 cells (maximum expression detected was ~1700 copies/cell in a MED23 peptide). Higher abundance peptides dominate discovery analyses, so in the case of RPMI-7951, where there were not really high abundant peptides present, discovery analyses were able to pick up more peptides of low abundance. Of note, neither cell line detected endogenous levels of any of the three PMEL (gp100) peptides, suggesting the cells did not present pMHCs derived from PMEL at levels above ~1 copy-per-cell.

One peptide of particular interest was the PRUNE2 derived epitope, “ALFDGDPHL,” which showed the highest change in expression in A375 cells in discovery, TMT-labeled analyses (2.6x with 100 nM and 10.5x with 1 μM MEKi). In SureQuant MHC analysis, endogenous levels of this epitope were below the 1 fmol limit of detection (<80 copies/cell) and interpolated to be ~22 copies/cell.

5-3-3 Iso18 quantitation in human tumors

To evaluate whether the absolute quantitation levels measured *in vitro* in human cell lines were comparable to levels present in patient tumors, we applied the SureQuant MHC Iso18 method to a human HLA-A2*01+ melanoma punch biopsy. The biopsy was homogenized,

and 5 mg of tumor lysate was used, equivalent to the protein quantity used in cell line experiments (**Figure 5-17**). 1-3H Iso18 hipMHCs were added to the lysate, followed by an immunoprecipitation & size exclusion filtration of endogenous and heavy isotope labeled pMHCs. The isolated peptides were then split and analyzed two ways: a SureQuant MHC targeted analysis for quantification of the Iso18 peptide panel, and a label-free discovery analysis to profile a larger portion of the immunopeptidome.

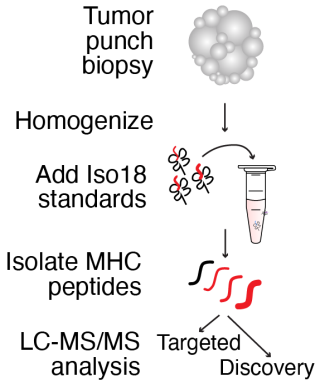

***Figure 5-17**. Experimental setup for SureQuant MHC and discovery analyses of human tumors.*

In a single injection comprised of just 25% of the peptide mixture, 5,039 unique pMHCs were identified which demonstrated the characteristic length distribution for class I MHCs (**Figure 5-18-A**). Of interest, 8 peptides in the Iso18 panel were identified, a majority of which were in the top 25% of peptide abundances (**Figure 5-18-B**). The two most abundant epitopes, ALFDGDPHL (PRUNE2) and RLLGTEFQV (SLC45A2), were also two of the most abundant in SKMEL5 cells. We investigated whether, similar to discovery analyses of melanoma cell lines, pMHCs derived from known tumor associate antigens (TAAs) exhibited significant enrichment among all pMHCs. pMHCs were rank ordered by precursor ion abundance, and we identified significant ($p<0.001$) TAA enrichment in highly abundant pMHCs (**Figure 5-18-C**). To verify this

result was not due to an overrepresentation of TAA-derived peptides in the dataset, we randomly scrambled the peptide's ranked order and performed the same analysis. The results were not significant (p=0.21), conforming that TAA-derived peptides are enriched among peptides of the highest abundances in this patient tumor sample.

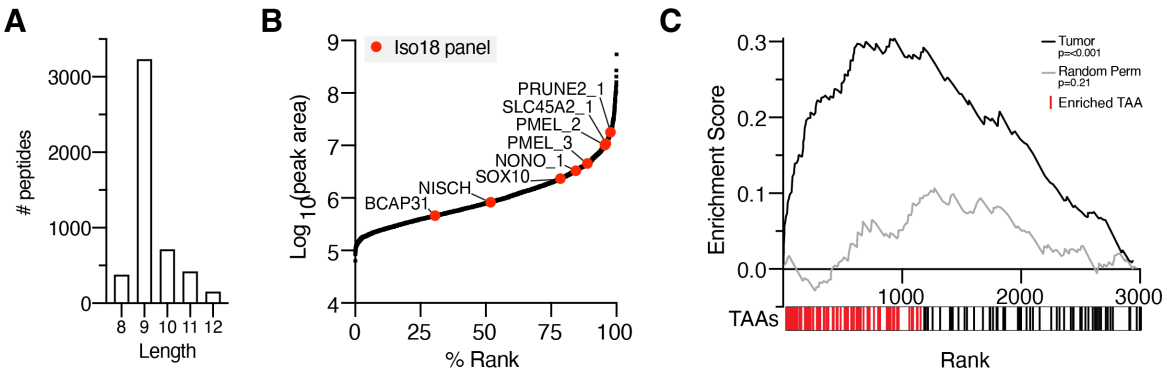

Figure 5-18. *Discovery data of tumor pMHC analysis.* ***A*** *Length distribution of tumor pMHCs.* ***B*** *Discovery pMHCs, rank ordered by integrated precursor ion peak area. Highlighted red nodes represent Iso18 panel peptides. PRUNE2_1 = ALFDGDPHL, SLC45A2_1 = RLLGTEFQV, PMEL_2 = ALDGGNKHFL, PMEL_3 = SLADTNSLAVV, NONO_1 = TLAEIAKVEL.* ***C*** *Enrichment plot for tumor associated antigen (TAA)-derived peptides within the discovery analysis, rank ordered by abundance. Enriched TAAs are shown in red, and a randomized analysis of the ranked list is shown in grey.*

We next performed the targeted SureQuant MHC analysis of the Iso18 panel. In line with the *in-vivo* analyses, summed abundances of transition areas roughly follow expected ratios (**Figure 5-19-A**). For RLLGTEFQV, the endogenous level falls within the standard curve, for a concentration of 16.7 fmol (**Figure 5-19-B**).

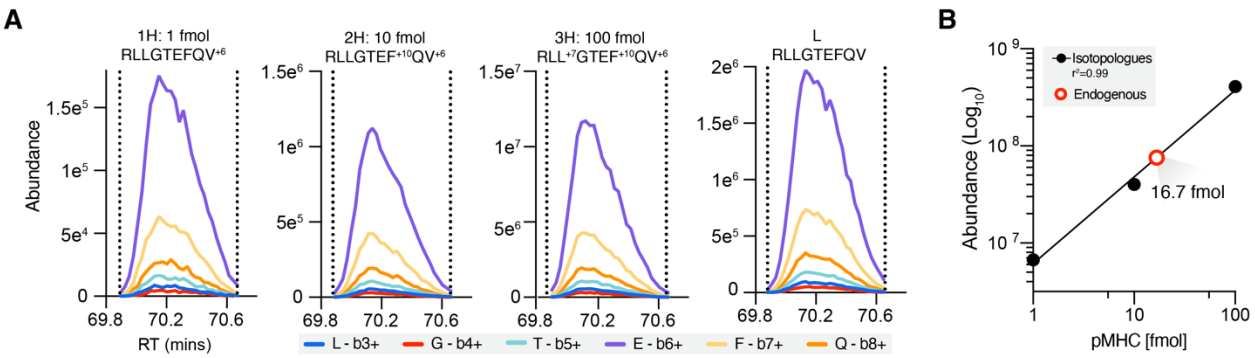

***Figure 5-19**. SLC45A2 absolute quantification in tumor sample. **A** Product ion traces for 1-3H and endogenous (L) SLC45A2-derived peptide, RLLGTEFQV. **B** Linear fit of summed intensities (r^2=0.994) of the 1-3H standards, and quantification of endogenous level from standard curve for RLLGTEFQV.*

As tumors represent a heterogenous composition of cell types including antigen presenting immune cells, it is challenging to accurately discern the number of tumor cells in each punch biopsy. Therefore, we elected to express the total amount of each peptide as a fraction of the bulk sample to enable comparison across patients and to SKMEL5 cells, which similarly utilized 5 mg cell lysate.

Between 2 and 17 pMHCs were quantifiable across tumors, with only 2 peptides identified across the entire tumor cohort (**Figure 5-20-A**). A comparison of pMHC concentrations both across and within tumors highlight the heterogeneity of antigen presentation. For example, the BCAP31 peptide ranged from 1-44 fmol across tumors, whereas both NONO-derived peptides were detected below 10 fmol in all instances. Perhaps most striking are the 8 peptides that were only identified in four or fewer tumors, particularly those derived from common TAAs like “SLADTNSLAVV”, a PMEL peptide identified in just 3 tumors. As all tumors were HLA-A2*01+, these data showcase the diversity of endogenous pMHC presentation among tumors even with a common allele. The inter-patient heterogeneity revealed by our analysis points to the need for targeted assays like SureQuant-IsoMHC to verify and quantify expression of antigens used in targeted immunotherapies which may serve to better stratify eligible patients and enhance personalized therapeutic approaches.

To assess the sensitivity of SureQuant-IsoMHC in clinical samples, we performed data dependent acquisition (DDA) on another aliquot of the isolated tumor peptides to determine whether the

Iso18 targets could have been identified in discovery-mode workflows (Dataset S4). While 8 Iso18 targets were identified in discovery mode in T1 (**Figure 5-20-B**), most tumors had between 0 and 2 Iso18 target identifications (**Figure 5-20-C**). Indeed, most peptides quantified below 1 fmol with SureQuant-IsoMHC were not identified in the discovery analyses (**Figure 5-20-B**), confirming the bias of DDA towards higher abundant epitopes. Moreover, T8, which used just 1.1 mg of tumor lysate input, had 0 Iso18 identifications with DDA and 7 with SureQuant-IsoMHC, highlighting the method's sensitivity in detecting and quantifying low-abundance epitopes.

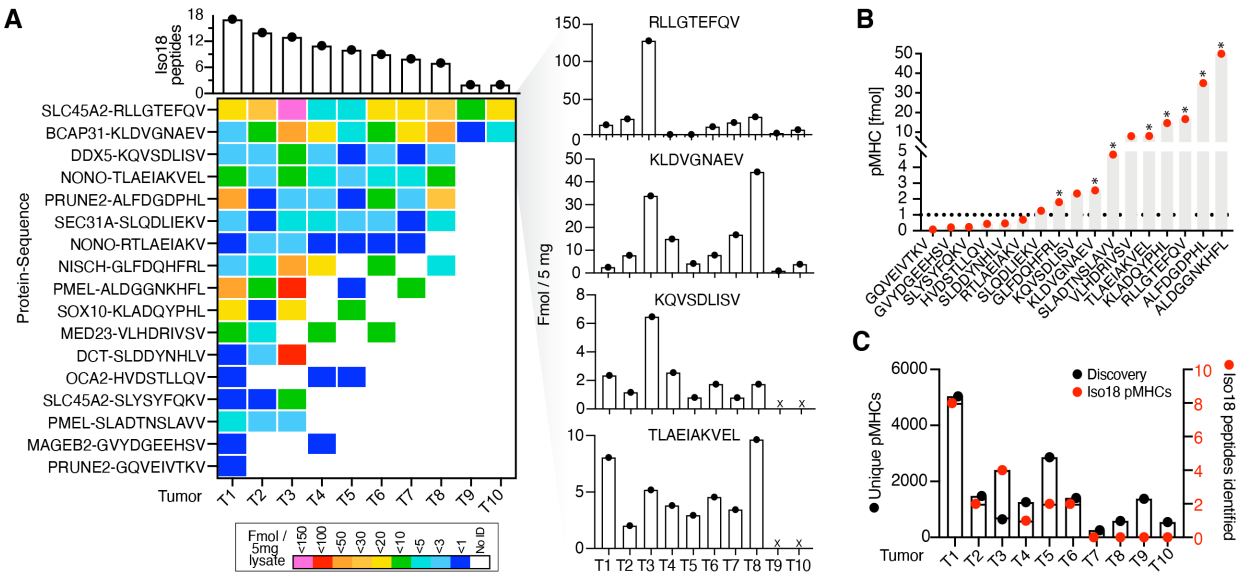

Figure 5-20. *SureQuant quantification in human tumors.* ***A*** *Peptide concentration per 5 mg lysate.* ***B*** *T1 Iso18 concentrations. Dotted line is lowest calibration point, *=pMHCs identified with DDA.* ***C*** *Number of unique peptides (left, black) and Iso18 panel peptides (right, red) identified with DDA.*

Of interest, tumor levels of the SLC45A2-derived peptide, RLLGTEFQV, are higher than A375 and RPMI-7951 levels (even with MEK treatment), but not nearly as high as the levels identified in SKMEL5 cells (**Figure 5-21**). Under the assumption that 5 mg of tumor lysate contains approximately the same number of cells as an *in vitro* sample, this amounts to ~1500 molecules/cell. Treatment with a MEK inhibitor may have increase expression several fold,

making it potentially targetable by antibody-based immunotherapies. The PRUNE2 derived peptide, ALFDGDPHL, has expression levels of similar to those seen in DMSO treated SKMEL5 cells, again suggesting that MEK inhibition may increase the expression to augment its ability to be targeted by immunotherapies requiring high expression.

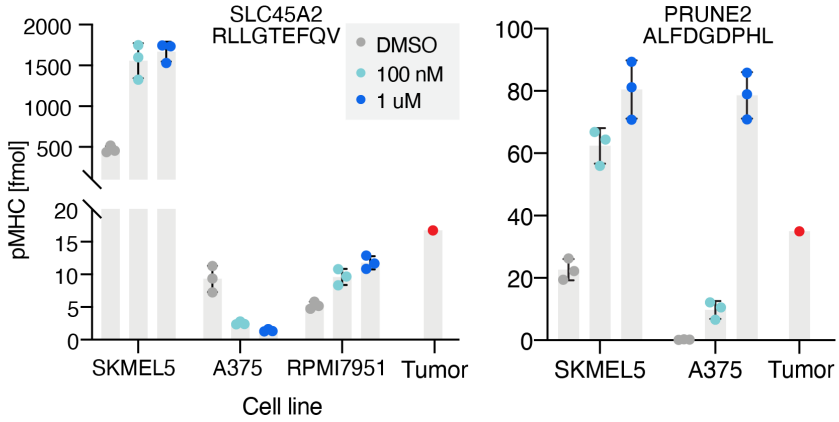

Figure 5-21. *Iso18 concentration estimates in tumor sample.* ***A*** *Iso18 pMHC concentrations in human tumor sample. Dotted notes the lower limit of quantitation at 1 fmol. *pMHCs identified in the discovery analysis.* ***B*** *Cell line and tumor concentrations of SLC45A2 and PRUNE2-derived peptides.*

5-4 Discussion

Accurate absolute quantification of endogenous pMHCs is critical for informing what type of targeted immunotherapy may be most effective. Furthermore, profiling how expression levels change with different perturbagens can identify treatment-modulated antigen targets whose expression levels can be selectively modulated for optimal therapeutic targeting. Previous estimates have relied on exogenous standards or pMHC-specific antibodies for quantitative estimates, both of which have limitations. To enable high sensitivity, reproducibility, and quantitative accuracy in measuring pMHC expression levels, we utilized a panel of 72 isotopologues, profiling 18 TAA pMHC targets that were previously identified in multiplexed discovery analyses as peptides modulated by MEK inhibitor treatment. Using IS-PRM, enabled by SureQuant acquisition, we utilized one isotopologue as a trigger peptide and the remaining three were incorporated into hipMHCs to generate an embedded standard curve for each analysis. Validation of this methodology demonstrated its robust sensitivity, quantifying pMHCs at 10 attomole concentration and application to *in vitro* and *in vivo* samples showcased successful targeting of lowly abundant endogenous pMHCs not identified in discovery analyses.

This work highlighted the broad range of expression levels between pMHCs within a single cell line and across cell lines. Furthermore, this data challenges the literature's reports of cell line expression of class I molecules being 500,000 copies/cell.[46,400] In SKMEL5 cells, a single pMHC (RLLGTEFQV) had untreated, endogenous expression levels of 40,000 copies/cell, representing 8% of the proposed immunopeptidome. MEK inhibition further increases expression levels to 150,000 copies/cell. While we did not find this peptide to be presented at as high of expression levels in the other analyzed samples, it does suggest that there is wide variability in cell expression levels, and perturbagens can greatly modulate total

and pMHC-specific expression. Characterization of pMHC expression across more targets and a wider cell line and *in-vivo* derived panel will further elucidate the upper and lower bounds of pMHC expression.

Generally, using IS- PRM is an effective approach for identifying lowly abundant pMHCs, and this general framework could be applied to identify predicted neoantigens or viral epitopes with high confidence. Other future uses of the isotopologue SureQuant-MHC approach may be to use absolute quantification estimates to better define thresholds of antigen presentation required for optimal targeted immunotherapy responses. For example, TAP-deficient T2 lymphoblast cells could be loaded with different concentrations of peptide, and SureQuant MHC could be applied to determine the number of molecules on average presented by each cell. This characterized range of expression could then be used it evaluate optimal pMHC presentation levels for various types of targeted immunotherapies, including bi-specific T cell engagers (BiTES), or antibody-drug conjugates (ADCs).

5-5 Materials & Methods

5-5-1 Cell culture

SKMEL5, A375, and RPMI-7951cell lines were obtained from ATCC [ATCC HTB-70, CRL-1619, and HTB-66, respectively] and maintained in DMEM medium (Corning supplemented with 10% FBS (Gibco) and 1% penicillin/streptomycin (Gibco). Cells were routinely tested for mycoplasma contamination, and maintained in 37 °C, 5% CO_2. Cultured cells were seeded in 10 cm plates, allowed to adhere overnight, and treated for 72h with binimetinib (Selleck Chemicals), or DMSO vehicle control. At the time of harvest, cells were washed with 1x PBS, and lifted using 0.05% Trypsin-EDTA (Gibco). Cells were pelleted at 500 g for 5 minutes, washed twice more in 1x PBS, and pelleted again. Cells were resuspended in 1 mL MHC lysis buffer [20 nM Tris-HCl pH 8.0, 150 mM NaCl, 0.2 mM PMSO, 1% CHAPS, and 1x HALT Protease/Phosphatase Inhibitor Cocktail (Thermo Scientific)], followed by brief sonication (3 x 10 second microtip sonicator pulses) to disrupt cell membranes. Lysate was cleared by centrifugation at 5000 g for 5 minutes and quantified using bicinchoninic acid (BCA) protein assay kit (Pierce).

5-5-2 Human Tumors

Frozen tumor punch biopsies were generously provided by Dr. Ryan Sullivan. Tumors were homogenized in 1 mL MHC lysis buffer, cleared by centrifugation (5000 g for 5 min at 4°C), and protein concentration was measured by BCA assay.

5-5-3 Peptide synthesis

Isotopologue peptides were purchased from Thermo Scientific Custom Peptide synthesis service. All synthetic peptides used in this study were produced as a PEPotec Custom

Peptide Libraries using FMOC solid-phase technology. Peptides were stored in either 1% DMSO for UV-mediated peptide exchange or 5% acetonitrile for peptides exogenously added. Heavy isotope labeled amino acids used for synthesis are listed in

Table 5-3, and labeled amino acids and mass shifts are listed in **Table 5-4**.

Peptides used for HLA-A2*01 binding affinity assay were were synthesized at the MIT Biopolymers and Proteomics Lab using standard Fmoc chemistry using an Intavis model MultiPep peptide synthesizer with HATU activation and 5 μmol chemistry cycles. Starting resin used was Fmoc-Amide Resin (Applied Biosystems). Cleavage from resin and simultaneous amino acid side chain deprotection was accomplished using: trifluoroacetic acid (81.5% v/v); phenol (5% v/v); water (5% v/v); thioanisole (5% v/v); 1,2-ethanedithiol (2.5% v/v); 1% triisopropylsilane for 1.5 hr. Standard Fmoc amino acids were procured from NovaBiochem.

Peptides were quality controlled by mass spectrometry and reverse phase chromatography using a Bruker MiroFlex MALDI-TOF and Agilent model 1100 HPLC system with a Vydac C18 column [300 angstrom, 5 micron, 2.1 x 150 mm] at 300 μL/min monitoring at 210 and 280 nm with a trifluoroacetic acid/ H_2O/MeCN mobile phase survey gradient.

5-5-4 Flow cytometry

T2 cells were seeded at a concentration of $1e^6$ cells/mL in round bottom plates, and media was supplemented with synthetic peptide standard at defined concentrations. Cells were incubated with peptide at 37 °C for 16-8 hours. Next, cells were harvested, washed 1x with ice cold PBS supplemented with 1% FBS and 0.1% sodium azide (flow buffer) and incubated with fluorophore-conjugated HLA-A2*01 specific antibody (BB7.2, Biolegend, cat # 343303) at 0.5 μg mL^{-1} in flow buffer for 30 minutes on ice. Cells were washed 1x with flow buffer and resuspended with propidium iodide. Analyses were performed on an LSRII (BD Biosciences) and data analyzed using FlowJo (version 10.6.2).

5-5-5 UV-mediated peptide exchange for hipMHCs

UV-mediated peptide exchange was performed using recombinant, biotinylated Flex-T HLA-A*02:01 monomers (BioLegend), using a modified version of the commercial protocol. Briefly, 2 µL of 500 µM peptide stock, 2 µL of Flex-T monomer, and 34 µL of 1X PBS were combined in a 96-well U bottom plate. On ice, plates were illuminated with ultraviolet light (365 nm) for 30 minutes, followed by a 30 minute incubation at 37 °C protected from light. Concentration of stable complexes following peptide exchange was quantified using the Flex-T HLA class I ELISA assay (Biolegend) per manufacturer's instructions for HLA-A*02:01. ELISA results were acquired using a Tecan plate reader Infinite 200 with Tecan icontrol version 1.7.1.12.

5-5-6 Peptide MHC isolation

Peptide MHCs were isolated from 5 mg of cell lysate (~5-7.5e^6 cells) per condition with immunoprecipitation (IP) and size exclusion filtration, as previously described.[188] Briefly, for each condition 0.25 mg of pan-specific anti-human MHC Class I (HLA-A, HLA-B, HLA-C) antibody (clone W6/32, Bio X Cell [cat # BE0079]) was bound to 20 µL FastFlow Protein A Sepharose bead slurry (GE Healthcare) for 3 hours rotating at 4 °C. Beads were washed 2x with IP buffer (20 nM Tris-HCl pH 8.0, 150 mM NaCl) prior to lysate and isotopologue hipMHC addition, and incubated rotating overnight at 4 °C to isolate pMHCs. Beads were washed with 1x TBS and water, and pMHCs were eluted in 10% formic acid for 20 minutes at room temperature (RT). Peptides were isolated from antibody and MHC molecules using a passivated 10K molecule weight cutoff filter (PALL Life Science), lyophilized, and stored at -80 °C. Prior to analysis, 250 fmol of each 4H trigger peptide was exogenously added to the peptide mixture, with the exception of GLFDQHFRL and AMLGTHTMEV, where 2.5 pmol was added due to poor intensity response.

5-5-7 Mass spectrometry data acquisition

For all SureQuant MHC analyses, samples were analyzed using an Orbitrap Exploris 480 mass spectrometer (Thermo Scientific) coupled with an UltiMate 3000 RSLC Nano LC system (Dionex), Nanospray Flex ion source (Thermo Scientific), and column oven heater (Sonation). The injection volume of pMHC sample was directly loaded onto a 10-15 cm analytical capillary chromatography column with an integrated electrospray tip (~1 µm orifice), prepared and packed in house (50 µm ID × 20 cm & 1.9 µM C18 beads, ReproSil-Pur).

Survey analyses

Peptides were eluted using a gradient with 6-25% buffer B (70% Acetonitrile, 0.1% formic acid) for 53 minutes, 25-45% for 12 minutes, 45-97% for 3 minutes, and 97% to 3% for 1 minute. Standard mass spectrometry parameters were as follows: spray voltage, 2.0 kV; no sheath or auxiliary gas flow; heated capillary temperature, 275 °C. The Exploris was operated in data dependent acquisition (DDA) mode with an inclusion list. Full scan mass spectra (300-1500 m/z, 120,000 resolution) were detected in the orbitrap analyzer after accumulation of $3e^6$ ions (normalized AGC target of 300%) or 50 ms. For every full scan, up to 20 ions were subsequently isolated if the m/z was within +/- 5 ppm of targets on the inclusion list (4H peptide precursor ions, Table 5-5) and reached a minimum intensity threshold of $1e^6$. Ions were collected with a maximum injection time of 10s, normalized AGC target = 1000%, and fragmented by higher energy collisional dissociation (HCD) with a collision energy (CE): 30%.

SureQuant MHC targeted analyses

The custom SureQuant acquisition template available in Thermo Orbitrap Exploris Series 2.0 was utilized for this method build. All the acquisition parameters for each series of isotopologues are located within a distinct 4-node branch stemming from a full scan node, therefore 18 branches are included in the method. MS1 scan parameters. In each branch, the peptide m/z and intensity thresholds are defined in the “Targeted Mass” filter node. Next, parameters for the low resolution, IS peptide MS^2 scan are defined, followed by the “Targeted Mass Trigger” filter node, which defines the 6 product ions used for pseudo-spectral matching. To connect each set of product ions within the targeted mass trigger node to a given precursor mass, we utilize the group ID feature to define the precursor m/z associated with each group of product ions is related to. Finally, along with the scan parameters for the four MS2 scans of the endogenous and 1-3H peptides, we define the isolation offset (m/z) within each node.

Standard mass spectrometry parameters for SureQuant acquisition are as follows: spray voltage: 1.6kV, no sheath or auxiliary gas flow, heated capillary temperature: 280°C. Full-scan mass spectra were collected with a scan range: 350-1200 m/z, AGC target value: 300% ($3e^6$), maximum IT: 50 ms, resolution: 120,000.

4H peptides matching the m/z (within 6 ppm) and exceeding the intensity threshold defined on the inclusion list were isolated [isolation window 1 m/z] and fragmented [nCE: 27%] by HCD with a scan range: 150-1700 m/z, maximum IT: 10 ms, AGC target value: 1000% ($1e^6$), resolution: 7,500. A product ion trigger filter next performs pseudo-spectral matching, only triggering an MS^2 event of the endogenous, target peptide at the defined mass offset if $n \geq 5$ product ions are detected from the defined list. If triggered, the subsequent light,1H, 2H, and 3H peptides MS^2 scans are initiated at the defined mass offsets, and scan parameters have the same CE, scan range, and AGC target as the heavy trigger peptide, with a higher maximum injection time and resolution (for example, max IT: 250 ms, resolution, 120,000). Triggered MS^2 scans are performed in the following order: Light, 1H, 2H, and 3H.

Discovery tumor analyses

Standard mass spectrometry parameters were as follows: spray voltage, 2.0 kV; no sheath or auxiliary gas flow; heated capillary temperature, 275 °C. The Exploris was operated in data dependent acquisition (DDA) mode. Peptides were eluted using a gradient with 6-25% buffer B (70% Acetonitrile, 0.1% formic acid) for 75 minutes, 25-45% for 5 minutes, 45-100% for 5 minutes, hold for 1 minutes, and 100% to 3% for 2 minutes.

Full scan mass spectra (350-1200 m/z, 60,000 resolution) were detected in the orbitrap analyzer after accumulation of $3e^6$ ions (normalized AGC target of 300%) or 25 ms. For every full scan, MS^2 were collected during a 3 second cycle time. Ions were isolated (0.4 m/z isolation width) for a maximum of 150 ms or 75% AGC target, and fragmented by HCD with 30% CE at a resolution of 45,000. Charge states < 2 and > 4 were excluded, and precursors were excluded from selection for 30 seconds if fragmented n=2 times within 20 second window.

5-5-8 SureQuant MHC data analysis

Peak area ratios of the endogenous light peptides and corresponding 1-3H isotopologue internal standards for the 6 selected product ions were exported from Skyline (version 20.2.1.28).[139] Transition areas were summed for all ions that that were quantifiable across L and 1-3H peptides. 1-3H peptides were used to generate a standard curve with a linear fit, from which endogenous pMHC concentrations were calculated.

5-6 Acknowledgements

We thank Aaron Gajadhar, Bhavin Patel, and Sebastien Gallien, and Andreas Huhmer from Thermo Fisher Scientific for providing project and methodological guidance, along with

financial support, and Eric Berg from 21st Century Biochemicals for the peptide synthesis and validation.

5-7 Supplementary Figures

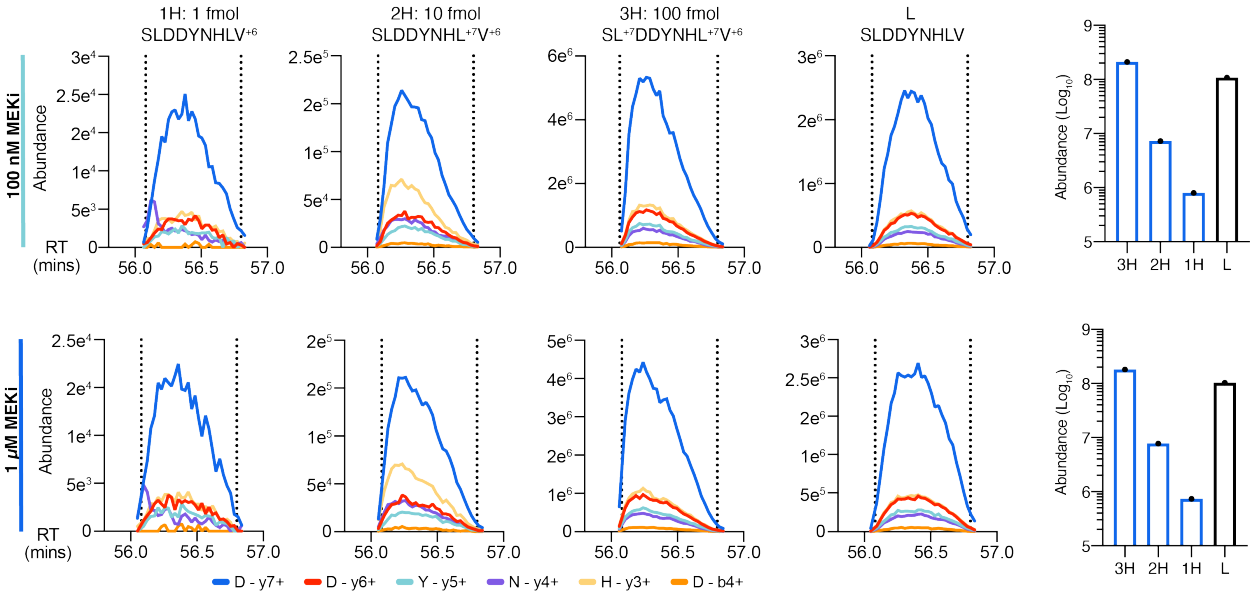

Supplementary Figure 5-1*. Transitions for 1-3H and L peptides for 100 nM (top) and 1 uM MEKi treated SKMEL5 cells (left). Summed product ion abundances for each peptide (right).*

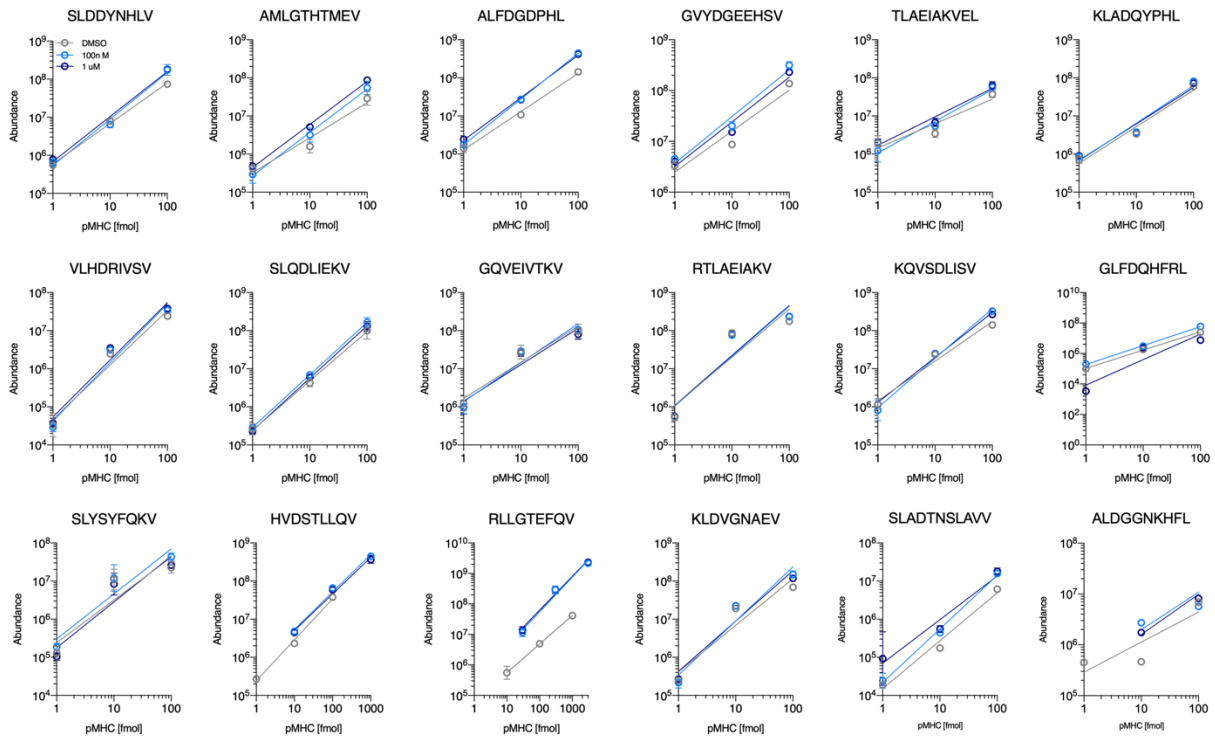

Supplementary Figure 5-2. *Standard curves with linear fit for each Iso18 peptide/treatment condition in SKMEL5 cells. Error bars represent standard deviation.*

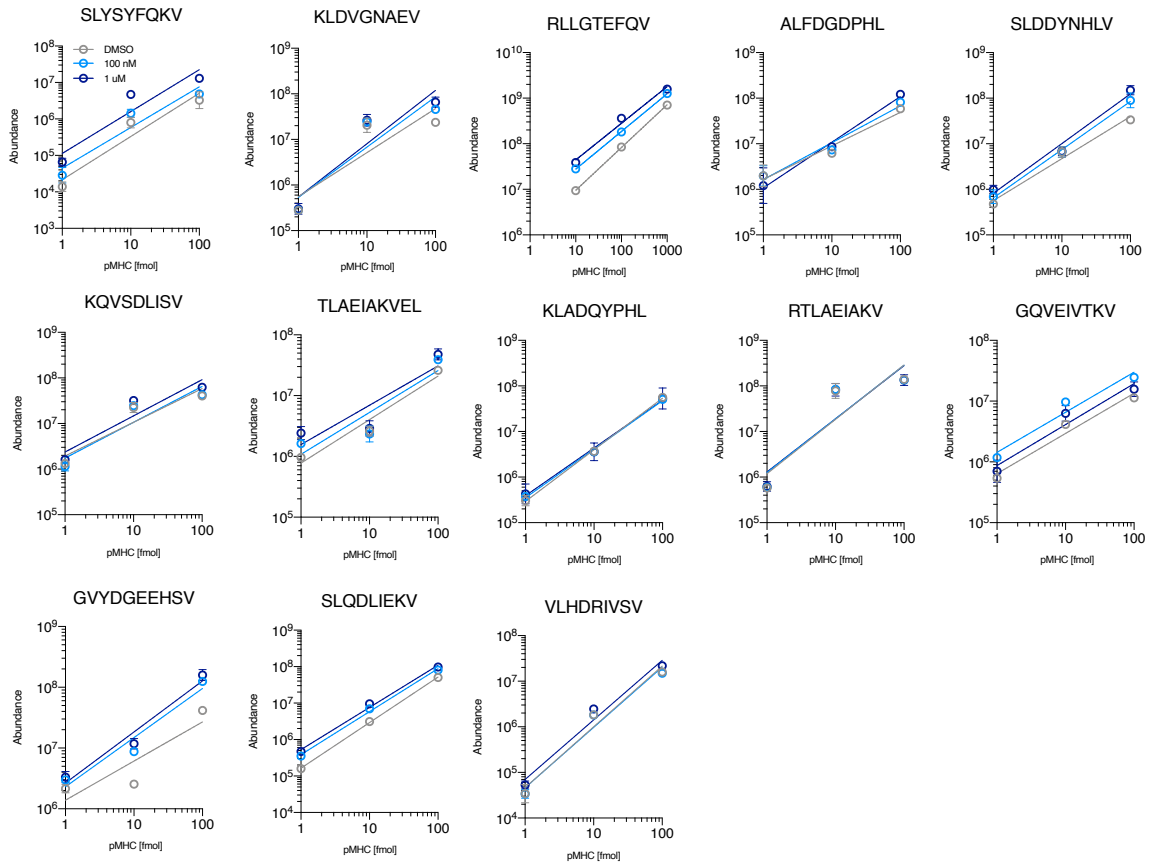

Supplementary Figure 5-3. *Standard curves with linear fit for each Iso18 peptide/treatment condition in A375 cells. Error bars represent standard deviation.*

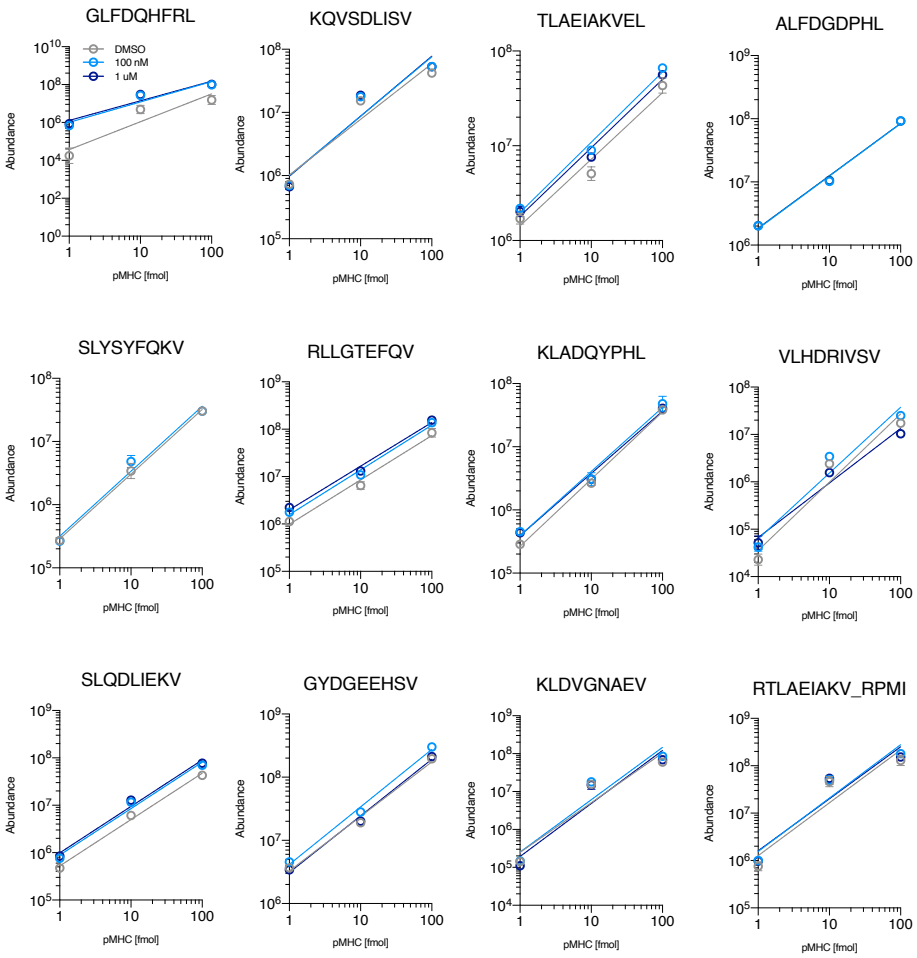

Supplementary Figure 5-4*. Standard curves with linear fit for each Iso18 peptide/treatment condition in RPMI-7951 cells. Error bars represent standard deviation.*

5-8 Tables

***Table 5-1**. HLA-A2*01 peptides synthesized for T2 binding analysis. Yield is in in mg, as measured by the biopolymers core facility.*

Peptide ID	Sequence	N-term	Well	Yield
PMEL1	ALDGGNKHFL-COOH	""NH2"	D2	5.2
DCT	SLDDYNHLV-COOH	""NH2"	D3	3.1
DDX5	KQVSDLISV-COOH	""NH2"	D4	3.1
NISCH	GLFDQHFRL-COOH	""NH2"	D5	4.6
SOX10	KLADQYPHL-COOH	""NH2"	D6	5.8
PMEL2	KTWGQYWQV-COOH	""NH2"	D7	4
VIM	KLLEGEESRISL-COOH	""NH2"	D8	6.5
HNRNPL	GLIDGVVEA-COOH	""NH2"	D9	1.7
NONO1	RTLAEIAKV-COOH	""NH2"	D10	3.9
SEC31A	SLQDLIEKV-COOH	""NH2"	D11	1.9
NONO2	TLAEIAKVEL-COOH	""NH2"	D12	1.9
BCAP31	KLDVGNAEV-COOH	""NH2"	E1	3.6
RPL10A	FLASESLIKQI-COOH	""NH2"	E2	3.3
IMP3	ALLDKLYAL-COOH	""NH2"	E3	2.4
KTN1	VLAEELHKV-COOH	""NH2"	E4	3.3
OCA2	HVDSTLLQV-COOH	""NH2"	E5	2.1
IRS2phospho	RVAS(pS)PTSGVK-COOH	""NH2"	E6	3.1
IRS2	RVASPTSGVK-COOH	""NH2"	E7	3.2
PRUNE2_1	ALFDGDPHL-COOH	""NH2"	E8	3.6
PCNA	ALKDLINEA-COOH	""NH2"	E9	3.5
TCF12	RLDDAIHVL-COOH	""NH2"	E10	3.4
HNRNPC	SLLENLEKI-COOH	""NH2"	E11	2.1
SNRNP200	GLIEIISNA-COOH	""NH2"	E12	1.3
INF2	ALDTSNVMV-COOH	""NH2"	F1	2.1
SLC45A2	SLYSYFQKV-COOH	""NH2"	F2	4.1
NUP98	ALWGHLKEL-COOH	""NH2"	F3	3.8
CAPRIN1	SLLDEFYKL-COOH	""NH2"	F4	2.6
COPG1	AIVDKVPSV-COOH	""NH2"	F5	2.1
FAM126A	ALDDIIYRA-COOH	""NH2"	F6	2.9
PRUNE2_2	GQVEIVTKV-COOH	""NH2"	F7	2.1
TPR	KIIDIQEKV-COOH	""NH2"	F8	3.2
S100A11	GQLDFSEFL-COOH	""NH2"	F9	2.8
ASB6	SLAEKIQAL-COOH	""NH2"	F10	2.1
PI4KB	KLYDGFQYL-COOH	""NH2"	F11	5.7
ITGAV	KLQEVGQVSV-COOH	""NH2"	F12	4.1
FLNA	ALAGDQPSV-COOH	""NH2"	G1	1.6
DST	FIWENIHTL-COOH	""NH2"	G2	3.3
DAB2	ILDDQTNKL-COOH	""NH2"	G3	2.2
CD59	SLSEKTVLL-COOH	""NH2"	G4	1.4

Table 5-1 continued.

EIF3F	ALNEKLVNL-COOH	""NH2"	G5	2.8
MED23	VLHDRIVSV-COOH	""NH2"	G6	3.8
CCT6A	ALSKEGIVAL-COOH	""NH2"	G7	2.6
CAD	GLADKVYFL-COOH	""NH2"	G8	2.1
COPA	KLNDLIQRL-COOH	""NH2"	G9	3.2
GNAS	ALWEDEGVRA-COOH	""NH2"	G10	3.2
DHX9	KVFDPVPVGV-COOH	""NH2"	G11	3.4
MYL6	KVLDFEHFL-COOH	""NH2"	G12	1.8
MYO5A	SLQEEIAKL-COOH	""NH2"	H1	2
RETSAT	SLAEVLQQL-COOH	""NH2"	H2	2.1
RIF1	KLISELQKL-COOH	""NH2"	H3	2
WDR19	ALFEGKVQL-COOH	""NH2"	H4	1.6
FluPosCtrl	GILGFVFTL-COOH	""NH2"	H5	<1
MLANAlowCtrl	AAGIGILTV-COOH	""NH2"	H6	1.7

***Table 5-2**. Iso18 peptide panel and predicted pMHC binding affinities to HLA-A2*01.*

Gene	Peptide	Length	Predicted affinity [nM]
PMEL1	ALDGGNKHFL	10	243.8
DCT	SLDDYNHLV	9	3.9
DDX5	KQVSDLISV	9	19.7
NISCH	GLFDQHFRL	9	4.7
NONO	TLAEIAKVEL	10	66.3
OCA2	HVDSTLLQV	9	479.1
PRUNE2	ALFDGDPHL	9	6.4
SLC45A2	SLYSYFQKV	9	5.1
SLC45A2	RLLGTEFQV	9	9.8
SOX10	KLADQYPHL	9	7.2
NONO	RTLAEIAKV	9	218.2
BCAP31	KLDVGNAEV	9	22.6
PRUNE2	GQVEIVTKV	9	66.9
MAGEB2	GVYDGEEHSV	10	386.5
PMEL	SLADTNSLAVV	11	86.7
PMEL	AMLGTHTMEV	9	13.9
SEC31A	SLQDLIEKV	9	12.7
MED23	VLHDRIVSV	9	7.4

Table 5-3. *Heavy isotope labeled amino acids used for synthesis.*

Amino acid (s)	Modification	Mass offset
I	13C6, 15N1	7.017
L	13C6, 15N1	7.017
F	13C9, 15N1	10.027
Y	13C9, 15N1	10.027
K	13C6, 15N2	8.014
V	13C3, 15N1	4.007
A	13C3, 15N1	4.007
G	13C2, 15N1	3.004
R	13C6, 15N4	10.008
P	13C5, 15N1	6.014

Table 5-4. *Isotopologue m/z and mass offsets for triggering.*

Peptide Name	Sequence	MW	Mass shift	Heavy Amino acid	MW	Mass Offset	m/z offset
Charge						3	
Endogenous						32.076	-10.692
Peptide 1 - 1H	ALDGGNKHF(L)	1077.567	+7	L: 13C6, 15N1	539.284	25.059	-8.353
Peptide 1 -2H	ALDGGNKH(F)(L)	1087.595	+17	F: 13C9, 15N1	544.297	15.031	-5.010
Peptide 1 - 3H	ALDGGN(K)H(F)(L)	1095.609	+25	K: 13C6, 15N2	548.304	7.017	-2.339
Peptide 1 - 4H	A(L)DGGN(K)H(F)(L)	1102.626	+32	L: 13C6, 15N1	551.813		
Charge						3	
Endogenous						28.069	14.034
Peptide 2 - 1H	SLDDYNHL(V)	1080.511	+6	V: 13C3, 15N1	540.756	24.062	12.031
Peptide 2 -2H	SLDDYNH(L)(V)	1087.529	+13	L: 13C6, 15N1	544.264	17.044	8.522
Peptide 2 - 3H	S(L)DDYNH(L)(V)	1094.546	+20	L: 13C6, 15N1	547.773	10.027	5.014
Peptide 2 - 4H	S(L)DD(Y)NH(L)(V)	1104.545	+30	Y: 13C9, 15N1	552.773		
Charge						2	
Endogenous						23.046	11.523
Peptide 3 - 1H	KQVSDLIS(V)	993.573	+6	V: 13C3, 15N1	497.287	19.038	9.519
Peptide 3 -2H	KQVSD(L)IS(V)	1000.590	+13	L: 13C6, 15N1	500.795	12.021	6.011
Peptide 3 - 3H	KQ(V)SD(L)IS(V)	1006.604	+19	V: 13C3, 15N1	503.802	8.014	4.007
Peptide 3 - 4H	(K)Q(V)SD(L)IS(V)	1014.618	+27	K: 13C6, 15N2	507.809		
Charge						2	
Endogenous						37.080	12.360
Peptide 4 - 1H	GLFDQHFR(L)	1138.599	+7	L: 13C6, 15N1	569.800	30.063	10.021
Peptide 4 -2H	GLFDQHF(R)(L)	1148.607	+17	R: 13C6, 15N4	574.804	20.054	6.685
Peptide 4 - 3H	GLFDQH(F)(R)(L)	1158.635	+27	F: 13C9, 15N1	579.817	10.027	3.342
Peptide 4 - 4H	GL(F)DQH(F)(R)(L)	1168.662	+37	F: 13C9, 15N1	584.831		
Charge						2	
Endogenous						26.056	13.028
Peptide 6 - 1H	TLAEIAKVE(L)	1092.650	+7	L: 13C6, 15N1	546.825	19.038	9.519
Peptide 6 -2H	TLAEIAK(V)E(L)	1098.664	+13	V: 13C3, 15N1	549.832	15.031	7.516
Peptide 6 - 3H	TLAEIA(K)(V)E(L)	1106.678	+21	K: 13C6, 15N2	553.839	7.017	3.509
Peptide 6 - 4H	TLAE(I)A(K)(V)E(L)	1113.695	+28	I: 13C6, 15N1	557.347		
Charge						2	
Endogenous						22.049	11.024
Peptide 7 - 1H	HVDSTLLQ(V)	1016.553	+6	V: 13C3, 15N1	508.776	18.041	9.021
Peptide 7 -2H	HVDSTL(L)Q(V)	1023.570	+13	L: 13C6, 15N1	512.285	11.024	5.512
Peptide 7 - 3H	HVDST(L)(L)Q(V)	1030.587	+20	L: 13C6, 15N1	515.794	4.007	2.004
Peptide 7 - 4H	H(V)DST(L)(L)Q(V)	1036.601	+26	V: 13C3, 15N1	518.800		

Table 5-4 continued

Peptide Name	Sequence	MW	Mass shift	Heavy Amino acid	m/z	Mass Offset	m/z offset
Charge						2	
Endogenous						30.075	15.038
Peptide 8 - 1H	ALFDGDPH(L)	990.488	+7	L: 13C6, 15N1	495.744	23.058	11.529
Peptide 8 -2H	ALFDGD(P)H(L)	996.502	+13	P: 13C5, 15N1	498.751	17.044	8.522
Peptide 8 - 3H	AL(F)DGD(P)H(L)	1006.529	+23	F: 13C9, 15N1	503.764	7.017	3.509
Peptide 8 - 4H	A(L)(F)DGD(P)H(L)	1013.546	+30	L: 13C6, 15N1	507.273		
Charge						2	
Endogenous						29.066	14.533
Peptide 9 - 1H	SLYSYFQK(V)	1139.589	+6	V: 13C3, 15N1	570.294	25.059	12.529
Peptide 9 -2H	SLYSYFQ(K)(V)	1147.603	+14	K: 13C6, 15N2	574.302	17.044	8.522
Peptide 9 - 3H	SLYSY(F)Q(K)(V)	1157.630	+24	F: 13C9, 15N1	579.315	7.017	3.509
Peptide 9 - 4H	S(L)YSY(F)Q(K)(V)	1164.648	+31	L: 13C6, 15N1	582.824		
Charge						2	
Endogenous						28.069	14.034
Peptide 10 - 1H	RLLGTEFQ(V)	1067.600	+6	V: 13C3, 15N1	534.300	24.062	12.031
Peptide 10 -2H	RLLGTE(F)Q(V)	1077.627	+16	F: 13C9, 15N1	539.314	14.034	7.017
Peptide 10 - 3H	RL(L)GTE(F)Q(V)	1084.644	+23	L: 13C6, 15N1	542.822	7.017	3.509
Peptide 10 - 4H	R(L)(L)GTE(F)Q(V)	1091.662	+30	L: 13C6, 15N1	546.331		
Charge						2	
Endogenous						28.062	14.031
Peptide 11 - 1H	KLADQYPH(L)	1090.588	+7	L: 13C6, 15N1	545.794	21.045	10.523
Peptide 11 -2H	KLADQY(P)H(L)	1096.602	+13	P: 13C5, 15N1	548.801	15.031	7.516
Peptide 11 - 3H	K(L)ADQY(P)H(L)	1103.619	+20	L: 13C6, 15N1	552.309	8.014	4.007
Peptide 11 - 4H	(K)(L)ADQY(P)H(L)	1111.633	+28	K: 13C6, 15N2	556.317		
Charge						2	
Endogenous						29.047	14.523
Peptide 12 - 1H	RTLAEIAK(V)	1005.621	+6	V: 13C3, 15N1	503.310	25.040	12.520
Peptide 12 -2H	RTLAEIA(K)(V)	1013.635	+14	K: 13C6, 15N2	507.318	17.025	8.513
Peptide 12 - 3H	RT(L)AEIA(K)(V)	1020.652	+21	L: 13C6, 15N1	510.826	10.008	5.004
Peptide 12 - 4H	(R)T(L)AEIA(K)(V)	1030.661	+31	R: 13C6, 15N4	515.830		
Charge						2	
Endogenous						23.046	11.523
Peptide 13 - 1H	KLDVGNAE(V)	949.511	+6	V: 13C3, 15N1	475.255	19.038	9.519
Peptide 13 -2H	KLD(V)GNAE(V)	955.524	+12	V: 13C3, 15N1	478.262	15.031	7.516
Peptide 13 - 3H	K(L)D(V)GNAE(V)	962.542	+19	L: 13C6, 15N1	481.771	8.014	4.007
Peptide 13 - 4H	(K)(L)D(V)GNAE(V)	970.556	+27	K: 13C6, 15N2	485.778		

Table 5-4 continued

Peptide Name	Sequence	MW	Mass shift	Heavy Amino acid	m/z	Mass Offset	m/z offset
Charge						2	
Endogenous						23.046	11.523
Peptide 14 - 1H	GQVEIVTK(V)	977.578	+6	V: 13C3, 15N1	489.289	19.038	9.519
Peptide 14 -2H	GQVEIVT(K)(V)	985.593	+14	K: 13C6, 15N2	493.296	11.024	5.512
Peptide 14 - 3H	GQVEI(V)T(K)(V)	991.606	+20	V: 13C3, 15N1	496.303	7.017	3.509
Peptide 14 - 4H	GQVE(I)(V)T(K)(V)	998.624	+27	I: 13C6, 15N1	499.812		
Charge						2	
Endogenous						21.045	10.523
Peptide 15 - 1H	GVYDGEEHS(V)	1096.470	+6	V: 13C3, 15N1	548.735	17.038	8.519
Peptide 15 -2H	(G)VYD(G)EEHS(V)	1102.477	+12	G: 13C2, 15N1	551.739	14.034	7.017
Peptide 15 - 3H	(G)(V)YD(G)EEHS(V)	1108.491	+18	V: 13C3, 15N1	554.746	10.027	5.014
Peptide 15 - 4H	(G)(V)(Y)D(G)EEHS(V)	1118.491	+28	Y: 13C9, 15N1	559.745		
Charge						2	
Endogenous						22.049	11.024
Peptide 16 - 1H	SLADTNSLAV(V)	1094.585	+6	V: 13C3, 15N1	547.792	18.041	9.021
Peptide 16 -2H	SLADTNSLA(V)(V)	1100.598	+12	V: 13C3, 15N1	550.799	14.034	7.017
Peptide 16 - 3H	SLADTNS(L)A(V)(V)	1107.615	+19	L: 13C6, 15N1	554.308	7.017	3.509
Peptide 16 - 4H	S(L)ADTNS(L)A(V)(V)	1114.633	+26	L: 13C6, 15N1	557.816		
Charge						2	
Endogenous						21.045	10.523
Peptide 17 - 1H	AMLGTHTME(V)	1094.513	+6	V: 13C3, 15N1	547.756	17.038	8.519
Peptide 17 -2H	AM(L)GTHTME(V)	1101.530	+13	L: 13C6, 15N1	551.265	10.021	5.010
Peptide 17 - 3H	(A)M(L)GTHTME(V)	1105.537	+17	A: 13C3, 15N1	553.268	6.014	3.007
Peptide 17 - 4H	(A)M(L)GTHT(M)E(V)	1111.490	+23	M: 13C5, 15N1	556.245		
Charge						2	
Endogenous						26.056	13.028
Peptide 18 - 1H	SLQDLIEK(V)	1049.599	+6	V: 13C3, 15N1	525.300	22.049	11.024
Peptide 18 -2H	SLQDLIE(K)(V)	1057.614	+14	K: 13C6, 15N2	529.307	14.034	7.017
Peptide 18 - 3H	SLQD(L)IE(K)(V)	1064.631	+21	L: 13C6, 15N1	532.815	7.017	3.509
Peptide 18 - 4H	SLQD(L)(I)E(K)(V)	1071.648	+28	I: 13C6, 15N1	536.324		
Charge						3	
Endogenous						22.030	7.343
Peptide 20 - 1H	VLHDRIVS(V)	1042.616	+6	V: 13C3, 15N1	521.808	18.022	6.007
Peptide 20 -2H	VLHDRI(V)S(V)	1048.630	+12	V: 13C3, 15N1	524.815	14.015	4.672
Peptide 20 - 3H	VLHD(R)I(V)S(V)	1058.638	+22	R: 13C6, 15N4	529.819	4.007	1.336
Peptide 20 - 4H	(V)LHD(R)I(V)S(V)	1064.652	+28	V: 13C3, 15N1	532.826		

Table 5-5. *Targeted mass and product ions for SureQuant MHC method build. Group IDs are the precursor mass for each target.*

Modified Sequence	m/z	Charge	Ion
AL[+7]DGGNK[+8]HF[+10]L[+7]	368.549	3	precursor
	797.469	1	y7
	569.383	1	y4
	433.274	1	y3
	456.751	2	y8
	399.238	2	y7
	370.727	2	y6
SL[+7]DDY[+10]NHL[+7]V[+6]	553.294	2	precursor
	898.448	1	y7
	783.421	1	y6
	668.394	1	y5
	495.303	1	y4
	381.260	1	y3
	438.194	1	b4
K[+8]QV[+6]SDL[+7]ISV[+6]	508.317	2	precursor
	370.257	1	b3
	457.289	1	b4
	572.316	1	b5
	692.417	1	b6
	805.502	1	b7
	892.534	1	b8
GLF[+10]DQHF[+10]R[+10]L[+7]	390.561	3	precursor
	842.469	1	y6
	727.442	1	y5
	599.383	1	y4
	462.324	1	y3
	500.286	2	y7
	421.738	2	y6
TLAEI[+7]AK[+8]V[+6]EL[+7]	557.855	2	precursor
	900.571	1	y8
	829.534	1	y7
	700.491	1	y6
	580.390	1	y5
	509.353	1	y4
	373.244	1	y3
HV[+6]DSTL[+7]L[+7]QV[+6]	519.308	2	precursor
	358.175	1	b3
	445.207	1	b4
	546.255	1	b5
	666.356	1	b6
	786.458	1	b7
	914.516	1	b8

Table 5-5 continued

Modified Sequence	m/z	Charge	Ion
AL[+7]F[+10]DGDP[+6]HL[+7]	507.781	2	precursor
	943.517	1	y8
	823.416	1	y7
	666.320	1	y6
	551.293	1	y5
	494.271	1	y4
	379.245	1	y3
SL[+7]YSYF[+10]QK[+8]V[+6]	583.331	2	precursor
	958.522	1	y7
	795.459	1	y6
	708.427	1	y5
	545.363	1	y4
	388.268	1	y3
	458.236	1	b4
RL[+7]L[+7]GTEF[+10]QV[+6]	546.838	2	precursor
	397.311	1	b3
	454.332	1	b4
	555.380	1	b5
	684.423	1	b6
	841.518	1	b7
	969.577	1	b8
K[+8]L[+7]ADQYP[+6]HL[+7]	556.824	2	precursor
	976.532	1	y8
	856.431	1	y7
	785.393	1	y6
	542.308	1	y4
	379.245	1	y3
	734.404	1	b6
R[+10]TL[+7]AEIAK[+8]V[+6]	516.338	2	precursor
	388.266	1	b3
	459.303	1	b4
	588.345	1	b5
	701.429	1	b6
	772.466	1	b7
	908.576	1	b8
K[+8]L[+7]DV[+6]GNAEV[+6]	486.285	2	precursor
	372.245	1	b3
	477.327	1	b4
	534.348	1	b5
	648.391	1	b6
	719.428	1	b7
	848.471	1	b8

Table 5-5 continued.

Modified Sequence	m/z	Charge	Ion
GQVEI[+7]V[+6]TK[+8]V[+6]	500.319	2	precursor
	814.551	1	y7
	715.483	1	y6
	586.440	1	y5
	466.339	1	y4
	361.257	1	y3
	414.198	1	b4
G[+3]V[+6]Y[+10]DG[+3]EEHSV[+6]	560.267	2	precursor
	954.419	1	y8
	781.328	1	y7
	666.301	1	y6
	606.276	1	y5
	477.234	1	y4
	477.713	2	y8
SL[+7]ADTNSL[+7]AV[+6]V[+6]	558.324	2	precursor
	394.205	1	b4
	495.252	1	b5
	609.295	1	b6
	696.327	1	b7
	816.428	1	b8
	496.778	2	b10
A[+4]ML[+7]GTHTM[+6]EV[+6]	556.783	2	precursor
	906.474	1	y8
	786.373	1	y7
	729.351	1	y6
	628.304	1	y5
	622.321	1	b6
	723.369	1	b7
SLQDL[+7]I[+7]EK[+8]V[+6]	536.832	2	precursor
	872.540	1	y7
	744.481	1	y6
	629.454	1	y5
	509.353	1	y4
	389.252	1	y3
	444.209	1	b4
V[+6]LHDR[+10]IV[+6]SV[+6]	355.891	3	precursor
	424.250	2	y7
	356.232	1	b3
	637.369	1	b5
	750.453	1	b6
	375.730	2	b6
	428.271	2	b7

***Table 5-6**. Quantifiable transitions in 10 attomol 1H hipMHC experiment.*

Peptide	# of quantifiable transitions	Area
ALDGGNKHFL	6	1.49E+05
ALFDGDPHL	5	1.37E+06
AMLGTHTMEV	6	3.81E+04
GLFDQHFRL	6	2.13E+05
GQVEIVTKV	6	2.52E+06
GVYDGEEHSV	6	1.27E+05
HVDSTLLQV	6	1.90E+05
KLADQYPHL	6	9.31E+05
KLDVGNAEV	4	6.09E+05
KQVSDLISV	6	5.50E+06
RLLGTEFQV	6	1.12E+05
RTLAEIAKV	6	2.01E+07
SLADTNSLAVV	5	6.79E+04
SLDDYNHLV	6	2.15E+06
SLQDLIEKV	6	8.82E+04
SLYSYFQKV	6	1.71E+06
TLAEIAKVEL	6	1.79E+04
VLHDRIVSV	6	1.56E+07

CHAPTER 6: Selective antibody-based targeting of MEK inhibitor modulated peptide MHCs

6-1 Introduction

Antibody-based therapies have shown remarkable clinical success as cancer therapies over the past several decades due to their high target specificity, and more antibody (Ab) therapies continue to move through clinical development.[401] After binding to their target antigen through their variable fragment antigen-binding (Fab) regions, Abs can mediate Anti-tumor effects through a variety of different mechanisms. These include direct binding to receptors or ligands to block receptor activation and/or downstream signaling (ex. Herceptin, anti-HER2 Ab), complement or antibody dependent cellular cytotoxicity (CDC or ADCC) (ex. rituximab, anti-CD20 Ab), immune cell activation and recruitment (ex. Keytruda, anti-PD1), or toxicity from antibody-drug conjugate (ADC)-mediated toxin delivery (Kadcyla, anti-HER2 ADC). The major clinical advantage of therapeutic antibodies is that they can target antigens that are expressed at higher levels on tumor cells than non-tumor cells, however key limitations are that only surface antigens can be targeted, and if differential expression between tumor/healthy cells is not significant, antibodies can induce toxicity in healthy cells. [402]

Targeting peptide MHCs that present tumor associated antigens on the cell surface is an attractive application of antibody-based therapies, as non-tumor cells express much lower levels of tumor antigens. Antibodies targeting pMHCs are also referred to as TCR-like antibodies and can be utilized in a variety of ways to induce cytotoxicity. These include ADCC, CDC, and ADC, as previous described, along with strategies that redirect cytotoxic T cells. This can be accomplished by engineering chimeric antigen receptor (CAR) T cells, which combine signaling

TCR domains and Fv Ab regions to confer target specificity, or alternatively cytotoxic T cells can be recruited using bispecific T-cell engagers (BiTEs), which contain an anti-pMHC region and an anti-CD3 region to engage T cells and direct them against the TAA target.[403,404]

In 2000, Chames et al. reported the first antibody targeting a pMHC, also called a TCR-like antibody. This TCR-like antibody targeted a MAGE-A1 pMHC, generated using phage display.[405] The same technique was subsequently applied to develop TCR-like Abs against pMHCs derived from other well studied tumor antigens including gp100 (PMEL), MART-1, Tyrosinase (TYR), and viral epitopes like HIV, among others.[394,401,404,406–408] While initially used for pMHC visualization and flow-cytometry based quantitation of expression levels, a variety of therapeutic applications of TCR-like antibodies have now been developed. For each therapeutic strategy, assessment of optimal antigen expression levels/threshold for cytotoxicity is required, and in many studies increased antigen expression may improve therapeutic efficacy.

6-1-1 Bi-specific T cell engagers (BiTES)

BiTES therapies force the formation of an immunological synapse between tumor cells and T cells by binding CD3, an invariant signaling domain on the T cell receptor, one side of the molecule, and to a cell surface tumor antigen on the other side of the molecule.[409] This allows for cell lysis independent of the T cells' intrinsic antigen specificity and bypassing several common mechanisms of immune escape on the immune and tumor antigen fronts. One BiTE example is the FDA approved therapey, Blincyto, which reacts with the B-cell antigen CD19 for treatment of B-cell neoplasms.[410] One significant benefit of BiTEs over other TCR-mimic Abs is that they have a lower thresholds of epitope density for efficacy, though not as sensitive as CAR T therapies.[403]

A pMHC-specific BiTE described by Dao et al. targeted a WT1 epitope (ESK1) which has a low density of expression.[411] *In vitro* and *in vivo*, the ESK1-BiTE demonstrated T-cell cytotoxicity against WT1+ tumor cells and WT1+ NOD-SCID mice. The data also suggested ESK1-BiTE therapy may induce epitope spreading, providing a more durable therapeutic response than other pMHC-specific Ab therapies. BiTEs against melanoma tumor antigens with higher expression (NY-ESO-1) have also been developed and demonstrated specific lysis, however expression level thresholds for optimal BiTE efficacy have not thoroughly explored.[412]

6-1-2 Antibody dependent cellular cytotoxicity (ADCC)

ADCC occurs when antibodies bind antigens on the cell surface, and natural killer (NK) cells expressing CD16 FC receptors recognize and crosslink to the antibody bound to the antigen.[413] This activates NK cells, which allows them to lyse the target cells and initiates cytokine secretion like interferon gamma, which recruits additional adaptive immune cells. While NK cells are the main effector cell type, other Fc-receptor cells like monocytes, macrophages, granulocytes, and eosinophils also contribute to ADCC-mediated killing of target cells.[414]

Generally, studies have shown that higher expression levels of the target antigen improve cytotoxicity via ADCC. Niwa et al. generated a panel of tumor cell lines with CCR4 antigen expression levels ranging from ~1000 to 500,000 and evaluated ADCC-mediated cytotoxicity using anti-CCR4 IgG antibody and PBMCs from two healthy donors.[392] The cytotoxicity (^{51}Cr release assay) was dependent on concentration of IgG1 used and the CCR4 expression levels, with the highest cytotoxicity observed with 3 ug/mL IgG and the highest expression level tested of 54,000 binding sites per cell. Another assay was performed testing CD20 expression levels (~1000-600,000 sites/cell) and data showed similar findings. In both examples, cytotoxicity at 50% or better was not observed without 10,000 copies of the target

antigen per cell. ADCC activity of cetuximab, an IgG1 monoclonal antibody against EGFR, demonstrated improved activity in cells with higher surface expression of EGFR.[415] Together, these results suggest that higher antigen expression levels improve antibody-based therapeutics.

In 2006, Wittman et al. utilized a TCR-like Ab against an HLA-A2*01 restricted peptide derived from human chorionic gonadotropin beta (hCG-β), overexpressed in many breast cancer patients, to mediate ADCC.[416] Similar to the CCR4 and CD20 studies, cytotoxicity was dependent on the antibody concentration and antigen presentation levels. Several other TCR-like antibodies have been recently developed targeting pMHCs derived from tumor protein 53, macrophage migration inhibitor factor (MIF) and WT1, all overexpressed in tumor cells.[417–419] Several of these studies have shown a maximum lysis in endogenous cells (not peptide pulsed) of ~20%, suggesting higher expression levels are required for increased cell lysis.[417,419] Still, this work demonstrates the potential for ADCC with TCR-like Abs, and may favor highly abundant pMHCs such as the TAAs modulated by MEK inhibitor treatment previously described in this thesis.

6-1-3 Antibody-drug conjugates

Antibody-drug conjugates traditionally consist of three parts: The antibody (selective targeting unit), the drug (cytotoxic agent), and the chemical linker which connects the two. While there are different mechanisms of action, generally the Ab binds the target antigen, after which the entire ADC is endocytosed. Inside the cell, the linker is cleaved which releases the drug and induces apoptosis.[420] This mechanism of action suggests that the higher the antigen expression, the better the efficacy of the ADC due to increased drug payload being endocytoses into

cells.[421,422] Still, studies evaluating the relationship between target expression levels and ADC efficacy are limited.

A Phase II study in metastatic breast cancer of T-DM1, a MMAE conjugated HER2 targeting antibody (trastuzumab), showed a high objective response rate (36% vs 28%) in patients with HER2 expression levels high than the mean expression of the patient cohort, via reverse-transcriptase polymerase chain reaction.[423] Furthermore, the overall response rate was 33.8% in patients with HER2 positivity with an immunohistochemistry score 3+ versus 4.8% in patients with normal HER2 expression.[424] A study by Sharma et al. assessed the efficacy T-DM1 using a panel of HER2+ cell lines with expression levels ranging from 10,000-800,000 receptors/cell (assayed by QuantBrite beads) and found a strong linear relationship between HER2 receptor expression and released MMAE exposure inside cancer cells.[422] Another study showed that cytotoxicity of T-DM1 was 61% in cells with “high” expression of HER2 and 3% in low expressors, however the receptor levels per cell were not defined.[425]

Improved efficacy of ADCs has also been shown in vivo by combining ADCs with targeted therapy. For example, in melanoma BRAF/MEK inhibitors have been shown to increase AXL expression, thereby increasing efficacy of the anti-AXL ADC in a melanoma PDX model.[426] This further highlights the importance of high antigen expression for ADC efficacy, and supports the hypothesis that non-tumor cells with lower target antigen expression would not be susceptible to ADC-mediated cytotoxicity, whereas tumor cells with high expression may be. This feature makes targeting tumor antigen pMHCs attractive, as expression is substantially higher on tumor cells than normal cells, and can be further modulated with perturbagens, including targeted therapies like MEK inhibitors.

Interestingly, there is some debate regarding whether antigen-dependent internalization is required via the “bystander” effect, which describes the diffusible free drug cleaved by extracellular enzymes being internalized through FC-mediated phagocytosis by neighboring

cells, resulting in cell death.[421] This has been proposed in response to clinical data of the ADC targeting CD30, where CD30 surface expression is not predictive of response.[427] The "bystander" effect can also result in toxicity if healthy cells endocytose the drug. Different ADCs and payloads have different mechanisms of action, therefore the ADC properties, receptor expression levels, and receptor turnover all likely impact therapeutic efficacy, though this remains to be exhaustively explored.

Targeting of pMHCs with pMHC-specific ADCs was first described in a 1997 study using an hemagglutinin (HA)-specific Fab conjugated to the pseudomonas exotoxin (PE38), which showed specific killing of influenza infected cells in vitro.[428] The first tumor antigen application utilized gp100 specific Fabs fused to PE38 and targeted JY cells loaded with the gp100 peptide, which authors estimate to reach 150,000 copies/cell.[363,393] In this experiment, the IC_{50} was 0.5 ng/mL. In FM3D melanoma cells pulsed with peptide (expression level estimated 10,000 copies/cell), the IC_{50} was 200 ng/mL, highlighting the importance of higher antigen expression levels for improved cytotoxicity with ADCs. When applied to melanoma cell lines with endogenous expression, IC_{50}s were 20-100 ng/mL, though absolute expression levels on the cell lines utilized were not evaluated.

Lowe et al. explored the impact of target copy numbers on ADC efficacy by using two cell lines: MDA-MB-231 and SW620 which both express the target antigens of two ADCs at varying concentrations.[390] Expression levels as low as 40,000 copies/cell resulted in cell viability between 50-65% of the untreated control. However, expression levels of 2,000 to 20,000 copies/cell showed a smaller effect (~80% viability of control) and 1,000 copies/cell showed no change in viability. This suggests that expression levels of 2,000+ copies/cell are required to see an effect with an ADC, however high expression results in a larger effect. Cohen et al. estimated 20,000 copies/cell were required for ADC-mediated toxicity.[393] Of note, expression

levels in both studies were measured using flow cytometry, which may be less accurate than mass spectrometry-based platforms like SureQuant MHC.

While *in vitro* analyses of TCR-like Ab targeting have been well documented, *in vivo* studies remain limited. Recently, Lai et al. reported the development and use of a MART-1 targeting TCR-like ADC and displayed tumor-specific killing *in vitro* and in *in vivo* xenograft mouse models.[429] Of Note, authors demonstrate that a low dose of the ADC (5mg/kg) is more efficacious in reducing tumor burden when combined with trametinib, which increases expression of the targeted MART1 antigen. Unfortunately, this study did not determine copy numbers of the MART-1 peptide pre/post trametinib treatment in vitro or in vivo, however these data provide additional evidence that increased pMHC presentation improves ADC-pMHC mediated killing of tumor cells.

Taken together, ADCs targeting pMHCs have the potential to be highly effective but require high antigen expression levels for optimal results. Previous work described in this thesis describes the identification and quantification of tumor antigens with high expression levels. We hypothesized that these antigens may make for compelling ADC targets, and co-treatment with MEK inhibitors to upregulate expression may further improve therapeutic efficacy. To this end, we collaborated with Jim Wells and Nick Rettko from UCSF to develop pMHC-specific Abs against four selected targets and evaluated their use as ADCs in BRAF mutant melanoma.

6-2 Results

6-2-1 Target selection for pMHC-specific antibody development

We selected four peptide targets for pMHC-specific Ab development, which were chosen based on several factors that incorporated data from previous discovery and targeted analyses. “RLLGTEFQV” from SLC45A2, “ALFDGDPHL” from PRUNE2, “MLGTHTMEV” from PMEL

(gp100), and “SLDDYNHLV” from DCT (TYRP2). All four targets selected are predicted HLA-A2*01 binders and are 9 amino acids in length. Next, we prioritized targets that showed large changes in expression following MEK inhibitor treatment in SKMEL5 cells, as this was our cell line model system. With 1 μM binimetinib, the targets increased 3.4 to 6.4-fold in multiplexed discovery analyses (**Figure 6-1**). Previous results highlight the impact of ion suppression in labeled MHC analyses, therefore changes in expression may actually be quite a bit higher. A comparison of label free (LF) and TMT-labeled analyses of SKMEL5 cells +/- 100 nM MEKi showed that LF analyses had high fold changes in expression than labeled analyses, though to varying degrees (**Supplementary Figure 6-1**). The DCT peptide had a 2.46x change with TMT and a slightly larger 3.46x change with LF data, however the PMEL peptide had a much larger quantitative difference: 1.85x with TMT and 6.65x with LF. While some of dynamics of these differences may be attributed to the differences between samples analyzed, this data and our previous results show a significant role of ratio compression in multiplexed and LF pMHC data, underscoring that dynamic changes are likely larger than measured with mass spectrometry.

We also explored how other perturbagens that increase HLA expression alter the presentation levels of the selected pMHCs. We utilized results from previous analyses evaluating the pMHC repertoire response of IFN-γ stimulation and palbociclib treatment (CDK4/6 inhibitor) and found that MEK inhibition still had the largest effect on these antigens over IFN-γ stimulation, despite IFN-γ having a larger effect on bulk expression changes. Interestingly, CDK4/6 inhibitors minimally increased presentation of the target antigens, suggesting that MEK inhibitor treatment is the most robust way to selectively increase expression of our pMHC targets.

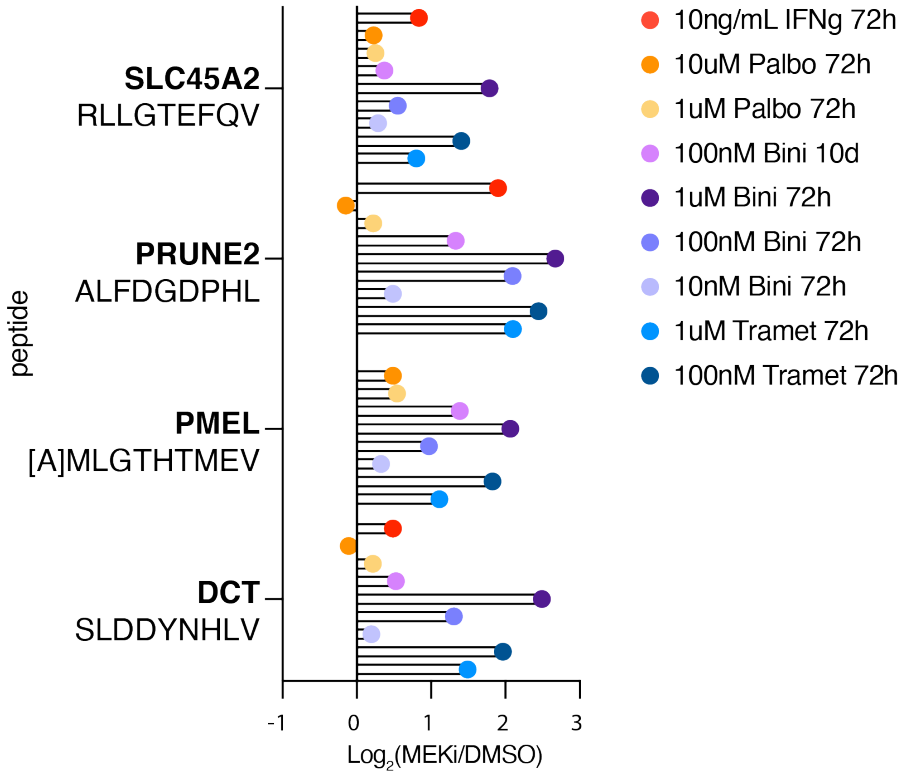

***Figure 6-1**. Change in pMHC expression of select targets across treatment conditions in multiplexed, discovery analyses. Palbo = palbociclib, CDK4/6 inhibitor. Bini = binimetinib, MEK inhibitor. Tramet = trametinib, MEK inhibitor.*

We also evaluated abundance levels by integrating the area under the curve of the precursor ion and found that in the SKMEL5 +/- 100 nM MEKi SLC45A2, DCT, and PRUNE2 all had abundances in the 99th percentile, and the PMEL peptide was in the 90th percentile of abundance (**Figure 6-2-A, Supplementary Figure 6-2**). This result was consistent across other SKMEL5 analyses, confirming all four peptides have high abundance relative to the other peptides identified in discovery analyses (**Figure 6-2**).

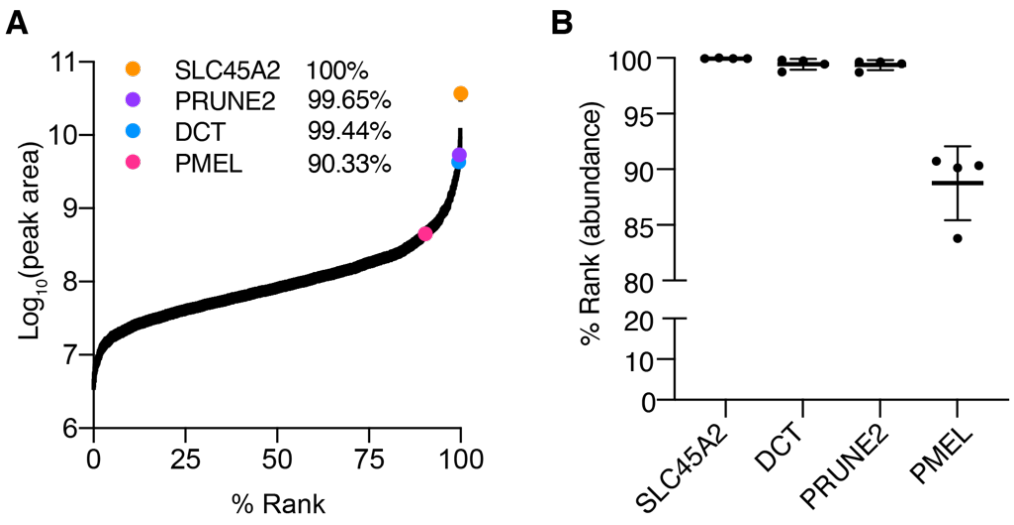

***Figure 6-2**. **A** Ranked abundance of pMHCs in SKMEL5 cells +/- 100 nM binimetinib. Antibody targets are highlighted in color, along with their % rank. **B** Mean ranked abundance of Ab targets across 4 discovery analyses: 10 nM, 100 nM, and 1 μM binimetinib, along with the 100 nM/ 1 μM trametinib analysis. μ=99.96%, 99.44%, 99.37%, and 88.75% for SLC45A2, DCT, PRUNE2, and PMEL, respectively. Error bars represent +/- standard deviation.*

Finally, we utilized data from the Iso18 panel for absolute quantification of target pMHCs and found the four selected had a wide range in presentation levels, spanning over three orders of magnitude (**Figure 6-3-A**). PMEL peptides had the largest change in presentation levels with MEKi, with approximately 200 copies/cell with DMSO treatment, and 1000+ with MEK inhibition, marking a 5-fold change. DCT and PRUNE2-derived peptides had similar expression levels, with 1000-2000 copies/cell with DMSO and 5000-7000 copies/cell with 100 nM or 1 μM MEKi. The SLC45A2 peptide had the highest level of expression, with ~36,000 copies/cell with DMSO treatment and over 10^5 with MEKi. These range in expression will allow for testing of different types of antibody-based pMHC therapies and aid in determining optimal thresholds therapeutic efficacy.

Not all target peptides were identified in the other HLA-A2*01+ BRAF mutant cell lines, implying either they were below the limit of detection (<1 copy/cell) or there was not sufficient

expression of the proteins the peptide was derived from. For example, no PMEL peptides were detected in A375 cells suggesting the PMEL protein is either absent or has low expression. SLC45A2 pMHC levels were the only peptide that showed an inverse trend in expression levels following MEKi in A375 cells, but expression increased in RPMI-7951 cells, though the copies/cell were substantially lower than SKMEL5 cells (~1000 copies/cell) (**Figure 6-3-B,C**). Both DCT and PRUNE2 peptides showed a substantial increase in copies/cell following MEKi, with DCT increasing from ~18 to ~1300 copies/cell and PRUNE2 from ~22 to ~8500 copies/cell following 1μM MEKi. The multiplexed discovery data showed mean increases in presentation of 8.5x and 10.5x of DCT and PRUNE2 peptides, respectively, which is much lower than the 74x and 378x changes in expression measured with SureQuant MHC analyses (**Supplementary Figure** 6-4). This further underscores the substantial impact of ion suppression in this dataset and identifies DCT and PRUNE2 as pMHCs whose expression is modulated by MEK inhibition to a much greater extent than originally anticipated and may be suitable targets for antibody-based therapies requiring high expression levels if primed with MEK inhibitor treatment.

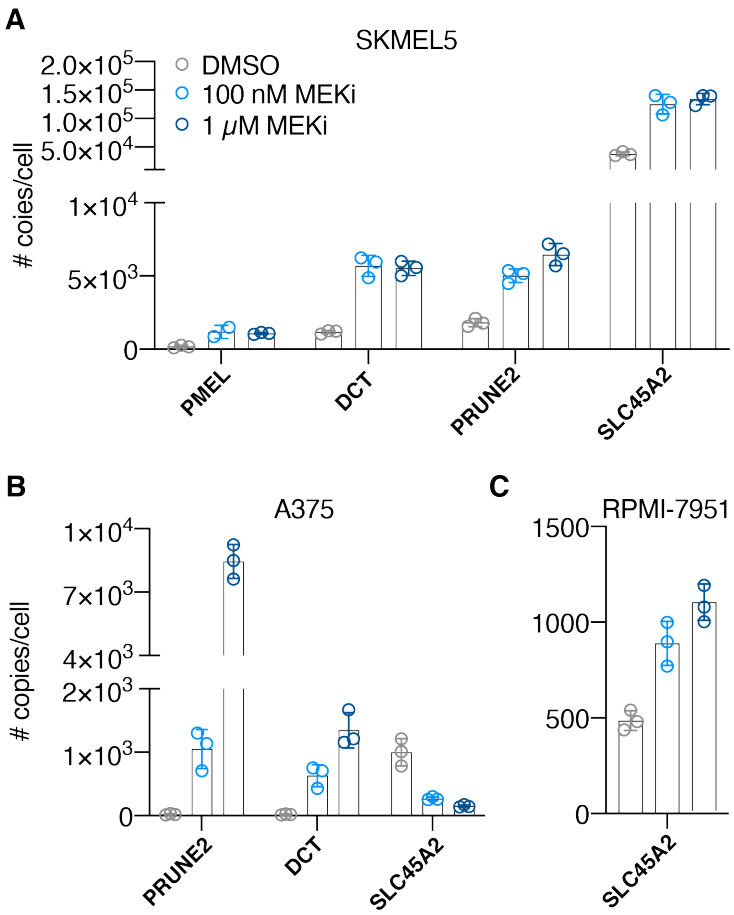

Figure 6-3*. Copies per cell estimates of target peptides for SKMEL5 cells (**A**), A375 cells (**B**), and RPMI-7951 cells (**C**) treated with 100 nM MEKi or 1 μM MEKi for 72 hours. Error bars represent +/- standard deviation from n=3 replicates.*

6-2-2 Generation of pMHC-specific Abs

To generate pMHC-specific Abs against the four targets of interest, we collaborated with Nick Rettko and Jim Wells, PhD. At UCSF. The work and methodology within this section is solely their contribution. First, we synthesized crude, synthetic peptides of the four targets and combined them with HLA-A2*01 and β2-Microglobulin for 3 days at 10°C to generate stable pMHC complexes. The pMHCs contained a TEC protease cleavage site and an AviTag for biotinylation, and refolded complexes were purified with size exclusion chromatography.

The Ab selection process is driven by a phage display library containing 10^{10} unique antibody fragment (Fab) clones (**Figure 6-4**). In the first round of selection, a negative selection is performed against a known HLA-A2*01 binding Flu peptide ("GILFGVFTL") and remove all the phage that do not bind the flu peptide. Next, a positive selection in the depleted library is performed against the antigen of interest. Elution of the Fab-phage is performed by using the TEV protease, and E. coli are then infected with whatever binds the target antigen so Fab-phage propagate to generate a new library enriched for antigen-binding Fab-phage.

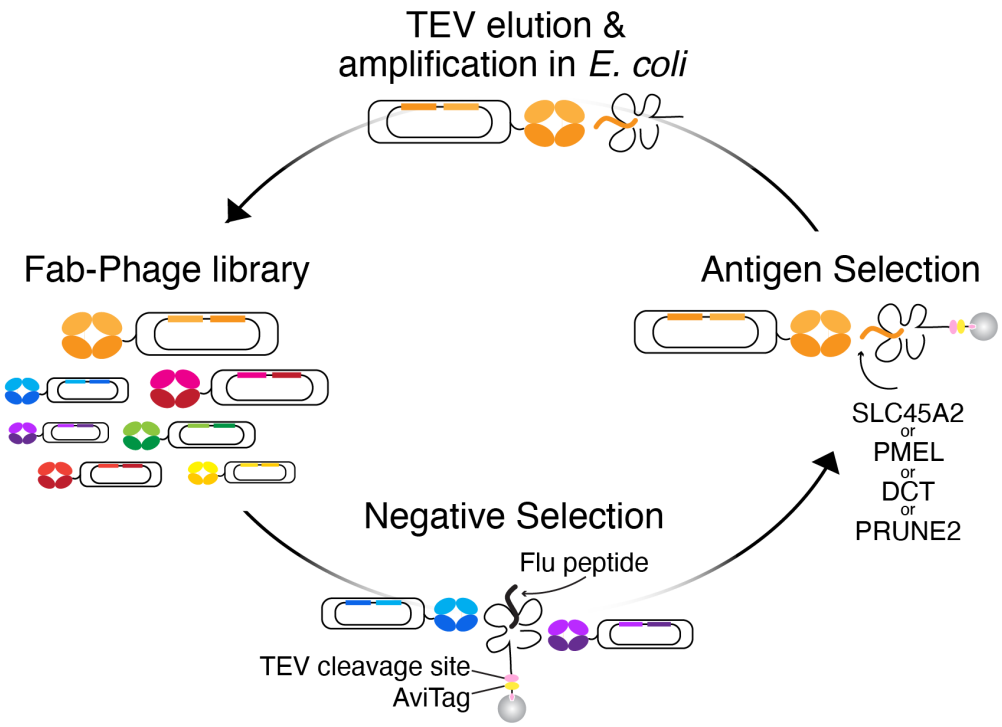

***Figure 6-4**. Schematic of phage display selection for pMHC-specific Fabs.*

In rounds 2-4 of selection, a negative selection with the Flu peptide is again performed first, With the remaining phage, 2 selections are performed in parallel (flu peptide and target antigen), and binding phage are amplified. Titers are measured to determine how many Fab-phage were eluted off of each antigen vs flu peptide to assess the level of enrichment. After 4

rounds of selection, phage are diluted such that a single phage clone infects a bacteria cell, allowing for propagation of single phage clones.

Next, an ELISA screen is performed on remaining single cell clones (four for each target). Briefly, 20 nM of the pMHC antigen target or flu peptide is immobilized on the plate, and the Fab-phage are added to each well and incubated for 30 minutes. An anti-phage HRB secondary is added to produce the ELISA signal, which is recorded to assess direct binding. For the competition ELISA, 20 nM pMHC are incubated with Fab-phage before adding the phage to the plate. If the ELISA signal from the competition assay is equal or less than the ELISA result from the direct binding experiment, the Fab affinity for the pMHC target is 20 nM or less. The clone with the highest direct binding score plus affinity ratio (competition/direct binding) for each target was selected as the optimal pMHC-specific Ab. The phage are then sequenced to determine the CDR sequences, and can be developed into full length IgGs.

6-2-3 pMHC-specific Abs demonstrate high specificity

To assess the pMHC specificity of selected clones, T2 cells were utilized which are defective in presenting exogenous antigens due to a deletion in genes encoding transporters associated with antigen presentation (TAP1/TAP2). The addition of exogenous peptide is taken up by cells and loaded onto newly synthetized MHC molecules, therefore T2 cells can be used to specifically present a single pMHC target. Target peptide or Flu peptide loaded T2 cells were assayed with flow cytometry using the pMHC-specific IgGs and Alexa-fluor 488 secondary antibodies. Impressively, only T2 cells loaded with the Ab targeted showed a substantial shift in fluorescence compared to DMSO or flu peptide loaded T2 cells, and antibodies did not show cross reactivity among the pMHC targets (**Figure 6-5**). N. Rettko performed an analogous experiment and found the results comparable.

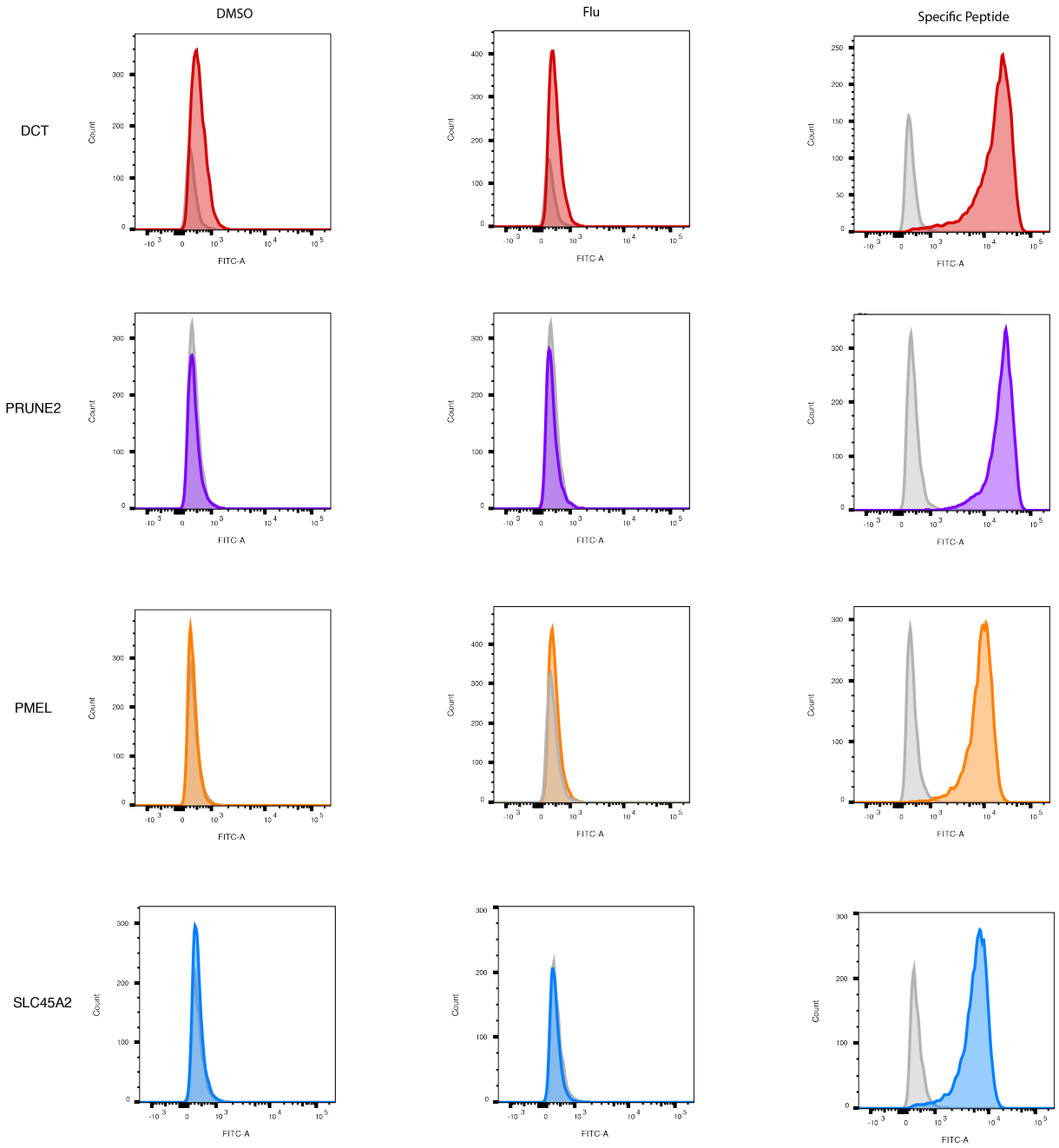

***Figure 6-5**. Flow cytometry analysis of T2 cells loaded with 100 nM target peptide or flu peptide and assayed with the pMHC-specific antibodies.*

6-2-4 pMHC-specific Ab recognition of SKMEL5 cells

We next investigated whether the pMHC-Abs could recognize target expression on SKMEL5 cells, and whether the signal would increase with MEKi treatment. We first verified the increase in expression with MEKi treatment of HLA-A2*01 peptides using flow cytometry (**Supplementary Figure 6-5**). Next, SKMEL5 cells treated with DMSO or 1 μM binimetinib for 72 hours were stained with pMHC specific Abs and measured by flow cytometry. No change in expression over the DMSO control was observed in for DCT, PMEL, and PRUNE2 peptides, but an increase in median fluorescence intensity was seen with the SLC45A2-specific pMHC and when a combination of all four antibodies was used (**Figure 6-6-A, B**). This result is consistent is with the SLC45A2 peptide having the highest expression levels.

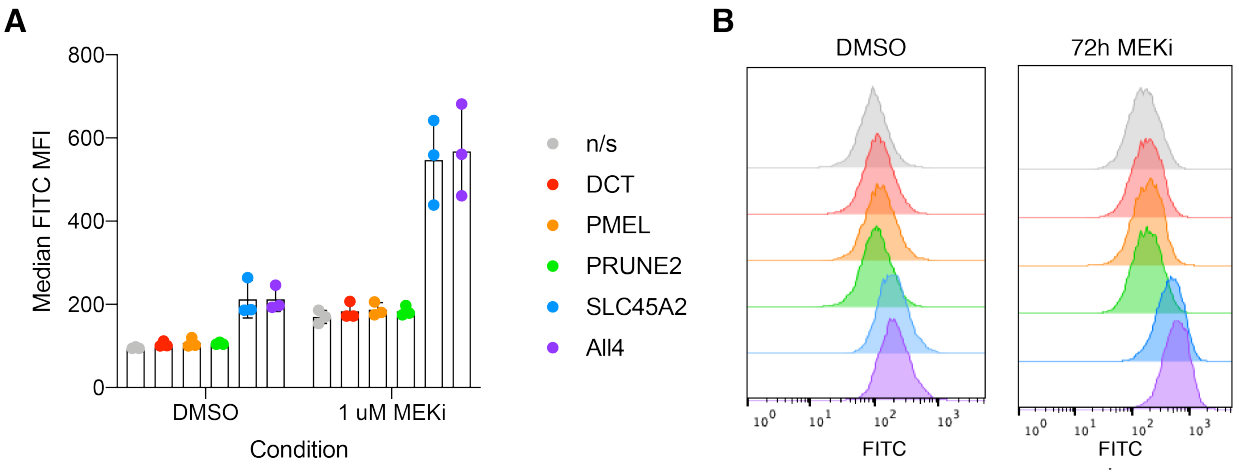

Figure 6-6**. Flow cytometry analysis using pMHC-Abs on SKMEL5 cells. **A** Median fluorescent intensity (MFI) for SKMEL5 cells stained with the pMHC specific Abs, n=3 for each condition. **B** Representative histograms from **Figure 6-6-A.

6-2-5 Antibody drug conjugate targeting of pMHCs

We next sought to determine whether targeting specific pMHCs with an antibody-drug conjugate (ADC) approach would be efficacious. In liu of a true ADC, we utilized the full length pMHC-specific IgGs with an IgG conjugated monomethyl auristatin F (MMAF) secondary antibody with a cleavable linker (**Figure 6-7-A**). MMAF is a cytotoxic small molecule which inhibits cell division by blocking tubulin polymerization.[430] The cleavable linker connecting MMAF to the Ab is stable in extracellular fluid, but can be cleaved by endosome cathepsins upon entering cells.

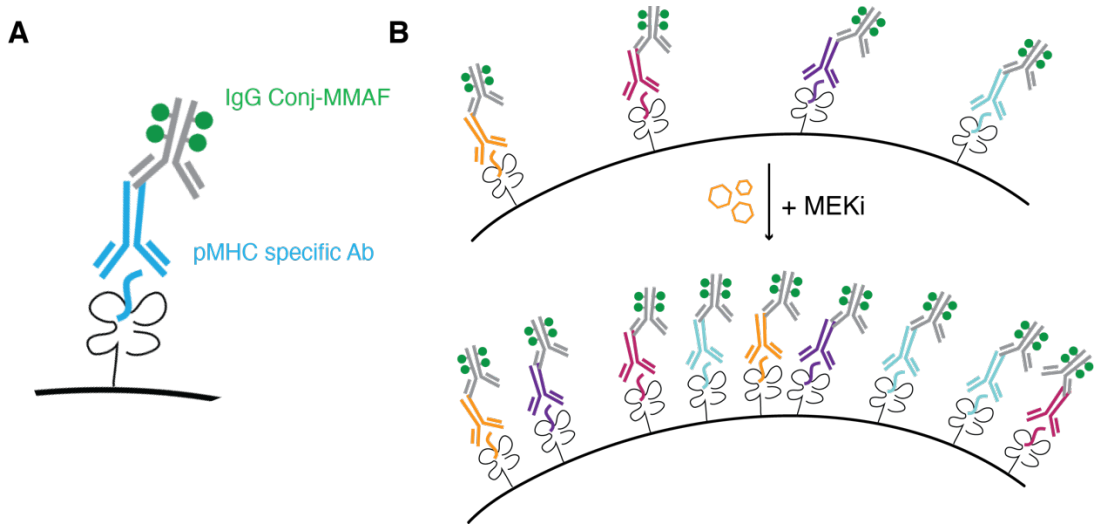

***Figure 6-7**. pMHC-ADC targeting scheme. **A** Schematic of ADC targeting using pMHC specific primary antibody and MMAF-conjugated secondary. **B** Schematic of ADC targeting with and without MEK inhibitor treatment.*

We first tested the pMHC-ADC approach on SKMEL5 cells, targeting the SLC45A2 pMHC as we know it has high expression with DMSO (~40,000 copies/cell) and even higher with MEK inhibitor treatment (100,000+ copies/cell). Higher expression may yield a higher drug

payload in cells and increase cytotoxicity (**Figure 6-7-B**). DMSO treated cells showed a 38% reduction in viability over untreated control cells with 30 nM Ab treatment, whereas cells pretreated with 1 μM binimetinib had a 47% reduction in cell viability, consistent with higher antigen target expression levels inducing higher cytotoxicity (**Figure 6-8**).

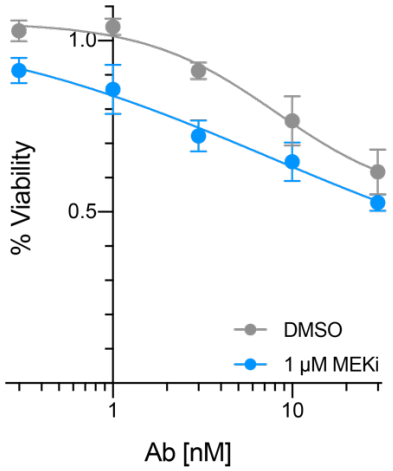

***Figure 6-8**. Cell viability response to SLC45A2 ADC (pMHC-specific Ab targeting with MMAF-conjugated secondary antibody in SKMEL5 cells). Error bars represent standard deviation for n=3 replicates.*

We next tested the PRUNE2 antibody against SKMEL5 cells (~2000/7000 copies/cell with DMSO/MEKi) and A375 cells (~20/8000 copies/cell). We find that for SKMEL5 cells, both treatment conditions result in ~40% reduction in cell viability (**Figure 6-9-A**). For A375 cells, DMSO treatment showed a 25% reduction in viability and 45% with MEKi, representing a substantial difference between the two conditions (**Figure 6-9-B**). A maximal reduction in viability of ~50% is consistent with high ADC treatment concentrations in other similar studies. Of note, while the same number of A375 cells were seeded for each analysis, the MEKi pre-treated cells exhibited much slower proliferation during the course of the assay, therefore it is possible some of the differences in viability are due to the cell populations having different

exposure levels to the MMAF secondary. Furthermore, the small decrease in viability observed in A375-treated DMSO cells may be due to toxicity of high concentrations of the Ab added, therefore subsequent analyses will include an additional control condition where cells are treated with the primary Ab but no secondary. Nevertheless, these preliminary results present compelling evidence that MEK inhibitors can be successfully combined with pMHC-specific ADCs for improved cell killing for high expressing antigens.

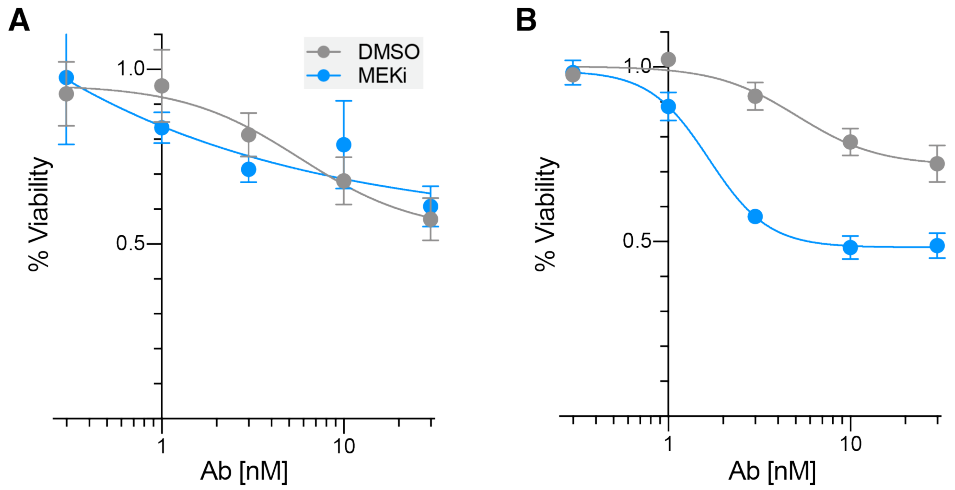

Figure 6-9*. Cell viability response to PRUNE2 ADC, i.e. pMHC-specific Ab targeting with MMAF-conjugated secondary antibody in* ***A*** *SKMEL5 cells and* ***B*** *A375 cells. Error bars represent standard deviation for n=4 replicates.*

6-3 Discussion

TCR-like antibody-based therapies represent a promising new treatment modality for selective killing of tumor cells by targeting tumor-specific or tumor-associated pMHCs. Our previous results using SureQuant MHC was able to provide absolute quantification of pMHC copies/cell for DMSO and MEKi treated cells, and this data highlighted the wide range in expression levels of endogenous pMHCs within and across cell lines. We sought to utilize this

absolute quantitative information to develop targeted pMHC-based therapies that were tailored to the defined expression levels. For high expressing antigens like SLC45A2, we demonstrate proof of concept in using an ADC against this pMHC target for tumor killing. Furthermore, we highlight the differential killing of tumor cells with MEKi treatment, confirming earlier studies that suggest higher expression levels increase ADC therapeutic efficacy.

Still, additional work is required to better understand how to utilize pMHC-specific ADCs. First, a deep understanding of the expression level threshold required for efficacy is needed. This could be accomplished by using SureQuant MHC to quantify copies/cell of T2 cells stimulated with different concentrations of peptide to create a panel of cells with varying expression levels as described by Cohen et al.,[431] followed by an ADC assay. Additionally, the temporal dynamics of ADCs require additional investigation. Cells were pre-treated with MEKi for 72 hours which showed superior results over cells co-treated with MEKi/ADCs, but the optimal dosing regimen beyond the initial 72 hours is unknown. Additional *in vitro* and *in vivo* studies will be informative in evaluating how best to combine MEK inhibitors and pMHC-targeted therapies.

There are many variables regarding the ADCs that can also be optimized to increase the PK/PD profile including the payload selection, the cleavable linker, chemical/immunophenotypic properties of the antibody, or intratumoral payload concentration. Furthermore, exploring the use of a of a bispecific antibody may improve targeting and therapeutic efficacy by increasing valency.[432,433]

One of the key limitations of utilizing ADCs and other targeted therapies are cohort selection for clinical trials. Many trials enroll patients without biomarker selection, and trials that do screen for target expression often rely on histology staining.[434] For some applications like HER2 expression, IHC may be sufficient. However, for pMHCs mRNA and protein expression

do not necessarily correlate with pMHC expression levels, therefore targeted assays to identify and quantify assess pMHC expression like SureQuant MHC is required.

Future work on this study also includes testing the existing antibodies' efficacy with ADCC and the development and testing of a BiTE therapy against one or two (bi-specific) pMHC targets, currently under development by N. Rettko. These two applications will also benefit from experiments with a T2 pMHC expression panel to identify optimal thresholds for efficacy. Together, these data will begin to elucidate the relationship between pMHC expression pMHC-specific Ab response to better understand which therapeutic modality to use based on a patient's pMHC expression levels.

6-4 Materials and Methods

6-4-1 Flow cytometry

All Analyses were performed on an LSRII (BD Biosciences) and data analyzed using FlowJo (version 10.6.2).

SKMEL5 cells

For analysis of cells by flow cytometry, cells were lifted with 0.05% Trypsin-EDTA and 10^6 cells/mL were spun at 300 g for 3 minutes, washed with ice cold PBS supplemented with 1% FBS and 0.1% sodium azide (flow buffer) and incubated with fluorophore-conjugated antibody at 0.5 µg mL^{-1} in flow buffer for 30 minutes on ice. After incubation, cells were washed again, and resuspended in flow buffer plus propidium iodide (PI) staining solution. Antibodies: Alexa Fluor 488 HLA-A2*01, clone BB7.2 [Biolegend, cat # 343303], fluorophore (488) conjugated pMHC-specific Abs. The gating strategy used for all experiments is located in the supplemental information in Stopfer et al.[188]

T2 pMHC-Ab validation

T2 cells were seeded at a concentration of $1e^6$ cells/mL in round bottom plates, and media was supplemented with synthetic peptide standard at defined concentration (30 nM for pMHC-specific Abs). Cells were incubated with peptide at 37°C for 16-8 hours. Cells were incubated with the primary pMHC-specific antibodies or IgG isotype control at 10 μg/mL concentration for 20 minutes on ice. Cells were washed with flow buffer and incubated with protein A-488 conjugate for 20 minutes (1:1000 dilution). Cells were washed again with flow buffer and resuspended in PI staining solution.

6-4-2 Antibody-drug conjugate assay

Cells were seeded in 10 cm dishes and allowed to adhere overnight. For 72 hours, cells were treated with DMSO or 1μM binimetinib. Five thousand cells per well of pre-treated cells were seeded in a 96 well plate and pMHC-specific primary antibodies were added at a dilution spanning 0-30 nM at n=3 or n=4 for 10 minutes at 37°C. Next, 10 nM of the MMAF-conjugated IgG secondary antibody with cleavable linker (Moradec, CAT# AH-102-AF) was added to each well and cells were incubated at 37°C for 72 hours. Cell viability was assayed using CellTiter-Glo luminescent cell viability assay (Promega), per manufacturer's instructions. Percent viability was determined as fraction of luminescence relative to the 0 nM primary Ab control. Dose response curves were fit with 4 parameter variable slope regression curve in Prism 9.0.0.

*Sample preparation, data acquisition, and data analysis for mass spectrometry analyses is described in the chapters where the data is first presented.

6-5 Acknowledgements

I'd like to thank Nick Rettko and Jim Wells from the University of California-San Francisco for the development of pMHC-specific antibodies, along with useful feedback and suggestions regarding this collaboration. I can confidently say my thesis work is more impactful and I am a better scientist having worked with the both of you. It is a joy to work with collaborators that are timely, courteous, and most important—passtionate

6-6 Supplementary Information

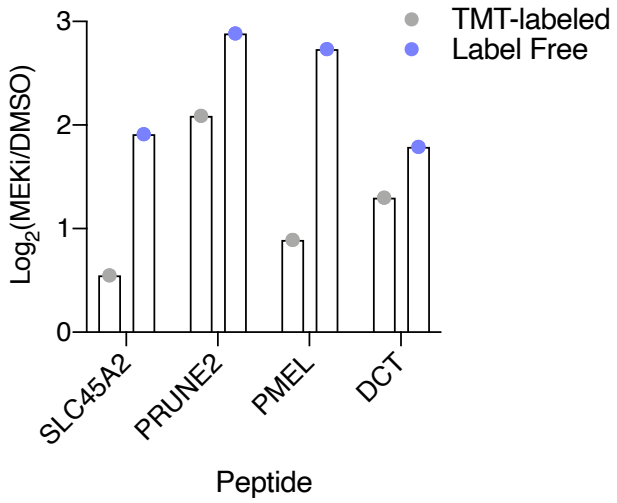

Supplementary Figure 6-1*. Comparison of changes in pMHC presentation levels between label free (purple) and TMT-labeled (grey) analyses of SKMEL5 cells treated with 100 nM MEKi.*

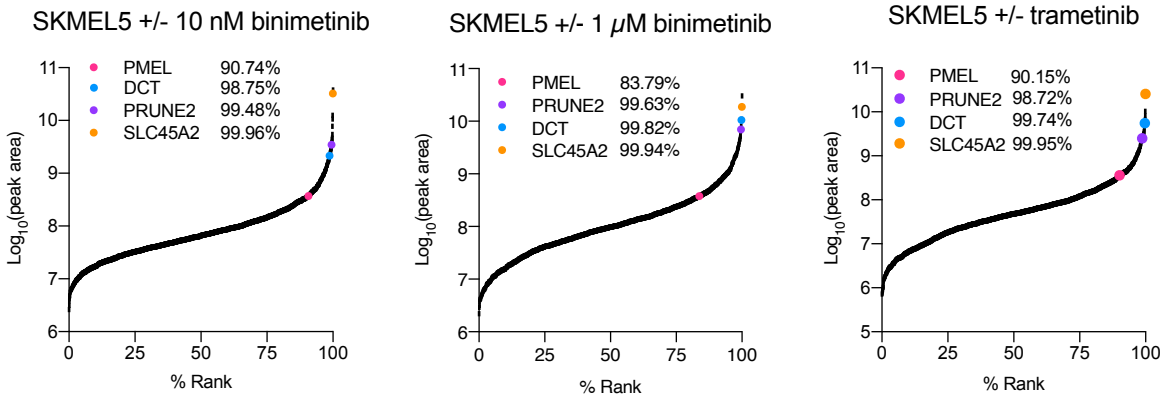

Supplementary Figure 6-2*. Ranked abundance of pMHCs in SKMEL5 cells +/- binimetinib or trametinib. Antibody targets are highlighted in color, along with their % rank.*

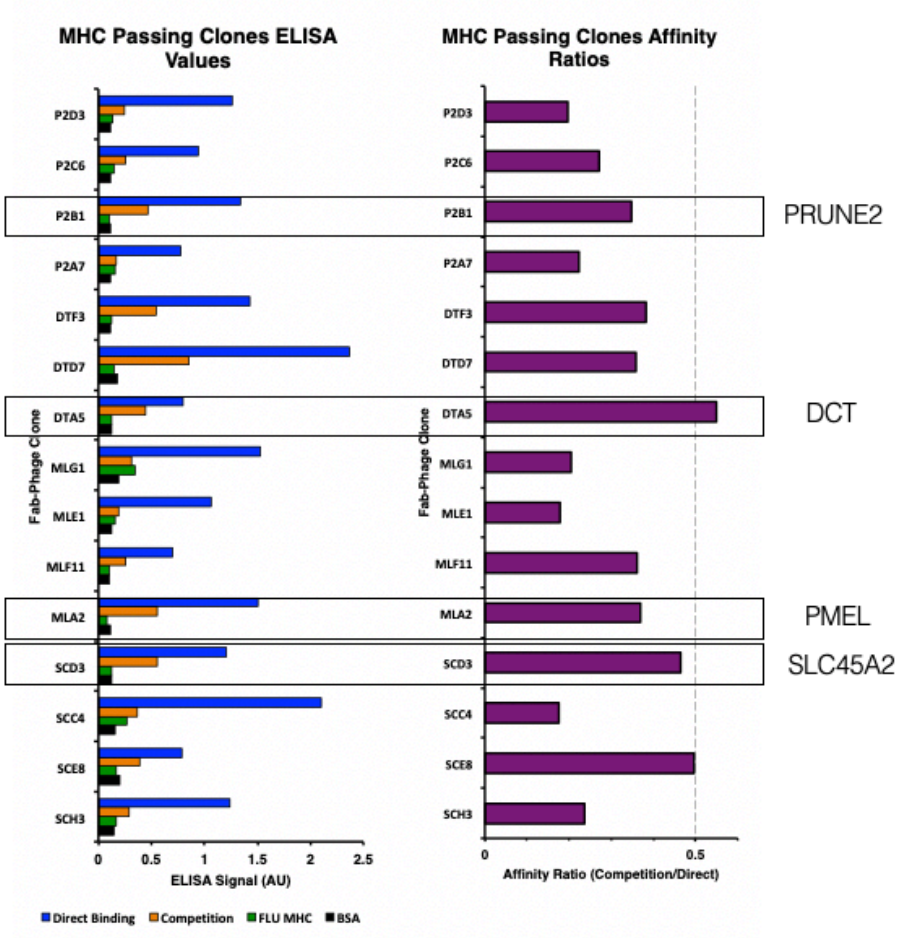

Supplementary Figure 6-3*. ELISA results for top four Fab-phage clones for each pMHC target. Selected clones are highlighted with a box. Figure and data curtesy of N. Rettko, UCSF.*

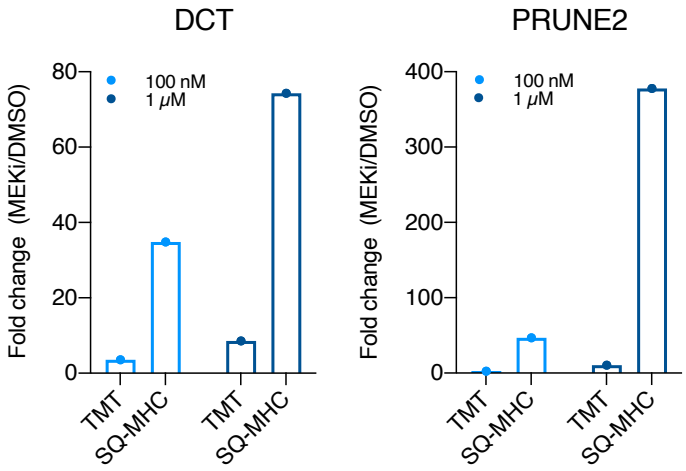

***Supplementary Figure** 6-4. Change in expression levels (DMSO vs. MEKi) in TMT-labeled analyses and SQ-MHC label free targeted quantitation.*

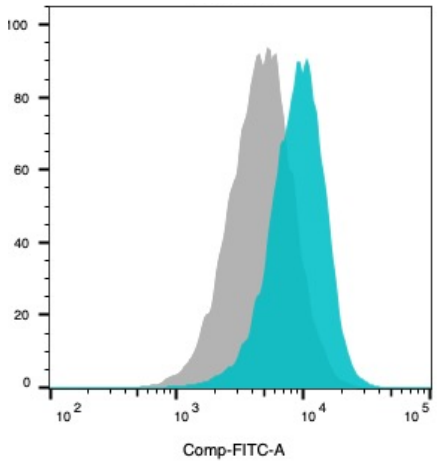

***Supplementary Figure 6-5**. Surface expression of HLA-A2*01 in SKMEL5 cells measured by flow cytometry for DMSO (grey) and 1 μM MEKi (teal).*

CHAPTER 7: Quantitative consequences of protein carriers in immunopeptidomics and tyrosine phosphorylation MS2 analyses

7-1 Introduction

Mass spectrometry (MS)-based proteomics has historically been limited to analyzing bulk cell populations, largely due to losses during sample processing and limited instrument sensitivity. In recent years, several platforms have achieved protein expression profiling in single cells (e.g., single-cell proteomics (SCP)), a notable advancement in proteomics. To overcome sensitivity limitations and acquire deep proteomics datasets, the majority of these platforms rely on isobaric labeling (*i.e.*, Tandem Mass Tags (TMT)) for sample multiplexing and a signal "boosting" sample, or "carrier proteome."[435–437] Carrier proteomes that have been utilized thus far contain a larger amount of protein than the non-carrier samples, an equivalent amount of protein but with a perturbation to increase the signal of interest[438], or both.[439] Because all isobaric labels have an identical intact mass, the inclusion of a carrier proteome increases the precursor ion intensity, enabling enhanced detection of low-input or low-level samples.

Use of a carrier proteome has also recently been applied to peptide major histocompatibility complex (pMHC) profiling (e.g., immunopeptidomics), and tyrosine phosphorylation (pTyr) analyses, both of which historically have required large sample inputs for sufficient signal detection by MS. For example, recent advances in pMHC profiling methods have decreased sample input requirements from $>10^9$ cells to $\sim10^7$ cells, yet even this lower boundary still represents a major limitation in the clinical translatability of the approach.[165,188] Clinical specimens, including fine needle biopsies, typically do not provide enough material for

deep pMHC profiling, and neoantigens are challenging to identify by MS, even with large sample quantities.[158] Similarly, profiling pTyr peptides is possible using several hundred micrograms of input protein per channel in a multiplexed analysis[384], but there is continued effort to reduce sample requirements to enable pTyr profiling of fine needle biopsies, tissue sections, or even single cells.

Inclusion of a protein carrier has resulted in an increased number of identifiable peptides in multiplexed immunopeptidomics analyses as well as multiplexed phosphotyrosine analyses. Ramarathinam et al. utilized increased protein material, cellular or patient-derived xenograft tumors as a protein carrier in class I pMHC experiments, while Chua et al. used a protein carrier that had been treated with pervanadate (PV) treatment to halt tyrosine phosphatase activity and thereby increase tyrosine phosphorylation levels.[439,440] However, the quantitative impact of boosting in both approaches remains poorly understood. Specifically, a carrier proteome may limit the instrument's dynamic range leading to reporter ion ratio compression and increase the number of missing values, thereby reducing data quality and/or data quantity, potentially altering biological interpretation.[441]

Several studies have begun to address these critical questions, albeit with limitations. For instance, experiments to assess ratio suppression typically evaluate whether constant ratios of protein input material are preserved in the presence of a protein carrier, which is not reflective of many biological systems where subtler changes in a subset of peptides demonstrate altered quantitation.[439,441] Studies have also evaluated whether principal component analysis (PCA) can resolve differences between two cell populations in the presence of various protein carrier-to-signal ratios. However, these experiments generally use distinct cell types or cell lines, which have higher heterogeneity in peptide quantitation.[435,439,441,442]

Here, we describe results from analyses comparing MS2-based quantitation with and without the inclusion of a 20x protein carrier in pMHC analyses and a high (~100x) or low (~9x)

carrier in pTyr analyses. We utilize EGF stimulation to drive a pTyr response in a subset of the tyrosine phosphoproteome, and titrated synthetic, isotopically labeled pMHCs along with CDK4/6 inhibitor treatment in pMHC experiments to shift the pMHC repertoire in pathways related to cell cycle control.[188,227] In both applications, protein carriers alter peptide quantitation, which inhibited our ability to interpret the biology. Using these data, we define existing limitations for MS2-based analyses using protein carriers and highlight areas for future exploration that may enhance the data quality through altered experimental design or acquisition framework.

7-2 Results

7-2-1 Characterizing ion suppression using synthetic, heavy isotope-labeled pMHCs

We prepared a set of 6 cell line-derived replicate samples comprised of $1x10^6$ cells per channel for the analysis without a protein carrier ("no-boost"), and a parallel experiment using 2x fewer cells per sample ($5x10^5$ cells) for the "pMHC-boost" analysis (**Figure 7-1-A**, **Supplementary Figure 7-1-A**). As a protein carrier, we utilized 2 samples of $2.5x10^6$ cells stimulated with 10 ng/mL interferon-gamma (IFN-γ) for 72h. IFN-γ stimulation increases pMHCs levels ~2x (**Supplementary Figure 7-1-B, C**), resulting in a ~10x boost per protein carrier sample and a combined signal-to-boost of ~20x, in line with recent published guidelines for SCP experiments.[441]

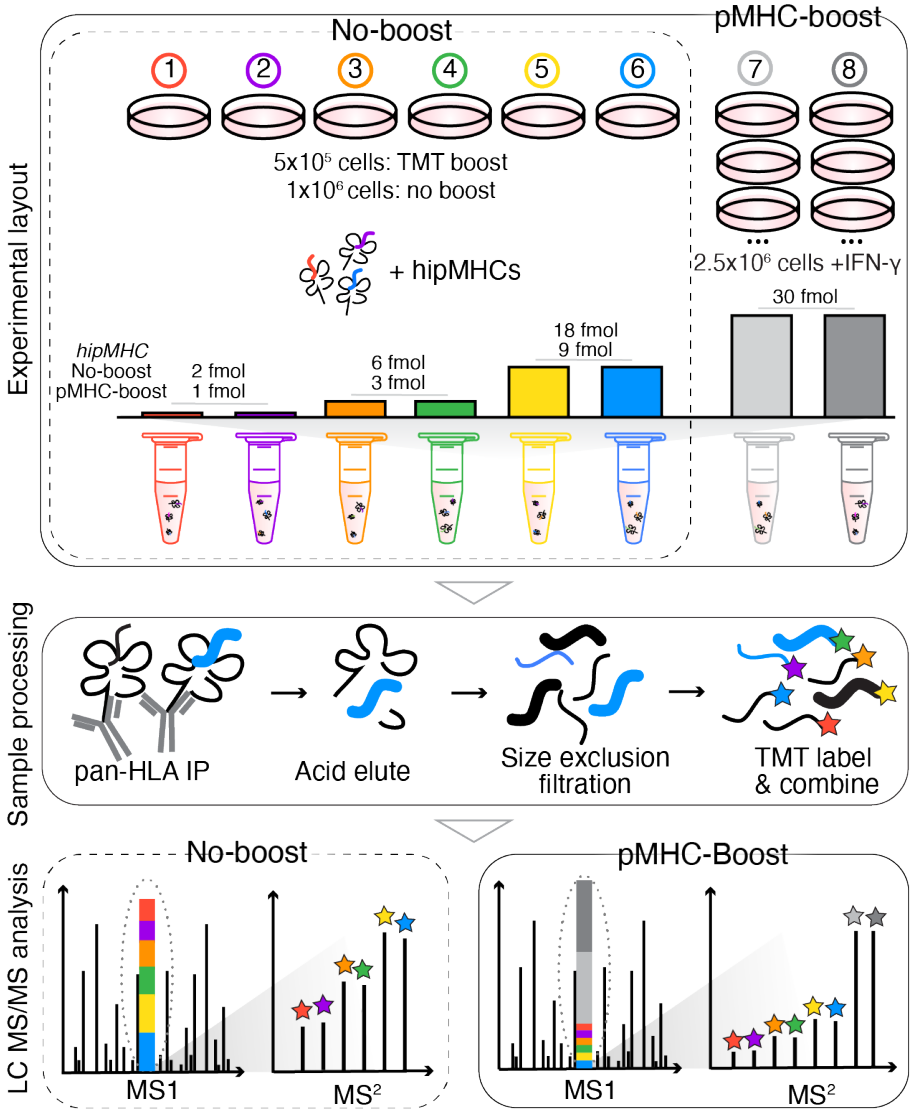

Figure 7-1. *Experimental setup of hipMHC quantitative immunopeptidomic analyses +/- protein carrier.*

To measure the ion suppression, we utilized a panel of six synthetic, heavy-isotope labeled pMHCs (hipMHCs), which were titrated into cell lysates prior to pMHC isolation to generate an internal standard curve, as previously described[188]. HipMHCs were added at a ratio of 1:1:3:3:9:9 across the 6 samples, with concentrations between 1, 3, and 9 fmol in the pMHC-boost analysis, and proportionally, 2, 6, and 18 fmol in the no-boost analysis. The protein carrier

channels each had 30 fmol of each hipMHC, 10x the median concentration used across non-protein carrier samples (**Supplementary Figure 7-1-A**).

After addition of hipMHCs, class I pMHC complexes were isolated from each sample by immunoprecipitation, acid elution, and size exclusion filtration. Peptides for each sample were subsequently labeled with TMT, combined, and analyzed by LC-MS/MS. From a single injection using just 25% of the labeled mixture, 3176 unique pMHCs were identified in the pMHC-boost sample, whereas 1619 were identified in the no-boost analysis (**Figure 7-2-A**). As expected, boosting with protein carrier enabled a strong increase in unique IDs using 50% less cellular input material for each channel. The peptides identified in both experiments followed expected length distributions (**Figure 7-2-B)**, with 97% and 97.9% of 9-mers predicted to be allelic binders in no-boost and pMHC-boost analyses, respectively (**Figure 7-2-C**). While both analyses had equivalent median coefficients of variation (CV) across replicates (**Figure 7-2-D**), PSMs in the boost analysis had a wider distribution of CV values. Together, these data suggest that while a 20x protein carrier improves the number of unique IDs while not altering peptide properties of the resultant dataset, use of a protein carrier may result in slightly higher quantitative variation. Of note, the proportion of missing values between the protein carrier and non-carrier samples in the pMHC boost analysis were comparable (4% of PSMs in no-boost, 8% in pMHC-boost), suggestive of sufficient ion sampling for a majority of peptides (**Supplementary Figure 7-1-D).**

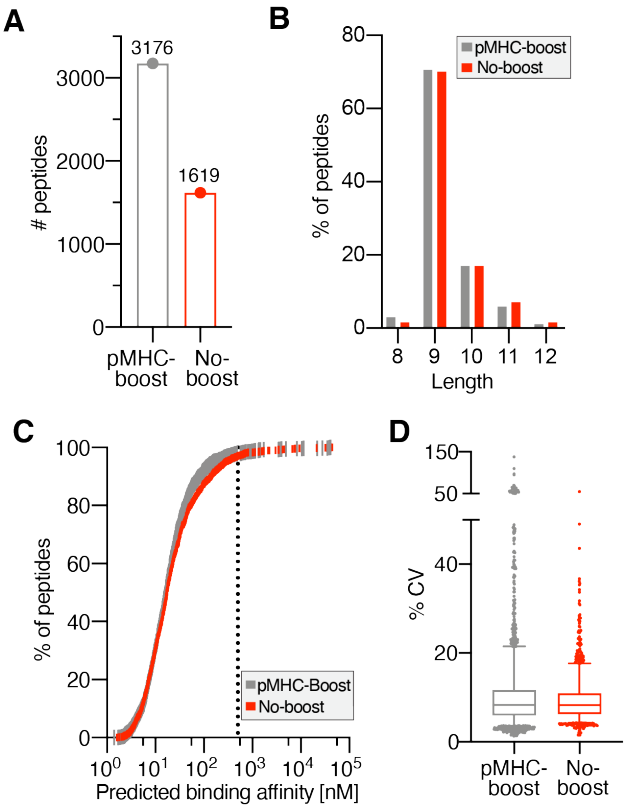

***Figure 7-2**. pMHC properties in pMHC-boost/no-boost analyses. **A** Number of unique pMHCs identified in a single analysis. **B** Length distribution of pMHCs. **C** Predicted binding affinity of 9-mers. 97.9% and 97.0% of 9-mers in the pMHC-boost and no-boost analyses, respectively, were predicted to have a binding affinity ≤500 nM (dotted line). **D** Coefficients of variation of pMHC-boost and no-boost analyses. Boxes outline the interquartile range, and whiskers the 5 and 95th percentiles. pMHC-boost median CV= 8.23%, no-boost = 8.30%. 95% PSMs have CV <17.7% (no-boost) and 21.5% (pMHC-boost).*

We next examined the intensity distributions across PSMs (**Figure 7-3-A**) and found that the protein carrier samples had 3.5-4x higher intensity than the other samples in the boost analysis. Our expected intensity ratios was ~10:1 (5x increase in sample in the protein carrier channels, coupled to a 2x increase in MHC expression due to IFN-g), and thus the observed peptide ratios demonstrate a ~2.5x reduction in signaling intensity, suggestive of ion suppression.

Ratios of the titrated hipMHCs were subsequently analyzed, and substantial ion suppression was observed in both analyses (**Figure 7-3-B**). In the no-boost analysis, the "GLFDQHFRL" peptide had a1.8x reduction in dynamic range, while the the "KLDVGNAEV" peptide had a 6.2x reduction.

Other hipMHC peptides fell between these two extremes. Although the hipMHC intensity ratios did not match expected values in the no-boost analysis, sample intensities increased with increasing concentration of hipMHC. In the boost analysis, almost all of the hipMHC standards had comparable reporter ion intensities across all samples, despite a 9x increase in peptide concentration, with "GLFDQHRFR," being the only exception (6.7x reduction in observed vs. expected dynamic range). Taken together, these data demonstrate that ion suppression exists in non-boost and boost experiments, however the presence of a protein carrier increased ion suppression to the extent that pMHCs up to 9-fold higher in concentration could not be differentiated via isobaric intensities. It is worth noting hipMHCs were added at relatively high concentrations, representing a range of ~1000-10,000 pMHCs/cell. Quantitative accuracy of endogenous pMHCs at lower presentation levels may be further negatively impacted by the presence of a protein carrier.

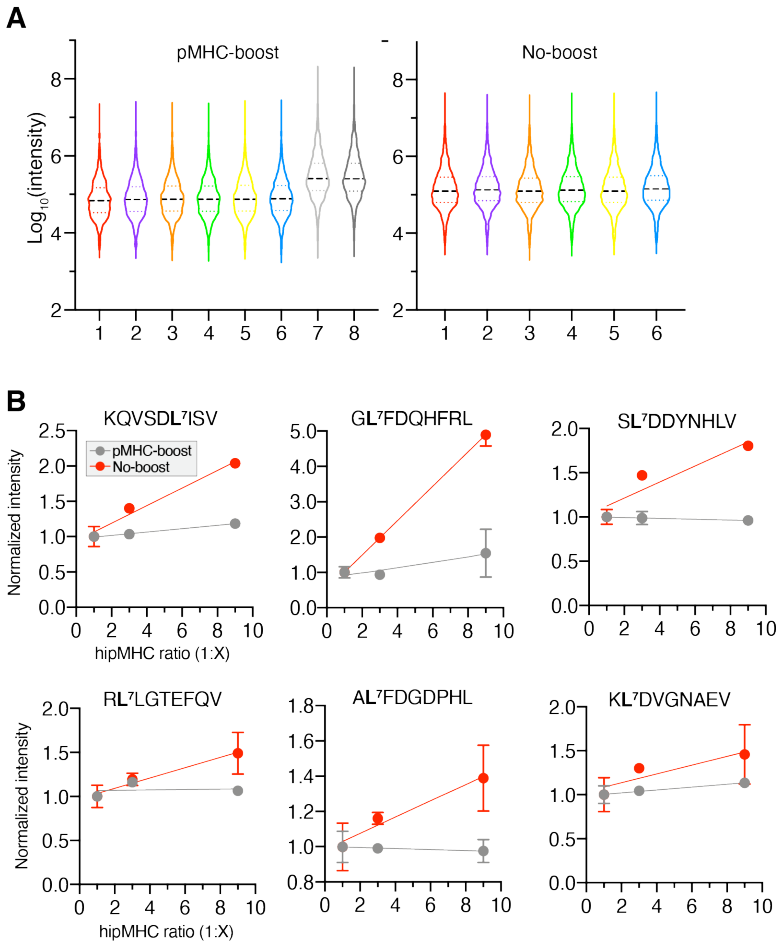

Figure 7-3. *Estimating ion suppression with hipMHCs.* ***A*** *Violin plots of reporter ion intensities for pMHC-boost (left) and no-boost (right) analyses. Median: black dashed line, quartiles: colored dotted line.* ***B*** *Reporter ion intensities of hipMHC peptides normalized to the mean signal of the 1 fmol (pMHC-boost) or 2 fmol (no-boost) samples. Solid line = linear fit, error bars = standard deviation.*

7-2-2 Protein carrier channel skews biological interpretation of palbociclib-induced pMHC repertoire alterations

To assess the accuracy of quantifying endogenous pMHCs in boost compared to non-boost analyses, we evaluated whether the presence of a protein carrier channel would affect data interpretation of melanoma cells treated with the CDK4/6 inhibitor palbociclib, which increases pMHC presentation and induces palbociclib-specific repertoire changes, as previously

described.[188] Cells were treated with DMSO or 10 μM palbociclib for 72h in triplicate, and analyzed alone or with an IFN-γ stimulated protein carrier channel for a combined 20x signal-to-boost ratio, using a similar set-up to the previous experiment (**Figure 7-4-A, Supplementary Figure 7-2**). Similar to the hipMHC experiment, "boosting" with a protein carrier yielded a greater number of unique peptides identified (**Figure 7-4B)**, with similar length distributions (**Figure 7-4-C**).

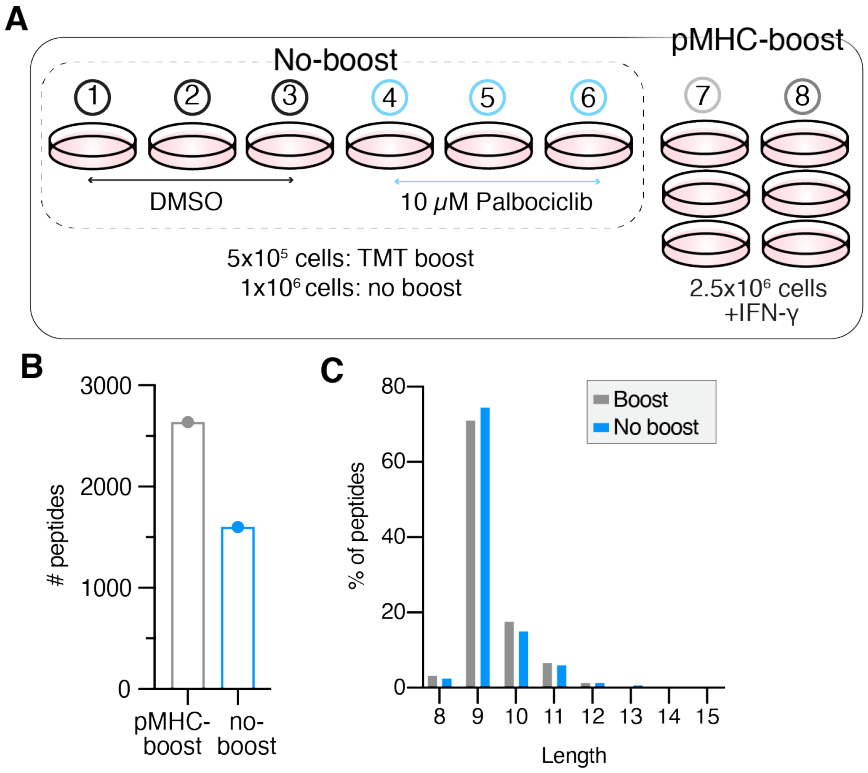

Figure 7-4*. pMHC-boost/no-boost comparison of cells treated with CDK4/6i.* ***A*** *Experimental setup of pMHC analyses +/- protein carrier with 72h DMSO or 10 μM palbociclib treatment.* ***B*** *Number of unique peptides identified in pMHC-boost (2637) and no-boost (1602) analyses.* ***C*** *Length distribution of pMHCs.*

However, while a majority of peptides showed an increase in presentation levels in the no-boost experiment (median fold change 1.17x) consistent with our previously reported results[188] (**Figure 7-5-A, B)**, peptides in the pMHC-boost experiment showed a narrower

distribution of changes, centered around a median fold change of just 1.05x. In line with this finding, principal component analysis showed superior separation of DMSO and palbociclib-treated samples in the no-boost analysis due (**Figure 7-5-C).**

To interrogate the data further, we considered the 1092 unique peptides quantified in both analyses (**Supplementary Figure 7-3-A**). We identified fewer peptides significantly increasing or decreasing in presentation in the boost analysis compared to the no-boost analysis (**Figure 7-5-D**), masking biological interpretation of the data. For example, 334 common peptides significantly increased in presentation in the no-boost analysis, while only 80 peptides in the boost analysis significantly increased. Of the 42 peptides significantly increased in the pMHC-boost analysis but not the no-boost analysis, 76% also showed an increase in expression in the no-boost analysis but did not achieve statiststical significance. The no-boost analysis had higher median coefficients of variation values than the boost analysis (**Supplementary Figure 7-3-B**), as ion suppression reduces variation in reporter-ion intensities, thereby increasing the likelihood of statistical significance. For example, the CSDE1-derived peptide, “KEVQDGIEL,” had an average fold-change of 1.36x in the no-boost analysis and 1.21x in the boost analysis, though the significance values were 0.06 and 0.05, respectively, narrowly missing our selected significance threshold.

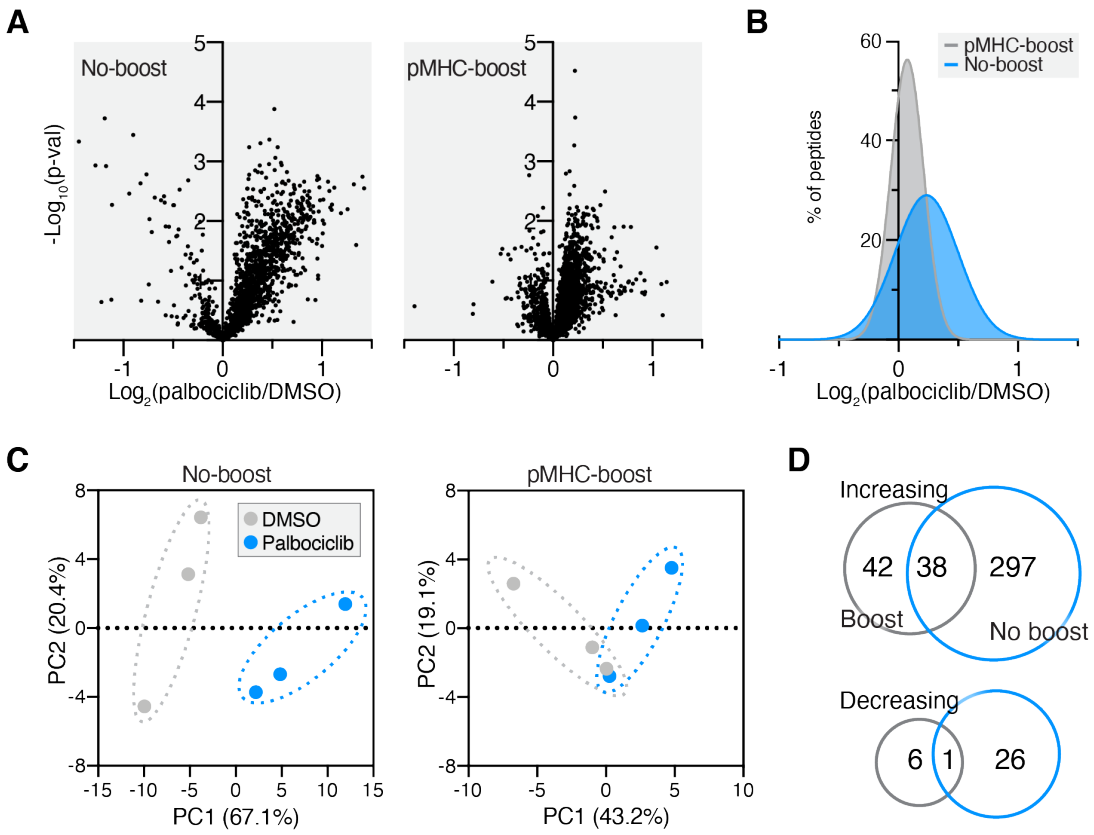

Figure 7-5*. Protein carrier suppresses CDK4/6i-induced pMHC changes.* ***A*** *Volcano plot displaying the log2(palbociclib/DMSO) of pMHCs (x-axis), where the fold change is calculated from the mean intensity of n=3 biological replicates per condition, versus significance (y-axis, mean adjusted p-value, unpaired two-sided t test).* ***B*** *Histogram distribution of unique pMHC fold change in expression.* ***C*** *Samples plotted by principal component 1 (PC1) and PC2 score for no-boost (left) and pMHC-boost (right) analysis, colored by treatment condition. Percentages are % variance explained by the plotted PC.* ***D*** *Venn diagram of peptides significantly increasing (upper) and decreasing (lower) with palbociclib treatment in the no-boost (blue) and pMHC-boost (grey) analyses.*

We next evaluated whether the altered quantitation in the boost analysis would change the previously described key findings of this analysis, namely that peptides derived from pathways known to be perturbed by CDK4/6 inhibition show significant positive enrichment (oxidative phosphorylation, OxPhos) and negative enrichment (G2M checkpoints and E2F targets).[188] To this end, we performed an enrichment analysis in the MSigDB Hallmarks gene

set database by rank ordering the gene names for pMHC source proteins in decreasing order of fold-change.[255,281,282] In the no-boost analysis, 10 μM palbociclib treatment showed significant enrichment in OxPhos, G2M checkpoints, and E2F targets, mirroring previously reported findings (**Figure 7-6-A, B**). None of the three pathways showed significant enrichment using the pMHC-boost dataset data. A comparison of E2F target peptides between the analyses illustrates this finding—most peptides with decreased expression in no-boost showed little change in expression in the presence of a protein carrier. (**Figure 7-6-C**). These data reaffirm that while utilizing a protein carrier channel can increase the number of peptides identified and quantified across samples using lower cellular input, ion suppression due to the presence of a protein carrier alters quantitative dynamics to the extent that known biological findings are masked, hiding relevant insight.

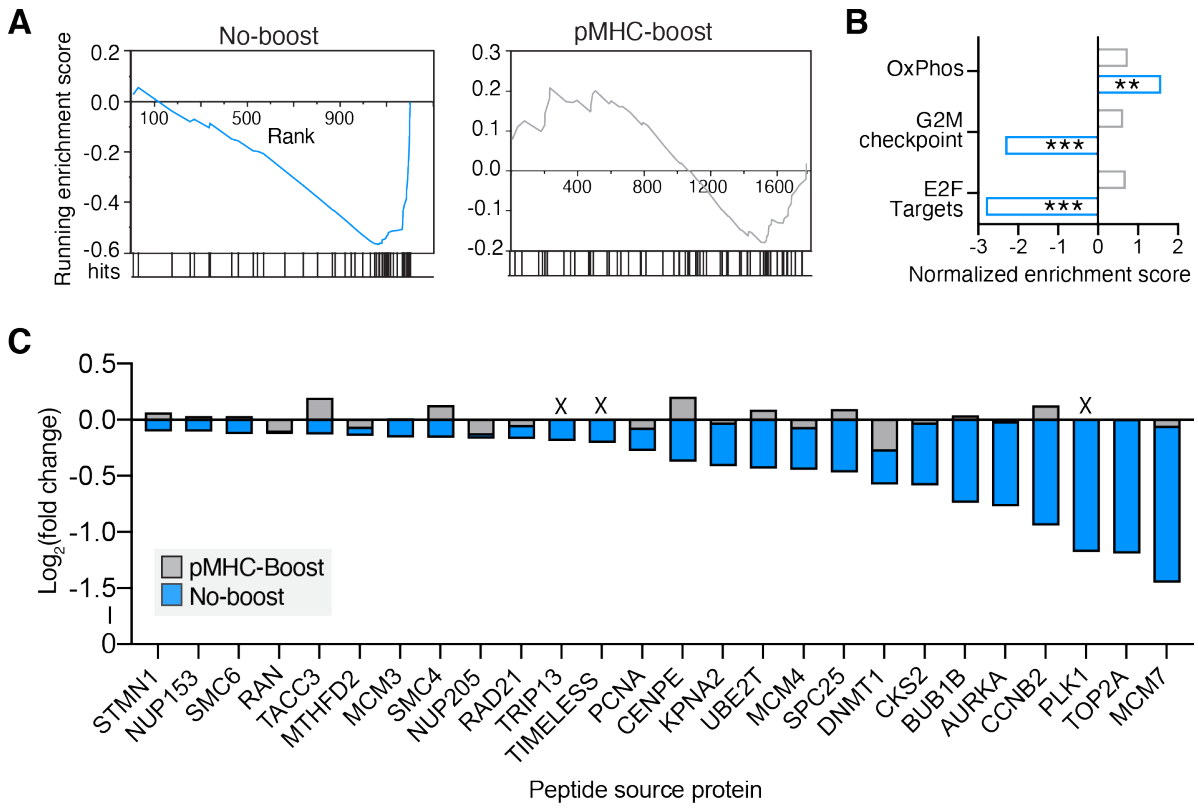

Figure 7-6. *Known pMHC response to CDK4/6i masked by presence of a protein carrier.* ***A*** *pMHC enrichment plots for E2F targets for the no-boost (grey, p=0.13, q=0.88) and pMHC-boost (blue, p<0.001, q<0.001) analyses. Hits mark pMHCs of source proteins mapping to E2F targets.* ***B*** *Normalized enrichment scores from enrichment analyses of pMHC-boost (grey) and no-boost (blue) datasets. Positive/negative scores represent directionality of pathway enrichment. Significant enrichment is noted by **p<0.01, ***p<0.001, with FDR-q values < 0.25.* ***C*** *Change in expression for E2F target pMHCs, plotted by source protein, with palbociclib treatment for the no-boost analysis and corresponding expression levels for the pMHC-boost analysis. X denotes pMHCs which were not quantified in the pMHC-boost analysis.*

7-2-3 Vanadate-treated protein carrier obscures pTyr data due to missing values and isotopic interference

To evaluate whether a protein carrier 'boosting' channel would impact quantitative accuracy in tyrosine phosphorylation analyses, we utilized A549 cells stimulated with 10 nM EGF for 0, 7, 15, 30, or 60 seconds to drive dynamic phosphorylation changes in the EGFR

signaling network.[227] As a protein carrier, A549 cells were incubated with pervanadate (PV) to halt tyrosine phosphatase activity, driving elevated pTyr signal (**Figure 7-7, Supplementary Figure 7-4**). Peptide amounts were selected to match the upper and lower limits of sample input utilized by Chua et al., however we elected to use a lower concentration of pervanadate (30 μM versus 500 μM).[439] Following tryptic digestion & standard sample procesing,100 μg of each EGF-stimulated sample was labeled with TMT, along with 1 mg of PV-treated sample in the "pTyr-boost" analysis. Tyrosine phosphorylated peptides were subsequently purified using two-step enrichment and analyzed by LC-MS/MS.

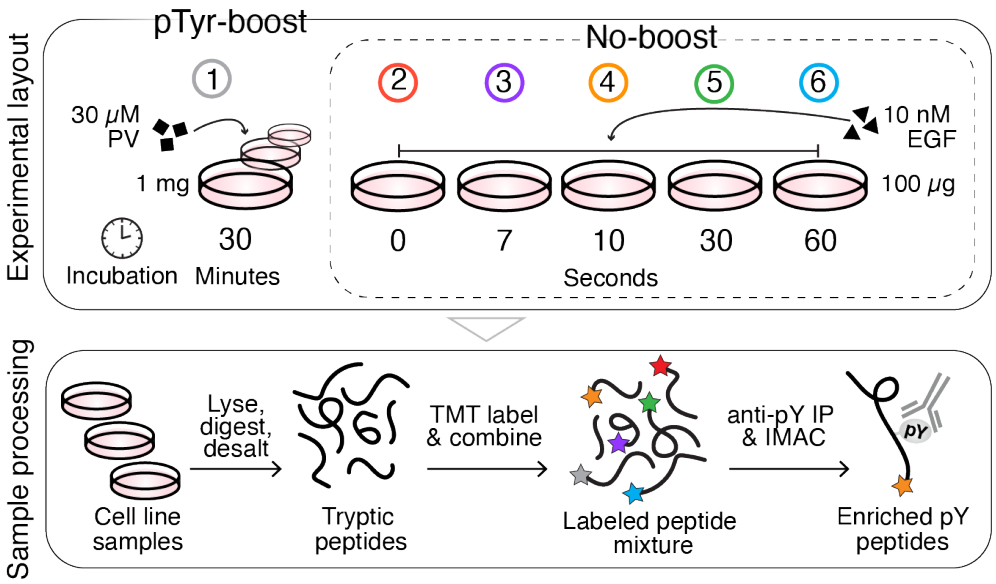

***Figure 7-7**. Schematic of pTyr-boost vs. no-boost experimental layout and pTyr peptide enrichment.*

As expected, signal intensity distributions showed a substantial increase (100-150x) in reporter ion signal for the PV-treated protein carrier sample over the EGF stimulated samples in the pTyr-boost analysis (**Figure 7-8-A**)**,** which is well outside the suggested protein carrier-to-signal range recommended for SCP boost experiments. Still, the pTyr-boost analysis identified a considerably higher number of unique pTyr peptides compared to the no-boost analysis (1831 vs. 328), however a majority of identified peptides were only quantified in the protein carrier channel, resulting in a large number of missing values (MVs) in the EGF-stimulated samples (64-91% of PSMs). Consequently, despite the greater number of overall pTyr-peptide identifications, the pTyr-boost analysis contained just 196 pTyr peptides quantifiable across all samples versus 321 in the no-boost analysis, suggesting inclusion of a protein carrier channel in this experimental setup reduces data quantity (**Figure 7-8-B**).

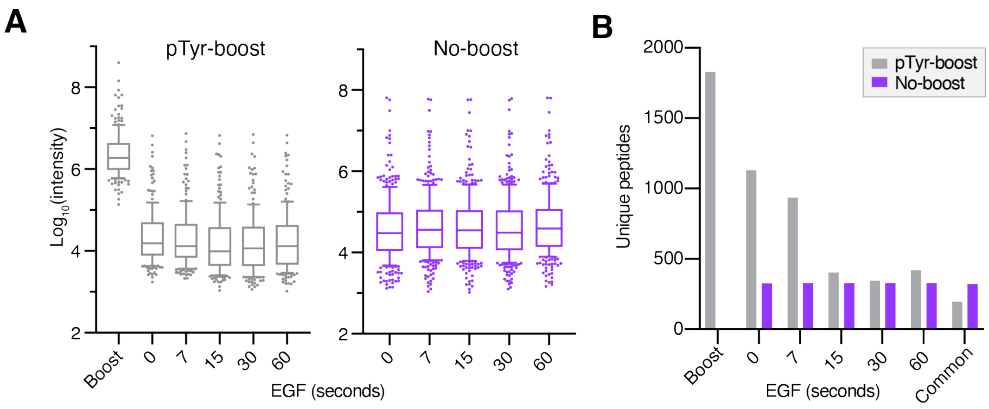

***Figure 7-8**. Protein carrier increases missing values. **A** Reporter ion intensities for pTyr-boost (left) and no-boost (right) analyses. Boxes outline the interquartile range, and whiskers the 10 and 90th percentiles. **B** Number of unique pTyr peptides identified in each sample.*

To assess whether the PV-treated protein carrier channel influenced the accuracy of the quantitative temporal signaling data data, the 98 peptides commonly quantified across both analyses were analyzed by hierarchical clustering, which identified several groups of peptides with distinct patterns of quantitative dynamics (**Figure 7-9**). Peptides in cluster A show increased pTyr with EGF stimulation over the 0 second control in both analyses, and include peptides derived from EGFR and adapter proteins GAB1 and SHC1 (**Figure 7-10**). While pTyr-boost and no-boost peptides have correlated quantitative dynamics there is noticeable ratio compression in the data from the pTyr-boost analysis in all but one of the cluster A peptides (SHC1-pY250, S3C). For example, we measure a 6.5-fold increase in the no-boost pTyr for GAB1-pY627 at 60 seconds following EGF stimulation, which reduces to a 2-fold change when analyzed with a protein carrier. While the same trend of increased phosphorylation with EGF stimulation is preserved between the analyses, subtler pTyr changes may be masked by the effects of ion suppression, as seen in the pMHC analyses.

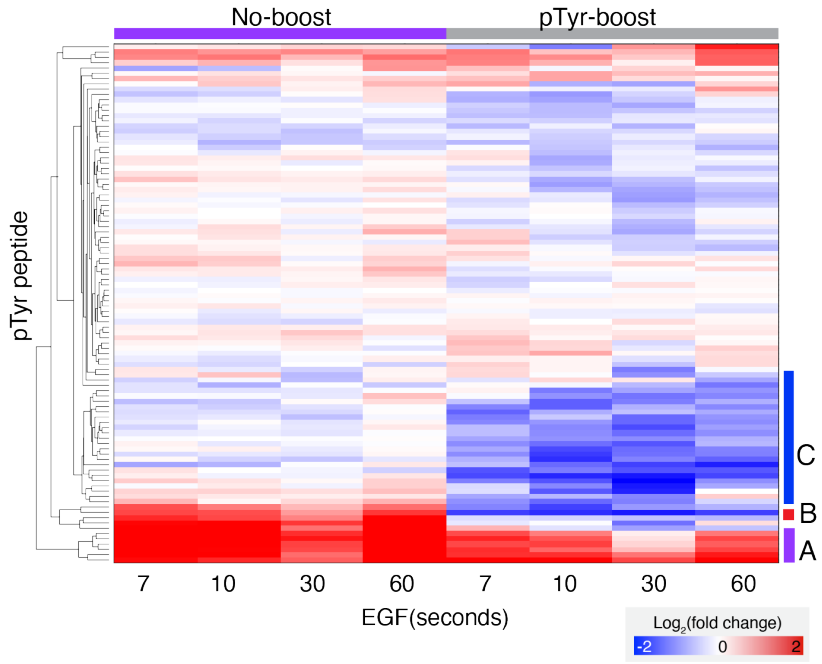

Figure 7-9. *Clustering of pTyr sites across pTyr-boost and no-boost analyses. Hierarchical clustering (Euclidean) of Log_2(fold change) values of pTyr sites identified in both analyses. Values are normalized to the 0 second EGF stimulated sample within each analysis.*

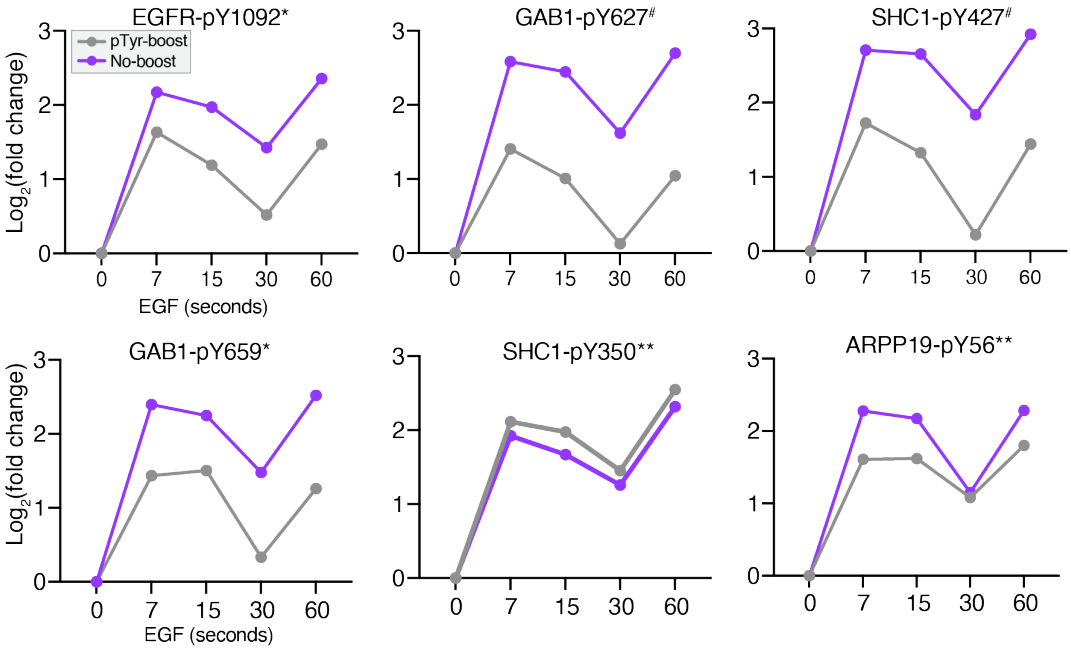

Figure 7-10. *Quantitative dynamics of cluster A peptides. Log_2(fold change) values of peptides in cluster A. Pearson correlation significance (two-tailed): *p<0.05, **p<0.01, #p < 0.1.*

In contrast to cluster A, peptides in cluster B demonstrated inverse phosphorylation trends (**Figure 7-11-A**), and 18 peptides in cluster C showed no change in pTyr in the no-boost analysis, and decreased pTyr in the pTyr-boost analysis (**Figure 7-11-B, C**). These differences in quantitation are particularly concerning and would likely alter biological interpretation of the dataset. We suspected the decrease in pTyr signal relative to the 0 second control in the pTyr-boost analysis may be a result of increased 0 second signal from isotopic interference of the protein carrier.

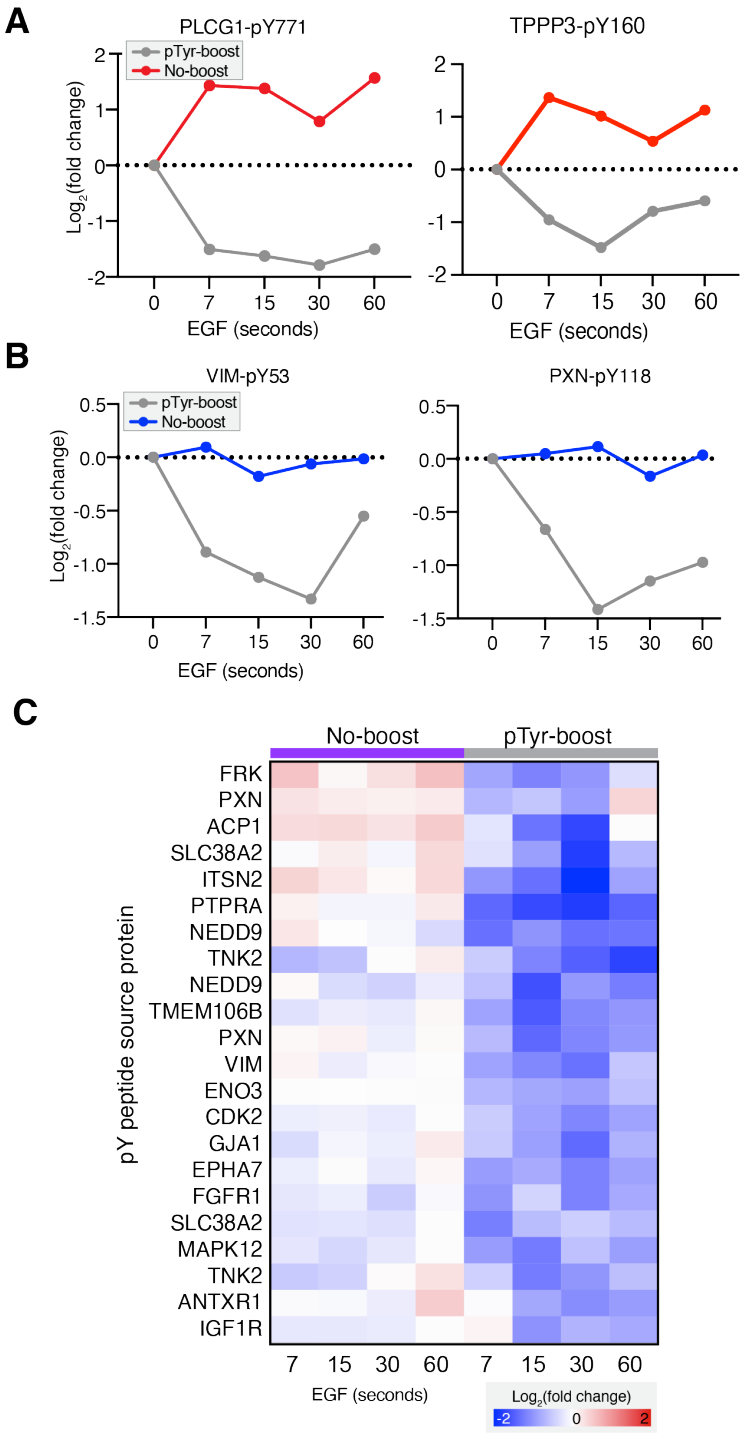

Figure 7-11. *Quantitative dynamics in cluster B/C peptides.* ***A-B*** *Log_2(fold change) values of peptides in cluster B (A) and cluster C (B).* ***C*** *Heatmap of Log_2(fold change) values in cluster C.*

Indeed, the 0 and 7 second EGF stimulated samples, located in the closest channel positions to the PV sample, had 1.4x and 1.3x higher mean reporter ion intensities than the 15, 30, and 60 second samples in the TMT-boost analysis, a trend that was not reflected in the no-boost analysis (**Figure 7-8-A**). We also observed the number of quantified peptides in 0 and 7 second samples were increased compared to the other samples**,** whereas the number of quantifiable peptides in the no-boost analysis were similar between samples, again suggestive of isotope interference from the protein carrier channel. Data reported by Chua et al. follow a similar trend: the two samples closest in position to the PV-treated protein carrier had an increased number of identifiable peptides versus a third replicate sample further away. To reduce the effects of isotopic leakage, we included empty channels in between the protein carrier and EGF stimulated samples (**Supplementary Figure 7-5**). While this strategy mitigated isotopic interference, it also decreased the number of TMT tags available for sample multiplexing, diminishing the throughput and utility of this approach (**Figure 7-12-A**). Furthermore, a large percentage of MVs and dynamic range suppression were still observed with this setup, suggesting that a boost-to-signal ratio of this magnitude may adversely affect the quantitative accuracy of the experiment, regardless of isotopic leakage (**Figure 7-12-B**).

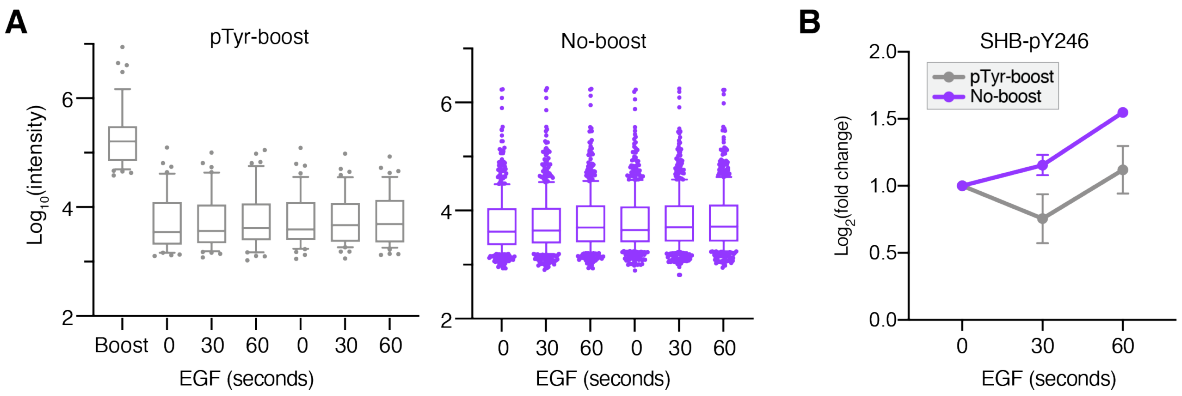

Figure 7-12. *Empty channels adjacent to protein carrier still yields high MVs.* ***A*** *Reporter ion intensities for pTyr-boost (left) and no-boost (right) analyses. Boxes outline the interquartile range, and whiskers the 10th and 90th percentiles.* ***B*** *Log_2(fold change) of pTyr levels in SHB-pY246; data is normalized to the 0 second control.*

7-2-4 Reduction in boost:signal ratio improves quantitative accuracy, still results in MVs

To evaluate whether a smaller carrier proteome would result in better quantitative accuracy and fewer MVs, we performed a 10-plex analysis consisting of 3 replicates of A549 cells were stimulated with 5 nM EGF for 0, 0.5, or 2 minutes (**Figure 7-13, Supplementary Figure 7-6**). One hundred μg of each sample was labeled with TMT along with a 900 μg protein carrier consisting of equal parts of each non-protein carrier sample in the pTyr-boost analysis for a boost-to-signal ratio of approximately 9x. This experimental setup should enhance detection of EGFR-mediated signaling, since the boosting protein carrier consists of EGF-stimulated samples.

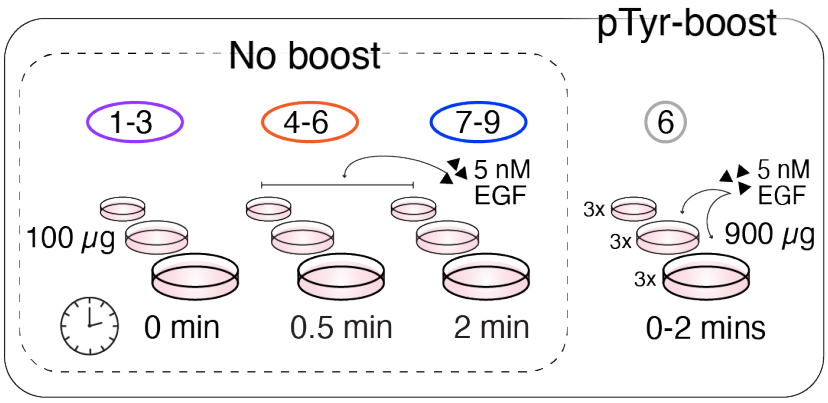

Figure 7-13. *Experimental layout of pTyr-boost and no-boost experiments with 9x protein carrier.*

Intensity distributions for each of the 9 EGF stimulated samples were similar in the boost and the no-boost analyses (**Figure 7-14-A**), while the protein carrier had a mean intensity 7.5-9x higher than the non-protein carrier samples near the expected ratio. In contrast to the results of the palbociclib-treated pMHC analysis, replicates in the boost experiment had higher median coefficients of variation (17-19%) than the no-boost analysis (10-12%), suggesting presence of the protein carrier decreases quantitative accuracy, possibly due to reduced ion sampling of the non-protein carrier samples, as previously described (**Figure 7-14-B**).[441]

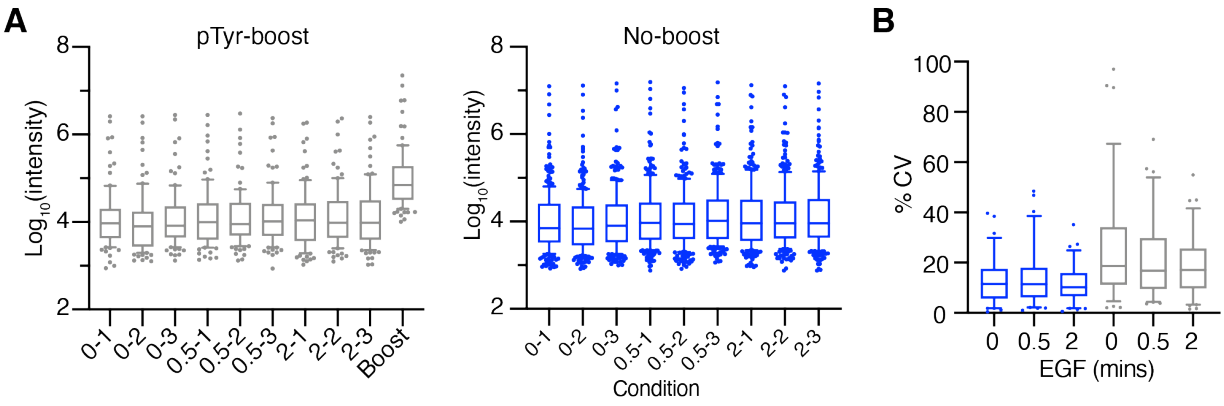

Figure 7-14. *Reporter ion intensities for 9x boost analysis. **A** Reporter ion intensities for no-boost (blue) and pTyr-boost (grey) analysis. Boxes outline the interquartile range, and whiskers the 10 and 90th percentiles. B Coefficients of variation of pTyr-boost (grey) and no-boost (blue) analyses. Boxes outline*

the interquartile range, and whiskers the 5 and 95th percentiles. pTyr-boost median CV: 10-12%, no-boost: 17-19%.

Similar to the PV-stimulated protein carrier pTyr analysis, there were more MVs when a protein carrier was included (35-59% of PSMs) (**Figure 7-15-A**). Despite this improvement, a greater number of pTyr peptides were quantifiable in the no-boost analysis versus the pTyr-boost analysis (282 vs. 91), suggesting the inclusion of a protein carrier still negatively affects data quantity in this context (**Figure 7-15-B**). Hierarchical clustering of the 79 peptides quantified in both analyses identified two clusters of peptides where pTyr levels increased or decreased with EGF stimulation over the 0-minute control (**Figure 7-16, Supplementary Figure 7-7-A, B**). While the quantitation of just three peptides in cluster A are significantly correlated ($p<0.05$), all cluster A/B peptides show comparable pTyr trends and with less ratio compression than the PV-stimulated pTyr-boost experiment (**Figure 7-17**).

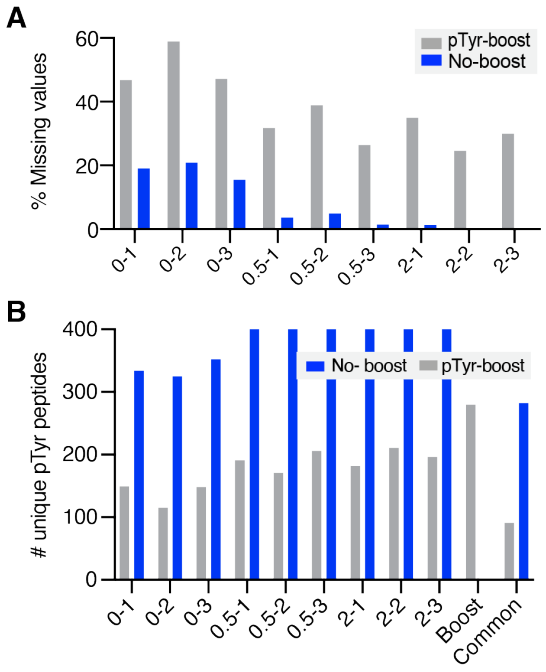

Figure 7-15. *Missing values in 9x boost analysis.* ***A*** *Percentage of total PSMs with missing values in each sample.* ***B*** *Number of unique, quantifiable pTyr peptides identified in each condition/analysis.*

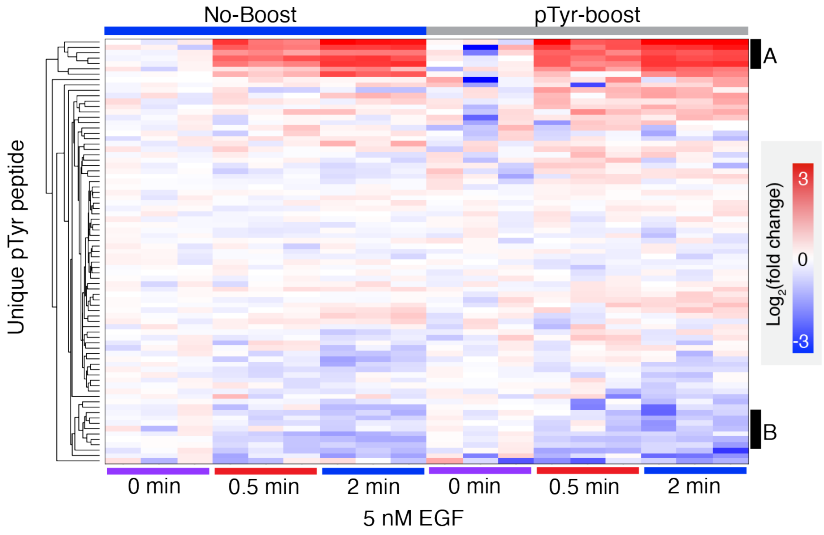

Figure 7-16. *Hierarchical clustering of peptides identified in both analyses, represented as log2(fold change) of each sample normalized to the mean reporter ion intensity of the 0-minute control.*

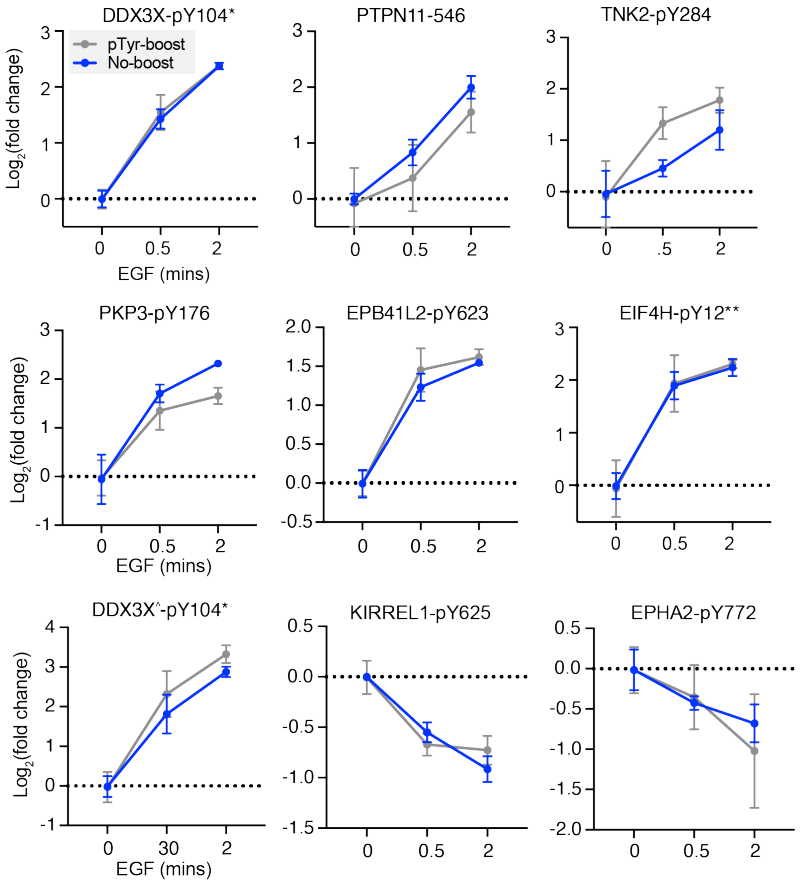

Figure 7-17*. Dynamics of select peptides in 9x boost and no-boost pTyr analyses. Log₂(fold change) of pTyr signal in selected peptides. Error bars represent +/- standard deviation. Pearson correlation significance (two-tailed): *p<0.05.*

Beyond the peptides identified in these clusters, we looked to see how many peptides had significant changes in pTyr at the 2-minute timepoint. Twenty-seven peptides in the no-boost analysis were significant versus 17 in pTyr-boost (**Figure 7-18-A**). Of the peptides that were not significant in the boost analysis, there was evidence of dynamic range suppression and altered quantitative dynamics (**Figure 7-18-B**) highlighting that not all peptides had comparable quantitation between the boost and no-boost analyses. In line with this observation, PCA revealed superior separation of the three treatment conditions in the no-boost analysis (**Figure 7-18-C**). Still, some separation was observed in the pTyr-boost analysis, suggesting

that a lower protein carrier-to-signal ratio offers some improvement in quantitative accuracy. Still, dynamic range suppression and large numbers of missing values were still observed, resulting in inferior data quantity and quality with the inclusion of a protein carrier.

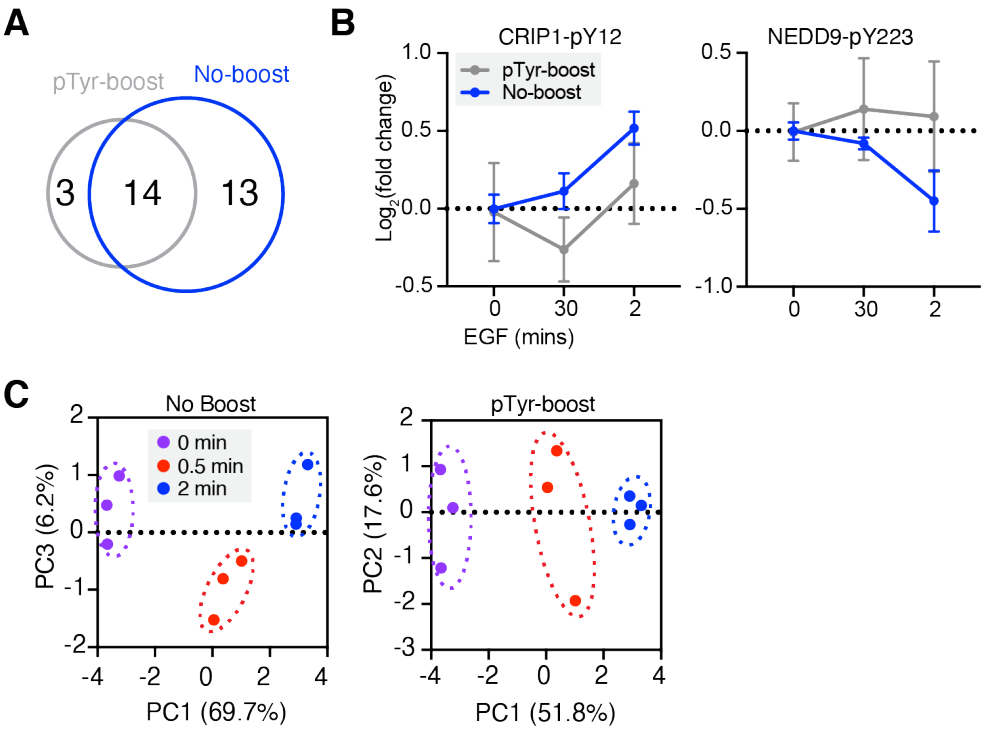

***Figure 7-18**. Dynamic range suppression with 9x protein carrier. **A** Venn diagram of peptides significantly increased or decreased with 2-minute EGF stimulation over the 0-minute control. **B** Log_2(fold change) of pTyr signal in selected peptides. Error bars represent +/- standard deviation. Pearson correlation significance (two-tailed): *p<0.05. **C** Samples plotted ted by principal component 1 (PC1) and PC2 score for no-boost analysis (left) and PC1 vs. PC3 for pTyr-boost analysis, colored by EGF stimulation condition. Percentages are % variance explained by the plotted PC. Alternate PCs are plotted in **Supplementary Figure 7-8**.*

7-3 Discussion

While the ability to reduce sample input and/or increase signal with a protein carrier is particularly appealing in immunopeptidomics and tyrosine phosphoproteomics, two applications

that are often limited by larger sample requirements, several critical limitations in MS^2-based analyses exist. First, despite selecting a signal-to-boost ratio within SCP guidelines (20x,[441] pMHC analyses suffered from high ratio compression, which masked dynamic alterations in pMHC expression levels and obscured known biological finding. Triple-stage mass spectrometry (MS^3) and/or high-field asymmetric waveform ion mobility spectrometry (FAIMS) has been shown to reduce ratio distortion, though this can come at a cost of sensitivity and data quantity.[154,443] Additional experiments, similar in format to those described here, will be useful in determining whether MS^3 can offer improved quantitative accuracy without compromising data quantity in this setting. To enable such comparisons, hipMHCs provide a useful tool to evaluate ion suppression in place of exogenously added peptide standards. Ratio compression was similarly observed in pTyr analyses and was adversely impacted by increased signal in the protein carrier channel. However, MS^3 is an unattractive solution due to its lower precision and fewer peptide identifications in phosphoproteomic applications compared to MS^2.[132]

Additionally, pTyr analyses specifically suffered from high numbers of MVs in protein carrier experiments, regardless of the boost-to-signal ratio. Chua et al. also observed high MVs, but interpolated reporter ion intensities using expected ratio construction, a strategy that is not applicable for analyzing biological systems where the quantitative dynamics are unknown. Increasing the AGC target or maximum ion injection time (IT) to increase the non-protein carrier ion count may reduce MVs, but 65% of PSMs with two or more missing values already reach the maximum IT (350 ms) at the current AGC target ($1e^5$), suggesting a significant increase in IT may be required for improvement. In turn, increasing IT and AGC targets will likely reduce the number of scans acquired and thus the number of identified peptides, though the balance between data quantity and data quality remains to be thoroughly explored in this application. Alternatively, decreasing the number of multiplexed samples would increase ions sampling of non-carrier samples, but limited multiplexing further reduces the utility of the assay.

These data illustrate that experiments leveraging protein carriers to generate quantitative data should rigorously evaluate the quantitative impact of the protein carrier (namely ion suppression, missing values, coefficients of variation, and isotope leakage) to avoid misinterpretation of biological data. Future studies exploring alternative instrument acquisition parameters and configurations will further illuminate whether protein carriers can be effectively used for quantitative studies in these applications, or whether improvements in sample preparation and instrument sensitivity may pave an alternative path forward in achieving high accuracy, high precision measurements without a signal boost.

7-4 Materials and Methods

7-4-1 Cell lines

SKMEL5 and A549 cell lines were obtained from ATCC [ATCC HTB-70 and CCL-185, respectively). Cells were maintained in DMEM medium (SKMEL5, Corning) and RPMI-1640 (Gibco, A549) supplemented with 10% FBS (Gibco) and 1% penicillin/streptomycin (Gibco). Cells were routinely tested for mycoplasma contamination, and maintained in 37°C, 5% CO_2. Experiments were performed on passages 4-8.

7-4-2 UV-mediated peptide exchange for hipMHCs

UV-mediated peptide exchange was performed using recombinant, biotinylated Flex-T HLA-A*02:01 monomers (BioLegend), using a modified version of the commercial protocol as previously described.[188] Concentration of stable complexes following peptide exchange was quantified using the Flex-T HLA class I ELISA assay (BioLegend) as per the manufacturer's

instructions. ELISA results were acquired using a Tecan plate reader Infinite 200 with Tecan icontrol version 1.7.1.12.

7-4-3 Synthetic peptide standards

Heavy leucine-containing peptides were synthesized at the MIT Biopolymers and Proteomics Lab using standard Fmoc chemistry using an Intavis model MultiPep peptide synthesizer with HATU activation and 5 μmol chemistry cycles. Starting resin used was Fmoc-Amide Resin (Applied Biosystems). Cleavage from resin and simultaneous amino acid side chain deprotection was accomplished using: trifluoroacetic acid (81.5% v/v); phenol (5% v/v); water (5% v/v); thioanisole (5% v/v); 1,2-ethanedithiol (2.5% v/v); 1% triisopropylsilane for 1.5 hr. Fmoc-Leu ($^{13}C_6$, ^{15}N) was obtained from Cambridge Isotope Laboratories, and standard Fmoc amino acids were from NovaBiochem.

Peptides were subjected to quality controlled by mass spectrometry and reverse phase chromatography using a Bruker MiroFlex MALDI-TOF and Agilent model 1100 HPLC system with a Vydac C18 column [300 angstrom, 5 micron, 2.1 x 150 mm] at 300 μL/min monitoring at 210 and 280 nm with a trifluoroacetic acid/ H_2O/MeCN mobile phase survey gradient.

7-4-4 Peptide MHC isolation & TMT labeling

Cells were seeded in 10 cm plates and treated the following day for 72 hours with DMSO control, palbociclib (Selleckchem, PD-0332991), 10 ng mL^{-1} human recombinant IFN-γ (ProSpec Bio). During harvest, cells were washed with 1x PBS, and lifted with 0.05% Trypsin-EDTA (Gibco). Cells were pelleted, washed with 1x PBS, pelleted again, and resuspended in lysis buffer [20 nM Tris-HCl pH 8.0, 150 mM NaCl, 0.2 mM PMSF, 1% CHAPS, and 1x HALT Protease/Phosphatase Inhibitor Cocktail (Thermo Fisher)], followed by brief sonication to disrupt

cell membranes. Lysate was cleared by centrifugation and quantified using bicinchoninic acid protein assay kit (Pierce).

Peptide MHCs were isolated by immunoprecipitation (IP), using 0.1 mg of pan-specific anti-human MHC Class I (HLA-A, HLA-B, HLA-C) antibody (clone W6/32, Bio X Cell [cat # BE0079]) per $1e^6$ cells, which was bound to 10 µL FastFlow Protein A Sepharose bead slurry (GE Healthcare) per $1e^6$ cells for 3 hours rotating at 4°C. Beads were washed 2x with IP buffer (20 nM Tris-HCl pH 8.0, 150 mM NaCl), after which lysate/hipMHCs were added and incubated rotating overnight at 4°C. Beads were washed with 1x TBS and water, and pMHCs were eluted in 10% formic acid for 20 minutes at room temperature (RT). Peptides were isolated from antibody and MHC molecules using a passivated 10K molecule weight cutoff filters (PALL Life Science), lyophilized, and stored at -80°C prior to TMT labeling.

To label pMHCs, 50 µg of pre-aliquoted Tandem Mass Tag 6-plex (TMT-6, Thermo Scientific) was resuspended in 30 µL anhydrous acetonitrile, and lyophilized peptides were resuspended in 100 µL 150 mM triethylammonium bicarbonate, 50% ethanol. TMT/peptide mixtures were incubated on a shaker for 1 hour at RT, followed by 15 minutes of vacuum centrifugation. Samples were next combined and centrifuged to dryness. Sample cleanup was performed using solid-pot solid-phase enhanced sample preparation (SP3) as previously described. After combining labeled samples, we washed tubes 2x with 25% acetonitrile (MeCN) in 0.1% acetic acid (AcOH) and added it to the labeled mixture, which was subsequently centrifuged to dryness. Sample cleanup was subsequently performed using single-pot solid-phase-enhanced sample preparation (SP3), as previously described.[188,290]

7-4-5 pTyr sample preparation

A549 cells were seeded in 10 cm plates and serum depleted for 72 hours prior to analysis. In EGF stimulation experiments, cells were stimulated with 5 or 10 nM EGF

(PeproTech), flash frozen in liquid nitrogen, and lysed in 8M urea. Pervanadate treated cells were incubated for 30 minutes with 30 μM pervanadate at 37°C and were subsequently washed 1X with ice cold 1X PBS and lysed in 8M urea.

Lysates were cleared by centrifugation at 5000 g for 5 min at 4°C and protein concentration was measured by bicinchoninic acid assay (BCA) (Pierce). Proteins were reduced with 10 mM dithiothreitol for 30 min at 56°C, alkylated with 55 mM iodoacetamide for 45 min at room temperature (RT) protected from light, and diluted 4-fold with 100 mM ammonium acetate, pH 8.9. Proteins were digested with sequencing grade modified trypsin (Promega) at an enzyme to substrate ratio of 1:50 overnight at RT. Enzymatic activity was quenched by acidifying with glacial acetic acid to 10% of the final solution volume, and peptides were desalted using C18 solid phase extraction cartridges (Sep-Pak Plus Short, Waters). Peptides were eluted with aqueous 60% acetonitrile in 0.1% acetic acid and dried using vacuum centrifugation. Protein concentration was again measured by BCA to account for variation in sample processing, and peptides were subsequently lyophilized.

Lyophilized peptides were labeled with TMT-10plex in ~35 mM HEPES and ~30% acetonitrile at pH 8.5 for 1 hour at room temperature. 100 ug aliquots utilized 400 μg TMT, 900 μg-1 mg aliquots used 1600 μg TMT. Labeling reactions were quenched with 0.3% of hydroxylamine, and samples were pooled, dried in vacuum centrifugation, and stored at -80°C prior to analysis.

Labeled peptide aliquots were resuspended in 400 µL of immunoprecipitation (IP) buffer [100 mM Tris-HCl, 0.3% NP-40, pH 7.4] and incubated with 60 µL protein G agarose bead slurry (Calbiochem) conjugated to an antibody cocktail containing 12 µg 4G10 (Millipore), 12 µg PT66 (Sigma) and 6 µg of pY100 (Cell Signaling Technologies), rotating overnight at 4°C. Beads were washed 1x with IP buffer, 3x with 100 mM Tri-HCl, pH 7.4, and eluted in 2 rounds of 25 µL 0.2%

TFA. Phosphopeptides were further enriched using High-Select Fe-NTA Phosphopeptide Enrichment Kit (Thermo Scientific) following manufacturer's instructions with minor adjustments. Modifications include reducing the peptide volume initially added to the Fe-NTA column (50 µL) and reducing the elution volume to 2 rounds of 20 µL elutions. Peptide elutions were dried down using vacuum centrifugation to <2 µL total volume and resuspended in 5% acetonitrile in 0.1% formic acid for a total volume of 10 µL.

7-4-6 MHC MS data acquisition

pMHC samples were analyzed using an Orbitrap Exploris 480 mass spectrometer (Thermo Scientific) coupled with an UltiMate 3000 RSLC Nano LC system (Dionex), Nanospray Flex ion source (Thermo Scientific), and column oven heater (Sonation). Samples were resuspended in 0.1% formic acid and directly loaded onto a 10-15 cm analytical capillary chromatography column with an integrated electrospray tip (~1 µm orifice), prepared and packed in house (50 µm ID × 20 cm & 1.9 µM C18 beads, ReproSil-Pur). Twenty-five percent of pMHC elutions were injected for each analysis. Peptides were eluted using a gradient with 8-25% buffer B (70% Acetonitrile, 0.1% formic acid) for 50 minutes, 25-35% for 25 minutes, 35-55% for 5 minutes, 55-100% for 2 minutes, hold for 1 minutes, and 100% to 3% for 2 minutes.

Standard mass spectrometry parameters were as follows: spray voltage, 2.0 kV; no sheath or auxiliary gas flow; heated capillary temperature, 275 °C. The Exploris was operated in data dependent acquisition (DDA) mode. Full scan mass spectra (350-1200 m/z, 60,000 resolution) were detected in the orbitrap analyzer after accumulation of $3e^6$ ions (normalized AGC target of 300%) or 25 ms. For every full scan, MS^2 were collected during a 3 second cycle time. Ions were isolated (0.4 m/z isolation width) for a maximum of 150 ms or 75% AGC target and fragmented by higher energy collision dissociation (HCD) with 32% normalized collision

energy (nCE) at a resolution of 45,000. Charge states < 2 and > 4 were excluded, and precursors were excluded from selection for 30 seconds if fragmented n=2 times within 20 second window.

7-4-7 pTyr MS data acquisition

LC-MS/MS analysis of pTyr peptides were performed on an Agilent 1260 liquid chromatography (LC) system coupled to a Q Exactive HF-X Hybrid Quadrupole-Orbitrap mass spectrometer (Thermo Fisher). Peptides were resuspended in 10 µL 0.1% acetic acid and onto an analytical capillary column with an integrated electrospray tip (~1 µm orifice) prepared in house ((50 µm ID × 12 cm with 5 µm C18 beads (YMC gel, ODS-AQ, 12 nm, S-5 µm, AQ12S05)). Peptides were eluted using a 140-minute gradient with 13-42% buffer B (70% Acetonitrile, 0.2M acetic acid) from 10-105 minutes and 42-60% buffer B from 105-115 minutes, 60-100% B from 115-122 minutes, and 100-0% B from 128-130 minutes at a flow rate of 0.2 mL/min for a flow split of approximately 10,000:1.

Standard mass spectrometry parameters were as follows: spray voltage, 2.5 kV; no sheath or auxiliary gas flow; heated capillary temperature, 250°C. The mass spectrometer was operated in data-dependent acquisition with following settings for MS1 scans: m/z range: 350-2000; resolution: 60,000; AGC target: $3e^6$; maximum injection time (max IT): 50 ms. The top 15 abundant ions were isolated (0.4 m/z) and fragmented by HCD with resolution: 60,000; AGC target: $1e^5$, max IT: 350 ms; nCE: 32%. Unassigned and charge states <+2 and >+6 were excluded, and dynamic exclusion was set to 20 seconds.

Crude peptide analysis was performed on a Q Exactive Plus hybrid quadropole-orbitrap mass spectrometer coupled to an Agilent 1260 LC system to correct for variation in peptide loadings across TMT channels using 2.5 kV no sheath or auxiliary gas flow; heated capillary temperature, 250°C. Approximately 30 ng of the supernatant from pTyr IP was loaded onto an

in-house packed precolumn (100 um ID x 10 cm) packed with 10 µm C18 beads (YMC gel, ODS-A, AA12S11) connected in series to an analytical column (as previously described) and analyzed with a 75 min LC gradient [0-30% B from 0-40 minutes, 30-60% B from 40-50 minutes, 60-100% B from 50-55 minutes, and 100-0% B from 60-65 minutes]. MS1 scans were performed with m/z range: 350-2000; resolution: 70,000; AGC target: $3e^6$; max IT: 50 ms. The top 10 abundant ions were isolated (isolation width 0.4 m/z) and fragmented (nCE = 33%) with 70,000 resolution, max IT 150 ms, AGC target $1e^5$. Unassigned, +1, and >+7 charge states were excluded, and dynamic exclusion was set to 30 seconds.

7-4-8 MHC MS search space and filtering

All mass spectra were analyzed with Proteome Discoverer (PD, version 2.5) and searched using Mascot (version 2.4) against the human SwissProt database. No enzyme was used, variable modifications were set to include oxidized methionine, static modifications included N-terminal and lysine TMT.

Heavy leucine-containing peptides were searched for separately with heavy leucine (+7), c-terminal amidation, and methionine oxidation as dynamic modifications against a custom database of the synthetic peptide standards. All analyses were filtered with the following criteria: search engine rank =1, isolation interference ≤ 30%, and length between 8 and 15 amino acids, ion score ≥ 15 and percolator q-value ≤ 0.05.

Reporter ion intensities of PSMs assigned to the same peptide sequence were summed, and reporter ion intensities were corrected using hipMHC intensity values (CDK4/6i analysis only) as previously described.[188] To evaluate differences between conditions, the $\log_2$ transformed ratio of arithmetic mean intensity for drug- and DMSO-treated samples (n=3) was

calculated. To determine if peptides were significantly increasing, an unpaired, 2-sided t-test was performed, and peptides with $p \leq 0.05$ were considered significantly increasing/decreasing.

7-4-9 pTyr MS search space and filtering

All mass spectra were analyzed with Proteome Discoverer (PD, version 2.5) and searched using Mascot (version 2.4) against the human SwissProt database. For pTyr analyses, Spectra were searched using the following parameters: enzyme: trypsin, maximum missed cleavages: 2, precursor mass tolerance: 10 ppm, fragment mass tolerance: 20 mmu. Static modifications included TMT-10-labeled lysine and N-terminal residues, as well as cysteine carbamidomethylation. Dynamic modifications included methionine oxidation, and tyrosine, serine, and threonine phosphorylation. Peptides were filtered with the following criteria: search engine rank =1, isolation interference ≤ 35%, ion score ≥ 20, and ≥1 tyrosine phosphorylated residue.

Crude peptide mixture was searched with the following parameters: enzyme: trypsin, maximum missed cleavages: 2, precursor mass tolerance: 10 ppm, fragment mass tolerance: 20 mmu. Static modifications included TMT-10-labeled lysine and N-terminal residues, as well as cysteine carbamidomethylation. Dynamic modifications included methionine oxidation. Peptides were filtered with the following criteria: search engine rank =1, ion score ≥ 20.

Peptide spectrum matches (PSMs) with phosphorylated tyrosine residues and no reporter ion missing values were filtered according to search engine rank = 1, ion score ≥ 20. Reporter ion intensities were summed across matching PSMs. Phosphotyrosine peptide reporter ion areas were corrected for variations in sample loading within each analysis using the median of peptide ratios in the crude peptide analysis for each channel relative to channel.

Quantitation is represented as the fold change between the mean reporter ion signal of the 0 second samples and the 30s/2m samples. PCA analysis was performed using Matlab R2019b.

7-4-10 Peptide MHC binding affinity

Binding affinity of pMHCs was estimated using NetMHCpan-4.0 against the allelic profile of SKMEL5 cells.[99,280] Only 9-mers were evaluated, and the minimum predicted affinity (nM) of each peptide was used to assign peptides to their best predicted allele. The threshold for binding was set to 500 nM.

7-4-11 Enrichment analyses

For pMHC pathway enrichment analyses, gene names from peptide source proteins were extracted and rank ordered according to the average $\log_2$ fold change over DMSO treated cells. In cases where more than one peptide mapped to the same source protein, the maximum/minimum was chosen, depending on the directionality of enrichment analysis. We utilized gene set enrichment analysis (GSEA) 4.0.3 pre-ranked tool against the Molecular Signatures Database hallmarks gene sets with 1000 permutations, weighted enrichment statistic (p=1), and a minimum gene size of 15 for pMHC analyses.[255,281,282] Results were filtered for FDR q-value ≤ 0.25, and nominal p-value ≤ 0.05.

7-5 Acknowledgements

Thank you to Jason Conage-Pough for collaborating on this project and for performing analysis and data interpretation for the pTyr-boost experiments. This research was supported in part by NIH grants R01EB027717, U54CA210180, and U01CA238720, as well as funding from MIT Center for Precision Cancer Medicine.

7-6 Supplementary Information

A

TMT label	Cell # No-boost	Cell # pMHC-boost	hipMHC (fmol) No-boost	hipMHC (fmol) pMHC-boost
126	$1e^6$	$5e^5$	2	1
127N	$1e^6$	X	2	X
127C	X	$5e^5$	X	1
128N	X	$5e^5$	X	3
128C	$1e^6$	X	6	X
129N	$1e^6$	$5e^5$	6	3
129C	X	$5e^5$	X	9
130N	X	$5e^5$	X	9
130C	$1e^6$	$2.5e^6$ + IFN-γ	18	30
131	$1e^6$	$2.5e^6$ + IFN-γ	18	30

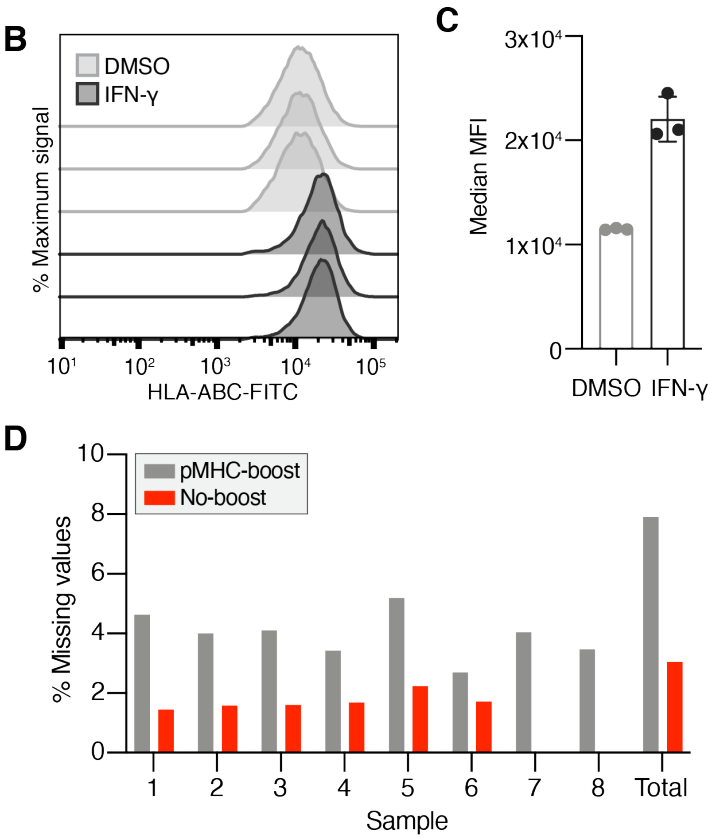

Supplementary Figure 7-1. ***A*** *Experimental setup of isobaric labels, cell number, and concentration of hipMHC added for each sample.* ***B*** *Flow cytometry analysis of surface HLA expression in SKMEL5 cells after 72h of DMSO or IFN-g treatment. Data are presented as % of maximum fluorescence intensity signal. N=3 biological replicates per treatment condition.* ***C*** *Median MFI of flow cytometry measurements in B. Error bars represent standard deviation from n=3 biological replicates.* ***D*** *Percentage of total PSMs with missing values in each sample.*

TMT label	Cell #		Condition	
	No boost	Boost	No boost	Boost
126	$1e^6$	$5e^5$	DMSO1	DMSO1
127N	$1e^6$	X	DMSO2	X
127C	X	$5e^5$	X	DMSO2
128N	X	$5e^5$	X	DMSO3
128C	$1e^6$	X	DMSO3	X
129N	$1e^6$	$5e^5$	Palbo1	Palbo1
129C	X	$5e^5$	X	Palbo2
130N	X	$5e^5$	X	Palbo3
130C	$1e^6$	$2.5e^6$ + IFN-γ	Palbo2	Boost1
131	$1e^6$	$2.5e^6$ + IFN-γ	Palbo3	Boost2

Supplementary Figure 7-2. *Experimental setup of isobaric labels, cell number, and treatment conditions.*

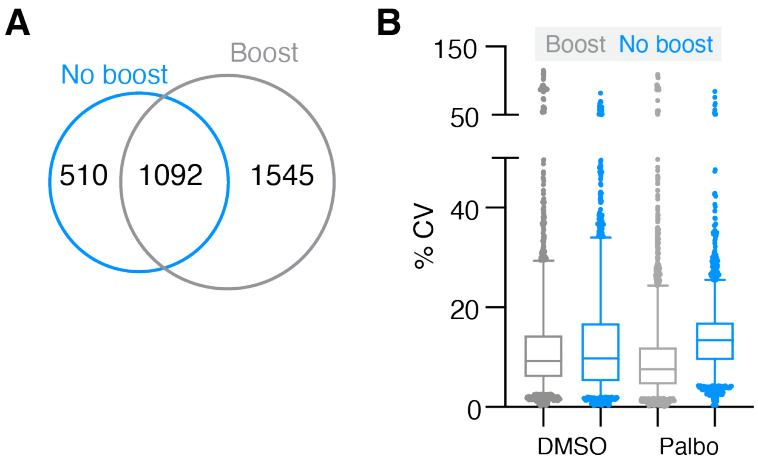

Supplementary Figure 7-3. ***A*** *Venn diagram of unique pMHC identified in the no-boost (blue) and pMHC-boost (grey) analysis.* ***B*** *Coefficients of variation of pMHC-boost and no-boost analyses. Boxes outline the interquartile range, and whiskers the 5 and 95th percentiles. pMHC-boost median CV: DMSO= 9.27%, palbociclib: 7.56%, no-boost DMSO = 9.72%, palbociclib = 13.39%.*

TMT label	Condition	
	No-boost	pTyr-boost
126	X	PV-boost
127	0 sec	0 sec
128	7 sec	7 sec
129	15 sec	15 sec
130	30 sec	30 sec
131	60 sec	60 sec

Supplementary Figure 7-4. *Experimental setup of isobaric labels and treatment conditions.*

TMT label	Condition	
	No-boost	pTyr-boost
126	X	PV-boost
127N	X	X
127C	X	X
128N	X	X
128C	0 sec	0 sec
129N	30 sec	30 sec
129C	60 sec	60 sec
130N	0 sec	0 sec
130C	30 sec	30 sec
131	60 sec	60 sec

Supplementary Figure 7-5*. Experimental setup of isobaric labels and treatment conditions.*

TMT label	Condition	
	No-boost	pTyr-boost
126	0-1	0-1
127N	0-2	0-2
127C	0-3	0-3
128N	0.5-1	0.5-1
128C	0.5-2	0.5-2
129N	0.5-3	0.5-3
129C	2-1	2-1
130N	2-2	2-2
130C	2-3	2-3
131	X	Boost

Supplementary Figure 7-6*. Experimental setup of isobaric labels and treatment conditions.*

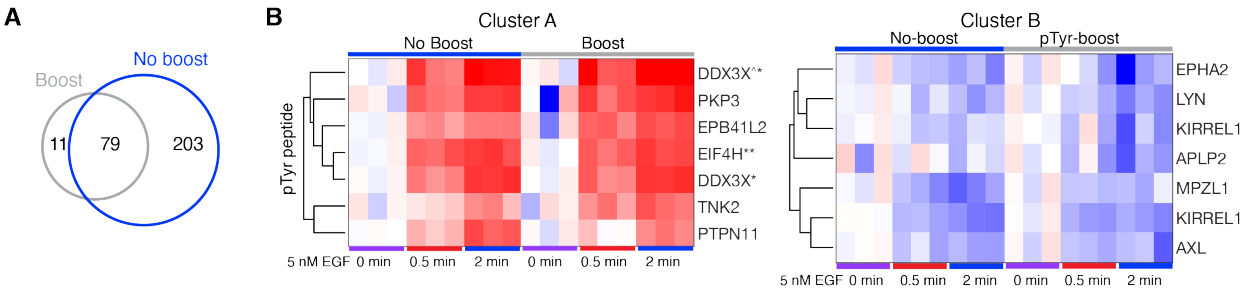

Supplementary Figure 7-7. A *Venn diagram of unique pTyr peptides in each analysis.* ***B*** *Clustergram of peptides in cluster A and B in Figure 4E. ^ denotes peptide miscleavage.*

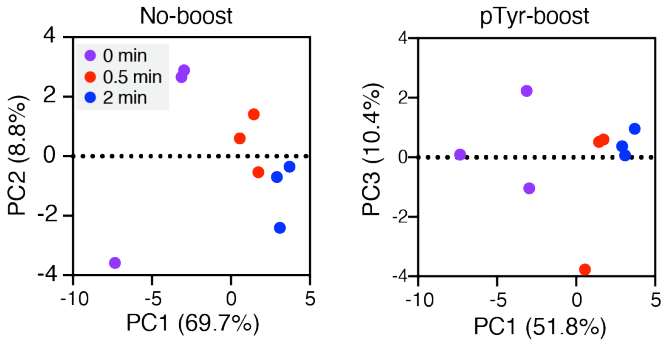

Supplementary Figure 7-8. *Samples plotted by principal component 1 (PC1) and PC2 score for no-boost analysis (left) and PC1 vs. PC3 for pTyr-boost analysis, colored by EGF stimulation condition. Percentages are % variance explained by the plotted PC.*

CHAPTER 8: Tumor-derived pMHCs cross presented by dendritic cells show bias in cellular compartment of source proteins

8-1 Dendritic cell cross presented peptides

As of late, the most successful immunotherapies rely on blocking co-inhibitory receptors like CTLA-4 and PD-1, “releasing the breaks” on the anti-tumor immune response and allowing for CD8+ T cell proliferation, activation, and killing of tumor cells.[444] However, T cell activity relies on efficient priming by professional antigen presenting cells such as dendritic cells (DCs).[445,446] DCs provide a link between the innate and adaptive immune system (**Figure 8-1**). In the tumor microenvironment, DCs ingest, process, and present peptide antigens on MHC-I and II molecules to adaptive immune cells.[447,448] Upon pMHC recognition by a naïve T-cell, assisted by costimulatory molecules, DCs can prime T cells to induce an immune response against tumor or infected cell types.[449] As a result, there is a great interest in understanding how to modulate DC function in cancer to improve the anti-tumor immune response.[450]

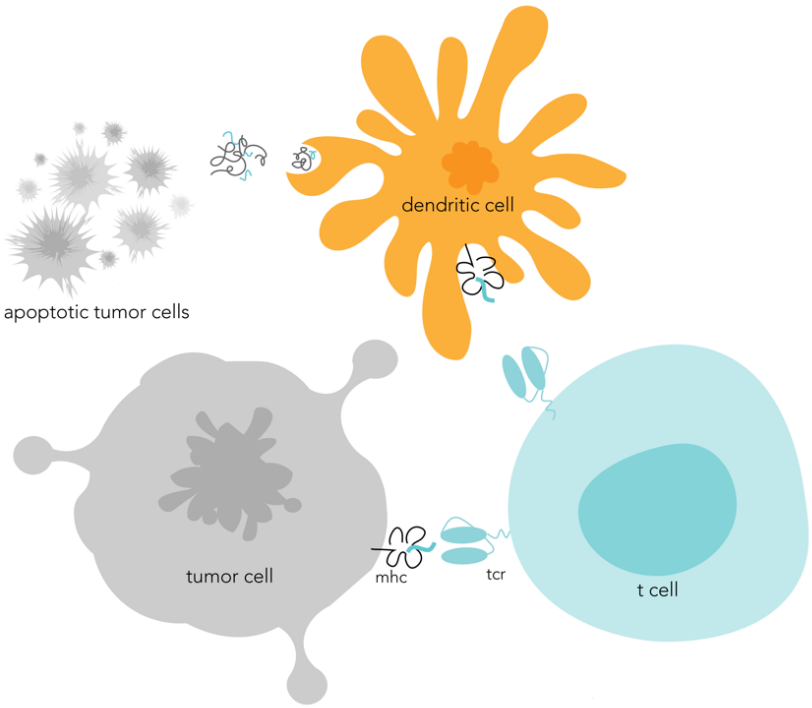

Figure 8-1. *Schematic of dendritic cells and their role in anti-tumor immunity.*

The molecular mechanisms of DC professing and presentation have been elucidated, however DCs utilize a variety of strategies for peptide cross presentation that differ in terms of peptide digestion and loading, peptide recognition, retention time in endolysosomes prior to processing, and more.[448,451–453] As a consequence, it is probably that cross-presented pMHC repertoire by DCs are biased in the sub-cellular compartments they sample. However, it remains poorly understood which peptides of apoptotic tumor material are cross presented and where they are derived from.[454] To date, only a single MS-based analysis has been performed to investigate cross-presented peptides, and their findings were focused solely on class II peptides and on validating prediction algorithms rather than improving the anti-tumor immune response.[60]

To this end, we began a collaboration with Stefani Spranger and Tim Fessenden to investigate cross presentation with the goal of understanding whether there is bias in the cellular

compartments cross-presented peptides are derived from. The experimental setup developed by Spranger and Fessenden relies on irradiated mouse B16F10 melanoma cells and dendritic cells. Unfortunately, traditional immunopeptidomics methods cannot distinguish between endogenous pMHCs and pMHCs derived from engulfed tumor material.

SILAC labeling one of the cell types provides an apart solution. However, unlike standard tryptic peptide-based proteomics experiments where lysine (K) and arginine (R) residues can be labeled, MHC peptides are non-tryptic and H-2K^{b}/H-2D^{b} mouse molecules do not contain K/R anchor residues. As a result, we developed a custom SILAC labeling scheme to explore tumor cell/DC cross presentation *in vitro (***Figure 8-2***)*.

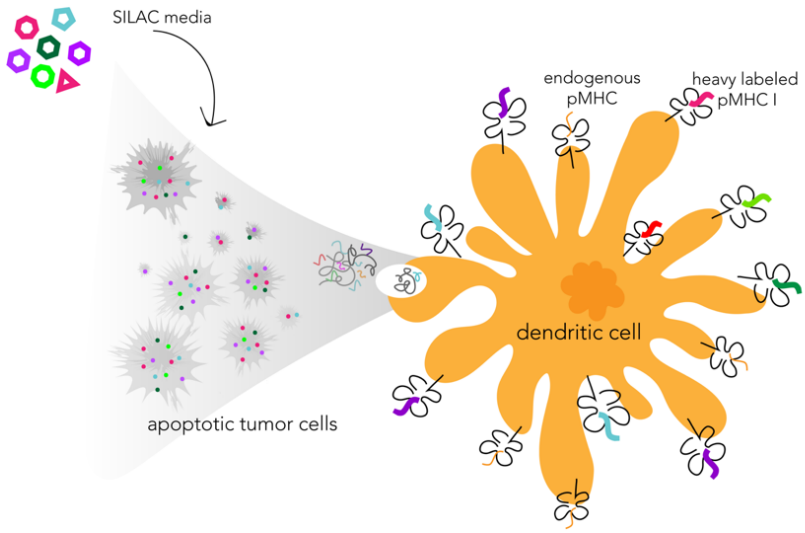

Figure 8-2*. Schematic of SILAC-labeled peptides cross presented on DCs.*

8-2 Results

8-2-1 Custom SILAC labeling scheme for H-2D^{b}/K^{b} pMHCs

To select which amino acids to heavy label, we analyzed previously generated data on MC38 cells[169], a mouse C57/BL6 colon adenocarcinoma- derived *in vitro* cell line which contains

the same allelic profile as B16F10 cells. We looked at which amino acids had the highest representation among pMHCs and found that 77% of H-2K^b/H-2D^b peptides contain leucine (L), followed by ~40% asparagine (N), and 46/36% for phenylalanine/tyrosine (F/Y) (**Figure 8-3-A**). If all four amino acids are labeled, our data estimates 98% of pMHCs will contain at least one heavy label (**Figure 8-3-B)**. Importantly, of the 10 pMHCs identified in MC38 cells that do not contain at least 1 of the four selected amino acids for SILAC labeling, 90% are not predicted to be a binder of H-2K^b/H-2Db.

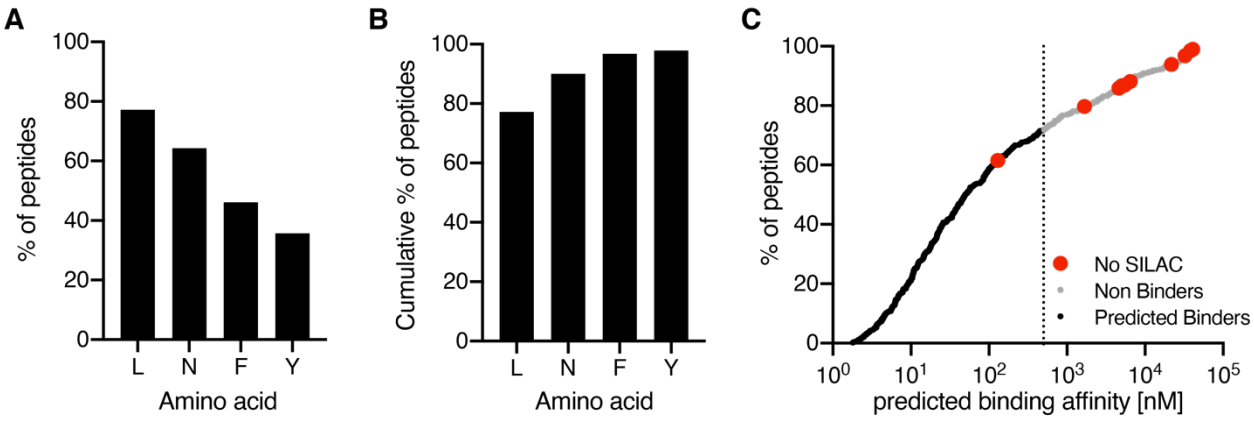

Figure 8-3*. Amino acid distribution in H-2K^b/H-2D^b pMHCs.* ***A*** *Fraction of peptides in MC38 analysis with each amino acid.* ***B*** *Cumulative fraction of peptides containing the labeled amino acid plus amino acids to the left. Ex. N = peptides with N and/or L.*

The amino acids selected for labeling align with published peptide motifs and anchor residues for these alleles: the fifth amino acid position in H-2K^b peptides shows a preference for F/Y, whereas the fifth position in H-2D^b show an enrichment for N (**Figure 8-4**). Both alleles have an enrichment for L as the last amino acid, which is consistent with L having the highest representation among pMHCs in our datasets.[455]

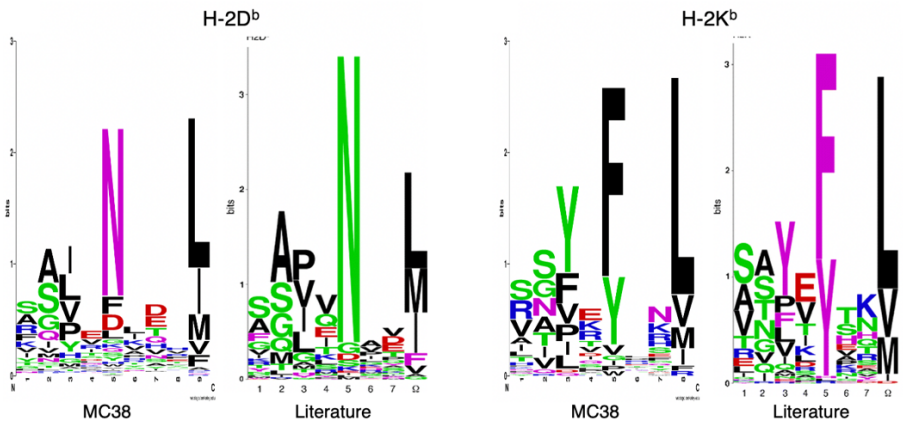

***Figure 8-4**. Sequence motifs of H-2 alleles in mice.*

8-2-2 IP antibody influences pMHC data quantity and quality

Critical to the success of this work, we discovered that the selection of antibody used for immunoprecipitation greatly influences the quality and quantity of pMHCs isolated. A pan mouse anti-H-2 antibody, documented to bind all H-2 haplotypes, pulled down a fraction (137) of peptides from IFN-γ stimulated B16F10 cells compared to using a combination of H-2Db/H-2Kb specific antibodies, which yielded 274 unique peptides (**Figure 8-5-A**). Of the total number of peptides isolated, only 50% were of the correct length (8-12 amino acids) in the pan H-2 analysis versus 72% in the allele-specific analysis (**Figure 8-5-B**). Importantly, allele-specific antibodies yielded peptides that matched known sequence motifs of D^b/K^b peptides, whereas the pan H-2 antibody did not show motif-specific enrichment (**Figure 8-5-C**). These results suggest that while using the pan-specific antibody is less expensive, its poor specificity requires the use of the allele-specific antibodies for high quality pMHC identifications.

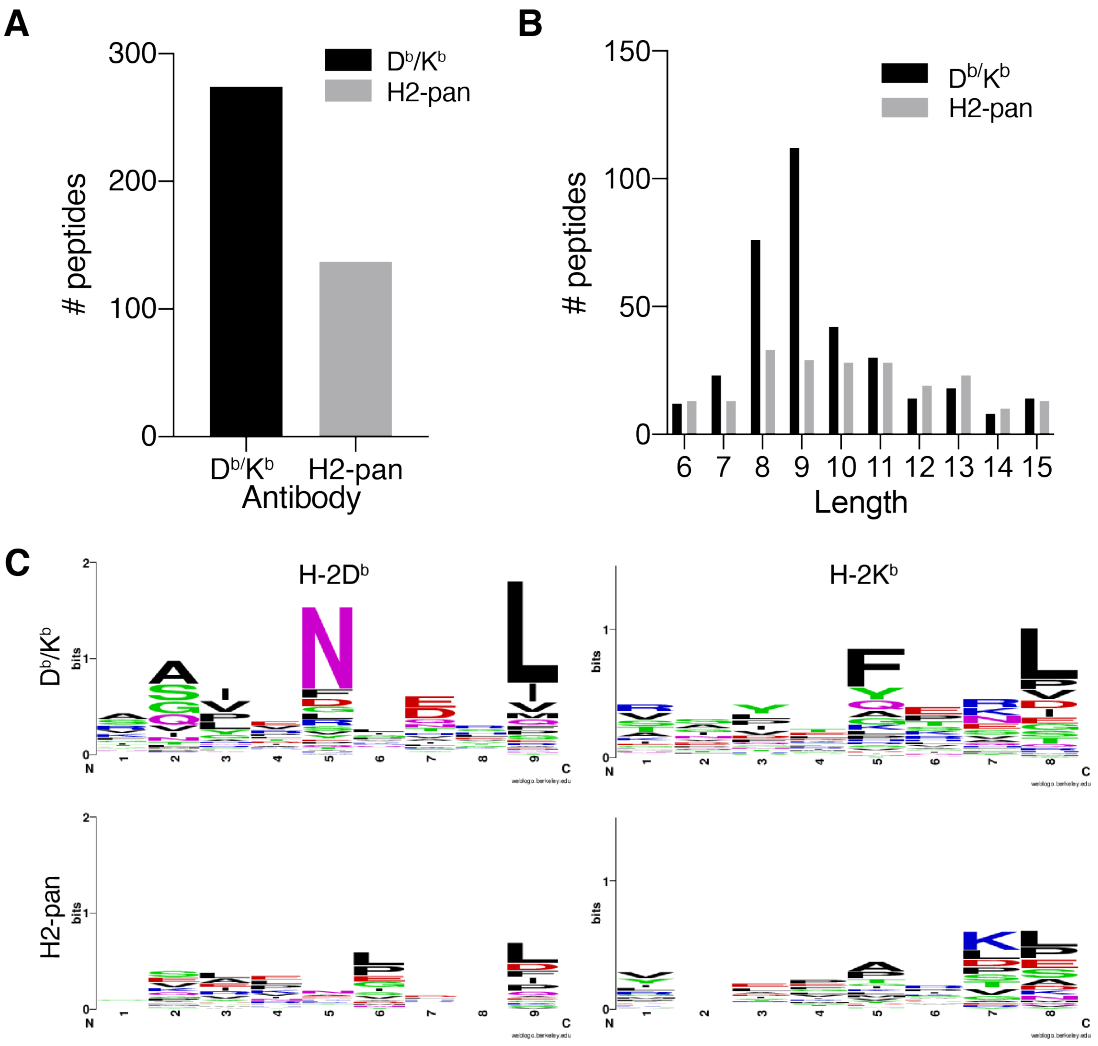

Figure 8-5*. Antibody comparison for IP of H-2D^b/K^b peptides.* ***A*** *Number of unique peptides identified.* ***B*** *Length distribution of pMHCs identified.* ***C*** *Weblogos of 8 and 9-mer peptides.*

8-2-3 Validation of cross presentation experimental workflow

To verify that we could detect cross-presented peptides by LC-MS/MS, we first utilized a B16F10 melanoma cell line engineered to present the SIY peptide, “SIYRYYGL,” which B16F10 cells and the DCs do not endogenously present. A LC-MS/MS analysis of B16-SIY cells demonstrated that the SIY peptide had the second highest abundance of all peptides present, with a tumor associated antigen peptides derived from DCT (gp100) having comparable intensity (**Figure 8-6-A**). Next, B16-SIY expressing cells were irradiated and incubated with

dendritic cells, after which class I pMHCs were isolated and analyzed by LC-MS/MS. Of the pMHCs on DCs, the SIY peptide was identified and was similarly one of the most abundant pMHCs presented (**Figure 8-6-B**), validating that cross presented peptides can be identified using this experimental platform.

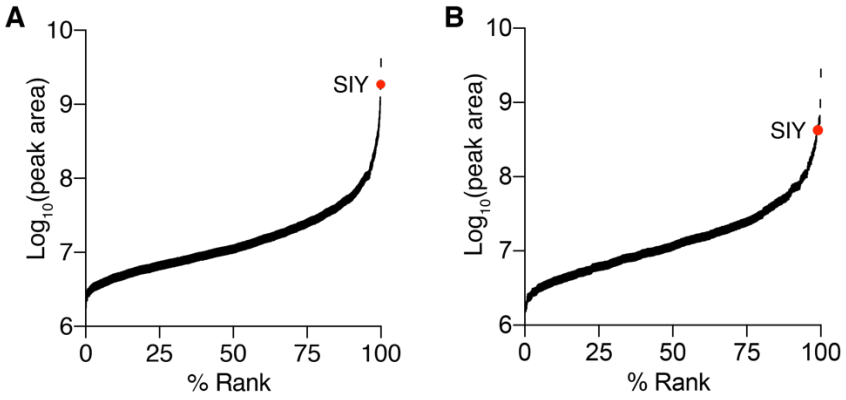

***Figure 8-6**. SIY pMHC abundance in B16F10 and DC cells. **A** pMHCs rank ordered by abundance (integrated precursor ion area for **A** B16F10 cells and **B** cross-presented/endogenous pMHCs on dendritic cells. The SIY peptide is highlighted in red, with a ranked abundance of 99.97% in B16F10 cells and 99.04% in DCs.*

8-2-4 Tumor-derived cross-presented peptides on DCs

To identify cross presented peptides, we first labeled B16F10 melanoma cells in the custom SILAC labeling media for ~6+ population doublings to reach near 100% SILAC incorporation. We tested SILAC incorporation by performing a tryptic digest of SILAC cells, and found that Y, F, N, and L amino acids were 98%, 99%, 91%, and 98% SILAC labeled, respectively. Labeled B16F10 cells were then irradiated and incubated with DCs, after which class I pMHCs were isolated by immunoprecipitation and purified with size exclusion filtration. We also analyzed the endogenous pMHCs presented by B16F10 cells.

B16F10 cells yielded 396 unique pMHCs, and DCs yielded 194 SILAC labeled pMHCs and 192 non-SILAC labeled pMHCs. Of the SILAC labeled "cross presented" peptides, only 10 were identified endogenously on B16 cells (**Table 8-1**). Furthermore, only 22 were predicted to be high affinity binders (< 2% rank) (

Peptide	Gene
FAPVNVTTEVK	EEF1A1
SAPENAVRM	GRCC10
ITQTLSDM	DNAH1
GGIQNVGHI	IMPDH2
VAGGAGLAVPG	PKD2
PEAPPPALPAGA	RYR1
YNIVGLRSN	MCCC1
GEPLQAAAS	F8A1
PMMVTKQENI	CDH13
NFASHAIVEDNV	PIGO

Table 8-2). Three of these high affinity binders are common to both B16 cells and cross-presented DCs, derived from EEG1A1, GRCC10 and IMPDH2.

To ensure that we were not isolating pMHCs from B16F10 cells, a separate experiment was performed where SILAC-labeled B2M knockout B16F10 cells were incubated with DCs, and pMHCs subsequently isolated. Without B2M, B16F10 cells cannot endogenous present pMHCs on the cell surface. The results yielded a 459 non-labeled pMHCs and 563 SILAC labeled, "cross-presented" peptides, 15 of which were predicted to be high affinity binders (**Table 8-3**). Two peptides were common to the high affinity binders in the initial cross-presentation analysis, including EEF1A1-derived peptide, "FAPVNVTTEVK," and VAT1-derived peptide, "RTVENVTVF."

8-2-5 Cytosolic peptides enriched amongst cross-presented repertoire

We next investigated whether the source proteins for cross-presented peptides were enriched amongst any cellular compartments. This analysis was led by Tim Fessenden, who found that peptides derived from cytosolic proteins were overrepresented amongst cross presented peptides, present at 60% (**Figure 8-7-A, B**). This is much higher than the fraction present in the endogenous repertoires of B16F10 and DC cells, where ~35% of peptides were derived from cytosolic proteins. A similar trend was observed on the B2M KO cells, though to a lesser extent (**Figure 8-7-C**). Intriguingly, Abelin et al. investigated cross presentation of peptides on DCs in human samples and found mitochondria and heat shock-derived peptides to be overrepresented, which are in disagreement with our *in vitro* mouse results.[60]

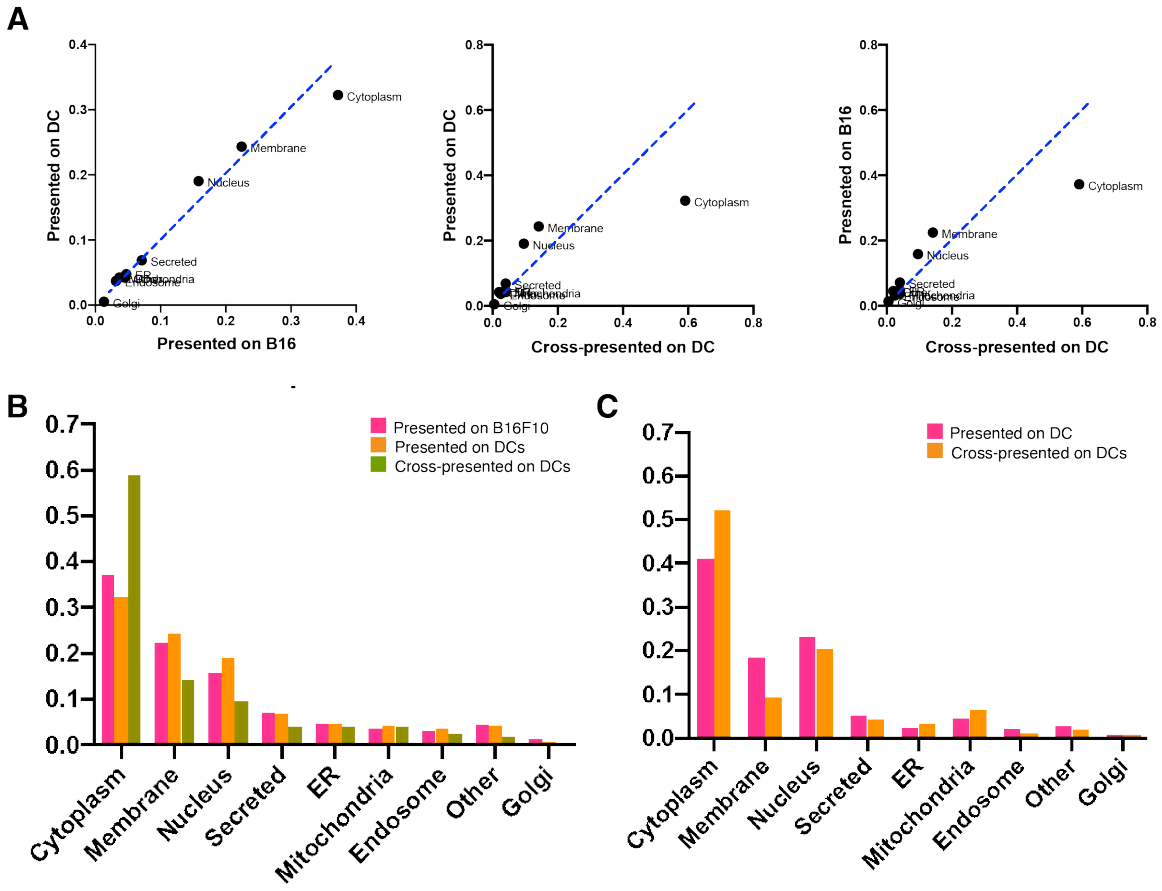

Figure 8-7*. Fraction of peptides derived from each cellular compartment (**A-C**). **A** Blue line represents a slope of 1, representing a 1:1 relationship between plotted conditions. **B** B2M B16F10 cells, **C**, B2M KO B16F10 cells. Image and analyses curtesy of T. Fessenden.*

8-3 Discussion

While the number of SILAC-labeled, cross presented peptides is relatively high, representing nearly 50% of all DC-presented peptides in both the B2M KO and wild-type analysis, very few of these peptides are predicted be high affinity binders. In fact, a lower proportion of peptides identified on DCs are predicted to be binders in comparison to B16F10 cells (**Figure 8-8**).

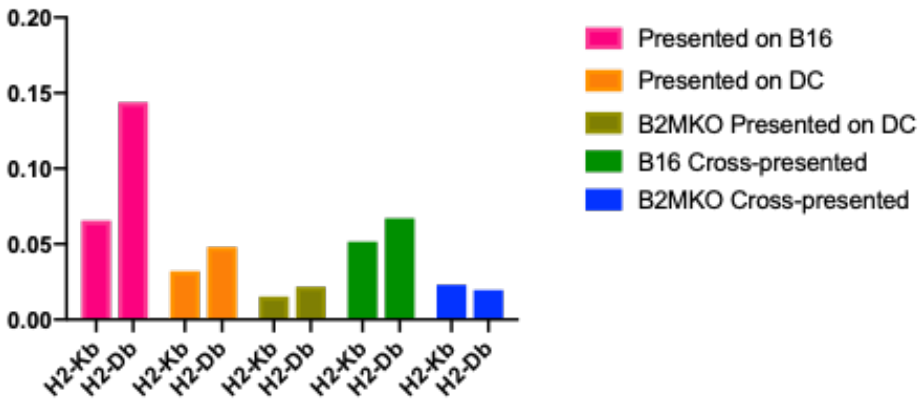

***Figure 8-8**. Fraction of pMHCs predicted to bind to D^b/K^b alleles from each analysis. Image and analysis curtesy of T. Fessenden.*

It is possible that the prediction algorithms generally perform poorly for these alleles, however this seems unlikely as pMHCs isolated MC38 cells showed ~60% of peptides were predicted to be high affinity binders. Still, this is lower than our analyses of well-studied human alleles, where binding affinity predictions for humans approach 95% or higher. One explanation may be that the prediction algorithms in panNetMHC are trained on datasets derived from common H-2D^b/K^b cell lines like B16F10 and MC38 and perform more poorly on cells presented by DCs. Additionally, it is possible DCs are able to present peptides of lower affinity. *In vitro* binding affinity assays fail to always predict the immunodominant T cell response observed *in vivo*, therefore identified pMHCs with low predicted affinity should still be considered in the context of this project.

Another explanation for the low quantity of predicted binders is the lower MHC presentation levels on these cells. In lieu of an abundance of high intensity endogenous peptides, more non-specific peptides may be identified by LC-MS/MS. These analyses identified several hundred pMHCs, whereas our human analyses identify several thousand. Perhaps

many endogenously presented peptides are below the limit of detection, wherein advancements in sample preparation and instrument sensitivity may improve yields in applications such as this.

Future studies related to this project by the Spranger lab include the use of a functional cross-presentation assay, where Cas9 gene editing is used to generate tumor cell lines that express the model antigen SIY linked to a fluorescent protein, tagged to proteins endogenously expressed in particular cellular compartments. Live cell microscopy can then be utilized to visualize cell debris and DC engulfment, and quantitative mass spectrometry can be used to compare the efficiency of cross presentation of the model antigen derived from different cellular compartments. Additional experiments will aim to apply cytotoxic therapy that may augment presentation of cross-presented antigens derived from particular cellular compartments that may be leveraged to selectively modulate antigen cross-presentation in cancer for efficient priming of T cells.

8-4 Materials and Methods

8-4-1 Cell culture

B16F10 mouse melanoma cells were obtained from ATCC (CRL-6475) and maintained in DMEM medium (Corning) supplemented with 10% FBS (Gibco) and 1% penicillin/streptomycin (Gibco). Cells were routinely tested for mycoplasma contamination, and maintained in 37 °C, 5% CO_2.

For antibody optimization experiments, cells were seeded in T-175 flasks (CELLSTAR) and stimulated with 10 ng/mL of recombinant mouse IFN-γ (Thermo Scientific, CAT# PMC4034) for 24 hours prior to cell harvesting and lysis.

8-4-2 SILAC media preparation

Adapted from a protocol prepared by Joshua Mesfin.

Reagents

-DMEM without Amino Acids (Powdered, US Biological, d9800-13)

-Normal Amino Acids

- L-Arginine hydrochloride *(Sigma Aldrich cat. No. A6969-25G)*
- L-Cystine 2HCl *(Sigma Aldrich cat. No. C6727-25G)*
- L-Histidine hydrochloride-H2O (*Sigma Aldrich cat. No. H6034-25G)*
- L-Isoleucine *(Sigma Aldrich cat. No. I7403-25G)*
- L-Lysine hydrochloride *(Sigma Aldrich cat. No. L8662-25G)*
- L-Methionine *(Sigma Aldrich cat. No. M5308-10MG)*
- L-Serine *(Sigma Aldrich cat. No. S4311-25G)*
- L-Threonine *(Sigma Aldrich cat. No. T8441-25G)*
- L-Tryptophan *(Sigma Aldrich cat. No. T8941-25G)*
- L-Valine *(Sigma Aldrich cat. No. V0513-25G)*
- Glycine *(Sigma Aldrich cat. No. G5417-100G)*

-Heavy labelled amino acids

- Tyrosine *(Sigma Aldrich cat. No. 492868-100MG)*
- Asparagine *(Sigma Aldrich cat. No. 641960-250MG)*
- Phenylalanine *(Sigma Aldrich cat. No. 490091-250MG)*
- Leucine *(Sigma Aldrich cat. No. 608068-100MG)*

-D-Glucose (*Sigma Aldrich cat. No. G8270-100G)*
-L-Glutamine *(Sigma Aldrich cat No. G7513-100ML)*

Protocol

1. Determine amount of each amino acid to add for desired media volume. Concentrations are based off of Corning DMEM media formulation.

Normal Amino Acids	**Corning Stock (mg/L)**
Glycine	30
L-Arginine hydrochloride	84
L-Cystine 2HCl	62.57
L-Histidine hydrochloride-H2O	30
L-Isoleucine	42
L-Lysine hydrochloride	146.2
L-Methionine	30
L-Serine	42
L-Threonine	95.2
L-Tryptophan	16
L-Valine	94

SILAC Amino Acids	**Corning Stock (mg/L)**
Tyrosine	103.79
Leucine	104.8
Phenylalanine	66
Asparagine *(Non Essential Amino Acid)*	52.848

Glucose	**Conc (g/L)**
Needed Conc of Glucose (g/L)	4.5
DMEM stock concentration (g/L)	1

2. Calculate the amount of glucose needed to add to master mix. Multiply the difference of needed concentration of glucose (4.5 g/L) and the stock of glucose in DMEM powder (1 g/L) by the desired volume.
    - For a final volume of 1 L, (4.5-1)*1 = 3.5 g to be added to the master mix.
3. Calculate the final concentration of L-glutamine to add to DMEM.

- Dissolve master mix of amino acids and D-glucose in L-glutamine (stock is 2.93 g/L).
- For a final volume of 1 L, the needed concentration of L-glutamine is 584 mg.

It is recommended to aliquot a master mix of amino acids and glucose in L-glutamine.

4. For a final volume of 1000 mL, dissolve 8.32 g of DMEM powder into 800-900 mL of ddH_2O, stirring gently until completely soluble. If the desired volume is different, dissolve a proportional amount (1000/desired volume) of DMEM powder.
5. Add master mixture of amino acids and L-glutamine to media. Mix until completely soluble.
6. If needed, add sodium bicarbonate to increase pH by 0.1-0.3. Using a pH probe, check the pH of the media is 7.4. Mix until completely soluble.
7. Add remaining amount of ddH_2O to get to the desired volume.
8. Bring dissolved DMEM into TC hood and filter media (0.2 μm, Corning) with vacuum filtration.

8-4-3 pMHC isolation

pMHCs were isolated from whole cell lysate as previously described.[169] Briefly, cells were pelleted, washed twice with 1X PBS, and resuspended in lysis buffer buffer [20 nM Tris-HCl pH 8.0, 150 mM NaCl, 0.2 mM PMSO, 1% CHAPS, and 1x HALT Protease/Phosphatase Inhibitor Cocktail (Thermo Scientific)], followed by brief sonication. Lysate was cleared by centrifugation and incubated with Protein A Sepharose bead conjugated to the anti-MHC antibody overnight, rotating at 4°C. Peptides were eluted with 10% acetic acid, filtered using 10K molecular weight cutoff filters, lyophilized, and stored at -80°C prior to analysis. A total of 250 ug of antibody was used for each analysis, split 125 ug H-2K^b/H-2D^b for allele-specific Ab analysis.

Antibodies: H-2D^{b} monoclonal antibody (Thermo Scientific, clone B22-249.R1, CAT# MA5-17992), H-2K^{b} monoclonal antibody (BioXcell, clone Y-3, CAT# BE0172), MHC Class I (H-2) (BioXcell, clone M1/42.3.9.8, CAT# BE0077).

8-4-4 LC-MS/MS data acquisition

pMHC samples were analyzed using an Exploris 480 Hybrid Quadrupole-Orbitrap mass spectrometer (Thermo Scientific) coupled with an UltiMate 3000 RSLC Nano LC system (Dionex), Nanospray Flex ion source (Thermo Scientific), and column oven heater (Sonation). Samples were resuspended in 0.1% formic acid and directly loaded onto a 10-15 cm analytical capillary chromatography column with an integrated electrospray tip (~1 µm orifice), prepared and packed in house (50 µm ID × 20 cm & 1.9 µM C18 beads, ReproSil-Pur). pMHC elutions were injected in four 15% fractions for improved coverage of the immunopeptidome with the exception of the SIY analysis, where one fraction containing 30% of the pMHC elution was used.

Peptides were eluted using a gradient with 6-25% buffer B (70% Acetonitrile, 0.1% formic acid) for 75 minutes, 25-45% for 5 minutes, 45-100% for 2 minutes, hold for 1 minute, and 100% to 2% for 2 minutes. Standard mass spectrometry parameters were as follows: spray voltage, 2.0 kV; no sheath or auxiliary gas flow; heated capillary temperature, 275 °C. The Exploris was operated in data dependent acquisition (DDA) mode. Full scan mass spectra (350-1200 m/z, 60,000 resolution) were detected in the orbitrap analyzer after accumulation of 3e^{6} ions (normalized AGC target of 300%) or 25 ms. For every full scan, MS^{2} were collected during a 3 second cycle time. Ions were isolated (0.4 m/z isolation width) for a maximum of 250 ms or 75% AGC target and fragmented by HCD with 30% collision energy at a resolution of 60,000.

Charge states < 2 and > 4 were excluded, and precursors were excluded from selection for 30 seconds if fragmented n=2 times within 20 second window.

8-4-5 pMHC data analysis

All mass spectra were analyzed with Proteome Discoverer (PD, version 2.5) and searched using Mascot (version 2.4) against the human SwissProt database. Non-SILAC labeled pMHCs were searched with variable F/Y/L/N modifications, and peptides with any heavy labeled amino acids were filtered out. Peptides were further filtered according to the following criteria: length = 8-15 amino acids, ion score ≥ 15, isolation interference ≤ 30%, search engine rank = 1. SILAC labeled peptides were identified by searching with F/Y/L/N static modifications and filtered according to the same criteria. pMHCs with 100% incorporation of SILAC-labeled F/Y/L/N in search results with variable modifications were compared against the pMHCs identified with static modification search criteria, which yielded an overlap of 146 peptides (87% of variable peptides). Peptides with incomplete SILAC labeling were ignored. Binding affinity prediction was performed using PanNetMHC 4.0 against H-2Kb and H2-Db. Peptides with a %rank < 2% were considered as binders.

**All cell compartment analyses were performed by Tim Fessenden; therefore, related methods are not described in this thesis.*

8-5 Acknowledgements

I'd like to first thank Joshua Mesfin, a talented undergraduate I had the privilege of training and working with, for his work in developing and piloting the SILAC labeling protocol. I'd also like to thank Tim Fessenden for being an enthusiastic and brilliant collaborator, always

bringing new ideas, analysis techniques, and papers I've never seen before to my attention. Finally, I'd like to thank Stefani Spranger, whose deep knowledge and background in dendritic cell research led to the initial idea of this project, and from whom I've learned a great deal from about immunology.

8-6 Tables

***Table 8-1**. Peptides identified in B16F10 and X-presented DCs.*

Peptide	Gene
FAPVNVTTEVK	EEF1A1
SAPENAVRM	GRCC10
ITQTLSDM	DNAH1
GGIQNVGHI	IMPDH2
VAGGAGLAVPG	PKD2
PEAPPPALPAGA	RYR1
YNIVGLRSN	MCCC1
GEPLQAAAS	F8A1
PMMVTKQENI	CDH13
NFASHAIVEDNV	PIGO

***Table 8-2**. High affinity, cross presented peptides on DCs.*

Peptide	Min rank	nM	Gene
NSIRNLDTI	0.0043	4.6463	ATXN10
ASVLNVNHI	0.0078	16.406	ANKRD17
INFDFPKL	0.0087	5.5085	DDX6
SAPENAVRM	0.0088	23.4417	GRCC10
KAPDNRETL	0.0115	41.7685	STT3B
TSVRFTQL	0.0184	10.0975	NOSIP
VAFDFTKV	0.0204	10.7461	PICALM
SQPVNPHSL	0.0237	80.6889	ZSWIM8
GGIQNVGHI	0.0449	173.2446	IMPDH2
TGPSNVDKL	0.0464	181.4227	CHEK1
RTVENVTVF	0.0545	218.574	VAT1
SAPRNFVENF	0.0736	276.711	ELP2
VNFEFPEF	0.0792	31.6201	RPS7
VNFEKMRM	0.0976	38.4143	RAPGEF4
RAVANETGAFF	0.1871	751.6148	VCP
VQNKNSSYF	0.2199	907.1068	TUBB5
AAPADNSEL	0.2826	1224.0697	OSBP2
FAPVNVTTEVK	0.459	1973.6716	EEF1A1
RMYKMVIV	0.9612	470.804	PTPRB
QISEFSFL	1.0647	528.8588	MTMR4
KIQLYQGI	1.702	928.3353	EGFL6
VATYIPGI	1.9476	1098.7549	DOLK

***Table 8-3**. High affinity binders in B2M-KO B16F10 cells X-presented on DCs.*

Peptide	Gene	% Rank	Affinity (nM)
RTVENVTVF	VAT1	0.0545	218.574
YQVINWRL	UGT3A1	0.3188	1387.1729
FAPVNVTTEVK	EEF1A1	0.459	1973.6716
YQVAKGMAFL	KIT	0.6151	2683.0674
TLLRDRDEL	ERP44	0.7864	3470.5002
SAPRHGSL	RPL3	0.793	360.5833
RGFLSAGF	STARD8	0.828	382.8167
RVPTPNVSVV	GAPDH	0.9965	4427.6226
AQVMSLSTIL	NR2C2	1.0402	4596.3198
VGYQHGRTVF	PNPLA7	1.0885	541.7628
KVVKVANVSLL	RPS23	1.3944	6001.354
RMQSKEYPV	TBX5	1.7257	5887.3853
VTPQNGLASGI	GLIS1	1.7285	7140.7314
SGYQRDGYQQNF	CAPRIN1	1.78	978.0981
RSFSTSVV	ATP5PO	2.0773	1193.9838

“The flexibility and potential of mass spectrometry remains to be fully exploited, and the creativity of mass spectrometry researchers is only limited by the questions they are asking.”

S. Sidoli, K Kulej, and B. Garcia
Why proteomics is not the new genomics and the future of mass spectrometry in cell biology (2016)

CHAPTER 9: Conclusions and future directions

In this thesis, I present a collection of mass spectrometry-based platforms that aim to address existing methodological limitations in tyrosine phosphoproteomics and immunopeptidomics and generate novel datasets that advance the field of cancer research. However, there are many more opportunities for method advancements and applications using the tools and techniques described herein.

9-1 Future directions

9-1-1 SureQuant pTyr panel extension for targeted pTyr profiling

This thesis describes the development of a targeted pTyr assay, utilizing 340 tyrosine phosphorylated peptide targets to capture key nodes on a handful of tyrosine-mediated signaling pathways. While we demonstrate the utility of this limited panel, broader coverage is required for a deeper understanding of a sample's signaling state. To this end, I analyzed over 10 discovery pTyr mass spectrometry analyses generated in the laboratory on a variety of different cancer types to generate a list of over 2,000 unique pTyr sites. Using this expanded list, a new panel of over 1,000 sites was curated (led by Cameron Flower), and a subset of this larger panel has been synthesized in collaboration with Thermo Fisher for SureQuant pTyr 2.0. This broader panel, in combination with new data analysis and visualization tools (also led by Cameron Flower), and advancements in sample preparation techniques (led by Ishwar Kohale) holds the potential to rapidly and reproducibly characterize and identify therapeutic targets in human tumors. Other future work may focus on the development of an automated platform to

process and analyze tumors with SureQuant pTyr, which greatly advance the feasibility of this technique integrating into clinical settings.

9-1-2 Expanding our understanding of therapy-induced pMHC changes in cancer

While the bulk of this thesis focuses on the pMHC repertoire-induced alterations driven by MEK and CDK4/6 inhibitors in melanoma, there is a vast opportunity for expansion of multiplexed, quantitative, immunopeptidomics to profile repertoire responses to different classes of therapies (chemotherapy, targeted therapies, cytokines, checkpoint blockade) across different cancer types. In collaboration with Alex Jaegar, we profiled the pMHC response to HSP90 inhibitors, and found that a sub-cytotoxic dose (but not a higher dose) increased antigen presentation, further highlighting the potential of therapeutic agents to modulate immunogenicity.[169] Expansion of analyses in this area may be particularly informative in cancers that are historically viewed as “immunologically cold,” with little to no immunogenicity such as ovarian cancer tumors, which are generally unresponsive to therapies that enhance the immune response like immune checkpoint blockade.[456,457]

Enhancing immunogenicity can transform a non-responsive tumor into a responsive tumor, and one possible way to boost tumor immunogenicity is through upregulation of HLA molecules with anti-cancer therapies.[458] Immunogenicity is also influence by the tumor microenvironment, such as efficient presentation of antigens by dendritic cells, another axis that can be modulated to improve the anti-cancer immune response.[459] As demonstrated by the novel methods developed in in chapters 3, 4, and 8, immunopeptidomics data can generate data which informs our understanding of tumor immunity.

Furthermore, future studies interrogating the temporal dynamics of the repertoire’s response is required, as clinical use of targeted therapies is generally not limited to a single

dose. While an initial study described in SKMEL5 cells treated for 10 days of therapy showed a sustained increase in antigen expression, evaluating later timepoints and dosing regimens will be informative. If cells are dosed with drug for 7 days and then taken off drug for 7 days, does HLA expression and repertoire alterations remain? If cells become resistant to therapy, how does that affect the repertoire? Furthermore, evaluating which order combination therapies should be administered also requires additional investigation.

9-1-3 Reducing sample input in immunopeptidomics

One of the major limitations in immunopeptidomics is the quantity of sample input required for pMHC profiling. While the number of cells required has dropped by several orders of magnitude over the past several decades, deep pMHC profiling still requires high cell numbers, and limited quantity *in vivo* samples like fine needle biopsies still do not provide enough material.

Still, the number of pMHCs I've been able to measure from the same quantity of lysate in MDA-MD-231 cells has increased significantly over the course of my PhD, due to improvements in instrument sensitivity, parameter optimization, and chromatography. To further reduce sample inputs and increase throughput of analysis, I believe miniaturizing and automating pMHC sample processing is required. This may come in the format of a 96/384 well plate or microfluidic platform. Inspiration may also come from single cell platforms like nanopots, which similarly aim to reduce sample handling and volumes to increase protein yields from very limited starting material.[460] Optimally, all processing steps including IP, peptide isolation, and labeling will be done in a single platform.

Indeed, profiling pMHCs on limited sample, particularly single cells have exciting potential. The field has largely been limited to analyses of bulk pMHc profiling, which is unlikely

to capture intratumoral heterogeneity. Recently, Demmers et al. profiled pMHC repertoires on organoids derived from single cell clones, representing the first paper investigating cell-to-cell differences in pMHC repertoires.[177] While the data highlighted potential clonal differences in expression levels, analyses were performed with label-free quantification, and differences in peptides identified and expression levels could simply be explained by run-to-run variation. In lieu of single-cell methods, this approach may prove valuable when combined with the relative and absolute quantification methods described in this work to determine cell-to-cell variation in pMHC expression. Several interesting applications come to mind, including analyzing the repertoires on different drug-resistant cell clones, metastases of the same tumor, or even to characterize the variation in targeted immunotherapy antigen targets, to better understand what proportion of a cell population may be susceptible to therapeutic targeting.

9-1-4 Additional applications of SureQuant MHC

Applying the SureQuant IS-PRM framework to immunopeptidomics was utilized in this thesis to perform absolute quantification estimates of select antigens. However, this framework can be adjusted and applied to a range of applications in immunopeptidomics. One area for future work, described in Chapter 6, is using SureQuant MHC to generate a panel of cells with varying expression levels for evaluating optimal thresholds of expression required for targeted immunotherapy efficacy.

Another useful application of SureQuant MHC is in estimating sample losses. As a preliminary experiment, I utilized two isotopologues to estimate pMHC losses associated with sample processing by comparing the intensities peptide isotopologues added exogenously prior to analysis with isotopologue added as hipMHCs prior to immunoprecipitation (**Figure 9-1**). I found that losses at 1 fmol concentration (~100 copies/cell in this experimental setup) ranged

from 19-92%, underscoring our previous claims that exogenous peptide standards cannot be used for absolute quantification estimates. Future work may involve testing the range of losses using differing sample input amounts or peptides of different properties (chemical, binding affinity) to better understand existing limitations in immunopeptidomics, as well as to test and compare new sample processing and analysis platforms.

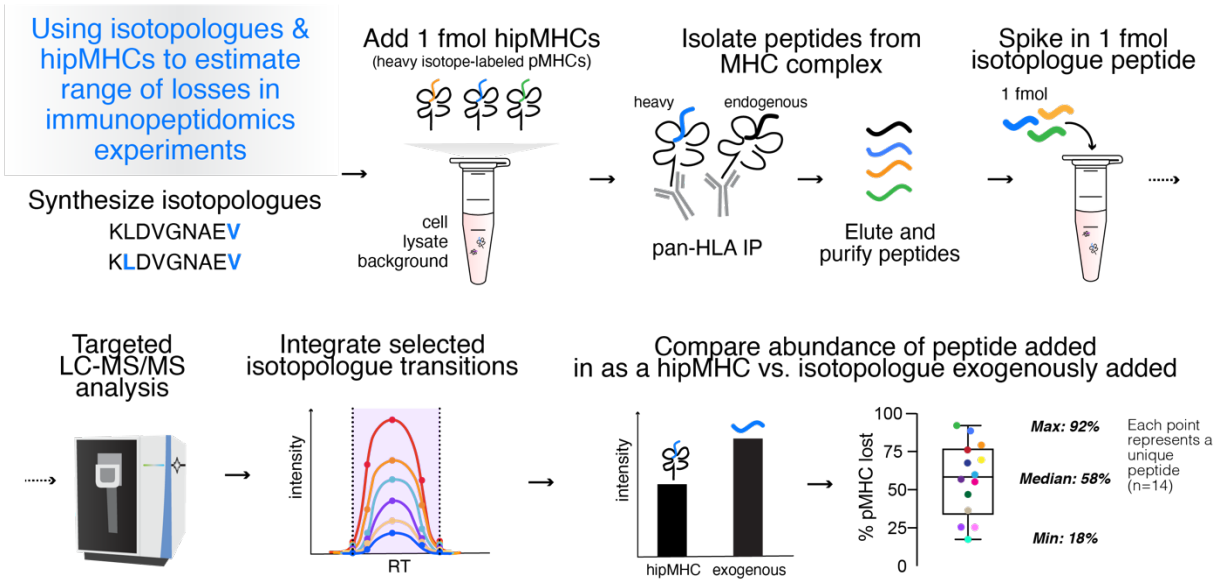

***Figure 9-1**. Isotopologues estimate pMHC sample processing losses.*

Apart from absolute quantification with isotopologues, the SureQuant MHC framework may be effectively used for targeted identification of antigens of interest. This may be relevant in clinical settings to identify whether a tumor presents a particular epitope essential to a targeted immunotherapy, as current methods for patient profiling rely largely on allelic profiling and target transcript/protein expression. Additionally, we describe in Chapter 5 our findings that peptides < 100 copies/cell were not identified in a discovery analysis of human tumors, whereas the same peptides were easily identified using our targeted method. We also show that we can detect peptides at < 1 copy/cell using fewer than $1e^7$ cells, highlighting the potential using SureQuant

MHC in identifying low-abundance antigens. This is particularly relevant for neoantigen identification, which are historically challenging to identify by LC-MS/MS.

9-1-5 Combatting ion suppression in pMHC analyses

One significant limitation in the MS^2-based immunopeptidomics workflow described in Chapter 3 is dynamic range suppression, where a known 10-fold change appears as a 3-fold change with reporter ion intensities. The SureQuant MHC data showed that in some cases, changes as large as 40-80x were compressed to 10-fold changes, suggesting ~10x is the dynamic range limit for pMHC analyses in this setting. HipMHCs are a useful tool for estimating ion suppression, however data described in Chapter 2 shows that all peptides are differently impacted by ion suppression, likely related to their abundance, chemical properties, and the peptides that co-elute around them. While hipMHCs and SureQuant MHC can be used to identify the magnitude of expression level changes, synthesizing the isotopically labeled standards for every target of interest is expensive and not scalable.

One possible avenue to improve ion suppression is to use SPS-MS^3, which has been shown in other contexts to reduce dynamic range compression. While SPS-MS^3 has been applied in immunopeptidomics in a few cases[180,440], an important study will be to perform a comparative analysis between MS^2 and MS^3-based analyses to evaluate differences in ion suppression, pMHC properties, and whether MS^3 analysis result in more losses, as is the case in pTyr analyses. hipMHCs standards can be leveraged for controlled comparisons of both losses and ion suppression. Additionally, we evaluated the quantitative impact of using a protein carrier channel for pMHC analyses, which is suggested as a way to circumvent existing limitations in sample input requirements, but we find that the protein carrier obscures quantitation in MS^2-based analyses. Comparing the use of a protein carrier in MS^2 versus MS^3

will be critical to determining whether use of a protein carrier may offer a way forward under certain applications.

9-2 Concluding remarks

In conclusion, proteomics holds great potential to expand our understanding of disease biology, identify biomarkers, and be used for clinical therapeutic selection in cancer research and beyond. Mass spectrometers offer a powerful and versatile tool for obtaining this information, and creative implementations and methodological designs continue to offer new data types. It is my sincere hope that innovations in sample processing and analysis automation, as well as continued advancements in instrument sensitivity, bring MS closer to widespread clinical adoption in the coming decade. Targeted acquisition platforms like SureQuant are an important step, and studies demonstrating their utility will hopefully pave the way for the integration of proteomics into clinical decision making.

References

1. Hanahan, D. & Weinberg, R. A. Hallmarks of cancer: The next generation. *Cell* vol. 144 646–674 (2011).
2. Sever, R. & Brugge, J. S. Signal transduction in cancer. *Cold Spring Harb. Perspect. Med.* **5**, (2015).
3. American Cancer Society. *Cancer Facts & Figures 2019*. (2019).
4. Jackson, S. P. & Bartek, J. The DNA-damage response in human biology and disease. *Nature* vol. 461 1071–1078 (2009).
5. Baskar, R., Lee, K. A., Yeo, R. & Yeoh, K. W. Cancer and radiation therapy: Current advances and future directions. *International Journal of Medical Sciences* vol. 9 193–199 (2012).
6. DeVita, V. T. & Chu, E. A history of cancer chemotherapy. *Cancer Research* vol. 68 8643–8653 (2008).
7. Huang, C. Y., Ju, D. T., Chang, C. F., Muralidhar Reddy, P. & Velmurugan, B. K. A review on the effects of current chemotherapy drugs and natural agents in treating non-small cell lung cancer. *BioMedicine (France)* vol. 7 12–23 (2017).
8. Luke, J. J. & Schwartz, G. K. Chemotherapy in the management of advanced cutaneous malignant melanoma. *Clin. Dermatol.* **31**, 290–297 (2013).
9. Nedeljković, M. & Damjanović, A. Mechanisms of Chemotherapy Resistance in Triple-Negative Breast Cancer-How We Can Rise to the Challenge. *Cells* vol. 8 (2019).
10. Zeng, S. *et al.* Chemoresistance in pancreatic cancer. *International Journal of Molecular Sciences* vol. 20 (2019).
11. Da Ros, M. *et al.* Glioblastoma chemoresistance: the double play by microenvironment and blood-brain barrier. *International Journal of Molecular Sciences* vol. 19 (2018).
12. Morgan, G. W., Ward, R. & Barton, M. The contribution of cytotoxic chemotherapy to 5-year survival in adult malignancies. *Clin. Oncol.* **16**, 549–560 (2004).
13. Pathak, A., Tanwar, S., Kumar, V. & Banarjee, B. D. Present and Future Prospect of Small Molecule & Related Targeted Therapy Against Human Cancer. *Vivechan Int. J. Res.* **9**, 36–49 (2018).
14. Flaherty, K. T. *et al.* Inhibition of Mutated, Activated BRAF in Metastatic Melanoma. *N. Engl. J. Med.* **363**, 809–819 (2010).
15. Chapman, P. B. *et al.* Improved Survival with Vemurafenib in Melanoma with BRAF V600E Mutation. *N. Engl. J. Med.* **364**, 2507–2516 (2011).
16. Maemondo, M. *et al.* Gefitinib or Chemotherapy for Non–Small-Cell Lung Cancer with Mutated EGFR. *N. Engl. J. Med.* **362**, 2380–2388 (2010).
17. Goldberg, R. M., Venook, A. P. & Schilsky, R. L. Cetuximab in the treatment of colorectal cancer. *Clin. Adv. Hematol. Oncol.* **2**, 2040–2048 (2004).
18. Slamon, D. J. *et al.* Use of Chemotherapy plus a Monoclonal Antibody against HER2 for Metastatic Breast Cancer That Overexpresses HER2. *N. Engl. J. Med.* **344**, 783–792 (2001).
19. Robert, C. *et al.* Improved Overall Survival in Melanoma with Combined Dabrafenib and Trametinib. *N. Engl. J. Med.* **372**, 30–39 (2015).
20. Yaffe, M. B. Why geneticists stole cancer research even though cancer is primarily a signaling disease. *Sci. Signal.* **12**, (2019).
21. Sabnis, A. J. & Bivona, T. G. Principles of Resistance to Targeted Cancer Therapy: Lessons from Basic and Translational Cancer Biology. *Trends in Molecular Medicine* vol. 25 185–197 (2019).

22. Wei, S. C., Duffy, C. R. & Allison, J. P. Fundamental mechanisms of immune checkpoint blockade therapy. *Cancer Discovery* vol. 8 1069–1086 (2018).
23. Esfahani, K. *et al.* A review of cancer immunotherapy: From the past, to the present, to the future. *Curr. Oncol.* **27**, 87–97 (2020).
24. Overman, M. J. *et al.* Nivolumab in patients with metastatic DNA mismatch repair-deficient or microsatellite instability-high colorectal cancer (CheckMate 142): an open-label, multicentre, phase 2 study. *Lancet Oncol.* **18**, 1182–1191 (2017).
25. Le, D. T. *et al.* PD-1 Blockade in Tumors with Mismatch-Repair Deficiency. *N. Engl. J. Med.* **372**, 2509–2520 (2015).
26. de Charette, M., Marabelle, A. & Houot, R. Turning tumour cells into antigen presenting cells: The next step to improve cancer immunotherapy? *European Journal of Cancer* vol. 68 134–147 (2016).
27. Javeed, A. *et al.* Paclitaxel and immune system. *European Journal of Pharmaceutical Sciences* vol. 38 283–290 (2009).
28. Galluzzi, L., Humeau, J., Buqué, A., Zitvogel, L. & Kroemer, G. Immunostimulation with chemotherapy in the era of immune checkpoint inhibitors. *Nature Reviews Clinical Oncology* vol. 17 (2020).
29. Ko, E. C. & Formenti, S. C. Radiotherapy and checkpoint inhibitors: a winning new combination? *Therapeutic Advances in Medical Oncology* vol. 10 (2018).
30. Wang, Y. *et al.* The reciprocity between radiotherapy and cancer immunotherapy. *Clinical Cancer Research* vol. 25 1709–1717 (2019).
31. Brea, E. J. *et al.* Kinase regulation of human MHC class i molecule expression on cancer cells. *Cancer Immunol. Res.* **4**, 936–947 (2016).
32. Sumimoto, H., Imabayashi, F., Iwata, T. & Kawakami, Y. The BRAF-MAPK signaling pathway is essential for cancer-immune evasion in human melanoma cells. *J. Exp. Med.* **203**, 1651–6 (2006).
33. Khalili, J. S. *et al.* Oncogenic BRAF(V600E) promotes stromal cell-mediated immunosuppression via induction of interleukin-1 in melanoma. *Clin. Cancer Res.* **18**, 5329–5340 (2012).
34. Pollack, B. P., Sapkota, B. & Cartee, T. V. Epidermal growth factor receptor inhibition augments the expression of MHC class I and II genes. *Clin. Cancer Res.* **17**, 4400–13 (2011).
35. Kulkarni, A., Natarajan, S. K., Chandrasekar, V., Pandey, P. R. & Sengupta, S. Combining Immune Checkpoint Inhibitors and Kinase-Inhibiting Supramolecular Therapeutics for Enhanced Anticancer Efficacy. *ACS Nano* **10**, 9227–9242 (2016).
36. Chaganty, B. K. R. *et al.* Trastuzumab upregulates expression of HLA-ABC and T cell costimulatory molecules through engagement of natural killer cells and stimulation of IFNγ secretion. *Oncoimmunology* **5**, (2016).
37. Franklin, D. A., James, J. L., Axelrod, M. L. & Balko, J. M. MEK inhibition activates STAT signaling to increase breast cancer immunogenicity via MHC-I expression. *Cancer Drug Resist.* **3**, 603–612 (2020).
38. Zhou, F. Molecular mechanisms of IFN-γ to up-regulate MHC class i antigen processing and presentation. *International Reviews of Immunology* vol. 28 239–260 (2009).
39. Zaidi, M. R. & Merlino, G. The two faces of interferon-γ in cancer. *Clinical Cancer Research* vol. 17 6118–6124 (2011).
40. Hamilton, E. & Infante, J. R. Targeting CDK4/6 in patients with cancer. *Cancer Treatment Reviews* vol. 45 129–138 (2016).
41. Schettini, F. *et al.* CDK 4/6 inhibitors as single agent in advanced solid tumors. *Front. Oncol.* **8**, 608 (2018).

42. Deng, J. *et al.* CDK4/6 inhibition augments antitumor immunity by enhancing T-cell activation. *Cancer Discov.* **8**, 216–233 (2018).
43. Esteva, F. J., Hubbard-Lucey, V. M., Tang, J. & Pusztai, L. Immunotherapy and targeted therapy combinations in metastatic breast cancer. *The Lancet Oncology* vol. 20 e175–e186 (2019).
44. Sullivan, R. J. *et al.* Atezolizumab plus cobimetinib and vemurafenib in BRAF-mutated melanoma patients. *Nature Medicine* vol. 25 929–935 (2019).
45. Ascierto, P. A. *et al.* Dabrafenib, trametinib and pembrolizumab or placebo in BRAF-mutant melanoma. *Nature Medicine* vol. 25 941–946 (2019).
46. Neefjes, J., Jongsma, M. L. M., Paul, P. & Bakke, O. Towards a systems understanding of MHC class I and MHC class II antigen presentation. *Nat. Rev. Immunol.* **11**, 823–36 (2011).
47. Wearsch, P. A. & Cresswell, P. The quality control of MHC class I peptide loading. *Current Opinion in Cell Biology* vol. 20 624–631 (2008).
48. Neefjes, J., Jongsma, M. L. M., Paul, P. & Bakke, O. Towards a systems understanding of MHC class i and MHC class II antigen presentation. *Nature Reviews Immunology* vol. 11 823–836 (2011).
49. Hassan, C. *et al.* Naturally processed non-canonical HLA-A∗02:01 presented peptides. *J. Biol. Chem.* **290**, 2593–2603 (2015).
50. Fernando, M. M. A. *et al.* Defining the Role of the MHC in Autoimmunity: A Review and Pooled Analysis. *PLoS Genet.* **4**, e1000024 (2008).
51. Alter, I., Gragert, L., Fingerson, S., Maiers, M. & Louzoun, Y. HLA class I haplotype diversity is consistent with selection for frequent existing haplotypes. *PLoS Comput. Biol.* **13**, e1005693 (2017).
52. Sidney, J. *et al.* Several HLA alleles share overlapping peptide specificities. *J. Immunol.* **154**, 247–24759 (1995).
53. Hansen, T. H. & Bouvier, M. MHC class I antigen presentation: learning from viral evasion strategies. *Nat. Rev. Immunol.* **9**, 503–513 (2009).
54. Carrington, M. & O'Brien, S. J. The Influence of HLA Genotype on AIDS. *Annual Review of Medicine* vol. 54 535–551 (2003).
55. Romieu-Mourez, R., François, M., Boivin, M.-N., Stagg, J. & Galipeau, J. Regulation of MHC Class II Expression and Antigen Processing in Murine and Human Mesenchymal Stromal Cells by IFN-γ, TGF-β, and Cell Density. *J. Immunol.* **179**, 1549–1558 (2007).
56. Wieczorek, M. *et al.* Major histocompatibility complex (MHC) class I and MHC class II proteins: Conformational plasticity in antigen presentation. *Frontiers in Immunology* vol. 8 1 (2017).
57. Busch, R., Doebele, R. C., Patil, N. S., Pashine, A. & Mellins, E. D. Accessory molecules for MHC class II peptide loading. *Current Opinion in Immunology* vol. 12 99–106 (2000).
58. Shin, J. S. *et al.* Surface expression of MHC class II in dendritic cells is controlled by regulated ubiquitination. *Nature* **444**, 115–118 (2006).
59. Lotem, M. *et al.* Presentation of tumor antigens by dendritic cells genetically modified with viral and nonviral vectors. *J. Immunother.* **29**, 616–627 (2006).
60. Abelin, J. G. *et al.* Defining HLA-II Ligand Processing and Binding Rules with Mass Spectrometry Enhances Cancer Epitope Prediction. *Immunity* **51**, 766-779.e17 (2019).
61. Melero, I. *et al.* Therapeutic vaccines for cancer: An overview of clinical trials. *Nature Reviews Clinical Oncology* vol. 11 509–524 (2014).
62. Yang, B., Jeang, J., Yang, A., Wu, T. C. & Hung, C. F. DNA vaccine for cancer immunotherapy. *Hum. Vaccines Immunother.* **10**, 3153–3164 (2014).
63. He, Q. *et al.* TCR-like antibodies in cancer immunotherapy. *J. Hematol. Oncol.* **12**, 99

(2019).
64. Van Der Bruggen, P. *et al.* A gene encoding an antigen recognized by cytolytic T lymphocytes on a human melanoma. *Science (80-.).* **254**, 1643–1647 (1991).
65. Lucas, S. *et al.* Identification of a new MAGE gene with tumor-specific expression by representational difference analysis. *Cancer Res.* **58**, 743–752 (1998).
66. Fiszer, D. & Kurpisz, M. Major histocompatibility complex expression on human, male germ cells: A review. *Am. J. Reprod. Immunol.* **40**, 172–176 (1998).
67. Van den Eynde, B. *et al.* A new family of genes coding for an antigen recognized by autologous cytolytic T lymphocytes on a human melanoma. *J. Exp. Med.* **182**, 689–698 (1995).
68. Akers, S. N., Odunsi, K. & Karpf, A. R. Regulation of cancer germline antigen gene expression: Implications for cancer immunotherapy. *Future Oncology* vol. 6 717–732 (2010).
69. Thomson, T. M. *et al.* Differentiation antigens of melanocytes and melanoma: analysis of melanosome and cell surface markers of human pigmented cells with monoclonal antibodies. *J. Invest. Dermatol.* **90**, 459–466 (1988).
70. Kirkin, A. F., Dzhandzhugazyan, K. & Zeuthen, J. The Immunogenic Properties of Melanoma-Associated Antigens Recognized by Cytotoxic T Lymphocytes. *Exp. Clin. Immunogenet.* **15**, 19–32 (1998).
71. Brichard, V. *et al.* The tyrosinase gene codes for an antigen recognized by autologous cytolytic T lymphocytes on HLA-A2 melanomas. *J. Exp. Med.* **178**, 489–495 (1993).
72. Coulie, P. G., Van Den Eynde, B. J., Van Der Bruggen, P. & Boon, T. Tumour antigens recognized by T lymphocytes: At the core of cancer immunotherapy. *Nature Reviews Cancer* vol. 14 135–146 (2014).
73. Fisk, B., Blevins, T. L., Wharton, J. T. & Ioannides, C. G. Identification of an immunodominant peptide of HER-2/neu protooncogene recognized by ovarian tumor-specific cytotoxic t lymphocyte lines. *J. Exp. Med.* **181**, 2109–2117 (1995).
74. Inoue, K. *et al.* Aberrant overexpression of the Wilms tumor gene (WT1) in human leukemia. *Blood* **89**, 1405–1412 (1997).
75. Braun, M. W. & Iwakuma, T. Regulation of cytotoxic T-cell responses by p53 in cancer. *Translational Cancer Research* vol. 5 692–697 (2016).
76. Schwartzentruber, D. J. *et al.* gp100 Peptide Vaccine and Interleukin-2 in Patients with Advanced Melanoma. *N. Engl. J. Med.* **364**, 2119–2127 (2011).
77. Dreno, B. *et al.* MAGE-A3 immunotherapeutic as adjuvant therapy for patients with resected, MAGE-A3-positive, stage III melanoma (DERMA): a double-blind, randomised, placebo-controlled, phase 3 trial. *Lancet Oncol.* **19**, 916–929 (2018).
78. Huang, J. *et al.* A single peptide-major histocompatibility complex ligand triggers digital cytokine secretion in CD4 + T cells. (2013) doi:10.1016/j.immuni.2013.08.036.
79. Morgan, R. A. *et al.* Cancer regression and neurological toxicity following anti-MAGE-A3 TCR gene therapy. *J. Immunother.* **36**, 133–151 (2013).
80. Brossart, P. The Role of Antigen Spreading in the Efficacy of Immunotherapies. (2020) doi:10.1158/1078-0432.CCR-20-0305.
81. De Martel, C. *et al.* Global burden of cancers attributable to infections in 2008: A review and synthetic analysis. *Lancet Oncol.* **13**, 607–615 (2012).
82. Emens, L. A. Cancer vaccines: On the threshold of success. *Expert Opinion on Emerging Drugs* vol. 13 295–308 (2008).
83. Tashiro, H. & Brenner, M. K. Immunotherapy against cancer-related viruses. *Cell Research* vol. 27 59–73 (2017).
84. Schiller, J. T., Castellsagué, X. & Garland, S. M. A review of clinical trials of human

papillomavirus prophylactic vaccines. *Vaccine* vol. 30 F123 (2012).
85. Hemminki, O., Dos Santos, J. M. & Hemminki, A. Oncolytic viruses for cancer immunotherapy. *Journal of Hematology and Oncology* vol. 13 84 (2020).
86. Macedo, N., Miller, D. M., Haq, R. & Kaufman, H. L. Clinical landscape of oncolytic virus research in 2020. *Journal for ImmunoTherapy of Cancer* vol. 8 1486 (2020).
87. Andtbacka, R. H. I. *et al.* Final analyses of OPTiM: a randomized phase III trial of talimogene laherparepvec versus granulocyte-macrophage colony-stimulating factor in unresectable stage III–IV melanoma. *J. Immunother. Cancer* **7**, 145 (2019).
88. Conry, R. M., Westbrook, B., McKee, S. & Norwood, T. G. Talimogene laherparepvec: First in class oncolytic virotherapy. *Human Vaccines and Immunotherapeutics* vol. 14 839–846 (2018).
89. Peng, M. *et al.* Neoantigen vaccine: An emerging tumor immunotherapy. *Molecular Cancer* vol. 18 1–14 (2019).
90. Chen, D. S. & Mellman, I. Elements of cancer immunity and the cancer-immune set point. *Nature* vol. 541 321–330 (2017).
91. Snyder, A. *et al.* Genetic Basis for Clinical Response to CTLA-4 Blockade in Melanoma. *N. Engl. J. Med.* **371**, 2189–2199 (2014).
92. Wang, Q. J. *et al.* Identification of T-cell receptors targeting KRAS-mutated human tumors. *Cancer Immunol. Res.* **4**, 204–214 (2016).
93. Lo, W. *et al.* Immunologic recognition of a shared p53 mutated neoantigen in a patient with metastatic colorectal cancer. *Cancer Immunol. Res.* **7**, 534–543 (2019).
94. Racle, J. *et al.* Robust prediction of HLA class II epitopes by deep motif deconvolution of immunopeptidomes. *Nat. Biotechnol.* **37**, 1283–1286 (2019).
95. Bulik-Sullivan, B. *et al.* Deep learning using tumor HLA peptide mass spectrometry datasets improves neoantigen identification. *Nat. Biotechnol.* **37**, 55–71 (2019).
96. O'Donnell, T. J. *et al.* MHCflurry: Open-Source Class I MHC Binding Affinity Prediction. *Cell Syst.* **7**, 129-132.e4 (2018).
97. Zhou, Z. *et al.* TSNAD: An integrated software for cancer somatic mutation and tumour-specific neoantigen detection. *R. Soc. Open Sci.* **4**, (2017).
98. Zhang, J., Mardis, E. R. & Maher, C. A. INTEGRATE-neo: A pipeline for personalized gene fusion neoantigen discovery. *Bioinformatics* **33**, 555–557 (2017).
99. Jurtz, V. *et al.* NetMHCpan-4.0: Improved Peptide–MHC Class I Interaction Predictions Integrating Eluted Ligand and Peptide Binding Affinity Data. *J. Immunol.* **199**, 3360–3368 (2017).
100. Schumacher, T. N. & Schreiber, R. D. Neoantigens in cancer immunotherapy. *Science* vol. 348 69–74 (2015).
101. The problem with neoantigen prediction. *Nature Biotechnology* vol. 35 97 (2017).
102. Ott, P. A. *et al.* An immunogenic personal neoantigen vaccine for patients with melanoma. *Nature* **547**, 217–221 (2017).
103. Sahin, U. *et al.* Personalized RNA mutanome vaccines mobilize poly-specific therapeutic immunity against cancer. *Nature* **547**, 222–226 (2017).
104. Matsushita, H. *et al.* Cancer exome analysis reveals a T-cell-dependent mechanism of cancer immunoediting. *Nature* **482**, 400–404 (2012).
105. Garrido, F., Aptsiauri, N., Doorduijn, E. M., Garcia Lora, A. M. & van Hall, T. The urgent need to recover MHC class I in cancers for effective immunotherapy. *Current Opinion in Immunology* vol. 39 44–51 (2016).
106. Marabelle, A. *et al.* Association of tumour mutational burden with outcomes in patients with advanced solid tumours treated with pembrolizumab: prospective biomarker analysis of the multicohort, open-label, phase 2 KEYNOTE-158 study. *Lancet Oncol.* **21**, 1353–

1365 (2020).
107. Kim, J. Y. *et al.* Tumor mutational burden and efficacy of immune checkpoint inhibitors: A systematic review and meta-analysis. *Cancers (Basel).* **11**, 11 (2019).
108. Karpanen, T. & Olweus, J. The potential of donor T-cell repertoires in neoantigen-targeted cancer immunotherapy. *Frontiers in Immunology* vol. 8 (2017).
109. Granados, D. P. *et al.* Impact of genomic polymorphisms on the repertoire of human MHC class I-associated peptides. *Nat. Commun.* **5**, 1–14 (2014).
110. Vigneron, N. *et al.* An Antigenic Peptide Produced by Peptide Splicing in the Proteasome. *Science (80-.).* **304**, 587–590 (2004).
111. Hanada, K. I., Yewdell, J. W. & Yang, J. C. Immune recognition of a human renal cancer antigen through post-translational protein splicing. *Nature* **427**, 252–256 (2004).
112. Ebstein, F. *et al.* Proteasomes generate spliced epitopes by two different mechanisms and as efficiently as non-spliced epitopes. *Sci. Rep.* **6**, 1–12 (2016).
113. Faridi, P. *et al.* A subset of HLA-I peptides are not genomically templated: Evidence for cis- and trans-spliced peptide ligands. *Sci. Immunol.* **3**, (2018).
114. Mylonas, R. *et al.* Estimating the contribution of proteasomal spliced peptides to the HLA-I ligandome. *Mol. Cell. Proteomics* **17**, 2347–2357 (2018).
115. Laumont, C. M. *et al.* Noncoding regions are the main source of targetable tumor-specific antigens. *Sci. Transl. Med.* **10**, (2018).
116. Chong, C. *et al.* Integrated proteogenomic deep sequencing and analytics accurately identify non-canonical peptides in tumor immunopeptidomes. *Nat. Commun.* **11**, (2020).
117. Glish, G. L. & Vachet, R. W. The basics of mass spectrometry in the twenty-first century. *Nature Reviews Drug Discovery* vol. 2 140–150 (2003).
118. Karas, M., Bachmann, D., Bahr, U. & Hillenkamp, F. Matrix-assisted ultraviolet laser desorption of non-volatile compounds. *Int. J. Mass Spectrom. Ion Process.* **78**, 53–68 (1987).
119. Yamashita, M. & Fenn, J. B. Electrospray ion source. Another variation on the free-jet theme. *J. Phys. Chem.* **88**, 4451–4459 (1984).
120. Smith, R. D., Bruce, J. E., Wu, Q. & Lei, Q. P. New mass spectrometric methods for the study of noncovalent associations of biopolymers. *Chem. Soc. Rev.* **26**, 191 (1997).
121. Pitt, J. J. Principles and applications of liquid chromatography-mass spectrometry in clinical biochemistry. *Clin. Biochem. Rev.* **30**, 19–34 (2009).
122. Mcluckey, S. A. *Principles of Collisional Activation in Analytical Mass Spectrometry*. (1992) doi:10.1021/JASMS.8B00290.
123. Glish, G. L. Multiple stage mass spectrometry: The next generation tandem mass spectrometry experiment. *Analyst* **119**, 533–537 (1994).
124. Makarov, A. Electrostatic axially harmonic orbital trapping: A high-performance technique of mass analysis. *Anal. Chem.* **72**, 1156–1162 (2000).
125. Guo, J. & Huan, T. Comparison of Full-Scan, Data-Dependent, and Data-Independent Acquisition Modes in Liquid Chromatography-Mass Spectrometry Based Untargeted Metabolomics. *Anal. Chem.* **92**, 8072–8080 (2020).
126. Tabb, D. L. *et al.* Repeatability and Reproducibility in Proteomic Identifications by Liquid Chromatography-Tandem Mass Spectrometry. doi:10.1021/pr9006365.
127. Michalski, A., Cox, J. & Mann, M. More than 100,000 detectable peptide species elute in single shotgun proteomics runs but the majority is inaccessible to data-dependent LC-MS/MS. *J. Proteome Res.* **10**, 1785–1793 (2011).
128. Liu, H., Sadygov, R. G. & Yates, J. R. A model for random sampling and estimation of relative protein abundance in shotgun proteomics. *Anal. Chem.* **76**, 4193–4201 (2004).
129. Deutsch, E. W. *et al.* Expanding the Use of Spectral Libraries in Proteomics. *Journal of*

Proteome Research vol. 17 4051–4060 (2018).
130. Navarro, P. *et al.* A multicenter study benchmarks software tools for label-free proteome quantification. *Nat. Biotechnol.* **34**, 1130–1136 (2016).
131. Bilbao, A. *et al.* Processing strategies and software solutions for data-independent acquisition in mass spectrometry. *Proteomics* **15**, 964–980 (2015).
132. Hogrebe, A. *et al.* Benchmarking common quantification strategies for large-scale phosphoproteomics. *Nat. Commun.* **9**, (2018).
133. Demichev, V., Messner, C. B., Vernardis, S. I., Lilley, K. S. & Ralser, M. DIA-NN: neural networks and interference correction enable deep proteome coverage in high throughput. *Nat. Methods* **17**, 41–44 (2020).
134. Vaca Jacome, A. S. *et al.* Avant-garde: an automated data-driven DIA data curation tool. *Nat. Methods* (2020) doi:10.1038/s41592-020-00986-4.
135. Gallien, S., Duriez, E., Demeure, K. & Domon, B. Selectivity of LC-MS/MS analysis: Implication for proteomics experiments. *J. Proteomics* **81**, 148–158 (2013).
136. Domon, B. Considerations on selected reaction monitoring experiments: Implications for the selectivity and accuracy of measurements. *Proteomics - Clin. Appl.* **6**, 609–614 (2012).
137. Gallien, S. *et al.* Targeted proteomic quantification on quadrupole-orbitrap mass spectrometer. *Mol. Cell. Proteomics* **11**, 1709–1723 (2012).
138. Peterson, A. C., Russell, J. D., Bailey, D. J., Westphall, M. S. & Coon, J. J. Parallel Reaction Monitoring for High Resolution and High Mass Accuracy Quantitative, Targeted Proteomics* □ S. (2012) doi:10.1074/mcp.O112.020131.
139. MacLean, B. *et al.* Skyline: An open source document editor for creating and analyzing targeted proteomics experiments. *Bioinformatics* **26**, 966–968 (2010).
140. Gallien, S., Bourmaud, A., Kim, S. Y. & Domon, B. Technical considerations for large-scale parallel reaction monitoring analysis. *J. Proteomics* **100**, 147–159 (2014).
141. Gallien, S., Kim, S. Y. & Domon, B. Large-scale targeted proteomics using internal standard triggered-parallel reaction monitoring (IS-PRM). *Mol. Cell. Proteomics* **14**, 1630–1644 (2015).
142. Ong, S. E. & Mann, M. Mass Spectrometry–Based Proteomics Turns Quantitative. *Nat. Chem. Biol.* **1**, 252–262 (2005).
143. Pappireddi, N., Martin, L. & Wühr, M. A Review on Quantitative Multiplexed Proteomics. *ChemBioChem* vol. 20 1210–1224 (2019).
144. Cox, J. *et al.* Accurate proteome-wide label-free quantification by delayed normalization and maximal peptide ratio extraction, termed MaxLFQ. *Mol. Cell. Proteomics* **13**, 2513–2526 (2014).
145. Ong, S. E. *et al.* Stable isotope labeling by amino acids in cell culture, SILAC, as a simple and accurate approach to expression proteomics. *Mol. Cell. Proteomics* **1**, 376–386 (2002).
146. Li, Z. *et al.* Systematic comparison of label-free, metabolic labeling, and isobaric chemical labeling for quantitative proteomics on LTQ orbitrap velos. in *Journal of Proteome Research* vol. 11 1582–1590 (J Proteome Res, 2012).
147. Rothenberg, D. A. *et al.* A Proteomics Approach to Profiling the Temporal Translational Response to Stress and Growth. *ISCIENCE* **9**, 367–381 (2018).
148. Thompson, A. *et al.* Tandem mass tags: A novel quantification strategy for comparative analysis of complex protein mixtures by MS/MS. *Anal. Chem.* **75**, 1895–1904 (2003).
149. Ross, P. L. *et al.* Multiplexed protein quantitation in Saccharomyces cerevisiae using amine-reactive isobaric tagging reagents. *Mol. Cell. Proteomics* **3**, 1154–1169 (2004).
150. Brenes, A., Hukelmann, J., Bensaddek, D. & Lamond, A. I. Multibatch TMT Reveals

False Positives, Batch Effects, and Missing Values Correspondence. *Mol. Cell. Proteomics* **18**, (2019).
151. Maes, E. *et al.* CONSTANd : A normalization method for isobaric labeled spectra by constrained optimization. *Mol. Cell. Proteomics* **15**, 2779–2790 (2016).
152. Altelaar, A. F. M. *et al.* Benchmarking stable isotope labeling based quantitative proteomics. *J. Proteomics* **88**, 14–26 (2013).
153. Wühr, M. *et al.* Accurate multiplexed proteomics at the MS2 level using the complement reporter ion cluster. *Anal. Chem.* **84**, 9214–9221 (2012).
154. Ting, L., Rad, R., Gygi, S. P. & Haas, W. MS3 eliminates ratio distortion in isobaric multiplexed quantitative proteomics. *Nat. Methods* **8**, 937–940 (2011).
155. Hunt, D. F. *et al.* Characterization of peptides bound to the class I MHC molecule HLA-A2.1 by mass spectrometry. *Science (80-.).* **255**, 1261–1263 (1992).
156. Depontieu, F. R. *et al.* Identification of tumor-associated, MHC class II-restricted phosphopeptides as targets for immunotherapy. *Proc. Natl. Acad. Sci. U. S. A.* **106**, 12073–8 (2009).
157. Bassani-Sternberg, M., Pletscher-Frankild, S., Jensen, L. J. & Mann, M. Mass spectrometry of human leukocyte antigen class I peptidomes reveals strong effects of protein abundance and turnover on antigen presentation. *Mol. Cell. Proteomics* **14**, 658–73 (2015).
158. Bassani-Sternberg, M. *et al.* Direct identification of clinically relevant neoepitopes presented on native human melanoma tissue by mass spectrometry. *Nat. Commun.* **7**, 13404 (2016).
159. Storkus, W. J., Zeh, H. J., Salter, R. D. & Lotze, M. T. Identification of T-Cell epitopes: Rapid isolation of class i-presented peptides from viable cells by mild acid elution. *J. Immunother.* **14**, 94–103 (1993).
160. Giam, K. *et al.* A comprehensive analysis of peptides presented by HLA-A1. *Tissue Antigens* **85**, 492–496 (2015).
161. Abelin, J. G. *et al.* Mass Spectrometry Profiling of HLA-Associated Peptidomes in Mono-allelic Cells Enables More Accurate Epitope Prediction. *Immunity* **46**, 315–326 (2017).
162. Purcell, A. W., Ramarathinam, S. H. & Ternette, N. Mass spectrometry–based identification of MHC-bound peptides for immunopeptidomics. *Nat. Protoc.* **14**, 1687–1707 (2019).
163. Gloger, A., Ritz, D., Fugmann, T. & Neri, D. Mass spectrometric analysis of the HLA class I peptidome of melanoma cell lines as a promising tool for the identification of putative tumor-associated HLA epitopes Europe PMC Funders Group. *Cancer Immunol Immunother* **65**, 1377–1393 (2016).
164. Wang, Q. *et al.* Direct detection and quantification of neoantigens. *Cancer Immunol. Res.* **7**, 1748–1754 (2019).
165. Chong, C. *et al.* High-throughput and sensitive immunopeptidomics platform reveals profound interferon γ-mediated remodeling of the human leukocyte antigen (HLA) ligandome. *Mol. Cell. Proteomics* **17**, 533–548 (2018).
166. Heather, J. M. *et al.* Murine xenograft bioreactors for human immunopeptidome discovery. *Sci. Rep.* **9**, (2019).
167. Mancette Rijensky, N. *et al. Identification of tumor antigens in the HLA peptidome of patient-derived xenograft tumors in mouse*.
168. Jensen, S. M., Potts, G. K., Ready, D. B. & Patterson, M. J. Specific MHC-I Peptides Are Induced Using PROTACs. *Front. Immunol.* **9**, (2018).
169. Jaeger, A. M. *et al.* Rebalancing protein homeostasis enhances tumor antigen presentation. *Clin. Cancer Res.* **25**, 6392–6405 (2019).

170. Loffler, M. W. *et al.* Mapping the HLA ligandome of colorectal cancer reveals an imprint of malignant cell transformation. *Cancer Res.* **78**, 4627–4641 (2018).
171. Lippolis, J. D. *et al.* Analysis of MHC Class II Antigen Processing by Quantitation of Peptides that Constitute Nested Sets. *J. Immunol.* **169**, 5089–5097 (2002).
172. Álvaro-Benito, M., Morrison, E., Abualrous, E. T., Kuropka, B. & Freund, C. Quantification of HLA-DM-dependent major histocompatibility complex of class II immunopeptidomes by the peptide landscape antigenic epitope alignment utility. *Front. Immunol.* **9**, 872 (2018).
173. Caron, E. *et al.* The MHC i immunopeptidome conveys to the cell surface an integrative view of cellular regulation. *Mol. Syst. Biol.* **7**, 533 (2011).
174. Javitt, A. *et al.* Pro-inflammatory cytokines alter the immunopeptidome landscape by modulation of HLA-B expression. *Front. Immunol.* **10**, 141 (2019).
175. Goncalves, G. *et al.* IFNγ Modulates the Immunopeptidome of Triple Negative Breast Cancer Cells by Enhancing and Diversifying Antigen Processing and Presentation. *Front. Immunol.* **12**, 645770 (2021).
176. Murphy, J. P. *et al.* Therapy-Induced MHC I Ligands Shape Neo-Antitumor CD8 T Cell Responses during Oncolytic Virus-Based Cancer Immunotherapy. *J. Proteome Res.* **18**, 2666–2675 (2019).
177. Demmers, L. C. *et al.* Single-cell derived tumor organoids display diversity in HLA class I peptide presentation. *Nat. Commun.* **11**, 1–10 (2020).
178. Bourdetsky, D., Schmelzer, C. E. H. & Admon, A. The nature and extent of contributions by defective ribosome products to the HLA peptidome. *Proc. Natl. Acad. Sci. U. S. A.* **111**, (2014).
179. Milner, E., Barnea, E., Beer, I. & Admon, A. The turnover kinetics of major histocompatibility complex peptides of human cancer cells. *Mol. Cell. Proteomics* **5**, 357–365 (2006).
180. Murphy, J. P. *et al.* Multiplexed Relative Quantitation with Isobaric Tagging Mass Spectrometry Reveals Class I Major Histocompatibility Complex Ligand Dynamics in Response to Doxorubicin. *Anal. Chem.* **91**, 5106–5115 (2019).
181. Bogunovic, B., Srinivasan, P., Ueda, Y., Tomita, Y. & Maric, M. Comparative quantitative mass spectrometry analysis of MHC class II-associated peptides reveals a role of GILT in formation of self-peptide repertoire. *PLoS One* **5**, 10599 (2010).
182. Shetty, V. *et al.* Quantitative immunoproteomics analysis reveals novel MHC class I presented peptides in cisplatin-resistant ovarian cancer cells. *J. Proteomics* **75**, 3270–3290 (2012).
183. Hassan, C. *et al.* Accurate quantitation of MHC-bound peptides by application of isotopically labeled peptide MHC complexes. *J. Proteomics* **109**, 240–244 (2014).
184. Li, J. *et al.* TMTpro-18plex: The Expanded and Complete Set of TMTpro Reagents for Sample Multiplexing. *J. Proteome Res.* **20**, 2964–2972 (2021).
185. Weingarten-Gabbay, S. *et al.* Profiling SARS-CoV-2 HLA-I peptidome reveals T cell epitopes from out-of-frame ORFs. *Cell* (2021) doi:10.1016/j.cell.2021.05.046.
186. Pollock, S. B. *et al.* Sensitive and quantitative detection of MHC-I displayed neoepitopes using a semi-automated workflow and TOMAHAQ mass spectrometry. *bioRxiv* 2020.12.16.423097 (2020) doi:10.1101/2020.12.16.423097.
187. Pfammatter, S. *et al.* Extending the Comprehensiveness of Immunopeptidome Analyses Using Isobaric Peptide Labeling. (2020) doi:10.1021/acs.analchem.0c01545.
188. Stopfer, L. E., Mesfin, J. M., Joughin, B. A., Lauffenburger, D. A. & White, F. M. Multiplexed relative and absolute quantitative immunopeptidomics reveals MHC I repertoire alterations induced by CDK4/6 inhibition. *Nat. Commun.* **11**, 1–14 (2020).
189. Khoury, G. A., Baliban, R. C. & Floudas, C. A. Proteome-wide post-translational

modification statistics: Frequency analysis and curation of the swiss-prot database. *Sci. Rep.* **1**, 1–5 (2011).
190. Duan, G. & Walther, D. The Roles of Post-translational Modifications in the Context of Protein Interaction Networks. *PLoS Comput. Biol.* **11**, 1004049 (2015).
191. Blume-Jensen, P. & Hunter, T. Oncogenic kinase signalling. *Nature* vol. 411 355–365 (2001).
192. Ardito, F., Giuliani, M., Perrone, D., Troiano, G. & Muzio, L. Lo. The crucial role of protein phosphorylation in cell signalingand its use as targeted therapy (Review). *International Journal of Molecular Medicine* vol. 40 271–280 (2017).
193. Lawrence, R. T., Searle, B. C., Llovet, A. & Villén, J. Plug-and-play analysis of the human phosphoproteome by targeted high-resolution mass spectrometry. *Nat. Methods* **13**, 431–434 (2016).
194. Bhullar, K. S. *et al.* Kinase-targeted cancer therapies: Progress, challenges and future directions. *Molecular Cancer* vol. 17 (2018).
195. Rikova, K. *et al.* Global Survey of Phosphotyrosine Signaling Identifies Oncogenic Kinases in Lung Cancer. *Cell* **131**, 1190–1203 (2007).
196. Emdal, K. B. *et al.* Characterization of In Vivo Resistance to Osimertinib and JNJ-61186372, an EGFR/Met Bispecific Antibody, Reveals Unique and Consensus Mechanisms of Resistance. *Mol. Cancer Ther.* **16**, 2572–2585 (2017).
197. Macbeath, G. Protein microarrays and proteomics. (2002) doi:10.1038/ng1037.
198. Eduati, F. *et al.* Drug resistance mechanisms in colorectal cancer dissected with cell type-specific dynamic logic models. *Cancer Res.* **77**, 3364–3375 (2017).
199. Ficarro, S. B. *et al.* Phosphoproteome analysis by mass spectrometry and its application to Saccharomyces cerevisiae. *Nat. Biotechnol.* **20**, 301–305 (2002).
200. Rush, J. *et al.* Immunoaffinity profiling of tyrosine phosphorylation in cancer cells. *Nat. Biotechnol.* **23**, 94–101 (2005).
201. Kettenbach, A. N. & Gerber, S. A. Rapid and reproducible single-stage phosphopeptide enrichment of complex peptide mixtures: Application to general and phosphotyrosine-specific phosphoproteomics experiments. *Anal. Chem.* **83**, 7635–7644 (2011).
202. Bian, Y. *et al.* Ultra-deep tyrosine phosphoproteomics enabled by a phosphotyrosine superbinder. *Nat. Chem. Biol.* **12**, 959–966 (2016).
203. Zoumaro-Djayoon, A. D., Heck, A. J. R. & Muñoz, J. Targeted analysis of tyrosine phosphorylation by immuno-affinity enrichment of tyrosine phosphorylated peptides prior to mass spectrometric analysis. *Methods* **56**, 268–274 (2012).
204. Engholm-Keller, K. & Larsen, M. R. Technologies and challenges in large-scale phosphoproteomics. *Proteomics* **13**, 910–931 (2013).
205. Zhang, Y. *et al.* Time-resolved Mass Spectrometry of Tyrosine Phosphorylation Sites in the Epidermal Growth Factor Receptor Signaling Network Reveals Dynamic Modules* □ S. *Mol. Cell. Proteomics* **4**, 1240–1250 (2005).
206. Kim, J.-E. & White, F. M. Quantitative Analysis of Phosphotyrosine Signaling Networks Triggered by CD3 and CD28 Costimulation in Jurkat Cells. *J. Immunol.* **176**, 2833–2843 (2006).
207. Randall, E. C. *et al.* Integrated mapping of pharmacokinetics and pharmacodynamics in a patient-derived xenograft model of glioblastoma. *Nat. Commun.* **9**, (2018).
208. Hochgräfe, F. *et al.* Tyrosine phosphorylation profiling reveals the signaling network characteristics of basal breast cancer cells. *Cancer Res.* **70**, 9391–9401 (2010).
209. De Graaf, E. L. *et al.* Signal Transduction Reaction Monitoring Deciphers Site-Specific PI3K-mTOR/MAPK Pathway Dynamics in Oncogene-Induced Senescence. *J. Proteome Res.* **14**, 2906–2914 (2015).

210. Parker, B. L. *et al.* Targeted phosphoproteomics of insulin signaling using data-independent acquisition mass spectrometry. *Sci. Signal.* **8**, rs6–rs6 (2015).
211. Soste, M. *et al.* A sentinel protein assay for simultaneously quantifying cellular processes. *Nat. Methods* **11**, 1045–1048 (2014).
212. Wolf-Yadlin, A., Hautaniemi, S., Lauffenburger, D. A. & White, F. M. Multiple reaction monitoring for robust quantitative proteomic analysis of cellular signaling networks. *Proc. Natl. Acad. Sci. U. S. A.* **104**, 5860–5865 (2007).
213. Curran, T. G., Zhang, Y., Ma, D. J., Sarkaria, J. N. & White, F. M. MARQUIS: A multiplex method for absolute quantification of peptides and posttranslational modifications. *Nat. Commun.* **6**, 5924 (2015).
214. White, F. M. & Wolf-Yadlin, A. Methods for the Analysis of Protein Phosphorylation–Mediated Cellular Signaling Networks. *Annu. Rev. Anal. Chem.* **9**, 295–315 (2016).
215. Lemmon, M. A. & Schlessinger, J. Cell signaling by receptor tyrosine kinases. *Cell* vol. 141 1117–1134 (2010).
216. Groves, J. T. & Kuriyan, J. Molecular mechanisms in signal transduction at the membrane. *Nature Structural and Molecular Biology* vol. 17 659–665 (2010).
217. Hunter, T. & Sefton, B. M. Transforming gene product of Rous sarcoma virus phosphorylates tyrosine. *Proc. Natl. Acad. Sci. U. S. A.* **77**, 1311–1315 (1980).
218. Sharma, K. *et al.* Ultradeep Human Phosphoproteome Reveals a Distinct Regulatory Nature of Tyr and Ser/Thr-Based Signaling. *Cell Rep.* **8**, 1583–1594 (2014).
219. Amit, I., Wides, R. & Yarden, Y. Evolvable signaling networks of receptor tyrosine kinases: Relevance of robustness to malignancy and to cancer therapy. *Molecular Systems Biology* vol. 3 (2007).
220. Du, W. & Elemento, O. Cancer systems biology: Embracing complexity to develop better anticancer therapeutic strategies. *Oncogene* **34**, 3215–3225 (2015).
221. Drake, J. M. *et al.* Oncogene-specific activation of tyrosine kinase networks during prostate cancer progression. *Proc. Natl. Acad. Sci. U. S. A.* **109**, 1643–1648 (2012).
222. Vasaikar, S. *et al.* Proteogenomic Analysis of Human Colon Cancer Reveals New Therapeutic Opportunities. *Cell* **177**, 1035-1049.e19 (2019).
223. Osinalde, N., Aloria, K., Omaetxebarria, M. J. & Kratchmarova, I. Targeted mass spectrometry: An emerging powerful approach to unblock the bottleneck in phosphoproteomics. *Journal of Chromatography B: Analytical Technologies in the Biomedical and Life Sciences* vols 1055–1056 29–38 (2017).
224. Zhang, Y. *et al.* Time-resolved mass spectrometry of tyrosine phosphorylation sites in the epidermal growth factor receptor signaling network reveals dynamic modules. *Mol. Cell. Proteomics* **4**, 1240–50 (2005).
225. Labots, M. *et al.* Phosphotyrosine-based-phosphoproteomics scaled-down to biopsy level for analysis of individual tumor biology and treatment selection. *J. Proteomics* **162**, 99–107 (2017).
226. Schmidlin, T. *et al.* Assessment of SRM, MRM 3 , and DIA for the targeted analysis of phosphorylation dynamics in non-small cell lung cancer. *Proteomics* **16**, 2193–2205 (2016).
227. Reddy, R. J. *et al.* Early signaling dynamics of the epidermal growth factor receptor. *Proc. Natl. Acad. Sci. U. S. A.* **113**, 3114–3119 (2016).
228. Xie, Y. H., Chen, Y. X. & Fang, J. Y. Comprehensive review of targeted therapy for colorectal cancer. *Signal Transduction and Targeted Therapy* vol. 5 1–30 (2020).
229. Sandhu, J., Lavingia, V. & Fakih, M. Systemic treatment for metastatic colorectal cancer in the era of precision medicine. *Journal of Surgical Oncology* vol. 119 564–582 (2019).
230. Montagner, A. *et al.* A novel role for Gab1 and SHP2 in epidermal growth factor-induced

Ras activation. *J. Biol. Chem.* **280**, 5350–5360 (2005).
231. Zhang, B. *et al.* Proteogenomic characterization of human colon and rectal cancer. *Nature* **513**, 382–387 (2014).
232. Guinney, J. *et al.* The consensus molecular subtypes of colorectal cancer. *Nat. Med.* **21**, 1350–1356 (2015).
233. Strasser, S. D. *et al.* Substrate-based kinase activity inference identifies MK2 as driver of colitis. *Integr. Biol.* **11**, 301–314 (2019).
234. Parseghian, C. M. *et al.* Dual inhibition of EGFR and c-Src by cetuximab and dasatinib combined with FOLFOX chemotherapy in patients with metastatic colorectal cancer. *Clin. Cancer Res.* **23**, 4146–4154 (2017).
235. Spano, J.-P. *et al.* Impact of EGFR expression on colorectal cancer patient prognosis and survival. *Ann. Oncol.* **16**, 102–108 (2005).
236. Amado, R. G. *et al.* Wild-type KRAS is required for panitumumab efficacy in patients with metastatic colorectal cancer. *J. Clin. Oncol.* **26**, 1626–1634 (2008).
237. Van Cutsem, E. *et al.* Cetuximab and Chemotherapy as Initial Treatment for Metastatic Colorectal Cancer. *N. Engl. J. Med.* **360**, 1408–1417 (2009).
238. Douillard, J.-Y. *et al.* Panitumumab–FOLFOX4 Treatment and *RAS* Mutations in Colorectal Cancer. *N. Engl. J. Med.* **369**, 1023–1034 (2013).
239. Giordano, G., Remo, A., Porras, A. & Pancione, M. Immune resistance and egfr antagonists in colorectal cancer. *Cancers* vol. 11 (2019).
240. Martins, M., Mansinho, A., Cruz-Duarte, R., Martins, S. L. & Costa, L. Anti-EGFR therapy to treat metastatic colorectal cancer: Not for all. in *Advances in Experimental Medicine and Biology* vol. 1110 113–131 (Springer New York LLC, 2018).
241. Yang, M. *et al.* Repurposing EGFR inhibitor utility in colorectal cancer in mutant APC and TP53 subpopulations. *Cancer Epidemiol. Biomarkers Prev.* **28**, 1141–1152 (2019).
242. Overman, M. J. *et al.* Durable clinical benefit with nivolumab plus ipilimumab in DNA mismatch repair-deficient/microsatellite instability-high metastatic colorectal cancer. *J. Clin. Oncol.* **36**, 773–779 (2018).
243. Guidoboni, M. *et al.* Microsatellite instability and high content of activated cytotoxic lymphocytes identify colon cancer patients with a favorable prognosis. *Am. J. Pathol.* **159**, 297–304 (2001).
244. Llosa, N. J. *et al.* The vigorous immune microenvironment of microsatellite instable colon cancer is balanced by multiple counter-inhibitory checkpoints. *Cancer Discov.* **5**, 43–51 (2015).
245. Sahin, I. H. *et al.* Immune checkpoint inhibitors for the treatment of MSI-H/MMR-D colorectal cancer and a perspective on resistance mechanisms. *British Journal of Cancer* vol. 121 809–818 (2019).
246. Pagès, F. *et al.* International validation of the consensus Immunoscore for the classification of colon cancer: a prognostic and accuracy study. *Lancet* **391**, 2128–2139 (2018).
247. Domingo, E. *et al.* Somatic POLE proofreading domain mutation, immune response, and prognosis in colorectal cancer: a retrospective, pooled biomarker study. *Lancet Gastroenterol. Hepatol.* **1**, 207–216 (2016).
248. Ni, L. & Lu, J. Interferon gamma in cancer immunotherapy. *Cancer Medicine* vol. 7 4509–4516 (2018).
249. Gustafson, K. S. & Ginder, G. D. Interferon-γ induction of the human leukocyte antigen-E gene is mediated through binding of a complex containing STAT1α to a distinct interferon-γ- responsive element. *J. Biol. Chem.* **271**, 20035–20046 (1996).
250. Rodríguez, J. A. HLA-mediated tumor escape mechanisms that may impair

immunotherapy clinical outcomes via T-cell activation (Review). *Oncology Letters* vol. 14 4415–4427 (2017).
251. Mojic, M., Takeda, K. & Hayakawa, Y. The dark side of IFN-γ: Its role in promoting cancer immunoevasion. *International Journal of Molecular Sciences* vol. 19 (2018).
252. Yoshihara, K. *et al.* Inferring tumour purity and stromal and immune cell admixture from expression data. *Nat. Commun.* **4**, 1–11 (2013).
253. Yu, Q. *et al.* Sample multiplexing for targeted pathway proteomics in aging mice. *Proc. Natl. Acad. Sci.* **117**, 201919410 (2020).
254. Carr, S. A. *et al.* Targeted peptide measurements in biology and medicine: Best practices for mass spectrometry-based assay development using a fit-for-purpose approach. *Mol. Cell. Proteomics* **13**, 907–917 (2014).
255. Subramanian, A. *et al.* Gene set enrichment analysis: A knowledge-based approach for interpreting genome-wide expression profiles. *Proc. Natl. Acad. Sci. U. S. A.* **102**, 15545–15550 (2005).
256. Szklarczyk, D. *et al.* STRING v11: Protein-protein association networks with increased coverage, supporting functional discovery in genome-wide experimental datasets. *Nucleic Acids Res.* **47**, D607–D613 (2019).
257. Shannon, P. *et al.* Cytoscape: A software Environment for integrated models of biomolecular interaction networks. *Genome Res.* **13**, 2498–2504 (2003).
258. Caron, E. *et al.* The MHC i immunopeptidome conveys to the cell surface an integrative view of cellular regulation. *Mol. Syst. Biol.* **7**, 533 (2011).
259. Sharma, P., Hu-Lieskovan, S., Wargo, J. A. & Ribas, A. Primary, Adaptive, and Acquired Resistance to Cancer Immunotherapy. *Cell* vol. 168 707–723 (2017).
260. Martins, F. *et al.* Adverse effects of immune-checkpoint inhibitors: epidemiology, management and surveillance. *Nature Reviews Clinical Oncology* vol. 16 563–580 (2019).
261. Reits, E. A. *et al.* Radiation modulates the peptide repertoire, enhances MHC class I expression, and induces successful antitumor immunotherapy. *J. Exp. Med.* **203**, 1259–1271 (2006).
262. Liu, W. M., Fowler, D. W., Smith, P. & Dalgleish, A. G. Pre-treatment with chemotherapy can enhance the antigenicity and immunogenicity of tumours by promoting adaptive immune responses. *Br. J. Cancer* **102**, 115–123 (2010).
263. Goel, S. *et al.* CDK4/6 inhibition triggers anti-tumour immunity. *Nature* **548**, 471–475 (2017).
264. Khodadoust, M. S. *et al.* Antigen presentation profiling reveals recognition of lymphoma immunoglobulin neoantigens. *Nature* **543**, 723–727 (2017).
265. Schittenhelm, R. B., Sian, T. C. C. L. K., Wilmann, P. G., Dudek, N. L. & Purcell, A. W. Revisiting the Arthritogenic Peptide Theory: Quantitative Not Qualitative Changes in the Peptide Repertoire of HLA-B27 Allotypes. *Arthritis Rheumatol.* **67**, 702–713 (2015).
266. Hogan, K. T. *et al.* Use of selected reaction monitoring mass spectrometry for the detection of specific MHC class I peptide antigens on A3 supertype family members. *Cancer Immunol. Immunother.* **54**, 359–371 (2005).
267. Tan, C. T., Croft, N. P., Dudek, N. L., Williamson, N. A. & Purcell, A. W. Direct quantitation of MHC-bound peptide epitopes by selected reaction monitoring. *Proteomics* **11**, 2336–2340 (2011).
268. Wu, T. *et al.* Quantification of epitope abundance reveals the effect of direct and cross-presentation on influenza CTL responses. *Nat. Commun.* **10**, (2019).
269. Bozzacco, L. *et al.* Mass spectrometry analysis and quantitation of peptides presented on the MHC II molecules of mouse spleen dendritic cells. *J. Proteome Res.* **10**, 5016–5030

(2011).
270. Bijen, H. M. *et al.* Specific T Cell Responses against Minor Histocompatibility Antigens Cannot Generally Be Explained by Absence of Their Allelic Counterparts on the Cell Surface. *Proteomics* **18**, (2018).
271. Yang, Y., Xiang, Z., Ertl, H. C. J. & Wilson, J. M. Upregulation of class I major histocompatibility complex antigens by interferon γ is necessary for T-cell-mediated elimination of recombinant adenovirus-infected hepatocytes in vivo. *Proc. Natl. Acad. Sci. U. S. A.* **92**, 7257–7261 (1995).
272. Rodenko, B. *et al.* Generation of peptide-MHC class I complexes through UV-mediated ligand exchange. *Nat. Protoc.* **1**, 1120–1132 (2006).
273. Bassani-Sternberg, M. *et al.* Deciphering HLA-I motifs across HLA peptidomes improves neo-antigen predictions and identifies allostery regulating HLA specificity. *PLoS Comput. Biol.* **13**, (2017).
274. Nyamao, R. M., Wu, J., Yu, L., Xiao, X. & Zhang, F. M. Roles of DDX5 in the tumorigenesis, proliferation, differentiation, metastasis and pathway regulation of human malignancies. *Biochimica et Biophysica Acta - Reviews on Cancer* vol. 1871 85–98 (2019).
275. Choi, Y. J. & Anders, L. Signaling through cyclin D-dependent kinases. *Oncogene* vol. 33 1890–1903 (2014).
276. Donati, G., Montanaro, L. & Derenzini, M. Ribosome biogenesis and control of cell proliferation: p53 is not alone. *Cancer Research* vol. 72 1602–1607 (2012).
277. Franco, J., Balaji, U., Freinkman, E., Witkiewicz, A. K. & Knudsen, E. S. Metabolic Reprogramming of Pancreatic Cancer Mediated by CDK4/6 Inhibition Elicits Unique Vulnerabilities. *Cell Rep.* **14**, 979–990 (2016).
278. Zarling, A. L. *et al.* Identification of class I MHC-associated phosphopeptides as targets for cancer immunotherapy. *Proc. Natl. Acad. Sci. U. S. A.* **103**, 14889–94 (2006).
279. Zarling, A. L. *et al.* MHC-restricted phosphopeptides from insulin receptor substrate-2 and CDC25b offer broad-based immunotherapeutic agents for cancer. *Cancer Res.* **74**, 6784–95 (2014).
280. Scholtalbers, J. *et al.* TCLP: an online cancer cell line catalogue integrating HLA type, predicted neo-epitopes, virus and gene expression. *Genome Med.* **7**, 118 (2015).
281. Mootha, V. K. *et al.* PGC-1α-responsive genes involved in oxidative phosphorylation are coordinately downregulated in human diabetes. *Nat. Genet.* **34**, 267–273 (2003).
282. Liberzon, A. *et al.* The Molecular Signatures Database Hallmark Gene Set Collection. *Cell Syst.* **1**, 417–425 (2015).
283. Hashizume, R. *et al.* Inhibition of DNA damage repair by the CDK4/6 inhibitor palbociclib delays irradiated intracranial atypical teratoid rhabdoid tumor and glioblastoma xenograft regrowth. *Neuro. Oncol.* **18**, 1519–1528 (2016).
284. Huang, J. *et al.* Article A Single Peptide-Major Histocompatibility Complex Ligand Triggers Digital Cytokine Secretion in CD4 + T Cells. *Immunity* **39**, 846–857 (2013).
285. Ellerman, D. Bispecific T-cell engagers: Towards understanding variables influencing the in vitro potency and tumor selectivity and their modulation to enhance their efficacy and safety. *Methods* **154**, 102–117 (2019).
286. Moritz, A. *et al.* High-throughput peptide-MHC complex generation and kinetic screenings of TCRs with peptide-receptive HLA-A*02:01 molecules. *Sci. Immunol.* **4**, (2019).
287. Harel, M. *et al.* Proteomics of Melanoma Response to Immunotherapy Reveals Mitochondrial Dependence. *Cell* **179**, 236-250.e18 (2019).
288. Yu, C. *et al.* Combination of immunotherapy with targeted therapy: Theory and practice in metastatic melanoma. *Frontiers in Immunology* vol. 10 (2019).

289. McGranahan, T., Therkelsen, K. E., Ahmad, S. & Nagpal, S. Current State of Immunotherapy for Treatment of Glioblastoma. *Current Treatment Options in Oncology* vol. 20 (2019).
290. Browne, C. M. *et al.* A Chemoproteomic Strategy for Direct and Proteome-Wide Covalent Inhibitor Target-Site Identification. *J. Am. Chem. Soc.* **141**, 191–203 (2019).
291. Dobin, A. *et al.* STAR: Ultrafast universal RNA-seq aligner. *Bioinformatics* **29**, 15–21 (2013).
292. Li, H. *et al.* The Sequence Alignment/Map format and SAMtools. *Bioinformatics* **25**, 2078–2079 (2009).
293. Li, B. & Dewey, C. N. RSEM: accurate transcript quantification from RNA-Seq data with or without a reference genome. *BMC Bioinformatics* **12**, 323 (2011).
294. Anders, S. & Huber, W. Differential expression analysis for sequence count data. *Genome Biol.* **11**, R106 (2010).
295. Boegel, S., Löwer, M., Bukur, T., Sahin, U. & Castle, J. C. A catalog of HLA type, HLA expression, and neoepitope candidates in human cancer cell lines. *Oncoimmunology* **3**, (2014).
296. Crooks, G. E., Hon, G., Chandonia, J. M. & Brenner, S. E. WebLogo: A sequence logo generator. *Genome Res.* **14**, 1188–1190 (2004).
297. Ashburner, M. *et al.* Gene ontology: Tool for the unification of biology. *Nature Genetics* vol. 25 25–29 (2000).
298. Hartman, M. L. & Czyz, M. MITF in melanoma: mechanisms behind its expression and activity. *Cell. Mol. Life Sci.* **72**, 1249–60 (2015).
299. Skin Cancer Facts and Statistics. *Skin Cancer Foundation* 1–13 (2017).
300. Serrone, L., Zeuli, M., Sega, F. M. & Cognetti, F. Dacarbazine-based chemotherapy for metastatic melanoma: Thirty-year experience overview. *J. Exp. Clin. Cancer Res.* **19**, 21–34 (2000).
301. Davies, H. *et al.* Mutations of the BRAF gene in human cancer. *Nature* **417**, 949–954 (2002).
302. Ascierto, P. A. *et al.* The role of BRAF V600 mutation in melanoma. *Journal of Translational Medicine* vol. 10 85 (2012).
303. Maurer, G., Tarkowski, B. & Baccarini, M. Raf kinases in cancer-roles and therapeutic opportunities. *Oncogene* vol. 30 3477–3488 (2011).
304. Pratilas, C. A. *et al.* V600EBRAF is associated with disabled feedback inhibition of RAF-MEK signaling and elevated transcriptional output of the pathway. *Proc. Natl. Acad. Sci. U. S. A.* **106**, 4519–4524 (2009).
305. Muñoz-Couselo, E., Adelantado, E. Z., Ortiz, C., García, J. S. & Perez-Garcia, J. NRAS-mutant melanoma: Current challenges and future prospect. *OncoTargets and Therapy* vol. 10 3941–3947 (2017).
306. Johnson, D. B. & Puzanov, I. Treatment of NRAS-mutant melanoma. **16**, 15 (2015).
307. Bos, J. L. ras Oncogenes in Human Cancer: A Review. *Cancer Res.* **49**, (1989).
308. Nissan, M. H. *et al.* Loss of NF1 in cutaneous melanoma is associated with RAS activation and MEK dependence. *Cancer Res.* **74**, 2340–50 (2014).
309. Cuenda, A., Lozano, J., Wellbrock, C. & Arozarena, I. The Complexity of the ERK/MAP-Kinase Pathway and the Treatment of Melanoma Skin Cancer THE ERK/MAP-KINASE PATHWAY IS A CRUCIAL REGULATOR OF MELANOCYTE PROLIFERATION AND DIFFERENTIATION. *Front. Cell Dev. Biol. Cell Dev. Biol* **4**, (2016).
310. Yajima, I. *et al.* RAS/RAF/MEK/ERK and PI3K/PTEN/AKT Signaling in Malignant Melanoma Progression and Therapy. *Dermatol. Res. Pract.* **2012**, 354191 (2012).
311. Lito, P., Rosen, N. & Solit, D. B. Tumor adaptation and resistance to RAF inhibitors.

doi:10.1038/nm.3392.
312. Hooijkaas, A. I., Gadiot, J., Van Der Valk, M., Mooi, W. J. & Blank, C. U. Targeting BRAF V600E in an Inducible Murine Model of Melanoma. *AJPA* **181**, 785–794 (2012).
313. Lim, S. Y., Menzies, A. M. & Rizos, H. Mechanisms and strategies to overcome resistance to molecularly targeted therapy for melanoma. *Cancer* **123**, 2118–2129 (2017).
314. Flaherty, K. T. *et al.* Improved Survival with MEK Inhibition in BRAF-Mutated Melanoma. *N. Engl. J. Med.* **367**, 107–114 (2012).
315. Sullivan, R. J., Lorusso, P. M. & Flaherty, K. T. The intersection of immune-directed and molecularly targeted therapy in advanced melanoma: where we have been, are, and will be. *Clin. Cancer Res.* **19**, 5283–91 (2013).
316. Johannessen, C. M. *et al.* COT drives resistance to RAF inhibition through MAP kinase pathway reactivation. *Nature* **468**, 968–72 (2010).
317. Long, G. V. *et al.* COMBI-d: A randomized, double-blinded, Phase III study comparing the combination of dabrafenib and trametinib to dabrafenib and trametinib placebo as first-line therapy in patients (pts) with unresectable or metastatic BRAF V600E/K mutation-positive cutaneous melanoma . *J. Clin. Oncol.* **32**, 9011–9011 (2014).
318. Grob, J. J. *et al.* Comparison of dabrafenib and trametinib combination therapy with vemurafenib monotherapy on health-related quality of life in patients with unresectable or metastatic cutaneous BRAF Val600-mutation-positive melanoma (COMBI-v): Results of a phase 3, open-label, randomised trial. *Lancet Oncol.* **16**, 1389–1398 (2015).
319. Kim, K. B. *et al.* Phase II study of the MEK1/MEK2 inhibitor trametinib in patients with metastatic BRAF-mutant cutaneous melanoma previously treated with or without a BRAF inhibitor. *J. Clin. Oncol.* **31**, 482–489 (2013).
320. Larkin, J. *et al.* Combined Vemurafenib and Cobimetinib in *BRAF* -Mutated Melanoma. *N. Engl. J. Med.* **371**, 1867–1876 (2014).
321. Dummer, R. *et al.* Encorafenib plus binimetinib versus vemurafenib or encorafenib in patients with BRAF-mutant melanoma (COLUMBUS): a multicentre, open-label, randomised phase 3 trial. *Lancet Oncol.* **19**, 603–615 (2018).
322. Long, G. V. *et al.* Combined BRAF and MEK Inhibition versus BRAF Inhibition Alone in Melanoma. *N. Engl. J. Med.* **371**, 1877–1888 (2014).
323. Robert, C. *et al.* Five-Year Outcomes with Dabrafenib plus Trametinib in Metastatic Melanoma. *N. Engl. J. Med.* **381**, 626–636 (2019).
324. Long, G. V. *et al.* Increased MAPK reactivation in early resistance to dabrafenib/trametinib combination therapy of BRAF-mutant metastatic melanoma. *Nat. Commun.* **5**, (2014).
325. Poulikakos, P. I., Zhang, C., Bollag, G., Shokat, K. M. & Rosen, N. RAF inhibitors transactivate RAF dimers and ERK signalling in cells with wild-type BRAF. *Nature* **464**, 427–430 (2010).
326. LoRusso, P. M. *et al.* Phase I pharmacokinetic and pharmacodynamic study of the oral MAPK/ERK kinase inhibitor PD-0325901 in patients with advanced cancers. *Clin. Cancer Res.* **16**, 1924–1937 (2010).
327. Gupta, A. *et al.* DOC-MEK: A double-blind randomized phase II trial of docetaxel with or without selumetinib in wild-type BRAF advanced melanoma. *Ann. Oncol.* **25**, 968–974 (2014).
328. Kirkwood, J. M. *et al.* Phase II, open-label, randomized trial of the MEK1/2 inhibitor selumetinib as monotherapy versus temozolomide in patients with advanced melanoma. *Clin. Cancer Res.* **18**, 555–567 (2012).
329. Falchook, G. S. *et al.* Activity of the oral MEK inhibitor trametinib in patients with

advanced melanoma: A phase 1 dose-escalation trial. *Lancet Oncol.* **13**, 782–789 (2012).
330. Dummer, R. *et al.* Binimetinib versus dacarbazine in patients with advanced NRAS-mutant melanoma (NEMO): a multicentre, open-label, randomised, phase 3 trial. *www.thelancet.com/oncology* (2017) doi:10.1016/S1470-2045(17)30180-8.
331. Inman, S. Binimetinib Application for NRAS-Mutant Melanoma Withdrawn. 61–62 (2017).
332. Bedard, P. L. *et al.* A Phase Ib Dose-Escalation Study of the Oral Pan-PI3K Inhibitor Buparlisib (BKM120) in Combination with the Oral MEK1/2 Inhibitor Trametinib (GSK1120212) in Patients with Selected Advanced Solid Tumors. *Clin. Cancer Res.* **21**, (2015).
333. Mcdermott, D. *et al.* Anti-Tumour Treatment Durable benefit and the potential for long-term survival with immunotherapy in advanced melanoma. (2014) doi:10.1016/j.ctrv.2014.06.012.
334. Rosenberg, S. A., Mulé, J. J., Spiess, P. J., Reichert, C. M. & Schwarz, S. L. Regression of established pulmonary metastases and subcutaneous tumor mediated by the systemic administration of high-dose recombinant interleukin 2. *J. Exp. Med.* **161**, 1169–88 (1985).
335. Cho, H. *et al.* Apoptosis inhibitor-5 overexpression is associated with tumor progression and poor prognosis in patients with cervical cancer. *BMC Cancer* **14**, 545 (2014).
336. M, K. D. & Gros, G. Le. The role of CTLA-4 in the regulation of T cell immune responses. *Immunol. Cell Biol.* **77**, 1–10 (1999).
337. Fife, B. T. & Bluestone, J. A. Control of peripheral T-cell tolerance and autoimmunity via the CTLA-4 and PD-1 pathways. *Immunol. Rev.* **224**, 166–182 (2008).
338. Hodi, F. S. *et al.* Improved Survival with Ipilimumab in Patients with Metastatic Melanoma. *N. Engl. J. Med.* **363**, 711–723 (2010).
339. Fellne, C. Ipilimumab (Yervoy) prolongs survival in advanced melanoma: Serious side effects and a hefty price tag may limit its use. *P T* **37**, 503 (2012).
340. Topalian, S. L. *et al.* Safety, Activity, and Immune Correlates of Anti–PD-1 Antibody in Cancer. *N. Engl. J. Med.* **366**, 2443–2454 (2012).
341. Robert, C. *et al.* Nivolumab in Previously Untreated Melanoma without BRAF Mutation . *N. Engl. J. Med.* **372**, 320–330 (2015).
342. Larkin, J. *et al.* Combined Nivolumab and Ipilimumab or Monotherapy in Untreated Melanoma. *N. Engl. J. Med.* **373**, 23–34 (2015).
343. Postow, M. A. *et al.* Nivolumab and Ipilimumab versus Ipilimumab in Untreated Melanoma. *N. Engl. J. Med.* **372**, 2006–2017 (2015).
344. Zeynep Eroglu, A. R. Combination therapy with BRAF and MEK inhibitors for melanoma: latest evidence and place in therapy. *Ther. Adv. Med. Oncol. Ther Adv Med Oncol* **8**, 48–56 (2016).
345. Weiss, S. A., Wolchok, J. D. & Sznol, M. Immunotherapy of melanoma: Facts and hopes. *Clinical Cancer Research* vol. 25 5191–5201 (2019).
346. Callahan, M. K. *et al.* Nivolumab plus ipilimumab in patients with advanced melanoma: Updated survival, response, and safety data in a phase i dose-escalation study. in *Journal of Clinical Oncology* vol. 36 391–398 (American Society of Clinical Oncology, 2018).
347. Kim, T. *et al.* Combining targeted therapy and immune checkpoint inhibitors in the treatment of metastatic melanoma. *Cancer Biol. Med.* **11**, 237–46 (2014).
348. Aris, M. & Barrio, M. M. Combining immunotherapy with oncogene-targeted therapy: a new road for melanoma treatment. *Front. Immunol.* **6**, 46 (2015).
349. Boni, A. *et al.* Selective BRAFV600E Inhibition Enhances T-Cell Recognition of Melanoma without Affecting Lymphocyte Function. *Cancer Res.* **70**, (2010).
350. Hu-Lieskovan, S. *et al.* Improved antitumor activity of immunotherapy with BRAF and

MEK inhibitors in BRAF V600E melanoma. doi:10.1126/scitranslmed.aaa4691.
351. Homet Moreno, B., Mok, S., Comin-Anduix, B., Hu-Lieskovan, S. & Ribas, A. Combined treatment with dabrafenib and trametinib with immune-stimulating antibodies for BRAF mutant melanoma. *Oncoimmunology* **5**, e1052212 (2016).
352. Kono, M. *et al.* Role of the Mitogen-Activated Protein Kinase Signaling Pathway in the Regulation of Human Melanocytic Antigen Expression. *Mol. Cancer Res.* **4**, (2006).
353. Frederick, D. T. *et al.* BRAF inhibition is associated with enhanced melanoma antigen expression and a more favorable tumor microenvironment in patients with metastatic melanoma. *Clin. Cancer Res.* **19**, 1225–31 (2013).
354. Ribas, A. *et al.* Combined BRAF and MEK inhibition with PD-1 blockade immunotherapy in BRAF-mutant melanoma. *Nat. Med.* **25**, 936–940 (2019).
355. Jakob, J. A. *et al.* NRAS mutation status is an independent prognostic factor in metastatic melanoma. *Cancer* **118**, 4014–23 (2012).
356. Johnson, D. B. *et al.* Impact of NRAS mutations for patients with advanced melanoma treated with immune therapies. *Cancer Immunol. Res.* **3**, 288–295 (2015).
357. Kirchberger, M. C. *et al.* MEK inhibition may increase survival of NRAS-mutated melanoma patients treated with checkpoint blockade: Results of a retrospective multicentre analysis of 364 patients. *Eur. J. Cancer* **98**, 10–16 (2018).
358. Keller, H. R. *et al.* Overcoming resistance to targeted therapy with immunotherapy and combination therapy for metastatic melanoma. *Oncotarget* **5**, (2015).
359. Vella, L. J. *et al.* The kinase inhibitors dabrafenib and trametinib affect isolated immune cell populations. *Oncoimmunology* **3**, e946367 (2014).
360. Andersen, R. S. *et al.* Dissection of T-cell antigen specificity in human melanoma. *Cancer Res.* **72**, 1642–50 (2012).
361. Van der Bruggen, P. *et al.* Tumor-specific shared antigenic peptides recognized by human T cells. *Immunol. Rev.* **188**, 51–64 (2002).
362. Vita, R. *et al.* The Immune Epitope Database (IEDB): 2018 update. *Nucleic Acids Res.* **47**, D339–D343 (2019).
363. Klechevsky, E. *et al.* Antitumor activity of immunotoxins with T-cell receptor-like specificity against human melanoma xenografts. *Cancer Res.* **68**, 6360–6367 (2008).
364. Middleton, M. R. *et al.* Tebentafusp, A TCR/Anti-CD3 Bispecific Fusion Protein Targeting gp100, Potently Activated Antitumor Immune Responses in Patients with Metastatic Melanoma. *Clin. Cancer Res.* **26**, 5869–5878 (2020).
365. Yang, L. & Ding, J. L. MEK1/2 inhibitors unlock the constrained interferon response in macrophages through IRF1 signaling. *Front. Immunol.* **10**, 2020 (2019).
366. Zhang, Y., Chen, Y., Liu, Z. & Lai, R. ERK is a negative feedback regulator for IFN-γ/STAT1 signaling by promoting STAT1 ubiquitination. *BMC Cancer* **18**, 613 (2018).
367. Van Den, P. J., Sam, E., Gobin, J. P., Van Zutphen, M. & Woltman, A. M. *IFN-Stimulated Response Element HLA Class I Genes Through the Transactivation of Classical and Nonclassical*. *J Immunol References* vol. 163 (1999).
368. Castro, F., Cardoso, A. P., Gonçalves, R. M., Serre, K. & Oliveira, M. J. Interferon-gamma at the crossroads of tumor immune surveillance or evasion. *Frontiers in Immunology* vol. 9 1 (2018).
369. Kang, S. H. *et al.* Inhibition of MEK with trametinib enhances the efficacy of anti-PD-L1 inhibitor by regulating anti-tumor immunity in head and neck squamous cell carcinoma. *Oncoimmunology* **8**, (2019).
370. Grzegrzolka, J. *et al.* Expression of EMT markers SLUG and TWIST in breast cancer. *Anticancer Res.* **35**, 3961–3968 (2015).
371. Fenouille, N. *et al.* The epithelial-mesenchymal transition (EMT) regulatory factor SLUG

(SNAI2) is a downstream target of SPARC and AKT in promoting melanoma cell invasion. *PLoS One* **7**, (2012).
372. Feldkoren, B., Hutchinson, R., Rapaport, Y., Mahajan, A. & Margulis, V. Integrin signaling potentiates transforming growth factor-beta 1 (TGF-β1) dependent down-regulation of E-Cadherin expression – Important implications for epithelial to mesenchymal transition (EMT) in renal cell carcinoma. *Exp. Cell Res.* **355**, 57–66 (2017).
373. Liu, C. Y., Lin, H. H., Tang, M. J. & Wang, Y. K. Vimentin contributes to epithelial-mesenchymal transition ancer cell mechanics by mediating cytoskeletal organization and focal adhesion maturation. *Oncotarget* **6**, 15966–15983 (2015).
374. Kitai, H. & Ebi, H. Key roles of EMT for adaptive resistance to MEK inhibitor in KRAS mutant lung cancer. *Small GTPases* vol. 8 172–176 (2017).
375. Sale, M. J. *et al.* MEK1/2 inhibitor withdrawal reverses acquired resistance driven by BRAF V600E amplification whereas KRAS G13D amplification promotes EMT-chemoresistance. *Nat. Commun.* **10**, (2019).
376. Sterneck, E., Poria, D. K. & Balamurugan, K. Slug and E-Cadherin: Stealth Accomplices? *Front. Mol. Biosci.* **7**, 138 (2020).
377. Shirley, S. H. *et al.* Slug expression during melanoma progression. *Am. J. Pathol.* **180**, 2479–2489 (2012).
378. Caramel, J. *et al.* A Switch in the Expression of Embryonic EMT-Inducers Drives the Development of Malignant Melanoma. *Cancer Cell* **24**, 466–480 (2013).
379. Tulchinsky, E., Howard Pringle, J., Caramel, J. & Ansieau, S. Plasticity of melanoma and EMT-TF reprogramming. *Oncotarget* vol. 5 1–2 (2014).
380. Denecker, G. *et al.* Identification of a ZEB2-MITF-ZEB1 transcriptional network that controls melanogenesis and melanoma progression. *Cell Death Differ.* **21**, 1250–1261 (2014).
381. Peng, J. *et al.* A proteomics approach to understanding protein ubiquitination. *Nat. Biotechnol.* **21**, 921–926 (2003).
382. Kim, J. Y. *et al.* Phosphoproteomics reveals MAPK inhibitors enhance MET-and EGFR-driven AKT signaling in KRAS-mutant lung cancer. *Mol. Cancer Res.* **14**, 1019–1029 (2016).
383. Akbani, R. *et al.* Genomic Classification of Cutaneous Melanoma. *Cell* **161**, 1681–1696 (2015).
384. Dittmann, A. *et al.* High-fat diet in a mouse insulin-resistant model induces widespread rewiring of the phosphotyrosine signaling network. *Mol. Syst. Biol.* **15**, (2019).
385. Udeshi, N. D., Mertins, P., Svinkina, T. & Carr, S. A. Large-scale identification of ubiquitination sites by mass spectrometry. *Nat. Protoc.* **8**, 1950–1960 (2013).
386. Rose, C. M. *et al.* Highly Multiplexed Quantitative Mass Spectrometry Analysis of Ubiquitylomes. *Cell Syst.* **3**, 395-403.e4 (2016).
387. Christinck, E. R., Luscher, M. A., Barber, B. H. & Williams, D. B. Peptide binding to class I MHC on living cells and quantitation of complexes required for CTL lysis. *Nature* **352**, 67–70 (1991).
388. Harding, C. V. & Unanue, E. R. Quantitation of antigen-presenting cell MHC class II/peptide complexes necessary for T-cell stimulation. *Nature* **346**, 574–576 (1990).
389. Bossi, G. *et al.* Examining the presentation of tumor-associated antigens on peptide-pulsed T2 cells. *Oncoimmunology* **2**, e26840 (2013).
390. Lowe, D. B. *et al.* TCR-like antibody drug conjugates mediate killing of tumor cells with low peptide/HLA targets. *MAbs* **9**, 603–614 (2017).
391. Liddy, N. *et al.* Monoclonal TCR-redirected tumor cell killing. *Nat. Med.* **18**, 980–987 (2012).

392. Niwa, R. *et al.* Enhanced natural killer cell binding and activation by low-fucose IgG1 antibody results in potent antibody-dependent cellular cytotoxicity induction at lower antigen density. *Clin. Cancer Res.* **11**, 2327–2336 (2005).
393. Cohen, C. J., Denkberg, G., Lev, A., Epel, M. & Reiter, Y. Recombinant antibodies with MHC-restricted, peptide-specific, T-cell receptor-like specificity: New tools to study antigen presentation and TCR-peptide-MHC interactions. in *Journal of Molecular Recognition* vol. 16 324–332 (2003).
394. Denkberg, G., Lev, A., Eisenbach, L., Benhar, I. & Reiter, Y. Selective Targeting of Melanoma and APCs Using a Recombinant Antibody with TCR-Like Specificity Directed Toward a Melanoma Differentiation Antigen. *J. Immunol.* **171**, 2197–2207 (2003).
395. Park, J. *et al.* SLC45A2: A melanoma antigen with high tumor selectivity and reduced potential for autoimmune toxicity. *Cancer Immunol. Res.* **5**, 618–629 (2017).
396. Salameh, A. *et al.* PRUNE2 is a human prostate cancer suppressor regulated by the intronic long noncoding RNA PCA3. *Proc. Natl. Acad. Sci. U. S. A.* **112**, 8403–8408 (2015).
397. Cheray, M. *et al.* KLRC3, a Natural Killer receptor gene, is a key factor involved in glioblastoma tumourigenesis and aggressiveness. *J. Cell. Mol. Med.* **21**, 244–253 (2017).
398. Harris, J. L. *et al.* BMCC1 Is an AP-2 Associated Endosomal Protein in Prostate Cancer Cells. *PLoS One* **8**, 73880 (2013).
399. Hassan, C. *et al.* Accurate quantitation of MHC-bound peptides by application of isotopically labeled peptide MHC complexes. (2014) doi:10.1016/j.jprot.2014.07.009.
400. Mester, G., Hoffmann, V. & Stevanović, S. Insights into MHC class I antigen processing gained from large-scale analysis of class I ligands. *Cellular and Molecular Life Sciences* vol. 68 1521–1532 (2011).
401. He, Q. *et al.* TCR-like antibodies in cancer immunotherapy. *Journal of Hematology and Oncology* vol. 12 99 (2019).
402. Chalouni, C. & Doll, S. Fate of Antibody-Drug Conjugates in Cancer Cells. *Journal of Experimental and Clinical Cancer Research* vol. 37 (2018).
403. Slaney, C. Y., Wang, P., Darcy, P. K. & Kershaw, M. H. CARs versus BiTEs: A Comparison between T Cell-Redirection Strategies for Cancer Treatment. (2018) doi:10.1158/2159-8290.CD-18-0297.
404. Høydahl, L. S., Frick, R., Sandlie, I. & Løset, G. Å. Targeting the MHC Ligandome by Use of TCR-Like Antibodies. *Antibodies* **8**, 32 (2019).
405. Chames, P., Hufton, S. E., Coulie, P. G., Uchanska-Ziegler, B. & Hoogenboom, H. R. Direct selection of a human antibody fragment directed against the tumor T-cell epitope HLA-A1-MAGE-A1 from a nonimmunized phage-Fab library. *Proc. Natl. Acad. Sci. U. S. A.* **97**, 7969–7974 (2000).
406. Michaeli, Y. *et al.* Expression Hierarchy of T Cell Epitopes from Melanoma Differentiation Antigens: Unexpected High Level Presentation of Tyrosinase-HLA-A2 Complexes Revealed by Peptide-Specific, MHC-Restricted, TCR-Like Antibodies 1. *J. Immunol.* **182**, 6328–6341 (2009).
407. Held, G. *et al.* MHC-peptide-specific antibodies reveal inefficient presentation of an HLA-A*0201-restricted, Melan-A-derived peptide after active intracellular processing. *Eur. J. Immunol.* **37**, 2008–2017 (2007).
408. Nunoya, J. I. *et al.* Short communication: Generation of recombinant monoclonal antibodies against an immunodominant HLA-A*2402-restricted HIV type 1 CTL Epitope. *AIDS Res. Hum. Retroviruses* **25**, 897–904 (2009).
409. Frankel, S. R. & Baeuerle, P. A. Targeting T cells to tumor cells using bispecific antibodies. *Current Opinion in Chemical Biology* vol. 17 385–392 (2013).

410. Nagorsen, D. & Baeuerle, P. A. Immunomodulatory therapy of cancer with T cell-engaging BiTE antibody blinatumomab. *Experimental Cell Research* vol. 317 1255–1260 (2011).
411. Dao, T. *et al.* Therapeutic bispecific T-cell engager antibody targeting the intracellular oncoprotein WT1. *Nat. Biotechnol.* **33**, 1079–1086 (2015).
412. Maruta, M. *et al.* Direct comparison of target-reactivity and cross-reactivity induced by CAR- and BiTE-redirected T cells for the development of antibody-based T-cell therapy. *Sci. Rep.* **9**, (2019).
413. Wang, W., Erbe, A. K., Hank, J. A., Morris, Z. S. & Sondel, P. M. NK cell-mediated antibody-dependent cellular cytotoxicity in cancer immunotherapy. *Frontiers in Immunology* vol. 6 1 (2015).
414. Hendriks, D., Choi, G., de Bruyn, M., Wiersma, V. R. & Bremer, E. Antibody-Based Cancer Therapy: Successful Agents and Novel Approaches. in *International Review of Cell and Molecular Biology* vol. 331 289–383 (Elsevier Inc., 2017).
415. Seo, Y. *et al.* Cetuximab-mediated ADCC activity is correlated with the cell surface expression level of EGFR but not with the KRAS/BRAF mutational status in colorectal cancer. *Oncol. Rep.* **31**, 2115–2122 (2014).
416. Wittman, V. P. *et al.* Antibody Targeting to a Class I MHC-Peptide Epitope Promotes Tumor Cell Death. *J. Immunol.* **177**, 4187–4195 (2006).
417. Li, D. *et al.* Development of a T-cell receptor mimic antibody against wild-type p53 for cancer immunotherapy. *Cancer Res.* **77**, 2699–2711 (2017).
418. Hawkins, O. *et al.* An HLA-Presented Fragment of Macrophage Migration Inhibitory Factor Is a Therapeutic Target for Invasive Breast Cancer. *J. Immunol.* **186**, 6607–6616 (2011).
419. Zhao, Q. *et al.* Affinity maturation of T-cell receptor-like antibodies for Wilms tumor 1 peptide greatly enhances therapeutic potential. *Leukemia* **29**, 2238–2247 (2015).
420. Johansson, M. P., Maaheimo, H. & Ekholm, F. S. New insight on the structural features of the cytotoxic auristatins MMAE and MMAF revealed by combined NMR spectroscopy and quantum chemical modelling. *Sci. Rep.* **7**, (2017).
421. Staudacher, A. H. & Brown, M. P. Antibody drug conjugates and bystander killing: is antigen-dependent internalisation required. *British Journal of Cancer* vol. 117 1736–1742 (2017).
422. Sharma, S., Li, Z., Bussing, D. & Shah, D. K. Evaluation of quantitative relationship between target expression and antibody-drug conjugate exposure inside cancer cells. *Drug Metab. Dispos.* **48**, 368–377 (2020).
423. Perez, E. A. *et al.* Relationship between HER2 expression and efficacy with first-line trastuzumab emtansine compared with trastuzumab plus docetaxel in TDM4450g: A randomized phase II study of patients with previously untreated HER2-positive metastatic breast cancer. *Breast Cancer Res.* **16**, (2014).
424. Burris, H. A. *et al.* Phase II study of the antibody drug conjugate trastuzumab-DM1 for the treatment of human epidermal growth factor receptor 2 (HER2) -positive breast cancer after prior HER2-directed therapy. *J. Clin. Oncol.* **29**, 398–405 (2011).
425. English, D. P. *et al.* T-DM1, a novel antibody–drug conjugate, is highly effective against primary HER2 overexpressing uterine serous carcinoma in vitro and in vivo. *Cancer Med.* **3**, 1256–1265 (2014).
426. Boshuizen, J. *et al.* Cooperative targeting of melanoma heterogeneity with an AXL antibody-drug conjugate and BRAF/MEK inhibitors. *Nat. Med.* **24**, 203–212 (2018).
427. Jacobsen, E. D. *et al.* Brentuximab vedotin demonstrates objective responses in a phase 2 study of relapsed/refractory DLBCL with variable CD30 expression. *Blood* **125**, 1394–

1402 (2015).
428. Reiter, Y., Di Carlo, A., Fugger, L., Engberg, J. & Pastan, I. Peptide-specific killing of antigen-presenting cells by a recombinant antibody-toxin fusion protein targeted to major histocompatibility complex/peptide class I complexes with T cell receptor-like specificity. *Proc. Natl. Acad. Sci. U. S. A.* **94**, 4631–4636 (1997).
429. Lai, J. *et al.* Elimination of melanoma by sortase A-generated TCR-like antibody-drug conjugates (TL-ADCs) targeting intracellular melanoma antigen MART-1. *Biomaterials* **178**, 158–169 (2018).
430. Waight, A. B. *et al.* Structural basis of microtubule destabilization by potent auristatin anti-mitotics. *PLoS One* **11**, (2016).
431. Cohen, C. J. *et al.* Direct Phenotypic Analysis of Human MHC Class I Antigen Presentation: Visualization, Quantitation, and In Situ Detection of Human Viral Epitopes Using Peptide-Specific, MHC-Restricted Human Recombinant Antibodies. *J. Immunol.* **170**, 4349–4361 (2003).
432. Tang, H. *et al.* The analysis of key factors related to ADCS structural design. *Frontiers in Pharmacology* vol. 10 (2019).
433. Maruani, A. Bispecifics and antibody–drug conjugates: A positive synergy. *Drug Discovery Today: Technologies* vol. 30 55–61 (2018).
434. Makawita, S. & Meric-Bernstam, F. Antibody-Drug Conjugates: Patient and Treatment Selection. *Am. Soc. Clin. Oncol. Educ. B.* 105–114 (2020) doi:10.1200/edbk_280775.
435. Budnik, B., Levy, E., Harmange, G. & Slavov, N. SCoPE-MS: mass spectrometry of single mammalian cells quantifies proteome heterogeneity during cell differentiation. *Genome Biol.* **19**, 161 (2018).
436. Yi, L. *et al.* Boosting to Amplify Signal with Isobaric Labeling (BASIL) Strategy for Comprehensive Quantitative Phosphoproteomic Characterization of Small Populations of Cells. *Anal. Chem.* **91**, 5794–5801 (2019).
437. Dou, M. *et al.* High-Throughput Single Cell Proteomics Enabled by Multiplex Isobaric Labeling in a Nanodroplet Sample Preparation Platform. (2019) doi:10.1021/acs.analchem.9b03349.
438. Klann, K., Tascher, G. & Münch, C. Functional Translatome Proteomics Reveal Converging and Dose-Dependent Regulation by mTORC1 and eIF2α. *Mol. Cell* **77**, 913-925.e4 (2020).
439. Chua, X. Y. *et al.* Tandem mass tag approach utilizing pervanadate BOOST channels delivers deeper quantitative characterization of the tyrosine phosphoproteome. *Mol. Cell. Proteomics* **19**, 730–743 (2020).
440. Ramarathinam, S. H. *et al.* A peptide-signal amplification strategy for the detection and validation of neoepitope presentation on cancer biopsies. *bioRxiv* 2020.06.12.145276 (2020) doi:10.1101/2020.06.12.145276.
441. Cheung, T. K. *et al.* Defining the carrier proteome limit for single-cell proteomics. *Nat. Methods* (2020) doi:10.1038/s41592-020-01002-5.
442. Tsai, C. F. *et al.* An Improved Boosting to Amplify Signal with Isobaric Labeling (iBASIL) Strategy for Precise Quantitative Single-cell Proteomics. *Mol. Cell. Proteomics* **19**, 828–838 (2020).
443. Schweppe, D. K., Rusin, S. F., Gygi, S. P. & Paulo, J. A. Optimized Workflow for Multiplexed Phosphorylation Analysis of TMT-Labeled Peptides Using High-Field Asymmetric Waveform Ion Mobility Spectrometry. *J. Proteome Res.* **19**, 554–560 (2020).
444. Robert, C. A decade of immune-checkpoint inhibitors in cancer therapy. *Nature Communications* vol. 11 1–3 (2020).
445. Durgeau, A., Virk, Y., Corgnac, S. & Mami-Chouaib, F. Recent advances in targeting CD8

T-cell immunity for more effective cancer immunotherapy. *Frontiers in Immunology* vol. 9 (2018).
446. Fu, C. & Jiang, A. Dendritic Cells and CD8 T Cell Immunity in Tumor Microenvironment. *Frontiers in immunology* vol. 9 3059 (2018).
447. Wculek, S. K. *et al.* Dendritic cells in cancer immunology and immunotherapy. *Nature Reviews Immunology* vol. 20 7–24 (2020).
448. Gutiérrez-Martínez, E. *et al.* Cross-presentation of cell-associated antigens by MHC class I in dendritic cell subsets. *Frontiers in Immunology* vol. 6 1 (2015).
449. Guermonprez, P., Valladeau, J., Zitvogel, L., Théry, C. & Amigorena, S. Antigen presentation and T cell stimulation by dendritic cells. *Annual Review of Immunology* vol. 20 621–667 (2002).
450. Steinman, R. M. Decisions about dendritic cells: Past, present, and future. *Annual Review of Immunology* vol. 30 1–22 (2012).
451. Reboulet, R. A., Hennies, C. M., Garcia, Z., Nierkens, S. & Janssen, E. M. Prolonged Antigen Storage Endows Merocytic Dendritic Cells with Enhanced Capacity To Prime Anti-Tumor Responses in Tumor-Bearing Mice. *J. Immunol.* **185**, 3337–3347 (2010).
452. Burgdorf, S., Schölz, C., Kautz, A., Tampé, R. & Kurts, C. Spatial and mechanistic separation of cross-presentation and endogenous antigen presentation. *Nat. Immunol.* **9**, 558–566 (2008).
453. Reimann, J. & Schirmbeck, R. Alternative pathways for processing exogenous and endogenous antigens that can generate peptides for MHC class I-restricted presentation. *Immunol. Rev.* **172**, 131–152 (1999).
454. Vyas, J. M., Van Der Veen, A. G. & Ploegh, H. L. The known unknowns of antigen processing and presentation. *Nature Reviews Immunology* vol. 8 607–618 (2008).
455. Delgado, J. C., Escobar, H., Crockett, D. K., Reyes-Vargas, E. & Jensen, P. E. Identification of naturally processed ligands in the C57BL/6 mouse using large-scale mass spectrometric peptide sequencing and bioinformatics prediction. *Immunogenetics* **61**, 241–246 (2009).
456. Duan, Q., Zhang, H., Zheng, J. & Zhang, L. Turning Cold into Hot: Firing up the Tumor Microenvironment. *Trends in Cancer* vol. 6 605–618 (2020).
457. Ghisoni, E., Imbimbo, M., Zimmermann, S. & Valabrega, G. Ovarian cancer immunotherapy: Turning up the heat. *Int. J. Mol. Sci.* **20**, (2019).
458. Wang, S., He, Z., Wang, X., Li, H. & Liu, X. S. Antigen presentation and tumor immunogenicity in cancer immunotherapy response prediction. *Elife* **8**, (2019).
459. Mellman, I. & Steinman, R. M. Dendritic cells: Specialized and regulated antigen processing machines. *Cell* vol. 106 255–258 (2001).
460. Zhu, Y. *et al.* Nanodroplet processing platform for deep and quantitative proteome profiling of 10-100 mammalian cells. *Nat. Commun.* **9**, (2018).